CHANGES IN DNA METHYLATION PATTERNS IN MAMMALS WITH SENESCENCE, AGEING AND ENERGY RESTRICTION

Sofia Lisanti

Thesis submitted for the degree of Doctor of Philosophy

Institute for Ageing and Health

Newcastle University, UK

September 2013

Abstract

DNA methylation is a reversible and inheritable chemical modification which involves the addition of a methyl group to DNA catalyzed by DNA methyltransferases (DNMTs), resulting in the conversion of the cytosine to 5'-methylcytosine, where the cytosine residue is followed by a guanine residue (CpG).
In mammals, there are unusually dense clusters of CpG dinucleotides in the promoters of genes which are called "CpG islands". For many housekeeping genes, these CpG islands are unmethylated in normal healthy tissue. However, CpG islands methylation is often associated with gene silencing and changed patterns of DNA methylation, associated with altered patterns of gene transcription, contribute to the aetiology of several diseases and to ageing.

The overall aim of this project was to characterise the changes in DNA methylation which are observed during cell senescence (in the human cell line MRC-5) and during ageing and in response to dietary energy restriction (in various mice tissues). For this purpose: i) global DNA methylation was quantified using various techniques (ELISA, LINE-1, B1 and LUMA assays and HPLC); ii) site-specific genome-wide screening for methylation changes was performed using the MeDIP technique followed by hybridization to DNA microarrays; iii) validation of the results for selected candidates was performed by pyrosequencing and iv) investigation of mitochondrial DNA methylation was conducted using bisulphite-modified-DNA PCR direct sequencing. Effects of senescence on gene expression were assessed by transcriptome microarrays and by RT-qPCR studies. During the study, previously established methods for the investigation of global DNA methylation (LUMA) and site-specific methylation (MeDIP) were improved.

Whilst global DNA methylation changes were detectable in senescence and after short-term dietary energy restriction, *DNMT*s/*Dnmt*s expression changes were observed in senescence, ageing and following dietary energy restriction and were tissue- and treatment-specific. In parallel, site-specific aberrant DNA methylation was found in the promoters of the genes *CTTN*, *GLIPR2*, *NPTX1* and *SLC39A14* in replicative senescent MRC-5 human fibroblasts. These changes were validated by pyrosequencing and were accompanied by changes in expression of the corresponding genes. Also, in a pilot study, promoter methylation of several cell cycle genes was altered in replicative senescence with associated changes in gene expression. Concordant methylation changes were found

in the promoters of 47 gene in ageing mouse and heart tissues including the genes *Wnt5a*, *Map4k5*, *Apcdd1*, *Chp2* and *Rasgrp2*. In addition, dietary energy restriction counteracted the age-related DNA methylation changes in the promoters of 40 genes, including *Aifm1*, *Irf8*, *Rarg*, *Nmi*, *Maf1*, *Rab33a* and *Fxn* in mouse liver. Finally, mitochondrial DNA methylation studies revealed that senescence affected the DNA methylation patterns of the MT-*COI* and MT-*ND1* gene coding sequences in MRC-5 fibroblasts whilst ageing affected the DNA methylation pattern of the D-Loop region in mouse liver, but this was not reversed by dietary energy restriction.

Pathway analysis revealed that senescence- and age-related aberrant DNA methylation affected genes involved in inter-cellular communication, stress response, malignant transformation, cellular development/proliferation control, cell growth/differentiation and survival, apoptosis and immune response. As these genes contribute to the maintenance of cellular and tissue homeostasis, these findings suggest a potential role for altered DNA methylation in the aetiology of senescence and ageing. On the other hand, short-term dietary energy restriction modulated some of the age-related aberrant DNA methylation patterns of the ageing mouse liver, in particular those in promoters of genes involved in apoptosis regulation, inflammatory and immune response to viral infections, transcription regulation, vesicle trafficking and mitochondrial iron transport and respiration. Finally, mitochondrial DNA aberrant methylation - found to occur at genes belonging to Complex IV and to Complex I - may contribute to the accumulation of hazardous superoxide species in senescent cells whilst DNA aberrant methylation at the D-Loop mitochondrial regulatory region may contribute to age-related mitochondrial dysfunction.

In conclusion, these findings suggest that altered DNA methylation may have a role in the aetiology of senescence and ageing and that some of the effects of dietary energy restriction in slowing down the ageing process and also delaying the onset of age-related diseases may occur via epigenetic mechanisms, including amelioration of age-related aberrations in patterns of DNA methylation.

Dedication

Dedicated to my dear daddy, my first teacher. I'm sure he would be proud of me, if he were here.

Dedicato al mio papà, il mio primo maestro. Sono sicura che sarebbe fiero di me, se fosse qui.

Without haste, but without rest.
Johann Wolfgang von Goethe

Senza fretta, ma senza sosta.
Johann Wolfgang von Goethe

Acknowledgements

I would like to thank my supervisors – Prof. John Mathers, Prof. Thomas von Zglinicki and Prof. Dario Altieri – and my panel members – Prof. Dianne Ford and Prof. Caroline Relton - for their professional guidance, useful critiques and constructive recommendations on this project.

I would also like to thank Dr. Michiel Adriaens for his valuable support with the statistical and bioinformatics analysis and my labmates for all the helpful discussions.

I would also like to extend my thanks to the technicians of the Animal Facility of the Institute for Ageing and Health and to Dr. Kerry Cameron for valuable support during the animal study.

Finally, a special thanks to my parents, to Dr. Michele Tavecchio and to Dr. Sabine Langie for their encouragement and patience throughout my studies.

Abbreviations

$(dT)_{18}$	Deoxythymidine oligonucleotide
(KG)n	Lysine-glycine repeat
5mC	5'-Methyl-Cytosine
A	Adenine
A.	*Acholeplasma*
A260	Absorbance reading at 260 nm
Ab	Antibody
ACME	Algorithm for Capturing Microarray Enrichment
AL	*Ad libitum*
AMP	Adenosine monophosphate
ANOVA	ANalysis Of VAriance
AP	Alkaline Phosphatase
APS	Ammonium Persulphate
ATCC	American Tissue Culture Collection
ATP	Adenosine triphosphate
BM	Bisulphite Modification/Bisulphite Modified
BMI	Body Mass Index
bp	Base pairs
BSA	Bovine Serum Albumine
C	Carbon
C	Cytosine
C. elegans	*Caenorhabditis elegans*
CALERIE	Comprehensive Assessment of Long-term Effects of Reducing Intake of Energy
cDNA	Complementary DNA
ChIP	Chromatin ImmunoPrecipitation
CoA	Coenzyme A
COBRA	COmbined Bisulphite Restriction Assay
CpG	Cytosine-phosphate-Guanosine
Cq	Cycle for quantification
CR	Calorie restriction/Calorie restricted

CRS	Caloric Restriction Society
Ct	Threshold cycle
CV	Coefficient of Variation
D. melanogaster	*Drosophila melanogaster*
dam^{-}	DNA Adenine methylation methylase deficient
DAPI	4',6-diamidino-2-phenylindole
dcm^{-}	DNA Cytosine methylation methylase deficient
DDR	DNA Damage Response
D-Loop	Displacement Loop
DMEM	Dulbecco/Vogt modified Eagle's minimal essential medium
DMF	Dimethylformamide
DMSO	Dimethylsulphoxide
DNA	Deoxyribonucleic acid
DNMT/*Dnmt*	Human DNA Methyltransferase/Murine DNA Methyltransferase
dNTP(s)	Deoxynucleotide(s) triphosphate
DRA	Dialysis Related Amyloidosis
E	Glutamic acid
E	Efficiency of amplification
E. coli	*Escherichia coli*
ECM	Extra-Cellular Matrix
EDTA	Ethylendiaminetetraacetic acid
ELS	Essential Lifespan of a Species
ER	Estrogen Receptor
ER	Dietary energy restriction/restricted
ESIPS	Early Stress-Induced Premature Senescence/Senescent
ESME	Epigenetic Sequencing MEthylation analysis software
EtOH	Ethanol
FBS	Fetal Bovine Serum
FD	Fast Digest
FOR	Forward primer
FR	Free Radicals
G	Guanine
G	Glycine
Gal	Galactosidase

GCRMA	GeneChip Robust Multi-Array Analysis
gDNA	Genomic DNA
GH	Growth Hormone
GHRKO	Growth Hormone Knock Out
GO	Gene Ontology
GTP	Guanosine-5'-triphosphate
h	Human
HDL	High-Density Lipoprotein
HF	High Fidelity
HG	Human Genome
HPLC	High Performance Liquid Chromatography
HSP	Heavy Strand Promoter
ICR	Imprinted Control Region
IgG	Immunoglobulin G
IP	ImmunoPrecipitation
IRS	Insulin Receptor Substrates
IVM	*In Vitro* Methylation/Methylated
K	Lysine
Kb	Kilobase
LB	Luria-Bertani
LDL	Low-Density Lipoprotein
Leu	Leucine
LINE	Long Interspersed Nuclear Element
LncRNA	Long non-coding RNA
LSP	Light Strand Promoter
LTR	Long Terminal Repeats
LUMA	LUminometric Methylation Assay
Lys	Lysine
m	Murine
M.	*Mycoplasma*
m.o.	Months old
MALDI-TOF	Matrix-Assisted Laser Desorption/Ionization-Time Of Flight
MAR	Matrix Attached Regions
mC	Methyl-Cytosine

MCS	Multiple Cloning Site
mdC	Methyl-deoxy-Cytidine
MDRE	Methylation-Dependent Restriction Enzyme
MeDIP	Methylated DNA ImmunoPrecipitation
MEM	Minimum Essential Medium
MHV	Mouse Hepatitis Virus
miR/miRNA	Micro RNA
mRNA	Messenger RNA
MSDK	Methylation-Specific Digital Karyotyping
mSEAP	Murine Secreted Alkaline Phosphatase
MS-HRM	Methylation-Sensitive High Resolution Melting
MSP	Methylation Specific PCR
MSRE	Methylation-Sensitive Restriction Enzymes
mt	Mitochondrial
N	Nitrogen
n	Number
N. furzeri	*Nothobranchius furzeri*
n.s.	Not significant
NaAc	Sodium Acetate
NAD	Nicotinamide adenine dinucleotide
NADH	Nicotinamide adenine dinucleotide (hydrogen)
ncRNA	non-coding RNA
NLS	Nuclear Localization Signal
O_H	Heavy strand origin of replication
OIS	Oncogene-Induced Senescence
O_L	Light strand origin of replication
P	Phosphate
p	Probability
PAGE	Polyacrylamide gel electrophoresis
pAn	PolyAdenylation
PBS	Phosphate Buffer Saline
PCR	Polymerase Chain Reaction
P_H	Heavy strand promoter site
PHD	Plant HomeoDomain motif

piRNA	Piwi-interacting RNA
P_L	Light strand promoter site
PPi	PyroPhosphate
qPCR	Quantitative PCR
r	Representation factor
R^2	Coefficient of determination
RBC	Red Blood Cells
RefSeq	REFerence SEQuence
REV	Reverse primer
RLGS	Restriction Landmark Genome Scanning
RLU	Relative Luminescence Units
RNA	Ribonucleic acid
ROS	Reactive Oxygen Species
rpm	Revolutions per minute
rRNA	Ribosomal RNA
RS	Replicative Senescence/Senescence
RT	Reverse Transcription
RT-qPCR	Reverse Transcriptase Quantitative PCR
S	Sulphur
S. cerevisiae	*Saccharomyces cerevisiae*
SAHF	Senescence Associated Heterochromatin Foci
SAM	S-Adenosyl-Methionine
SASP	Senescent-Associated-Secretory Phenotype
SA-β-GAL	Senescent-Associated-β-Galactosidase
SD	Standard Deviation
SDS	Sodium Dodecyl Sulphate
SEM	Standard Error of the Mean
Ser	Serine
SINE	Short Interspersed Nuclear Elements
siRNA	Small interfering RNA
SNP	Single Nucleotide Polymorphism
SOC	Super Optimal broth with Catabolite repression
sscDNA	Single-Strand Complementary DNA
T	Thymine

Taq	*Thermus aquaticus*
TBE	Tris/Borate/EDTA
TE	Tris-HCl/EDTA
TERM	Transcription TERMination region
Tris-HCl	Tris(hydroxymethyl)aminomethane Hydrochloride
tRNA	Transfer RNA
U	Uracil
UV	Ultra violet
V	Valine
WGA	Whole genome amplification
XCI	X-Chromosome Inactivation
X-gal	5-bromo-4-chloro-3-indolyl-ß-D-galactopyranoside
YC	Young Confluent
Zeo	Zeocin
α	Apyrase
ρ	Spearman's rank correlation coefficient or Pearson's correlation coefficient

Contents

List of Figures

List of Tables

Chapter 1. Introduction

1.1 Epidemiology of ageing

The world population is increasingly growing older; in the developed countries this is the result of a decline in the leading causes of mortality in combination with a decline in the number of births (Ferrucci et al., 2008). According to the most recent data of the World Health Organization (WHO, 2013), in 2011 in the UK:

- life expectancy at birth was 80 years (compared with 76 years in 1990)
- the probability of dying between the age of 15 and 60 was 0.09% (against 0.13% in 1990)
- the median age of the population was 40 years
- the percentage of the population aged under 15 years old was 17%
- the percentage of the population aged over 60 years old was 23%
- the annual growth rate was 0.5%

The increase in life expectancy is the result of better life conditions and of the progress of the medical sciences, but brings new social, economic and medical challenges, which modern society is not entirely equipped to cope with. In fact, older people often face chronic and/or progressive age-related diseases (see Table 1.1, (Ferrucci et al., 2008)) which may cause severe disability, have a major impact on the quality of life, may require long-term care need and are common causes of death (see Figure 1.1).

Table 1.1. Most commonly reported chronic conditions per 100 persons aged > 65 in 2005 (from (Ferrucci et al., 2008)).

Condition	**Men**	**Women**
Hypertension	44.6	51.1
Arthritis diagnosis	40.4	51.4
Chronic joint symptoms	39.7	47.7
Coronary heart disease	24.3	16.5
Cancer (any type)	23.2	17.5
Vision impairment	14.9	18.7

Diabetes	16.9	14.7
Sinusitis	11.5	16.0
Ulcers	13.1	10.4
Hearing impairment	14.8	8.4
Stroke	8.9	8.2
Emphysema	6.3	4.1
Chronic bronchitis	4.5	6.3
Kidney disorders	4.1	3.9
Liver disease	1.4	1.4

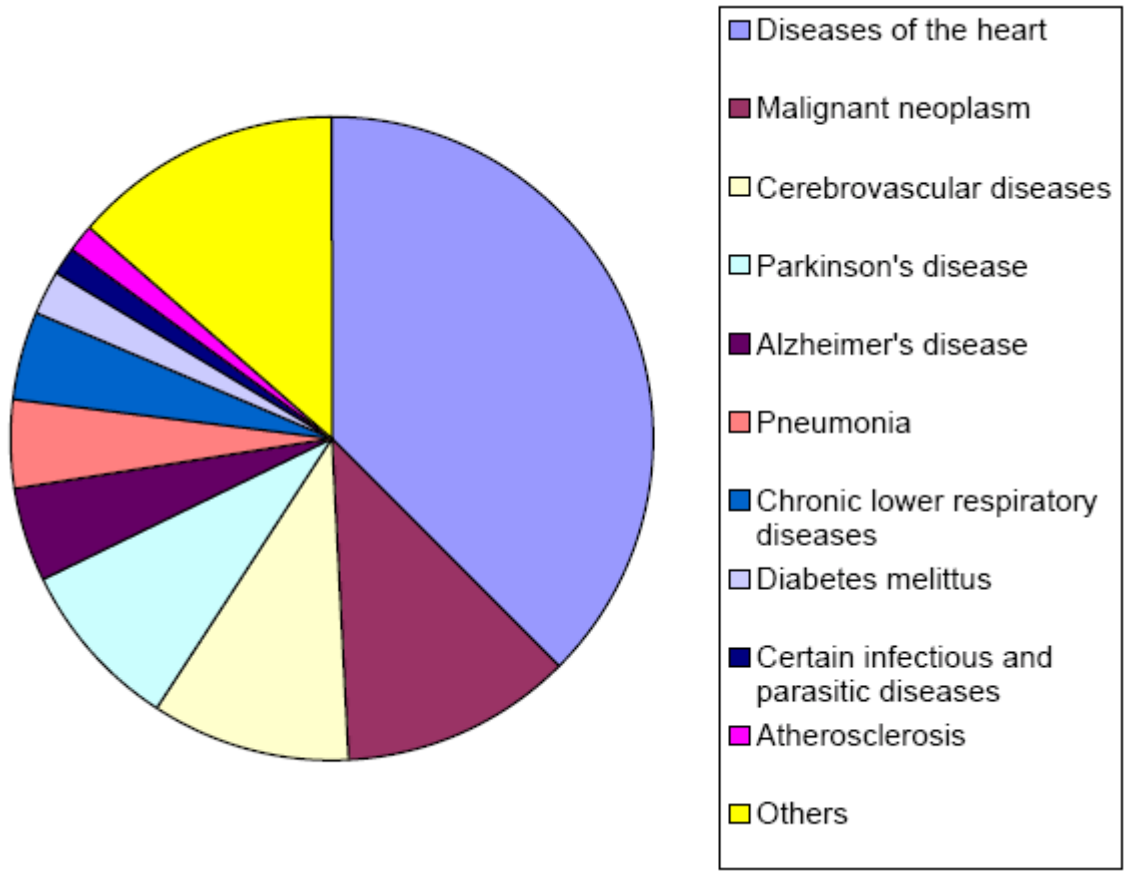

Figure 1.1. Death by underlying or multiple cause, expressed in rates per 100,000 people, for the 2001 US population aged 85 and older (from the National Center for Health Statistics, Data Warehouse on Trends in Health and Aging).

Ageing is a main factor in the development of cancer, cardiovascular and neurodegenerative disorders (Niccoli and Partridge, 2012), although other factors can contribute to their onset; for example, genetic factors such as *APOE4* genotype predispose to Alzheimer's disease (Blennow et al., 2006) and mutations in the leucine-

rich repeat kinase 2 (*LRRK2*) gene to Parkinson's disease (Lesage and Brice, 2009). Lifestyle choices can also have a major impact in the onset of age-related diseases: cholesterol-rich, fat-rich and glucose-rich diets and being overweight or obese have long being associated with the risk of cardiovascular disease, type 2 diabetes, cancers and dementia (Everitt et al., 2006). There is therefore evidence that a healthy diet, together with weight control and exercise, can help in the prevention of age-related diseases (Aballay et al., 2013), resulting in increased life expectancy and in an improvement of the overall quality of life of older people. In particular, there is a strong evidence that adherence to a Mediterranian eating pattern is associated with reduced mortality and lower risk of age-related diseases (Sofi et al., 2010). Elucidating more risk factors that are implicated in the development of age-related diseases, and their reduction or elimination, can also help to achieve these goals.

1.2 Definitions and theories of biological ageing

In biology, ageing is described as a complex and progressive process which takes place in living organisms over time and is characterised by:

- an exponential increase in mortality with age;
- physiological changes leading to functional decline;
- increased susceptibility to many common diseases (summarized in Table 1.1 and Figure 1.1)

and can be defined as:

- the accumulation of changes which lead an organism to death (Medawar, 1952);
- a gradual deterioration of physiological functions (Partridge and Mangel, 1999);
- the irreversible process of loss of viability and increase in vulnerability (Comfort, 1964).

Many hypotheses have been formulated to explain the ageing process, but none of them seems to be able to describe all aspects of the process (Lopez-Otin et al., 2013). This is due to the extensive heterogeneity of ageing between species and between individual organisms within a species - from the macroscopical to the microscopical level - and also

to the impact of different stochastic events. Rattan (Rattan, 2006) concluded that "ageing has no universal cause, phenotype and consequence, except death".
The following sections summarise some of the hypothesis that scientists have formulated to try to explain the ageing process.

1.2.1 The evolutionary principle

The evolutionary principle is based upon the Darwinian definition of essential lifespan of a species (ELS), which is defined as the time that an organism requires to reproduce itself and therefore guarantee the continuity of its species (Rattan and Clark, 2005).
In general, species that quickly develop to adulthood and have a high potential of reproduction have a short ELS, while species that grow slowly and produce few offspring have a long ELS. In a protected environment, such as modern societies for humans or laboratories for mice, living organisms can live longer than their ELS and it is in this further period of life that ageing occurs (Rattan, 2006).

1.2.2 The molecular principle

The molecular theories state that ageing occurs because of progressive accumulation of damaged and damaging molecules and macromolecules within cells and tissues; some examples of those are:

- reactive oxygen species (ROS) and free radicals (FR) generated by exposure to external oxidising agents (e.g. UV rays), or by increased internal production due to reduced mitochondria respiratory capacity (Passos and von Zglinicki, 2005). As an example, the resulting lipid peroxidation products exert cytotoxic and genotoxic effects (Niki et al., 2005);
- long lived-proteins which do not undergo turnover e.g. crystallin, collagen and elastin. Since they may persist for a long time within tissues, these proteins are particularly prone to the accumulation of damage and this damage may affect tissue function and contribute to ageing (Toyama and Hetzer, 2013);
- insoluble proteins that accumulate in the intra and extracellular spaces are also thought to contribute to the ageing process: Hallen (Hallen, 2002) hypothesized that biological ageing could depend on this deleterious accumulation of proteins

that have escaped from proteolytic degradation, which impairs intracellular transport mechanisms.

Glycation – the covalent binding of glucose to proteins - contributes to this process and has been linked with increased risk of diseases such as diabetes, cataract, Alzheimer's, dialysis related amyloidosis (DRA) and atherosclerosis (Suji and Sivakami, 2004);

- errors in the transfer of genetic information from DNA through replication, transcription, translation and in post-transcriptional and post-translational modifications (Rattan, 2006);
- protein errors, which have been widely studied in attempts to understand ageing. The induction of translational errors can accelerate the ageing process in human cells (Holliday, 1996; Rattan, 1996) and in bacteria (Nystrom, 2002). Conversely, increasing the accuracy of the translation machinery, has led to a longer lifespan (Silar and Picard, 1994; Silar et al., 2000; Holbrook and Menninger, 2002).

1.2.3 The genetics principle

Many attempts have been made to identify gerontogenes, that is genes directly involved in the process of ageing, but there seems to be no genes with the specific purpose of causing ageing (Rattan, 1996; Johnson, 2002); nonetheless, it has been demonstrated that mutations in genes encoding for kinases, kinases receptors, transcription factors, DNA helicases, membrane glucosidases, GTP-binding proteins coupled receptors, chaperons, and products involved in cell cycle checkpoints and energy metabolism pathways can affect life span and/or cause premature ageing in humans (Kenyon, 2005; Martin, 2005; Christensen et al., 2006). In addition, altered epigenetics patterns which may cause dysregulation of gene expression is common in age-related diseases and this issue will be discussed in detail later in this Chapter.

1.2.4 The homeodynamics principle

A living organism can be considered as a dynamic system, which responds to external stimuli through internal reassessments. This reassessment is called homeodynamics, that is "stability through change" (Rattan, 2006).

Examples of biological pathways involved in assuring homeodynamics include:

- pathways of nuclear and mitochondrial DNA repair;

- processes for sensing and responding to intra- and extra-cellular stressors;
- pathways for the removal and degradation of defective proteins;
- antioxidative and enzymic defences against reactive oxygen species (ROS);
- processes for the detoxification of harmful chemicals ingested in the diet or entering the body via the lungs or skin;
- cellular and humoral immune responses against pathogens and parasites, including apoptosis;
- processes of wound healing and tissue regeneration.

Over time, organisms become progressively less efficient in maintaining homeostasis; therefore, accumulation of damage and progressively less efficient mechanisms of self-defence may contribute to the ageing process.

1.2.5 The disposable soma theory

Every organism has finite resources and therefore needs to "budget" its metabolic resources between the demands for somatic maintenance and those of growth and reproduction. According to the disposable soma theory, because of the dominant requirement for reproduction, natural selection favours a strategy that invests fewer resources in maintenance of somatic cells and tissues than are necessary for indefinite survival (Kirkwood, 1977).

From Drenos (Drenos and Kirkwood, 2005):

"The disposable soma theory thus closes the gap between mechanistic and evolutionary theories of ageing by suggesting that ageing results from progressive accumulation of molecular and cellular damage, as a direct consequence of evolved limitations in the genetic settings of maintenance and repair functions".

1.3 Cellular senescence

Cellular senescence is defined as an irreversible cell cycle arrest state which was first described in normal human diploid cell cultures by Hayflick and Moorhead (Hayflick and Moorhead, 1961; Hayflick, 1965), who observed that these cells, when cultured under optimal conditions, could only perform a limited number of divisions, or population doublings, the so-called "Hayflick limit". Hayflick and Moorhead identified three different phases undergone by primary cells in culture: a first stage of slow proliferation,

during which the culture is established (phase I), a second stage of rapid growth (phase II) and a third stage, characterized by progressive reduction in rate of cell proliferation, culminating in an inevitable and irreversible arrest of cells growth during which cells remained metabolically active (Hayflick and Moorhead, 1961).

Cellular senescence is characterized by morphological changes, chromatin structure reorganization and specific gene expression profiles. In particular, cells become larger and show increased granularity (Nishio et al., 2001) and the formation of senescence associated heterochromatin foci (SAHF) is observed (Zhang et al., 2007). Gene expression changes in senescence are strongly cell line specific, one example being the chronic inflammatory phenotype seen in senescent fibroblasts (Shelton et al., 1999). Table 1 summarizes the main categories of senescence, with two major types termed replicative senescence and premature senescence respectively, and further subtypes of the latter class, termed stress-induced premature senescence, oncogene-induced senescence and PTEN loss induced cellular senescence (Vargas et al., 2012). However, it must be noted that this classification does not refer to independent molecular mechanisms of senescence, but only to the different terminologies adopted by various authors.

Replicative senescence is typical of cells which stop proliferating as a consequence of telomere shortening and have reached their Hayflick limit (Wright and Shay, 2001). Telomeres are single-stranded DNA stretches located at the end of chromosomes and are formed by TTAGGG repeats folded back on themselves, so that no single-stranded regions of DNA, which could be sensed as DNA damage, are detectable (Moyzis et al., 1988; Meyne et al., 1989). The main function of telomeres is the maintenance of genome integrity, through the protection of chromosome ends from degradation and the prevention of chromosome ends fusion upon replication (Chakhparonian and Wellinger, 2003; Bailey and Murnane, 2006). The inability of DNA polymerase to replicate telomeric sequences (Wright and Shay, 2000), combined with the repression of TERT enzyme (Telomerase Reverse Transcriptase, a ribonucleoprotein polymerase that maintains telomere ends by addition of the telomere repeat) in postnatal somatic cells and to oxidative stress (von Zglinicki, 2002; Kawanishi and Oikawa, 2004), leads to progressive erosion of telomeres with each cell division. This shortening has been strongly associated with cellular senescence (Sherr, 2000) and a functional link is suggested by the fact that most cell lines which overexpress TERT escape senescence (Bodnar et al., 1998; Vaziri and Benchimol, 1998; Yang et al., 1999) and are therefore termed “immortalized”.

The other senescence categories refer to senescence states which are telomere shortening independent. This is the case for oncogene-induced senescence, which is promoted by the overexpression of oncogenes (Gorgoulis and Halazonetis, 2010) and for stress-induced premature senescence, which can be triggered by several kinds of stress, such as DNA damage, suboptimal culture conditions and oxidative stress (Chen and Ames, 1994; Di Leonardo et al., 1994; Chen et al., 1995; Robles and Adami, 1998; Rodier et al., 2009). However, in some instances, replicative and stress-induced senescence might overlap: this is the case of oxidative stress, that contributes to telomeres shortening in fibroblasts (von Zglinicki et al., 1995; von Zglinicki, 2002; Von Zglinicki, 2003).
PTEN-loss induced senescence is considered a separate process by some authors because, although sharing several features with oncogene-induced senescence, it does not require activation of the DNA damage response or hyper-proliferative activity to be induced (Shelton et al., 1999).
All these types of senescence have in common transcriptional activation of the RB-E2F complex response, which ultimately leads to the irreversible arrest of the cell cycle.

Table 1.2. Summary of senescence categories; the classification refers to the triggering mechanism (adapted from (Vargas et al., 2012)).

Type of senescence	**Mechanism**
Replicative senescence	Senescence dependent on telomere length and blocked by hTert expression.
Premature senescence	Any senescence that is not replicative.
Stress-induced premature senescence	Senescence induced by several kinds of stresses, such as DNA damage, oxidative stress and culture conditions.
Oncogene-induced senescence (OIS)	Senescence induced by oncogenes such as Ras^{G12V}, cMYC or $BRaf^{V600E}$; involves signalling pathways such as p38MAPK and the DNA damage response.
PTEN loss-induced cellular senescence	Shares several features with OIS but can also be induced through mechanisms that do not involve DNA Damage Response or p53 signalling.

Several transducers commonly mediate the activation of the senescence programmes (Lowe et al., 2004), e.g. the DNA damage response proteins 53BP1, NBS1, MDC1, ATM and ATR (d'Adda di Fagagna et al., 2003), p53 (Fujita et al., 2009), $p16^{INK4A}$ and RB (Ben-Porath and Weinberg, 2005; Campisi, 2005). These are summarized in Figure 1.2.

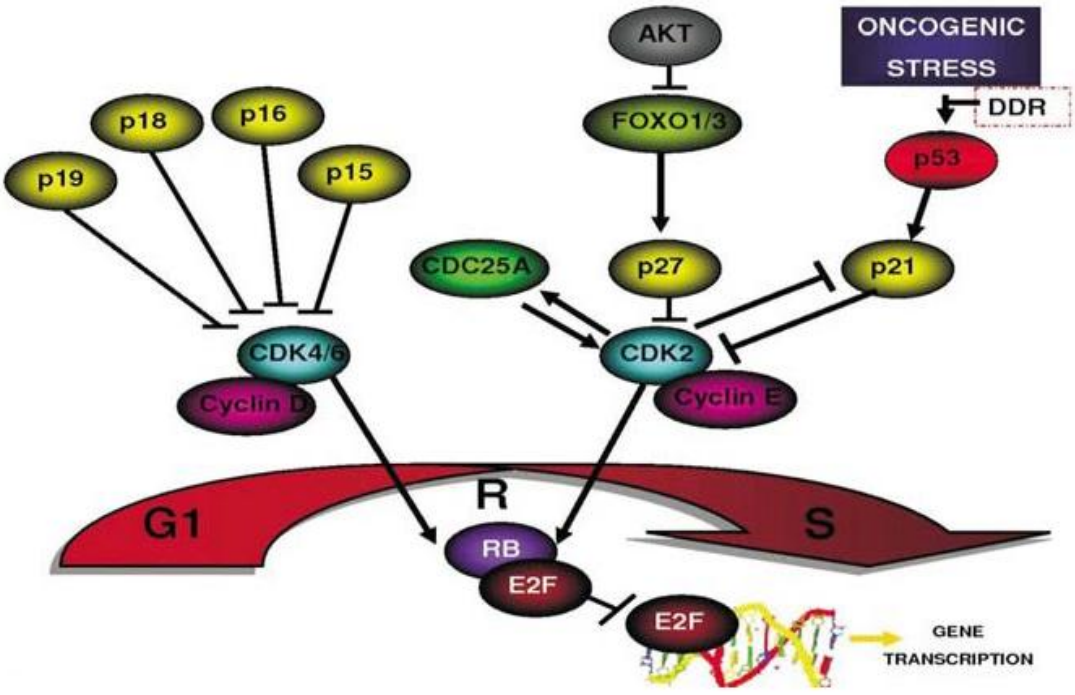

Figure 1.2. Molecular pathways triggering cell senescence (adapted from (Vargas et al., 2012)). Several signal transducers are involved in the activation of the senescence programme, including inhibitors of the expression and/or the activity of cyclins (p15, p16, p18, p19, p21, p27 and p53), cell division cycles (CDCs) and cyclin-dependent kinases (CDKs) and DNA Damage Response proteins.

1.3.1 Biomarkers of cellular senescence

Numerous biomarkers have been used to identify senescent cells *in vitro*, but, to date, none of them alone is sufficient to identify a senescent state (Kuilman et al., 2010). Together with the above mentioned activated (phosphorylated) transducers, morphological changes and the appearance of senescence-associated heterochromatic foci (SAHF), the following other biomarkers are also used to identify senescent cells:

- induction of Senescence Associated-β-Galactosidase (SA-β-GAL) activity (Dimri et al., 1995) at pH = 6, a suboptimal condition for non-senescent cells, for which pH = 4 is optimal for enzyme activity;
- increased mitochondrial Reactive Oxygen Species (ROS) content (Lu and Finkel, 2008; Moiseeva et al., 2009; Lawless et al., 2010; Lawless et al., 2012);
- telomere shortening (Cristofalo et al., 2004);

- telomere-associated DNA damage response (Herbig et al., 2006; Hewitt et al., 2012).

1.3.2 The senescence secretome and cellular senescence in vivo

Senescent cells secrete several cytokines and chemokines (Campisi, 2005) and therefore communicate with neighbouring cells through what it is termed the senescent-associated-secretory phenotype (SASP) (Coppe et al., 2008; Rodier et al., 2009). As previously mentioned, fibroblasts undergoing senescence show a strong inflammatory response (Shelton et al., 1999) which, depending on the genetic context of the cells "receiving the message", can result in a pro-oncogenic response (Krtolica et al., 2001). Communication with neighbouring cells can also be mediated by ROS and induce senescence in normal cells (the so-called senescent cell bystander effect) (Nelson et al., 2012). Once established, the senescence phenotype is stabilized and maintained by a long-term activation of p21, with the induction of mitochondrial dysfunction and ROS production, which, in turns, contribute to persistent DNA damage and to a continuous DNA damage response (Passos et al., 2010). In addition, chemokines (Acosta et al., 2008) and interleukins (Kuilman et al., 2008) contribute to the reinforcement of senescence through a self-amplifying secretory mechanism.

The accumulation of senescent cells can be detected in vivo in ageing organisms. For example, SA-β-GAL activity at pH = 6 has been described in the skin of the older people (Dimri et al., 1995) and in endothelial cells from atherosclerosis patients (Foreman and Tang, 2003), whilst decreased telomere length has been correlated with chondrocyte senescence in osteoarthritis (Price et al., 2002). Partial confirmation of the utility of these putative markers of senescence in vivo is provided by findings from a study of dermal fibroblasts from ageing compared with young baboons, which showed increased markers of DNA damage and of heterochromatinization localized at telomeres and accompanied by increased $p16^{INK4A}$ expression (Herbig et al., 2006). DNA damage foci - in particular accumulation of γ-H2A.X foci (see section 1.4.1) – have been observed in ageing mice lung, spleen, dermis, liver and gut epithelium. This accumulation, a major trigger of senescence, seemed to be associated with tissue sections subjected to higher oxidative stress (e.g. centrilobular area of the liver), but not necessarily to telemore shortening (e.g. intestine crypts), suggesting that stress-dependent senescence might contribute to ageing of some tissues in a telemore-independent manner (Wang et al., 2009). Post-mitotic cells, such as neurons, progressively show several senescence markers in ageing mice

(Senescence Associated-β-Galactosidase activity, ROS and inflammatory chemokines production) as a consequence of a DNA damage response (Jurk et al., 2012).
Cellular senescence is regarded as an important regulator of tissues homeostasis and constitutes a barrier against tumour formation by preventing uncontrolled cell proliferation (Wright and Shay, 2001). However despite the evidence that senescent cells accumulate in ageing tissues, their role in contributing to the ageing phenotype has remained under debate for a long time. Recent findings have demonstrated that clearance of $p16^{Ink4a}$-expressing cells (used as a marker for senescence) delays the onset of age-related phenotypes in certain mouse tissues (Baker et al., 2011), thus suggesting that the accumulation of senescent cells within a tissue has a causal role in the ageing process.

1.4 Epigenetics

Epigenetics is defined as "the inheritance of changes in gene function without any changes in the DNA nucleotide sequence" (Fraga and Esteller, 2007).
Epigenetics plays important roles in biological processes, one example of which is cellular differentiation, as reviewed in (Mohn and Schubeler, 2009). All the nucleated cells in an organism contain the same genomic DNA, but only some genes are expressed in a given tissue, while other genes are silenced. These differential patterns of gene expression underpin the phenotypic heterogeneity of cell types within a higher organism. The three best known epigenetic mechanisms are histone modifications, DNA methylation and non-coding RNAs.

1.4.1 Histone modifications

Within the nucleus, DNA is wrapped around an octet of globular proteins called histones. This structure is called the nucleosome and it is constituted by two copies of each of the core histone proteins (H2A, H2B, H3 and H4) and 146 bp of double-stranded superhelical DNA. Nucleosomes are the basic unit of DNA packaging in eukaryotic cells, indespensable for the storage of genetic information in cell nuclei and are connected to each other by a short stretch of DNA (up to 80 bp) and one copy of the linker histone H1 (Luger et al., 1997).
The ends of histones which protrude from the globular core are known as histone tails and several amino acid residues in these tails are post-translationally modified. The most characterised histone modifications are acetylation, methylation, phosphorylation and

ubiquitination. Whilst more than 60 such modifications have been detected so far using different methodologies (Kouzarides, 2007), the function of most of them is still unknown. They can be classified into two main groups:

- activating modifications, which are related to chromatin accessibility and transcriptional activity, even if not directly;
- repressive modifications, which are related to heterochromatin and genes repression.

This is only a general classification. Indeed, in many cases a single histone modification has different functions depending on modifications of other amino acid residues nearby. The first described histone modification was acetylation (Phillips, 1963), which is often associated with active gene transcription (Zentner and Henikoff, 2013). Typically, core histones are acetylated at several lysine residues by specific enzymes termed Histone Acetyltransferases (HATs) and the mechanism proposed for gene transcription activation is based on the fact that acetylation counteracts the positive charge of lysines, inhibiting interactions between histones and DNA in the nucleosomes and rendering the DNA more accessible to transcriptional complexes (Zentner and Henikoff, 2013).
Another well characterized histone modification is methylation, which occurs not only at lysine residues within core histones, but also at arginines (Bedford and Clarke, 2009). Methylation can be a single modification (monomethylation) or a multiple modification (di- or trimethylation). These modifications have been associated with both transcriptional activation and repression, depending on the residue on which they occur. However, their direct effect on regulation of transcription may be relatively small (Lenstra et al., 2011; Jiang et al., 2011) and regulation of gene expression may be indirect, through modulation of histone affinity for protein complexes involved in the transcription process (Taverna et al., 2007; Schmitges et al., 2011).
Phosphorylation is another well characterized histone modification and it is thought to affect transcription through a similar mechanism of action as for acetylation, i.e. through directly modifying the charge on the histone tail and rendering DNA more accessible for transcription (Banerjee and Chakravarti, 2011). Histones are phosphorylated in many contexts. For example, phosphorylation of the histone variant H2A.X at Ser139 following double-strand breaks (indicated as γ-H2A.X) recruits the repair complexes at the sites of damage and it is used widely as a marker for DNA damage (Paull et al., 2000; Sharma et al., 2012).

With the use of Chromatin Immunoprecipitation techniques, many other histone modifications have been identified; a comprehensive guide to the known histone modifications can be found at the "Human Histone Modification Database" (http://bioinfo.hrbmu.edu.cn/hhmd) (Zhang et al., 2010). However, for most of them, functions and/or mechanisms of action are still to be fully elucidated.

1.4.2 DNA Methylation and DNA Methyltransferases

DNA methylation is a reversible and heritable chemical modification which involves the addition of a methyl group to DNA, described for the first time in calf thymus (Hotchkiss, 1948). In mammals this addition of methyl groups occurs exclusively on Cytosines within CpG dinucleotides (i.e. where a Cytosine residue is followed by guanine residue) and it results in the conversion of the Cytosine to 5'-methylCytosine.

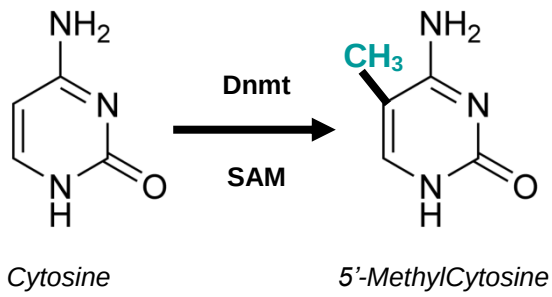

Figure 1.3. Cytosine methylation to 5'-MethylCytosine. The reaction is catalysed by a DNA MethylTransferase (DNMT) in the presence of S-Adenosyl-methyonine.

Figure 1.3 shows the Cytosine methylation reaction, which is catalysed by a group of enzymes called DNA Methyltransferases (Dnmts), responsible to transfer a methyl group from the donor S-adenosyl-methionine (SAM) to the 5' carbon of an unmethylated Cytosine.

The class of DNA Methyltransferases includes enzymes that share similarities within the C-terminal catalytic domains, but little homology at the N-terminal domains (see Figure 1.4).

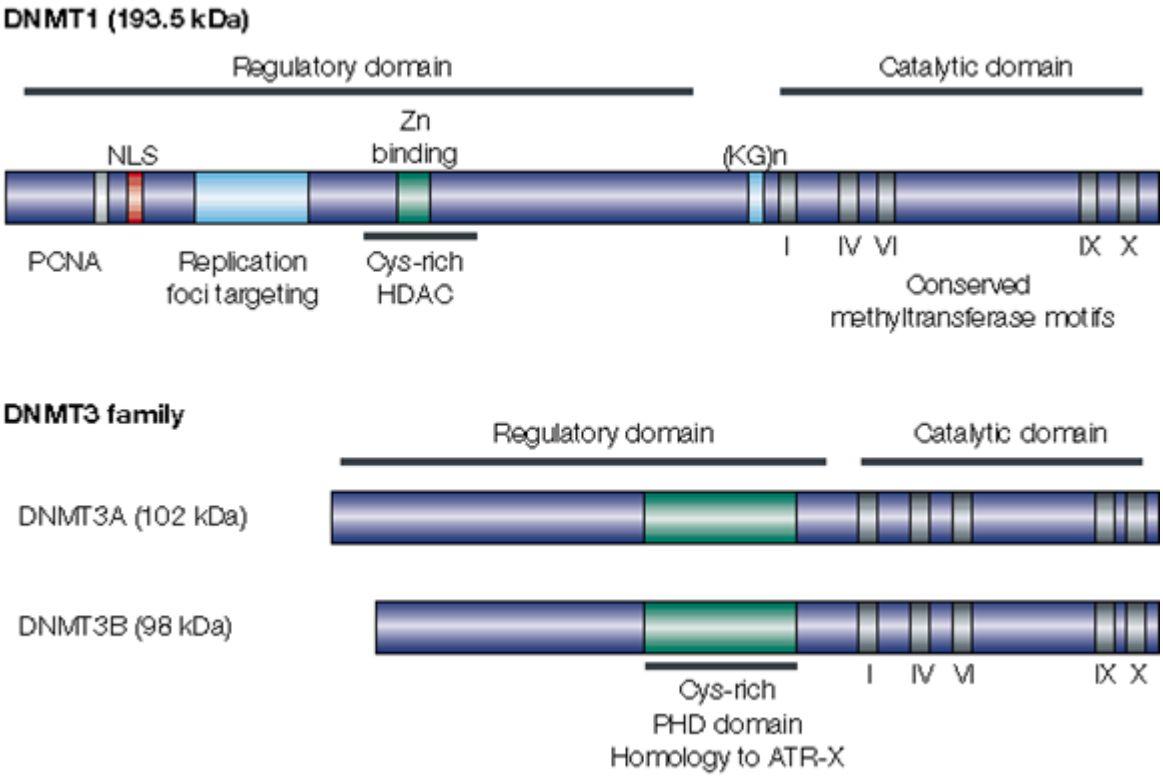

Figure 1.4. Organization of the three main mammalian DNA Methyltransferases. The Roman numerals in the C-terminal part indicate the amino acids motifs that show strong homology to prokaryotic DNA-(Cytosine-C5)-MTase (from (Robertson and Wolffe, 2000). PCNA = proliferating cell nuclear antigen interaction domain; NLS = nuclear localization signal; (KG)n = lysine-glycine repeat hinge region; HDAC = histone deacetylase interaction domain; PHD = plant homeodomain motif that shows homology to the ATR-X (α-thalassaemia, mental retardation, X-linked) gene.

Dnmt1 was the first DNA methyltransferase to be discovered (Gruenbaum et al., 1982) and is commonly termed "the maintenance Dnmt" since it binds to the daughter strand of DNA during replication and methylates it according to the pattern of methylation marks on the parental strand. This assures the inheritance of the methylome (the totality, and patterns, of methylated DNA sites) during cell replication (reviewed by (Hermann et al., 2004a)).

Group 3 includes Dnmt3A and Dnmt3B, which are de novo methylases (reviewed by (Hermann et al., 2004a), and Dnmt3L, which is expressed only in germ cells. Although the latter has not been shown to have methyltransferase activity, it is essential to set the correct imprinting in oocytes and prospermatogonia (Bourc'his et al., 2001; Hata et al., 2002) and it has also been identified as a stimulator of the activity of Dnmt3a (Chedin et al., 2002).

The formerly termed Dnmt2 is the most conserved Dnmt, but the least known enzyme of this family. Its structure allows us to classify it as a Dnmt but, to date, there is no evidence that it has any methyltransferase activity and, even though it is expressed ubiquitously, it seems not to be essential for survival (Goll and Bestor, 2005). Since the discovery that this enzyme is able to methylate Cytosine-38 residue of aspartic acid transfer RNA (Goll et al., 2006), it is has been renamed tRNA aspartic acid methyltransferase 1 (TRDMT1).

In mammals, DNA methylation marks are found throughout their genomes e.g. in transposable elements, gene bodies and intergenic regions.
Although overall the CpG dinucleotide is under-represented in the genome, there are unusually dense clusters of CpG dinucleotides in certain areas of the genome, which are called "CpG islands". In mathematical terms, they are defined as sequences longer than 200 bp with CG content of at least 55% and a ratio observed/expected of CpG frequency of at least 0.6 (Takai and Jones, 2002). However, in order to avoid false positives in the identification of CpG islands, it has become a standard to consider as CpG islands sequences to which the above criteria apply, but with a minimum length of 500 bp (Illingworth et al., 2008). Islands predicted using these methods have been seen to overlap promoter regions of 50%-60% of human genes (Wang and Leung, 2004), thus suggesting that DNA methylation plays a role in the regulation of gene expression; in fact, DNA methylation is associated with gene silencing: methylated Cytosines can either physically impede the binding of transcription factors or bind methyl-CpG-binding domain proteins which in turns recruit other proteins, such as histone deacetylases, and inactivate chromatin, as reviewed by (Zou et al., 2012).

Many functions for DNA methylation have been hypothesized and some have been demonstrated.
The first group includes:

- evolution: spontaneous mutations are the biological driver for evolution so it is logical to assume that DNA methylation could be a mechanism for "increasing genetic and biological diversity" (Cooper and Gerber-Huber, 1985);
- apoptosis: "the suicidal function" of Cytosines methylation could be due to the high mutational rates at these sites, thus leading to progressive genome instability and to programmed cell death (Mazin, 2009).

In the second group of functions there are:

- dosage compensation in mammals. While males have only one X chromosome, females have two. DNA methylation randomly silences one of the female X chromosomes so that there is the same amount of X-related gene products in individuals of both sexes. This process is called X-chromosome inactivation (XCI) and starts in early mammalian development (Heard and Disteche, 2006);
- genomic imprinting. This term refers to the fact that, in placental mammals, some autosomal genes are expressed from only one of the two parental alleles, i.e. parent-of-origin specific expression. Usually, imprinted genes are found in clusters where they are controlled by a unique imprinted control region (ICR) rich in CpG, which are methylated in one of the two strands (Spahn and Barlow, 2003). The methylated allele is transcriptionally silent;
- genome defence from molecular parasites. About 45% of the human genome and 37% of the mouse genome is composed of transposable elements, which include Long Terminal Repeats (LTR)-Retrotransposons, Long and Short Interspersed Nuclear Elements (LINE and SINE, respectively) and DNA transposons. These sequences could interfere with the regulation of gene expression and genome structure by means of insertions, deletions, inversions and translocations of genomic sequences. However, this potential damage is prevented by methylation of most Cytosines within CpG dinucleotides in these repeat regions and most of them resides in heterochromatin regions (Kim et al., 2009b);
- development and cell/tissue differentiation: reprogramming of methylation patterns occurs during different stages of mammalian development. In primordial germ cells there is a global demethylation, while in preimplantation embryos a remethylation occurs (Reik et al., 2001; Cantone and Fisher, 2013);
- chromatin remodelling and regulation of gene expression: approximately half of mammalian genes have CpG islands in their promoter regions (Antequera and Bird, 1993); DNA methylation can suppress their transcription preventing the binding of transcription factors or promoting the binding methyl-CpG-binding proteins (i.e. MeCP2, MBD2), which draw in situ chromatin inactivators (i.e. histone deacetylases and methyltransferases) (Richardson, 2003).

Altered patterns of DNA methylation are observed frequently in many common pathologies and include the following:

- hypomethylation and demethylation, which are associated with some chronic autoimmunodiseases, such as Systemic Lupus Erythematosus (Rahman and Isenberg, 2008) and tumours which develop in several tissues/organs, including stomach, kidney, colon, pancreas, liver, uterus, lung and cervix (Hirst and Marra, 2009). Demethylation is associated with vascular disease (Castro et al., 2003), congenital anomalies of the central nervous system and schizophrenia and other personality disorders (Susser et al., 1996; Hoek et al., 1998; Nishioka et al., 2012; Byrne et al., 2013);
- hypermethylation, which is also seen in cancer development and it is likely to be causal for tumourigenesis when it occurs in the promoter regions of tumour suppressor genes (because it silences the tumour suppressor gene) or of DNA repair genes such as *MLH1* (when gene silencing leads to the accumulation of DNA damage and can be detected via instability of DNA repeat sequences) (Esteller et al., 1998). Similar effects are seen in Fragile X Syndrome (Crawford et al., 2001);
- specific genetic defects, which are observed in genes encoding components of the DNA methylation machinery. For example, Prader-Willi Syndrome and Angleman Syndrome are due to loss of imprinting and are characterised by mental retardation and behavioural abnormalities (Lossie et al., 2001; Nicholls and Knepper, 2001; Goldstone, 2004).

1.4.3 Noncoding RNAs

The term noncoding RNAs (ncRNAs) refers to a wide set of functional RNA molecules that do not encode a protein product. The first RNAs belonging to this category to be identified were RNAs involved in the translation process, such as ribosomal RNAs (rRNAs) (Palade, 1955) and transfer RNAs (tRNAs) (Hoagland et al., 1958). More recently, several other species of noncoding RNAs were discovered which can be generally divided into two main categories - small noncoding RNAs and long noncoding RNAs - . These are of particular interest for epigenetics because they have been shown to be involved in post-transcriptional gene silencing (reviewed in (Castel and Martienssen, 2013). In the first category we can find microRNAs (miRNAs), small interference RNAs (siRNAs) and Piwi-interacting RNAs (piRNAs).

MiRNAs are short non-coding RNAs about 22 nucleotides long which can inhibit the translation of messenger RNAs by binding - through base-pairing complementarity - to

their 3'-untranslated region and targeting them for degradation or affecting their stability (Esquela-Kerscher and Slack, 2006). They are transcribed by RNA polymerase II (Lee et al., 2004) or may derive from splicing of introns (Berezikov et al., 2007). To date, >1000 human miRNAs have been described and miRNAs target many mRNAs (Griffiths-Jones et al., 2008). As a consequence, miRNAs are implicated in the regulation of many cellular processes including development, cell cycle regulation, differentiation, energy metabolism, tumour suppression and apoptosis, as reviewed in (Grillari and Grillari-Voglauer, 2010). There is increasing interest in miRNAs not least because of the recent discovery that miRNAs-encoding loci can be polymorphic and that SNPs and translocations at these loci are correlated with certain diseases and phenotypes (Duan et al., 2009). Thus, these small molecules have become potential new therapeutic targets (Mishra et al., 2009; Mishra and Bertino, 2009).

SiRNAs are short double-stranded RNAs (20-25 bp) which are not encoded by specific genes (as miRNAs are), but are produced from the cleavage of long double-stranded and small hairpin RNAs; these reactions are catalysed by the endoribonuclease Dicer (Bernstein et al., 2001). SiRNAs most known function is transcriptional gene silencing through base-pairing complementarity, as reviewed in (Castel and Martienssen, 2013). Surprisingly, in humans, siRNAs can also activate gene expression by targeting specific promoters (Li et al., 2006).

PiRNAs are the most abundant small noncoding RNAs, are 26 to 31 nucleotides long and are encoded in clusters throughout the genome (Seto et al., 2007). PiRNAs interact with Piwi proteins to form RNA-protein complexes, which have been related to epigenetic and post-transcriptional gene silencing in germ line cells (specifically in the testis for mammals) (Siomi et al., 2011). Because of their sequence complementarity to transposons, piRNAs are thought to specifically silence transposons, contributing to genome stability (Malone and Hannon, 2009).

LncRNAs are very abundant in the genome (Carninci et al., 2005) and lack or have a small open reading frame (ORF) (Dinger et al., 2008). However, some mRNAs can also function as lncRNAs, thus showing bifunctionality (Dinger et al., 2011). LncRNAs are transcribed in the same way as mRNAs (Guttman et al., 2009) and can be found throughout the genome within intergenic regions and often clustered with mRNAs (Carninci et al., 2005). Despite the abundance of these molecules, only about 100 of them have been functionally annotated so far (Amaral et al., 2011). Known functions of lncRNAs include gene-specific transcription regulation (by targeting and modulation of transcriptional activators or repressors and different components of the transcription

machinery (Goodrich and Kugel, 2006)), post-transcriptional regulation (by base complementarity to a target mRNA. As a consequence, lncRNAs might influence all the steps in mRNA processing, such as splicing (Beltran et al., 2008) and translation (Centonze et al., 2007), epigenetic regulation (by modification of the accessibility to chromatin accessibility of modifying proteins (Rinn et al., 2007)), participation in the imprinting process (Pauler et al., 2007) and in X-chromosome inactivation occurring in females (Morey et al., 2004) and possibly by contributing to telemore stability and integrity (Azzalin et al., 2007)).

1.5 DNA methylation in senescence and ageing

The first studies focusing on epigenetics of ageing have demonstrated a significant reduction of in the global 5mC content occurring in mouse, hamster and human fibroblasts with time in culture (Wilson and Jones, 1983) and also in a variety of ageing mammalian tissues (Zin'kovskaia et al., 1978; Wilson et al., 1987; Golbus et al., 1990; Singhal et al., 1987), although this is tissue-specific (Thompson et al., 2010). This loss of methylation could be explained if considering the following observations:

- there is a gradual loss of repetitive DNA regions (such as telomeres) over time; these regions contain a significant proportion of the 5mC in mammalian genomes (Fraga et al., 2005);
- DNMT1 level decreases with age (Zhang et al., 2002b);
- there is a loss of fidelity and efficacy of DNMT1 with age (Casillas et al., 2003);
- DNMT1 targeting by cofactors is progressively impaired with age (Casillas et al., 2003).

Despite the global loss of methylation, ageing cells show aberrant patterns of hypermethylation in some gene promoters and, therefore, altered gene expression levels. Pioneering studies have detected promoter hypermethylation of *MLH1* and *p14ARF* (Shen et al., 2003), *ER, MYOD1, IGF2* and *N33* (Issa et al., 1994; Issa et al., 1996; Ahuja et al., 1998) genes in ageing tissues. Interestingly, those promoters are also aberrantly hypermethylated in cancer, corroborating the assumption that ageing is a primary risk factor for cancer (Fraga and Esteller, 2007; Tapp et al., 2013).
Another characteristic of ageing tissues and cells is the progressive accumulation of mutations at CpG methylation sites, which are the most common hotspots for C>T and

G>A transitions in human genes; in addition, these sites are target for most spontaneous G>C/T and C>A/G transversions, deletions, insertions, tandem, multiple and complex mutations (Cooper and Krawczak, 1989; Walsh and Xu, 2006; Mazin, 2009).
It is known that single base substitutions contribute to cancer development (Cooper and Youssoufian, 1988; Mazin, 1995; Walsh and Xu, 2006), so the age-related accumulation of such mutations helps explain why malignant neoplasia is a common cause of death among older people (see Figure 1.1).
Figure 1.5 shows some epigenetics differences between a young (healthy) cell and an aged cell. Young cells are characterised by dense methylation of repetitive sequences, unmethylated CpG islands of housekeeping genes and high levels of monoacetylated Lys16 and trimethylated Lys20 of H4. In contrast, aged cells show lower Cytosine methylation in repetitive regions and hypermethylation in promoter regions, together with decreased SIRT1 histone deacetylase activity. The resulting changes in gene expression and in genome stability lead to a decreased proliferation/lifespan of the cells.

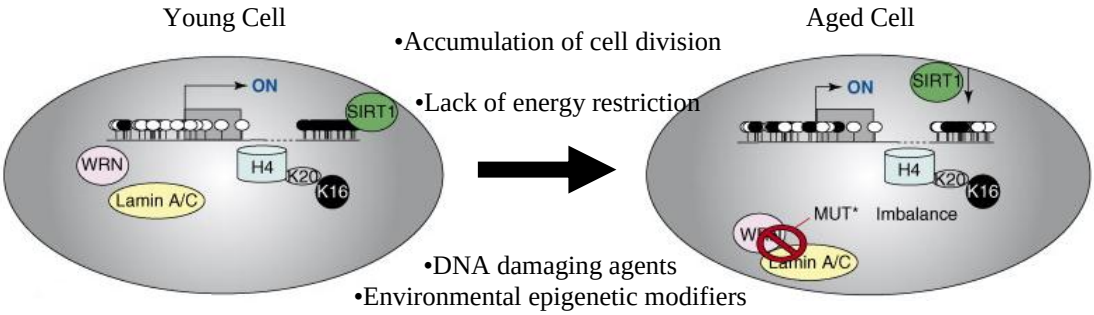

Figure 1.5. Epigenomes of young and aged cells. White and black circles are unmethylated and methylated Cytosines, respectively (adapted from (Fraga and Esteller, 2007).

Lamin A/C and WRN in Figure 1.5 are proteins involved in the development of two "progeroid" syndromes, in which affected patients show clinical features resembling premature ageing, such as cataracts, type 2 diabetes, osteoporosis, arteriosclerosis, hypogonadism and susceptibility to cancer at young age.
The lamin A/C gene encodes for lamins A and C - deriving from alternative RNA splicings - which are involved in the positioning of subchromosome domains in the organisation of chromatin. Hutchinson-Gilford progeria is caused by a point germline mutation in this gene (Taddei et al., 2004), with the direct consequence of nuclear disorganization.

Werner syndrome is caused by an autosomal recessive mutation in *WRN* gene, which encodes a member of the RecQ family helicases, known to be involved in maintaining genome stability (Brosh and Bohr, 2002). Werner syndrome patients have defects in DNA replication and repair pathways.

Recently, it has been shown that these syndromes can also be caused by epigenetic inactivation of the same genes (Fraga and Esteller, 2007). This is stimulating research interest in epigenomic alterations and their relationships with ageing and in the possibility of slowing ageing, or reduce its adverse effects, through targeting these age-related epigenomics events.

1.6 Dietary Energy Restriction

The first study aimed to investigate the effect of dietary energy restriction on mammalian lifespan was conducted on rats as early as 1935. McCay and colleagues found that feeding rats and mice with reduced dietary energy intake, but making sure that the diet provided adequate and balanced amounts of all nutrients, prolonged average and maximum lifespan of the animals of both sexes by 30%-40% and delayed the onset of age-related diseases (McCay et al., 1989).

Since then, dietary energy restriction (ER) without malnutrition has become a powerful and well established tool to study the positive effects that reduced food intake has on lifespan, both in lower and in higher eukaryotes.

ER has been used extensively in longevity studies on *Saccharomyces cerevisiae*, also known as budding yeast, a single-cell organism in which it is easily possible to monitor replicative lifespan - the number of daughter cells generated by a mother cell - and chronological lifespan - the lifespan of a non-dividing cell. In these studies, dietary energy restriction is achieved by diminishing the growing media glucose concentration, e.g. down from the usual 2% to 0.05%. Such experiments showed that both replicative and chronological lifespan were increased up to 3-fold compared with controls (Lin et al., 2000; Kaeberlein et al., 2005; Smith et al., 2007; Wei et al., 2008). Starvation by substituting the growing media with water doubled the chronological lifespan, but affected replicative capacity of the cells (Longo et al., 1997; Wei et al., 2008).

As reviewed in (Mair and Dillin, 2008), in the nematode worm *Caenorhabditis elegans*, dietary restriction is achieved by removing the bacterial feeding layer (axenic culture), or diluting it, and also by genetic manipulations that, for example, introduce defects in the pharyngeal pumping capacity and so limits the amount of food intake. Such dietary

restriction extends lifespan of *C. elegans* by 2 to 3-fold compared with controls (Fontana et al., 2010).

In the fruit fly, dietary energy restriction is achieved by diluting the food (Chapman and Partridge, 1996; Bass et al., 2007) and it can yield a 2-fold increase in lifespan (Fontana et al., 2010).

In mammals, the most of dietary energy restriction studies have been performed on rodents, where this manipulation has increased lifespan by up to 60% and has delayed the onset of age-realated diseases (Anderson et al., 2009). However, a reduced dietary energy intake has also been demonstrated to have deleterious effects, such as impairment of the ability to heal wounds in long term dietary energy restricted mice (Reed et al., 1996) and increased susceptibility to infections (Kristan, 2008). Animals genetic background seems to play a major role in the response to dietary energy restriction which, in some cases, resulted in a shorter lifespan (Swindell, 2012; Liao et al., 2013).

In primates, a long term study (20+ years) is being conducted on rhesus monkeys and recently published results demonstrated that dietary energy restriction of 30% decreased age-related mortality (Colman et al., 2009). Dietary energy restricted animals showed a lower incidence of neoplasia formation and cardiovascular disease, compared with normal fed individuals, and none of them developed diabetes; in addition, reduced oxidative damage, inflammation and brain atrophy were observed. However, another study conducted on rhesus monkeys showed no significant improvement of survival outcomes in dietary energy restricted animals compared with control group animals (Mattison et al., 2012). Austad (Austad, 2012) commented on these contrasting results suggesting that those could be due to differences in the diet compositions or to the fact that in the second study the control group was not fed an *ad libitum* diet, but a diet which would prevent obesity, therefore being partially dietary energy restricted. The author suggests that, if this proved true, the effects of dietary energy restriction could be beneficial for overweight individuals, but only minimal for people who already maintain a healthy body weight.

For both practical and technical reasons, long-term randomized studies of effects of ER in humans have not been carried out. However, there have been a number of short-term studies of dietary energy restriction in humans. For example, Fontana and colleagues reported that adults from both sexes exposed to dietary energy restriction lasting 1 or 6 years showed lower serum levels of atherosclerosis risk factors, such as LDL cholesterol, ratio total cholesterol/HDL cholesterol, triglycerides and fasting glucose and insulin (Fontana et al., 2004; Fontana et al., 2007). In the latter study, the authors concluded that

20% dietary energy restriction has the same beneficial effects in lowering levels of atherosclerosis risk factors as a 20% increase in energy expenditure. Both interventions were found to decrease the amount of oxidative damage to DNA and RNA in white blood cells.

The CALERIE project (Comprehensive Assessment of Long-Term Effects of Reducing Calorie Intake) has concluded Phase I with three pilot studies in which healthy and non-obese subjects were subjected to 6 to 12 months of 20-25% dietary energy restriction; results were similar to those reported by Fontana and colleagues (Racette et al., 2006; Heilbronn et al., 2006; Rochon et al., 2011; Meydani et al., 2011).

Members of the Caloric Restriction Society (CRS) showed, together with lower serum levels of atherosclerosis factors, also lower plasma level of TNFα, a proinflammatory cytokine (Fontana et al., 2004; Holloszy and Fontana, 2007). Interpretation of these results is not straight forward because members of the CRS are self-selected and the apparent effects of dietary energy restriction may be confounded by other lifestyle factors, notably physical activity and smoking behavior, and/or by genetic factors, which may influence willingness to join the CRS.

Recent studies have correlated the Body Mass Index (BMI, a measure of general adiposity based on an individual's weight and height) to mortality and found that the latter was lowest at BMI included between at about 22.5–25, while it increased in a direct proportional manner at BMIs higher than 25 and in an inverse proportional manner at BMIs lower than 22.5, mainly due to smoking-related diseases (Prospective Studies et al., 2009). Maintaing a healthy body weight throughtout life might therefore help reducing the risk of age-related diseases; this can be achieved by eating a balanced diet and practising regular exercise (Handschin and Spiegelman, 2008).

1.6.1 Molecular mechanisms of dietary energy restriction-mediated increased lifespan

Age-related changes seem to be tissue specific (Anderson and Weindruch, 2010); nonetheless there are some that seem to play a pivotal role in the synchronization of the ageing process at a whole organism level (Zahn et al., 2007). Dietary energy restriction counteracts the most common ones, such as increased expression of genes involved in the immune and inflammatory responses and mitochondrial dysfunction (Park and Prolla, 2005; de Magalhaes et al., 2009).

Many pathways and molecular mechanisms have been suggested to be mediators of this action and of the resulting extended and healthier lifespan; so far, the most characterized

ones are the TOR signalling pathway, the IGF/insulin pathway, adiponectin expression and epigenetics mechanisms - DNA methylation and histone acetylation/deacetylation and miRNA expression, as reviewed by (Ribaric, 2012) -. DNA methylation will be discussed in Chapter 1.6.

Figure 1.6 summarizes the engagement of the TOR and IGF1 signalling pathways in various organisms subjected to dietary energy restriction.

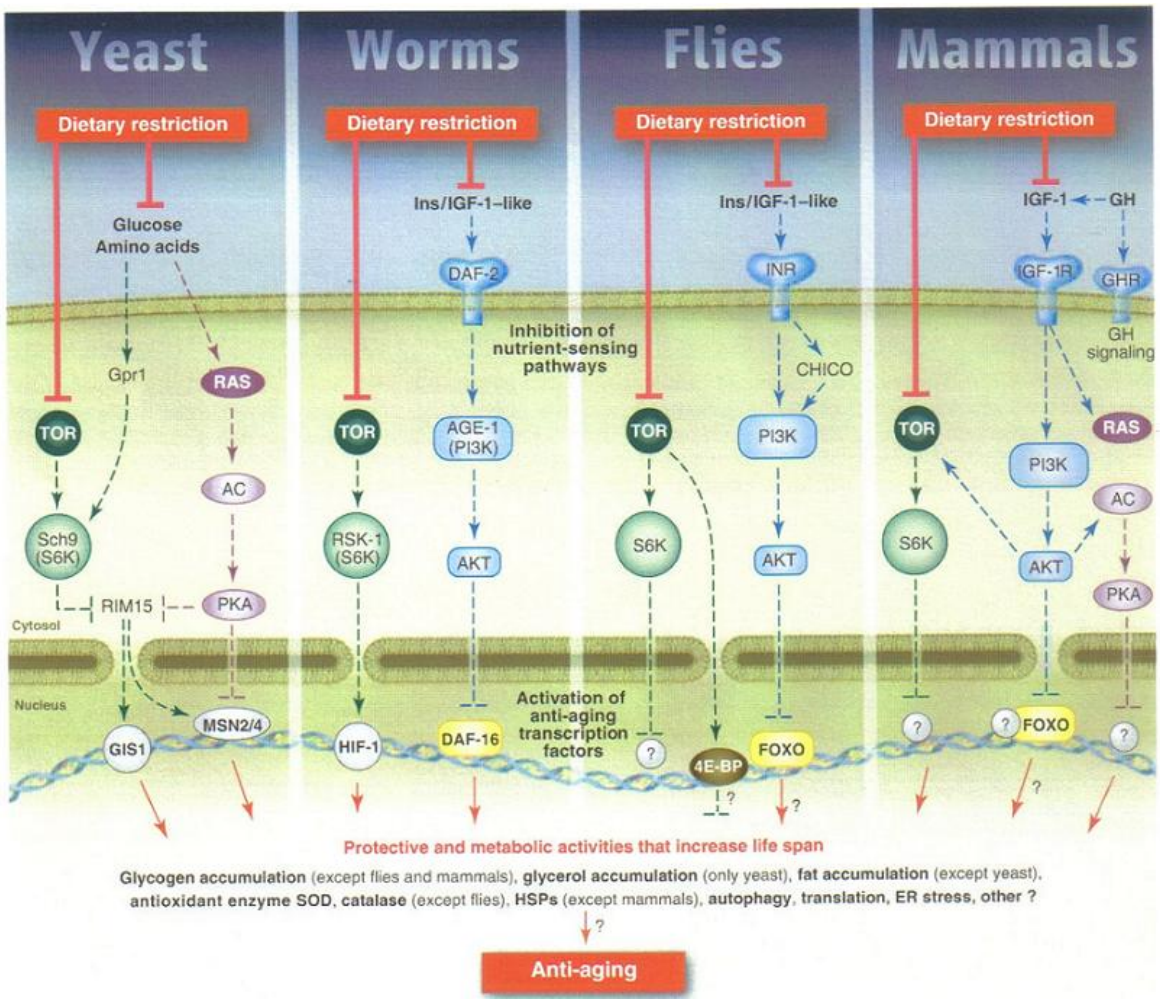

Figure 1.6. Nutrient signalling pathways involved in the dietary energy restriction-mediated lifespan extension in lower and higher eukaryotes. From (Fontana et al., 2010).

TOR signalling pathway and its ageing promoting action is conserved in yeast, worms, flies and mice (Fontana et al., 2010); this pathway is a master regulator of protein synthesis, contributing to cell growth and proliferation (Hay and Sonenberg, 2004). Reduced levels of cellular aminoacids, as it occurs under dietary energy restriction conditions, inhibit TOR activity and promote a longer lifespan, partially by increasing autophagy (Yen and Klionsky, 2008).

In yeasts, the inhibition of the TOR signalling pathway and the resulting inactivation of its downstream target SCH9 have been linked to extented lifespan, which correlates with altered protein synthesis (Kaeberlein et al., 2005; Powers et al., 2006).
In mammals, mTOR (mechanistic TOR, formerly mammalian TOR) forms two big protein complexes, named mTORC1 and mTORC2. mTORC1 is the most known one and acts as a stress sensor: when conditions of nutrient depletion (Blommaart et al., 1995), energy decrease or hypoxia (Inoki et al., 2003) or growth factors unbalance occur within the cells, mTORC1 becomes inactivated and unable to phosphorylate its numerous effectors, as reviewed in (Laplante and Sabatini, 2012). The same effects are seen when the complex is genetically targeted, as in the case of deletion of TOR1 in yeasts (Kaeberlein et al., 2005; Powers et al., 2006; Wei et al., 2008) or pharmacologically targeted with rapamycin (Powers et al., 2006) again in yeasts, but also in mice (Harrison et al., 2009). In this latter study, rapamycin fed mice showed a slower ageing rate compared with control, which was associated with decreased tissue degeneration.
Although the downstream effector responsible in modulating ageing is still unknown, it has been observed that reduction in the activity of S6K1 is correlated with an increase in lifespan of various species (Kapahi et al., 2010) and that overexpression of 4E-BP1 extends lifespan in flies under normal diet conditions, while its loss does not extend it under a dietary energy restriction regimen (Zid et al., 2009). As reviewed in (Kapahi et al., 2010) the effect of these mediators is believed to be due to the impairment of the translational process.
Rapamycin has also been shown to decelerate cellular senescence and to be able to reverse the senescence phenotype in human and rodents cell lines (Demidenko et al., 2009), thus reinforcing the existence of a link between cellular senescence and ageing; further confirmations arise from studies showing that dietary energy restriction - which usually extends lifespan and delays age-related diseases onset - inhibits cellular senescence in vivo (Wang et al., 2009).

The insulin/IGF1 signalling pathway seems to be another evolutionarily conserved mediator of the beneficial effects of dietary energy restriction on longevity. Studies in worms have shown that a reduced activity of this pathway, which could be achieved by diminishing food intake, increases lifespan, as it does in flies and rodents (Johnson, 2008; Piper et al., 2008; Bartke, 2005). However, in humans dietary energy restriction has not been demonstrated to decrease IGF1 serum levels without being combined to a restriction of the protein intake (Fontana et al., 2008).

IGF1 and insulin inhibit a class of transcription factors termed FOXOs (forkhead box O) by translocating them from the nucleus through various insulin receptor substrates (IRS) and kinases (PDPK1, PTDINS-3K); FOXOs control several cellular functions such as cell cycle, apoptosis, differentiation and the expression of DNA repair related genes and genes involved in the stress response, therefore their up-regulation is considered one of the mechanism through which dietary energy restriction mediates lifespan increase (Qin et al., 2008).
Nonetheless, although low levels of IGF1 and mutations of the IGF1 receptor gene are associated with longevity in humans (Bonafe et al., 2003; Suh et al., 2008), there is increasing evidence that the insulin/IGF1 signalling pathway inhibition could be only a secondary cell response towards increased lifespan dietary energy restriction mediated: in fact, GHRKO (Growth Hormone Knock Out) mice showed only a minimal extension of lifespan (and only females) when subjected to dietary energy restriction in comparison with *ad libitum* fed mice controls (Bonkowski et al., 2006), corroborating the hypothesis that GH signalling could be crucial to delayed ageing in mammals, with the inhibition of the Insulin/IGF1 pathway being only its secondary effect (Brown-Borg and Bartke, 2012).

Adiponectin is a hormone secreted by adipocytes of the white adipose tissue; it has been shown to promote fatty acid oxidation within this tissue and to reduce the accumulation of lipids in other tissues (Zhu et al., 2007). It is also implicated in the control of glucose metabolism and thus it suppresses metabolic perturbations which could lead to the development of some age-related diseases, such as obesity, type 2 diabetes, atherosclerosis and metabolic syndrome (Ukkola and Santaniemi, 2002; Diez and Iglesias, 2003; Renaldi et al., 2009). Adiponectin plasma levels are inversely correlated to the amount of body fat in adults (Ukkola and Santaniemi, 2002; Meier and Gressner, 2004), so that under dietary energy restriction regimen, an increase of its plasma concentration is observed (Shinmura et al., 2007). High levels of circulating adiponectin stimulate AMPK, which, in turns, favours mitochondrial biogenesis and energy production (Civitarese et al., 2006). The beneficial effects of the adiponectin increased plasma levels are also mediated by the inhibition of proinflammatory cytokines, such as TNFα (Fernandez-Real et al., 2003; Aldhahi and Hamdy, 2003; Ouchi et al., 2003); in fact, at least two different dietary energy restriction studies conducted in humans have demonstrated decreased serum or plasma levels of C-reactive protein (an inflammation

positive acute-phase protein) of the subjects compared with controls (Fontana et al., 2004; Fontana et al., 2007).

Histone modifications play a major role in the regulation of chromatin structure, rendering it more or less accessible to transcription factors and thus regulating gene expression (Clayton et al., 2006). Histone acetylation/deacetylation are among the most studied histone modifications and they're carried out by histone acetyltransferases (HATs) and Histone deacetylases (HDACs), two classes of enzymes which transfer an acetyl group from the acetyl CoA coenzyme or remove it, respectively.
Dietary energy restriction increases HDAC activity in human cell culture models and this is associated with expression changes of $p16^{INK4\alpha}$ and hTERT (Meyerson et al., 1997; Kanaya et al., 1998; Li et al., 2010). SIRT1, a class III NAD^+ dependent histone deacetylase, is thought to have a main role in mediating the increase in lifespan under dietary energy restriction conditions: its expression has been shown to increase in rats subjected to dietary energy restriction (Guarente and Picard, 2005) and this is likely due to inhibition of p53 and FOXOs, which ameliorate cellular stress resistance (Luo et al., 2001; Langley et al., 2002; Brunet et al., 2004; Motta et al., 2004) and also by regulation of PGC-1α, a known regulator of mitochondrial biogenesis (Vega et al., 2000; Schilling et al., 2006). Interestingly, SIRT1 is able to deacetylate also non-histone substrates (Guarente and Picard, 2005; Wakeling et al., 2009) as in the case of p53 (Luo et al., 2001; Langley et al., 2002; Vaziri et al., 2001) and FOXO proteins (Brunet et al., 2004; Motta et al., 2004), hence directly impairing apoptosis and senescence.

Given their high number of targets, miRNAs are being studied to understand their implications in the modulation of the ageing process through gene expression regulation. Figure 1.7 presents a summary of the known miRNAs that regulate genes belonging to the high conserved ageing pathways discussed above.

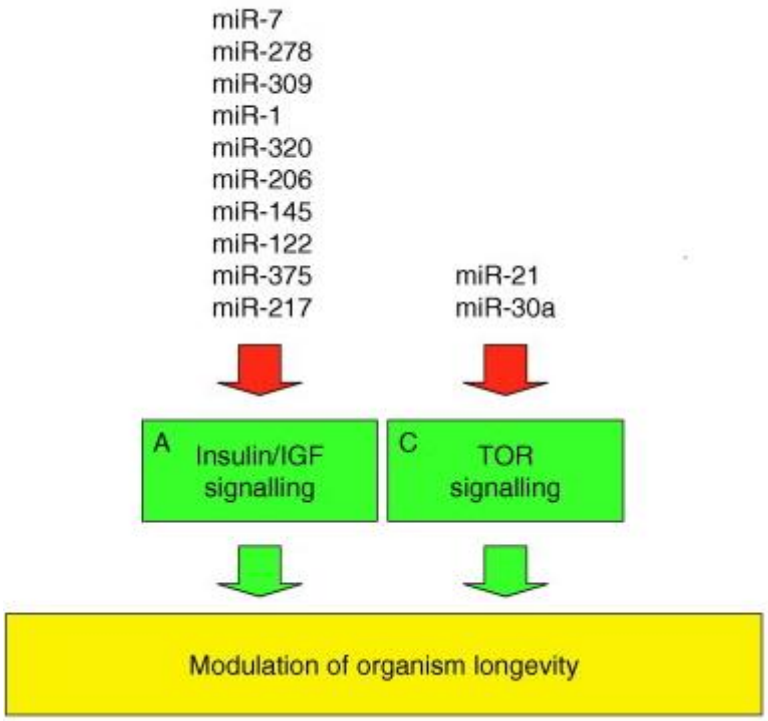

Figure 1.7. miRNAs involved in the regulation of conserved ageing pathways genes. Adapted from (Grillari and Grillari-Voglauer, 2010).

Dietary energy restriction has been shown to change expression levels of some miRNA in mice, which correlated with the reduction of risk factors for age-related diseases: a recent genome-wide study conducted on murine serum identified circulating miRNAs belonging to pathways relevant to ageing and whose serum levels were increased with age and decreased by ER (Dhahbi et al., 2013). Another study showed that miR-203 increased in dietary energy restricted mice breast tissue, thus decreasing expression of two proteins involved in tumourigenesis and invasiveness, i.e. CAV1 and p63 (Orom et al., 2012). A further example is the decrease in the BCL2-targeting miR30, miR34a and miR-181a observed in the brain of dietary energy restricted mice; the resulting increase in BCL2 expression and decrease in the activity of BAX and Caspases 3 and 9, which are associated with a reduction in apoptosis (Khanna et al., 2011), could slow down the onset and progression of neurodegenerative diseases, indeed characterized by high expression of both BAX and Caspase 3 (Paradis et al., 1996; Louneva et al., 2008).

Anderson and colleagues have proposed a model which integrates the contributions of all the above discussed molecular mechanisms (and DNA methylation, discussed in the next section) in mediating the increase of lifespan through dietary energy restriction (Figure

1.8). In essence, it is proposed that cells respond to the diminished food (and energy) intake by activating master regulators within nutrient-sensing pathways which drive a shift in energy metabolism, decreasing the rate of ageing hence securing longevity (Anderson et al., 2009).

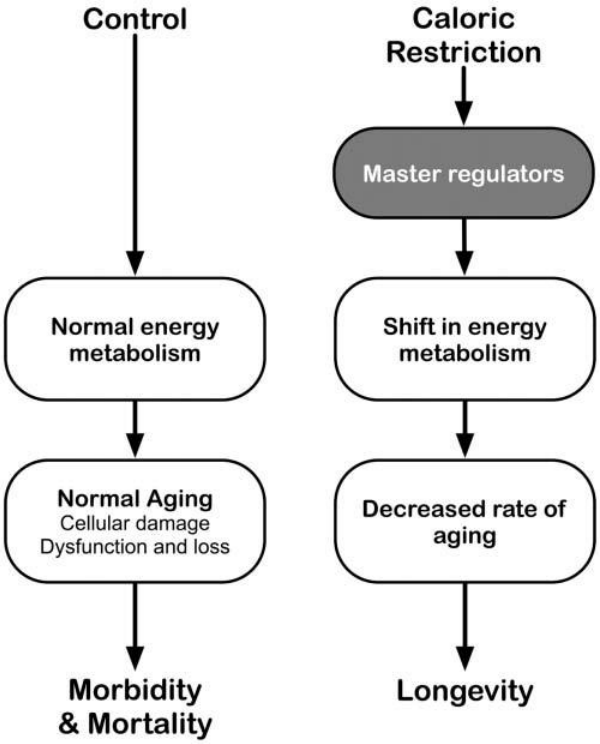

Figure 1.8. Model of interaction between nutrient-sensing pathways in response to dietary energy restriction. From (Anderson et al., 2009).

1.6.2 Dietary modulation of the epigenome

Diet can modulate the epigenome, as reviewed in (McKay and Mathers, 2011). Between the dietary components that are able to mimic the effects of dietary energy restriction, resveratrol (3,5,4'-trihydroxy-*trans*-stilbene) has been identified as the most potent enhancer of SIRT1 (a deacetylase) *in vitro* (Howitz et al., 2003). It has been shown to extend lifespan of various invertebrate and vertebrate species - *S. cerevisiae, C. elegans, D. melanogaster* and *N. furzeri* (Howitz et al., 2003; Wood et al., 2004; Viswanathan et al., 2005; Baur et al., 2006; Valenzano et al., 2006) - and to revert the effects of a high-fat diet in mice, inducing effects associated with a healthier lifespan, such as increased insulin sensitivity, reduced insulin-like growth factor-1 (IGF-I) levels, increased AMP-activated protein kinase (AMPK) and peroxisome proliferator-activated

receptor-γ coactivator 1α (PGC-1α) activity, increased mitochondrial number, and improved motor function (Baur et al., 2006). However, no change in levels of free fatty acids and cholesterol or effects on lifespan were observed when comparing the control mice group with the high-fat diet group. Other studies on mice have confirmed the lack of resveratrol-dependent improval on lifespan (Pearson et al., 2008; Miller et al., 2011). Studies in humans have demonstrated the positive effects on insulin and metabolic functions (Crandall et al., 2012; Timmers et al., 2011).
The effects of resveratrol on longevity in higher-order animals may not be apparent in complex organisms due to experimental factors or because the effects of dietary energy restriction involve several degrees of interactions other than the one activated by resveratrol alone (Hector et al., 2012).

1.7 DNA methylation and dietary energy restriction

As already outlined in section 1.5, generally there is a global demethylation and a local hypermethylation within ageing tissues. Diet can greatly influence those aberrant patterns and beneficial effects have already been demonstrated for folate and vitamin B12, choline, as reviewed by (McKay and Mathers, 2011) and by dietary energy restriction, as reviewed by (Li et al., 2011). In particular, dietary energy restriction exerts its ageing-delaying action increasing genome stability (Vaquero and Reinberg, 2009; Munoz-Najar and Sedivy, 2011) by reverting age-related aberrant methylation patterns (or preventing them) at specific genomic loci, rather than globally (Munoz-Najar and Sedivy, 2011). Examples of genes promoters in which those changes are seen include age-related and cancer-related genes promoters, thus reinforcing the importance of a healthy diet in the prevention and in the onset delaying of age-related diseases and ageing itself.
Dietary energy restriction was shown to increase promoter methylation of the proto-oncogene H-ras in rats pancreas compared with *ad libitum* fed controls, thus decreasing gene expression (Hass et al., 1993); the same hypermethylation/down-regulation has been seen for the tumour suppressor and ageing/senescence associated gene $p16^{INK4A}$ in an *in vitro* model (Li et al., 2010; Li and Tollefsbol, 2011). Two recent studies have identified three human genomic loci in which DNA methylation significantly changes after short dietary energy restriction regimens; these are the promoters of the genes *ATP10, WT1* (Milagro et al., 2011) and *TNFα* (Campion et al., 2009), which have been proposed as early indicators for dietary energy restriction response.

1.8 Mitochondrial DNA (mtDNA) and mtDNA methylation

Mitochondria are small size organelles often referred to as the cell "power plants": they're in fact responsible for the production of ATP, the cells main energy, through a process called oxidative phosphorylation.

Mitochondria have their own genome, called mitochondrial DNA (mtDNA), which is a small, circular, double-stranded DNA molecule, that replicates independently from the nuclear genome and shows some peculiarities, such as a complete maternal inheritance in vertebrates (with few exceptions) (Giles et al., 1980) and the use of alternative start codons to the conventional AUG: AUA and AUU are common in humans, while AUA, AUU and AUC are common in mice, as reviewed by (Osawa et al., 1992) and (Jukes and Osawa, 1993).

MtDNA molecules are composed of a light strand (C rich) and a heavy strand (G rich), which are both transcribed to produce polycistronic RNAs and replicate starting from a triple-stranded structure called D-Loop, which constitutes the origin of replication (reviewed by (Shadel and Clayton, 1997)). They are organized in clusters, in the so called nucleoids, which are devoid of histones (Satoh and Kuroiwa, 1991).

Despite the high numbers of proteins required for mitochondrial functions, only 13 of them are encoded by the mitochondrial DNA; those are polypeptidic components of the oxidative phosphorylation chain, the main metabolic pathway involved in ATP production. The other genes featured in this small molecule encode for 22 transfer RNAs and for the small and large subunit of the ribosomal RNA (Anderson et al., 1981).

MtDNA is of particular interest in the context of ageing studies because spontaneous deletions in its sequence have been observed to arise with normal ageing, especially in postmitotic tissues, such as brain, skeletal muscle and heart (Cortopassi et al., 1992; Corral-Debrinski et al., 1992; Simonetti et al., 1992; Meissner et al., 2008). These deletions are also found in the substantia nigra of Parkison's disease patients, leading to the hypothesis that the resulting mitochondrial defect and bioenergetics unbalance could be causal for the development of the disease (Bender et al., 2006; Kraytsberg et al., 2006).

As it happens in the nuclear genome, CpG sites are underrepresented and not evenly distributed in both human (Figure 1.9) and murine mitochondrial genome (Chinnery et al., 2012).

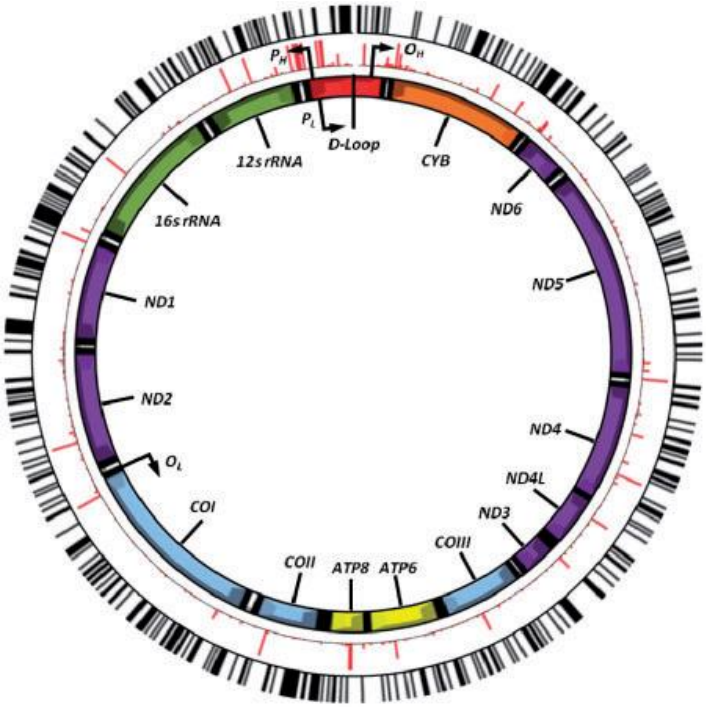

Figure 1.9. Organization of the human mitochondrial genome (centre) and distribution of CpG sites in its context (black outer ring). The intermediate red ring shows positions and relative frequencies of mtDNA variants. O_H = heavy strand origin of replication; O_L = light strand origin of replication; P_H = heavy strand promoter site; P_L = light strand promoter site (from (Chinnery et al., 2012)).

The first evidence of the existence of methylated Cytosines within mtDNA molecules came from an *in vitro* study conducted on a mouse cell culture model, in which the authors detected very low levels of global mtDNA methylation (between 3% and 5%) (Pollack et al., 1984). In a more recent publication, the four main regulatory regions within the human mtDNA have been analysed - the transcription termination region (TERM) within the $tRNA^{Leu(UUR)}$, the heavy and light strand promoters (HSP and LSP) and the origin of replication of the light strand (O_L) - and have been found to be protected from methylation during *in vitro* methylation assays performed with prokaryotic DNA methyltransferases (Rebelo et al., 2009). The authors noticed an inverse correlation between methylation rate and protein occupancy and concluded that DNA regions associated to proteins (including transcription factors) are less accessible to DNA methyltransferases and therefore protected from methylation, seemingly being transcriptionally active (Rebelo et al., 2009). Although mtDNA methylation has been investigated and demontstrated in other studies, both in humans and rodents (Nass, 1973; Shmookler Reis and Goldstein, 1983; Pollack et al., 1984; Hecht et al., 1984; Maekawa et

al., 2004), it was not until recently that there's been proof of the existence of a mitochondrial isoform of DNMT1, which is able to bind mtDNA and methylate it (Shock et al., 2011). In this study, the authors concluded that, as DNMT1 is the only DNMT present in human and mice mitochondria, this must also have *de novo* methylase activity, contrary to what previously believed by the scientific community.
Albeit some studies have demonstrated the inefficacy of aberrant mtDNA methylation patterns as markers for cancer diagnosis and prognosis (Maekawa et al., 2004), new technologies pave the way to more precise quantification of DNA methylation, so it is possible that this opinion could be reversed in the future.

1.9 Methodology

A wide number of laboratory techniques have been developed to study DNA methylation and nowadays it is possible to focus on specific DNA regions and to carry out genome-wide analysis.
The principles upon which these techniques are based include the following:

- separation of Cytosines and 5mC according to their different size;
- use of restriction enzymes: a methyl-sensitive restriction enzyme is used to digest unmethylated CpGs, enriching for methylated DNA sequences;
- bisulphite conversion: bisulphite treatment selectively deaminates unmethylated Cytosines to uracils;
- affinity purification: an antibody or a methyl-binding protein that recognize 5-methylcytidine is used to immunoprecipitate the methylated fraction of the sample.

1.9.1 Quantification of Global DNA Methylation in Mammals

One of the first methods for detecting global methylation in mammalian genomes is HPLC (High Performance Liquid Chromatography) after DNA digestion into single nucleotides. The chromatography column contains a stationary phase which separates each nucleotide according to its size; Cytosines, which are lighter than 5mCytosines will be therefore eluted earlier. The instrument produces a real time graph with peaks corresponding to the different nucleotides; in addition, the area of each peak is proportional to its content in the original sample (Kuo et al., 1980).

This method is highly quantitative and reproducible, but it requires large amounts of starting material (DNA) and it does not give any indication about the location of the methylations in the genome analysed.

Three more common methods for global methylation quantification take advantage of the fact that the majority of methylated CpG sites in mammalian genomes resides in repetitive regions; therefore, quantifying them can give an estimate of the overall methylation content of the sample analysed.
The first step of the Alu and LINE-1 assays for human DNA (Yang et al., 2004) and of the B1 assay for mouse DNA (Jeong and Lee, 2005) is the bisulphite conversion of the DNA (Clark et al., 1994) (Figure 1.10), followed by PCR of the bisulphite modified DNA:

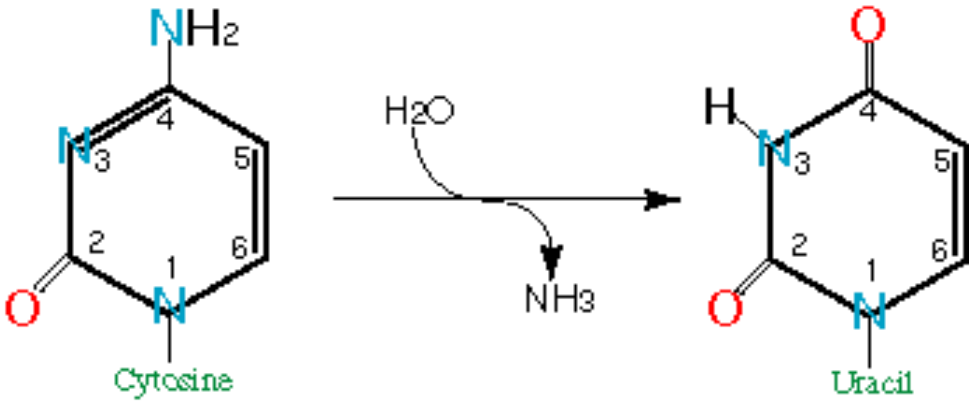

Figure 1.10. Deamination of Cytosine to Uracil, which is commonly termed Bisulphite Conversion, as it is carried out in the presence of Sodium Bisulphite.

In the Alu and LINE-1 methods, the changes in the BM-DNA PCR products are investigated by Pyrosequencing (Ronaghi et al., 1996) or by means of *MboI* and *HinfI* restriction enzymes, which cut only methylated Cytosines. The digestion products are loaded on polyacrylamide gel and analyzed by densitometry: the ratio between the intensity of the bands is the ratio methylated: unmethylated CpG sites. This last part of the method has previously been used for studying methylation at specific loci and it is known as COBRA (Combined Bisulphite Restriction Analysis) assay (Xiong and Laird, 1997).

In the original B1 assay (Jeong and Lee, 2005), after bisulphite modification, a methylation specific PCR (MSP) is performed: two couple of primers are designed to amplify either the unconverted (methylated) or the converted (unmethylated) DNA, so that it is possible to estimate the ratio between methylated and unmethylated Cytosines by densitometry on the resulting PCR products (Herman et al., 1996). PCR products can also be analysed by Pyrosequencing to obtain a more quantitative measurement.

Compared with HPLC, PCR based methods are less expensive and require a minimal amount of starting material, but they do provide only approximate methylation levels.

The LUMA assay (Karimi et al., 2006a; Karimi et al., 2006b) is based upon the use of the isoschizomeres *MspI* and *HpaII*, which recognise the same sequence (CCGG), but cut in different ways according to its methylation state: *MspI* cuts the sequence regardless of methylation status whereas *HpaII* cuts only at sites where the internal C is not methylated. The digestions are run in parallel on the same sample and then loaded in a Pyrosequencer. In the instrument, a known sequence of nucleotide is dispensed and luciferin is converted to light in a proportional amount to the number of cuts that each enzyme has done.

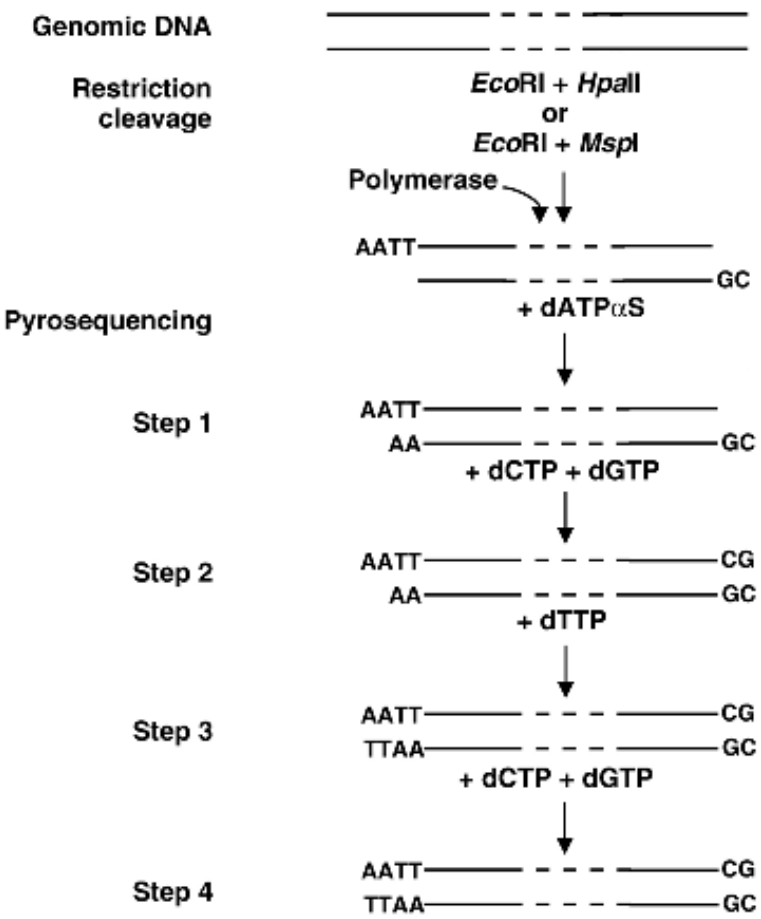

Figure 1.11. Steps involved in the LUMA assay (adapted from (Karimi et al., 2006b).

1.9.2 Detection and Quantification of Site Specific Methylation

Several methods have been developed to assess the methylation state of specific DNA loci and nowadays it is possible to test several of them in once and even performing genome-wide methylation analysis.

The COBRA (COmbined Bisulfite Restriction Analysis) assay, already described briefly above, can be used to test a specific sequence. In brief the assay involves the preparation of bisulphite modified DNA, amplification and then cutting with a methyl sensitive enzyme. After electrophoresis on Ethidium Bromide acrilamyde gel, the percentage of fully methylated restriction sites can be calculated from the brightness ratio between the cleaved PCR product and the total amount of PCR product.

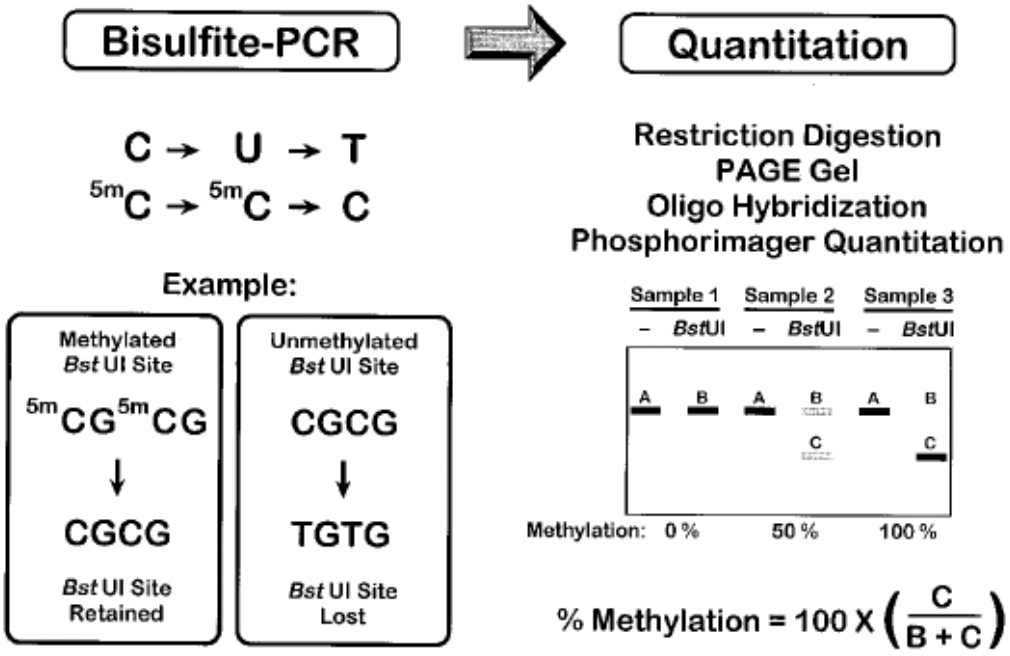

Figure 1.12. Outline of the COBRA assay (from (Xiong and Laird, 1997).

Pyrosequencing is a technology based upon sequencing by synthesis (Ronaghi et al., 1996).

In the context of DNA methylation studies, it can be used to detect and quantitate bisulphite converted and unconverted Cytosines using a biotin labelled sequencing primer. The primer is hybridized to the single-stranded bisulphite treated template, and incubated with the enzymes (DNA polymerase, ATP sulfurylase, luciferase, apyrase) and the substrates (adenosine 5' phosphosulfate or APS and luciferin).

When the first complementary dNTP is added to the reaction mixture, DNA polymerase catalyzes its incorporation into the DNA strand. Each incorporation event is accompanied by release of pyrophosphate (PPi) in a quantity equimolar to the amount of incorporated nucleotide.

ATP sulfurylase converts PPi to ATP in the presence of APS; this reaction drives the luciferase-mediated conversion of luciferin to oxyluciferin, which generates visible light in amounts that are proportional to the amount of ATP. The light produced is then detected by a camera and seen as a peak in a graph called Pyrogram. The height of each peak (light signal) is proportional to the number of nucleotides incorporated.

Apyrase continuously degrades unincorporated nucleotides and ATP. When degradation is complete, another nucleotide is added.

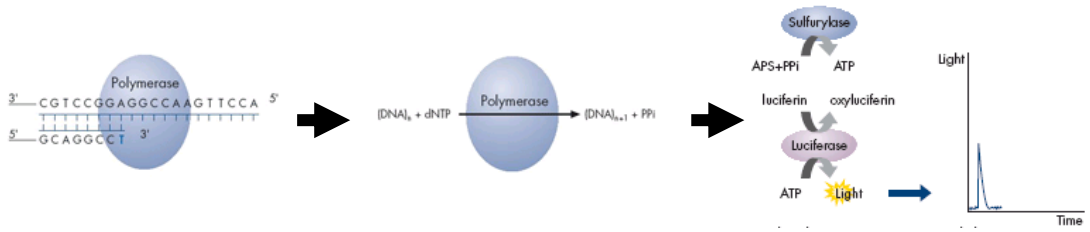

Figure 1.13. Steps of the Pyrosequencing technology.

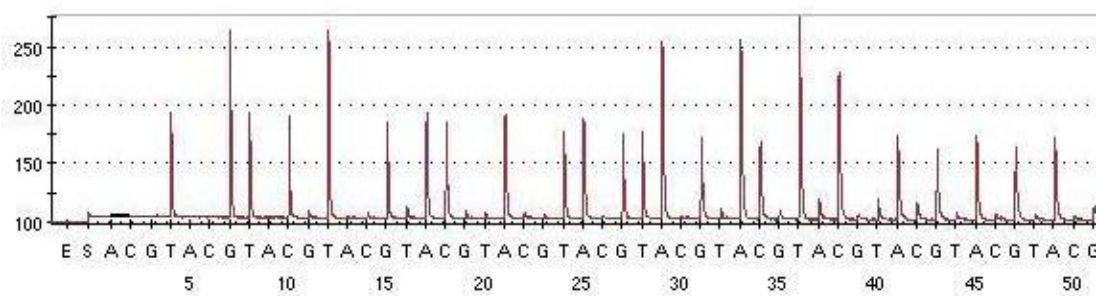

Figure 1.14. Example of a DNA Pyrogram.

In the MeDIP (Methylated DNA ImmunoPrecipitation) technique (Weber et al., 2005; Weber et al., 2007), total genomic DNA is sonicated into fragments, which are then immunoprecipitated with an antibody that recognises 5'-MethylCytidine. The starting sample, called Input, contains both methylated and unmethylated fragments, while the MeDIP sample mainly contains methylated fragments.

After the IP reaction, the two samples can be labelled with different dyes and co-hybridized as a two colour experiment array containing a very large number of probes. In this way it is possible to have a genome-wide assessment of methylation status. Samples can also be analysed with specific primers in PCR or by Real Time PCR to calculate the relative enrichment of a specific sequence between the MeDIP and its relative Input.

This technique will be described in further details in Chapter 4 – Standardization and quality control for the Methylated DNA Immunoprecipitation technique -.

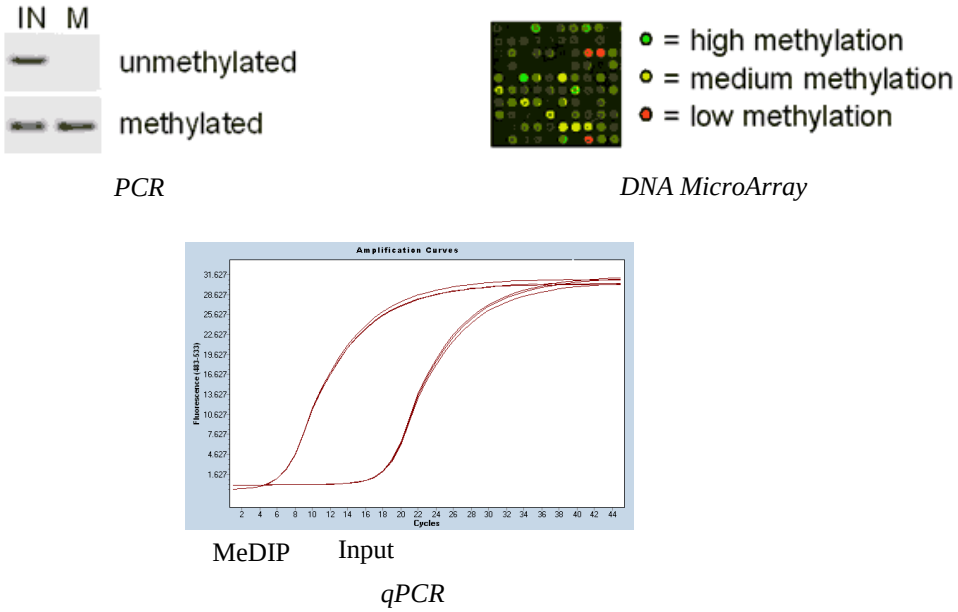

Figure 1.15. Different molecular biology techniques used in the analysis of methylated versus unmethylated DNA sequences after affinity enrichment.

Several other methods for DNA methylation quantification have been developed from previously established ones; between those

- the MethylLight technique (Eads et al., 2000): a variation of the MSP in which Real Time PCR is used for methylation quantification of the samples under investigation;
- the Methyscreen technique (Holemon et al., 2007): an assay that utilizes a combined restriction from both methylation-sensitive restriction enzymes (MSREs) and methylation-dependent restriction enzymes (MDREs), followed by qPCR;
- cloning and sequencing of BM-DNA PCR products (Frommer et al., 1992): BM-PCR product are cloned into a vector, transfected, grown with a selection antibiotic and single clones are sequenced. This method allowes for allele-specific methylation quantification if a sufficient numbers of clones are sequenced;
- MALDI-TOF Mass Spectrometry of BM-DNA PCR products (Ehrich et al., 2005): in this method a region of interest is amplified with primers containg a T7 RNA polymerase tag, *in vitro* translated with T7 polymerase and subsequently cut with a ribonuclease; the digestion products are then quantified in a mass spectrometer;

- Restriction Landmark Genome Scanning (RLGS) (Costello et al., 2002): this technique uses a mixture of methyl-sensitive restriction enzymes and then radioactive labelling of the genomic DNA under investigations, followed by a two-dimensional electrophoresis of the labelled restriction fragments, and allows for the methylation quantification of several (thousands) CpG sites at a time;
- Methylation-Specific Digital Karyotyping (MSDK) (Hu et al., 2005): methylation-sensitive enzymes are used to cut genomic DNA and the resulting fragments are then sequenced and mapped to the genome; this technique requires large amounts of DNA;
- libraries construction (Rollins et al., 2006): in this method, genomic DNA is cut either with a methyl-sensitive enzyme or a methyl-independent enzyme to produce fragments which are ligated into a plasmid, tranformed into *E. coli* to obtain colonies which will be sequenced;
- direct sequencing: various algorithms have been developed for the analyses of BM-PCR products sequenced directly with the Sanger method (Sanger and Coulson, 1975), allowing for rapid screening of multiple CpG sites in sequences of DNA which can go up to 500-600 bp; a few examples are: (Jiang et al.; Lewin et al., 2004; Leakey et al., 2008);
- Methylation-sensitive High Resolution Melting (MS-HRM) (Wojdacz and Dobrovic, 2007): this method apply the use of High Resolution Melting technology post-qPCR to detect methylation levels as low as 0.1%.

Figure 1.16 summarizes the most common methods for the study of DNA methylation.

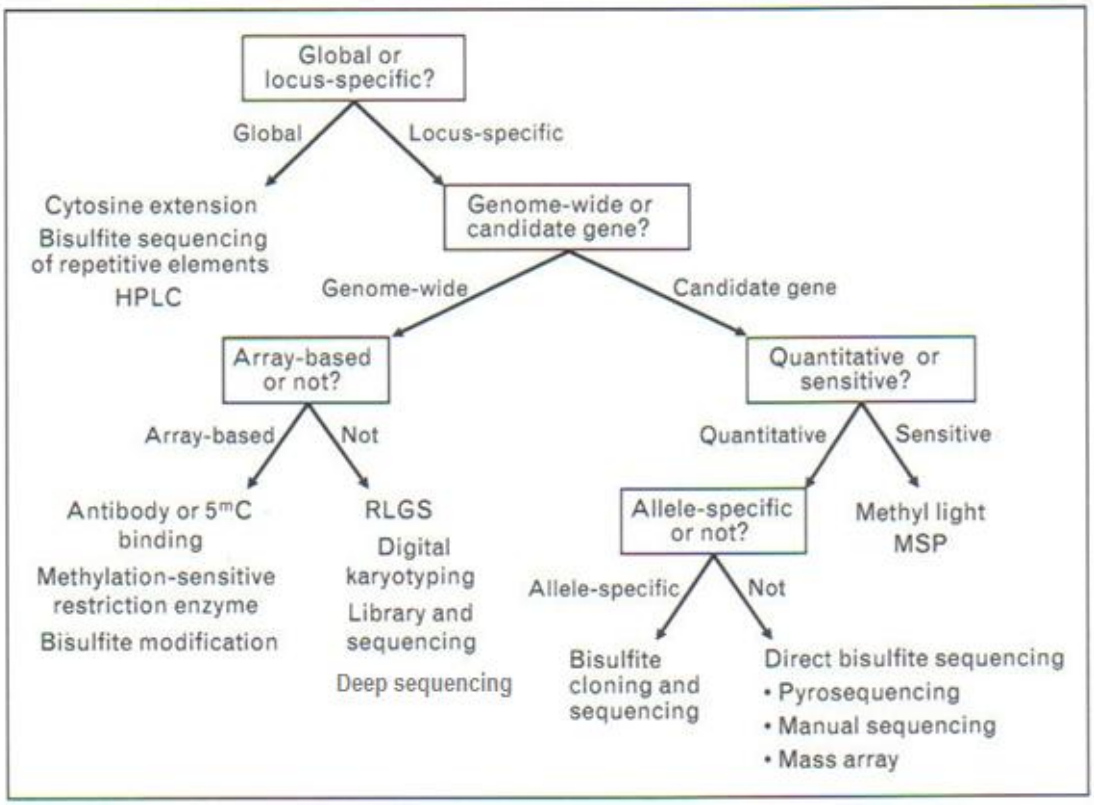

Figure 1.16. Summary of the most common methods for the study of DNA methylation. HPLC = High Performance Liquid Chromatography; RLGS = Restriction Landmark Genomic Scanning; MSP = Methyl Specific PCR (modified from (Shen and Waterland, 2007).

1.10 Aims and objectives of the study

The aim of this project was to characterise the changes in DNA methylation which occur in cellular senescence, during ageing and in response to dietary energy restriction; the human cell line MRC-5 and various tissues from ageing and dietary energy restricted mice were used to this purpose. Specific objectives for the study were:

Objective 1: measurement of global 5'-mC methylation level and assessment of *DNMT*s/*Dnmt*s gene expression in senescence, ageing and dietary energy restriction conditions. Methylation studies were conducted using an ELISA-based assay, BM followed by PCR of repetitive regions (human LINE-1, murine B1 element), the LUMA assay and HPLC, while gene expression studies were conducted using RT-qPCR (Chapter 3).

Objective 2: Establishment and validation of the MeDIP technique for whole genome DNA methylation studies (Chapter 4).

Objective 3: Characterisation and quantification of genome-wide promoter methylation and of gene expression in replicative senescent and premature senescent compared with young replicative MRC-5 human lung fibroblasts using the MeDIP technique and BM-PCR followed by pyrosequencing for methylation studies and RT-qPCR for gene expression studies (Chapter 5).

Objective 4: Comparison of genome-wide promoter methylation in heart and liver from young and ageing mice and assessement of the impact of dietary energy restriction (ER) in mice on genome-wide promoter methylation in liver using the MeDIP technique (Chapter 6).

Objective 5: Quantitative analysis of DNA methylation in selected mitochondrial genomic regions in i) DNA from replicative senescent and premature senescent compared with young replicative MRC-5 human lung fibroblasts, ii) liver from ageing mice vs their young counterparts and iii) liver from dietary energy restricted mice vs liver from *ad libitum* fed mice using BM-PCR followed by direct sequencing (Chapter 7).

Chapter 2. Materials and Methods

2.1 Cell culture

MRC-5 human lung fibroblasts (Jacobs et al., 1970) (ATCC, CCL-171) and LN-229 human glioblastoma epithelial cells (ATCC, CRL-2611) were cultured at 37°C in 5% CO_2 atmosphere in DMEM High Glucose Medium (Gibco) supplemented with 10% Fetal Bovine Serum (FBS; Lonza), 100 U/mL Penicillin and 100 µg/mL Streptomycin (Mediatech). Culture media was replenished every 3 to 4 days. When confluent, cells were washed with Phosphate Buffer Saline (PBS; Mediatech; 17 mM KH_2PO_4, 5 mM Na_2HPO_4, 150 mM NaCl, pH 7.4) and trypsinized for 5 minutes at 37°C. Trypsin was neutralized with 2 volumes of complete media, cells collected into a polypropylene conical tube, centrifuged at 500 x g for 5 minutes at room temperature and subcultured at a ratio of 1:4 with fresh medium. Cell stocks were prepared resuspending 3 x 10^6 cells in 1 mL of freezing solution (DMEM medium containing 60% of FBS and 10% DMSO), storing for at least one day at -80° C and then transferring in liquid nitrogen for future use. When needed, cells were thawed in 37° C warm water, resuspended in 5 mL of complete medium, centrifuged and cultured with fresh medium.

Cell cultures were tested periodically for mycoplasma contamination by PCR using the Bioo Scientific Mycoplasma Primer Sets. Primer set A amplified a 569 bp conserved region of *M. orale*, *M. salivarium*, *M. hominis*, *M. hyorhinis*, *M. fermentans*, *M. gallisepticum* and *A. laidlawii*; primer set B amplified a 698 bp conserved region of *M. genitalium*, *M. hyponeumoniae* and *M. flocculare*. To prepare the PCR templates, 500 µL of conditioned media were centrifuged at 800 g for 5 minutes and transferred 400 µL of the supernatant to another tube; after a second centrifugation step at 12000 rpm, 10 minutes, 4° C, 350 µL of the supernatant were discarded. The remaining 50 µL were diluted 1:2 with water and 5 µL were used for PCR in a final volume of 25 µL with 300 nM final concentration of either primer set A or B and Maxima Hot Start PCR Master Mix (Fermentas). Reaction conditions were as follows:

95° C, 4 minutes
95° C, 30 seconds
55° C, 30 seconds
72° C, 1 minute
} 35 cycles
72° C, 10 minutes.

PCR products were loaded in 1% agarose/TBE gel with 0.4 µg/mL of Ethidium Bromide and PCR products analyzed. Cell lines that showed positive in at least one of the reactions were discarded and a new aliquot of cells was thawed and kept in culture.
To compare replicating cells with premature senescent cells and replicative senescent cells, without cell cycle bias, 100% confluent cells were harvested after 30 population doublings (Young Confluent samples, YC). Premature senescent cells were prepared by irradiating subconfluent cells with 20 Gy of γ-radiation and harvesting after 48 hours (early stress-induced premature senescent samples, ESIPS samples); replicative senescent cells were prepared by culturing cells until they reached the Hayflick limit (Hayflick, 1979) (Replicative Senescent samples, RS). Growth curves were produced counting the average number of cells in three 1 mm^2 cells of an improved Neubauer haemocytometer and applying the formula in (Lawless et al., 2010) to calculate the cells population doublings.
For all downstream applications, cell pellets were washed 3 times with cold PBS, centrifuged at 800 x g for 5 minutes and stored at -80°C until use.

2.1.1 Beta Gal senescence associated assay

Cells were plated in 12 wells plates containing round sterile cover glasses and allowed to settle for 2 days. The Senescence β-Galactosidase Staining Kit (Cell Signaling) was used as follows: growth medium was removed, cells were rinsed twice with PBS and fixed with 500 µL of Fixative Solution 1x (2% formaldehyde, 0.2% glutaraldehyde in PBS) for 15 minutes at room temperature. After 2 rinses with PBS, 500 µL of β-Galactosidase Staining Solution (465 µL 1x Staining Solution, 5 µL Staining Supplement A and B, 25 µL of X-gal 20 mg/mL in DMF, pH 6) were added and plates were incubated at 37° C in a dry incubator for 4 to 6 hours and monitored frequently for the development of blue colour. Cover glasses were mounted and the slides were counterstained with DAPI on frosted slides with Vectashield Mounting Medium with DAPI (1.5 µg/mL, Vector Laboratories) and photographed using a UV-visible light microscope.

2.2 Sampling of mouse tissues

Heart and colon tissues were obtained from male C57Bl/6 mice aged 3 and 32 months old; livers were collected from male ICRFa mice at 7, 17 and 30 months of age fed *ad libitum* fed (AL) and from male mice at 17 months of age that were dietary energy

restricted (ER) by feeding 60% of food relative to the AL animals for the last three months of their life (Cameron et al., 2011). ICFRa mice are a long-established sub-strain of C57Bl/6, which had been selected for use in studies of intrinsic ageing because it is free from specific age-associated pathologies and thus provides a good general model of ageing (Rowlatt, 1979). Some of the ICRFa animals acquired MHV seropositivity which, in the opinion of the unit's veterinarian, was due to transient cross-infection from another imported stock. No significant symptoms of active infection were noted in the aged animals and there was no indication of lesions in the liver or gut upon dissection. Furthermore, in spite of the seropositivity, longevity did not appear to have been compromised (data not shown). I used only the distal part/rectum of the colon because it appears to less affected by the virus in asymptomatic infections (Baker, 1998). Three animals per group were killed by neck dislocation, colons were flushed with PBS and cut in half, livers were divided into lobes and heart dissected as a whole.
Tissues were snap-frozen in liquid nitrogen and then kept at -80'C. To ensure representative tissue sampling and to help with tissue lysis, the frozen tissues were pulverized using a mortar and a pestle cooled in liquid nitrogen.

2.3 Genomic DNA (gDNA) extraction

Cell pellets (1 to 5 x 10^6) and ground samples (10 to 50 mg) were digested overnight at 56° C in 500 µL of the following solution:

50 mM Tris HCl (pH = 8)
12.5 mM EDTA
0.5% SDS
0.03 U/µL Proteinase K (Fermentas).

Lysates were then mixed with one volume of a solution 24:1 chloroform: isoamyl alcohol (Sigma Aldrich) and centrifuged in 2 mL PhaseLock Heavy tubes (5 Prime) at 13000 rpm for 5 minutes to allow separation of the phases. The acqueous phase, which contained the nucleic acids, was recovered and RNA digested for 30 minutes at 37'C with RNase A/T1 mix (Fermentas) at a final concentration of 80µg/mL RNAse A and 0.2 U/mL RNase T1. DNA was then precipitated at room temperature by adding 1/10 of volume of NaAc 3M, 1 volume of isopropanol and 40 µg glycogen (Fermentas). After centrifugation at 13000 rpm for 5 minutes, pellets were washed twice with 500 µL EtOH 70%, air dried for 10

minutes and resuspended in 50 µL of TE buffer (10 mM Tris HCl pH = 8, 1 mM EDTA). 200 ng of each extraction were checked on 1% agarose/TBE gel for integrity and absence of RNA contamination.

Heart samples were not washed at the dissection stage so it was necessary to perform a double step of red blood cell lysis with 500 µL RBC Lysis Solution purchased from QIAgen. In initial trials (where this RBC lysis step was not done), the spectrophotometric reading of the extracted DNA showed a low 260/230 ratio, probably due to the catalysis of haemoglobin into bilirubin and its yellow colour was clearly visible in the DNA suspension.

2.4 RNA extraction

For RNA extractions, I developed a protocol combining a lysis step in TriReagent (Ambion) and a purification step using the E.Z.N.A. Total RNA Kit I (Omega Bio-Tek). Cell pellets (1 to 5 x 10^6) and ground samples (10 to 50 mg) were homogenised with a hand-held homogenizer in 500 µL of TRiReagent solution to assure a complete lysis of the samples in a RNA denaturing environment; 100 µL 1, 3-BromoChloroPropane (Sigma Aldrich) were added to the lysates and, after centrifugation (12000 g, 10 minutes, 4° C), the aqueous phase (containing RNA) was recovered. The RNA-containing solution was mixed with 200 µL TRK lysis buffer from the kit and 300 µL 100% EtOH and loaded into the columns. From this point on, the manufacturers' protocol was followed, except in the elution step where I used 1mM sodium citrate instead of water, because it keeps the RNA more stable. This method has allowed me to obtain maximum RNA yields and purity. Concentrations of RNA in samples were quantified spectrophotometrically (Nanodrop 2000) and 500 ng of each extraction were checked on 1% agarose/TBE gel and 1 uL was loaded on the Agilent Bionalyzer. Both methods indicate the integrity level of the nucleic acid.

2.5 DNA and RNA quantification by means of nucleic acids stains

For most of the applications, DNA and RNA were quantified spectrophotometrically using a Nanodrop 2000 (Thermo Scientific). However, in some cases, e.g. where the nucleic acids quantifications were used directly to normalize assays values or the amounts to be quantified were lower than the detection linearity range of the Nanodrop (4 ng/µL), a more precise quantification method based upon the use of SYBR nucleic acids stains

was developed. For DNA, 1 µL of each sample was dispensed into a 96-well Black Clear-Bottom Plate (Corning Costar), 200 µL of a 1:1000 dilution of SYBR Green I (10000x in DMSO, Invitrogen) in TE buffer was added; a standard curve with 1:2 serial dilution of Lambda DNA (Fermentas) ranging from 1 ng/µL to 512 ng/ µL was prepared and read together with the samples.
For RNA, 1 µL of each sample was dispensed in a 96-well Black Clear-Bottom Plate (Corning Costar), 200 µL of a 1:10000 dilution of SYBR Green II (10000x in DMSO, Invitrogen) in TE buffer was added; the standard curve was prepared with 1:2 serial dilution of ssRNA Ladder (New England Biolabs) ranging from 3.9 ng/µL to 500 ng/ µL was prepared and read together with the samples.
Fluorescence was read in a microplate reader with the following settings:

Excitation: 485 nm
Emission: 535 nm
Integration time: 1 s;

sample concentration was calculated from the standard curve equation.

2.6 Methylated DNA Immunoprecipitation (MeDIP)

2.6.1 Samples sonication

10 µg gDNA was diluted to 450 µL with TE buffer and sonicated in cold water for 2 min at 20% pulse and 5 Volts of power output with an Ultrasonic Homogenizer 4710 Series (Cole-Parmer Instrument Co.). Extent of sonication was assessed by loading 15 µL of sample on 1% agarose/TBE gel with 0.4 µg/mL of Ethidium Bromide. Successfully fragmented DNA samples (fragment size ranging from 200 bp to 1000 bp) were concentrated with the DNA Clean & Concentrator – 25 kit (Zymo Research) as follows: 2 volumes of DNA Binding Buffer were added to each sonicated DNA sample and the mixture was transferred into a Zymo-Spin Column; after centrifugation at 13000 rpm for 1 minute, the flow-through was discarded and 2 washes with 300 µL of reconstituted Wash Buffer (6 mL concentrated Wash Buffer plus 24 mL 100% ethanol) performed, followed by centrifugation at 13000 rpm for 1 minute. DNAs were eluted with 50 µL in

TE buffer after an incubation at room temperature for 1 minute. All centrifugation steps were carried out at room temperature.

2.6.2 Spike Positive and Negative Control Preparation

Both Positive and Negative Controls were prepared from Lambda Phage gDNA *dam*$^-$ *dcm*$^-$ (Fermentas) by PCR and were about 600 bp in length (average size of fragments for immunoprecipitation). Fragment A starts at base 2576 and ends at base 3200 of the Lambda phage genome and contains 41 CpG sites, while Fragment B starts at base 919 and ends at base 1524 and contains 35 CpG sites.
Reactions were set up in a total volume of 20 µL with 10 ng template DNA, 500 nM final primers concentration (see Table 1 for sequences) and FastTaq Mix (Fermentas). PCR conditions were as follows:

95°C, 1 minute
95°C, 1 second
60°C, 15 seconds } 30 cycles
72°C for 10 seconds.

Table 2.1. Primer sequences for λ DNA Fragment A and B preparation.

Primer Sequences	**Amplicon Length**
Fragm. A FOR1 - AGC AAC CAA CAA GAA AAC ACT Fragm. A REV1 - TCA TCC TCG GCA AAC TCT TT	625
Fragm. B FOR1 - GTG AGG TGA ATG TGG TGA AGT Fragm. B REV1 - TCG CAG AGA TAA AAC ACG CT	606

PCR products were loaded on agarose/TBE gel 1% plus 0.4% of Ethidium Bromide, excised and purified with the GeneJet PCR Purification kit (Fermentas) as follows: 1 volume of Binding Buffer was added to the PCR reaction and, after thorough vortexing, the mixture was loaded into a GeneJET PCR purification column and centrifuged at 13000 rpm. The flow-through was discarded and the column washed with 700 µL of Wash Buffer reconstituted as indicated by the manufacturer (9 mL of concentrated buffer plus 45 mL of 100% ethanol). The column was then centrifuged for an additional minute

to remove any residual ethanol and purified DNA eluted in 30 µL of Elution Buffer, centrifuging at 13000 rpm for 1 minute, after 1 minute of incubation at room temperature. To prepare the fully methylated positive control, Lambda DNA Fragment A was *in vitro* methylated with M.SssI (New England BioLabs) as follows:

1 µg DNA
5 µL NEBuffer 2
1 µL S-adenosylmethionine (32 mM)
Water to 50 µL, 37° C, 4 hours.

The reaction was re-purified with the GeneJet PCR Purification kit (Fermentas) and DNA eluted in 30 µL of TE buffer. *In vitro* methylated fragment A (Positive Control) and unmethylated fragment B (Negative Control) were then diluted to 10 ng/µL in TE buffer and stored as single-use aliquots at -20°C. To determine if those were suitable controls, I digested 200 ng of each with the isoschizomers *MspI* and *HpaII* and also with the methylation sensitive enzyme *AciI* (all enzymes were purchased as Fast Enzymes form Fermentas). Reactions were set up as follows:

200 ng DNA
2 µL Green FD buffer
1 µL of *MspI* or *HpaII* or *AciI*
Water to 20 µL, 37° C, 1 hour.

Digestions were loaded on 2% MetaPhor High Resolution Agarose/TBE (Lonza) gel with 0.4 µg/mL of Ethidium Bromide.

2.6.3 Immunoprecipitation

4 µg of the sonicated DNA were diluted in a final volume of 450 µL with TE buffer and 40 ng of Positive Control and 40 ng of Negative Control (Lisanti et al., 2012) were added up to a total volume of 495 µL. Samples were denatured at 99º C for 10 minutes in a thermocycler and then immediately cooled in ice for 10 minutes; 45 µL of them were kept at 4º C as Inputs.
After the addition of 51 µL of 10x IP buffer (100 mM Na-Phosphate pH 7.0; 1.4 M NaCl; 0.5 % Triton X-100) and 12 µL of mouse monoclonal 5-methylcytidine antibody

100 mg/mL (Eurogentec), the reaction mixture was incubated for 2 h on a rotating wheel at 4º C.

For each sample, 48 µL of Invitrogen Dynabeads M-280 sheep anti-mouse IgG were washed twice with 800 µL of 1x IP buffer, 5 minutes, at room temperature with shaking, re-suspended in 48 µL of 1x IP buffer and added to the primary Ab-DNA complexes.

A further incubation of 2 hours on a rotating wheel at 4º C was performed. The beads were recovered and washed 3 times at room temperature with 700 µL of 1x IP buffer (10 mM Na-Phosphate pH 7.0; 140 mM NaCl; 0.05 % Triton X-100) for 10 minutes with shaking and the bound DNA was eluted with 70 µg of Proteinase K (Roche) in 250 µL of Proteinase K buffer (50 mM Tris-HCl pH 8; 10 mM EDTA; 0.5% SDS).

The immunoprecipitated fractions were purified with the DNA Clean & Concentrator –5 kit (Zymo Research) as follows: 5 volumes of DNA Binding Buffer were added to each sonicated DNA sample and the mixture was transferred into a Zymo-Spin Column; after centrifugation at 13000 rpm for 1 minute, the flow-through was discarded and 2 washes with 300 µL of reconstituted Wash Buffer (6 mL concentrated Wash Buffer plus 24 mL 100% ethanol) performed, followed by centrifugation at 13000 rm for 1 minute. DNAs were eluted with 15 µL in TE buffer after an incubation at room temperature for 1 minute. All centrifugation steps were carried out at room temperature.

Purified DNA samples were spectrophotometrically quantified using a Nanodrop 2000 Thermo Scientific).

Each MeDIP experiment yielded approximately 5% of the starting amount of DNA.

2.6.4 Test for the specificity of the immunoprecipitation

A preliminary PCR was performed on the Input and MeDIped samples to assess if the immunoprecipitation worked successfully. The primers pairs used were also designed to work for Real Time qPCR (see Table 2) and were used at a final concentration of 250 nM each, with 2 ng of Input or MeDIP sample and Fast Hot Start Taq PCR Master Mix from Fermentas. The reactions were carried out up to 15 cycles, to make sure that the amplification was still in the exponential phase. Cycling conditions were as follows:

95º C 1 minute

95º C 1 second
60º C 3 seconds
} 15 cycles

72º C 10 minutes

PCR products were loaded and analyzed on 2% agarose/TBE gel plus 0.4% of Ethidium Bromide. Primer sequences are listed in Table 2.

2.7 Whole Genome Amplification (WGA)

Whole Genome Amplification (WGA) was necessary to obtain enough material to be analysed by Real Time qPCR and DNA MicroArray. The GenomePlex WGA2 kit (Sigma Aldrich) was used according to the manufacturer's protocol, but omitting the initial DNA fragmentation, as our samples were already fragmented because of the sonication step. The kit is based upon the linker adaptor approach: each end of the small fragments of genomic DNA is ligated to an adaptor (library preparation) and these known adaptor sequences are used as priming sites for the following PCR reaction (library amplification).
For the library preparation reaction mixtures were prepared and incubated as follows:

4 µL Library Preparation Buffer
2 µL Library Stabilization Solution
22 µL Input or MeDIP sample (2 ng/µL), 95º C for 2 minutes, followed by cooling in ice.

After the addition of 2 µL of Library Preparation Enzyme, samples were incubated in a thermocycler as follows:

16º C 20 minutes
24º C 20 minutes
37º C 20 minutes
75º C 5 minutes.

Libraries were cooled in ice and a mix containing the following reagents was added:
15 µL 10x Amplification Master Mix

95 µL Nuclease-free Water
10 µL WGA DNA Polymerase
The amplification mixes were incubated as follows:

95º C 3 minutes
94º C 15 seconds } 14 cycles
65º C 5 minutes.

Reactions were cleaned up with the GenElute PCR Clean-Up kit (Sigma Aldrich) and eluted in 50 µL of water and quantified at the Nanodrop 2000 (Thermo Scientific). 500 µg of reaction product were loaded on 1% agarose/TBE gel to check fragments size, which should reflect the one of the Input material before the Whole Genome Amplification process.
In general, WGA generated between 300-700 fold amplification of the starting amount.

2.8 Quantitative PCR (qPCR)

The relative enrichment methylated fraction/unmethylated fraction between MeDIP and Input samples can be calculated from qPCR data using the Pfaffl method (Pfaffl, 2001) or the simplified ΔΔCt method (Livak and Schmittgen, 2001). In this study, I used the first method, which accounts for differences in amplification efficiency of the primer pairs used.
To design and perform all qPCR assays the Minimum Information for Publication of Quantitative Real-Time PCR Experiments Guidelines (Bustin et al., 2009) were followed. Primer pairs were designed to have an annealing temperature of 60°C and to produce amplicons of 90 to 150 bp (with the Thermo Scientific webtool Reviewer: http://www.thermoscientificbio.com/webtools/reviewer/) and in-silico tested to confirm a unique amplification product at http://genome.ucsc.edu/. Efficiency and linearity of amplification were calculated from 10-fold or 5-fold dilution curves of the template DNA; each primer pair was also tested in 3 different final concentrations (100 nM, 200 nM, 300 nM). PCR reactions were carried out in triplicate in a LightCycler 480 (Roche) with 1 µL of template and Maxima SYBR Green qPCR Master Mix (Fermentas) in the following conditions:

95°C for 10 minutes
95°C for 15 seconds } 45 cycles
60°C for 1 minute

Melting curves were obtained as follows:

95°C for 5 seconds
65°C for 1 minute
from 65°C to 97°C, with a ramp rate of 0.11° C/second.

The acquisition of the fluorescence signal was set as a single reading during the annealing step and as a continuous reading during the melting curve. Primer concentrations were 300 nM for the endogenous gene assays and 100 nM for the spiked positive and negative control assays. For the dilution curves, template DNA was Lambda Phage gDNA *dam*$^-$ *dcm*$^-$ (Fermentas) for spike controls assays (dilutions ranging from 500 ng/µL to 50 fg/µL), gDNA from young confluent MRC-5 (dilutions ranging from 200 ng/µL to 200 pg/µL) for human gene specific assays, gDNA from 3 months old mouse liver (dilutions ranging from 200 ng/µL to 200 pg/µL) and sscDNA obtained by reverse transcription of 500 ng of total RNA from 3 months old mouse liver (dilutions ranging from 1:2 to 1:2000).
PCR products were also loaded in 2% agarose/TBE gel plus 0.4% of Ethidium Bromide to confirm the presence of a unique DNA band.
Table 2 and 3 list the sequences for the primers used in the qPCR assays. Dilution curves and melt curves for each primers pair are shown in Appendix A.

Table 2.2. Primers sequences for λ DNA Spike Positive and Negative Controls specificity test and qPCRs.

Primer Sequences	**Amplicon Length**
Fragm. A FOR2 – TAC AGA AAG ACG GAC GAA GG Fragm. A REV2 - TGG TGG GCG TTT TCA TAC AT	143
Fragm. B FOR2 - TTC GTG ATA TTC CGT CGC TG Fragm. B REV2 - AGT TTT TTG CCG CTT TAC CG	132

Table 2.3. Primers sequences for qPCR on MeDIP samples. The symbol "*" indicate primers previously used in (Weber et al., 2005).

Specificity	Primers Sequences	Amplicon Length
Human	**H19 ICR *** FOR - GAGCCGCACCAGATCTTCAG REV - TTGGTGGAACACACTGTGATCA	134 bp
Human	**HIST1H2BA** FOR - TGTTTGTTTACTTGGCGAGAC REV - GGTTACACAGCACTTTCCAG	91 bp
Human	**GAPDH** FOR - CTCTCTCCCATCCCTTCTCC REV - CAAGTTGCCTGTCCTTCCTA	91 bp
Human	**CD7** FOR - CACGCATGGAGTCAAGTG REV - CACGCATGTGCAGAGATG	132 bp
Human	**DCHS1** FOR - GAGAGATCAAGCAGAAGGGG REV - TCTTTTTCCCAACCGTCATCT	131 bp
Human	**MLNR** FOR - TTGTGGTGCTCTTGGTGGAT REV - TCTTCACTTTCTTCCTTTACCCA	127 bp
Human	**OR5AP2** FOR - TCTGATGTTTTCTGGTTCTCTTG REV - AGATTGTAAGAATGAGTAGGCATC	112 bp
Human	**PRDM8** FOR - ACTTTCATCTCTTCTATCTCAACAC REV - ATGGCATTCATTAGCACGGG	177 bp
Human	**RAB5C** FOR - CTCCAGATCAGCGAGTTCAC REV - TGGAAGAAGGCAGAGGATTG	104 bp
Mouse	**H19 ICR *** FOR - ACATTCACACGAGCATCCAGG REV - GCTCTTTAGGTTTGGCGCAAT	146 bp
Mouse	**Hist1h2ba** FOR - TAAGGTGCTGAAACAAGTGCA REV - ATGTCTGTCACAAAGGAGTTCA	81 bp

Mouse	**Actb** FOR - TTTCTGTCACTCTTCTCTTAGGT REV - AGGTCTTTACGGATGTCAACG	97 bp
Mouse	**Gapdh** FOR - CTCTGCTCCTCCCTGTTCC REV - TCCCTAGACCCGTACAGTGC	133 bp

2.9 PCR cloning

To confirm the identity of the qPCR products for human *H19, HIST1H2BA, GAPDH* and murine *H19, Hist1h2ba, Actb* and *Gapdh*, amplicons were cloned into a blunt linearized plasmid for sequencing using the CloneJET PCR Cloning kit (Fermentas). Ligation mixtures were prepared as follows:

1 µL non-purified PCR product
10 µL Reaction Buffer 2x
1 µL pJET1.2/blunt Cloning Vector (50 ng/µL)
T4 DNA Ligase
water to 20 µL, incubation at room temperature for 5 minutes.

A parallel control reaction was set up including all the components except the PCR product. For each ligation, one 50 µL aliquot of *E.coli* Subcloning Efficiency DH5α Chemically Competent Cells (Invitrogen) was thawed in ice and gently resuspended; after the addition of 5 µL of the ligations, the suspensions were incubated in ice for 30 minutes, at 42° C in a water bath for 20 seconds and again in ice for at least 2 minutes. 950 µL of SOC medium (Mediatech Inc.; 2% peptone, 0.5% Yeast extract, 10mM NaCl, 2.5mM KCl, 10mM $MgCl_2$, 10mM $MgSO_4$, 20 mM glucose) were added, followed by a 1 hour incubation at 37° C with orbital shaking at 220 rpm. 1/10 of the transformation was spread onto LB Miller agar plates (1% Tryptone, 0.5% Yeast extract, 0.05% Sodium chloride, 1.5% Agar) containing 50 µg/mL of Ampicillin (Sigma Aldirch) as a selection antibiotic and incubated at 37° C overnight.

2.9.1 Screening and confirmation of the cloning products

A preliminary colony PCR screening was performed to detect *E.coli* colonies containing successfully cloned PCR products setting up the reactions as follows:

5 µL of bacteria colony resuspended in 50 µL of water
300 nM of each primer
12.5 µL HotStart Maxima PCR Master Mix 2x (Fermentas)
water to 25 µL.

Primer sequences are listed below:

pJET1.2 FOR: CGACTCACTATAGGGAGAGCGGC
pJET1.2 REV: AAGAACATCGATTTTCCATGGCAG;

Reactions were incubated as follows:

95° C for 4 minutes
95° C for 30 seconds
60° C for 30 seconds
72° C for 9 seconds
} 30 cycles
72° C for 10 minutes.

5 µl of each PCR product were loaded into 2% agarose/TBE gel with 0.4 µg/mL of Ethidium Bromide and electrophoresed.
Among the clones that showed successful amplification, two were chosen at random for plasmid DNA extraction, restriction digestion analysis and sequencing confirmation. 5 mL of a selected clone culture in LB Miller medium (1% Tryptone, 0.5% Yeast extract, 0.05% Sodium chloride) plus 100 µg/mL Ampicillin (Sigma Aldrich) were incubated overnight at 37° C with orbital shaking at 220 rpm. The morning after, bacteria cells were centrifuged at 3500 rpm for 15 minutes at 4° C, medium discarded and plasmid DNA was extracted using the GeneJET Plasmid Miniprep Kit (Fermentas) as follows: pelleted cells were resuspended in 250 µL of Resuspension Solution (containing 0.1 µg/µL of RNase A) and transferred to a microcentrifuge tube, 250 µL of Lysis Solution was added, the mixture inverted several times and incubated at room temperature for 5 minutes. After the addition of 350 µL of Neutralization Solution and several inversions, samples were centrifuged at 13000 rpm for 5 minutes and supernatant loaded into a GeneJET spin column to be further centrifuged at 13000 rpm for 1 minute. Plasmid DNA, now bound to the silica column, was washed twice with 500 µL of Wash Solution (reconstituted adding 70 mL of ethanol 100% to 100 mL of the supplied concentrated Wash Buffer) and

centrifuged at 13000 rpm for 1 minute. An additional centrifugation step was performed to remove residual ethanol from the column. Plasmid DNA was eluted with 50 µL of Elution Buffer after 2 minutes of incubation at room temperature, followed by centrifugation at 13000 rpm for 1 minute. All centrifugation steps were carried out at room temperature.
Restriction digestion analysis was set up using the same enzymes used for cloning, as follows:

1 µg plasmid DNA
2 µL FastDigest Green Buffer 2x
1 µL FastDigest BglII (Fermentas)
water to 20 µL, incubation at 37° C for 1 hour.

Digests were loaded into 1% agarose/TBE gel plus 0.4 µg/mL of Ethidium Bromide to assess the release of the cloned promoters from the vector backbone.
To confirm the sequence of the cloned products, 1 µg of each plasmid DNA was sequenced with both Forward and Reverse pJET1.2 primers in an ABI 3130xl sequencer; sequences were then aligned with the expected promoter sequences with the aid of the webtool Chromas, Version 2.33 (Technelysium, South Brisbane, Australia).

2.10 Whole Genome Amplification (WGA) Bias Assessment

To determine whether the WGA process introduced any methylation-related bias, Fragment A and B were prepared to be used as Negative Control and Positive Control, respectively. Briefly, Fragment B was *in vitro* methylated as described in section 2.6.2, while Fragment A was left unmethylated. A MeDIP reaction was set up with the usual Positive and Negative Controls and a parallel one was set up with the controls prepared as stated above. WGA was performed as described in section 2.7, relative enrichments of Controls was determined by qPCR (see section 2.8) also in Pre-WGA mixtures and compared. To determine whether WGA introduced any sequence-related bias, four additional Lambda DNA fragments of various sizes (in the range of the sonicated gDNAs size – 200 to 1000 bp) were prepared by PCR and spiked in one of the samples at the usual 1:100 ratio. Again, qPCR was performed on both Pre-WGA and Post-WGA mixtures and the relative enrichments compared. Primers sequences for fragments preparation and qPCR are listed in Table 2.4.

Table 2.4. Primers sequences for λ DNA Fragment Spikes preparation (pairs 1) and qPCRs (pairs 2) for the assessment of Whole Genome Amplification length related bias.

Primer Sequences	**Amplicon Length**
Spike 208 FOR1 - CGTTTCCTTTCTCTGTTTTTGTC Spike 208 REV1 - CAATTTCAGCATCCCTTTCGG	208
Spike 208 FOR2 - CAATGGAAGTCAACAAAAAGCA Spike 208 REV2 - CATAAAGCACCTCATTACCCTT	126
Spike 400 FOR1 - CCATCAATAAAACCTATACCCGC Spike 400 REV1 - AGTATTTTTTTCCTGCCATCCAC	400
Spike 400 FOR2 - CGAAACAAAAACGGGGTTTAC Spike 400 REV2 - TTATTCGGGAAGTGAACGGC	128
Spike 800 FOR1 - GGCGAATGACCAAAGAGACT Spike 800 REV1 - ATAAAAAAATCCCGTAAAAAAAGCC	800
Spike 800 FOR2 - GACGAGACGAAAAAACGGAC Spike 800 REV2 - CGTAAAAAAAGCCGCACAGG	99
Spike 1000 FOR1 - CATAAAAGGTCTTGAGCAGGC Spike 1000 REV1 - CGGCATTGTAGGATTTGGTAC	1000
Spike 1000 FOR2 – TGTTTTTGATGAGGCGGATTTT Spike 1000 REV2 - TGAGCAGGCAGGAAAACTTC	126

2.11 MeDIP arrays and data analyses

To obtain DNA methylation data, 3 µg of WGA Input and MeDIP samples were sent to Nimblegen Roche, where they were labelled with Cy3 and Cy5, respectively, and hybridized onto HG18_RefSeq_promoter Arrays (human samples) or MM9_CpG_Refseq_promoter Arrays (murine samples). For the HG18_RefSeq_promoter Arrays, tiling of promoter regions was based on human RefSeq genes (HG18; NCBI Build 36) and included 2200 bp upstream and 500 bp downstream of the transcriptional start, with an interval spacing of 100 bp between probes. For the MM9_CpG_Refseq_promoter Arrays, tiling of promoter regions was based on refFlat file downloaded from UCSC on May 19th 2009 and included 2960 bp upstream and 740 bp downstream of the transcriptional start, with an interval spacing of 100 bp between probes.

Data analyses were carried out by M. Adriaens (Maastricht University, The Netherlands).

2.11.1 Data preprocessing

For the analysis of the MeDIP microarray data, the *enrichR* package was used, running in R (version 2.15.1) with Bioconductor (version 2.10). A full description of all functions and required packages is available from http://www.bigcat.unimaas.nl/wiki/index.php/EnrichR.

After importing the files containing the raw probe intensities (Nimblegen PAIR-files) into R, quality control was performed using the *arrayQualityMetrics* package (Kauffmann et al., 2009), revealing no data quality issues. Raw data were normalized using T-quantile normalization, performed separately on the channels, and separately on each experimental group (Adriaens et al., 2012). Nimblegen employs two-channel microarray technology, where one channel contains the MeDIP enriched sample and the other channel contains a total DNA reference sample. Hence after normalization, for each microarray the $\log_2$ ratios between the MeDIP enriched channel and the total DNA channel were calculated and used thereafter as relative probe intensities.

2.11.2 Enrichment analysis

To quantify the relative degree of DNA methylation, enrichment analysis was applied using a sliding window approach. A window is defined as the genomic region centred on a probe and containing all neighbouring probes within a span of 750 bp. The null hypothesis is that the normalized intensities of a set of probes in a window are sampled from the null distribution, defined as the distribution of all probe intensities in the dataset. The alternative hypothesis is that probe intensities in the window are drawn from a distribution that has a higher mean than the null distribution. The procedure is similar to the ACME approach (Scacheri et al., 2006), the difference being that here a one-sided two-sample Kolmogorov-Smirnov test is performed using the normalized probe intensities directly, instead of a χ^2-test on dichotomized probe values, acquired by setting a specific intensity cut-off. The test applied here is more appropriate for the continuous nature of DNA methylation data, whereas the standard procedure in ACME was designed to take account of the binary nature of DNA binding events in most ChIP-on-chip experiments (Adriaens et al., 2012). It is important to note that for this analysis, replicate measurements were pooled for each experimental group. After the enrichment analysis, the resulting p-values were negative $\log_{10}$-transformed to yield enrichment scores. In accordance with the manufacturer's protocol, if a window has an enrichment score of 2 or higher, it is considered enriched, indicating some degree of DNA methylation in the

window region. The higher the enrichment score, the more likely the relative degree of DNA methylation is high.

2.11.3 Identification of differentially methylated regions

For each promoter region on the microarray, the most enriched region for each experimental group plus the corresponding regions in the other two experimental groups were returned. To assess differences in DNA methylation between experimental groups, differential enrichment analysis was performed by applying an ANOVA between each two groups, using all normalized probe intensities in the returned regions. As with the enrichment analysis, replicate measurements were pooled for each experimental group. A region of interest is defined as having a significant difference in probe intensities between any two experimental groups, with as large a difference as possible in enrichment score, preferably having an enrichment score lower than 2 in one condition and much higher than 2 in the other. Such regions were prime candidates for having functionally large differences in DNA methylation.

2.12 Transcriptome arrays and data analyses

To obtain gene expression data, RNA were extracted as previously described (see section 2.4) in triplicate and sent to Affymetrix for hybridization onto Affymetrix.GeneChip.NuGO_Hs1a520180 arrays.
Data analyses were carried out by M. Adriaens (Maastricht University, The Netherlands).

2.12.1 Data analyses

Files containing the raw probe intensities (Affymetrix CEL-files) were imported in the statistical programming language R (version 2.15.1) using standard Bioconductor (version 2.10) procedures (R-Core-Team, 2012; Gentleman et al., 2004). Quality control was performed using the standardized microarray quality control service offered on www.arrayanalysis.org (Eijssen et al., 2013), revealing no data quality issues. The data were normalized using the GCRMA (GeneChip Robust Multi-Array Analysis) normalization (Wu and Irizarry, 2004; Zhang et al., 2004) and annotated using the most up-to-date Entrez Gene based annotation available from the BrainArray project (Dai et al., 2005) of the University of Michigan (http://brainarray.mbni.med.umich.edu/).

Differences in gene expression between experimental groups were assessed using linear modelling and the empirical Bayes methods of the *limma* package (Smyth, 2004).

2.13 Reverse Transcription (RT) and RT-qPCR

To eliminate contaminating gDNA prior to reverse transcription, total RNAs were digested in duplicate reactions with DNaseI (Fermentas) as follows:

500 ng total RNA
1 µL DNAse I 10x buffer with 25 mM $MgCl_2$
0.5 U DNaseI, RNase-free
Water to 10 µL, 37° C for 30 minutes.

After the addition of 1 µL of EDTA 50 mM, samples were incubated at 65° C for 10 minutes and cooled in ice. A reverse transcription mix with the following composition was prepared with the reagents included in the Maxima Universal First Strand cDNA Synthesis kit (Fermentas) and added to each sample:

0.25 µL 100 µM oligo $(dT)_{18}$ primers
0.25 µL 100 µM random hexamers primers
1 µL 10 mM dNTP mix
4 µL 5x RT buffer
1 µL RiboLock RNase Inhibitor (20 u/µL)
Water to 8 µL.

1 µL of Maxima Reverse Transcriptase (200 u/µL) was added to one of the duplicate reaction and 1 µL of water was added to the second reaction, which was later used as no template control. Mixes were incubated as follows:

25° C for 10 minutes
50° C for 15 minutes
85° C for 5 minutes.

Single strand cDNAs (sscDNAs) and control reactions were diluted 1:20 with water and stored at -80° C until used as templates in qPCR assays; reactions were set up as

described in section 2.8 with primers listed in Table 2.5. Dilution curves and melt curves for each primer pair are shown in Appendix A.

Table 2.5. Primers sequences for RT-qPCR assays.

Specificity	**Primers Sequences**	**Amplicon Length**
Human	**DNMT1** FOR - AAACAAAGGGAAGGGCAAGG REV - AGAAAACACATCCAGGGTCC	118 bp
Human	**DNMT3A** FOR - GCCTCAATGTTACCCTGGAA REV - CAGCAGATGGTGCAGTAGGA	127 bp
Human	**DNMT3B** FOR - CCCATTCGAGTCCTGTCATT REV - GGTTCCAACAGCAATGGACT	126 bp
Mouse	**Dnmt1** FOR - TGAGGAAGGCTACCTGGCTA REV - GTCTGCCATTTCTGCTCTCC	142 bp
Mouse	**Dnmt3a** FOR - ACCAGGCCACCTACAACAAG REV - GCTTGTTCTGCACTTCCACA	150 bp
Mouse	**Dnmt3b** FOR - GCATGAAGGCCAGATCAAAT REV - GCTTCCACCAATCACCAAGT	97 bp
Human	**CCNB2** FOR - GGAAGAGATATAAATGGACGCAT REV - TGGCTGAACCTGTAAAAATCG	135 bp
Human	**DLGAP5** FOR - ACTTTTTGTTTGGTTGAGGTTTC REV - AGACAGTGATTTCCTATGAGCA	133 bp
Human	**FANCG** FOR - TGGAGGGAAAAGAATGACCG REV - CCAAGGGAAGAACAGGAACA	163 bp
Human	**MMP3** FOR - GGACAAAGGATACAACAGGGA REV - GTGAGTGAGTGATAGAGTGGG	124 bp
Human	**PNMA2** FOR - AACCCGTCCATCAGTGTAGA	122 bp

	REV - ACCTTCTCTCCTTCCTCCTG	
Human	**TMSB15A** FOR - CGAACAGCCTTTCACGAGTC REV - GTCAAACTTCTCCACTTCCGA	92 bp
Human	**CTTN** FOR - GGATCGGATGGATAAGAATGC REV - TGATGTTACTTGTTTTGCTGGT	110 bp
Human	**GLIPR2** FOR - CACAATGAGTACCGGCAGAA REV - CCATCTATCAGCCACCTCCT	201 bp
Human	**NPTX1** FOR - CAAACTTTGCAATCGCTCAA REV - GATCCTTGAGGCTGTTGGTC	91 bp
Human	**SLC39A14** FOR - TGTCTCCAAGTCTGCAGTGG REV - AATGGCTGTGTCCATGATGA	113 bp
Human	**mtDNMT1** FOR - AGCAAACCGTGGAGCTTG REV - CAAACGGAGAGAGGCGATAC	134 bp
Mouse	**mtDnmt1** FOR - ATGGTCTTCCCCCACTCTCT REV - TGCAGACGACAGAACAGCTC	126 bp
Human	**B2M** FOR - CGCTACTCTCTCTTTCTGGC REV - AATTTGACTTTCCATTCTCTGCT	93 bp
Human	**GAPDH** FOR - TCAAGAAGGTGGTGAAGCAG REV - GTGTCGCTGTTGAAGTCAGA	97 bp
Human	**HPRT1** FOR - AAGTTTGTTGTAGGATATGCCC REV - GCTTTGTATTTTGCTTTTCCAGT	98 bp
Human	**UBE2B** FOR - TCTTAACATCAATTCAGTCTCTGC REV - ACTCTTTTCTCATATTCTCGTTTGT	109 bp
Mouse	**Actb** FOR - CCCAGAGCAAGAGAGGTATC REV - ATTGTAGAAGGTGTGGTGCC	104 bp
Mouse	**B2m** FOR - ATGCTGAAGAACGGGAAAAAAA REV - CAGTGTGAGCCAGGATATAGAA	91 bp

Mouse	**Gapdh** FOR - AGGACACTGAGCAAGAGAGG REV - TGTTATTATGGGGGTCTGGGA	91 bp
Mouse	**Hprt** FOR - AGGAGAGAAAGATGTGATTGATATT REV -TCCACTGAGCAAAACCTCTT	96 bp

2.14 LUminometric Methylation Assay (LUMA)

One of the methods applied to determine global DNA methylation content in the samples under study was the LUMA assay (Karimi et al., 2006a; Karimi et al., 2006b), with a small modification consisting in the substitution of the normalizer restriction enzyme *EcoRI* with *MunI*, as described in section 3.5. This modification was important in producing better standard curves (see section 3.3) and lower reading variability between replicates (data not shown) (Lisanti S., Omar W.A.W. et al., accepted).
gDNAs were double digested as follows:

600 ng gDNA
3.5 µL 10x Tango buffer (Fermentas)
0.6 µL *MspI* (or *HpaII*) 20 U/µL (Fermentas)
0.6 µL *MunI* 20 U/µL (Fermentas)
water to 35 µL, 37°C for 4 hours.

After the addition of 35µL of annealing buffer (Biotage), the digestions were distributed in triplicates (3x 20µL) in a 96-well PCR plate for analysis by pyrosequencing as described in section 2.20, in a PyroMark MD instrument, Biotage. The deoxynucleotide dispensation order was: GTGTCACATGTGTG and the percentage of global genome CpG methylation was calculated from the *HpaII/MspI* digestions ratio as follows:

[1 - [(*HpaII* ΣC / ΣA) / (*MunI* ΣC / ΣA)] / [(*MspI* ΣC / ΣA)/ *(MunI* ΣC / ΣA)] x 100 (adapted from (Karimi et al., 2006b)),

where C and A are the overhangs left by the restriction enzymes cuts.

2.15 Measurement of total 5'-methylCytosine content by means of High Performance Liquid Chromatography (HPLC)

For some of the samples, the genomic content of the nucleoside 5-methyl-2'-deoxycytidine by quantified by HPLC with UV detection as described (Rozhon et al., 2008) with minor modifications. These measurements were carried by S. De Prins, G. Jacobs and G. Koppen at the Environmental Risk and Health Unit of the Flemish Institute of Technological Research, Belgium.

Frozen tissues and cell pellets gDNAs were extracted as described in section 2.3 and digested overnight at 37° C with a mixture of DNaseI and Nuclease P1. Next, nucleotide monophosphates were dephosphorylated overnight at 37 °C with calf intestine alkaline phosphatase. The content of 5'methylCytosine was estimated using a Waters Acquity Ultra Performance Liquid Chromatography (UPLC) system. The HPLC protocol was based on isocratic separation using a Nucleosil SA cation exchange silica 150 x 4.6 mm x 5 µm column (Macherey-Nagel); the column temperature was maintained at 30 °C. The acidic mobile phase consisted of 50 mM ammonium acetate in 15% acetonitrile with a pH of 4.8 and the flow rate was 0.5 ml/min. Samples were cooled at 4 °C and 30 µl were injected in the column. UV detection was performed at 278 nm for mdC with a bandwith of 9.6 nm. Levels 5'mC were estimated based on the corresponding standard curve (2 – 0.008 µg/mL). A standard sample (0.5 µg/mL) was measured at the beginning, at the end and 3 additional times throughout the run to check for intra-assay variation.

2.16 Global DNA Methylation Colourimetric Assay

A second approach used to determine the total content of 5-methylCytosines in the samples under investigation was a colourimetric assay based upon the use of a capture and a detection antibody applied to the sample gDNA, followed by methylation quantification based on a standard curve prepared with increasing concentration of a control DNA samples of known methylation content. For this purpose, the MethylFlash Methylated DNA Quantification kit (Epigentek) was used.

gDNAs were quantified as described in section 2.5, diluted to a final volume of 8 µL with TE buffer, mixed to 80 µL of ME2 Binding Solution and dispensed in a clear 96-well plate. In parallel, 1 µL of ME3 (Negative Control, 20 ng/µL), 1 µL of the following dilutions of ME4 (Positive Control at 50% of methylation content, 20 ng/µL): 0.5 ng/µL, 1 ng/µL, 2 ng/µL, 5 ng/µL, 10 ng/µL, all in TE buffer, were also added to prepare a methylated DNA standard curve. Plates were sealed with Parafilm M and incubated at

37° C for 90 minutes. After removal of the ME2 Binding Solution, wells were washed with 150 µL of ME1 Wash Buffer 1x three times and 50 µL of ME5 Capture Antibody (1:1000 dilution in ME1 Wash Buffer 1x, to obtain a final concentration of 1 ng/µL) were added; plates were incubated at room temperature for 1 hour, followed by removal of diluted ME5 and 3 washes with 150 µL of ME1 Wash Buffer 1x. 50 µL of ME6 Detection Antibody (1:2000 dilution in ME1 Wash Buffer 1x, to obtain a final concentration of 0.2 ng/µL) were added and plates incubated at room temperature for 30 minutes. After four washes with 150 µL of ME1 Wash Buffer1 x, 50 µL of ME7 Enhancer Solution (1:5000 dilution in ME1 Wash Buffer 1x), plates were incubated at room temperature for 30 minutes and washed five times with 150 µL of ME1 Wash Buffer1 x; 100 µL of ME8 Developer Solution was added to each well, followed by 10 minutes of incubation at room temperature in the dark. The colourimetric reaction was stopped with the addition of 50 µL of ME9 Stop Solution and absorbance at 495 nm was recorded after 5, 10 and 15 minutes in a microplate reader. Coefficient of determination (R^2) of the standard curve was calculated for each time point and data readings corresponding to the R^2 closest to 1 were used for the calculation of the total methylation content in the samples, applying the following formulas:

5-mC (ng) = (sample OD – ME3 (Negative Control) OD) / Slope x 2,

where 2 is a normalization factor, as the ME4 Positive Control contains only 50% of 5-mC;

5-mC% = (5-mC amount (ng)) / (amount of input gDNA (ng)) x 100.

2.17 Bisulphite Modification (BM)

All bisulphite modification (BM) reactions were conducted using 350 ng of starting genomic DNA and the EZ DNA Methylation-Gold kit (Zymo Research). The CT Conversion Reagent was supplied in lyophilized aliquots and prepared adding 900 µL of water, 300 µL of M-Dilution Buffer and 50 µL of M-Dissolving Buffer for each aliquot, followed by vortexing for 10 minutes. Unused CT Conversion Reagent was stored at -20° C and warmed at 37° C for 10 minutes prior to use and used within a month from dissolution. M-Wash Buffer was prepared adding 96 mL of 100% ethanol to the supplied 24 mL of concentrated buffer.

gDNAs were diluted to 20 µL of final volume with TE buffer in PCR tubes and 130 µL of reconstituted CT Conversion Reagent were added; mixtures were incubated in a thermal cycler as follows:

98° C for 10 minutes
64° C for 2.5 hours
storage at 4° C for up to 20 hours.

600 µL of M-Binding Solution were added to Zymo-Spin IC Columns together with the samples and, after several inversions, columns were centrifuged at 13000 rpm for 1 minute at room temperature. The column was washed once with 100 µL of M-Wash Buffer and the bound DNA was desulphonated by the addition of 200 µL of M-Desulphonation Buffer, followed by 20 minutes of incubation at room temperature. The columns were washed twice with 200 µL of M-Wash Buffer and the BM-DNA eluted in 25 µL of M-Elution Buffer. BM-gDNAs were stored at -80° C until use and for up to 3 months.

2.18 Bisulphite modified DNA PCRs (BM-PCR)

Bisulphite modified DNA PCRs (BM-PCR) were set up as follows:

2 µL of BM-DNA
300 nM of each primer
12.5 µL of Maxima HotStart Taq Master Mix 2x (Fermentas)
water to 25 µL.

Primer pairs were designed to amplify sequences between 200 and 500 bases of length using the webtool MethPrimer (Li and Dahiya, 2002) and annealing temperatures were optimized by gradient PCR testing a range included between ±5° C of the single primers melting temperatures. Cycling conditions for each pair are listed in Table 2.6; an initial denaturation step (95° C for 4 minutes) and a final elongation step (72° C for 10 minutes) were performed for all the reactions and cycling programs were repeated 45 times.

Table 2.6. Primers sequences for BM-PCR. The symbol "*" indicates an assay for which template DNA was diluted 1:200 before use. The symbol "**" indicates primers previously used in (Jeong and Lee, 2005). The symbol "***" indicates an assay requiring a final concentration of 3.5 mM $MgCl_2$, instead of the usual 2 mM obtained by using the Maxima HotStart Taq Master Mix.

Specificity	**Primers Sequences**	**Cycling conditions**	**Amplicon Length**
λ-DNA	**Fragment A *** FOR - GGTATTGTATGATTTGATGATAGGTA REV - AATTAAACAACAAAACTACATCCAC	95º C, 30 sec 58.8º C, 30 sec 72ºC, 20 sec	325 bp
Human	**LINE-1** FOR -TTATTAGGGAGTGTTAGATAGTGGG REV -CCTCTAAACCAAATATAAAATATAATCTC	95º C, 30 sec 56.7º C, 30 sec 72ºC, 15 sec	245 bp
Mouse	**B1 element ** ** FOR - GGTGGTGGTGGTGGTTGAGATAG REV - AATAACACACACCTTTAATCCCAACACT	95º C, 30 sec 64.9º C, 30 sec 72ºC, 10 sec	155 bp
Human	**H19 ICR** FOR - TGGGTATTTTTGGAGGTTTTTTT REV -TCCCATAAATATCCTATTCCCAAA	95º C, 30 sec 56º C, 30 sec 72ºC, 15 sec	220 bp
Human	**HIST1H2BA** FOR - ATTTGTTATTTGATTGGTTGATGGT REV - ACACTTTCCAATACTCAACAACTCTT	95º C, 30 sec 58º C, 30 sec 72ºC, 15 sec	247 bp
Human	**GAPDH** FOR - TTAAAGGTTAGGTTGTAAATGTTAT REV - ATATTTAACCTCAAACCAAAATAC	95º C, 30 sec 55º C, 30 sec 72ºC, 15 sec	128 bp
Mouse	**H19 ICR** FOR – AAGGAGATTATGTTTTATTTTTGGA REV - CCACAACATTACCATTTATAAATTCC	95º C, 30 sec 56º C, 30 sec 72ºC, 15 sec	152 bp
Mouse	**Hist1h2ba** FOR - GAATTTTTTTGTGATAGATATTTT REV - CCTTTAAATTTATTATAAACCCTAC	95º C, 30 sec 52º C, 30 sec 72ºC, 15 sec	222 bp
Mouse	**Actb** FOR – GGAGAAGAGTTATGAGTTGTTTGA REV - TAAACTACAACTTACCCAAAAAAAA	95º C, 30 sec 56º C, 30 sec 72ºC, 15 sec	110 bp
Mouse	**Gapdh** FOR - GGGGAAATGAGAGAGGTTTAGTTAT REV - AAAAAACAAAAAACACCAAAAAAA	95º C, 30 sec 56º C, 30 sec 72ºC, 15 sec	183 bp

Human	**MT-COI** FOR - ATTTTTTATAAATTATAAAGATATTGGAAT REV - AAACTATTCAACCTATTCCTACTCC	95º C, 30 sec 55.4º C, 30 sec 72ºC, 23 sec	365 bp
Human	**MT-non coding region** FOR - TTGGGATTAGATATTTTATTATGTTTAGTT REV - ATAACCCATTTCTTACCACCTCATA	95º C, 30 sec 59.3º C, 30 sec 72ºC, 23 sec	297 bp
Human	**MT-ND1** FOR - ATGGTTAATTTTTTATTTTTTATTGTATTT REV - TAATTTAAATTTAATACTCACCCTAATCAA	95º C, 30 sec 57.5º C, 30 sec 72ºC, 23 sec	374 bp
Human	**MT-ND4 ***** FOR - TTTTTGAGTTAATAATTTAATATGATTAGT REV - ACTTCAAAAAATTTAAATAAAAATAACTAT	95º C, 30 sec 55.4º C, 30 sec 72ºC, 15 sec	361 bp
Human	**MT-ND5** FOR - GTTTTTTAAATATTTATTTATTTTTTTAAT REV - CCTAATTAAACTAATTTACCTACTACTACT	95º C, 30 sec 53º C, 30 sec 72ºC, 23 sec	336 bp
Mouse	**MT-D-Loop** ATTTGGTTTATTAATTTATTATTTTT CTATATACTATCCTTTCATACCTTAAC	95º C, 30 sec 46.1º C, 30 sec 72ºC, 19 sec	304 bp
Mouse	**MT-non coding region** GGAATGTTTAAAGGAAAGATTTAAAAAG TCAACCTCTTCACTAAAAAATCAATTT	95º C, 30 sec 50.6º C, 30 sec 72ºC, 19 sec	268 bp

2.19 BM-PCR sequencing and BM-cloning sequencing

BM-PCR products were treated to eliminate primers and nucleotides prior to sequencing (Werle et al., 1994), as follows:

5 µL PCR product containing 15 ng of DNA for each 100 bp of amplicon length
1 µL FastAP Thermosensitive Alkaline Phosphatase 1 u/µL (Fermentas)
0.5 µL Exonuclease I (Fermentas), incubate at 37°C for 15 minutes and at 85° C for 15 minutes.

Sequencing was performed with the Reverse primer (unless otherwise indicated) in an ABI 3130xl sequencer. Chromatograms were subject to visual quality control and areas with wide/overlapping peaks were excluded from subsequent analyses. A further quality control was performed with BiQ Analyzer software (Bock et al., 2005) to ensure a minimum of 70% identity match with the expected PCR product sequence and a minimum of 80% conversion rate of unmethylated Cytosines to thymines. For data

presented in Chapter 3 and Chapter 4, Cytosine methylation content was determined by applying the following formula:

% C Methylation = C peak height / (C peak height + T peak height) * 100 (Jiang et al.).

When direct sequencing did not pass BiQ quality controls or sequencing chromatograms were not optimal, the BM-PCR products were cloned as described above in section 2.9, plasmid DNA was purified from 10 clones and sequenced with the pJET1.2 FOR primer. Sequences were aligned as described above and aggregated methylation data graphs produced.
For data presented in Chapter 5 and Chapter 7, Cytosine methylation content was determined using Epigenetic Sequencing Methylation analysis software (ESME) (Lewin et al., 2004). This program calculates methylation levels by comparing the C to T peaks at CpG sites after alignment of the ABI sequencers trace files to a reference sequence (the unconverted PCR product) after having performed a quality control, normalised the signals and corrected for incomplete bisulphite conversion. Quality control output for all analyzed sequences is given in Appendix B.

2.20 Pyrosequencing

Predesigned assays for Pyrosequencing (PyroMark CpG Assays, including PCR and sequencing primers for Pyrosequencing analysis of gene-specific CpG methylation after DNA bisulfite conversion) were obtained from QIAgen Sciences, Germantown, MD. Primer sequences were protected from copyright, therefore are not known; Table 2.7 lists the available informations for those assays. Methylation standards measurements and pyrograms are presented in Appendix C.

Table 2.7. Specifications for PyroMark CpG Assays used in the present study. CpG sites under investigation are underlined. The symbol "*" indicates assays that required a final concentration of 3 nM of $MgCl_2$, instead of the usual 1.5 mM obtained by using the PyroMark PCR Master Mix.

Specificity	**Assay name** **Catalog Number**	**Amplicon Length**	**Sequence to analyse**
Human	Hs_CTTN_01 PM00151844	114 bp	GGGGGCACGGAGGGCTTGGGGCTGGGGTCCGCGGA
Human	Hs_GLIPR2_01* PM00141176	152 bp	GGCTGTCCTCGGGACAGCCGAGCGGGGCAAACTGCTTCGC
Human	Hs_NPTX1_03* PM00182035	78 bp	CAGCCCGGCTCCAAACGACCCCGGC
Human	Hs_NPTX1_07* PM00182063	181 bp	CGGGGGTCACCGGGCCGCCCCGCGTTTCTTAGATGTCCGT
Human	Hs_SLC39A14_01* PM00136598	125 bp	GGCTAGGCGGTGAGAGCTTCCCGCGT
Human	Hs_SLC39A14_02* PM00136605	261 bp	GAGCGGGCGCCGACCACAGCCAGGGCCGCGAGGCGC

To prepare samples for Pyrosequencing, gDNAs were bisulphite modified as described in section 2.17 and BM-PCR products were prepared in triplicate reactions using the PyroMark PCR Kit following the manufacturer's instructions, as follows:

2 µL BM DNA
25 µL PyroMark PCR Master Mix, 2x
2.5 µL CoralLoad Concentrate, 10x
2.5 µL Primers Mix 3 µM (including a Biotinylated Reverse Primer)
water to 25 µL.

Cycling conditions were:

95° C for 15 minutes
94° C for 30 seconds
56° C for 30 seconds — 45 cycles
72° C for 30 seconds
72° C for 10 minute.

10 µL of each PCR product were electrophoresed in a 2% agarose/TBE gel plus 0.4% of Ethidium Bromide to check for the presence of a unique band and samples leftovers were sent to EpigenDx, Hopkinton, MA, for Pyrosequencing in a PyroMark Q96 MD instrument. Briefly, the following mix was prepared for each biotinylated PCR product in a 96-well PCR plate:

10 µL biotinylated BM-DNA PCR product
2 µl GE Healthcare Streptavidin Sepharose High Performance beads
40 µl QIAgen PyroMark Binding Buffer
water to 80 µl.

PCR plates were sealed and mixed at 1400 rpm for 10 minutes at room temperature, allowing the immobilization of the PCR products to the streptavidin-coated beads. Strand separation was performed with the aid of probes applying vacuum in a PyroMark Q96 Vacuum Workstation by soaking the captured beads in 70% ethanol, then in PyroMark Denaturation Solution (QIAgen) and then in PyroMark Wash Solution (QIAgen); finally, beads were released into a PyroMark Plate containing 12 µL of 300 nM sequencing primer resuspended in PyroMark Annealing Buffer (QIAgen) in each well, heated at 80° C for 10 minutes, allowed to cool to room temperature and run into the instrument.
CpG sites that did not pass the instrument quality control were excluded from further analyses.

2.21 Promoter-reporter assays

2.21.1 Promoter identification and cloning

To determine whether the genomic regions that showed differential methylation could act as promoters for the related downstream genes, bioinformatics analyses were performed using the webtool http://genome.ucsc.edu/cgi-bin/hgBlat to determine the presence of regulatory elements (Transcription Factors Binding Sites, Transcription Start Sites in the proximity, Regulatory Regions and Polymorphisms). In addition, a high density of CpG dinucleotides was confirmed using the webtool http://www.ebi.ac.uk/Tools/emboss/cpgplot, applying the default criteria. As previously described, these genomic regions spanned a 750 bp size (the window size used for the bioinformatics analyses). A murine Secreted Embryonic Alkaline Phosphatase (mSEAP)

reporter plasmid without a promoter, an enhancer and completely devoid of CpG dinucleotides was obtained (Invivogen); the plasmid map is shown in Figure 2.1.

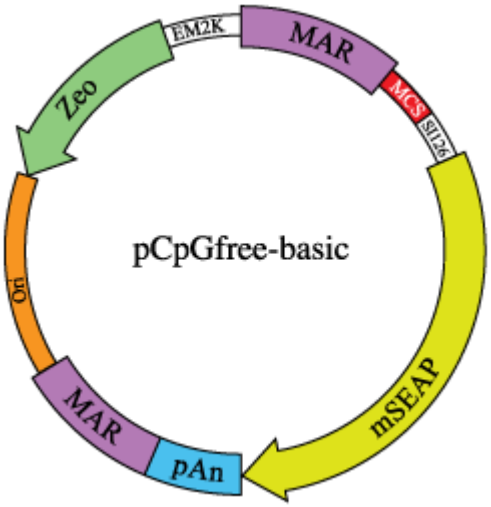

Figure 2.1. Map of the pCpGfree-basic plasmid (adapted from http://www.invivogen.com/pcpcgfree-basic).

The plasmid is 3837 bp in size and has the following features:

Ori: *E. coli* origin of replication R6K gamma ori (modified to eliminate all CpG sites), activated by the *pir* gene-activated protein ∏ (Wu et al., 1995);
EM2K: bacterial promoter EM7 (modified to eliminate all CpG sites);
Zeo: CpG-free synthetic allele of the Zeocin resistance gene;
mSEAPΔCpG: a modified version of the murine Secreted Embryonic Alkalyne Phosphatase without CpG sites;
pAn: CpG-free polyadenylation signal of the SV40 polyadenylation signal;
MAR: Matrix Attached Regions (Bode et al., 1996); this plasmid includes two naturally CpG-free MARs: one upstream of the IFNB*1* gene and one upstream of the HBB gene;
MCS: Multiple Cloning Site, featuring the following restriction sites form 5' to 3': SdaI, Bsp120I, AvrII, NsiI, Prpu10I, ScaI, BamHI, SpeI, HindIII.

The promoters of interest were PCR amplified from gDNA of replicative MRC-5 fibroblasts according to the following reaction set up:
200 ng of gDNA
300 nM of each primer

0.75 µL DMSO (final concentration 3%)
12.5 µL Phusion High-Fidelity PCR Master Mix 2x with HF Buffer (Finnzymes)
water to 25 µL.

Reactions were prepared in triplicates and incubated as follows:

98° C for 30 seconds
98° C for 10 seconds
71.5° C for 30 seconds } 30 cycles
72° C for 24 seconds
72° C for 10 minutes.

Primer sequences are listed in Table 2.8.

Table 2.8. Primers sequences for *CTTN* and *GLIPR2* promoters cloning; BamHI and HindIII restriction sites are underlines in the FOR and REV sequences, respectively.

Primer Sequences	**Amplicon Length**
CTTN Prom. FOR: CAGGGATCCCCGGGCGAGCTCTGCAGA CTTN Prom. REV: CAGAAGCTTCTTTCCTTGAGACCCCCCACACC	780
GLIPR2 Prom. FOR: CAGGGATCCCCCAGAGTCACCGGAGATGGG GLIPR2 Prom. REV: AGAAGCTTTGGCCTCCTGAAACAAAGCAGAAC	792

PCR products were electrophoresed in a 1% agarose/TBE gel plus 0.4% of Ethidium Bromide and DNA bands excised with the aid of a transilluminator. DNAs were purified using the GeneJET Gel Extraction Kit (Fermentas), according to the following protocol: 1 volume of Binding Buffer was added to the gel slice (volume: weight) and the mixture incubated at 60° C for 10 minutes to completely solubilize the gel. This solution was then transferred to a GeneJET purification column and centrifuged at 13000 rpm for 1 minute, the flow-through discarded and the column washed with 700 µL of Wash Buffer reconstituted as indicated by the manufacturer (9 mL of concentrated buffer plus 45 mL of 100% ethanol). The column was centrifuged for an additional minute to remove any residual ethanol and DNAs eluted in 30 µL of Elution Buffer, centrifuging at 13000 rpm for 1 minute, after 1 minute of incubation at room temperature.

Purified promoters were double digested as follows:

30 µL of purified DNA
3 µL Fast Digest Green Buffer 10x
1 µL Fast Digest BamHI (Fermentas)
1 µL Fast Digest HindIII (Fermentas)
water to 40 µL, incubate at 37° C for 1 hour.

A parallel digestion with the same enzymes and 1 µg of pCpG-free plasmid DNA was set up, electrophoresed and purified from gel with the GeneJET Gel Extraction Kit (Fermentas) as described above. The digested promoters were cleaned up using the DNA Clean & Concentrator-5 kit (Zymo Research), as described in section 2.6.3.
1 µL of each purified DNA was quantified on agarose/TBE gel by comparison with 1 µL of 1 Kb Plus DNA Ladder, ready-to-use (Fermentas).
The following equation was applied to calculate the optimal amount of fragment (digested promoter) to be incubated with the vector (digested plasmid) in a ligation reaction:

3 : 1 = amount of fragment (ng) / fragment size (bp) : vector amount (ng) / vector size (bp).

Ligation reactions were set up as follows:

50 ng of vector
30 ng of fragment (*CTTN* promoter or *GLIPR2* promoter)
2 µL T4 DNA Ligase Reaction Buffer
1 µL T4 DNA Ligase 0.4 U/mL (New England Biolabs)
water to 20 µL.

A parallel control ligation was set up with all reagents except the fragment (digested promoter). The reaction mixtures were incubated at room temperature for 2 hours and cleaned up using the DNA Clean & Concentrator-5 kit (Zymo Research) as described in section 2.6.3, but eluting in 10 µL of water.
Ligations were transformed as described in section 2.9, but using the *E.coli*, strain GT115 (Invivogen; genotype: F- mcrA Δ(mrr-hsdRMS-mcrBC) φ80lacZΔM15 ΔlacX74 recA1 rspL (StrA) endA1 Δdcm uidA(ΔMluI)::pir-116 ΔsbcC-sbcD), suitable for the replication

of plasmids featuring the R6K gamma ori. LB Lennox agar plates (Teknova; 1% Tryptone, 0.5% Yeast Extract, 0.5% Sodium Chloride, 2.0% Agar) containing 25 µg/mL Zeocin (Teknova) as a selection antibiotic were used for the colonies overnight growth.

2.21.2 Screening and confirmation of the cloning products

A preliminary colony PCR screening was performed to detect *E.coli* colonies containing successfully cloned promoters setting up the reactions as follows:

5 µL of bacteria colony resuspended in 50 µL of water
300 nM of each primer
1.25 µL DMSO (5% final concentration)
12.5 µL HotStart Maxima PCR Master Mix 2x (Fermentas)
water to 25 µL.

The Forward primer (FOR) was designed upstream of the plasmid multiple cloning site (MCS) and Reverse primer (REV) was designed downstream of the MCS; sequences are listed below:

pCpGfree-basic FOR: ACTGATTTTTGTTTATGTGAGC
pCpGfree-basic REV: GCAATAGCAGACAGGCAC;

Expected amplicon length was 953 bp for the *CTTN* promoter cloning and 965 for the *GLIPR2* promoter cloning.
Reactions were incubated as follows:

95° C for 4 minutes
95° C for 30 seconds ⎫
55° C for 30 seconds ⎬ 30 cycles
72° C for 48 seconds ⎭
72° C for 10 minutes.

5 µl of each PCR product were loaded into 1% agarose/TBE gel with 0.4 µg/mL of Ethidium Bromide and electrophoresed.

Among the clones that showed successful amplification, two were chosen at random for plasmid DNA extraction, restriction digestion analysis and sequencing confirmation. 5 mL of a selected clone culture in LB Lennox medium (Teknova; 1% Tryptone, 0.5% Yeast Extract, 1.0% Sodium Chloride, pH 7.5) plus 25 µg/mL Zeocin (Invitrogen) were incubated overnight at 37° C with orbital shaking at 220 rpm. The morning after, plasmid DNA was extracted using the GeneJET Plasmid Miniprep Kit (Fermentas) as described in section 2.9.1.
Restriction digestion analysis was set up using the same enzymes used for cloning, as follows:

1 µg plasmid DNA
2 µL FastDigest Green Buffer 2x
1 µL FastDigest BamHI (Fermentas)
1 µL FastDigest HindIII (Fermentas)
water to 20 µL, incubation at 37° C for 1 hour.

Digests were loaded into 1% agarose/TBE gel plus 0.4 µg/mL of Ethidium Bromide to assess the release of the cloned promoters from the vector backbone.
To confirm the sequence of the cloned products, 1 µg of each plasmid DNA was sequenced with both pCpGfree-basic primers in an ABI 3130xl sequencer and sequences aligned with the expected using the webtool Chromas, Version 2.33.

2.21.3 Preparation of promoter-reporter construct at increasing concentration of DNA methylation content

To study the effect of DNA methylation on gene expression for the promoters under investigation, fully methylated promoter-reporter construct were prepared as described in section 2.6.2 and purified with the GeneJet PCR Purification kit, as also described in section 2.6.2. To test the efficiency of *in vitro* methylation (IVM), 200 ng of the IVM constructs were digested with *MspI* and *HpaII* isoschizomers in parallel reactions, as described in section 2.6.2. Fully methylated and unmethylated constructs for the same cloned promoter were mixed to obtain 0%, 25%, 50%, 75% and 100% of CpG promoter final methylation content.

2.21.4 Transfection of cells

2.5 x 10^5 LN-229 cells were plated in 24 well plates the day before transfection in 500 µL of complete DMEM medium (Sigma Aldrich) supplemented with 10% FBS, 100 U/mL Penicillin and 100 µg/mL Streptomycin. 170 ng of each plasmid DNA (prepared as described in section 2.21.3) were added to 17 µL of Opti-MEM Reduced Serum Media (Invitrogen). In parallel, 1 µL of Lipofectamine Transfection Reagent (Invitrogen) was added to the same volume of Opti-MEM. Both mixes were incubated for 5 minutes at room temperature, combined and further incubated for 20 minutes at room temperature. After two washes with 1 mL of Opti-MEM, the growth medium was replaced with 200 µL of Opti-MEM, transfection mixes were added to the wells and plates were incubated for 5 hours at 37° C in a 5% CO_2 incubator. At the end of this incubation time, cells were washed twice with 1 mL of complete DMEM and placed in the incubator with 500 µL of complete DMEM until assayed (3 days after transfection).

2.21.5 Secreted Embryonic Alkaline Phosphatase (SEAP) Assay

SEAP levels can be measured in the conditioned media of cells transfected with a pCpGfree-basic plasmid in which a functional promoter was cloned at 5' end of the mSEAPΔCpG gene. For this purpose, the Secreted Alkaline Phosphatase Reporter Gene Assay Lit – Luminescence (Cayman Chemical Company) was used. 10 µL of each conditioned media were transferred to a 0.2 mL PCR tube and heated at 65° C for 30 minutes in a thermal cycler; this step inactivated endogenous alkaline phosphatase, but not the SEAP, which is stable at this temperature. Samples were equilibrated at room temperature, transferred to a white 96 well plate and 50 µL of Substrate were added to each well. After incubation at room temperature for 30 minutes, luminescence was read in a plate reader at intervals of 30 minutes for up to 3 hours. In parallel, a standard curve with serial dilutions of the Cell-Based Alkaline Phosphatase Standard 5U/mL was prepared (dilution curve range: 156.25 µU/mL to 1 µU/mL), using the culture medium used with the cells and performing the inactivation. The time point showing the standard curve best coefficient of determination (2 hours) was chosen for the data analysis. Data are shown setting as reference/normalization value the luminescence of the unmethylated sample.

2.22 Methylscreen

To perform a promoter methylation screening on cell cycle genes, I used the Methylscreen technology (Holemon et al., 2007). The following reagents were obtained from QIAgen:

EpiTect Methyl II DNA Restriction Kit (containing 5X Restriction Digestion Buffer, Enzyme A (Methylation-Sensitive) and Enzyme B (Methylation-Dependent)
RT² SYBR® Green qPCR Mastermix, catalog number 330520
qPCR plates containing pre-dispensed primers: Human Cell Cycle DNA Methylation PCR Array, Signature Panel: EAHS-201Z

Briefly, 1 µg of genomic DNA from each sample (replicative senescent and young confluent MRC-5) was split in 4 tubes and incubated overnight in a final volume of 30 µL at 37°C in the presence of 1X digestion buffer and:

1. No restriction enzymes (Mock digestion)
2. 1 µL Methylation Sensitive Enzyme (digestion A)
3. 1 µL Methylation Dependent Enzyme (digestion B)
4. 1 µL of both Methylation Sensitive and Dependent enzymes (digestion A+B)

After enzymes inactivation (65°C, 20 minutes), samples were prepared for qPCR as follows:

30 µL of either Mock digestion, digestion A, B or A+B
330 µL RT² SYBR® Green qPCR Mastermix
water to 660 µL.

According to the manufacturer's suggested layout, 25 µL of each mix were dispensed in the qPCR plates wells, which contained primers for amplification, and incubated as follows:

95° C for 10 minutes
99° C for 30 seconds
72° C for 1 minute
} 3 cycles

97° C for 15 seconds
72° C for 1 minute
] 40 cycles

Melting curves were obtained as described in section 2.8; the acquisition of the fluorescence signal was set as a single reading during the annealing step and as a continuous reading during the melting curve.
Methylation rates were calculated from the Cq values obtained after the Real Time qPCR run using an Excel template provided by the manufacturer.

2.23 Statistical analyses and data analysis of gene overlaps

Statistical analyses were performed using standard statistical software (Microsoft Office Excel® 2010; Systat Software SigmaPlot® for Windows Version 11.0 Build 11.0.1.80; Minitab® 16.1.0).

For gene overlaps in Chapter 5 and Chapter 6, representation factors and hypergeometric probabilities were calculated.The representation factor (r) indicated whether the number of common genes was higher ($r > 1$), equal ($r = 1$) or lower than what would be expected by chance ($r < 1$), if the genes were drawn from two independent lists of genes. The representation factor was calculated by applying the following formula:

$$r = X / [(n \times D) / N],$$

where X was the number of common genes, n was the number of gene in one list, D was the number of genes in the other list and N was the total number of genes.

The hypergeometric probability (h) indicated the probability that the number of common genes resulted in greater than or equal to X overlaps and it was calculated by applying the following formula:

$$h (\geq X; N, n, D) = [DCX] [N\text{-}DCn\text{-}X] / [NCn],$$

where X was the number of genes common between groups, n was the number of genes in one list, D the number of genes in the other list, N the total number of genes and DCX is the number of combinations of D things, taken X at a time.

Chapter 3. Effects of senescence, ageing and dietary energy restriction on expression of DNA Methyltransferases and global DNA methylation

3.1 Outline

Altered global DNA methylation content (hypomethylation and hypermethylation) is a feature of several conditions. Global hypomethylation of DNA is associated with some chronic autoimmunodiseases (Rahman and Isenberg, 2008) and tumours (Hirst and Marra, 2009). In contrast, hypermethylation of the promoter regions of tumour suppressor genes and of DNA repair genes, such as *MLH1*, causes gene silencing and contributes causally to tumourigenesis (Jones and Baylin, 2002). Similar effects are seen in Fragile X Syndrome (Crawford et al., 2001; Penagarikano et al., 2007). Altered patterns of DNA methylation are also observed during ageing (Thompson et al., 2010), some of which correlate with age-related frailty (Bellizzi et al., 2012) and other age-related phenotypes (Bell et al., 2012).

Although CpG islands are present in mammalian genomes and overlap promoter regions of 50%-60% of human genes (Wang and Leung, 2004) - thus suggesting that DNA methylation plays a role in the regulation of gene expression - most of the DNA methylation in mammalian genomes is found in repetitive elements, such as transposons and endogenous retroviruses (Schulz et al., 2006). Transposable elements, which include Long Terminal Repeats (LTR)-Retrotransposons, Long and Short Interspersed Nuclear Elements (LINE and SINE, respectively) and DNA transposons constitute about 45% of the human and 37% of the mouse genome, as reviewed in (Burns and Boeke, 2012). These sequences could interfere with the regulation of gene expression and genome structure by means of insertions, deletions, inversions and translocations of genomic sequences. However, this potential damage is prevented by high levels of CpG methylation (Schulz et al., 2006; Kim et al., 2009b) and this methylation is thought to contribute to genome stability.

HPLC-based assays (outlined in section 1.8.1) were one of the first methods developed to quantify global Cytosine methylation. Although HPLC has the advantage of being both robust and sensitive, this technique is relatively laborious and requires relatively large amounts of starting DNA, so alternative methods aimed at the estimation of global methylation content of DNA have been established. These alternative assays are based on estimating the methylation content of genomic repeats by e.g. pyrosequencing or by direct

sequencing after bisulfite modification of DNA or on the use of methylation-sensitive enzymes. Although these alternative assays actually measure site-specific methylation, they may provide researchers with useful estimates of global DNA methylation (because these repeats domains constitute a large part of the genome) and their advantages include the small amount of starting material (DNA) needed and the widespread availability of the appropriate technologies.

In this chapter, I first measured the relative expression of the genes that encode for the enzymes that catalyze the addition of a methyl group to the 5' position on Cytosines residues in DNA in the context of CpG dinucleotides (DNA Methyltransferases; DNMTs, Dnmts) in young replicative (YC) and senescent (ESIPS, RS) cells in culture, in young and ageing heart, colon and liver samples from mice and in liver samples from *ad libitum* fed and dietary energy restricted mice. Secondly, I measured the global DNA methylation content of each of the samples using different experimental approaches. Finally, I investigated potential releationships between *DNMT*s/*Dnmt*s expression and estimates of global DNA methylation content of the cells and tissues.

3.2 Assessment of the senescence state of MRC-5 cells

Before starting with the methylation experiments, it was important to determine whether the cell cultures showed the expected expression pattern of a widely utilized senescence-associated marker i.e. β-Gal senescence-associated expression at pH = 6. For this purpose, I stained young confluent (YC), early stress-induced premature senescent (ESIPS; 20 Gy, harvesting after 48 hours) and replicative senescent (RS) MRC-5 cells, as described in section 2.1.1. For the latter samples, replicative senescence was determined by the aid of growth curves, generated as described in section 2.1. As shown in Figure 3.1, no β-Gal expression was detected under the experimental conditions in both YC and ESIPS cells, while an intense cytoplasmic and perinuclear β-Gal expression was detected in RS cells. This provided further confirmation of the suitability of my RS and YC cell cultures for further studies. In a previously published report, MRC-5 fibroblasts irradiated with 10 or 40 Gy and harvested after 72 hours stained positively, but weakly, for β-Gal (Bluwstein et al., 2013), thus it is possible that my irradiated cells (ESIPS) stained negative for β-Gal simply because I harvested at an earlier timepoint. As shown later in this thesis (see Chapter 5 and CD insert), I obtained proof of the senescent state of my irradiated (ESIPS) MRC-5 fibroblasts by transcriptome analyses. These observations

suggest that, although a widely used marker for senescence, the β-Gal increased activity at pH 6 is not an essential marker for senescence.

A

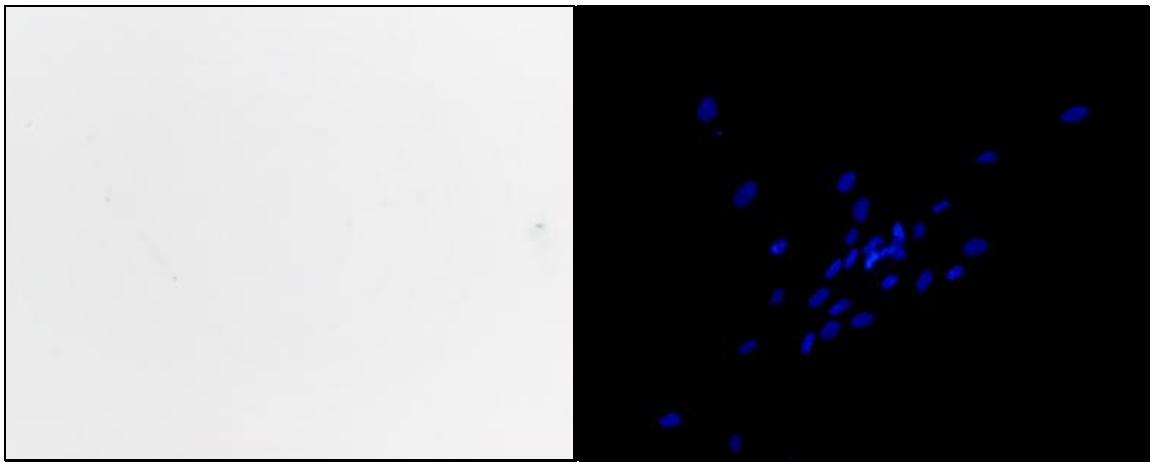

B

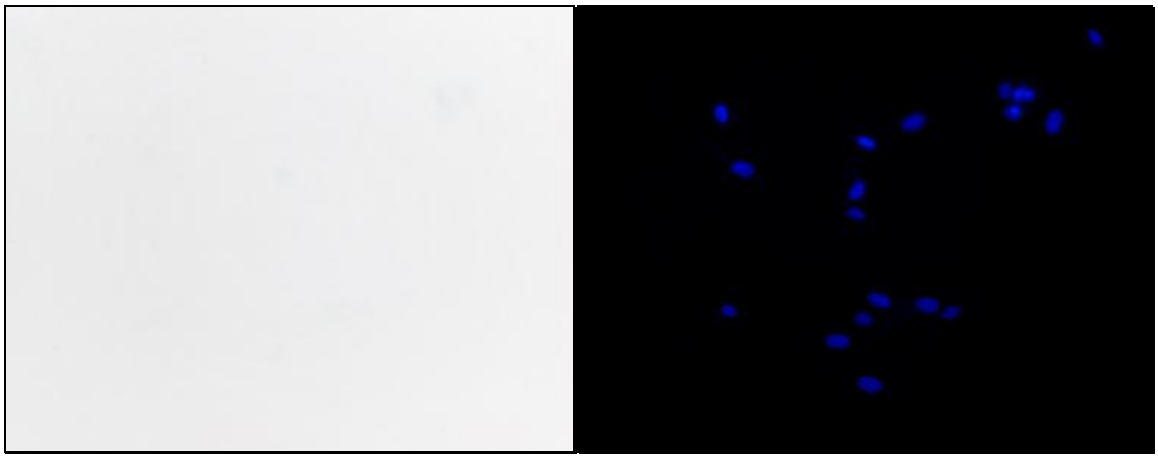

C

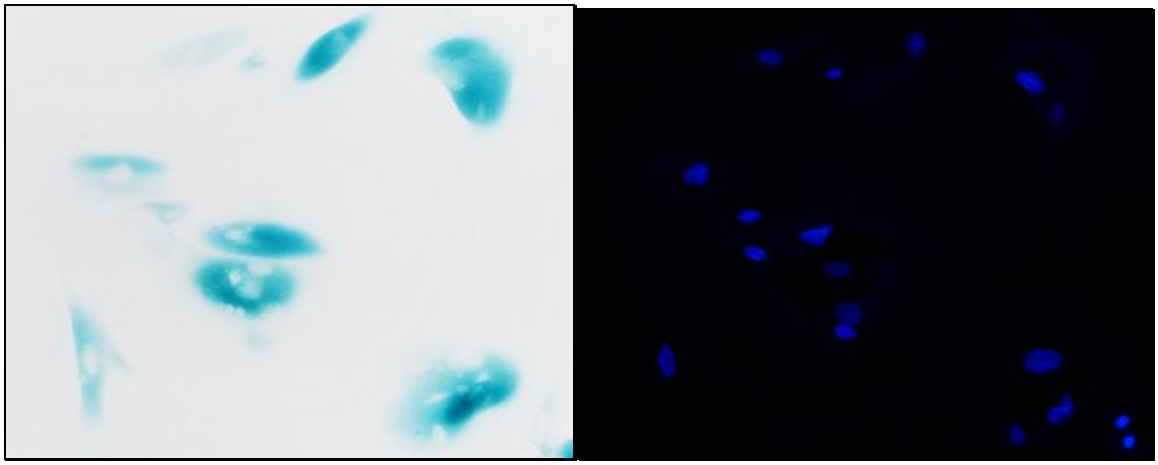

Figure 3.1. β-Gal senescence-associated assay performed on young confluent (panel A), early stress-induced premature senescent (20 Gy, harvesting after 48 h; panel B) and replicative senescent MRC-5 cells (panel C). Left pictures show β-Gal cytoplasmic and perinuclear stainings and right pictures show DAPI staining of the cell nuclei in the same fields.

3.3 DNA Methyltransferases expression in senescent cells and in ageing and dietary energy restricted mouse livers

As a first approach to study global DNA methylation changes occuring in senescence, and in response to ageing and to dietary energy restriction (ER), I quantified the expression of the three main DNA Methyltransferases (*DNMT1*/*Dnmt1*, *DNMT3A*/*Dnmt3a* and *DNMT3B*/*Dnmt3b*) at the mRNA level. I designed and performed assays for Reverse Transcription quantitative PCR assays (RT-qPCR; see sections 2.4 and 2.13, Table 2.5 and Appendix A for details) and normalized the data using the Pfaffl method (Pfaffl, 2001), choosing as normalizer the gene that showed the lowest Cq (cycle for quantification) standard deviation between the samples under investigation. The normalizers tested were *ACTB*, *B2M*, *GAPDH* and *UBE2B* for the MRC-5 cells assays and *B2m*, *Hmbs*, *Hprt* and *Gapdh* for murine samples. The chosen normalizers for the qPCR calculations were *GAPDH* for the cells-based assays, *Gapdh* for the heart and colon assays and *B2m* for the liver assays.
Expression of *DNMT*s was significantly down-regulated in RS (*DNMT1* fold change = 0.61, *DNMT3A* fold change = 0.38 and *DNMT3B* = 0.51) and also in ESIPS cells (*DNMT1* fold change = 0.54 and *DNMT3A* fold change = 0.52) each compared with YC cells, with the only exception of *DNMT3B*, which showed a similar, but not significant trend (data shown in Figure 3.2). Significant changes in expression were observed for the *de novo* methylase *Dnmt3b* and for *Dnmt1*, which were down-regulated by ageing in the liver (fold change = 0.56) and colon (fold change = 0.64) when compared with young counterparts, whereas *Dnmt3b* was significantly up-regulated in liver with short-term dietary energy restriction (fold change = 8.05) (data shown in Figure 3.3 and 3.4, respectively) compared with *ad libitum* diet. Colon or heart samples from dietary energy restricted mice were not available; this precluded the investigation of effects in those tissues.

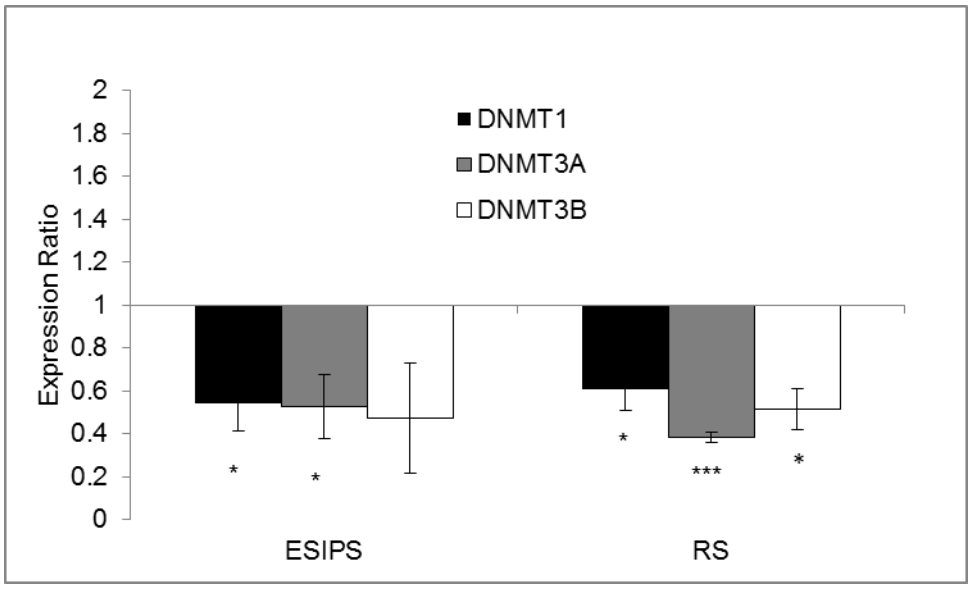

*Figure 3.2. DNMTs expression at mRNA levels in early stress-induced premature senescence (ESIPS) and replicative senescence (RS) compared with young confluent MRC-5 fibroblasts. Data are shown as average expression ratios using GAPDH as normalizer; error bars indicate ± SD of n =3 biological replicates. * = p < 0.05; ** = p < 0.01; *** = p < 0.001 for student's unpaired t-test.*

A

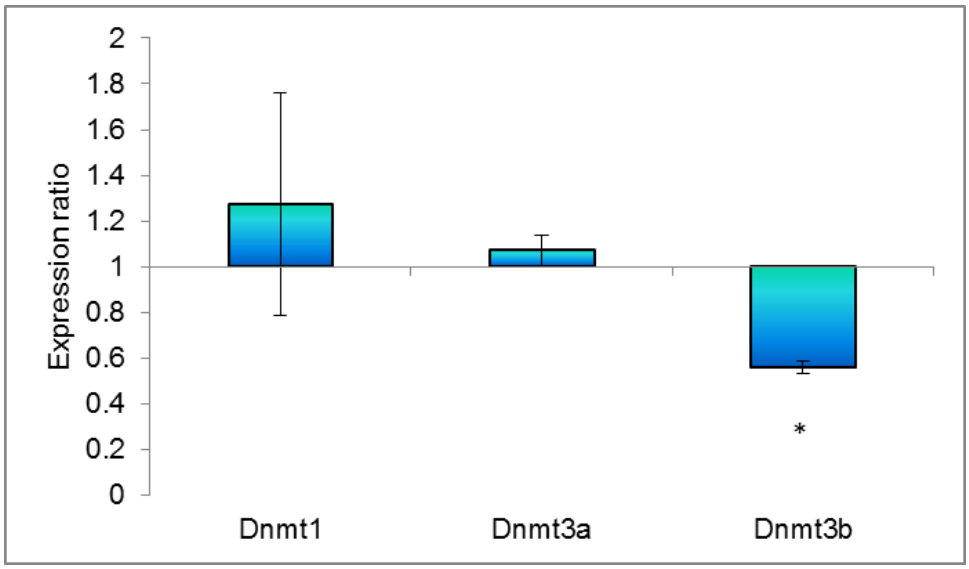

B

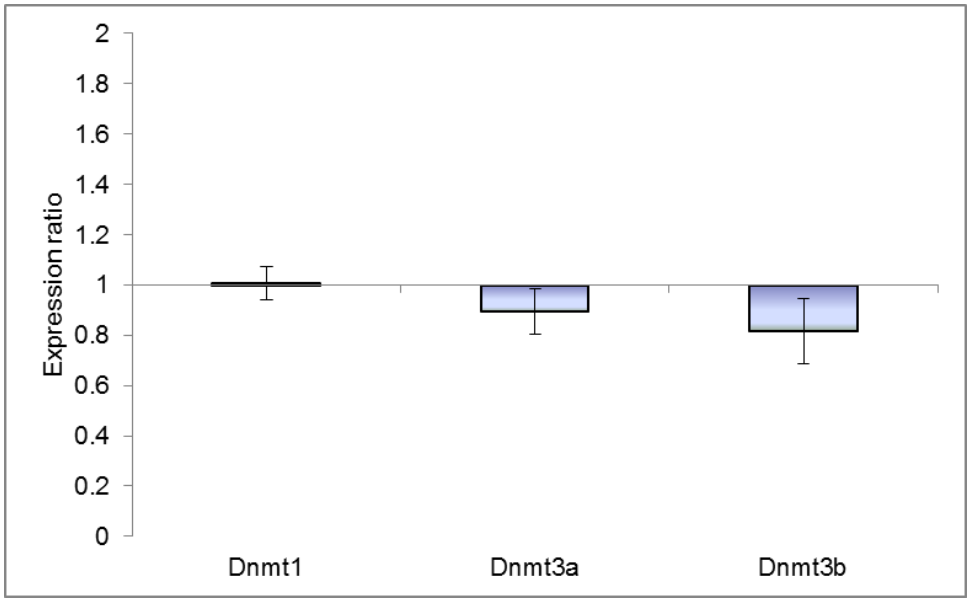

C

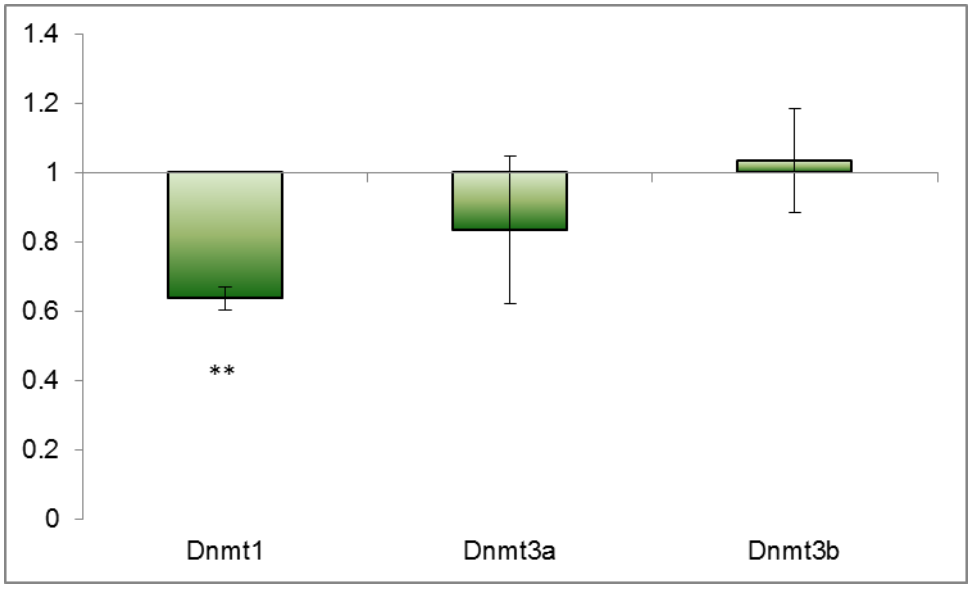

*Figure 3.3. Dnmts expression at mRNA levels in ageing (32 m.o.) mouse liver (panel A), heart (panel B) and colon (panel C) compared with their young (3 m.o.) counterparts. Data are shown as average expression ratios using B2m as normalizer for livers and Gapdh for heart and colon samples; error bars indicate ± SD of n =3 biological replicates. * = p < 0.05; ** = p < 0.01 for student's unpaired t-test.*

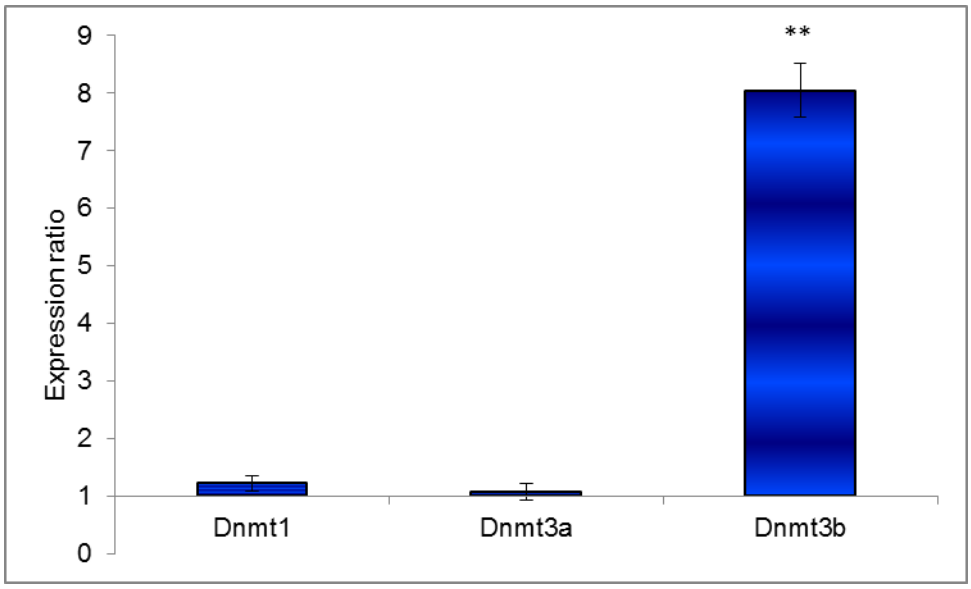

*Figure 3.4. Dnmts expression at mRNA levels in dietary energy restricted mouse liver compared with ad libitum fed mice livers. Data are shown as average expression ratios using B2m as normalizer; error bars indicate ± SD of n =3 biological replicates. ** = p < 0.01 for student's unpaired t-test.*

3.4 Global DNA methylation content in senescent cells vs young replicative cells and effects of ageing and dietary energy restriction on global DNA methylation in mouse livers

To measure the global DNA methylation content in my samples, I used four different approaches: a colourimetric ELISA-based method (MethylFlash Methylated DNA Quantification Kit, Epigentek) and a PCR based method (LINE-1 assay for human cells samples and B1 element assay for mice samples). I then quantified global methylation in subsets of my samples using a methyl-sensitive restriction enzyme based assay followed by Pyrosequencing (LUMA) and by the gold standard for global methylation content measurement (HPLC) to further validate my results. Experimental procedures and reagents are described in sections 2.14, 2.15, 2.16, 2.17, 2.19 and Table 2.6.

3.4.1 Global DNA methylation measurement by means of an ELISA-based colourimetric assay

For these measurements, I first established a standard curve with dilutions of DNA of known methylation content (provided with the kit) and determined the reading time point

which resulted in a coefficient of determination (R^2) as close as possible to 1. For this purpose, I chose 3 time points included within the time frame for reading suggested by the manufacturer (between 2 to 15 minutes); these were 5 minutes, 10 minutes and 15 minutes. The best linearity curve was obtained after 5 minutes from colour development (see Figure 3.5), hence sample readings obtained at this time point were used for the global methylation content amount calculations, applying the following formula:

5-mC (ng) = (sample OD –Negative Control OD) / Slope x 2,

where 2 is a normalization factor, as the Positive Control used for the standard curve preparation contains only 50% of 5-methylCytosines.

The percentage of 5-methylCytosine content was then calculated as follows:
5-mC% = (5-mC amount (ng)) / (amount of input gDNA (ng)) x 100.

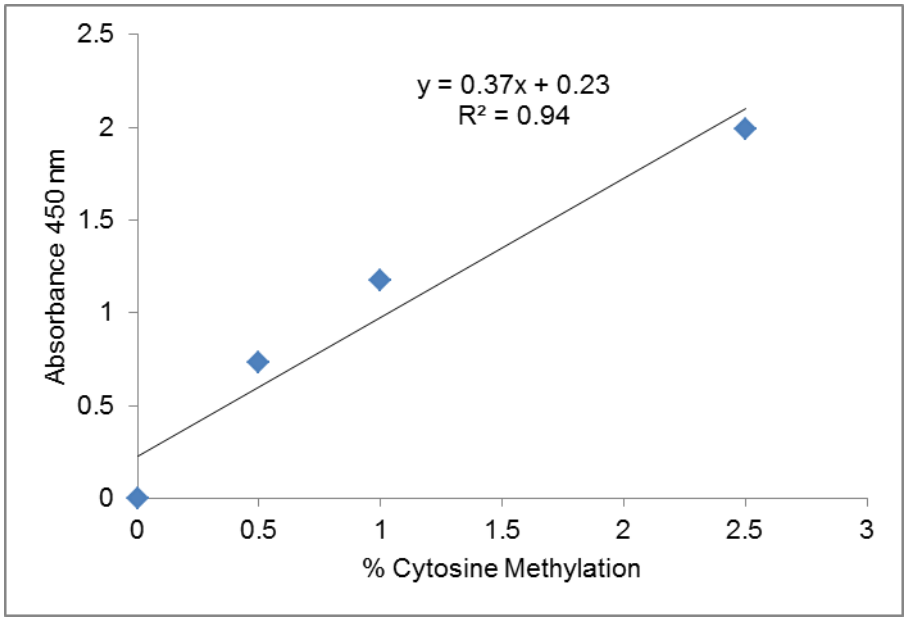

Figure 3.5. Example of linearity curve for global methylation colourimetric assay using the Epigentek MethylFlash Methylated DNA Quantification Kit; data were collected after 5 minutes of colour development. The line equation was used for samples global methylation content calculations.

Figure 3.6 summarises the results of global DNA methylation obtained using this technique in human cells. There was a trend for global methylation to decrease in the

order YC > ESIPS > RS, but these differences were not statistically significant because of the relatively high inter-sample differences for these assays. Global DNA methylation was relatively similar in all 3 mouse tissues (heart, liver and colon) examined (Figure 3.7) Perhaps surprisingly, global DNA methylation tended to be higher in tissues from the older compared with the younger mice but this difference was not statistically significant, when considering each single tissue separately in the statistical analysis, or when both age and tissue were included as factors in a two-way ANOVA (Figure 3.7).

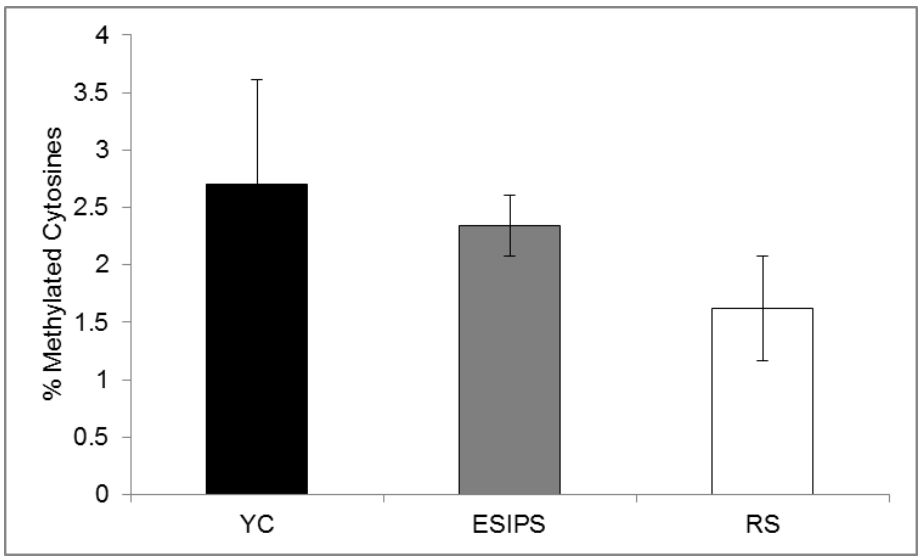

Figure 3.6. ELISA-based colourimetric global methylation assay results for young confluent (YC), early stress-induced premature senescent (ESIPS) and replicative senescent (RS) MRC-5 cells. Results are shown as average percentage of 5-methylCytosine content. Error bars show ± SD, n = 4 biological replicates.

A

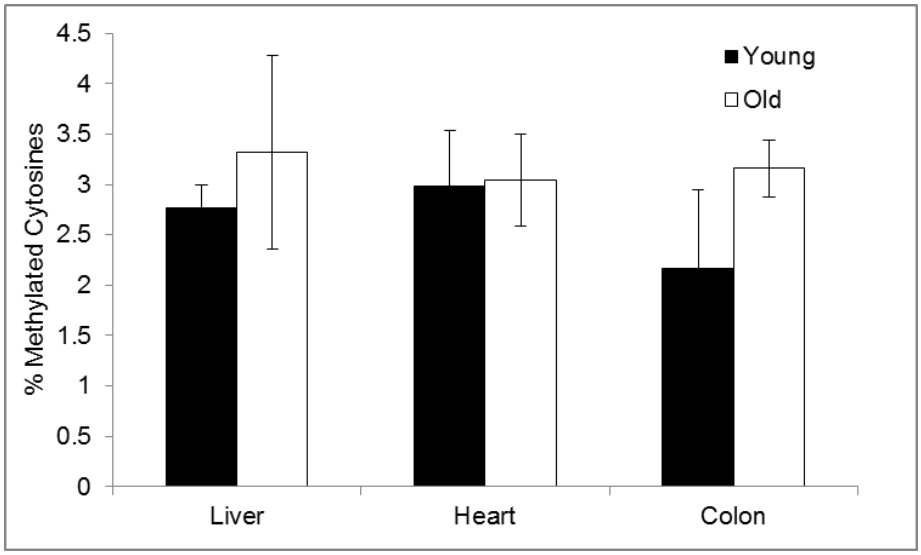

B

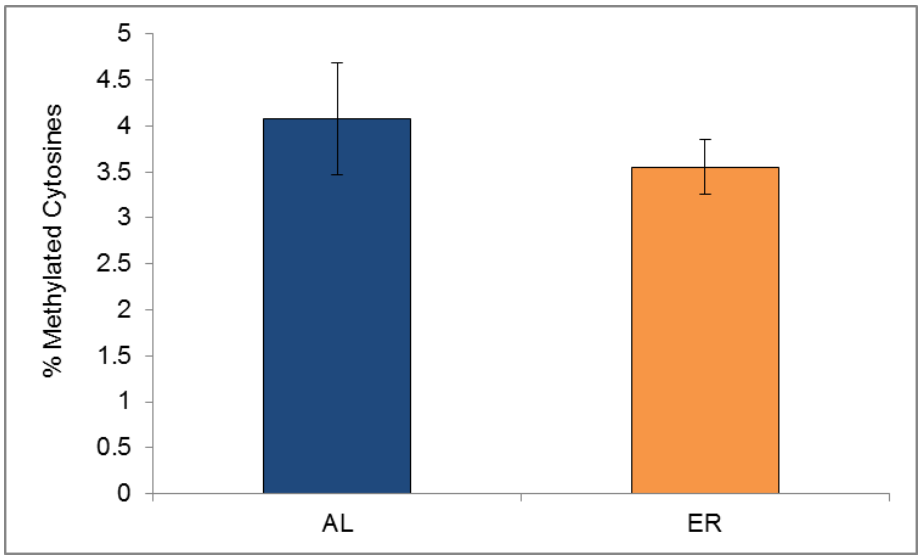

Figure 3.7. ELISA-based colourimetric global methylation assay on mouse tissues. Panel A: global methylation content for young vs old murine livers, hearts and colons; panel B: global methylation content for livers from ad libitum (AL) vs dietary energy restricted mice (ER). Results are shown as average percentage of 5-methylCytosine content. Error bars show ± SD, n = 3 biological replicates.

3.4.2 Repetitive elements methylation measurements as surrogates for global DNA methylation content measurements: LINE-1 and B1 element assays

Given the high variability between replicates seen with the ELISA-based method for estimating global DNA methylation, I moved on to a different methodology and designed a direct sequencing assay to monitor 12 CpG sites within the human LINE-1 Long Interspersed Element, which, with about 500000 copies per genome, is the most highly represented domain in the human genome (Yang et al., 2004). For murine samples, I used an already published assay to monitor 3 CpG sites within the mouse B1 short interspersed element, of which there are about 30000 copies in the murine genome (Jeong and Lee, 2005). Genomic regions of interest are illustrated in Figure 3.9 and 3.11, respectively, while experimental procedures, reaction conditions and primer sequences are listed in sections 2.17, 2.18 and 2.19 and Table 2.6.

I used a Bisulphite Modified (BM) DNA PCR direct sequencing technique to quantify methylation at each of the CpG sites within the region of interest. To assess the suitability of this method, I monitored 1 CpG site of know methylation level in the Lambda DNA Fragment A sequence (see section 4.2). To prepare a methylated fragment, I *in vitro* methylated Fragment A, as described in section 2.6.2 and mixed the unmethylated and the fully methylated preparations in different proportions to obtain mixtures with the following methylation levels: 0%, 5%, 25%, 50%, 75%, 95% and 100%. Then I PCR-amplified the mixtures using the primer pairs and reaction conditions listed in Table 2.6. The linearity curve for observed vs expected methylation is shown in Figure 3.8. Although the measured methylation content was lower than expected for the CpG of interest (reaching only 85% instead of 100%) - probably due to incomplete *in vitro* methylation of the starting DNA – the assay showed a good linearity ($R^2 = 0.98$) and the technique was therefore deemed suitable for the assay.

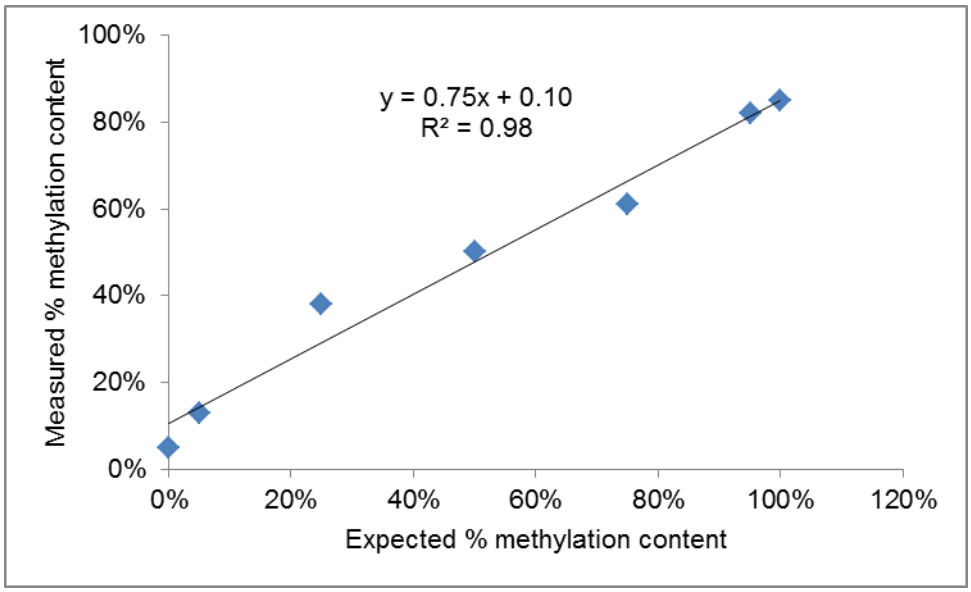

Figure 3.8. Optimization of Bisulphite Modified (BM) DNA PCR direct sequencing. Observed vs expected methylation of 1 CpG site within a Lambda DNA sequence (Fragment A, see section 4.2).

Human LINE-1 transposon (L1Hs) DNA
GenBank: X58075.1

1 gggggaggag ccaagatggc cgaataggaa cagctccggt ctacagctcc cagcgtgagc
61 gacgcagaag acgggtgatt tctgcatttc catctgaggt accgggttca tctcactagg
121 gagtgccaga cagtgggcgc aggccactgt gtgcgcgcac cgtgcgcgag ccgaagcagg
181 gcgaggcatt gcctcacctg ggaagcgcaa ggggtcaggg agttcccttt ccgagtcaaa
241 gaaaggggtg acggacgcac ctggaaaatc gggtcactcc cacccgaata ttgcgctttt
301 cagaccggct taagaaacgg cgcaccacga gactatatcc cacacctggc tcagagggtc
361 ctacgcccac ggaatctcgc tgattgctag cacagcagtc tgagatcaaa ctgcaaggcg
421 gcaacgaggc tgggggaggg gcgcccgcca ttgcccaggc ttgcttaggt aaacaaagca
481 gccgggaagc tcgaactggg tggagcccac cacagctcaa ggaggcctac ctgcctctgt
541 aggctccacc tctgggggca gggcacagac aaacaaaaag acagcagtaa cctctgcaga
601 cttaagtgtc cctgtctgac agctttgaag agagcagtgg ttctcccagc acgcagctgg
661 agatctgaga acgggcagac tgcctcctca agtgggtccc tgacccctga cccccgagca
721 gcctaactgg gaggcacccc ccagcagggc acactgacac ctcacacggc agggtattcc
781 aacagacctg cagctgaggg tcctgtctgt tagaaggaaa actaacaacc agaaaggaca
841 tctacacgaa aacccatctg tacatcacca tcatcaaaga ccaaaagtag ataaaaccac
901 aaagatgggg aaaaaacaga acagaaaaac tggaaactct aaaacgcaga ggccctctcc

961 tcctccaaag gaacgcagtt cctcaccagc aacagaacaa agctggatgg agaatgattt
1021 tgacgagctg agagaagaag gcttcagacg atcaaattac tctgagctac aggaggacat
1081 tcaaaccaaa ggcaaagaag ttgaaaactt tgaaaaaaat ttagaagaat gtataactag
1141 aataacc

Figure 3.9 LINE-1 transposon sequence as published in (Crowther et al., 1991). Genomic regions used as priming sites for methylation studies are underlined; CpG sites investigated in this study are indicated in bold orange font.

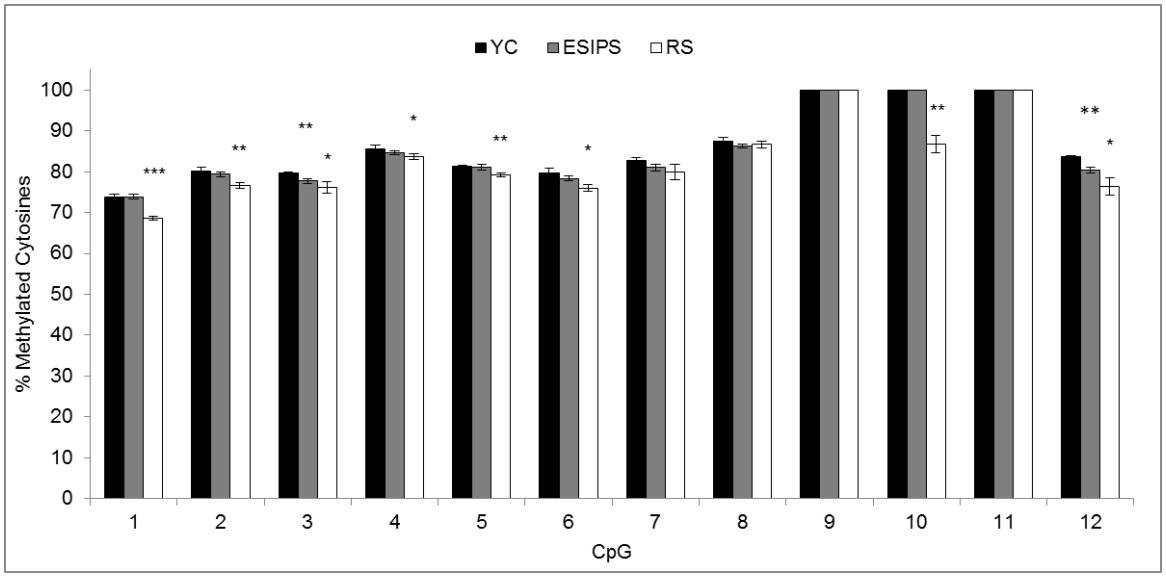

*Figure 3.10. Human LINE-1 CpG methylation quantification by means of bisulphite modified DNA PCR direct sequencing in young confluent (YC), early stress-induced premature senescent (ESIPS) and replicative senescent (RS) MRC-5 fibroblasts. Bars represent average Cytosine methylation for n = 3 biological replicates, error bars show ±SD. * = p < 0.05; ** = p < 0.01; *** = p < 0.001 for student's unpaired t-test.*

Using the LINE-1 assay, I observed that methylation differed between individual CpG sites across the region of interest being at or close to 100% for CpG sites 9 to11 and approximately 70% at CpG site 1. There was significant demethylation at 8 out of 12 of the tested CpGs for RS compared with YC MRC-5 and in 2 CpGs in ESIPS compared with YC MRC-5 cells. The extent of decrease in methylation at single CpG sites ranged from 2% to 13% for RS compared with YC cells and from 2% to 3% for ESIPS compared with YC cells.

Methylation of the 3 CpG sites within the murine B1 element ranged from 51% to 80% (see Figure 3.11 for sequence). None of the 3 CpG sites analyzed showed different levels of methylation between age groups for liver, heart and colon samples (Figure 3.12, panels A, B and C, respectively) or between dietary groups (Figure 3.12). However, absolute methylation values across this B1 repeat region differed significantly between tissue types, with heart showing the lowest methylation (51% to 76%), liver showing intermediate methylation (64% to 79%) and colon being the most highly methylated tissue (68% to 80%), as calculated by ANOVA followed by Holm-Sidak or Kruskal-Wallis ANOVA, followed by Dunn's multiple comparisons test (data not shown).

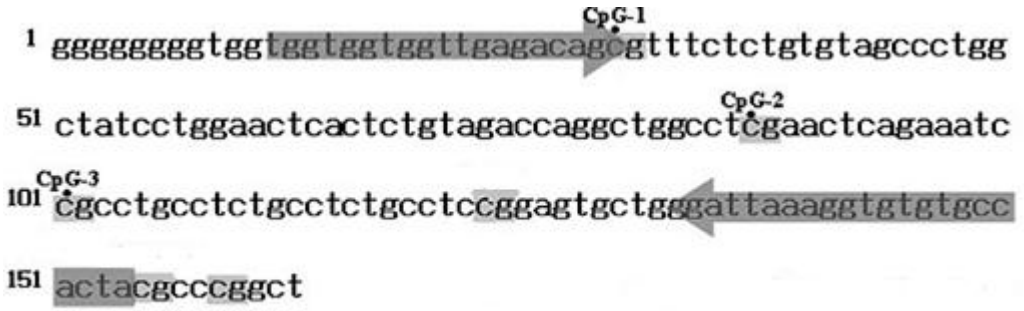

Figure 3.11. Murine B1 Short Interspersed Nuclear Element (SINE) sequence. Genomic regions used as priming sites for methylation studies are highlighted in dark grey; CpG sites are highlighted in light grey and CpG sites investigated in this study are marked with a black dot and a progressive number. Adapted from (Jeong and Lee, 2005).

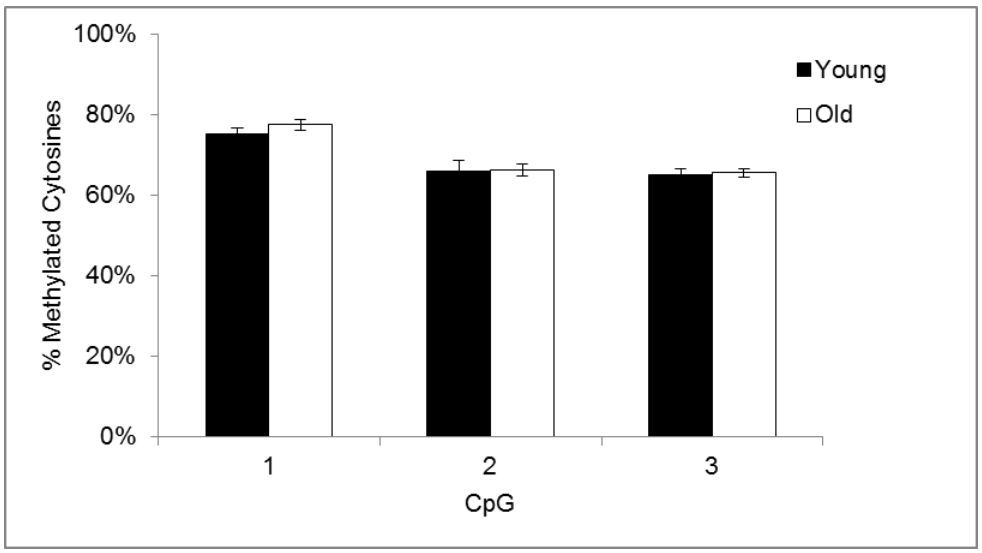

A

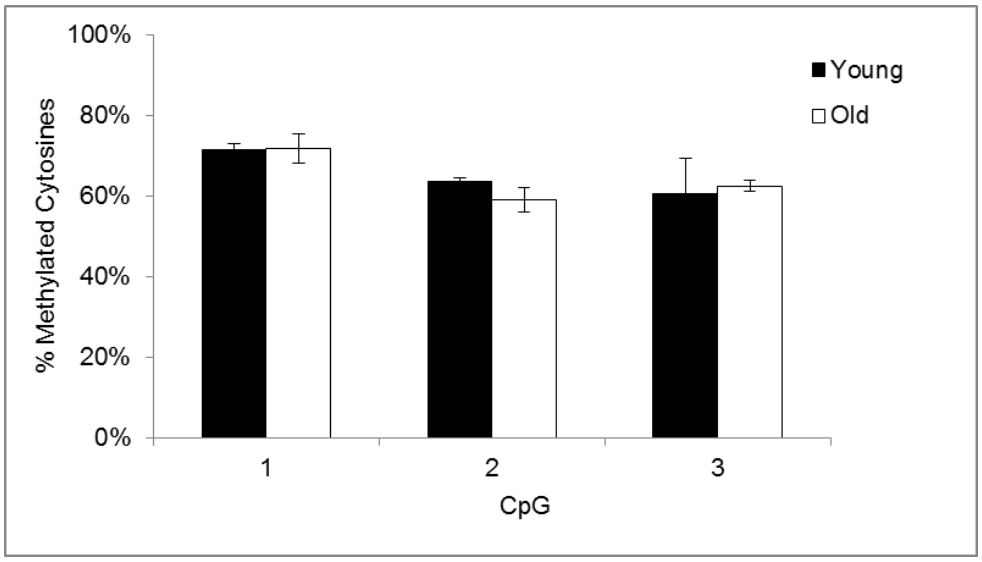

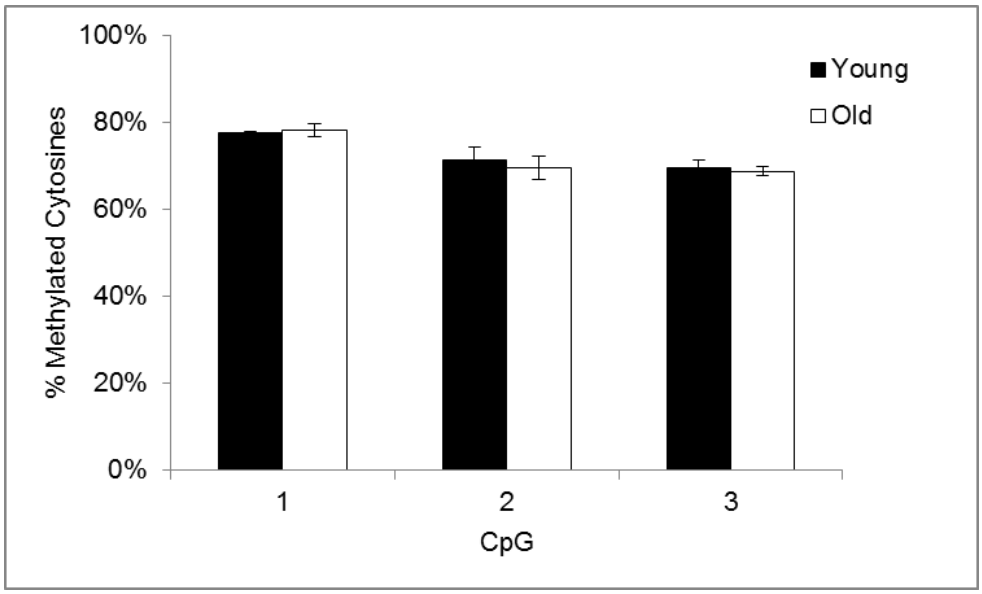

Figure 3.12. Quantification of murine B1 element CpG methylation by bisulphite modified DNA PCR direct sequencing in young (3 m.o.) and old (32 m.o.) mouse livers (panel A), hearts (panel B) and colons (panel C). Bars represent average Cytosine methylation for n = 3 biological replicates, error bars show ±SD.

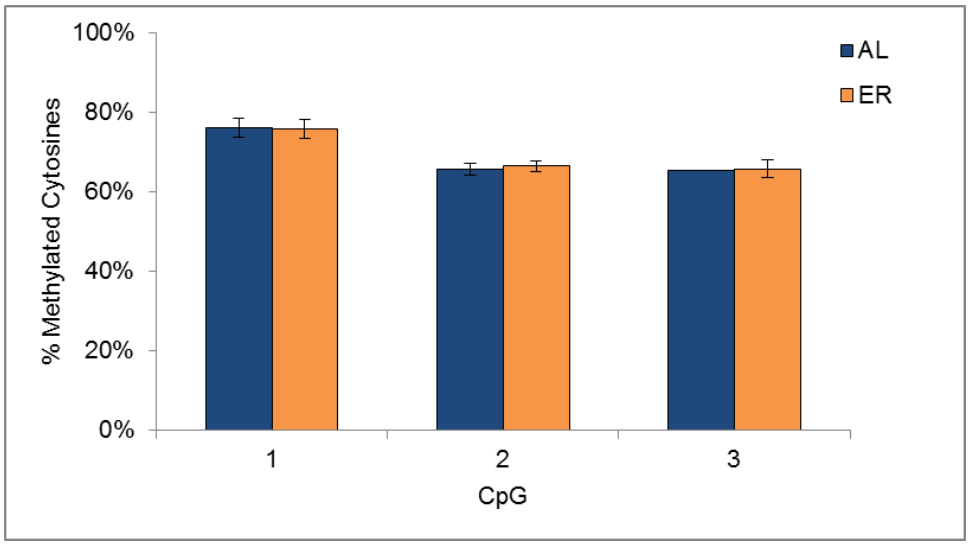

Figure 3.13. Quantification of murine B1 element CpG methylation by bisulphite modified DNA PCR direct sequencing in ad libitum fed (AL) and dietary energy restricted (ER) mouse livers. Bars represent average Cytosine methylation for n = 3 biological replicates, error bars show ±SD.

3.5 Use of methylation-dependent isoschizomers to estimate global methylation content and confirmation of the results by HPLC

Two further approaches were used to quantify global DNA methylation on a subset of samples. Based on the amount of material available, the chosen samples were DNAs isolated from young and old mouse liver and colon and liver from *ad libitum* and dietary energy restricted mice. The additional analytical approaches used included the LUminometeric Methylation Assay - LUMA- (Karimi et al., 2006a; Karimi et al., 2006b), which has been described in sections 1.8.1; experimental procedures are given in section 2.14. Briefly, this assay is based upon the use of the isoschizomeres *MspI* and *HpaII*, which recognise and cut the same sequence (CC↓GG), but with differential cutting according to its methylation state: *MspI* cuts the sequence regardless of methylation status, whereas *HpaII* cuts only at sites where the internal C is not methylated. The digestions are run in parallel on the same sample and then the extent of cutting is quantified in a pyrosequencer. Each reaction is performed in combination with another enzyme cutting at a separate site which theoretically is not affected by methylation (that is, not containing CpG dinucleotides) and that acts as a loading normalizer. *EcoRI* is used as the normalizator in the published method (Karimi et al., 2006b).

In setting up this assay in our laboratory, I repeated the validations performed previously by Karimi at al. including quantification of Lambda DNA at different levels of methylation to produce a standard curve. However, I noticed high variability in the reading produced by the pyrosequencer instrument and the calculated coefficients of determination were never higher than 0.8 (data not shown).
To address this issue, I first checked on agarose/TBE gel the Lambda DNA digestions products and, surprisingly, I found that the *EcoRI* enzyme pattern of digestion was different from what expected. Computational analyses predicted that there should be no bands visible below 3 Kb, but this was not what was observed (Figure 3.13).

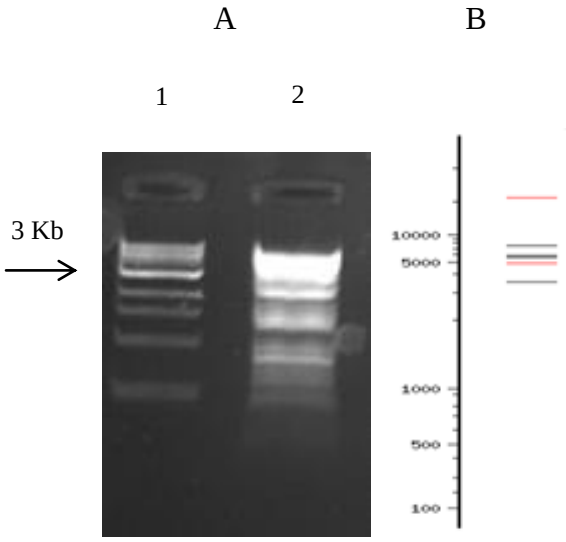

Fig. 3.14: Lambda Phage DNA digestion patterns with EcoRI restriction enzyme (panel A, lane 2; lane 1 is 1 Kb DNA ladder) and virtual agarose/TBE gel showing EcoRI digestion of unmethylated Lambda DNA (panel B, adapted from NEBcutter, http://tools.neb.com/NEBcutter2/).

The *EcoRI* altered digestion pattern was probably due to high star activity of the enzyme. It is well established that many restriction endonucleases show "relaxed" activity when the template DNA is "overdigested" (i.e. incubation for more than one hour with more than 5 U/µg DNA) and/or when the digestion in set up in a non-optimal buffer (see http://www.thermoscientificbio.com/restriction-enzymes/ecori/). These conditions were all satisfied by Karimi's method, in which the reactions are run for 4h, the enzyme concentration is 25U/µg DNA and 1x Tango Buffer is not recommended for *EcoRI* digestion by the manufacturers (Fermentas).

As previously published, *EcoRI* restriction site is G↓AATTC, while in conditions of relaxed specificity it can be N↓AATTN, where N can be any base (Bishop, 1979). Theoretically, this should not influence the results of the LUMA, because the overhangs left after the cuts are all AATT, but I think it is possible that the higher number of cuts could affect the reading of the Pyrosequencer instrument. In addition, cutting by *EcoRI* is impaired by CpG methylation when the initial G in the recognition site is preceded by a methylated C (Figure 3.15) (see http://www.thermoscientificbio.com/restriction-enzymes/ecori/). I therefore substituted *EcoRI* with another enzyme leaving the same overhangs, but which was not showing any star activity under the experimental conditions applied. *MunI*, which cuts C↓AATTG was a commercially available candidate, so I validated the method including it as normalizer in my assays (Lisanti S., Omar W.A.W. et al., accepted). Figure 3.16 compares LUMA validation curves generated by using either *EcoRI* (panel A) or *MunI* as normalizers (panel B) (W. A. W. Omar, Newcastle University, personal communication): *MunI* normalization resulted in an improved linearity of the relationship of observed vs expected methylation *EcoRI* ($R^2 > 0.99$ and $R^2 > 0.93$, respectively). In addition, I noticed that *EcoRI* normalization was C-biased (tended to overestimate methylation) for low methylation content standards and T-biased (tended to underestimate methylation) for high methylation content standards. As shown in Figure 3.16, panel B, when using *MunI* normalization, measured methylation percentages were very close to the expected methylation levels.

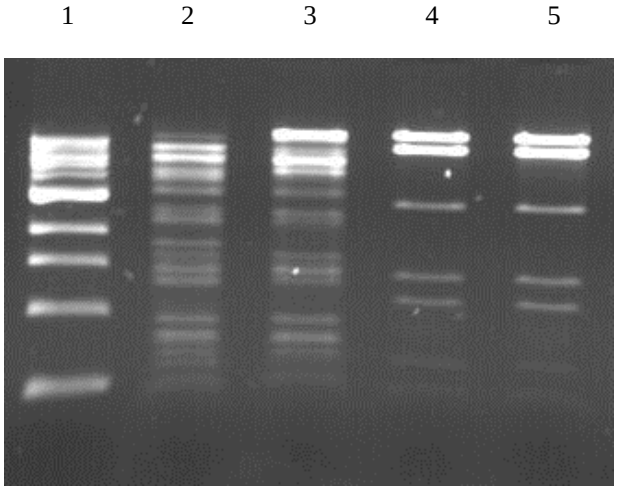

Figure 3.15. Fragment sizes after cutting unmethylated and methylated Lambda Phage DNA with EcoRI and MunI restriction enzymes. Lane 1 = 1 Kb DNA Ladder; Lane 2 and 3 = EcoRI digestion patterns on unmethylated and methylated Lambda DNA using the published LUMA protocol, respectively; Lane 4 and 5 = MunI digestion patterns for

unmethylated and methylated Lambda DNA using the published LUMA protocol (Karimi et al., 2006b), respectively.

A B

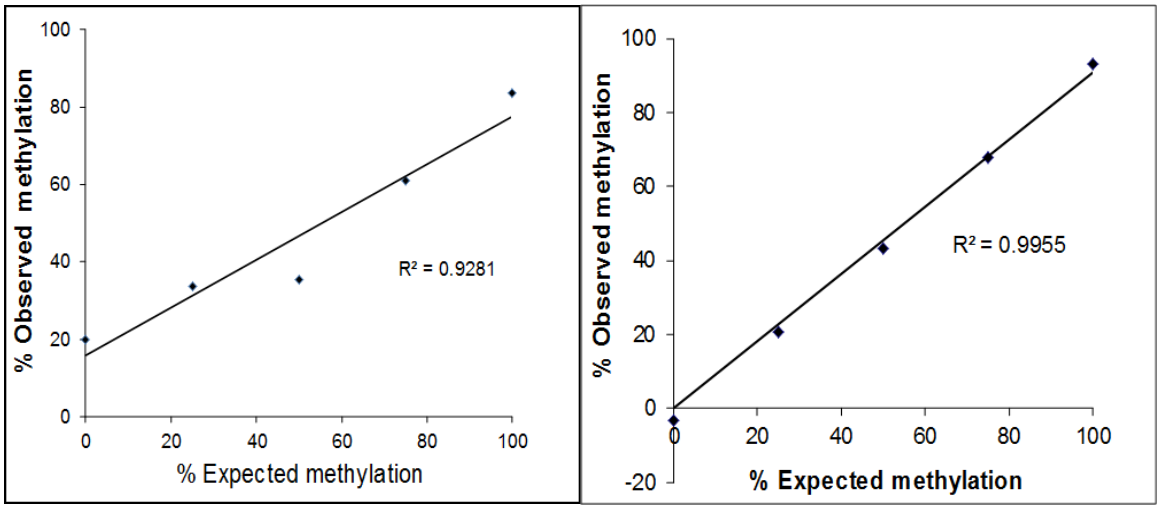

Figure 3.16. Plots of observed vs expected methylation for samples of Lambda DNA of known methylation content quantified using the LUMA Pyrosequencing assay. Data were normalized with EcoRI (Panel A) or MunI (Panel B); reactions were carried out for 4 h in the presence of 1x Tango Buffer (Fermentas) (W.A.W. Omar, Newcastle University, personal communication).

Having chosen *MunI* as normalizer, I used the modified LUMA assay to estimate global DNA methylation in liver and colon tissue from young and old mice. Global methylation was more variable for livers (means ranged between 64% and 70%) than for colon (means ranged between 72% and 73%) (Figure 3.17 and Figure 3.18). There was no detectable difference in methylation for either liver or colon for old compared with young mice (Figure 3.17, panels A and B, respectively). However, dietary energy restriction significantly decreased global DNA methylation by 6% ($p = 0.026$) in murine liver (Figure 3.18).

A

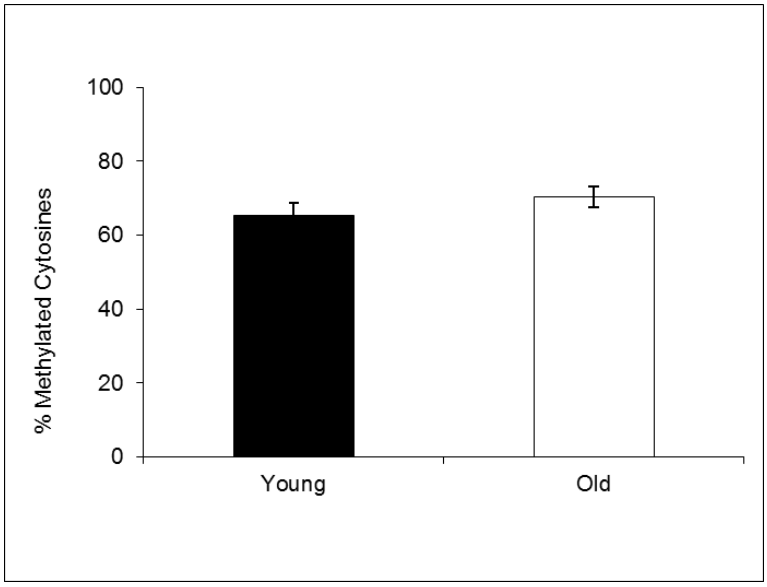

B

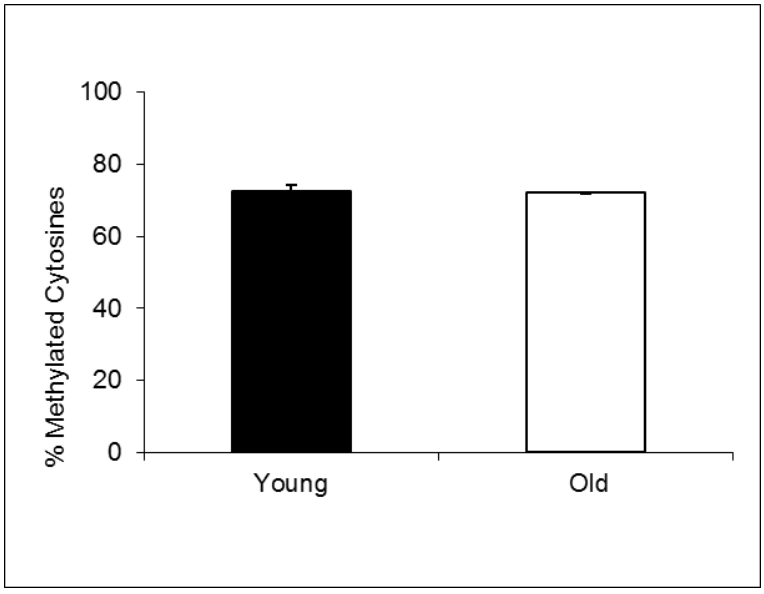

Figure 3.17. Global DNA methylation estimated using a modified Luminometric Methylation assay for young (3 m.o.) and old (32 m.o.) mouse liver (panel A) and colon DNA (panel B). Bars represent average Cytosine methylation for n = 3 biological replicates, error bars show ± SD.

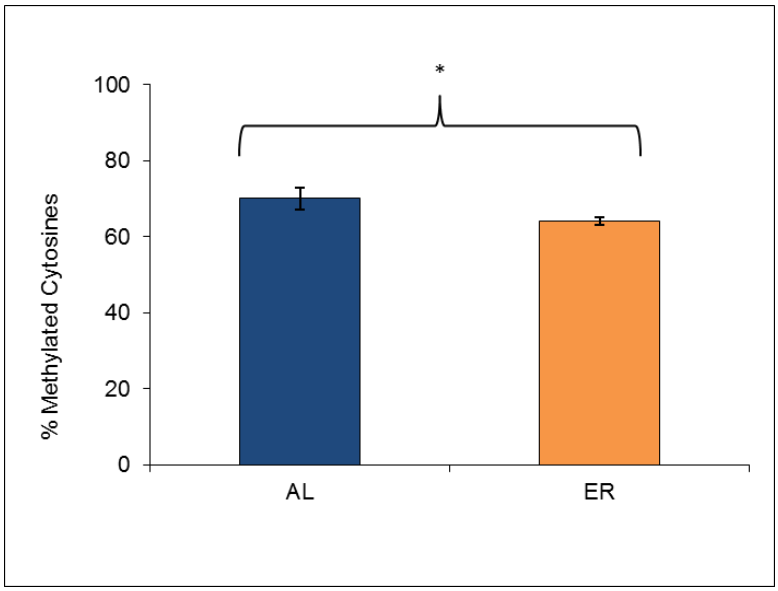

*Figure 3.18. Global DNA methylation estimated using a modified Luminometric Methylation assay for ad libitum fed (AL) and dietary energy restricted (ER) mouse liver DNA. Bars represent average Cytosine methylation for n = 3 biological replicates, error bars show ± SD. * = $p < 0.05$ for student's unpaired t-test.*

Finally, I estimated global DNA methylation using the gold standard HPLC approach, which quantifies 5'-methylCytosine directly in hydrolised DNA (see section 1.8.1 for the technique outline and section 2.15 for the experimental procedures). This work was undertaken in collaboration with the Environmental Risk and Health Unit of the Flemish Institute of Technological Research (Belgium), using the ageing liver samples, which were the ones from which I had the highest amount of available DNA. This assay showed that mean 5'-methylCytosine content of mouse liver DNA was approximately 3% of all Cytosines, with no detectable difference in methylation between age groups (Figure 3.19).

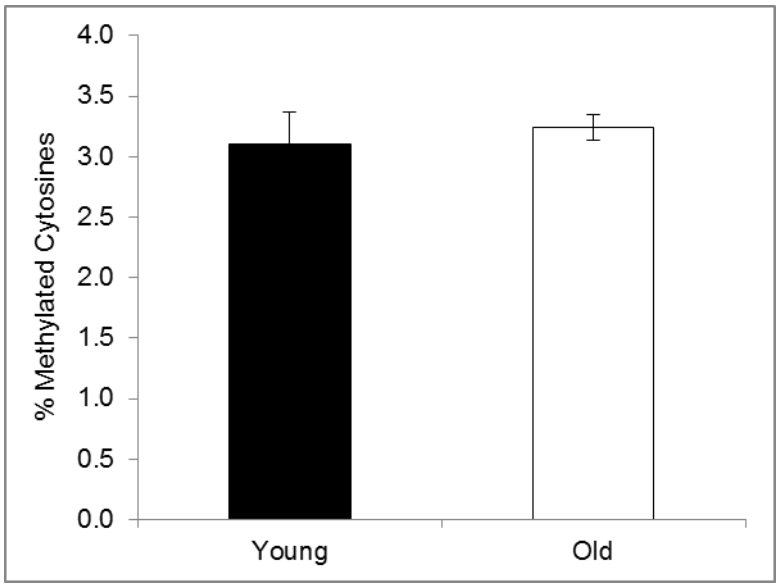

Figure 3.19. HPLC measurement of global methylated Cytosine content in young (3 m.o.) and old (32 m.o.) mouse liver DNA. Bars represent average percentage of methylated Cytosines on total Cytosine content for n = 3 biological replicates, error bars show ± SD.

3.6 Discussion

There is evidence that global methylation shows gender specific differences (El-Maarri et al., 2007) and that it alters during ageing (Bollati et al., 2009; Cedar and Bergman, 2012) and may be influenced by nutritional interventions such as dietary energy restriction (Mathers, 2006; Ribaric, 2012). Since DNA methylation is catalyzed by DNMT enzymes, we hypothesized that alterations of global DNA methylation in response to ageing and/or dietary restriction could be related to changes in expression of *DNMT*s. To test this hypothesis, expression of the best known DNMT enzymes at the mRNA level were quantified by RT-qPCR and global DNA methylation was assessed by a number of different assays which aimed to estimate DNA methylation content directly (ELISA-based colourimetric assay and HPLC) or indirectly (human LINE-1 and murine B1 element PCR-based assays and the LUMA assay).

DNMT1/Dnmt1 is the key maintenance methyltransferase, featuring a high preference (average 24 fold) for hemimethylated Cytosines within CpG sites compared with unmethylated ones (Hermann et al., 2004b). Most previous studies of expression of *DNMT*s/*Dnmt*s and global methylation have focused on *DNTM1*/*Dnmt1* gene expression only, although there is now compelling evidence that the maintenance of the correct methylation DNA pattern relies upon cooperation between the three main DNA-Methyltransferases and in particular upon the recognition of hemimethylated DNA by DNMT1/Dnmt1 and the specific localization of DNMT3A/Dnmt3a and DNMT3B/Dnmt3b to methylated DNA-containing chromatin regions (Kim et al., 2002). This cooperation between three DNMTs is believed to ensure high-fidelity for the process. For this reason, here I have quantified not only *DNMT1*/*Dnmt1*, but also *DNMT3A*/*Dnmt3a* and *DNMT3B*/*Dnmt3b* expression and investigated relationships with global Cytosine methylation content of cells and tissues.

3.6.1 Summary of the main findings of expression of DNMTs/Dnmts and of global methylation in senescence, ageing and following dietary energy restriction

Table 3.1. Summary of main findings of expression of *DNMT*s in early stress-induced premature senescent (ESIPS) and replicative senescent (RS) compared with young confluent (YC) MRC-5 human fibroblasts. Data are expressed as average ratios using *GAPDH* as normalizer. * = $p < 0.05$; ** = $p < 0.01$; *** = $p < 0.001$ for student's unpaired t-test vs YC sample.

	ESIPS MRC-5 vs YC MRC-5	RS MRC-5 vs YC MRC-5
DNMT1 expression	0.54*	0.61*
DNMT3A expression	0.52*	0.38***
DNMT3B expression	0.47	0.51*

Table 3.2. Summary of main findings of estimates of global DNA methylation in young confluent (YC), early stress-induced premature senescent (ESIPS) and replicative senescent (RS) MRC-5 human fibroblasts. Data are expressed as percentage of methylated Cytosine within CpG dinucleotides. * = $p < 0.05$; ** = $p < 0.01$ for student's unpaired t-test vs YC sample; # = data refer to CpG no. 3; NP = not performed.

	YC MRC-5	ESIPS MRC-5	RS MRC-5
Global CpG methylation (ELISA)	3%	2%	2%
Global CpG methylation (LINE-1) #	80%	78%**	76%*

Table 3.3. Summary of main findings of expression of *Dnmt*s in heart, colon and liver from older animals compared with tissue from young animals and in liver from dietary energy restricted animals compared with tissue from *ad libitum* fed animals. Data are expressed as average ratios using *Gapdh* as normalizer for heart and colon samples and *B2m* as normalizers for liver samples. * = $p < 0.05$; ** = $p < 0.01$ for student's unpaired t-test vs Young or AL sample sample.

	Heart Old vs Young	Colon Old vs Young	Liver Old vs Young	Liver ER vs AL
Dnmt1 expression	1.01	0.64**	1.27	1.22
Dnmt3a expression	0.90	0.84	1.07	1.07
Dnmt3b expression	0.82	1.04	0.56*	8.05**

Table 3.4. Summary of main findings of estimates of global DNA methylation in heart, colon and liver from older animals compared with tissue from young animals and in liver from dietary energy restricted animals compared with tissue from *ad libitum* fed animals. Data are expressed as percentage of methylated Cytosine within CpG dinucleotides. * = $p < 0.05$ for student's unpaired t-test vs Young or AL sample sample; # = data refer to CpG no. 3; NP = not performed.

	Young heart	Old heart	Young colon	Old colon	Young liver	Old liver	AL liver	ER liver
Global CpG methylation (ELISA)	3%	3%	2%	3%	3%	3%	4%	4%
Global CpG methylation (B1 element)	71%	72%	78%	78%	75%	78%	76%	76%
Global CpG methylation (LUMA)	NP	NP	73%	72%	65%	70%	70%	64%*
Global CpG methylation (HPLC)	NP	NP	NP	NP	3%	3%	NP	NP

3.6.2 Changes in DNMTs gene expression and in global DNA methylation with replicative and premature senescence

In a common *in vitro* model of senescence, human MRC-5 fibroblasts, I found significant down-regulation of *DNMT1*, *DNMT3A* and *DNMT3B* when cells were cultured to reach replicative senescence (RS), and significant down-regulation in *DNMT1* and *DNMT3A* expression, together with a trend towards down-regulation for *DNMT3B* (albeit not significant), when cells were γ-irradiated to prompt stress-induced premature senescence (ESIPS). The expression ratios calculated from RT-qPCR data and presented in this Chapter mirror data obtained from whole genome transcriptomic analysis of the same samples (see CD insert). These data were partially consistent with a previous study in which when compared with replicative (young) cells, *DNMT1* was significantly down-regulated in both ESIPS and RS cells but *DNMT3A* was up-regulated in premature senescent cells only and *DNMT3B* was up-regulated in replicative senescent cells only, in human embryonic lung fibroblasts (HEF cells) (Zhang et al., 2008). Various causes could

contribute to the discrepancies in gene expression changes between the two studies, e.g. i) the dose-response specificity to different senescence-inducing insults – for example, (Zhang et al., 2008) have indeed used hydrogen peroxide and not γ-rays to this purpose - and ii) the different time-points of cell harvesting after senescence induction.

Using an ELISA-based method, I did not detect any significant DNA methylation changes occurring within senescence and premature senescence (although a progressive trend was seen towards demethylation), while a PCR-based method (LINE-1 assay) for quantifying global DNA methylation detected significant changes in 8 (RS) and in 2 (ESIPS) out of the 12 CpGs under investigation. Both assays showed a tendency for global DNA methylation to decrease from YC > ESIPS > RS. However, as presented in Figures 3.6 and 3.7, the ELISA-based assay showed high variability between measurements - probably because of low experimental consistency - whilst the LINE-1 showed very little variability (Figure 3.10). This assay variability probably explains why I was not able to detect significant changes in global DNA methylation using the ELISA-based method, while small, but significant changes in estimates for global DNA methylation were detected by the latter (LINE-1) assay. Interestingly, the specific CpG sites which showed decreased methylation in the LINE-1 experiments for ESIPS cells were the same CpG sites which were demethylated in replicative senescent cells. On the assumption that the "premature senescence" model used here is an intermediate step towards "late" senescence, these findings suggest that demethylation occuring during senescence is progressive. This is coherent with a previous study in which DNA global methylation (investigated using a cell immunofluorescence approach) diminished progressively with premature senescence and replicative senescence (Zhang et al., 2008).

3.6.3 Changes in Dnmts gene expression and in global DNA methylation with ageing and dietary energy restriction

Previous studies have demonstrated organ specificity in gene expression profiles during ageing (Weindruch et al., 2002), and, consistent with these observations, I found that *Dnmt*s expression changes with age were tissue-specific in ageing mice. The RT-qPCR data presented in this Chapter indicated that, compared with tissues from young mice, i) no changes in *Dnmt*s gene expression occurred in heart tissue, ii) there was a decrease in *Dnmt3b* gene expression in liver and iii) there was a decrease in *Dnmt1* gene expression in the colon tissue. In addition, a striking increase in *Dnmt3b* gene expression was

detected in liver tissue from dietary energy restricted animals compared with tissue from *ad libitum* fed animals. This was clearly opposed to the *Dnmt3b* gene expression down-regulation which occurred with ageing.
*Dnmt*s down-regulation associated with ageing has been documented in previous studies including human T cells - that showed down-regulation of *DNMT1* - (Zhang et al., 2002b), hematopoietic stem cells - that showed down-regulation of *DNMT3B* - (Chambers et al., 2007) and murine hippocampi - that showed down-regulation of *Dnmt3a*, isoform a2 - (Oliveira et al., 2012). As reviewed in (Li et al., 2011), such down-regulation of gene expression is opposed by dietary energy restriction. In summary, I believe that the greater expression of *Dnmt3b* seen in liver from dietary energy restricted animals, which is opposed to the down-regulation seen in ageing liver, may be one of the beneficial consequences of this dietary intervention which could contribute to the maintenance of a proper pattern of global DNA methylation.

Despite the observed changes in *Dnmt* expression, there were no detectable changes in global DNA methylation, as measured by an ELISA-based method. This lack of effect on global DNA methylation was confirmed by the results from other approaches to global DNA methylation estimation including measurement of methylation of the B1 element using PCR-based method, by the LUMA assay and by HPLC measurements of total 5'-MethylCytosine content of DNA for subsets of the samples. These findings are in contrast with previously published studies that have shown a general tendency of global DNA methylation to decrease with ageing in various murine tissues, including brain (Mays-Hoopes et al., 1986), liver (Barbot et al., 2002) and oocytes (Yue et al., 2012). However, a direct comparison of my data for liver with the data from (Barbot et al., 2002) is difficult because the latter were obtained using a different assay (a methyl-sensitive enzymes based assay followed by Southern Blot analysis) that measured the methylation content of a different repeat region (the intracisternal A-particle) in a different mouse strain (BALB/c). In this contest, strain-specific differences in liver DNA methylation response to ageing have already been documented (Counts et al., 1997).
To my knowledge, no studies that have investigated global DNA methylation changes with ageing in murine heart and colon have been previously published.

Using the LUMA assay, there was small, but significant decrease in global DNA methylation in livers from dietary energy restricted animals. However, this decrease was not confirmed by any of the other methods used to quantify global DNA methylation.

Global hypomethylation could be potentially harmful because it contributes to genome instability (Rodriguez et al., 2006). However, it is difficult to interpret my data from a functional perspective because the LUMA assay does not provide information on where in the genome the changes in methylation have occurred. LUMA does not measure methylation at repeat regions only but can detect changes in methylation in the context of any CCGG site within the genome, including gene promoters. If the reduced methylation occurred in gene promoters, my data could suggest that livers from dietary energy restricted animals have a higher transcriptional activity compared with livers from *ad libitum* fed animals (Razin and Cedar, 1991).

3.6.4 Comparisons between different methods for measurements/estimation of global DNA methylation content

Correlation analyses performed on the data set from the ELISA-based method and the one from the LINE-1 assay at the representative CpG no. 3 yielded a not significant Spearman and Pearson correlation coefficients (probably due to the small number of pairs of data); however regression analysis yielded a coefficient of determination of 0.93 (data not shown). In parallel, no significant Spearman or Pearson correlation coefficient yielded from comparisons of data sets produced with the various applied methods for global DNA methylation measurements on murine samples (probably due to the small number of pairs of data), whilst regression analyses analyses yielded the following coefficient of determination: i) ELISA-based method vs B1 element assay at the representative CpG no. 1 = 9.13×10^{-4}; ii) B1 element assay at the representative CpG no. 1 vs LUMA assay = 0.71 and ELISA-based method vs LUMA assay = 6.29×10^{-2} (data not shown). These data indicated that the data sets for measured global DNA methylation by LINE-1 assay and ELISA-based assay had a relationship very close to linearity for cell samples and that only data sets obtained by the B1 element and the LUMA assay had a relationship close to linearity for murine samples, respectively. A previous study has investigated correlations among assays for estimation of global DNA methylation in human white blood cells and found that those were highest for three repetitive elements methylation levels (ρ included between 0.39 and 0.64), whilst LUMA assay results were only modestly correlated with LINE1 (ρ included between 0.18 and 0.20) (Wu et al., 2011). Taken together, these results suggest that comparison between results arising from different global methylation measurement/estimation methods must be interpreted cautiously. The only comparison which I deem appropriate is the one between the

ELISA-based methods and the HPLC methods, which actually measure 5'-MethylCytosine content in a given sample, irrespective of its genomic location. For all other cases, one has to keep into consideration that each assay investigates different genomic regions (repeats or CCGG sites), so it is possible that results obtained by different methods for the same sample differ not only in the absolute measurements, but also in the detected differences (compare Figure 3.7, panel B and Figure 3.13 with Figure 3.18; compare Figure 3.7, panel A with Figure 3.10) (Lisanti S. Omar W.A.W., accepted).

None of the assays considered in this study is universally better than another: researchers need to determine which is the most suitable for their purposes e.g. which assay is capable of detecting differences between samples under certain conditions. In my opinion, as a rule of thumb, small differences are better detected by PCR-based assays and bigger differences by HPLC, ELISA-based assays or methyl-sensitive enzymes-based assays. This is because, although PCR-based methods rely upon the measurement of abundantly repeated regions, they nevertheless detect changes in specific regions, which could be counterbalanced by changes in the opposite direction in other genomic regions or simply be so small not to be detected at a global level.

HPLC data for the ageing livers showed little biological variability between samples (Figure 3.19); this which confirmed the previous assumption that ELISA-based measurements variations derive from technical variability. However, calculated methylation percentages were in the same range for both methods (around 3%), suggesting that the assays have similar sensitivity and confirming my assumption that results obtained with these techniques can be compared. If pipetting errors are an important source of inconsistency, then including an internal normalizator for DNA quantification (such as a total anti-Cytosine antibody or an in-well DAPI staining) might help to improve the reliability of ELISA-based methods. If this hypothesis proves right, such a modified assay could be developed as a useful and inexpensive alternative to the relatively laborious and high demanding HPLC-based techniques for quantifying global DNA methylation.

3.6.5 Correlation between DNMTs/Dnmts gene expression and global DNA methylation content

As discussed in section 3.6.2 and section 3.6.3, there was a positive correlation between *DNMT*s gene expression and global DNA methylation content in replicative senescence (for all the *DNMT*s) and in premature senescent cells (for *DNMT1*/*DNMT3A)*. These data are partially confirmed by a previous study in which authors found a positive correlation between *DNMT1* expression and global DNA methylation, but a negative correlation between *DNMT3B* and global DNA methylation (Zhang et al., 2008). Contrasting findings may be explained taking into account the different cell types and experimental settings, as previously discussed.

In contrast with the results from the cell-based work, there was no evidence of correlation between *Dnmt*s gene expression and global DNA methylation content with ageing in murine tissues. Previously published research has shown that heterozygous mice *Dnmt* $^{+/-}$ maintain levels of global DNA methylation in T cells which are comparable with those in wild type mice *Dnmt1*$^{+/+}$ (Ray et al., 2006). In parallel, mRNA levels for *Dnmt3a* and *Dnmt3b* increased with age, suggesting a compensatory mechanism that is capable of maintaining a global DNA methylation content which is characteristic of young cells (Ray et al., 2006). In my mouse study, tissue-specific changes in *Dnmt*s expression were not associated with global DNA methylation changes and it logical to postulate that this was probably because not all *Dnmt*s genes were affected in the same way and that compensatory mechanisms (one *Dnmt* increasing whilst another decreases) maintain global DNA methylation levels. In support to this hypothesis, it is of note that there was a direct correlation between *DNMT*s expression and global DNA methylation in replicative senescent cells. The measurement of protein levels, post-translational modifications and enzymatic activity changes could help in confirming this hypothesis; unfortunately, this was not possible for me because of lack of samples.

3.7 Conclusions

In the work described in this Chapter I found that:

- *DNMT*s/*Dnmt*s expression changes with senescence and ageing are tissue- and are treatment-specific;
- global DNA methylation content is decreased during *in vitro* replicative senescence, but does not seem to be affected by ageing in various mice tissues;

- global DNA methylation is decreased in mouse livers in response to dietary energy restriction;
- dietary energy restriction significantly counteracts the age-related *Dnmt3b* gene down-regulation in mouse liver
- comparisons of results from different methods for estimating global DNA methylation are not always possible because these measure different aspects of DNA methylation (e.g. methylation of repeat regions or methylation of cytosine residues in specific genomic sequences).

Related publication:

Comparison of methods for quantification of global DNA methylation in human cells and tissues. PLoS ONE 8(11): e79044. doi:10.1371/journal.pone.0079044.

Sofia Lisanti[1,2§], Wan A.W. Omar[1,4§], Bart Tomaszewski[1], Sofie De Prins[3], Griet Jacobs[3], Gudrun Koppen[3], John C. Mathers[1,2] and Sabine A.S. Langie[1,3*].

[1]Centre for Brain Ageing and Vitality, Institute for Ageing and Health, Human Nutrition Research Centre, Newcastle University, Campus for Ageing and Vitality, NE4 5PL, Newcastle upon Tyne, UK; [2]Centre for Integrated Systems Biology of Ageing and Nutrition, Institute for Ageing and Health, Newcastle University, Campus for Ageing and Vitality, NE4 5PL, Newcastle upon Tyne, UK; [3]Flemisch Institute of Technological Research, Environmental Risk and Health unit, Boeretang 200, 2400 Mol, Belgium. [4]Advance Medical and Dental Institute, Universiti Sains Malaysia, 13200 Kepala Batas, Penang, Malaysia.

§ = contributed equally
* = corresponding author

Chapter 4. Standardization and quality controls for the methylated DNA immunoprecipitation technique (MeDIP)

4.1 Outline

To study site specific methylation and how this varies in cellular senescence, ageing and dietary energy restricted animals, I chose to use the Methylated DNA Immunoprecipitation Technique (MeDIP) (Weber et al., 2005).

MeDIP is an affinity based technique in which single-stranded methylated DNA fragments are bound by an antibody directed against 5-methylCytidine and separated from unmethylated fragments. MeDIP processed samples are suitable for investigation of the methylation status of specific genomic loci and for performing genome-wide screening, when hybridized to DNA methylation microarrays or analyzed by deep sequencing. In such experiments, it is usual to assess the efficacy and repeatability of the MeDIP step by enrichment estimation of genomic regions expected to be heavily methylated in the samples under investigation. This is done from qPCR data, comparing the pairs MeDIP/Input and normalizing with genomic regions expected to be unmethylated. However, the methylation status of specific loci is not always known for particular samples under the conditions of the specific study, which may render the choice of genomic regions for quality control problematical. In addition, although MeDIP is a widely used tool in epigenetics studies, to my knowledge, no comprehensive studies on possible biases occurring during any of the procedure steps have been conducted so far, nor universally accepted quality controls have been developed.

I therefore proposed the introduction of external positive and negative controls ("spikes") (Lisanti et al., 2012) to test the methylated fraction enrichment of any MeDIPed/Input sample pairs; these can also be used to verify that each batch of samples is successfully enriched for methylated regions and to ensure experimental reproducibility between samples and experiments within laboratories and between laboratories. Figure 4.1 outlines the MeDIP protocol and the introduction of the spikes suggested in my study.

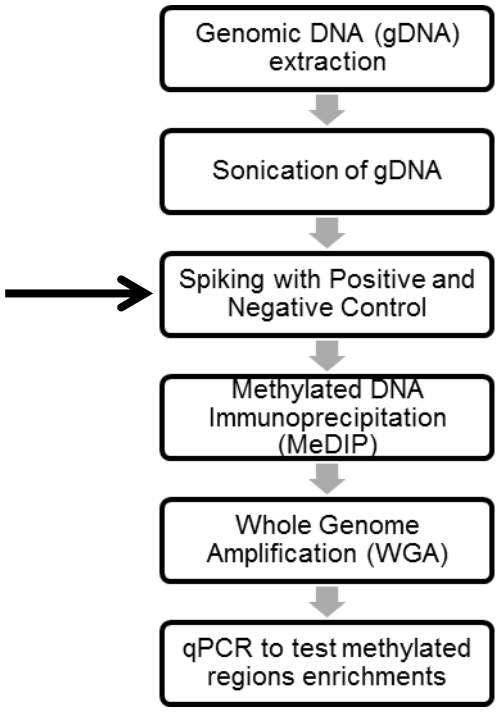

Figure 4.1. Methylated DNA Immunoprecipitation (MeDIP) protocol. The black arrow indicates the introduction of exogenous controls described in my study.

4.2 Development of internal controls for the MeDIP assays standardization and quality assessment

Two fragments (Fragment A and Fragment B, see Figure 4.2) of similar length (625 and 611 bp, respectively) and CpG content (41 and 35 CpG, respectively) were PCR amplified using primers and PCR conditions indicated in Table 2.1 and section 2.6.2. The fragments size was chosen to be the average size of the sonicated genomic DNA suitable for MeDIP (Weber et al., 2005; Weber et al., 2007).

Fragment A

AGCAACCAACAAGAAAACACTGGCAGATTACGCCCGTGCCTTATCCGGAGAG
GATGAATGACGCGACAGGAAGAACTTGCCGCTGCCCGTGCGGCACTGCATGA
CCTGATGACAGGTAAACGGGTGGCAACAGTACAGAAAGACGGACGAAGGGT
GGAGTTTACGGCCACTTCCGTGTCTGACCTGAAAAAATATATTGCAGAGCTG
GAAGTGCAGACCGGCATGACACAGCGACGCAGGGGACCTGCAGGATTTTATG
TATGAAAACGCCCACCATTCCCACCCTTCTGGGGCCGGACGGCATGACATCG
CTGCGCGAATATGCCGGTTATCACGGCGGTGGCAGCGGATTTGGAGGGCAGT

TGCGGTCGTGGAACCCACCGAGTGAAAGTGTGGATGCAGCCCTGTTGCCCAA
CTTTACCCGTGGCAATGCCCGCGCAGACGATCTGGTACGCAATAACGGCTAT
GCCGCCAACGCCATCCAGCTGCATCAGGATCATATCGTCGGGTCTTTTTTCCG
GCTCAGTCATCGCCCAAGCTGGCGCTATCTGGGCATCGGGGAGGAAGAAGCC
CGTGCCTTTTCCCGCGAGGTTGAAGCGGCATGGAAAGAGTTTGCCGAGGATG
A

Fragment B

GTGAATGTGGTGAAGTCTGCCCGTGTCGGTTATTCCAAAATGCTGCTGGGTGT
TTATGCCTACTTTATAGAGCATAAGCAGCGCAACACCCTTATCTGGTTGCCGA
CGGATGGTGATGCCGAGAACTTTATGAAAACCCACGTTGAGCCGACTATTCG
TGATATTCCGTCGCTGCTGGCGCTGGCCCCGTGGTATGGCAAAAAGCACCGG
GATAACACGCTCACCATGAAGCGTTTCACTAATGGGCGTGGCTTCTGGTGCCT
GGGCGGTAAAGCGGCAAAAAACTACCGTGAAAAGTCGGTGGATGTGGCGGG
TTATGATGAACTTGCTGCTTTTGATGATGATATTGAACAGGAAGGCTCTCCGA
CGTTCCTGGGTGACAAGCGTATTGAAGGCTCGGTCTGGCCAAAGTCCATCCGT
GGCTCCACGCCAAAAGTGAGAGGCACCTGTCAGATTGAGCGTGCAGCCAGTG
AATCCCCGCATTTTATGCGTTTTCATGTTGCCTGCCCGCATTGCGGGGAGGAG
CAGTATCTTAAATTTGGCGACAAAGAGACGCC GTTTGGCCTCAAATGGACGC
CGGATGACCCCTCCAGCGTGTTTTATCTCTGCGA

Figure 4.2. Sequences of the Lambda DNA Fragments used as spikes in my study. CpG sites are indicated by thick underlines, genomic regions used as priming sites for Fragments PCR amplification by dashed underlines and genomic regions used as priming sites for qPCR by wave underlines (see Table 2.1, Table 2.2, section 2.6.2 and section 2.8 for primer sequences and reaction conditions).

After PCR products purification, Fragment A was *In vitro* Methylated (IVM) using *E. coli* M.SssI methyltransferase, in the presence of S-Adenosyl Methionine (SAM), and used as Positive Control, while Fragment B (totally unmethylated) was used as Negative Control in subsequent MeDIP experiments. The efficiency of Fragment A IVM (Positive Control) was checked for 14 CpG sites by two methylation-sensitive restriction enzymes: *AciI*, which cuts blunt at CC↓CG sites (9 in the sequence) and *HpaII*, which cuts blunt at CC↓GG sites (5 in the sequence). Both enzymes cut DNA at the respective sequences only if the internal C is unmethylated. As a double check, I also used a third enzyme, the

HpaII-isoschizomer *MspI*, whose cutting is not affected by the internal C methylation. I ran the same set of digestions with Fragment B, which contains 6 *AciI* sites and 2 *MspI*/*HpaII* sites. As expected, Fragment A IVM was cut by *MspI* (Fig 4.3, lane 2), but uncut by Acil (lane 1) or by *HpaII* (lane 3): the agarose/TBE gel shows a single band of 625 bp long in these last two cases, as for the undigested fragment (lane 4). Full length Fragment B (lane 8), instead, was fully digested by *AciI*, *MspI* and *HpaII* (lanes 5, 6 and 7, respectively).

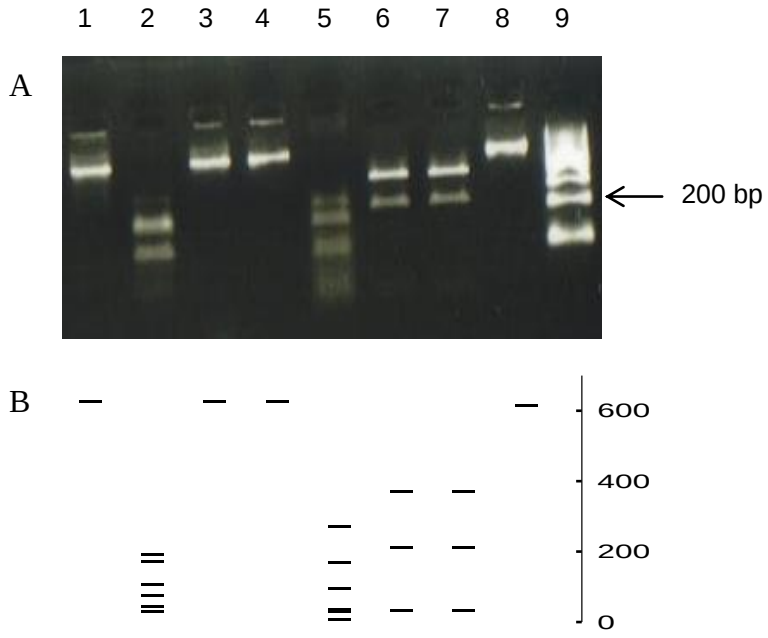

Figure 4.3. Digestion patterns of Positive and Negative Controls with the restriction enzymes AciI, MspI and HpaII on 2% Metaphor agarose/TBE gel. Panel A: lanes 1 and 5 = AciI digestions of Positive and Negative Control, respectively; lane 2 and 6 = MspI digestions of Positive and Negative Control; lanes 3 and 7 = HpaII digestions of Positive and Negative Control; lanes 4 and 8 = undigested Positive and Negative Control; lane 9 = 100 bp DNA Ladder. Panel B: virtual gel with the corresponding digestions patterns, as computed by the webtool http://tools.neb.com/NEBcutter2/.

I then designed qPCR assays to amplify short stretches of the Positive and Negative Controls (see Table 2.2 for sequences); these assays were subsequently used to quantify the enrichment of methylated regions in my MeDIPed samples compared with their related Input samples, according to the following formula (Pfaffl, 2001):

$$\text{Enrichment} = (E_{\text{Pos.Ctrl.}})^{\Delta Cq \text{ Pos. Ctrl. (Input - MeDIP)}} / (E_{\text{Neg. Ctrl.}})^{\Delta Cq \text{ Neg. Ctrl. (Input - MeDIP)}}.$$

I tested assays linearity on 10 fold dilutions of each control and calculated their efficiency of amplification from the line equation ($E = 10^{1/slope} - 1$) (Bustin et al., 2009) (see Appendix A for standard and melt curves). The amplification linearity ranged over at least eight orders of magnitude for both controls (500 pg/μL to 50 ag/μL) and the Cq values obtained were in an acceptable scale ($5 < Cq < 40$, data not shown). In addition, the amplification efficiencies were good for both Positive Control (0.82) and Negative Control (0.85). I concluded that the chosen primer pairs were suitable for quantification of both methylated and unmethylated DNA controls and for estimation of enrichment using the Pfaffl method. Also, as the two efficiencies were similar, the user could simplify the enrichment calculation using the ΔΔCq approximation method (Livak and Schmittgen, 2001).

The next step was to determine the optimal sample concentration to be used in the qPCR assays for quantification of the controls and to ensure that amplification efficiencies for the controls was similar when tested in the context of genomic DNA to be immunoprecipitated as when tested alone. I checked the amplification efficiencies of the controls in three 10-fold dilutions (100 pg/μL, 10 pg/μL and 1 pg/μL) of both Input and MeDIP samples from a randomly chosen immunoprecipitation experiment, which was conducted on gDNA from mouse liver. As shown in Figure 4.4, I observed very similar efficiencies (E) in the presence of both Input DNA and of methylation enriched (MeDIP) DNA for both Positive (panel A, E = 0.87 vs E = 0.81) and Negative Controls (panel B, E = 0.84 vs E = 0.87). I therefore concluded that:

- the presence of Input and MeDIP DNA fractions did not influence the amplification efficiencies of the chosen primer sets for the controls;
- 20 pg of template DNA was an acceptable amount for control PCR reactions to ensure that the answers are in the linear range of the assay.

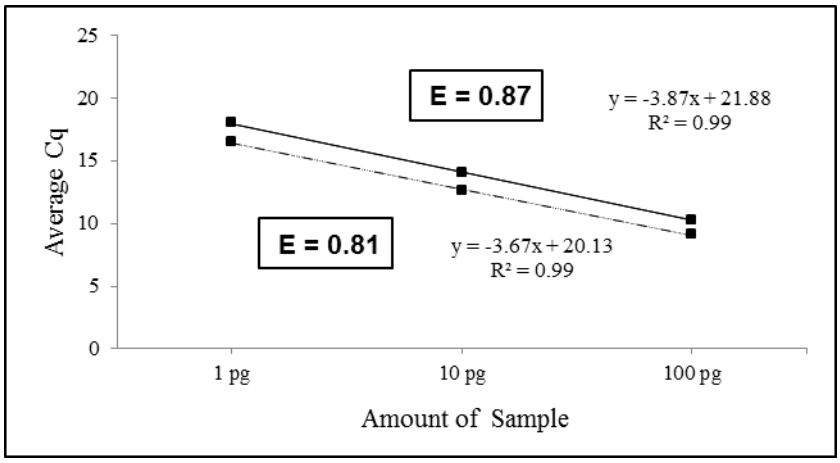

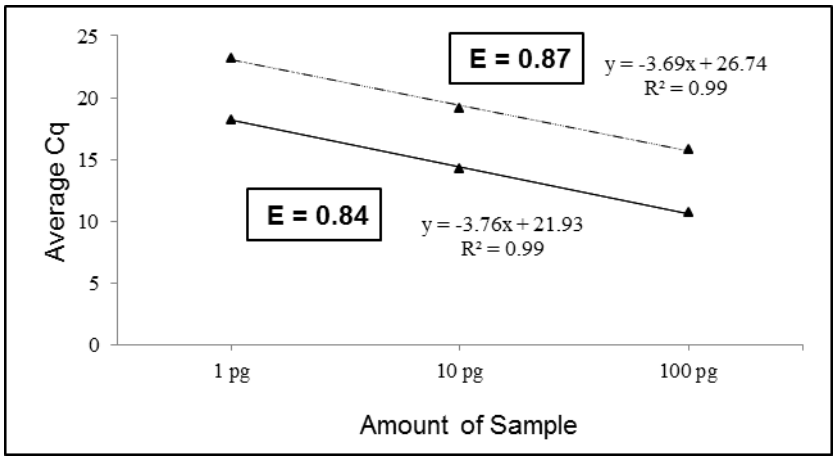

Figure 4.4. Positive (A) and Negative Control (B) qPCR assays linearity on 10-Fold Dilutions of the controls for MeDIP in the background of genomic DNA from mouse liver. Dashed lines show linear regression trendlines for Controls in the MeDIP samples and solid lines show trendlines for Controls in the Input samples. Efficiencies of amplification (E) are shown in the boxes.

In addition, I found that the chosen primer pairs did not result in amplification of any unspecific DNA sequences or in false priming of human and mouse gDNA with the template amount chosen for control PCR reactions (Figure 4.5).

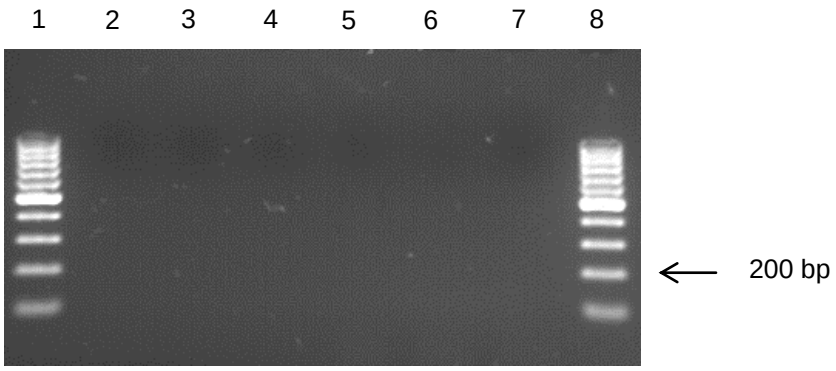

Figure 4.5. Absence of unspecific amplification of λ-DNA spike controls primer pairs 2 (see Table 2.2 for sequences) in human and murine genomic DNA. Lane 1 and 8 = 1 Kb DNA ladder; lane 2 and 3 = Positive Control end-point PCR (30 cycles) on human and murine gDNA respectively; lane 4 and 5 = Negative Control end-point PCR (30 cycles) on human and murine gDNA respectively; lane 6 and 7 = non-template reaction controls for Positive Control and Negative Control primers, respectively.

4.3 Sonication of Genomic DNA

The first step of the MeDIP procedure is fragmentation of the DNA to be immunoprecipitated; this is usually done by sonication, although DNase digestion or restriction endonucleases can be used. However, this last method does not produce random fragments, as it is dependent on the restriction enzyme pattern of digestion, and can therefore introduce biases.
For my experiments, I sonicated genomic DNAs as described in section 2.6.1 and ran a small amount on agarose/TBE gel to confirm:

- the integrity of each DNA sample;
- the absence of RNA.

The latter is critical to avoid antibody capture by 5-mC that is known to be present in this nucleic acid (Klagsbrun, 1973; Motorin et al., 2009; Cantara et al., 2010; Karijolich et al., 2010). Sonication patterns were assessed on agarose/TBE gels and optimally fragmented DNA samples, i.e., with fragment sizes 200 to 1000 bp (Weber et al., 2005; Weber et al., 2007) (Figure 4.6), were purified using silica columns. I chose this method of purification because it is faster than the ethanol-based precipitation method proposed in the original method (Weber et al., 2005; Weber et al., 2007).

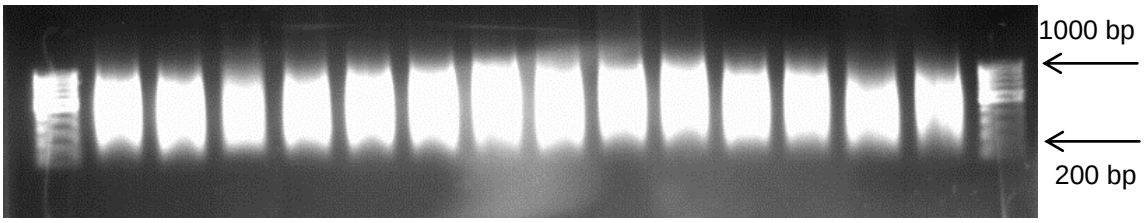

Figure 4.6. Example of correctly sonicated genomic DNA samples for MeDIP. First and last lanes are 1 Kb DNA Ladder.

4.4 Methylated DNA Immunoprecipitation and Spike Controls Enrichments

As described in detail in section 2.6.3, I spiked genomic DNA with both Positive and Negative Control fragments in the ratio 1:100 control: genomic DNA. This resulted in Cq values ranging from about 14 to 23 for all my subsequent qPCR assays (data not shown). From these data, I inferred that users of my approach could reduce the proportions of control "spikes" to as low as 1:10000 in proportion to the total amount of sample DNA being investigated; in fact, this would result in Cq values up to about 30, which fall within the linear range of the qPCR assays (Appendix A, Figure A.1 and Figure A.2). However, the spiked amount that I suggested was high enough to allow detection using a minimal amount of IP reactions and was low enough to result in average total controls occupancy of 5.07% for pre-Whole Genome Amplification (WGA) samples and 3.32% for post-WGA samples in the IPed samples (calculated from qPCR data, not shown). Since lambda DNA sequences do not share homology with human or mouse sequences (Butcher and Beck, 2010), they will not hybridize to human or mouse array chips and so will not interfere with downstream analysis. However, if deep sequencing is intended to be used for further interrogation of MeDIP samples, I suggest further optimization of the fragment lengths and amounts of spikes used to limit any potential redundancy in material to be sequenced (Butcher and Beck, 2010; Down et al., 2008; Feber et al., 2011).

4.5 Whole Genome Amplification

Whole Genome Amplification (WGA) is a necessary step in the preparation of MeDIP samples for arrays hybridization, deep sequencing or simple endogenous regions enrichment measurements in a MeDIPed specimen by means of qPCR. However, if my spiked controls are used, it is possible to assess the Positive Control/Negative Control enrichment both in the pairs MeDIP/Input both pre-WGA and post-WGA. Comparing pre- and post-WGA enrichments for all performed experiments, I noticed that the latter

were significantly lower ($p < 0.001$ for student's paired t-test) of about 32% than the related pre-WGA enrichments (Figure 4.7). This "loss" was manifest as an increase in the Cq values for the Positive Control of about 5 cycles, when the same sample (Input or MeDIP) was tested Pre-WGA and Post-WGA, while Cq values for the Negative Control remained similar pre- and post-WGA (data not shown). With the following experiments, I demonstrated that biases introduced by the WGA step were sequence specific and not dependent on the methylation state (Figure 4.8) or to the length of the target template (Figure 4.9).

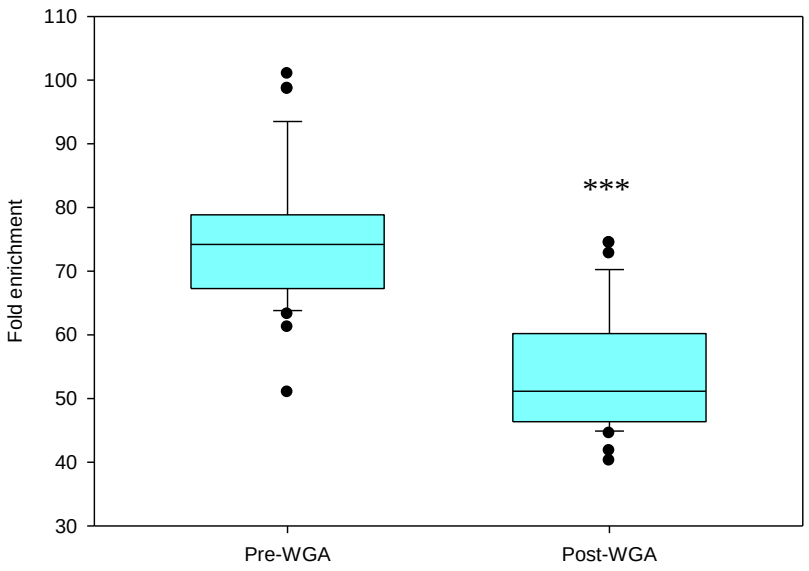

*Figure 4.7. Descriptive statistics for fold enrichments Positive Control/Negative Control Pre-WGA and Post-WGA. Box plots show the percentiles and the median of column data. Box outlines define the 25th and 75th percentiles, with a line at the median and whiskers indicate the 10th and 90th percentiles. *** = $p < 0.001$ for student's paired t-test, n = 33.*

In a first experiment, I *in vitro* methylated Fragment B and left Fragment A unmethylated (see Figure 4.8, panel A) and therefore used Fragment A as spiked negative control and Fragment B as positive control in one murine gDNA; the ratio between the sonicated DNA and the spikes was left constant at 100:1:1. I then proceeded to the WGA step and performed qPCR on pre- and post-WGA mixes. I noticed that the ratio of Fragment A: Fragment B after WGA was always about one sixth of the ratio before WGA, irrespective of the methylation status of the fragments (Figure 4.8, panel B), hence I concluded that WGA-related amplification biases were not due to the methylation status of a DNA sequence.

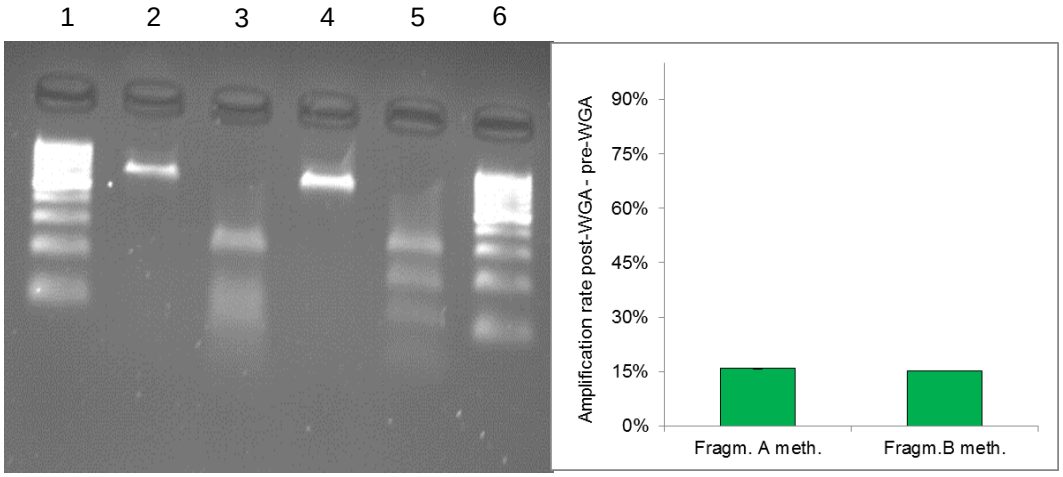

Figure 4.8. Left: digestion patterns of methylated and unmethylated Fragments A and B with the restriction enzymes AciI on 2% agarose/TBE gel. Lanes 2 and 3 = AciI digestions of Fragment A unmethylated and IVM, respectively; lane 4 and 5 = AciI digestions of Fragment B unmethylated and IVM, respectively; lanes 1 and 6 = 100 bp DNA Ladder. Right: amplification rate of Fragment A post-WGA/pre-WGA in a MeDIP experiment where either Fragment A (left bar) or Fragment B (right bar) act as methylated control in a MeDIP experiment. Error bars show ± SEM on 3 technical replicates.

In another experiment, I spiked three randomly chosen sonicated gDNAs with six Lambda DNA fragments of defined lengths (in the range suggested by the WGA kit manufacturer, which was 100 bp to 1000 bp) and measured the amplification rate of those post-WGA/pre-WGA. As shown in Figure 4.9, panel B, different fragments showed different amplification rates, but no correlation between fragment length and amplification rate could be found; rather surprisingly, the shortest fragment presented the lowest amplification rate after WGA. I concluded that WGA-related amplification biases were not due the fragment length; this was already obvious for Fragment A and B, which are of very similar length, but together with the observation resulting from the previous experiment, led me to the conclusion that biases occurring during the WGA process were sequence related. I hypothesize that the annealing/extension temperature of the standard amplification step in the WGA procedure might not provide enough energy to unfold stable hairpins and helixes in the context of certain DNA sequences (and, in fact, Fragment A has a lower folding ΔG compared with Fragment B, as computed using the webtool http://mfold.rna.albany.edu/?q=mfold/DNA-Folding-Form). I think that the

sequence-related amplification bias issue cannot be solved because of the complexity of the starting material: indeed it is possible to adjust the temperature for a specific target, but in doing so biases towards other targets might arise.

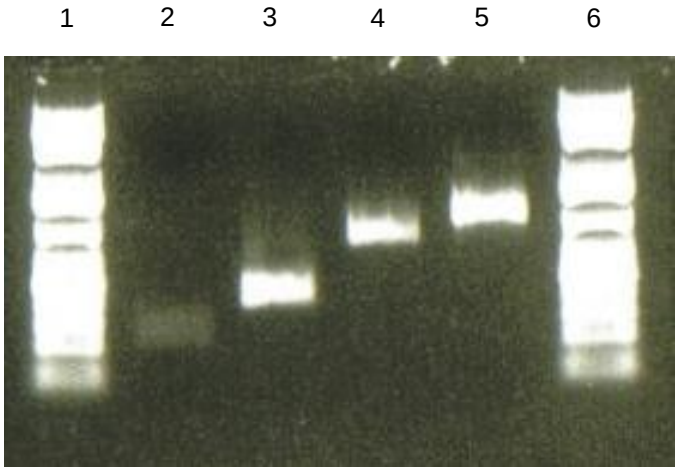

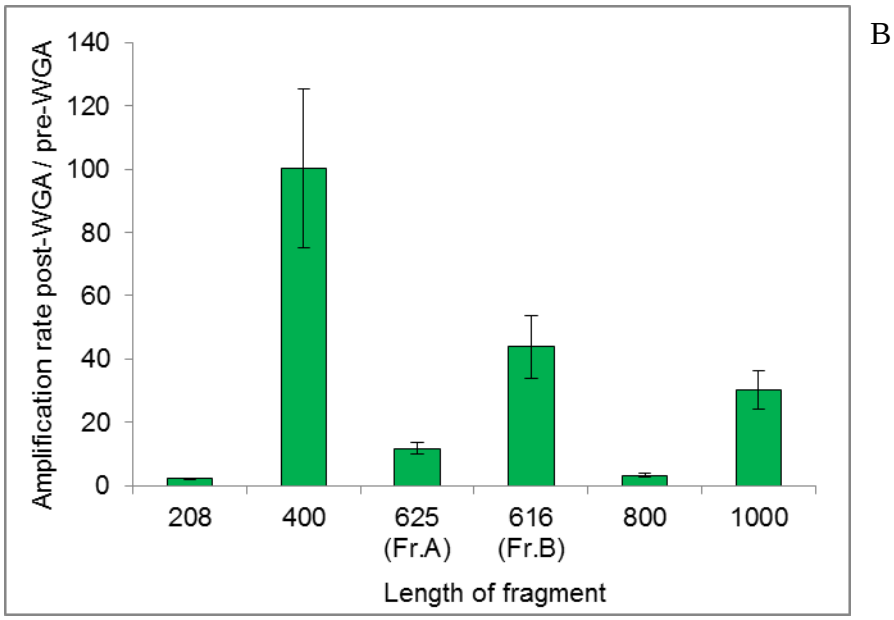

Figure 4.9. Panel A: preparation of Lambda DNA spikes of different length. Lanes 2, 3 and 4: Lambda DNA fragment of 208 bp, 400 bp and 1000 bp, respectively. Panel B: assessment of WGA amplification fragment length-related biases. Black bars represent the amplification rate Post-WGA/Pre-WGA of different length Lambda DNA fragments spiked in mouse genomic DNA. Error bars show ± SEM, n = 3. The table illustrates the primer sequences for λ DNA Fragment Spikes preparation (pairs 1) and qPCRs (pairs 2) for the assessment of Whole Genome Amplification length related bias.

Although having demonstrated that WGA introduced biases in the processed samples, I noticed good correlation between pre- and post-WGA enrichments (Spearman correlation coefficient of 0.59, $p < 0.001$, Figure 4.10, panel A) and high DNA yields (between 11 µg and 17.3 µg, Figure 4.10, panel B); I therefore concluded that this is a cheap and simple method to prepare sufficient amount of DNA from MeDIP samples; however, if WGA samples are to be used to quantitate enrichments of endogenous regions, I suggest the users to perform a preliminary experiment in order to assess the loss of amplification of the region of interest after WGA.

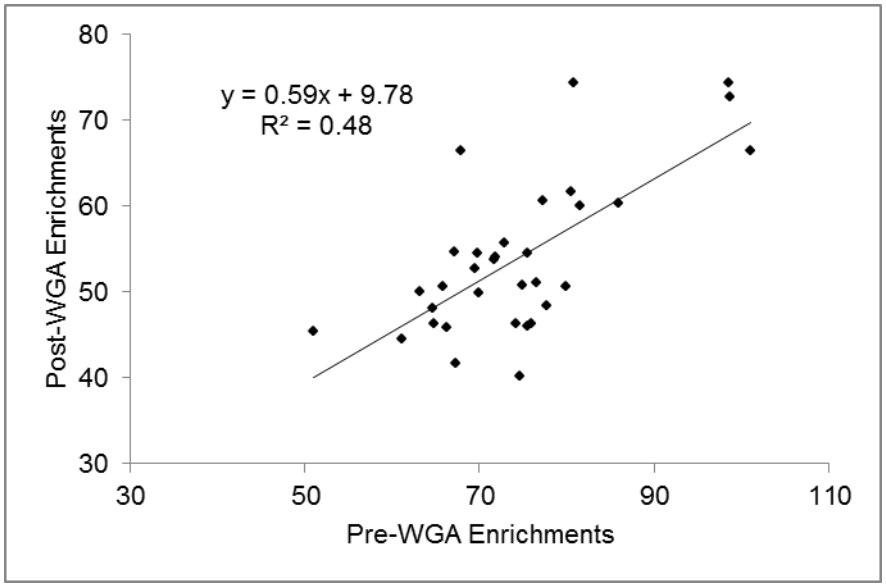

A

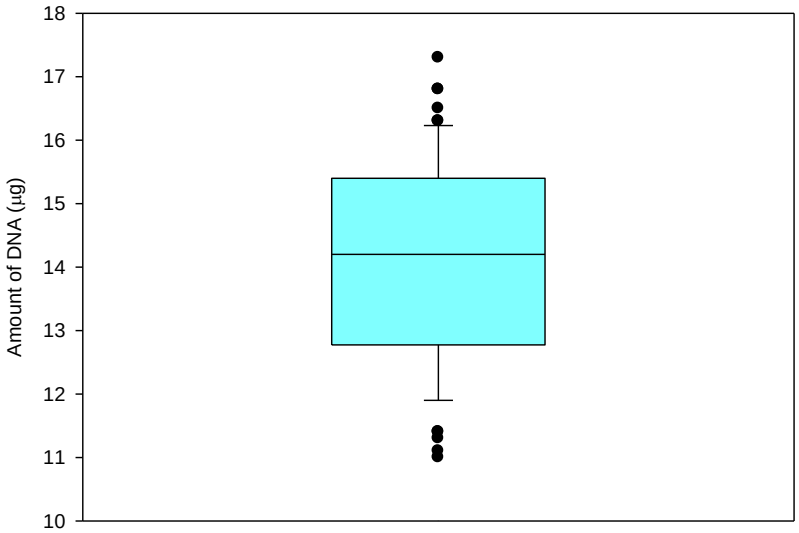

B

Figure 4.10. Linear regression for pairs of Pre-WGA and Post-WGA spike controls enrichments, n= 33 (panel A) and DNA yield obtained from WGA reactions for n = 66 samples; box plot shows the percentiles and the median of column data, box outlines define the 25th and 75th percentiles, with a line at the median and whiskers indicate the 10th and 90th percentiles.

4.6 Methylated endogenous regions enrichments assessments

After having demonstrated that the spiked controls were a useful tool in assessing efficiency and specificity of the MeDIP procedure in a variety of samples, I also wanted to demonstrate that my assays were reproducible, that endogenous methylated regions were enriched by MeDIP and that my Negative Control is an optimal normalizer in the enrichment calculations. In fact, usually housekeeping genes promoters are used as normalizers, assuming that these are either unmethylated or methylated to the same extent in all tissues; this is not always the case, as I demonstrated here, and can mislead the interpretation of results. On the contrary, my Negative Control, which is not methylated and so is in all the experiments, is an alternative and more suitable choice as a normalizer, whenever enrichments comparison needs to be done between samples.
I tested the reproducibility of all the performed assays and investigated the extent of the technical error on a subset of technical replicates, by comparing *GAPDH*-normalized enrichments of *H19* and *HIST1H2BA* genes with Positive Control/Negative Control enrichments in post-WGA samples. As inferred from the data in Figure 4.11, percentage coefficient of variations for these assays ranged from 6% to 15%, indicating that the technical error of assays of the spike controls was similar to that for endogenous regions. It is to be noted that *H19* enrichment was about half of *HIST1H2BA* enrichment; this is concordant with the fact that *H19* ia an imprinted gene, and so heavily methylated only on one of the parental alleles (Gao et al., 2002) and that MeDIP enrichments are proportional to the methylation content of the immunoprecipitated fragments (Weber et al., 2005).

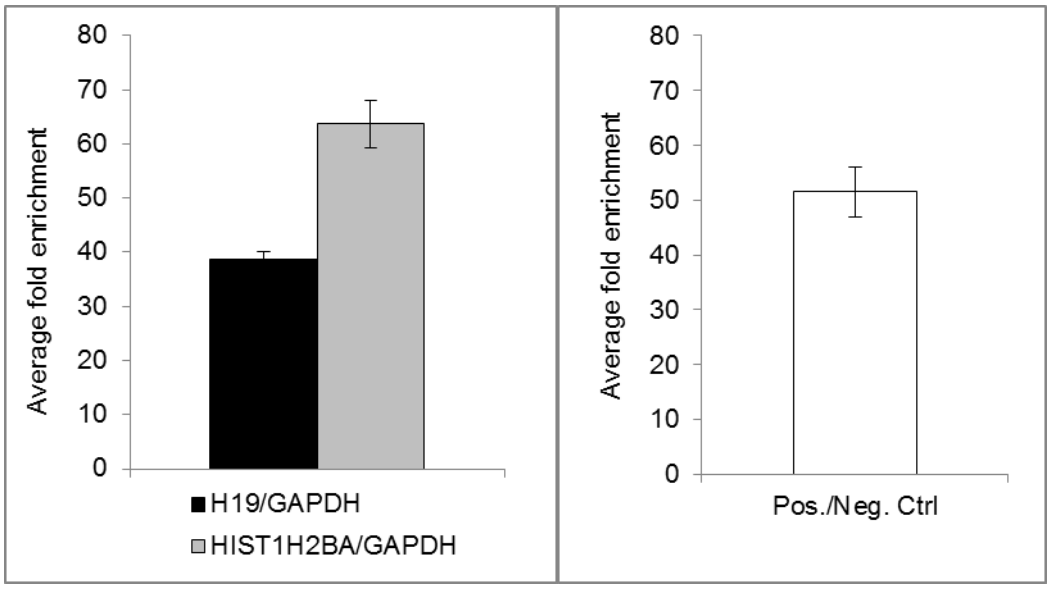

Figure 4.11. Gene specific enrichments after MeDIP followed by WGA for MRC-5 fibroblasts DNA. Left: enrichment of the MRC-5 internal genes H19 (black bar) and HIST1H2BA (grey bar), both normalized to GAPDH. Right: Positive/Negative Control Enrichment Post-WGA. Error bars show ± SEM, n = 3 technical replicates.

To demonstrate that endogenous normalizers could be a wrong choice in the enrichments calculations, I calculated enrichments in various murine MeDIPed samples for *H19* and *Hist1h2ba* genes and normalized those with either *Actb* or *Gapdh* promoter regions (Figure 4.12 A and B). Extent of the two different normalized enrichments was substantially different in some of the samples, while similar in others, indicating that the normalizer is a source of variation between biological replicates. In these experiments as well, *H19* enrichments were about half of *Hist1h2ba* enrichments, confirming what stated above for the cell line experiments.

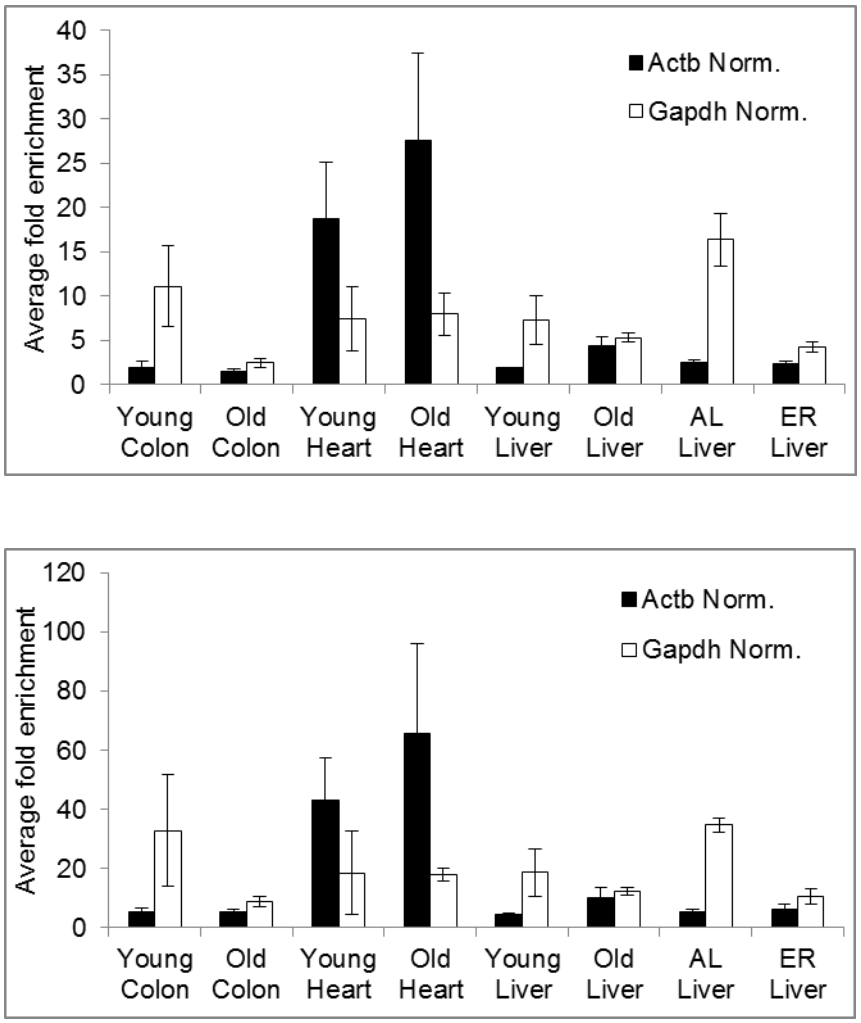

Figure 4.12. Gene specific enrichments for H19 (panel A) and Hist1h2ba (panel B) in mice tissues normalized to either Actb (black bars) or Gapdh (white bars). Data are mean ± SD, n = 3 biological replicates. AL = ad libitum fed, ER = dietary energy restricted.

I then illustrated cases where:

- normalization of endogenous gene enrichment by the Negative Control reduced experimental variability (Figure 4.13);
- normalization of endogenous gene enrichment by the Negative Control reduced the impact of tissue-specific methylation of the normalizer gene (Figure 4.14).

In Figure 4.13, left panel, enrichment following MeDIP was calculated from qPCR data after WGA from old mice heart gDNA for the endogenous gene *Hist1h2ba* with *Actb* as the normalizer and compared with estimate of enrichment obtained after normalization with the Negative Control. As shown in the right panel, normalization with the Negative

Control reduced considerably the coefficient of variation for the biological replicates (from 46% to 18%); this latter CV better represents the biological variability due to the methylated endogenous region.

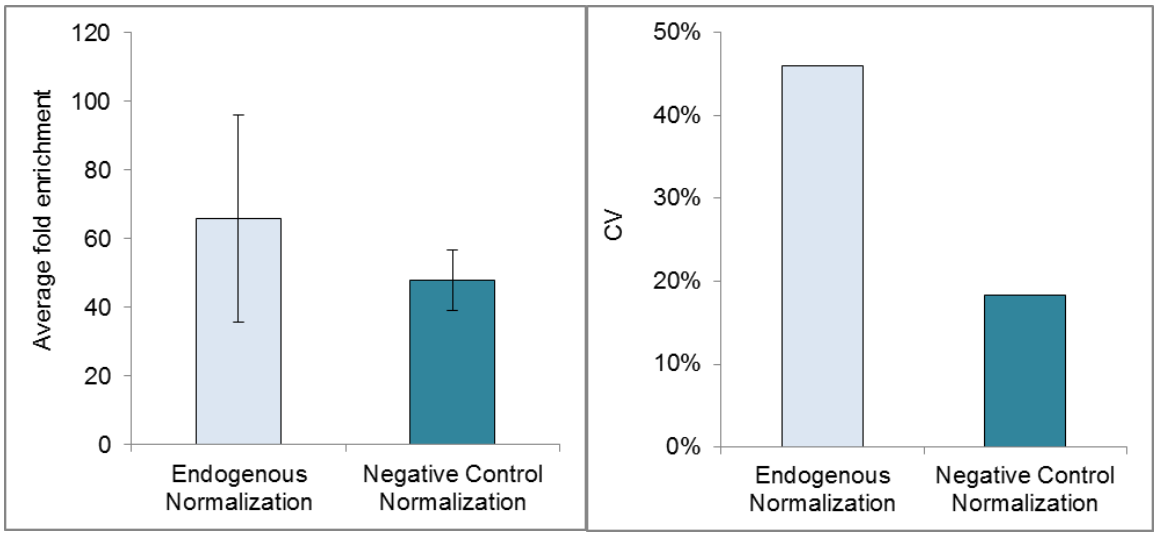

Figure 4.13. Normalization of endogenous gene enrichment by the Negative Control reduced experimental variability. Left panel: average fold enrichments for Hist1h2ba normalized with the endogenous region Actb (left column) or with the spiked Negative Control (right column) in old mice heart DNA. Data are mean ± SD, n = 3 biological replicates. Means are not significantly different (p = 0.41, student's unpaired t-test). Right panel: Black bars show Coefficients of Variation (CV) related to estimates in left panel.

Figure 4.14 presents instead data on enrichments of the endogenous gene *Hist1h2ba* from heart and colon genomic DNA from young mice using either *Actb* or the spiked Negative Control as the normalizer: the apparently tissue-specific difference in *Hist1h2ba* methylation between colon and heart was no longer significant when the Negative spike Control was used as the normalizer (left panel). Constancy between spiked controls enrichments is confirmed in the right panel, showing very similar degrees of enrichment post-WGA for DNA from the same samples.

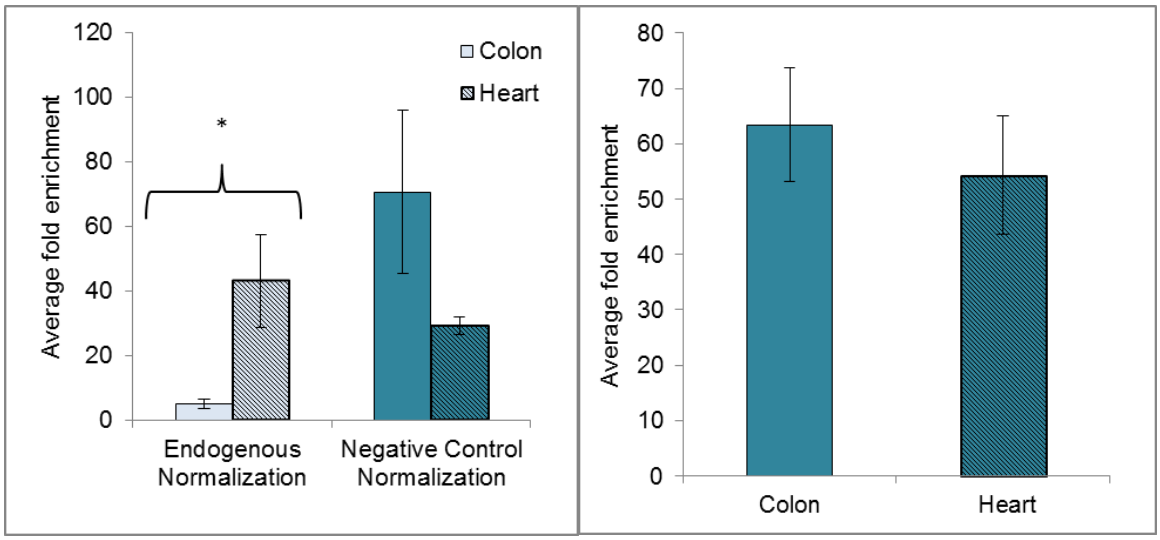

*Figure 4.14. Normalization of endogenous gene enrichment by the Negative Control reduced the impact of tissue-specific methylation of the normalizer gene. Left panel shows the comparison between gene specific enrichments for Hist1h2ba calculated with the endogenous normalizer Actb (light blue bars) and with the Negative Control (aqua bars) for Young Colon samples (empty bars) and Young Heart samples (dashed bars). Right panel shows Positive Control/Negative Control Enrichment Post-WGA. Data are mean ± SD, n = 3 biological replicates. * p = 0.04, student's unpaired t-test.*

4.7 Validation of the results by means of BM direct sequencing

With the goal to confirm the results showed in in Figure 4.14 by means of an alternative method, I chose the BM direct sequencing, already optimized in section 3.4.2 (see section 2.19 for experimental procedures). Briefly, primers for those assays were designed within 600 bp sequences (the average length of the fragments for immunoprecipitation) centered on the qPCR products of Figure 4.12, 4.13 and 4.14.

Results for the *Hist1h2ba* region are illustrated in Figure 4.15 and results for the endogenous normalizer *Actb* region are illustrated in Figure 4.16; this latter required cloning and subsequent sequencing of the BM-PCR products because of poor quality of some of the sequences reads.

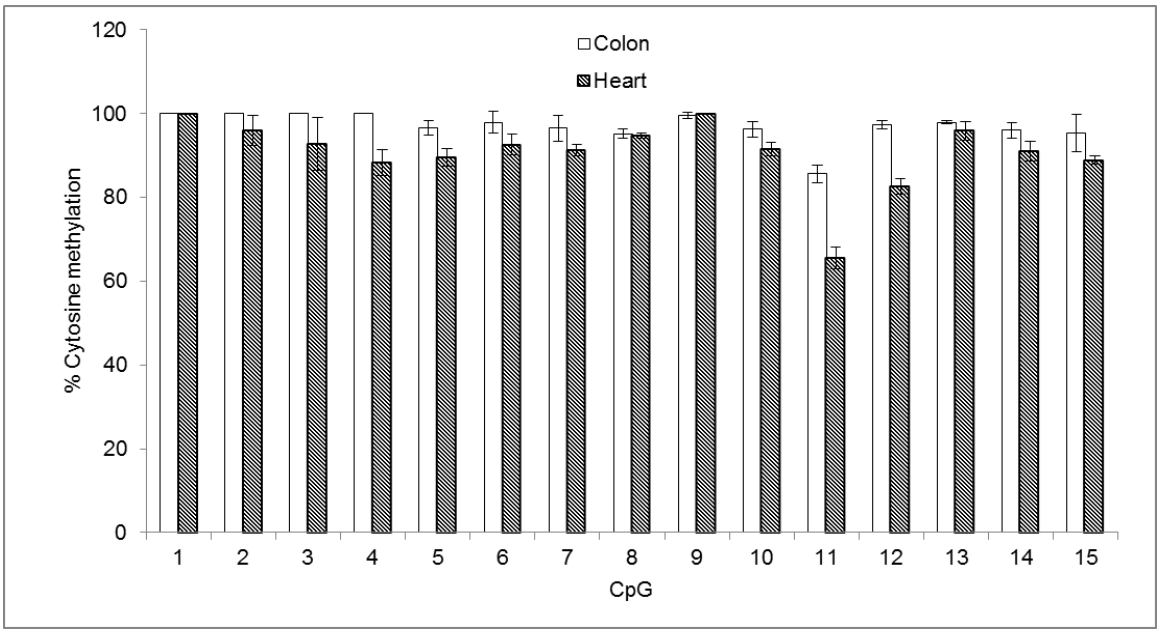

Figure 4.15. Direct BM sequencing of murine Hist1h2ba from colon and heart genomic DNA; data are mean ± SD, n = 3 biological replicates.

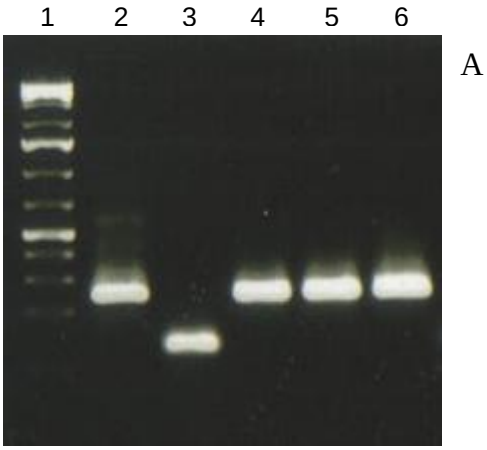

A

B

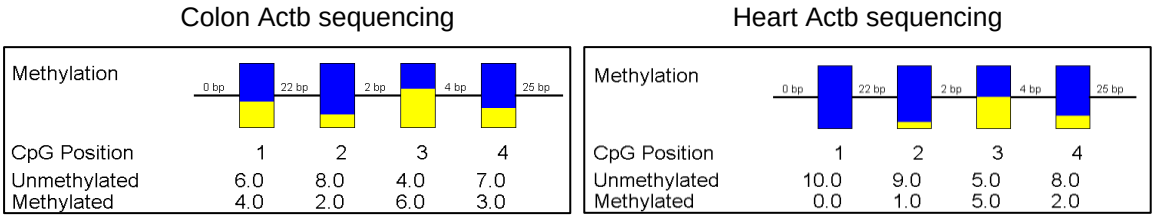

Figure 4.16. Panel A: colony PCR of Actb blunt cloning for one heart sample; lanes 2, 4, 5 and 6 = successfully cloned Actb sequence, lane 3 = amplification occurring with a colony transformed with an empty vector; lane 1 = 100 bp DNA ladder. Panel B: aggregate representation of methylation data obtained by BM cloning and sequencing for

one colon and one heart sample, respectively. The bars indicate the percentage of clones which showed unmethylated (blue) or methylated (yellow) Cytosines at the CpG sites analysed (adapted from BiQ Analyzer v2.00).

Heart samples showed lower methylation - especially at CpG no. 11 and 12 - in the *Hist1h2ba* region under investigation (Figure 4.15), and also lower methylation in the *Actb* region analyzed (Figure 4.16, panel B, right). The actual *Hist1h2ba* methylation is the one obtained when normalizing with the negative control, while the opposite result was obtained when normalizing with *Actb* (Figure 4.14, left panel), corroborating the need of proper choice of a normalizer for estimating and comparing methylation enrichments.

Using the same methodology, I also confirmed the methylation status of all the genomic regions previously tested by qPCR in a subset of samples; these results were in agreement with what seen by qPCR and are presented in Figure 4.17 and 4.18. Primers sequences and reaction conditions are given in Table 2.6.

Figure 4.17 shows the percentage of Cytosine methylation for MRC-5 fibroblasts in 3 technical replicates (left panels A, C and E). CVs ranged from 1% to 9% across 15 CpGs for *H19* and from 1% to 6% across 6 CpG for *HIST1H2BA*. This statistic could not be calculated for *GAPDH*, as bisulphite modification of this region resulted in complete C to T conversion, meaning that there was no detectable cytosine methylation across the 3 CpGs analyzed. The mean percentage methylation for all the CpG sites examined was 72% for *H19* (panel A, right), 94% for *HIST1H2BA* (Panel B, right) and 0 for *GAPDH* (data not shown). These data provided evidence that, as expected, *H19* was approximately hemi-methylated, *HIST1H2BA* was highly methylated and *GAPDH* was unmethylated. In addition, the ratio of mean methylation of *HIST1H2BA/H19* was similar to the *GAPDH* normalized mean enrichment ratio of *HIST1H2BA/H19* observed in my previous MeDIP-qPCR experiments (1.31 fold vs. 1.60 fold, respectively, see Figure 4.11 for comparison).

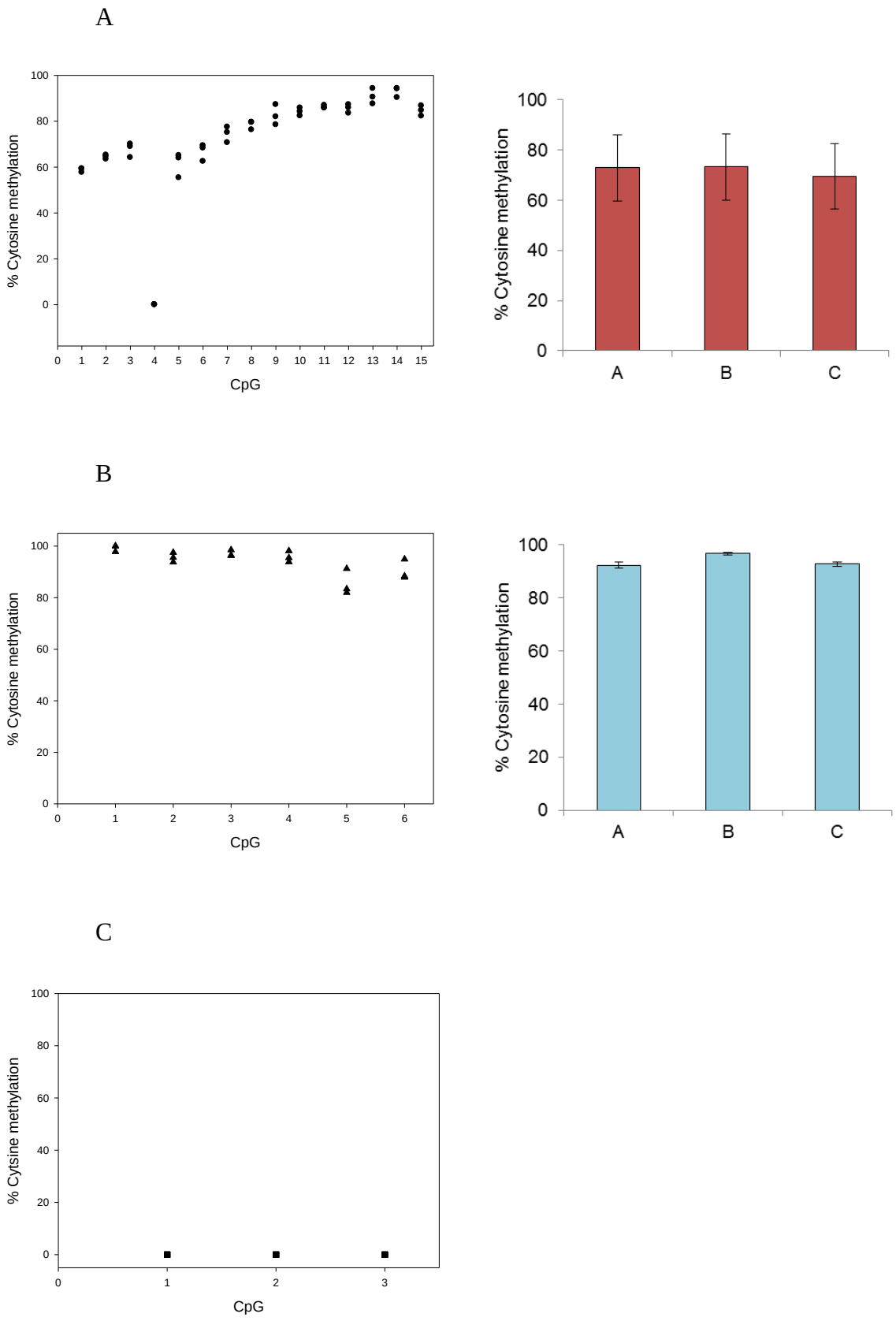

Figure 4.17. Cytosine methylation quantification by BM direct sequencing of human MRC-5 H19 (panel A), HIST1H2BA (panel B) and GAPDH regions (panel C). Panels on the left Y axes present data measured for 3 independent technical replicates. Panels on the right present average methylation ± SD across the CpG sites analysed.

Figure 4.18 (panels A to D) shows the percentage of Cytosine methylation in mouse colon. As for the human orthologous regions, mean percentage methylation in both young and old mice was about 70% in *H19* across 5 CpGs (panel A) and close to 100% in *Hist1h2ba* across 15 CpGs (panel B). Mean methylation of the housekeeping genes was approximately 70% across 3 CpGs for *Actb* (panel C) and 13% across 6 CpGs for *Gapdh* (panel D), consistent with the MeDIP-qPCR enrichments results, which were higher when normalized using *Gapdh* (Figure 4.12, panels A and B). Panel E shows the minimum and the maximum percentage CV calculated on the CpG analyzed, which spanned from 0 (*Hist1h2ba*) to 89% (*Gapdh*), also consistent with data presented in Figure 4.12, where *Gapdh* was the normalizer which showed the biggest SDs.

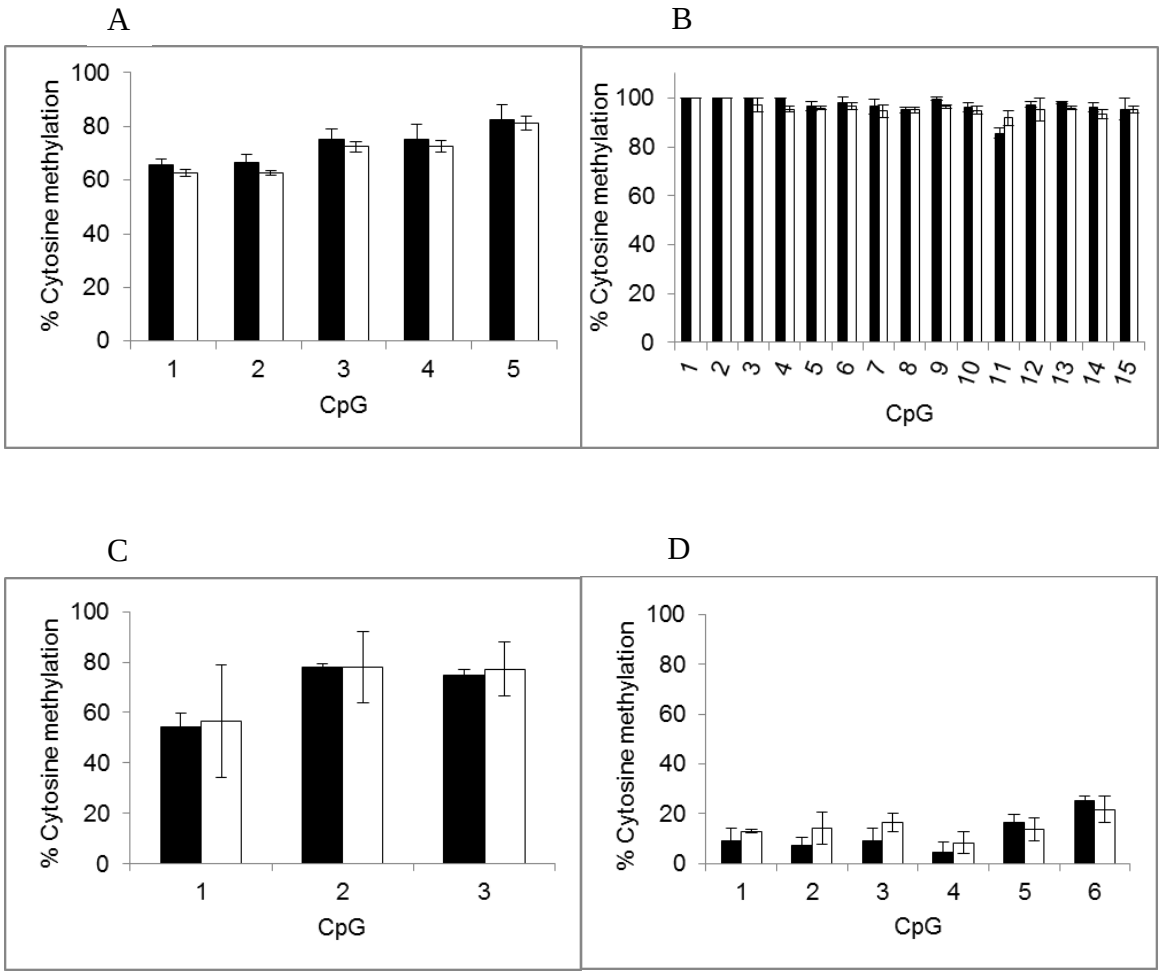

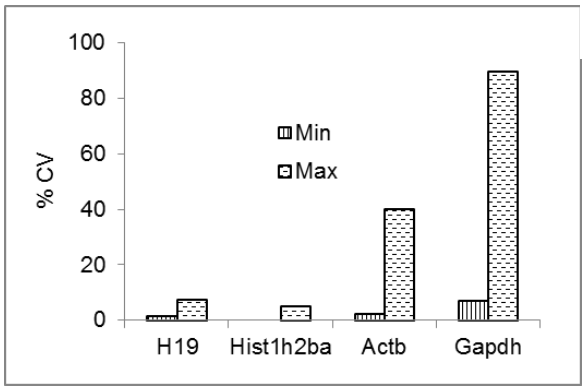

Figure 4.18. Cytosine methylation quantification by BM direct sequencing of H19 (panel A), Hist1h2ba (panel B), Actb (panel C) and Gapdh (panel D) regions of murine young (black bars) and old (grey bars) colon samples. Error bars present ± SD calculated on each single CpGs measurements of 3 biological replicates. Panel E shows minimum (white bars) and maximum (dashed bars) percentage CV determined on all the investigated CpGs measurements.

4.8 Discussion

In the present study, I developed standardization protocols and quality controls to assess the specificity, reproducibility and efficiency of the Methylated DNA Immunoprecipition (MeDIP) procedure. By the use of "spiked" positive and negative controls, I provided an economical and fast method for quantifying success in enrichment of samples processed using the MeDIP technique.

A common way to deal with enrichment data (ChIP or MeDIP), in particular in genome-wide (array) contexts, is to normalize to input DNA, as a "genome-wide methylation state"; however, I believe that the use of internal controls (spikes) is an additional advantage since this allows users to take account of other sources of variation, such as efficiency of immunoprecipitation. Those spikes were designed with careful attention to the defined length and methylCytosine content; technical details of their preparation and assessment of suitability are abundantly discussed within this Chapter.
When I checked for the presence of CpG islands in those spike controls using the software http://www.ebi.ac.uk/Tools/emboss/cpgplot/, I found one island of 520 bp in the Positive Control and one of 508 bp in the Negative Control; for prediction of CpG islands, I used the default settings of the program. I believe that my controls could well represent one methylated and one unmethylated CpG island from the human or murine genomes. In addition, since these Controls were not subjected to shearing (as prepared genomic DNA for MeDIP assays is), they had a constant length and number of methylated or unmethylated CpGs. Therefore their immunoprecipitation efficiency was constant and could be used with confidence to determine the consistency of the assays.

In principle it is possible, of course, to choose a genomic region with no CpG sites and to use it as a normalizer. However, we have to keep in mind that fragments for MeDIP are of different length (200 bp to 1000 bp) and that, consequently, target regions for qPCR are contained in a pool of these variable length fragments. Thus, to be absolutely certain that there are no CpGs in a template, we would have to choose quite a long genomic region without any CpG site, which will be much more difficult to find. Assuming that we wish to design a qPCR assay that amplifies an amplicon of 100 bp, we would have to go upstream and downstream in the genome for 900 bp in each direction without encountering a single CG site, with the fragment size range used; this seems unlikely to

happen. These considerations reinforce the utility of my method in circumventing normalization issues.

Common MeDIP follow-up techniques require more material than what is obtained from a typical immunoprecipitation (average yield is about 2% to 5% of the starting material); for example, semi-quantitative PCR and qPCR of a non-repetitive region usually necessitates of at least 10 ng-20 ng of gDNA for each replicate, while arrays hybridization and deep sequencing experiment require at least 3 µg-5µg DNA. Hence, WGA is often a mandatory step when preparing MeDIP samples starting from small amount of sonicated DNA (a typical quantity for an IP experiment is 1 to 10 µg, but smaller amounts have been successfully used). When I compared Positive Control enrichments pre- and post-WGA, I noticed that post-WGA enrichments were consistently lower by about 32% in all my assays; I found that this was due to unequal amplification efficiency of the WGA procedure of the fragments within a mix and I demonstrated that this bias was sequence-related and not due to the fragments length or methylation. It is possible to correct for it when estimating enrichment by qPCR, by simply calculating the amplification rate pre-WGA/post-WGA of a region of interest in a related sample, e.g. genomic DNA of the same species. Absolute methylation levels estimation is also possible when MeDIP followed by qPCR, by enrichment comparison of the region of interest with a known methylation content region with similar CpG density (efficiency of immunoprecipitation is in fact directly proportional to the amount of methylated Cytosines (Weber et al., 2005)). However, WGA biases cannot be corrected when performing MeDIP-arrays coupled experiments and regions which have enrichments affected by amplification bias could pass undetected.

The quantity of spikes used in my study resulted in a total of about 3% of occupancy in MeDIP prepared after the WGA step; this amount did not seem big enough to affect quality of the arrays hybridization (to which, anyway, λ DNA sequences would not bind). I did not have experience on deep sequencing techniques, but 3% seemed reasonably low for those as well, if we take into account that almost half of the human and more than one third of the murine genome are made up by repeats (Burns and Boeke, 2012), which are considered “background noise” in this kind of experiments. Here, genomic DNA could be spiked with the controls before the sonication step, as average DNA fragments length should be smaller than the 600 bp used for arrays hybridization (usually around 200 bp (Butcher and Beck, 2010)); in alternative, shorter spikes could be prepared. This second

solution seems preferable, as keeping costant the spike controls length ensures that CpG content, and consequently efficiency of immunoprecipitation, is always identical for each control molecule spiked in a MeDIP reaction, making enrichments comparison between samples more reliable.

Overall, my endogenous regions methylation enrichments data indicate that there may be considerable inter-animal variation in methylation of conventional housekeeping genes and that researchers need to be alert to the possibility that their treatments may influence the methylation status of such genes. These observations reinforce the need for an external normalizer to provide a more precise and unbiased normalization of enrichment data, if a qPCR approach is used after MeDIP assays; in this context, my spikes method can be used as a semi-quantitative predictor for the calculation of methylation fold changes in samples to be compared, it eliminates the issue of finding a good endogenous normalizer and can be applied to a variety of samples from different species.

Whenever *ACTB/Actb* or *GAPDH/Gapdh* are anyway chosen to be used as normalizers in qPCR assays using gDNA as template, I suggest researchers to assess whether the amplicons obtained correspond to a single genomic region; in fact, those genes have many pseudogenes and amplification of one or more of those could lead to confounding results, if the samples under investigation present a different content in methylation at those genomic locations. To exclude that this was happening in my assays, I double-checked my primers design making sure of their specificity by *in silico* PCR (using the webtool http://genome.ucsc.edu/cgi-bin/hgPcr?command=start), melt curve analyses (Appendix A) , agarose/TBE gel runs and full length sequencing of the cloned PCR products (see Appendix D).

4.9 Conclusions

In conclusion, the method developed in this study can be used:

- to test the reproducibility, specificity and efficiency of MeDIP assays;
- as a quality control in the screening of MeDIP processed samples prepared for hybridization to methylation microarrays;
- to minimize the risk of bias when making comparisons in the extent of methylation between treatments/conditions when there may be biological variation

not only in the DNA regions of interest, but also in the endogenous regions used as normalizers;

- to normalize calculations of enrichment when the methylation status of DNA domains of interest is not known. I anticipate that the test protocols and quality controls described in this report will have utility when comparing results of MeDIP procedures between samples and experiments within laboratories and between laboratories.

Related publication:

Standardization and quality controls for the methylated DNA immunoprecipitation technique. Epigenetics. 2012 Jun 1;7(6):615-25. doi: 10.4161/epi.20028. Epub 2012 Jun 1.

Sofia Lisanti*, Thomas von Zglinicki, John C. Mathers.

Centre for Integrated Systems Biology of Aging and Nutrition; Institute for Aging and Health; Newcastle University; Newcastle upon Tyne, UK.

* = corresponding author

Chapter 5. Identification of novel aberrantly methylated genomic regions in senescence and in early stress-induced premature senescence and effects of senescence on gene expression

5.1 Outline

Promoter-specific aberrant methylation was first described in cancer, with the first data published in the early ‘80s (Feinberg and Vogelstein, 1983). In the field of senescence and ageing, aberrant DNA methylation has become a top focus recently and nowadays databases for such data are readily available, one example being the “Epigenomics” section within PubMed database (http://www.ncbi.nlm.nih.gov/epigenomics/).
Since 1995, there has been evidence of site-specific aberrant CpG methylation associated with cellular senescence for genes whose expression is known to be dysregulated during senescence. For example, studies conducted on human fibroblasts primary cultures have detected intragenic hypermethylation of the proto-oncogene *MYC* (Halle et al., 1995), of rRNA genes (Machwe et al., 2000), of the h*TERT* promoter (Shin et al., 2003), of the *CDKN1A* (p21) promoter (Zheng et al., 2006) and of the intragenic sequence of the *CSNK2A1* gene (Kim et al., 2009a) in replicative senescent cells. With the establishment of microarray technology, it has been possible to undertake genome-wide profiling of CpG methylation, which has revealed aberrant methylation within promoter regions of homeobox genes and genes involved in cell differentiation (Bork et al., 2010), DNA replication and cell cycle (Koch et al., 2011; Choi et al., 2012). More recently, DNA methylation at specific CpG sites has been suggested as a molecular biomarker for senescence (Koch et al., 2012; Koch and Wagner, 2013).
On the other hand, studies which have investigated site specific DNA methylation changes occuring within premature senescence induced by ionizing radiations have found contrasting results. Some studies have reported aberrant promoter methylation of genes involved in the cell cycle, DNA repair, and apoptosis pathways (Antwih et al., 2013), whereas others have failed to detect evidence of senescence-associated DNA methylation changes (Koch et al., 2013).

This study was set up to screen for novel differentially methylated regions in replicative senescence (RS) and early stress premature induced senescence (ESIPS) compared with young confluent (YC) cells using the human lung fibroblasts cell line MRC-5 and to

assess whether those were associated with differential expression. To this purpose, I prepared 3 biological replicates for each sample type, isolated DNA and performed MeDIP, followed by hybridization onto Nimblegen DNA Methylation Arrays. In parallel, transcriptome data were obtained using AffimetrixData arrays. Arrays data analyses were conducted by M. Adriaeans, Maastricht University. Sample preparation, arrays and data analysis methods are described in sections 2.1, 2.3, 2.4, 2.6, 2.7, 2.8, 2.10, 2.11 and 2.12. In this Chapter, I describe, analyse and interpret the obtained genome-wide methylation and expression data. This includes consideration of genomic regions/genes which were altered in both RS and ESIPS cells when compared with YC cells and also consideration of the separate lists for each of the comparisons. Then from the RS vs YC cells list of comparison for both methylation and expression data, I chose 4 candidates for validation of methylation and gene expression. Briefly, methylation arrays and expression arrays data were sorted according to the observed fold changes and then bioinformatics analyses were performed to check for the presence of regulatory elements within the genomic regions identified by the methylation arrays (more details are given in section 5.6). Usually, there is an inverse correlation between promoter methylation and expression of the corresponding gene because when CpGs within a gene promoter are highly methylated this can impede the binding of transcription factors and therefore transcription of the related gene (Siegfried and Simon, 2010). However, cases have been reported where there is a positive correlation between promoter methylation and expression of the corresponding gene and authors have speculated that this may occur when highly methylated CpGs impair the binding of transcription repressors. One example is the *BIRC5* gene, where hypermethylation of the promoter inhibits the binding of its transcriptional repressor p53, leading to increased gene expression (Nabilsi et al., 2009). With this background, the candidates chosen for validation included examples where there were either negative correlation or positive correlation between DNA methylation and gene expression changes.

I concluded my study with a preliminary screening of methylation of the promoters of cell cycle genes, whose expression is known to be dysregulated in senescence (Rittling et al., 1986; Goldstein, 1990).

5.2 Genome-wide methylation of replicative senescent and early stress-induced premature senescent MRC-5 cells compared with young confluent cells

Figure 5.1 shows volcano plots for the genome-wide methylation data of RS compared with young confluent (YC) cells (left) and ESIPS compared with YC cells (right); significant hits lie above the blue line, which corresponds to the significance cut off (p = 0.05). Only 2.06% and 2.68% of probes showed significantly different methylation between the comparison groups (RS vs YC and ESIPS vs YC, respectively); these corresponded to 365 and 476 genomic regions. Of those, about 58% were hypomethylated and 42% were hypermethylated in RS vs YC cells, while 89% were hypomethylated and 11% were hypermethylated in ESIPS vs YC cells (data not shown). For a complete list of all the significant hits, see CD insert.

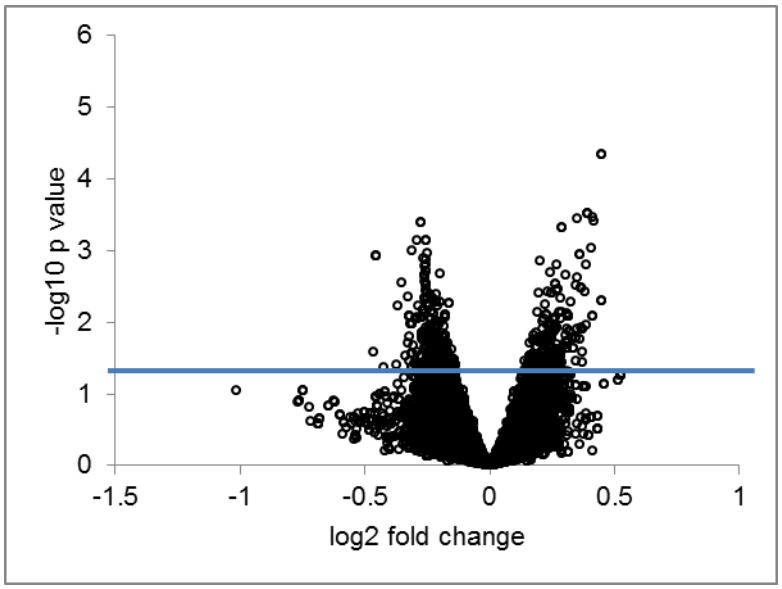

A

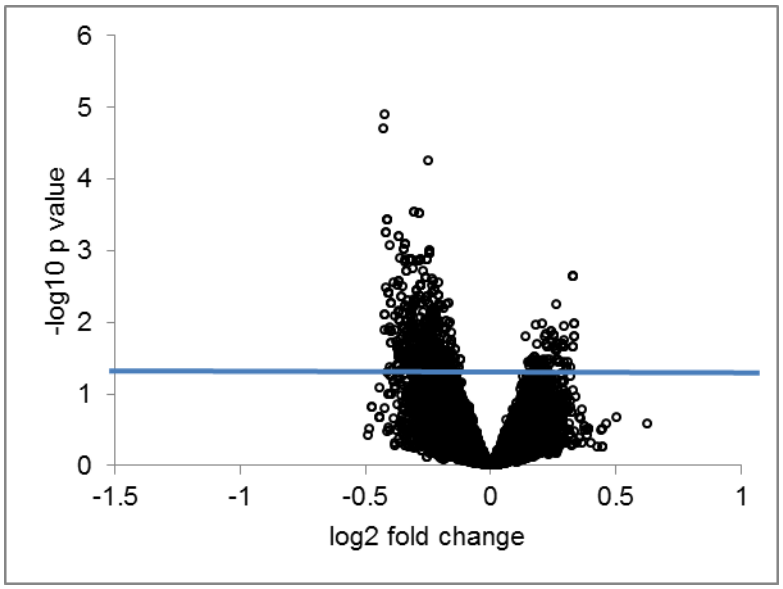

B

Figure 5.1. Descriptive statistics of MRC-5 cells DNA methylation data shown as volcano plots. Panel A: volcano plot showing the distribution significance/fold change of the methylation data for replicative senescent MRC-5 cells in comparison with young confluent cells; panel B: volcano plot showing the distribution significance/fold change of the methylation data for early stress-induced premature senescent MRC-5 cells in comparison with young confluent cells. Blue lines indicate the cut off above which the statistical significance criteria is met ($p < 0.05$ for student's unpaired t-test).

To determine whether there was a relationship between the methylation changes in the two pairs of comparison groups, I calculated the Spearman rank order correlation coefficient for all the significant differentially methylated Entrez Gene IDs in RS vs YC against all Entrez Gene IDs for ESIPS vs YC cells. As shown in Figure 5.2, panel A, this correlation was significant and positive, indicating that methylation changes occured in the same direction in the two groups. Figure 5.2, panel B, shows the analysis done with all significant differentially methylated Entrez Gene IDs in ESIPS vs YC against all Entrez Gene IDs for RS vs YC cells. Although still statistically significant, the Spearman rank order correlation coefficient for this dataset was much lower than in the previous case, but still indicated that methylation changes occured in the same direction.

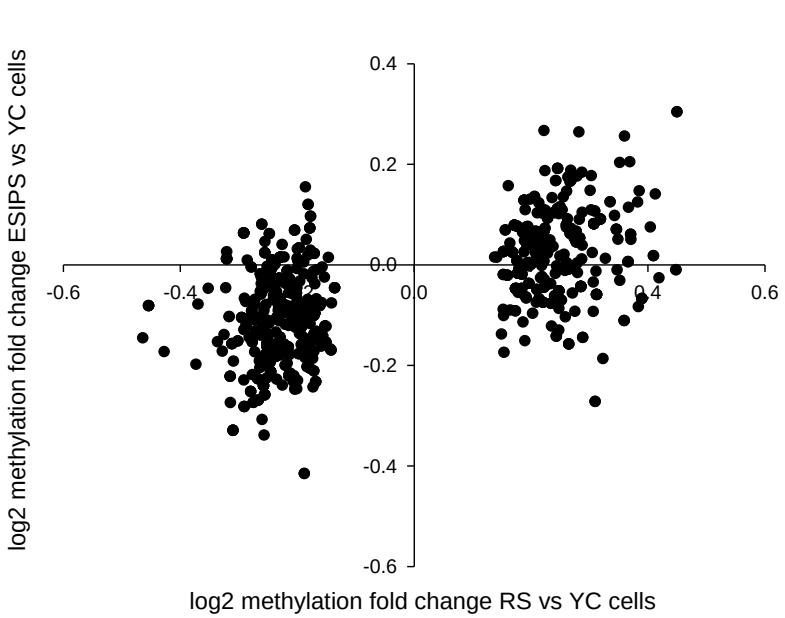

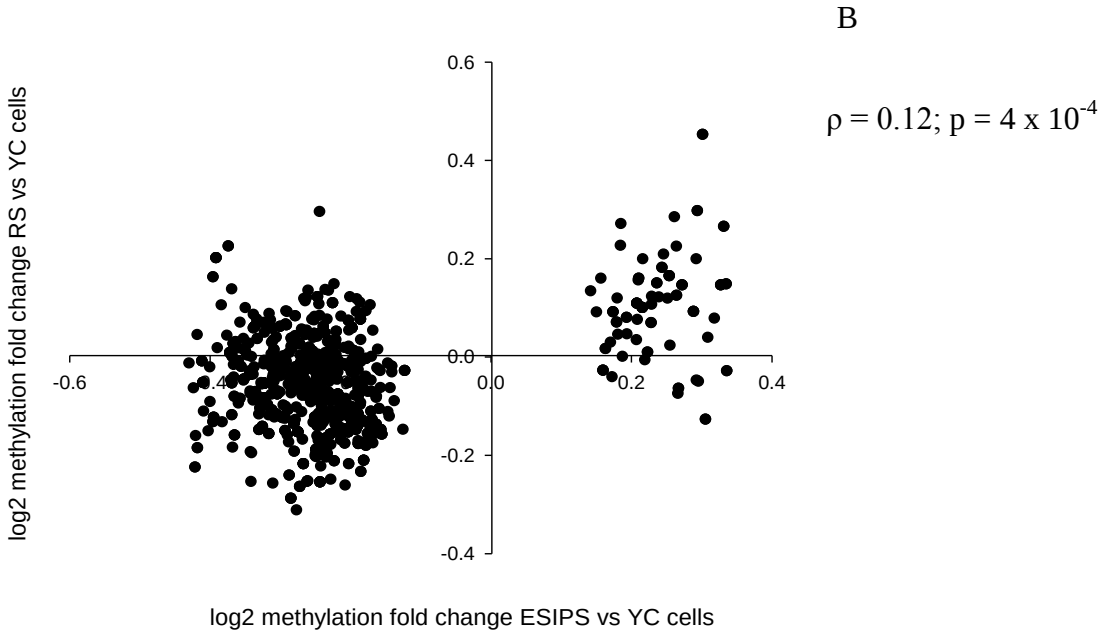

Figure 5.2. Descriptive statistics of MRC-5 cells DNA methylation data: correlation between replicative senescence and early stress-induced premature senescence methylation changes. Panel A: correlation between replicative senescent and early stress-induced premature senescent MRC-5 methylation data; panel B: correlation between early stress-induced premature senescent and replicative senescent MRC-5 methylation data. X-axes show only significant changes while y-axes show all methylation data. The Spearman's rank correlation coefficient (ρ) and the p value for significance are indicated at the top right of each panel.

I then identified 38 genomic regions with common behaviour, i.e. where the changes in methylation seen were similar for both RS vs YC and ESIPS vs YC comparisons. Of these 4 were hypermethylated and 34 were hypomethylated in both RS and ESIPS vs YC cells (Figure 5.3, Table 5.1 and 5.2). These numbers were higher than what would be expected by chance; in fact, the representation factors and hypergeometric probabilities were 9.07 and 9.11 x 10^{-4} for hypermethylation and 6.73 and 8.32 x 10^{-19} for hypomethylation repsectively.

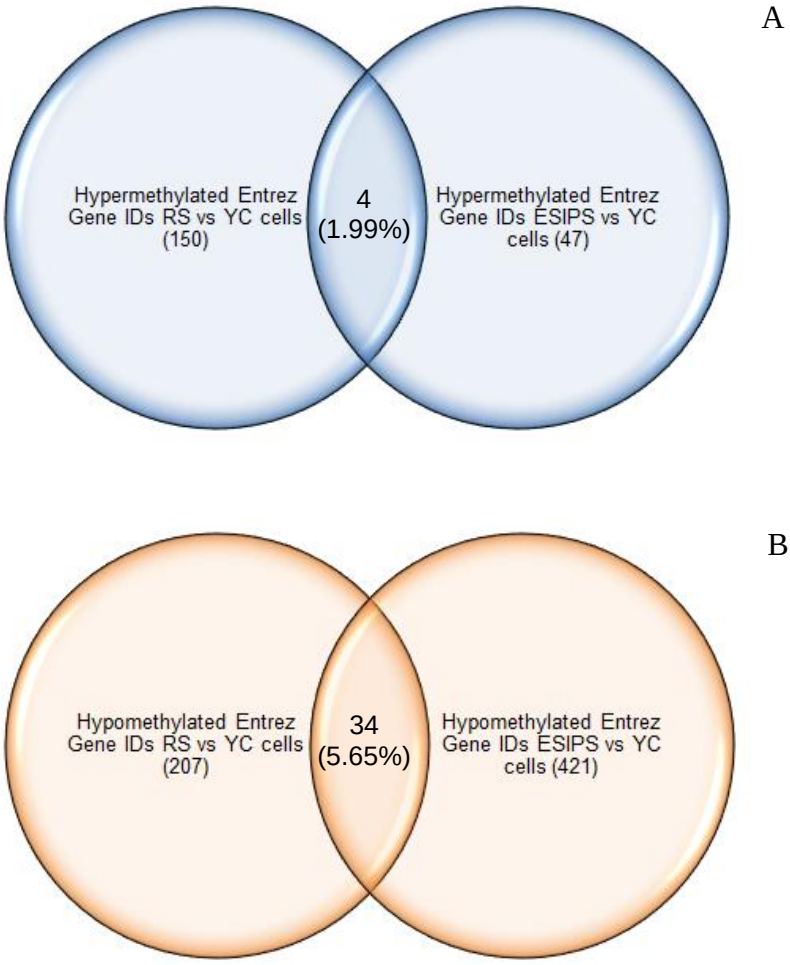

Figure 5.3. Descriptive statistics of MRC-5 cells DNA methylation data: common behaviour for methylation between replicative senescent and early stress-induced premature senescent cells compared with young confluent cells. Panel A: Venn diagram showing the number and percentage of significantly hypermethylated Entrez Gene IDs in common between replicative senescent and early stress-induced premature senescent cells in each case compared with young confluent cells; panel B: Venn diagram showing the number and percentage of significantly hypomethylated Entrez Gene IDs in common between replicative senescent and early stress-induced premature senescent cells in each case compared with young confluent cells.

Table 5.1. List of genes shown as their Entrez Gene IDs and official symbols which were significantly hypermethylated in both replicative senescent and early stress-induced premature senescent cells in each case when compared with young confluent cells.

Entrez Gene ID	**Gene Official Symbol**
924	CD7

3149	HMGB3
7580	ZNF32
27071	DAPP1

Table 5.2. List of genes shown as their Entrez Gene IDs and official symbols which were significantly hypomethylated in both replicative senescent and early stress-induced premature senescent cells in each case when compared with young confluent cells.

Entrez Gene ID	**Gene Official Symbol**
118	ADD1
818	CAMK2G
1634	DCN
2268	FGR
2972	BRF1
3895	KTN1
4121	MAN1A1
4359	MPZ
4833	NME4
4884	NPTX1
5534	PPP3R1
5830	PEX5
7483	WNT9A
10455	ECI2
10509	SEMA4B
22884	WDR37
23598	PATZ1
23641	LDOC1
26292	MYCBP
27164	SALL3
51646	YPEL5
55608	ANKRD10
56172	ANKH
57156	TMEM63C
57473	ZNF512B
80305	TRABD
80323	CCDC68
80331	DNAJ5C
84504	NKX6-2
128372	OR6N1

130271	PLEKHH2
220988	HNRNPA3
246330	PELI3
389136	VGLL3

Although pathway enrichment analyses using the full list of 38 genes did not produce any significant result, Gene Ontology (GO) terms enrichment analyses identified 7 molecular functions terms and 19 biological processes terms which were significantly enriched when using the list of common hypomethylated genes and 2 molecular functions terms and 1 biological processes term which were significantly enriched when using the list of common hypermethylated genes. Top hits were, respectively, calcium-dependent protein serine/threonine phosphatase activity and transmission of nerve impulse for hypomethylation and phosphatidylinositol-3,4-bisphosphate binding and homeostasis of number of cells within a tissue for hypermethylation.

To further unravel the biological meaning of the methylation data, I then considered the data sets for RS and ESIPS cells separately and ran pathway analyses on all significant differentially methylated Entrez Gene IDs (Appendix E, Table E.1 and Table E.2). Using data for replicative senescent cells yielded only one enriched canonical pathway, the Caspase 3 activation signalling, or TNFR1 signalling pathway (Table 5.3). However, analysis of data from the early induced stress premature senescent cells yielded 5 enriched canonical pathways which were the signalling events mediated by Class III Histondeacetylases, the JNK and NF-kB cascade, N-cadherin and SMAD2/3 signalling and the IFN-γ and VEGFR1 pathways (Table 5.4).

Table 5.3. Enriched pathways for significant differentially methylated Entrez Gene IDs between RS and YC MRC-5 cells.

Enriched Pathway	**Genes observed/total**	**p value**	**Hypomethylated genes/Hypermethylated genes**
TNF signalling	4/32	7.36×10^{-3}	2/2

Table 5.4. Enriched pathways for significant differentially methylated Entrez Gene IDs between ESIPS and YC MRC-5 cells.

Enriched pathway	**Genes observed/total**	**p value**	**Hypomethylated genes/Hypermethylated genes**
Signalling events mediated by HDAC Class III	16/40	5.60×10^{-15}	14/1
CD28 signalling (CD4 T cell receptor signalling (JNK cascade))	8/53	1.59×10^{-4}	8/0
N-cadherin signalling events	6/35	5.43×10^{-4}	6/0
Regulation of cytoplasmic and nuclear SMAD2/3 signalling	4/21	3.25×10^{-3}	4/0
IKK-NF-kappaB cascade (CD4 T cell receptor signalling)	8/94	7.14×10^{-3}	8/0
IFN-gamma pathway	5/43	9.09×10^{-3}	5/0
VEGFR1 specific signals	4/28	9.44×10^{-3}	4/0

5.3 Genome-wide gene expression of replicative senescent and early stress-induced premature senescent MRC-5 cells compared with young confluent cells

Figure 5.4 shows volcano plots for the genome-wide expression data of RS compared with young confluent (YC) cells (left) and ESIPS compared with YC cells (right), significant hits lie above the blue line, which corresponds to the significance cut off (p = 0.05). 32.84% and 16.82% of Entrez Gene IDs showed significant different expression between the comparison groups (RS vs YC and ESIPS vs YC, respectively); these corresponded to 5596 and 2866 genes. Of those, about 48% were up-regulated and 52% were down-regulated in RS vs YC cells, while about 52% were up-regulated and 48% were dowregulated in ESIPS vs YC cells (data not shown). For a complete list of all the significant hits see CD insert.

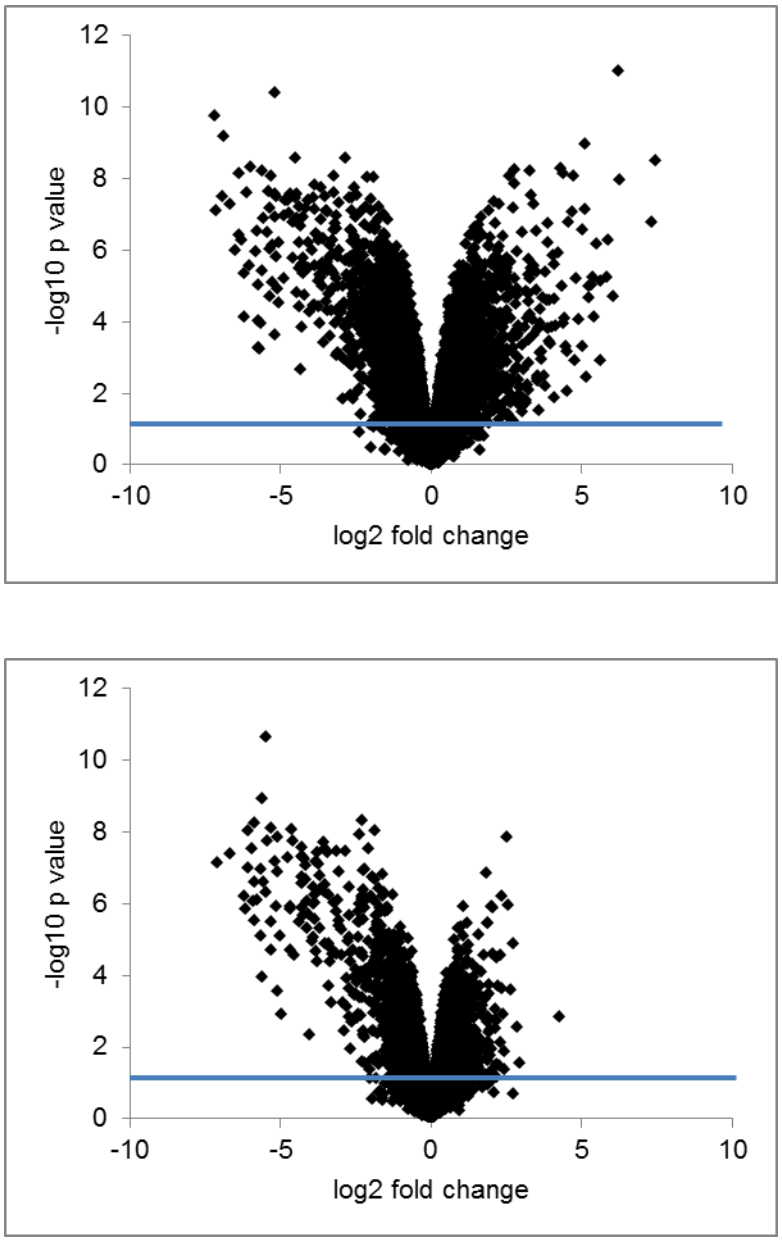

Figure 5.4. Descriptive statistics of MRC-5 cells gene expression data shown as volcano plots. Panel A: volcano plot showing the distribution significance/fold change of the expression data for replicative senescent MRC-5 cells in comparison with young confluent cells; the Panel B: volcano plot showing the distribution significance/fold change of the expression data for early stress-induced premature senescent MRC-5 cells in comparison with young confluent cells. Blue lines indicate the cut off above which the statistical significance criteria is met ($p < 0.05$ for unpaired student's t-test).

As for the equivalent genome-wide methylation data sets, to assess if there was a relationship between the expression changes of the two pairs of comparison groups, I calculated the Spearman rank order correlation coefficient for all the significant

differentially expressed Entrez Gene IDs in RS vs YC against all Entrez Gene IDs for ESIPS vs YC cells. As shown in Figure 5.5, left panel, this correlation was significant and positive. Figure 5.5, right panel, shows the same analysis done with all significant differentially expressed Entrez Gene IDs in ESIPS vs YC against all Entrez Gene IDs for RS vs YC cells: here, the Spearman rank order correlation coefficient was also significant and even higher than in the previous case. In both comparisons, the analyses indicated that expression changes occurred in the same direction in RS and ESIPS when compared with YC cells.

A

$\rho = 0.69$; $p = 2 \times 10^{-7}$

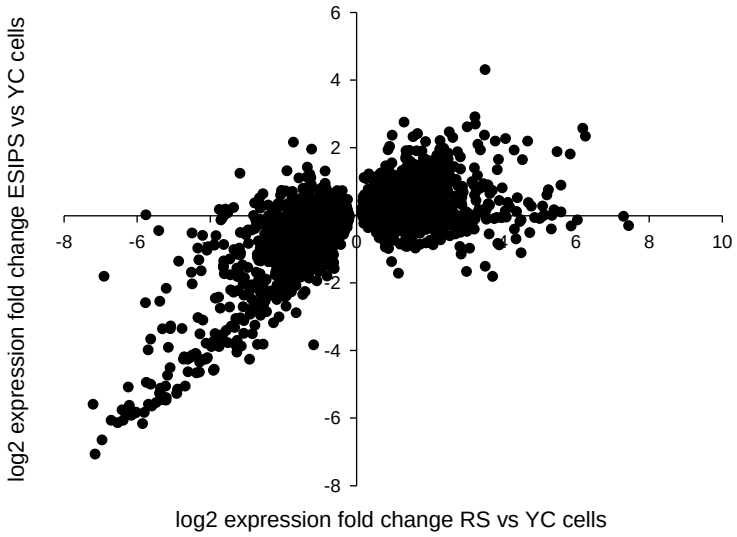

B

$\rho = 0.82$; $p = 2 \times 10^{-7}$

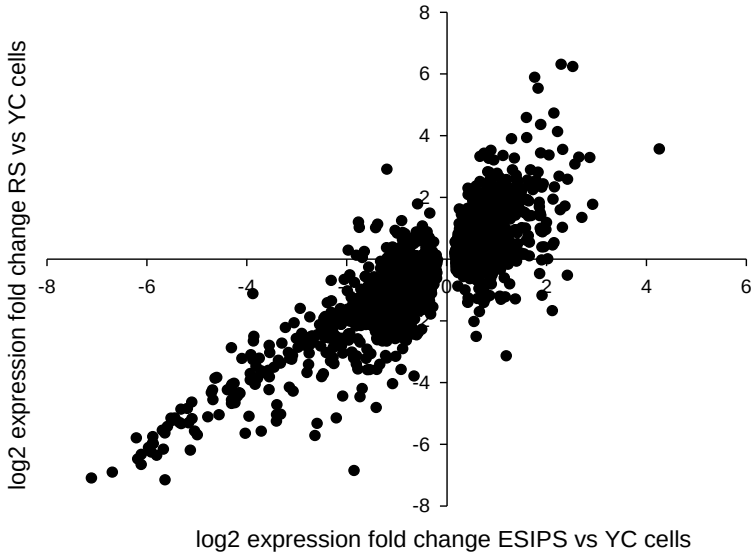

Figure 5.5. Descriptive statistics of MRC-5 cells gene expression data: correlation between replicative senescence and early stress-induced premature senescence expression changes. Panel A: correlation between replicative senescent and early stress-induced premature senescent MRC-5 expression data; Panel B: correlation between early stress-induced premature senescent and replicative senescent MRC-5 expression data. X-axes show only significant changes while y-axes show all expression data. The Spearman's rank correlation coefficient (ρ) and the p value for significance are indicated at the top right of each panel.

Comparison of the lists of significantly expressed Entrez Gene IDs revealed that 838 hits (25.37%) were commonly up-regulated, while 1072 hits (32.99%) were commonly down-regulated in both RS and ESIPS vs YC cells (Figure 5.6, panels A and B, respectively). Those numbers were higher than would be expected by chance; in fact, representation factors were 3.63 and 4.49 for up-regulation and down-regulation, respectively, and hypergeometric probability was 0 in both cases.

A

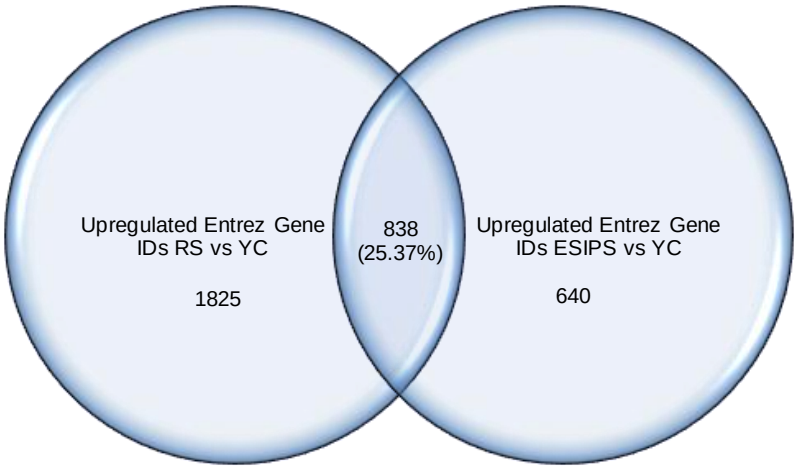

B

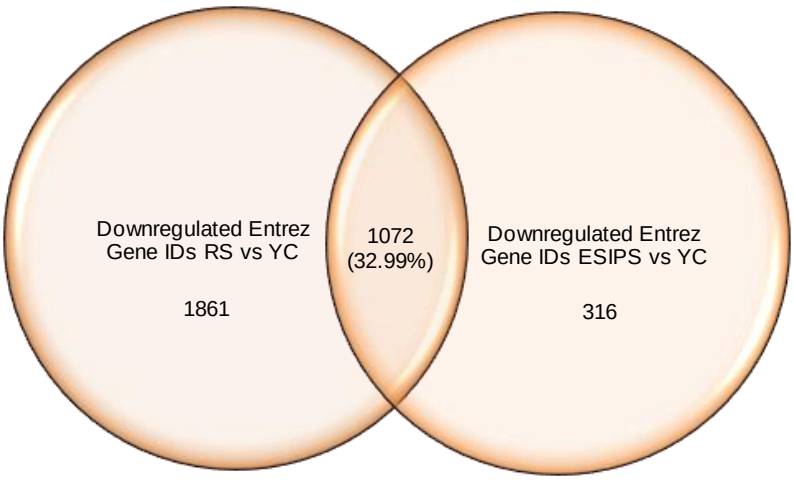

Figure 5.6. Descriptive statistics of MRC-5 cells gene expression data: common behaviour for expression between replicative senescent and early stress-induced premature senescent cells. Panel A: Venn diagram showing the number and percentage of significantly up-regulated Entrez Gene IDs in common between replicative senescent and early stress-induced premature senescent cells in each case compared with young confluent cells; Panel B: Venn diagram showing the number and percentage of significantly down-regulated Entrez Gene IDs in common between replicative senescent and early stress-induced premature senescent cells in each case compared with young confluent cells.

Pathway analyses performed using the gene expression data sets for RS and ESIPS cells separately revealed several commonly enriched terms, many of them being cell cycle regulation and cell growth related (Table 5.5 and Table 5.6).

Table 5.5. Enriched pathways for significant differentially expressed Entrez Gene IDs between RS and YC MRC-5 cells.

Enriched Pathway	**Genes observed/total**	**p value**	**Up-regulated genes/Down-regulated genes**
PLK1 signalling events	28/46	5.70×10^{-5}	4/24
cdk regulation of dna replication	14/18	9.46×10^{-5}	2/12
E2F transcription factor network	41/78	1.42×10^{-4}	7/34
ATR signalling pathway	24/40	2.66×10^{-4}	0/24
cell cycle: g1/s check point	18/28	4.86×10^{-4}	5/13
Effects of Botulinum toxin	8/9	7.12×10^{-4}	7/1
Aurora B signalling	23/40	8.33×10^{-4}	1/22
cyclins and cell cycle regulation	15/23	1.17×10^{-3}	8/7
Regulation of retinoblastoma protein	33/66	1.93×10^{-3}	12/21
spliceosomal assembly	7/8	1.97×10^{-3}	0/6
Hedgehog signalling events mediated by Gli proteins	25/48	3.32×10^{-3}	6/19
Regulation of Telomerase	35/73	3.53×10^{-3}	10/25
p73 transcription factor network	35/75	6.10×10^{-3}	14/21
mechanisms of transcriptional repression by dna methylation	10/15	6.51×10^{-3}	2/8
btg family proteins and cell cycle regulation	7/9	6.72×10^{-3}	2/5
Signalling events mediated by HDAC	33/71	8.24×10^{-3}	12/21

Class I			
BARD1 signalling events	18/34	9.78×10^{-3}	0/18

Table 5.6. Enriched pathways for significant differentially expressed Entrez Gene IDs between ESIPS and YC MRC-5 cells.

Enriched Pathway	**Genes observed/total**	**p value**	**Up-regulated genes/Down-regulated genes**
ATR signalling pathway	25/40	4.73×10^{-10}	4/21
PLK1 signalling events	23/46	7.26×10^{-7}	4/19
Aurora B signalling	20/40	3.92×10^{-6}	2/18
E2F transcription factor network	31/78	4.84×10^{-6}	3/28
cdk regulation of dna replication	12/18	7.21×10^{-6}	1/11
role of brca1 brca2 and atr in cancer susceptibility	12/22	1.23×10^{-4}	2/10
ATM pathway	15/36	8.03×10^{-4}	2/13
BARD1 signalling events	14/34	1.38×10^{-3}	1/14
Regulation of Telomerase	24/73	1.57×10^{-3}	7/17
Aurora A signalling	13/31	1.67×10^{-3}	4/9
estrogen responsive protein efp controls cell cycle and breast tumours growth	8/15	2.15×10^{-3}	2/6
cell cycle: g2/m checkpoint	10/22	2.81×10^{-3}	5/5
Caspase cascade in apoptosis	18/52	3.15×10^{-3}	8/10
p53 signalling pathway	7/13	3.85×10^{-3}	4/3
cyclins and cell cycle regulation	10/23	4.17×10^{-3}	4/6
FOXM1 transcription factor network	15/42	4.88×10^{-3}	2/13
brca1 dependent ub ligase activity	5/8	6.59×10^{-3}	0/5
Validated targets of C-MYC transcriptional activation	25/87	9.31×10^{-3}	3/22

5.4 Validation of data from methylation arrays by means of MeDIP-qPCR

To validate the array methylation data, I sorted both RS vs YC and ESIPS vs YC data sets applying a significance cut off ($p < 0.05$) and then selected the most significant hits that appeared in a CpG island of at least 50 bp. The presence of CpG islands was assessed using the webtool "CpG finder": http://www.ebi.ac.uk/Tools/emboss/cpgplot/. In this program, the default minimal length for CpG islands is set to 200 bp, but this parameter

was changed to 50 bp to make qPCR primer design easier under the chosen conditions (see section 2.8). Those regions were mapped to the *PRDM8* gene promoter for RS cells and the *DCHS1* gene promoter for ESIPS cells, respectively. To select additional candidates for both groups, I selected significant regions presenting CpG island computed as described above that also appeared among genes with the highest or lowest fold change and for which it was possible to design good qPCR assays. Those regions were mapped to the promoters of *CD7* and *RAB5C* genes for RS cells and *MLNR* and *OR5AP2* genes for ESIPS cells. The details of the qPCR reactions set up and conditions, primers sequences, dilution and melt curves for all assays are given in section 2.5, Table 2.3 and Appendix A. Results of these validations are shown in Figure 5.7 and, with two minor exceptions, were mostly in agreement with the methylation fold changes inferred from the methylation arrays, with a validation rate of 83.33% (see Table 5.7). The minor exceptions were the *PRDM8* and *RAB5C* gene promoters, where MeDIP-qPCR results revealed a significant hypermethylation when comparing either RS or ESIPS cells with YC cells, while the arrays did not show any significant methylation changes under the same conditions. However, it should be noted that the fold changes detected with both techniques were relatively small. In addition, whilst the arrays were performed for three separate immunoprecipitations (i.e. estimated fold changes are the average of 3 independent replicates), the MeDIP-qPCR was performed only on one sample and so the reliability of the latter measurement is likely to be lower.

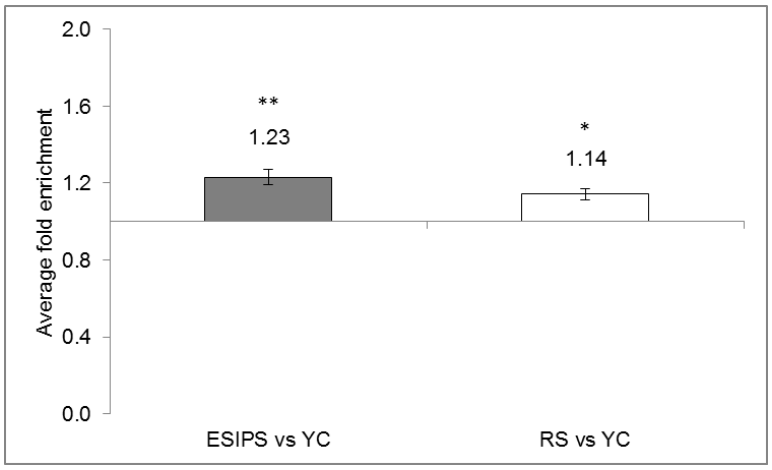

A

B

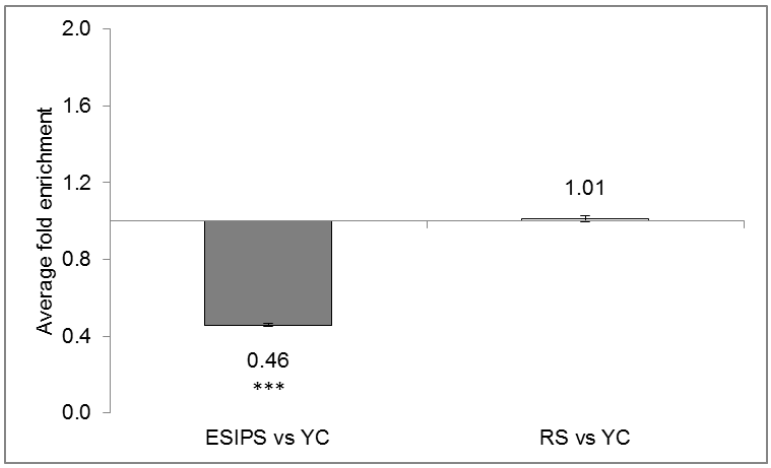
2.0
1.6
1.2
0.8
0.4
0.0
Average fold enrichment
1.01
0.46
***
ESIPS vs YC
RS vs YC

C

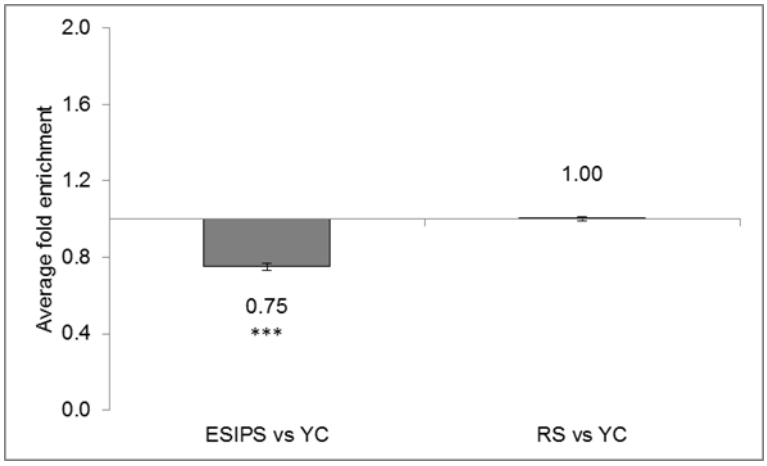
2.0
1.6
1.2
0.8
0.4
0.0
Average fold enrichment
1.00
0.75
***
ESIPS vs YC
RS vs YC

D

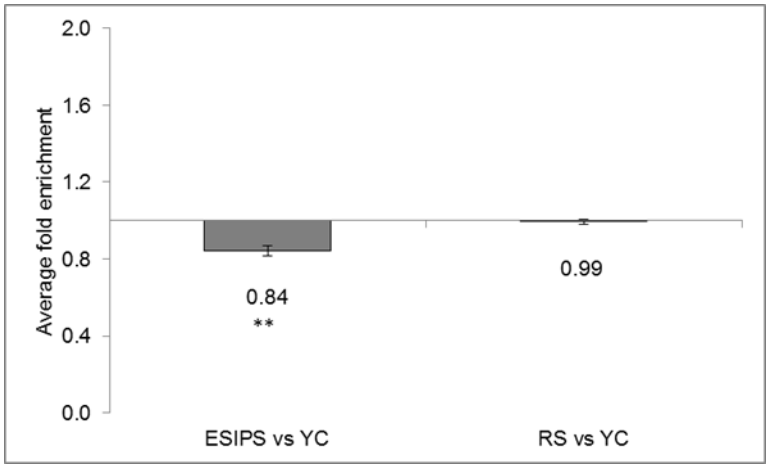
2.0
1.6
1.2
0.8
0.4
0.0
Average fold enrichment
0.99
0.84
**
ESIPS vs YC
RS vs YC

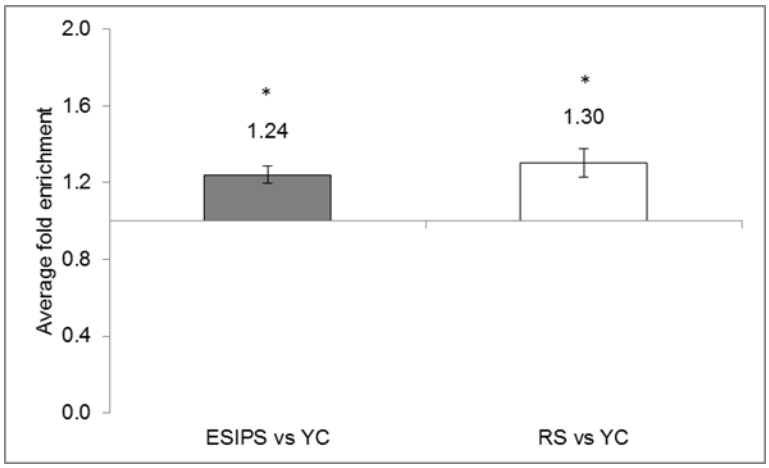

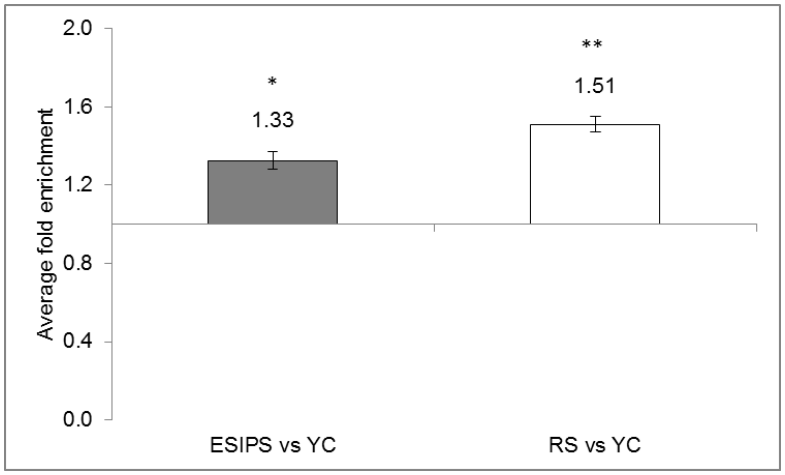

*Figure 5.7. DNA Methylation arrays validation by means of MeDIP-qPCR. Panels A, B, C, D, E and F show, respectively, methylation enrichment for CD7, DCHS1, MLNR, OR5AP2, PRDM8 and RAB5C genomic regions in MeDIPed samples compared with their related Inputs as calculated from qPCR data normalized on the Spike Negative Control content, as described in Chapter 4. Bar charts show average enrichment for one experiment; error bars show ± SEM of 3 technical replicates. * = p < 0.05; ** = p < 0.01; *** = p < 0.001 for student's unpaired t-test.*

Table 5.7. Methylation fold changes as calculated from Roche Nimblegen DNA Methylation Arrays and from MeDIP-qPCR assays for the MeDIP-qPCR validation candidates (see Figure 5.7). Unless otherwise indicated with (n.s.), values are statistically significant ($p < 0.05$ for student's unpaired t-test).

Genomic region	**ESIPS vs YC methylation fold change (array)**	**ESIPS vs YC methylation fold change (MeDIP-qPCR)**	**RS vs YC methylation fold change (array)**	**RS vs YC methylation fold change (MeDIP-qPCR)**
CD7	1.23	1.23	1.37	1.14
DCHS1	0.75	0.46	0.89 (n.s.)	1.01 (n.s.)
MLNR	0.77	0.75	1.07 (n.s.)	1.00 (n.s.)
OR5AP2	0.74	0.84	0.99 (n.s.)	0.99 (n.s.)
PRDM8	0.99 (n.s.)	1.24	1.37	1.30
RAB5C	1.11 (n.s.)	1.33	1.31	1.51

5.5 Validation of gene expression arrays by means of RT-qPCR

To validate the gene expression data, I selected candidates from both groups of comparison; these were the most significant differentially expressed Entrez Gene IDs, the significant IDs with the lowest fold change and the highest fold change. For the RS vs YC comparison, those were, respectively, *CCNB2*, *TMSB15A* and *PNMA2*, while for ESIPS vs YC comparison, these were *CCNB2*, *DLGAP5* and *MMP3*. As *CCNB2* was common to both groups, a further candidate was selected in *MMP3* by going down in the significance list for the ESIPS vs YC group. I then designed and optimized RT-qPCR assays; reactions set up and conditions, primers sequences, dilution and melt curves for all assays are given in section 2.13, Table 2.5 and Appendix A.

Figure 5.8 shows expression ratios normalized to *GAPDH* for the selected genes; although fold changes were substantially different from the ones calculated from the Affimetrix Gene Expression Arrays data sets, the trend of the changes was confirmed for all the validation candidates (see Table 5.8).

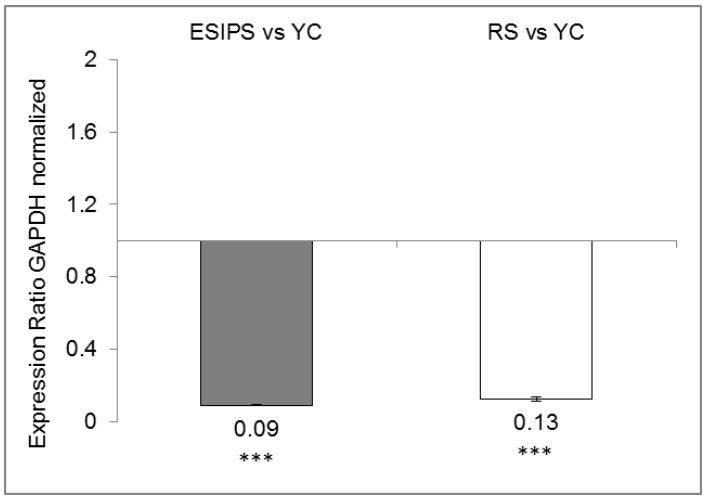
ESIPS vs YC
RS vs YC
Expression Ratio GAPDH normalized
2
1.6
1.2
0.8
0.4
0
0.09
***
0.13
***

A

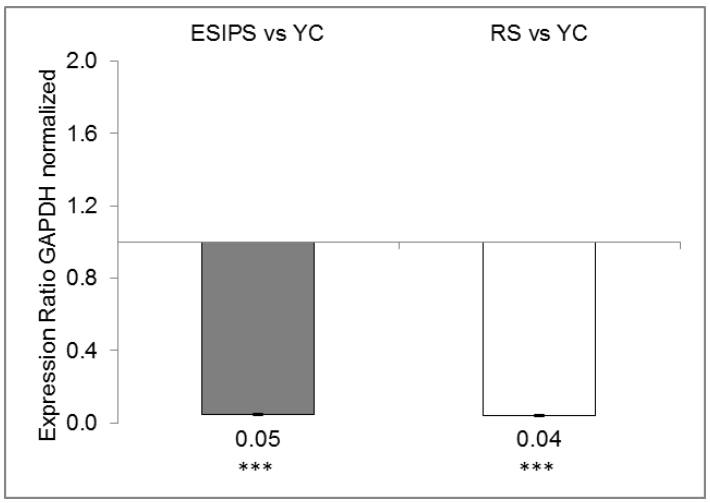
ESIPS vs YC
RS vs YC
Expression Ratio GAPDH normalized
2.0
1.6
1.2
0.8
0.4
0.0
0.05
***
0.04
***

B

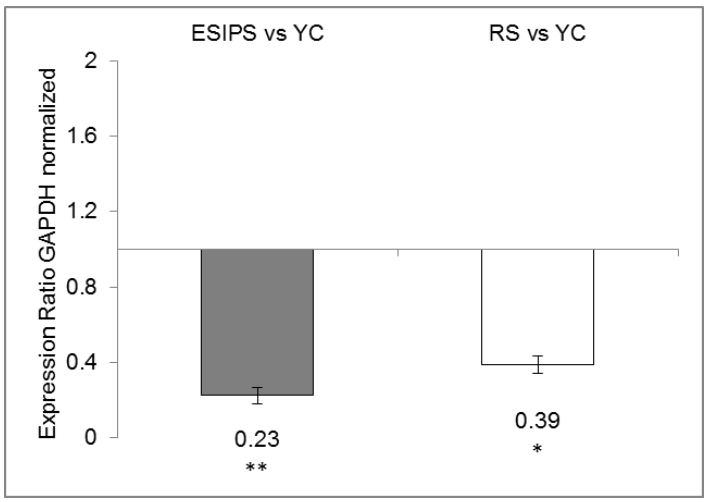
ESIPS vs YC
RS vs YC
Expression Ratio GAPDH normalized
2
1.6
1.2
0.8
0.4
0
0.23
**
0.39
*

C

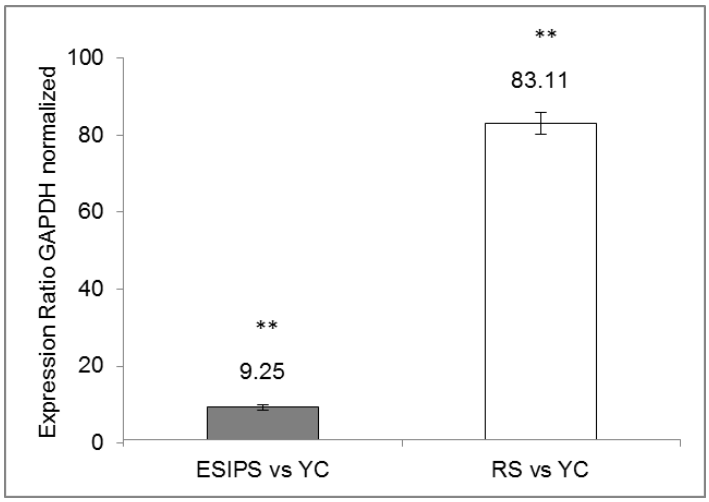

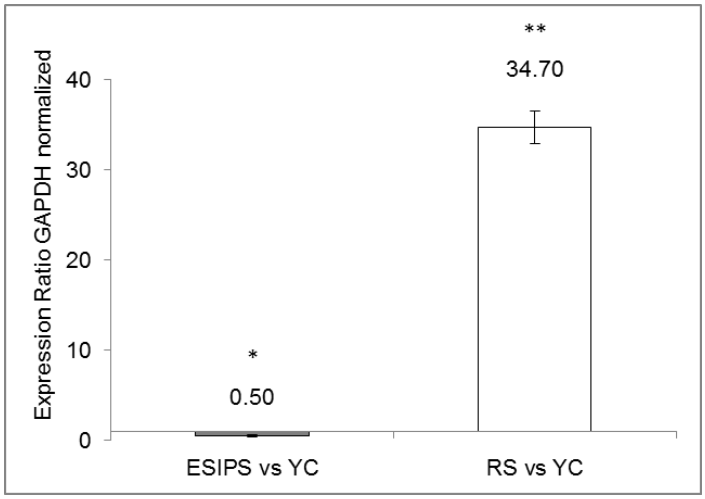

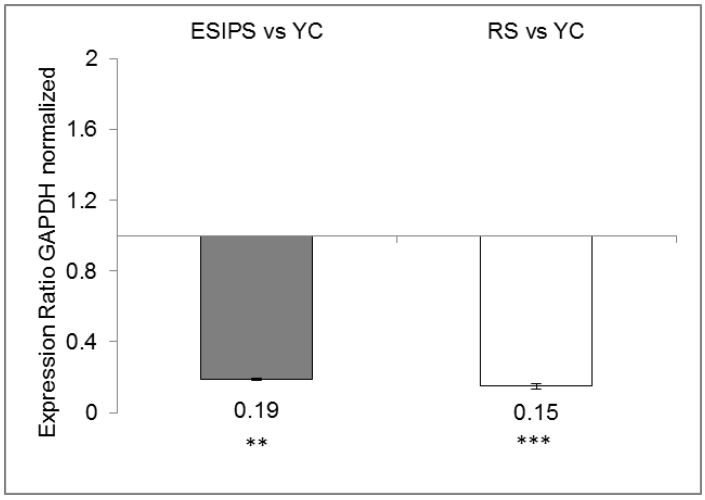

Figure 5.8. Validation of gene expression arrays by means of RT-qPCR. Panels A to F: CCNB2, DLGAP5, FANCG, MMP3, PNMA2, TMSB15A relative cDNA content in ESIPS and RS MRC-5 fibroblasts compared with YC fibroblasts; expression data are normalized

*on GAPDH cDNA content and plotted as average fold change of 3 technical replicates ± SEM. * = p < 0.05; ** = p < 0.01; *** = p < 0.001 for student's unpaired t-test.*

Table 5.8. Gene expression fold changes as calculated from Affimetrix Gene Expression Arrays and from RT-qPCR assays for the RT-qPCR validation candidates (see Figure 5.8). All the values shown in the Table are statistically significant ($p < 0.05$ for student's unpaired t-test).

Gene	**ESIPS vs YC expression fold change (array)**	**ESIPS vs YC expression fold change (RT-qPCR)**	**RS vs YC expression fold change (array)**	**RS vs YC expression fold change (RT-qPCR)**
CCNB2	0.02	0.09	0.03	0.13
DLGAP5	0.007	0.05	0.007	0.04
FANCG	0.2	0.23	0.2	0.39
MMP3	19.4	9.25	11.6	83.11
PNMA2	0.79	0.5	177	34.7
TMSB15A	0.02	0.19	0.007	0.15

5.6 Integration of methylation and expression arrays data sets and choice of regions of interest for combined methylation-expression functional studies

Having assessed the reliability of both arrays datasets, I wanted to determine whether changes in promoter methylation could be causal for changes in expression of the corresponding gene. For this purpose, I selected four genomic regions/genes of interest from the replicative senescent cells data which showed either the expected inverse correlation between methylation and gene expression or opposite than expected correlation i.e. direct correlation between methylation and gene expression. The selection process consisted of four steps:

1. the methylation data set for RS vs YC cells was sorted as described in section 2.11.3 to produce two lists of Entrez Gene IDs/regions of interest, one containing all hits showing either +2 or -2 of difference in enrichment score (list 1A) and one containing all hits showing enrichment score lower than 2 in one sample and higher than 2 in the other (list 1B);

2. all Entrez Gene IDs in list 1A and 1B which, in parallel, did not show any significant change in gene expression were excluded from next steps;
3. the resulting candidate genomic regions from point 2 were analyzed with the program PromoterInspector (available on the Genomatix platform: http://www.genomatix.de/) for the presence of experimentally verified or computed regulatory elements and only the positive ones were used in step 4;
4. the final selection was done choosing the genomic regions from step 3 for which pyrosequencing assays were commercially available.

The selection process yielded 4 Entrez Gene IDs/genomic regions of interest, whose methylation and expression data are summarized in Table 5.9. The candidate gene with the expected negative relationship between promoter methylation and gene expression expression was *CTTN* and the candidates with the contrasting positive relationship between methylation and gene expression were *GLIPR2*, *NPTX1* and *SLC39A14*.

Table 5.9. Entrez Gene IDs candidates for methylation-expression integration studies and functional studies. Unless indicated by (n.s.), fold changes are statistically significant ($p < 0.05$ for student's unpaired t-test).

Entrez Gene ID	**Gene symbol**	**Methylation fold change RS vs YC**	**Expression fold change RS vs YC**	**Methylation fold change ESIPS vs YC**	**Expression fold change ESIPS vs YC**
2017	*CTTN*	0.82	1.33	0.84 (n.s.)	1.25
152007	*GLIPR2*	0.83	0.57	0.94 (n.s.)	0.82 (n.s.)
4884	*NPTX1*	0.86	0.15	0.89 (n.s.)	0.78 (n.s.)
23516	*SLC39A14*	0.89	0.60	0.90 (n.s.)	0.90 (n.s.)

5.7 Pyrosequencing and gene expression analyses of genomic regions of interest

To investigate CpG methylation in the chosen candidates, I obtained pyrosequencing primers from QIAgen. The relevant assays and experimental conditions are described in section 2.20 and the outputs from quality controls are presented in Appendix C. To quantify gene expression for the same candidates, I designed and optimized RT-qPCR assays and the relevant experimental conditions, primers sequences, dilution curves and melt curves are presented in section 2.13, Table 2.5 and Appendix A.

Figure 5.9, Figure 5.11, Figure 5.13 and Figure 5.15 illustrate the genomic regions identified by the methylation arrays and the CpG sites investigated by the pyrosequencing assays; Figures 5.10, Figure 5.12, Figure 5.14 and Figure 5.16 present methylation and expression data obtained by pyrosequencing and RT-qPCR, respectively.

5.7.1. CTTN promoter CpG methylation and gene expression measurement

Figure 5.10 shows the pyrosequencing and RT-qPCR validation results for the first candidate gene, *CTTN*. The results showed significant hypermethylation at the second CpG under investigation for the comparison RS vs YC MRC-5 cells (panel A). This was opposite of what seen in the data from the methylation arrays, where hypomethylation was detected (see Table 5.9). Significant gene up-regulation was found for the RS vs YC comparison only (panel B), partially confirming the transcriptome data, where significant up-regulation was detected also for the ESIPS vs YC cells comparison (see Table 5.9).

>gi|51468880:467208-468208 Homo sapiens chromosome 11 genomic contig, reference assembly, genomic build 36.3

1 gcaggggggcg gggtcgcgcg gggacccggg tgcggccccg cccccgccct cggaaccggg

61 agtagagcct ggtgcctggg agcggctggc gcggcggaat ccagggccga cccgggccgg

121 accgacccca ggcggcggtg agcgagcgcg gcgtccgccc ggggtgcagg ccgggctctg

181 cttcttccct cctgtggcgt cgcctggccg cgaaagggga aggaagcggc ggccgcagcg

241 gtctcaccgc tcttccgctt gcggtttcgg gggccggggc agagtggcga ggctttcccg

301 gcctggggcg gggcagggcg agggccgggg gtccgcgagg gccacgagga cgggtctggg

361 cccaaggagg ccgggcaggg ggcaaggggg cacggagggc ttggggctgg ggtccgcgga

421 ggaaggttag aaaggggcca aattggggta tcagctctga ggggagggtc cctgggcgcc

481 gggggctcc agggcaggag aggggccagg ctgggagggg tcttgggtcc gagggaatag

541 gagaggggga tgggctccga gggggagggt attagggccc gagggagagg ggctgggcct

601 gtggggttcg ggggtctgag cggagggggc cggggttcga ggggccaagg aaggtgggtg

661 tgggggtct caaggaaagg gcgaggggtc tgagagggag gtgtctgggt gcagagggaa

721 agggatgagg tccgagggga ggagattggg

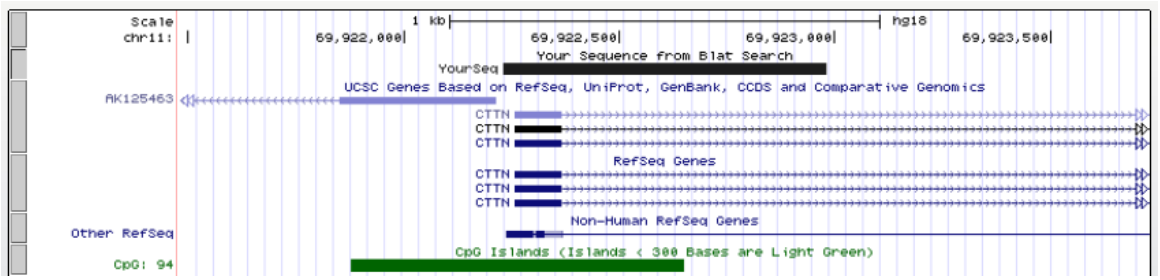

Figure 5.9. CTTN promoter sequence (top) and graphic genomic location (bottom, adapted from http://genome.ucsc.edu/cgi-bin/hgBlat) for differentially methylated region between RS and YC MRC-5 cells as identified by methylation arrays. The sequence and the CpG sites under investigation are underlined and indicated in orange bold font, respectively; TSSs are indicated in blue bold font.

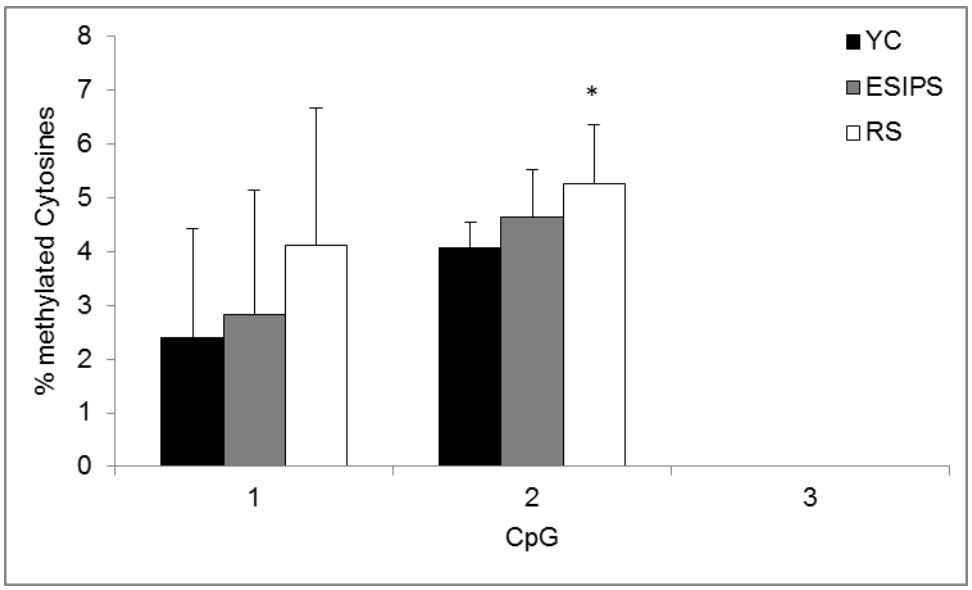

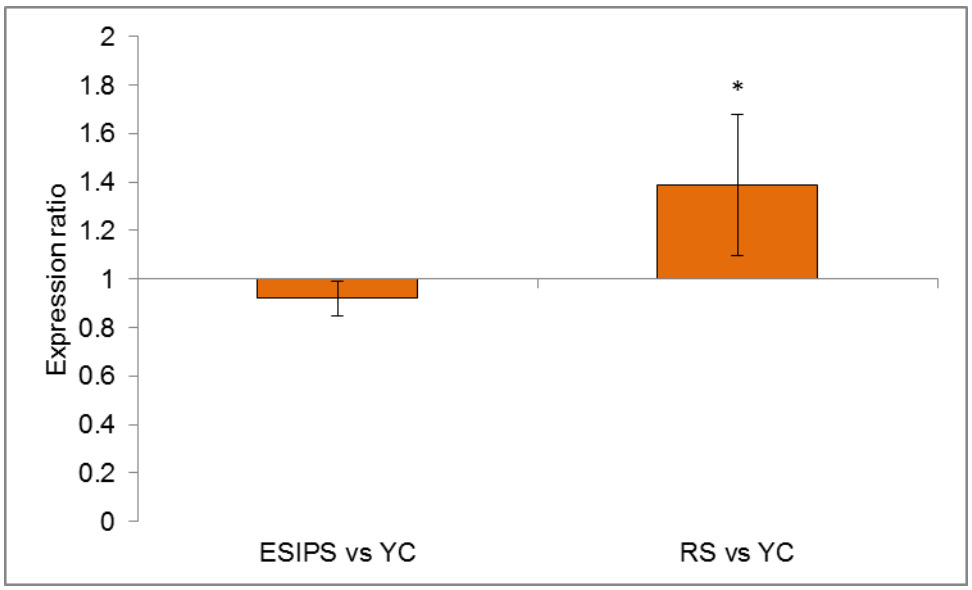

*Figure 5.10. CTTN promoter methylation (panel A) and gene expression (panel B) in replicative senescence and early stress-induced premature senescence. Bar chart in panel A shows average methylation of 3 CpG sites measured by pyrosequencing; error bars represent + SD for at least 8 combined biological and technical replicates. Bar chart in panel B shows gene expression GAPDH-normalized; error bars represent ± SD for 4 biological replicates. * = $p < 0.05$ for student's unpaired t-test.*

5.7.2. GLIPR2 promoter CpG methylation and gene expression measurement

Figure 5.12 shows the pyrosequencing and RT-qPCR validation results for the second candidate gene, *GLIPR2*. Although not significant, there was a trend towards hypermethylation trend in both ESIPS vs YC and RS vs YC cells comparisons (panel A). This was the opposite to what was expected from the methylation array, where hypomethylation was detected for theses comparisons (see Table 5.9). *GLIPR2* expression was down-regulated significantly for both pairs of comparison (panel B), confirming the transcriptome data for the RS vs YC comparison. Whilst the transcriptome array had identified a similar trend for ESIPS vs YC cells, this was not statistically significant (see Table 5.9).

>gi|89029256:36126241-36127241 Homo sapiens chromosome 9 genomic contig, reference assembly

1 gcgtgtccta ggagaggagc atccccctcc ccggaccagc cgccctccgg agcccagagt
61 caccggagat gggggcacac cccggggctg cgtgtgtcgt gtcaggccgc ggcagggaga
121 ggccgtcccc tggtggcgcc ggccggaacg cccctcgtgc cgcgaccgcg cgcccctctg
181 tcctcgccgc gcgtcggcgc agagcagcca cccggggccc agcaggcgcg ggcttcccca
241 cgcgccccgg gaagggacag ctcggtgtgg ggtccgggag gcttgagccc cgcggccgca
301 tccggggagc cctcggcagt cgcggagctg cttcccaggg gtgagctctc cgggaggccc
361 acggggtggc cccgggcgcc tccgccctca gctgtcgctc cttataaggc gggggccggg
421 cggcgccgga ggagggggccg cggcatcagc ccggtcctgg gctctggggc ggcgctgggc
481 cgggcgagcg cagtgcagcg cagccgcggg gagcgaggag cgcgcggagc cggccatggg
541 caagtcaggt gagcccgcgg gctcgcccgc tgcggaatgg ttcggaaccc cgcgctcccg
601 gacctcgccg tctccctcgt ccgccgcaag ccaggtcctg gggagtgcgg gagcccgggg
661 tgcgggtgga gggcgcgcgg gcggagcgcc ccggcgcggt ttccggggaa cccgggggga
721 aggcgagccc gagggaggcc cccgccggag agccggggat cgcgccaagt tgggcttccc
781 gaccctgagg ggctgcgcgc cgcggcccgc caaggcgtgg cttctgcttt gtttcaggag

841 gccagactta gagttggaaa agtcaccaaa gtgtgacaac agctctcgct g**cg**aagcagt

901 ttgccccgct cggctgtccc gaggacagcc ctgagcatcc ccctcatcca tttgttgttc

961 cttctctcct gagcgcccgc gccgtgccgg gctccccctg t

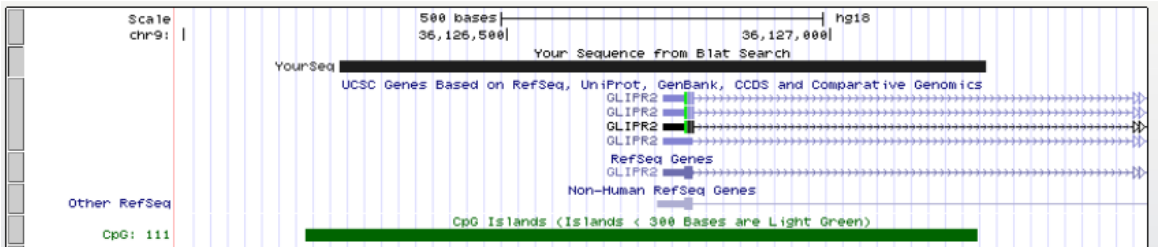

Figure 5.11. GLIPR2 promoter sequence (top) and graphic genomic location (bottom, adapted from http://genome.ucsc.edu/cgi-bin/hgBlat) for differentially methylated region between RS and YC MRC-5 cells as identified by methylation arrays. The sequence and the CpG sites under investigation are underlined and indicated in orange bold font, respectively; TSSs are indicated in blue bold font.

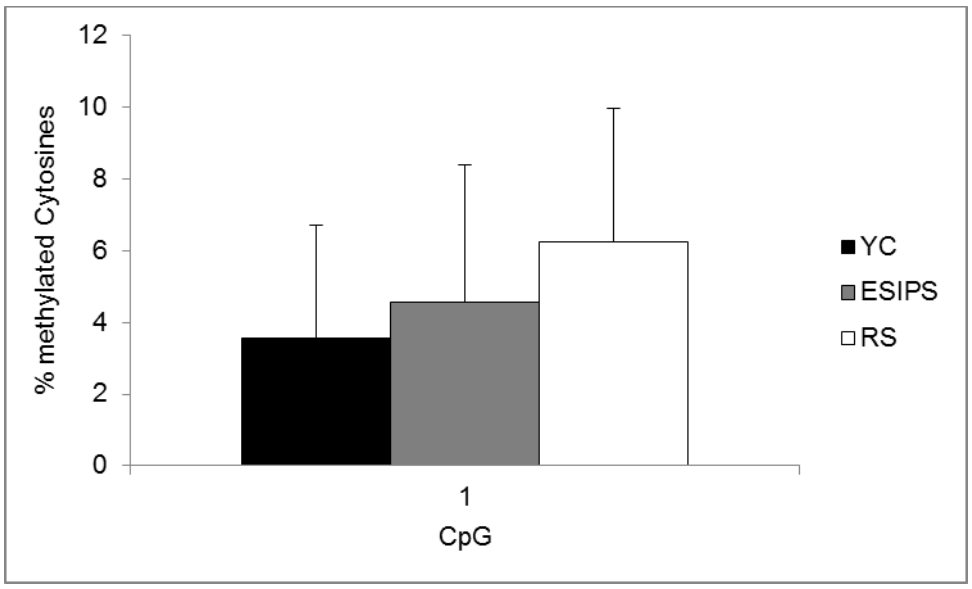

A

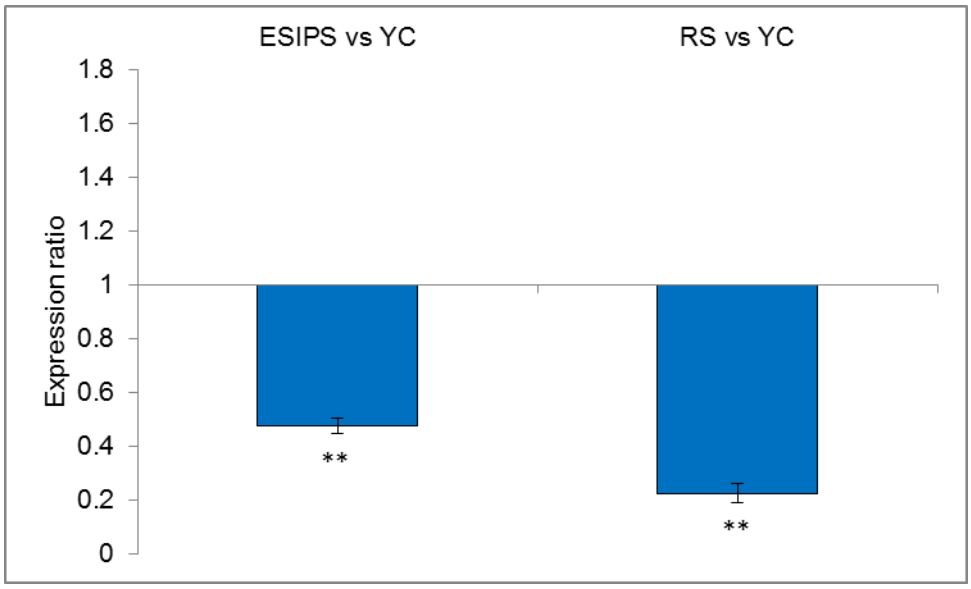

B

*Figure 5.12. GLIPR2 promoter methylation (panel A) and gene expression (panel B) in replicative senescence and early stress-induced premature senescence. Bar chart in panel A shows average methylation of 1 CpG site measured by pyrosequencing; error bars represent + SD for 9 between biological and technical replicates. Bar chart in panel B shows gene expression GAPDH-normalized; error bars represent ± SD for 4 biological replicates. ** = p < 0.001 for student's unpaired t-test.*

5.7.3. NPTX1 promoter CpG methylation and gene expression measurement

Figure 5.14 shows the pyrosequencing and RT-qPCR validation results for the third candidate gene, *NPTX1*: here, a significant hypomethylation was detected in 3 CpG sites for the comparison RS vs YC cells (panel A and panel B); this was in agreement with the the methylation array results (see Table 5.9). No significant gene down-regulation was found for the comparison RS vs YC cells (panel C), although down-regulation trend was detected (see Table 5.9).

>gi|37544588:c854818-854068 Homo sapiens chromosome 17 genomic contig, reference assembly, genomic build 36.3
1 cctggcaagg ggaagctgct ggagacgcgg gcggctgctc ccgcggggcc cccttccgaa
61 gcgccgctgc gaacgtccag ccccggcgac gccgcctgcc cgcgatcggg ccggcgccgc
121 ggacaggaaa ggctcgatca gctaggtctg cctccgagaa gtccccagcg ccccgcccgc
181 acggggtggg gactgacagt cccccgggga cggggccggg tccacagagc ccgggagctg
241 ggggagggga ggcgccgggg gccccgaccc gtgggaagtc cctgtaccca ggctgcccgg

301 cggcttctca atagcaca**cg** gacatctaag aaa**cgcg**ggg **cg**gcc**cg**gtg accccc**g**ctc

361 tggacttagt ggcgcc**g**cga ggccccactc cgagccgttg accaccgggc actcgggtgt

421 tgacgacctg ggtccttggg cacccagcc**c g**gctccaaa**c g**accc**gg**gcc caagggtgtt

481 cagtgcagcc aggagggccg aaccgaattc tatctcccgg acgcggtggt ttcccgcccg

541 cctggagccc cgtcggaggt tcggggacac cacgcaggtg gtccatcctc gagtccgggg

601 ccggagcccg acttccttcc ccctgagctc tcggagcctt cggggcagca gcgccggccc

661 aggcgggggc gggggaggag ggggccgcgg cagctcccag aaggcggggg ggacgcgagc

721 ggaggcagcc ccggtggcgc gctcgtgaga

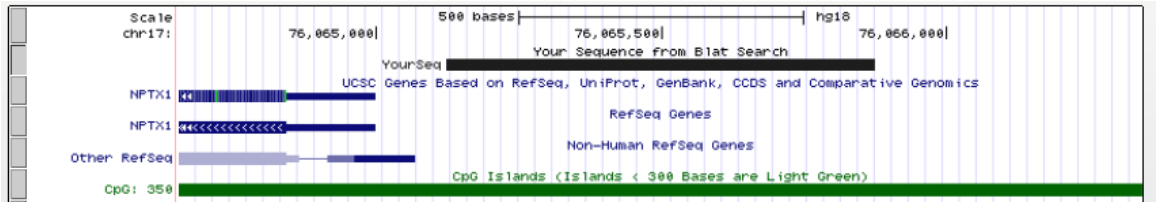

Figure 5.13. NPTX1 promoter sequence (top) and graphic genomic location (bottom, adapted from http://genome.ucsc.edu/cgi-bin/hgBlat) for differentiallly methylated region between RS and YC MRC-5 cells as identified by methylation arrays. The sequence and the CpG sites under investigation are underlined (smooth underline corresponds to assay NPTX1_03 and waved undeline corresponds to assay NPTX1_07) and indicated in orange bold font, respectively; TSS is indicated in blue bold font.

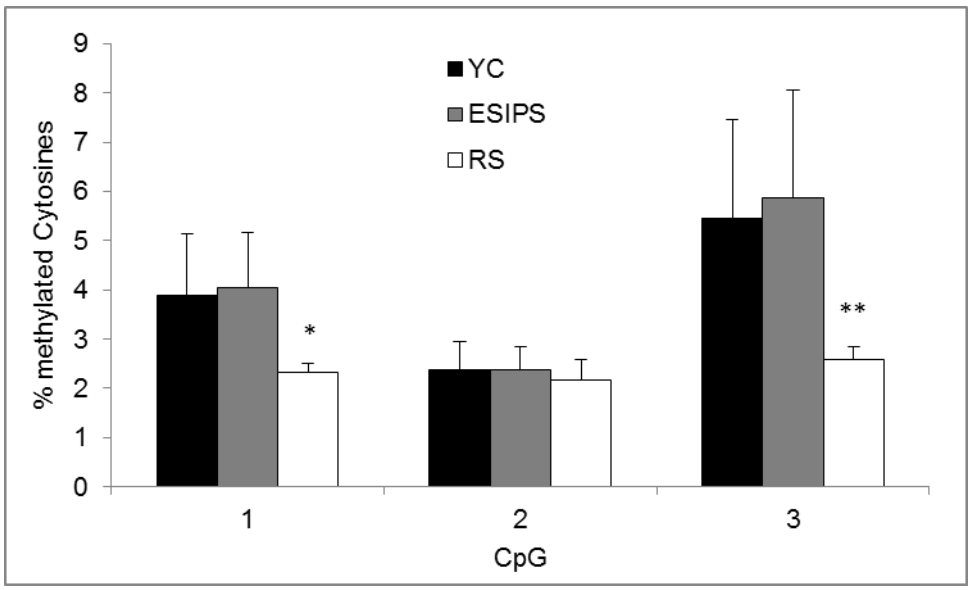

A

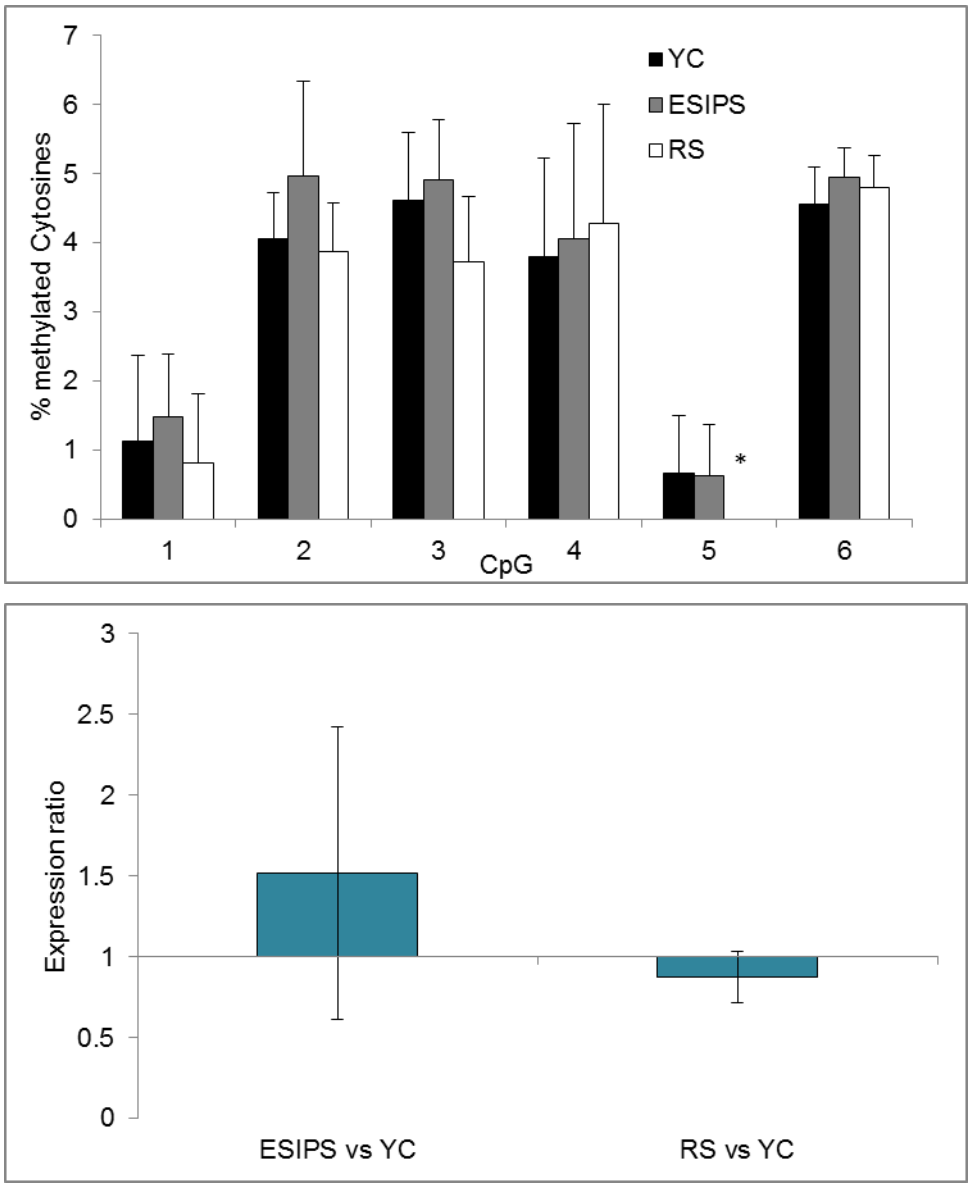

*Figure 5.14. NPTX1 promoter methylation (panel A and panel B) and gene expression (panel C) in replicative senescence and early stress-induced premature senescence. Bar charts in panel A and panel B show average methylation of 3 and 6 CpG sites as measured by pyrosequencing; error bars represent + SD for 9 between biological and technical replicates; * = $p < 0.05$; ** = $p < 0.01$ for Mann-Whitney rank sum test for the comparison RS vs YC. Bar chart in panel C shows gene expression GAPDH-normalized; error bars represent ± SD for 4 biological replicates.*

5.7.4. SLC39A14 promoter CpG methylation and gene expression measurement

Figure 5.16 shows the pyrosequencing and RT-qPCR validation results for the last candidate gene, *SLC39A14*: here, a significant hypomethylation was detected in one of

the CpG sites for the comparison RS vs YC cells (panel A); this was in agreement with the methylation array results (see Table 5.9). No significant gene down-regulation was found for the comparison RS vs YC cells (panel C), although a trend towards dowregulation was detected (see Table 5.9).

>gi|51466739:598730-599480 Homo sapiens chromosome 8 genomic contig, reference assembly, genomic build 36.3

1 gggagggaag agaaaagctt tttgggtgaa ccagaagtgg taaaatcaca ttcaaataga

61 gtgggtagga ctctcctcca gggggtgtgg ggtggaggct aggcggtgag agcttccgcc

121 gcccagggag caggtcttca cgggaggttt ccggaggcag gaggagcctg cgggtcctcg

181 ggagtcacgg ccggatgaag gatgggagcg ggccgccgacc acagccaggg ccgcggaggcg

241 caggagggcg caggctggcc aggtccccag cctgccggcc ccacgtggca gccccggggc

301 gagcggggcg ggccgggggc gggtccggcc gctgacgcgc cgggtatata gccgggcatg

361 cgcgcggtgc cggggccggg acgcagtgag gggggtcggc gcgcgtgtct acgcggacgc

421 accggctaag ctgcttctgc cgccgccggc cgcctgggac cttgcggtga ggctgcgcgg

481 ggccgaggcc gcctccgagc gccaggtgag ggcggggacg ccaagggccg cgggatgggc

541 agcggcggag gagccccgca ccccaggctg gggcagtggg tgggggcggg gacagccctg

601 cgccgaggac cgggcgccgc tcccgggcac cggcacacgc ccggacggct gggtggaggc

661 tgcacctggc cgtggtgccg cgctggcgag gggagaggtc aaggcgcggc ctgtccgcct

721 ggagggtgcg ggatgctaga gccgcagaag

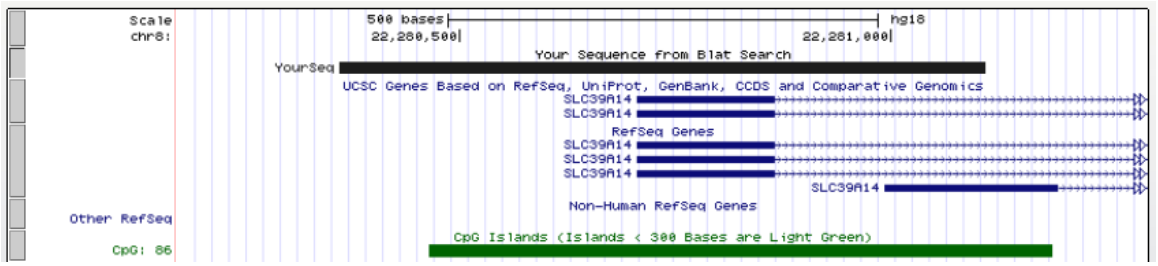

Figure 5.15. SLC39A14 promoter sequence (top) and graphic genomic location (bottom, adapted from http://genome.ucsc.edu/cgi-bin/hgBlat) for differentiallly methylated region between RS and YC MRC-5 cells as identified by methylation arrays. The sequences and the CpG sites under investigation are underlined (smooth underline corresponds to assay SLC39A14_01 and waved undeline corresponds to assay SLC39A14_02) and indicated in orange bold font, respectively; TSSs are indicated in blue bold font.

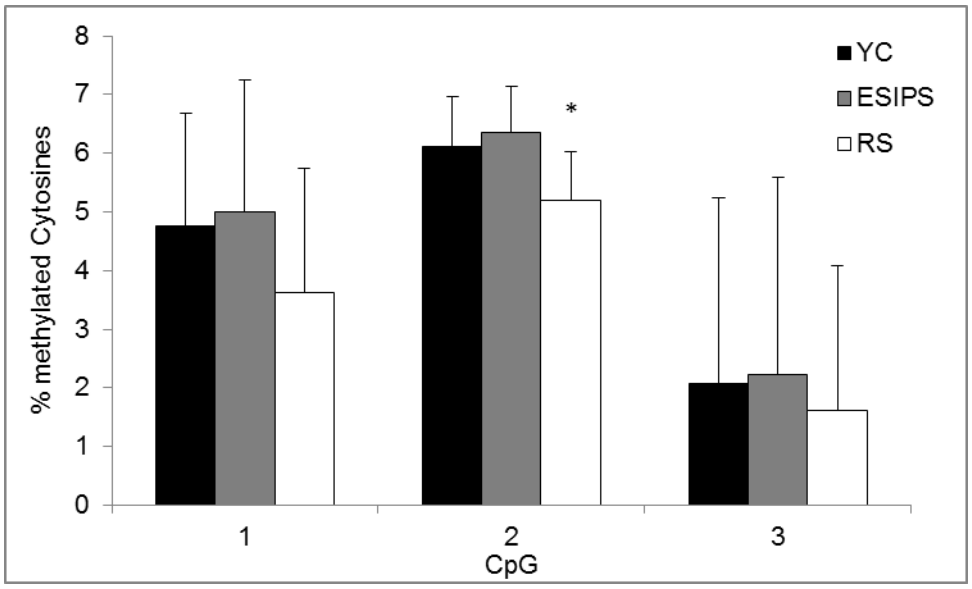
8
7
6
5
4
3
2
1
0
% methylated Cytosines
YC
ESIPS
RS
*
1
2
3
CpG

A

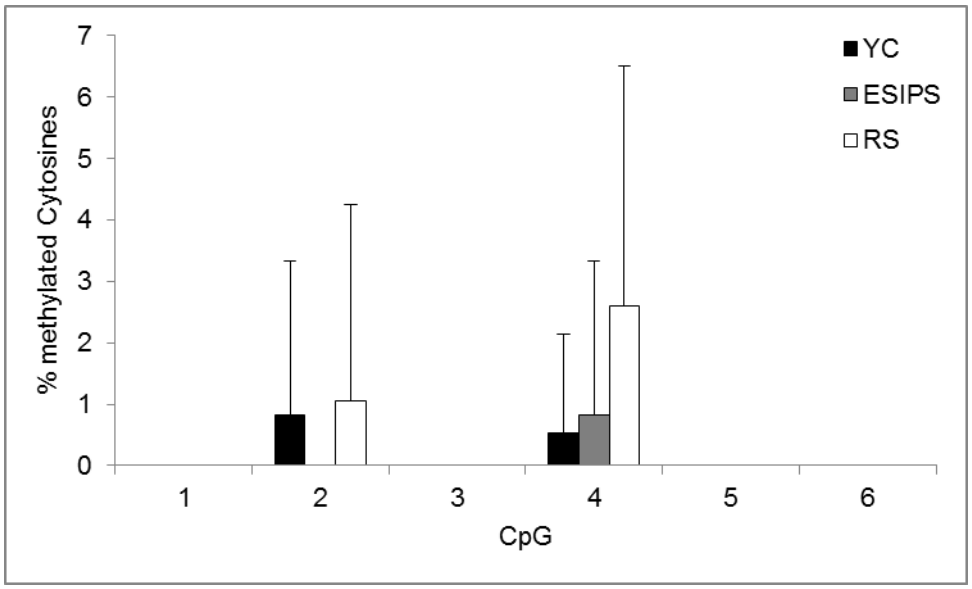
7
6
5
4
3
2
1
0
% methylated Cytosines
YC
ESIPS
RS
1
2
3
4
5
6
CpG

B

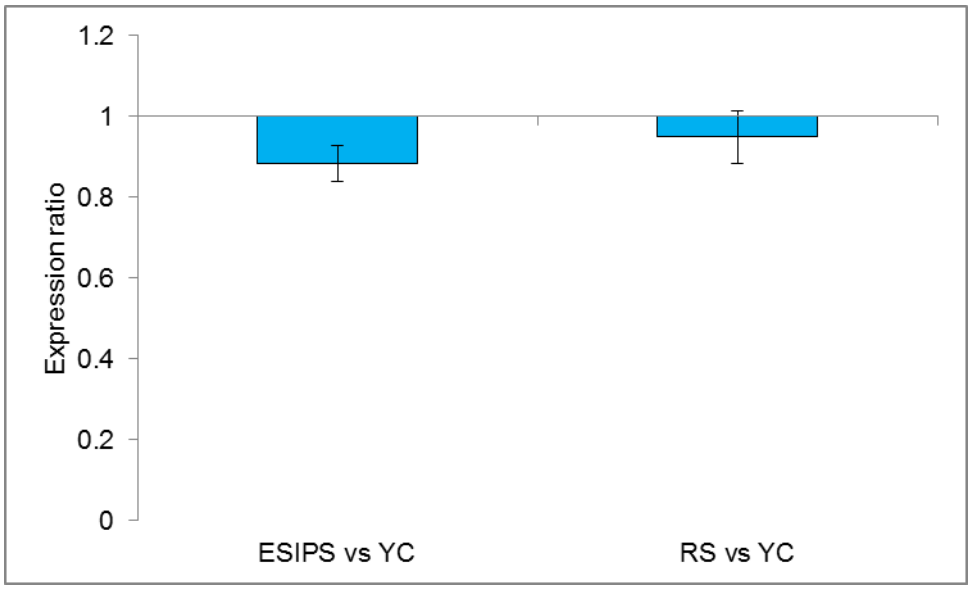
1.2
1
0.8
0.6
0.4
0.2
0
Expression ratio
ESIPS vs YC
RS vs YC

C

*Figure 5.16. SLC39A14 promoter methylation (panel A and panel B) and gene expression (panel C) in replicative senescence and early stress-induced premature senescence. Bar charts in panel A and panel B show average methylation of 3 and 6 CpG sites as measured by pyrosequencing; error bars represent + SD for 9 between biological and technical replicates; * = $p < 0.05$ for Mann-Whitney rank sum test for the comparison RS vs YC. Bar chart in panel C shows gene expression GAPDH-normalized; error bars represent ± SD for 4 biological replicates.*

5.8 Investigation, using a promoter-reporter assay, of the functional consequences of promoter methylation on gene expression

For *NPTX1* and *SLC39A14* the overall trends of the methylation and expression changes detected by means of arrays and pyrosequencing/RT-qPCR were confirmed, while for *CTTN* and *GLIPR2* this was validated only partially. To further investigate the effect of promoter methylation on gene expression, I optimized and applied the Secreted Embryonic Alkaline Phosphatase (SEAP) promoter-reporter assay, as described in section 2.21.

Briefly, the promoters of interest were cloned upstream of a murine Secreted Embryonic Alkaline Phosphatase gene in a plasmid without a promoter or an enhancer and which was completely devoid of CpG dinucleotides. This construct was *in vitro* methylated to produce a fully methylated product and then mixed with portions of the unmethylated construct in appropriate proportions to obtain mixtures with the following methylation levels: 0%, 25%, 50%, 75% and 100%. These mixtures were used to transfect LN-229 cells and the SEAP content (a measure of expression of the corresponding gene downstream of the cloned promoter) was measured in the media 3 days after transfection by a luminometer.

Figure 5.17 presents a dilution curve for assay of SEAP obtained with serial dilutions of a standard and shows that linearity of the assays was good ($R^2 > 0.99$) and spanned over at least four 5-fold dilutions. SEAP assays for the chosen promoters revealed that, for both promoters, methylation impaired the expression of the downstream gene in a manner that was directly proportional to the methylation content (Pearson correlation coefficients were -0.998 for CTTN and -0.875 for GLIPR2, see Figure 5.18).

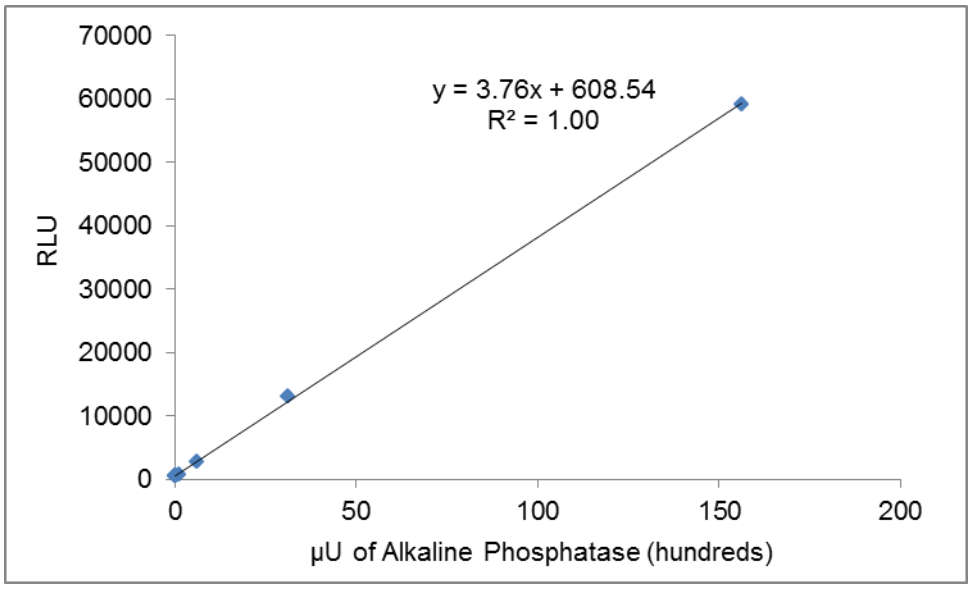

Figure 5.17. Standard curve for Secreted Embryonic Alkaline Phosphatase (SEAP) promoter-reporter assay. Luminescence of a standard serial dilutions was measured under the conditions used for all assays. RLU = relative luminescence units.

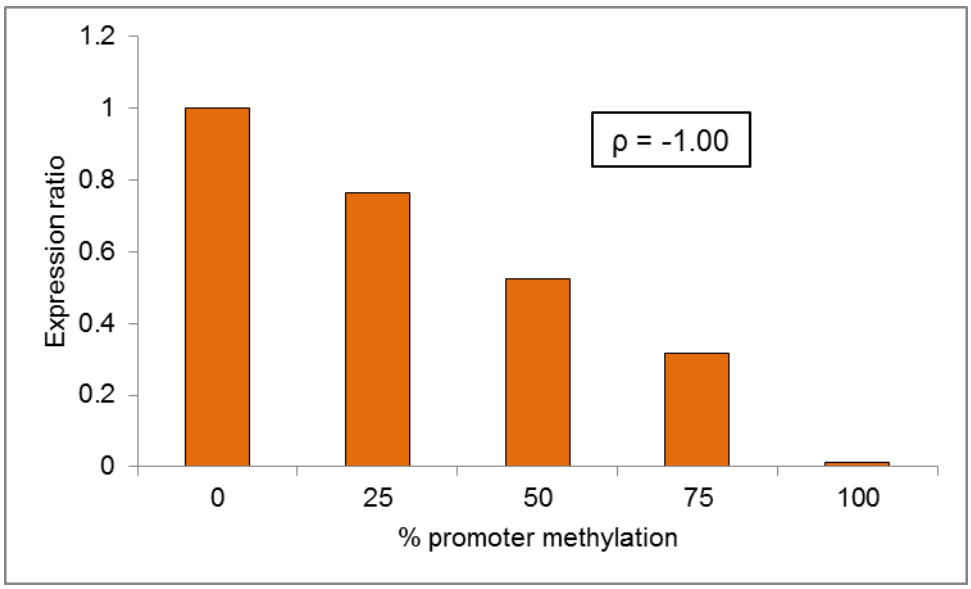

A

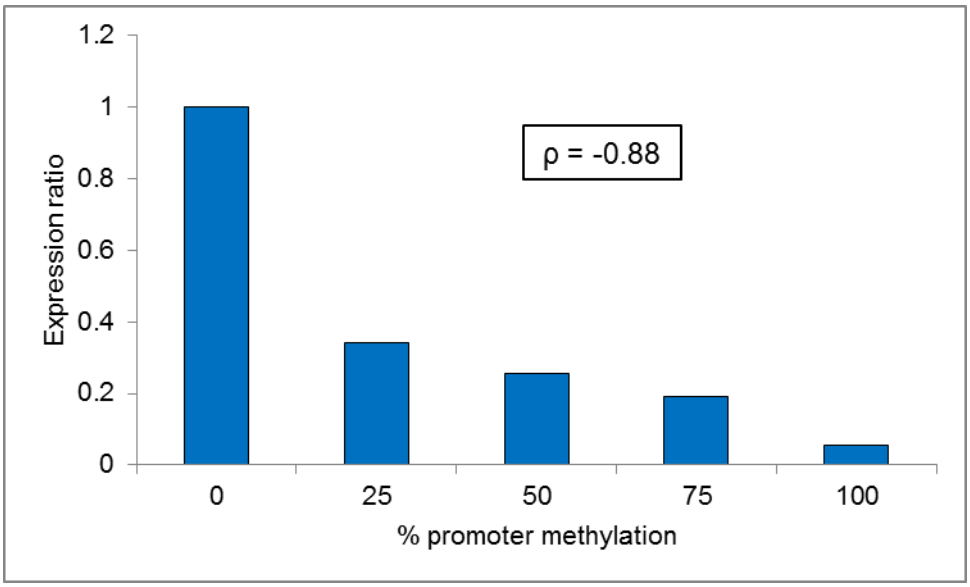

Figure 5.18. Relationship between CpG methylation content of the promoters of CTTN (panel A) and GLIPR2 (panel B) genes and expression. Estimates of expression of the reporter Secreted Embryonic Alkaline Phosphatase (SEAP) under the control of CTTN or GLIPR2 promoters with increasing methylation content are shown as luminescence readings normalized to the reading for the unmethylated promoter. The boxes inside the graphs show the Pearson correlation coefficients for the relationships between methylation and expression.

5.9 Screening of cell cycle genes promoter methylation in replicative senescence

To find further genomic regions of interest, I examined the expression data only and noted that one of the pathways which was most affected in both RS and ESIPS cells was the cell cycle pathway (see Table 5.5 and Table 5.6). I then screened genes in this pathway for altered methylation using the Methyl-Profiler DNA Methylation PCR array technology (QIAgen), as described in section 2.22. Briefly, this method is based on the digestion of the genomic DNA under investigation with methylation-sensitive and methylation-dependent restriction enzymes. Subsequent real-time qPCR allows the quantification of the uncut DNA. The relative DNA methylation content of a test sample compared with a control sample is then calculated with a comparative ΔCT calculation. Because of the high cost of the reagents, samples from RS and YC cells only were used in the screening. The method allowed me to screen the methylation status of 24 gene promoters involved in:

- G1 Phase and G1/S Transition: *CCND1*, *CCNE1*, *CDK4*, *CDKN1B* (p27KIP1);
- S Phase and DNA Replication: *MCM2*, *MCM4*;
- G2 Phase and G2/M Transition: *CCNB1*, *CDK5RAP1*, *CKS1B*;
- M Phase: *CCNF*, *MRE11A*, *RAD51*;
- Cell Cycle Checkpoint and Cell Cycle Arrest: *ATM*, *BRCA1*, *BRCA2*, *CDK2*, *CDKN1A* (p21CIP1/WAF1), *CDKN1B* (p27KIP1), *CHEK1*, *GADD45A*, *RAD17*, *RAD9A*, *TP53*;
- Regulation of Cell Cycle: *ATM*, *BRCA1*, *BRCA2*, *CCNB1*, *CCND1*, *CCNE1*, *CCNF*, *CDK2*, *CDK4*, *CDKN1A* (p21CIP1/WAF1), *CDKN1B* (p27KIP1), *CKS1B*, *GADD45A*, *RAD9A*, *RBL1*, *RBL2*, *TP53*.

Although efficiency of digestions were very good (the refractory fraction was always lower than 4% of the Input DNA, data not shown), I had to exclude 6 of the genes from the final analyses because their melt curves showed multiple peaks (data not shown), hence the specificity of amplification could not be proven. The excluded genes were: *CCNF*, *MCM2*, *MCM4*, *RAD17*, *BRCA2* and *CDKN1A*. For the remaining 18 genes, calculated estimates of promoter methylation data are summarized in Figure 5.19. The assay detected low levels of promoter methylation for all genes under investigation: in fact, the percentage of CpG methylation was always lower than 7% and 3% in RS and YC cells, respectively. There was no evidence of consistent trend towards hypomethylation or hypermethylation and, when comparing RS with YC cells, 10 of the gene promoters showed increased methylation (*CCNB1*, *CCNE1*, *CDK4*, *CDK5RAP1*, *CDKN1B*, *CHEK1*, *GADD45A*, *RAD51*, *RBL1* and *RBL2*) whilst other 7 showed lower methylation in the senescent cells (*ATM*, *BRCA1*, *CDK2*, *CSK1B*, *MRE11A*, *RAD9A*, *TP53*).

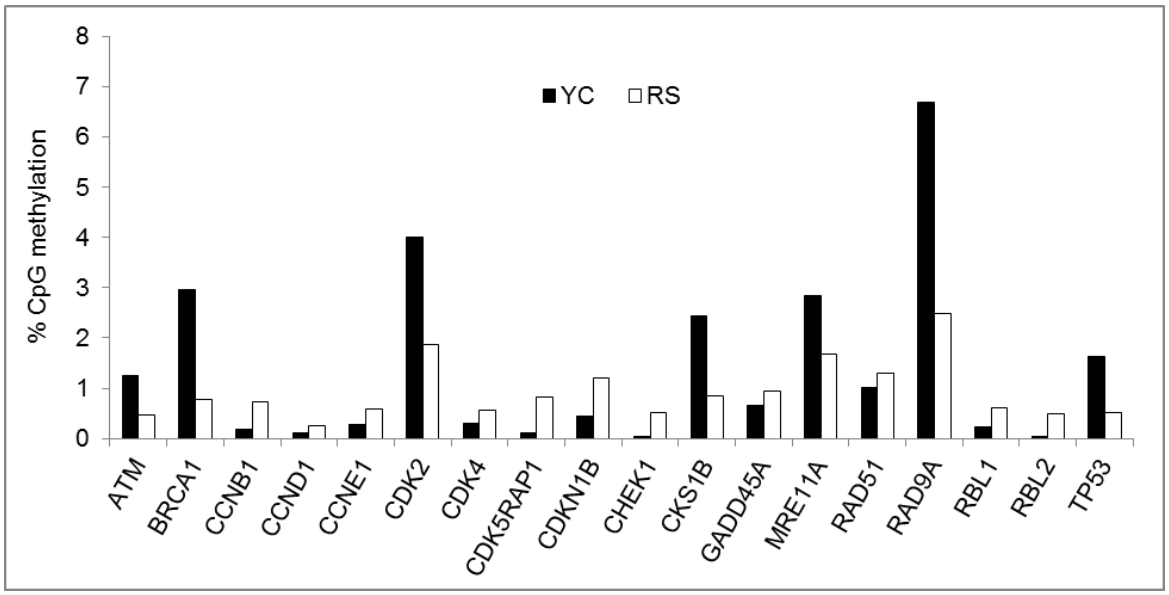

Figure 5.19. Young Replicative (YC) and Replicative Senescent (RS) MRC-5 fibroblasts CpG promoter methylation for cell cycle related genes measured by Methyl-Profiler DNA Methylation PCR array technology (QIAgen). Bars represent percentage methylation measured in one replicate and normalized as indicated by the manufacturer.

5.10 Discussion

This study was designed to use genome-wide array-based approaches to identify novel aberrantly methylated genomic regions in DNA from cells undergoing replicative senescence and to assess whether those changes could be causal for changes in gene expression. My model of choice was the cell line MRC-5 i.e. fibroblasts isolated from fetal human lung. A parallel screening was conducted on early stress premature induced senescent cells (γ-irradiated).

When compared with the control (DNA from YC cells), differentially methylated loci in DNA from early stress premature induced senescent cells were predominantly hypomethylated. In contrast, analysis of differentially methylated loci in DNA from RS cells revealed approximately equal numbers of hypomethylated and hypermethylated loci. This observation may indicate that demethylation of specific loci occurs more quickly than does hypermethylation of other loci and/or during the early stages of the senescent state induction. If such demethylation was linked with increased gene expression one might expect to see activation of the transcription of genes of the DNA repair and cell cycle control pathways.

I observed that a few genes (n = 38) showed similar methylation changes in the two data sets i.e. those for the RS vs YC and for the ESIPS vs YC comparisons; this finding is in contrast with a recently published study, in which authors found no senescence-associated DNA methylation changes upon irradiation of *in vitro* cultured fibroblasts (Koch et al., 2013). However, I found that hypergeometric probabilities were highly significant and representation factors were higher than 6 for both hypomethylation and hypermethylation, indicating that the gene methylation changes detected in common between early and late senescence were not due to chance. These short lists of Entrez Gene IDs did not reveal the identity of any significantly enriched pathway, suggesting that senescence-associated aberrant methylation involved single genes belonging to a number of pathways, but not to a single senescence-specific pathway. Further analysis of the enriched lists of differentially methylated Entrez Gene IDs for RS or ESIPS (see Appendix E, Table E.1 and Table E2, respectively) showed that although each comparisons featured different genes, both sets of differentially methylated genes were involved in similar biological processes. These processes included inflammation, cell proliferation, differentiation and apoptosis. This observation suggests that similar cellular response are induced by both replicative senescence (characterized by telomere shortening) and by the use of DNA

damaging agents (γ-rays) to induce early stress premature senescence, as reviewed by (Kuilman et al., 2010).

I also examined genome-wide changes in gene expression in exactly the same cells undergoing the same senescence-inducing procedures. These studies showed that, of the statistically significant changes, approximately half of the genes were down-regulated and half were up-regulated in both samples sets. Pathway analysis showed similar enrichments in the two sample sets, indicating that the genes expression changes associated with the senescent state are relatively constant from "early" senescence to "late" senescence. Previous studies have also shown similar transcriptome pathways enrichment in stress-induced senescent and replicative senescent cells; for example (Pascal et al., 2005) have shown enrichment of genes involved in growth arrest and senescence morphogenesis in both experimental conditions.

The observation that few common methylation changes and many common gene expression changes were detected in early and late senescence, may suggest that: i) a negligible part of the expression changes is ascribable to changes in methylation only and that other transcriptional mechanisms might be differentially involved during early and late senescence and that: ii) I was able to detect only a small part of the common occurring changes in methylation because the chosen array design did not include probes for CpG sites further away from the promoter regions e.g. in CpG island shores, shelves and open sea, which more recent work has suggested may be important in regulating gene expression (Irizarry et al., 2009).

In the following sections, I will give a brief description of the functions and summarize the current status of knowledge for the chosen candidates of methylation-expression and functional studies which were identified from my genome-wide analysis (see section 5.7). I will then continue with the discussion of the experimental results.

5.10.1 CTTN

As reviewed by (Weaver, 2008), the *CTTN* gene encodes for a cytoskeleton protein (cortactin, also known as EMS1), which is a regulator of the actin filaments assembly and is highly expressed in many cellular compartments, at sites of vesicles trafficking and at intercellular junctions. In particular, cortactin is abundantly found in podosomes, lamellipodia and invadopodia; those are subcellular structures responsible for the remodelling/degradation of the extra-cellular matrix (ECM) and ultimately cell motility.

Podosomes are found in normal cells that have to pass through tissue barriers, such as osteoclasts and macrophages, while lamellipodia and invadopodia are abundantly found within tumoural cells, where they contribute to aggressiveness and invasiveness. Cortactin overexpression is therefore a feature of many types of human cancers and is associated with poor prognosis; however this does not seem to be related to tumour initiation, but rather to tumour progression and metastatic potential, as demonstrated by i*n vivo* experiments in transgenic mice (van Rossum et al., 2006).

Frequently, aberrant cortactin expression results from the amplification of the chromosomal region 11q13.3 (Myllykangas et al., 2007), but other mechanisms could contribute to it; however, to my knowledge no previous report about promoter DNA methylation regulation of the *CTTN* gene expression have been published, nor studies that correlate *CTTN* expression with senescence or age. Hence, this is the first study showing that altered promoter DNA methylation may have a causal role in *CTTN* overexpression occurring within senescence.

CTTN gene overexpression seen in the transcriptome data set (see Table 5.9 and CD insert) was confirmed by RT-qPCR; on the other hand, pyrosequencing did not confirm *CTTN* promoter hypomethylation detected by the methylation arrays in the replicative senescent compared with young confluent MRC-5 (see Table 5.9 and CD insert). It is to be noted that I investigated a small number of the CpG sites included within the genomic area of interest identified by the methylation arrays (3 CpG sites out of 59, corresponding to about 5%), thus it is possible that the loss of methylation deteted by the arrays occurs in sites not included in the study; in addition, the only CpG site in which I found a significant methylation change between RS and YC cells showed opposite than expected behaviour, i.e. hypermethylation. This CpG site is contained within a DNA motif which shares high similarity with the transcriptional factor ETS1 binding sequence (97% of similarity, as calculated using the webtool Genomatix MatInspector (Cartharius et al., 2005)). As ETS1 can act as a transcriptional repressor (Hahne et al., 2009), I hypotesize that hypermethylation of this specific CpG site may impair ETS1 binding and thus contribute to the *CTTN* gene overexpression through diminished transcriptional repression. In parallel, ETS1 was also found to be down-regulated in replicative senescence from the transcriptome data (fold change 0.68, $p = 0.019$, data not shown), which could also be consistent with my hypothesis. In addition, promoter-reporter functional studies confirmed the hypothesis that CpG methylation could regulate expression for this gene (Figure 5.18, Panel A).

CTTN promoter aberrant methylation and the resulting overexpression occurring during senescence could: i) contribute to the invasive potential of cells capable of escaping the senescence barrier; ii) contribute to the enlarged and flattened morphology of senescent cells, which has been previously discussed in section 1.1 and was also found in my cell cultures (data not shown); iii) be one factors that contribute to increased risk of developing cancer with age.

The fact that the pattern hypomethylation/overexpression was not detected in stress premature induced senescent cells could be simply due to the early time point of harvesting. I predict that γ-irradiated cells harvested at a later time point would present a methylation/expression pattern similar to the one of replicative senescent cells, but further experiments need to be conducted to verify this hypothesis.

5.10.2 GLIPR2

Little is known about the function of the product of the *GLIPR2* gene (Golgi-associated plant pathogenesis-related protein 1 or glioma pathogenesis-related protein 2, also known as GAPR-1), which was discovered by two independent groups in 2002 (Eberle et al., 2002; Eisenberg et al., 2002). Upon translation, the protein is targeted to the Golgi, but there is no evidence of its presence in the COPI-vesicles (coat-protein vesicles), thus it does not seem to be involved in the transport of proteins between different Golgi cisternae (Eberle et al., 2002). The same authors found that GLIPR2 protein is preferentially expressed in rat immunocompetent cells and organs (leukocytes, monocytes, lung and spleen), but not detectable in tissues like liver, heart and adrenal glands, suggesting a potential role in the innate immune response; this assumption is corroborated by the fact that high level of GLIPR2 protein are also found in embryonic tissues and in the prostasomes, small membranous vesicles secreted by prostate epithelial cells which have been proposed to modulate immune cell response in the female reproductive tract and facilitate sperm motility (Aalberts et al., 2012).

Observational studies conducted in human peripheral chondrosarcomas specimens have shown that *GLIPR2* transcripts decrease in a proportional manner to increasing malignancy (Hameetman et al., 2006); in contrast, a study conducted in a mouse model for kidney fibrosis revealed that GLIPR2 protein is up-regulated in fibrotic kidneys compared with healthy controls. This overexpression is specific of epithelial cells, where it induces an epithelial-mesenchymal transition (EMT) (a process characterized by loss of

cell adhesion and increased cell motility), causing a cell morphology shift to fibroblastic phenotype (Baxter et al., 2007).

More recently, GLIPR2 has been identified as a negative regulator of autophagy, a cellular mechanism necessary for cell survival, differentiation and organism's development and defense from pathogens (Shoji-Kawata et al., 2013). As autophagy contributes to tissues homeostasis, its dysregulation could lead to the onset of infections, cancer, various diseases and also to ageing (Levine and Kroemer, 2008).

Although methylation arrays detected significant hypomethylation in the promoter of the *GLIPR2* gene in RS compared with YC MRC-5 fibroblasts (see Table 5.9 and CD insert), the subsequent attempt at validation using a pyrosequencing assay did not detect any significant change in methylation in the only CpG site investigated (Figure 5.12, Panel A). However, this was just CpG 1 site out of the 119 CpG sites found in the genomic area identified by methylation arrays and it is possible that methylation changes at this site were unrepresentative of the remainder of the genomic domain. RT-qPCR assays confirmed that expression was decreased during replicative senescence and also in early stress-induced premature senescent cells. For the latter, expression arrays had shown a trend towards transcriptional down-regulation although this was not statistically significant (Figure 5.12, Panel B; CD insert).

The functional study conducted using the promoter-reporter assay showed clearly that there was an inverse relationship between *GLIPR2* promoter methylation and gene expression (Figure 5.18, Panel B). This was in distinct contrast with the data from the genome-wide arrays, where hypomethylation was associated to decreased expression. Dependent on the specific CpG sites with altered methylation, it is possible that both hypermethylation and hypomethylation could be associated with gene down-regulation. A limitation of the data from methylation arrays is that it is not possible to identify which specific CpG sites show altered methylation. In contrast, pyrosequencing has considerable precision, but this approach has the limitation that each assay can interrogate only relatively few CpG sites. For this reason, it is difficult to provide a formal validation of the results of methylation arrays.

To my knowledge, this is the first study of the effects of senescence on promoter methylation or gene expression for the *GLIPR2* gene. This project has shown changes in DNA methylation (detected by the MeDIP technique) and in gene expression (detected by transcriptome arrays and RT-qPCR) for *GLIPR2* in response to induction of replicative senescence.

Changes in *GLIPR2* promoter methylation and the resulting gene down-regulation may contribute to a number of different processes known to occur in senescence, including: i) ageing of the innate immune system (Gomez et al., 2008), because of the above mentioned possible involvement of *GLIPR2* in the modulation of the immune system; ii) ECM degradation (Hornebeck, 2003), because GLIPR2 appears to act as an ECM deposition enhancer messenger, being a secreted protein whose up-regulation has been linked to fibrosis in the kidney (Baxter et al., 2007); this could also contribute to tumour metastatic potential by facilitating migration and invasion of transformed cells through a "relaxed" matrix and iii) enhancement of autophagy (Young et al., 2009), because GLIPR2 has been identified as a negative regulator of apoptosis (Shoji-Kawata et al., 2013).

5.10.3 NPTX1

The product of the gene *NPTX1*, neuronal pentraxin 1, was first discovered in 2000 and identified as a ligand of taipoxin, one of the most potent snake venom neurotoxins known (Kirkpatrick et al., 2000). *NPTX1* function remains still to be fully elucidated, although its high sequence homology to other well studied pentraxins genes lead to the hypothesis that it could be involved in the binding of diverse ligands during infection and inflammation processes, in the uptake of extracellular material and synaptic material during synapsis remodeling (Kirkpatrick et al., 2000). In addition, *NPTX1* has been shown to be rapidly up-regulated upon hypoxia conditions and to function as a mediator of cell death in primary cortical neuron (Hossain et al., 2004), to be necessary for normal structural and physiological maturation of the visual system (Bjartmar et al., 2006) and to be accumulated in dystrophic neurites of Alzheimer's disease patients and around amyloid plaques in the cerebral cortex and hippocampus of a mouse model of Alzheimer's disease, thus possibly contributing to the neurotoxicity of amyloid-beta accumulation (Abad et al., 2006). In addition, upon neuronal damage, *NPTX1* is overexpressed and targeted to the mitochondria, where it acts upstream of Bax and contributes to mitochondria fragmentation and apoptosis in cultured rat and mouse cerebellar granule neurons (Clayton et al., 2012).

Originally believed to be exclusively expressed in the brain, *NPTX1* has been also detected in several other tissues and cell types, including myogenic stem cell induced to differentiate (Wyzykowski et al., 2002) and in rat insulinoma β-cells (Brunner et al., 2007) and pancreatic tissue (Schvartz et al., 2012), where overexpression occurs in

glucotoxic conditions, suggesting that the protein might have a role as an apoptotic mediator upon stress, as in the nervous system.

With ageing, *NPTX1* overexpression has been seen to be associated with progressive accumulation of amyloid-beta in human seminal vesicles and to correlate with hemospermia (Furuya et al., 2005), but its function in the male reproductive tract is currently not known. In the same study, the authors speculated that, in addition to the pro-apoptotic function played also in other tissues, the protein could be involved in sperm-oocyte interactions and therefore have a role in the regulation of reproductive functions.

Interestingly, *NPTX1* has been recently identified as an effector of mTOR, being up-regulated by rapamycin - a known mTOR inhibitor - in a rare astrocytoma cell line, but not in normal human astrocytes (Tyburczy et al., 2010). In light of this consideration, *NPTX1* down-regulation could play a role in the senescence and ageing phenotypes, as a result of the mTOR pathway substained activity.

Various observational studies have found that *NPTX1* down-regulation associates with increased incidence of adenomas in mice (Stearns et al., 2012) and its promoter hypermethylation associates with human pancreatic cancer (Hagihara et al., 2004), colorectal cancer (Mori et al., 2011) and cervical cancer (Ongenaert et al., 2008; Yang et al., 2009), while no data are available so far on *NPTX1* promoter methylation occuring with senescence and ageing.

In my study, I detected significant hypomethylation of the *NPTX1* promoter and this was associated with a trend toward gene expression down-regulation (Figure 5.14; Table 5.9 and CD insert); this was in contrast with the aforesaid findings, which correlated instead promoter hypermethylation to decreased gene expression; however, hypomethylation could favour the binding of transcriptional repressors. To test this hypothesis, I performed computational analyses of the sequences investigated by pyrosequencing using the webtool Genomatix MatInspector, as already done for the *CTTN* promoter region. I found that CpG 1 within assay NPTX1_03 was contained within the binding domain of the transcription factor PLAGL1, which can act as activator or repressor (Abdollahi, 2007), and of PBF and E2F factors, which act synergistically to repress transcription (Boeckle et al., 2002). In addition, CpG 3 within the same assay was contained in the binding domain of RREB1 and ZIC2, both capable of transcription repressional activity (Flajollet et al., 2009; Pourebrahim et al., 2011). CpG 5 within assay number 7 was contained within the binding domain of the transcriptional repressor REST, which represses neuronal genes in non-neuronal tissues (Schoenherr et al., 1996); the same domain is shared by SP1 and

GLIS2, transcription factors which can both act as enhancers or repressors (Chu, 2012; Zhang et al., 2002a).
In light of these considerations, I can speculate that *NPTX1* promoter hypomethylation occuring with senescence can contribute to silencing of the *NPTX1* gene and, although the function of this gene in tissues outside of the nervous system is still to be fully elucidated, its down-regulation could have a role in the dysregulation of the apoptotic program and in the increase of the inflammatory response seen in a senescent scenario.

5.10.4 SLC39A14

SLC39A14 has been originally identified as a transmembrane zinc transporter protein (Taylor et al., 2005), which was up-regulated during adipocyte differentiation (Tominaga et al., 2005). Studies in mice models have confirmed its role in the differentiation and systemic growth: in fact, *Slc39a14* KO mice have reduced birth weight and size and show growth retardation, together with low plasma levels of GH, IGF and low Zn^{++} level in the pituitary gland (Hojyo et al., 2011).
In addition, SLC39A14 plays a major role in the acute-phase response: upon activation by IL-6 and IL-1 (master regulators of the immune and inflammatory response), *SLC39A14* mRNA levels increase, as does intracellular Zn^{++} uptake (Liuzzi et al., 2005; Lichten et al., 2009). This involvement is also supported by the fact that *SLC39A14* gene promoter contains response elements for several immune mediators (Liuzzi et al., 2005).
Different splicing isoforms (4A and 4B) with tissue-specific pattern of expression have been identified (Girijashanker et al., 2008); in addition, altered ratio between these two isoforms have been associated with adenomas and various cancers, with a marked predominance of isoform 4B on isoform 4A (Thorsen et al., 2011). Contribution to tumourigenesis of SLC39A14 isoform 4B is believed to be its high affinity for Cd^{++}, a potent carcinogen, and to the consequent increased intracellular Cadmium uptake.
A study on pigs demonstrated that SLC39A14 expression level was down-regulated with age; this is in agreement with my findings in senescent cells (Figure 5.16, Panel C, Table 5.9 and CD insert). However, no previous studies have been conducted on aberrant promoter methylation of this gene occuring during senescence and ageing. My pyrosequencing and RT-qPCR validation assays confirmed the significant trend hypomethylation/down-regulation detected by the genome-wide investigation for the comparison RS vs YC cells (Figure 5.16, Table 5.9 and CD insert).

Similarly to what previously done for the other candidate genes, I analyzed the genomic region investigated by the pyrosequencing assays with the webtool MatInspector and found that the hypomethylated CpG found within the SLC39A14_01 assay was contained in the binding motif of two transcription factors, MYT1L and GTF2B. MYT1L was found to be exclusively expressed in the nervous system (especially during development), the pituitary gland and testis (Jiang et al., 1996) and was not further kept in consideration. Very low *MYT1L* transcript levels in my samples were confirmed by transcriptome data, where the transcript featured at the 19th percentile, when ordering probes by increasing measured intensity (data not shown). GTF2B is a general transcription factor ubiquitely expressed and correlated with increased gene expression upon binding to recognition sites within promoters of many genes. In theory, hypomethylation should increase its binding and favour gene expression, but this is in contrast with my findings, where hypomethylation was associated with gene down-regulation; however, a study demonstrated that, in the presence of a p53-mediated transcriptional response (and this is the case of the senescence scenario), GTF2B transcriptional activity is attenuated (Shandilya et al., 2012). This could explain the absence of increased *SLC39A14* gene expression with promoter hypomethylation, but does not explain its down-regulation; I therefore concluded that a causal effect for promoter methylation on gene expression cannot be drawn referring only to this particular CpG site.
Down-regulation of the *SLC39A14* gene can contribute to decreased intracellular Zn uptake and participate in the pathogenesis of acute and chronic lung disease (Zalewski, 2006) and therefore to the loss of physiological function observed in this tissue with ageing; Zn depletion plays, in fact, a part in the increase of the susceptibility of lung tissue to oxidative stress (Taylor and Bray, 1991), alcohol-induced (Joshi et al., 2009), and sepsis-induced (Knoell et al., 2009) injury and triggers pro-apoptotic stimuli. In addition, down-regulation of the *SLC39A14* gene has been found in hepatoma cancer cell lines, where it occurs in the first stages of malignant transformation (Franklin et al., 2012); this could corroborate the assumption that cancer is mostly a disease of the ageing cell.

5.10.5. Methylation of the promoters of cell cycle genes in replicative senescence

The investigation of promoter methylation of the cell cycle genes in replicative senescent cells described in this chapter should be considered as pilot data only because the study was performed just once. In consequence, I could not perform any statistical evaluation of

the collected data and so results must be interpreted cautiously. In addition, the identities of the CpG sites which showed differential methylation between the two conditions (YC and RS cells) were not known. This is because the primers used in the methylation assay were copyright protected, and the genomic regions which they amplified could not be identified. This meant that a direct comparison of these results with those obtained from the methylation arrays was not possible. Whilst the MethylProfiler array investigates a 150-350 bp region known to be bound by transcription factors in the promoter of the chosen genes, this might not correspond completely with the region investigated in the methylation arrays. Also, although it was possible to compare changes in methylation with those in expression, conclusions about the causal relationship between changes in methylation and in gene expression could not be drawn. A possible experimental approach to address this issue could be based on the following two steps: i) PCR-cloning and then sequencing of selected qPCR products obtained from the MethylProfiler array assays. This would unravel specific genomic loci under investigation and ii) pyrosequencing of multiple CpG sites within the identifed genomic loci. This would provide information on the methylation status of specific CpG sites. This may help to establish a functional link between aberrant methylation and changes in gene expression occuring during senescence.

5.11 Conclusions

In the work described in this Chapter I found that:

- premature senescent and replicative senescent human lung fibroblasts share a small, but significant, number of changes in promoters DNA methylation when compared with young replicative cells. The genes affected in common include those which are involved in inflammation, cell proliferation, differentiation and apoptosis;
- premature senescent and replicative senescent human lung fibroblasts share a relatively large number of changes in gene expression when compared with young replicative cells. However, the direction of change in promoter methylation and in gene expression differed between the two pairs of comparisons, suggesting that different mechanisms for regulation of transcription may be involved in “early” and “late” senescence;

- for *CTTN*, *GLIPR2*, *NPTX1* and *SLC39A14* genes, both promoter methylation and gene expression was altered in replicative senescence. The functional studies (gene-reporter assays) that I carried out and/or the literature support the hypothesis that aberrant promoter methylation occurring with senescence may be causal for the related gene expression dysregulation of *CTTN* and *GLIPR2* which, in turn, could contribute to the senescent phenotype;
- in a pilot study, I observed that promoter methylation of a number of cell cycle genes is altered in replicative senescence and that this was associated with altered gene expression. However a causal (functional) relationship between these two states is still to be elucidated.

Manuscript under preparation

Chapter 6. Investigation of effects of ageing and of dietary energy restriction on genome-wide patterns of DNA methylation in mouse tissues

6.1 Outline

Evidence of age-dependent aberrant DNA methylation at specific CpG sites in mouse has been shown for several genes including the proto-oncogenes *Myc* (Ono et al., 1986; Ono et al., 1989), *Fos* (Uehara et al., 1989) and *Hras1* (Counts et al., 1997), for rRNA genes (Swisshelm et al., 1990), for genes involved in reproductive function (Liang et al., 2008), DNA repair (Conde-Perezprina et al., 2008) and cognitive function (Singh and Prasad, 2008) and for genes regulating the circadian rhythm (Zhang et al., 2013).
In parallel, aberrant patterns of gene expression which are characteristic of tissue ageing have been identified. These transcriptional changes contribute to progressive loss of cellular and tissue function with age (Lee et al., 2000; Zhang et al., 2003; Zahn et al., 2007; Edwards et al., 2007; Fridman and Tainsky, 2008; de Magalhaes et al., 2009; Kuilman et al., 2010). Some of these changes are counteracted by dietary energy restriction (Weindruch et al., 2001; Heilbronn and Ravussin, 2003).
DNA methylation occurring at gene promoters is often accompanied by silencing of the corresponding gene so that aberrant DNA methylation occurring with ageing may contribute to the ageing phenotype. At this stage it is uncertain whether this is causal for, or a consequence of, ageing itself. Identification of novel aberrantly methylated gene promoters in ageing and assessment of their methylation state in response to dietary energy restriction could help in discerning the mechanisms by which this dietary intervention counteracts the effect of ageing in multiple species. In addition, the outcomes of such research may be help to establish dietary interventions aimed at slowing down ageing and reducing the risk of age-related diseases.

This study aimed: i) to screen for age-associated DNA methylation changes in the promoters of all known mouse genes in DNA from heart and from liver and ii) to assess whether those changes were modified by short-term dietary energy restriction.
For the first part of the study, I chose heart and liver as 2 tissues with different proliferative characteristics. By focussing on DNA methylation changes which were common to both tissues I hoped to identify methylation changes that were not tissue-

specific i.e. to identify gene whose methylation status might be universally susceptible to ageing. In the second part of the study, I compared changes in DNA methylation in response to ageing with those in response to short-term dietary energy restriction (3 months). This work was restricted to liver only.

6.2 Effects of ageing on methylation patterns in DNA from mouse heart and liver

6.2.1 Overview of methylation changes observed in murine liver and heart tissues with ageing

Genomic DNA from 3 animals for each age group/tissue was prepared. Hearts were obtained from male C57Bl/6 mice aged 3 and 32 months old; livers were collected from male ICRFa mice at 7 and 30 months of age. DNA samples were processed using the MeDIP technique, whole genome amplified, subjected to quality control to test for methylation enrichment and hybridized to Nimblegen promoter arrays, as described earlier (see sections 2.6, 2.7, 2.8 and 2.11 for experimental details).
Figure 6.1, panel A and panel B, summarises the significant effects of age on genome-wide methylation in both heart and liver. In each case, "hypomethylation" indicates that DNA from the older tissue was significantly less methylated than that from the young animals whereas the converse was true for "hypermethylation". Only 5.05% and 6.68% of probes showed significantly different methylation between tissue from older animal vs tissue from young animal for heart and liver, respectively; these corresponded to 1007 and 1331 genomic regions. In both tissues, a greater proportion of the differentially methylated genes in older tissue were hypomethylated (62.26% and 55.52% of all significant methylation changes in heart and liver, respectively). For a complete list of all the significant hits, see CD insert.

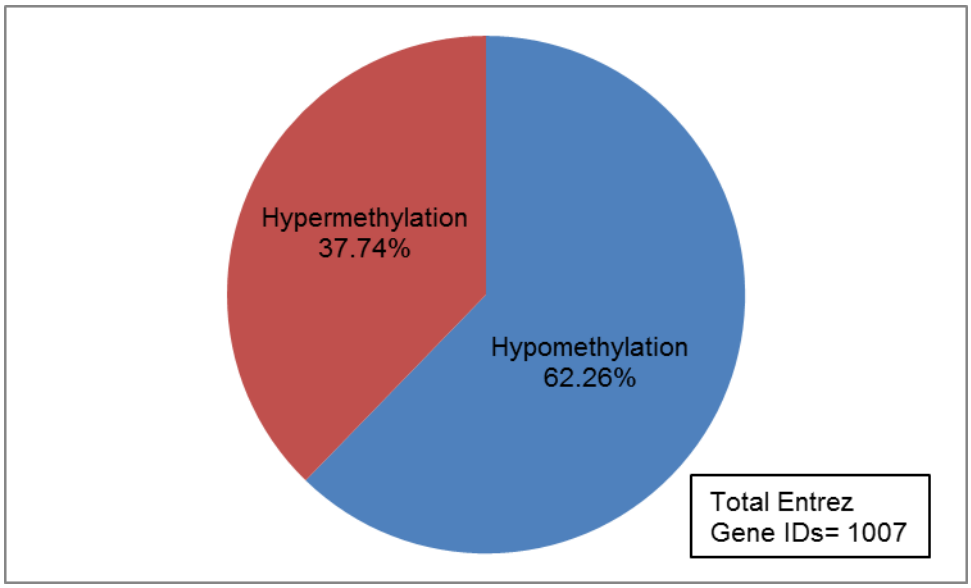

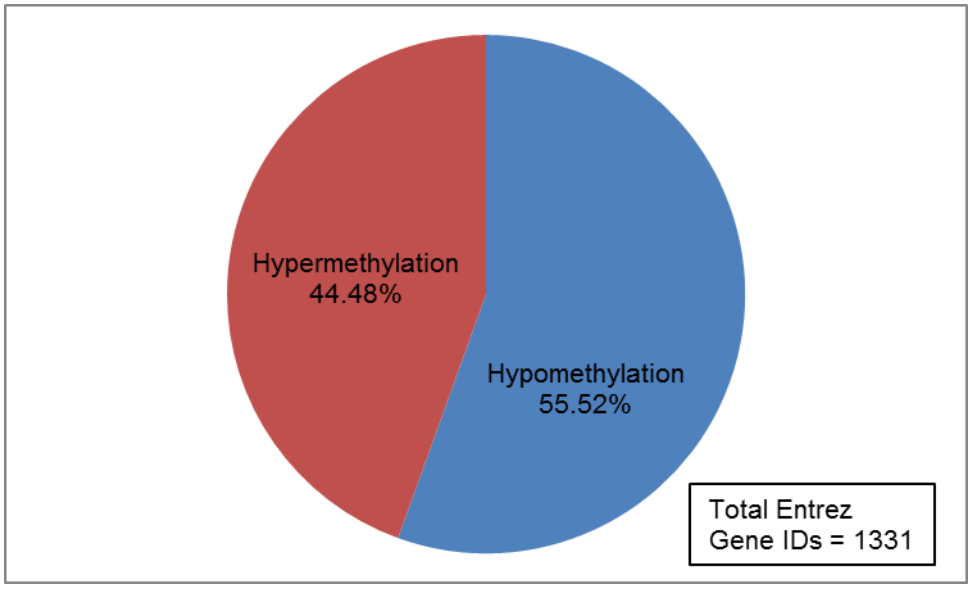

Figure 6.1. Significant effect of ageing on methylation in mouse heart (panel A) and liver (panel B). The pie charts illustrate the proportions of genes showing reduced (hypo) and greater (hyper) methylation in older when compared with young adults mice. The boxes in the bottom right of each panel indicate the total number of significant Entrez Gene IDs for which significant methylation changes were detected ($p < 0.05$ for student's unpaired t-test).

The list of common Entrez Gene IDs promoters affected by significant age-related DNA methylation changes in murine heart and liver contained 108 hits (Figure 6.2); this number exceeded what would be expected by chance; in fact, calculated representation factor and hypergeometric probability were 1.61 and 2.55×10^{-7}, respectively.

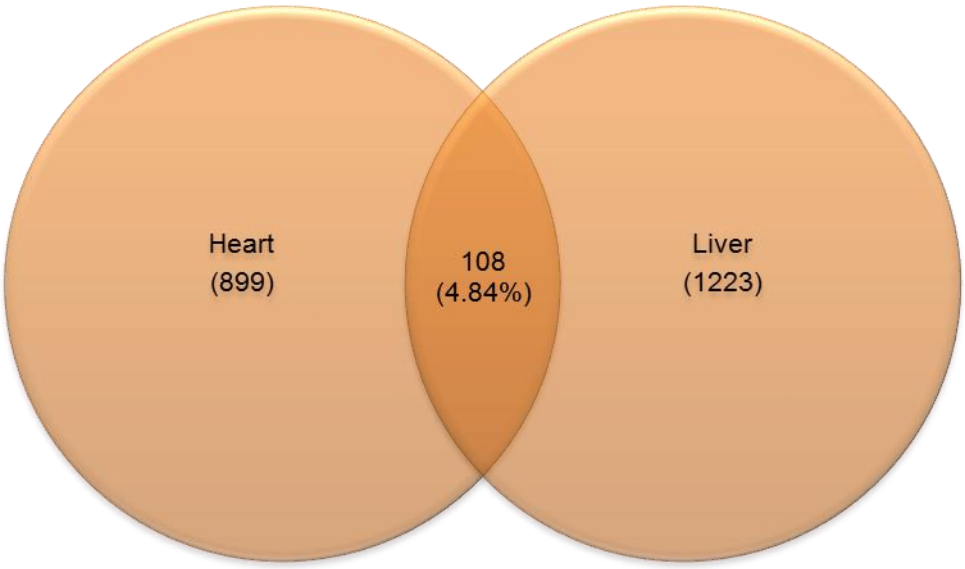

Figure 6.2. Common Entrez Gene IDs promoters affected by age-related DNA methylation changes in murine heart and liver shown as Venn diagram. Representation factor = 1.61; hypergeometric probability = 2.55 x 10 $^{-7}$.

These data indicated that there were more genes showing altered promoter methylation with ageing in both tissues than would have occurred by chance. The next steps were to determine whether i) the methylation changes occurred in the same or in opposite direction (i.e. hypermethylation or hypomethylation) and ii) the number of same-direction or opposite-direction changes was significant. To address this issue, I used the lists of significantly hypermethylated and hypomethylated Entrez Gene IDs promoters separately and compared each pair of data as described below. The analyses yielded the following results:

- Entrez Gene IDs that were significantly hypermethylated in both heart and liver tissue during ageing = 17 hits; representation factor of 1.51 and hypergeometric probability of 2.66 x 10 $^{-2}$ (Figure 6.3, panel A);
- Entrez Gene IDs that were significantly hypomethylated in both heart and liver tissue during ageing = 30 hits; representation factor of 1.29 and hypergeometric probability of 2.88 x 10 $^{-2}$ (Figure 6.3, panel B);
- Entrez Gene IDs that were significantly hypermethylated in heart tissue but significantly hypomethylated in liver tissue during ageing = 24 hits; representation factor of 1.70 and hypergeometric probability of 3.92 x 10 $^{-3}$ (Figure 6.3, panel C);

- Entrez Gene IDs that were significantly hypomethylated in heart tissue but significantly hypermethylated in liver tissue during ageing = 37 hits; representation factor of 1.99 and hypergeometric probability of 3.45×10^{-5} (Figure 6.3, panel D).

These results indicated that for all the pairs of datasets considered the number of hits in common i.e. those indicated by the intersections of the two circles in the Venn diagrams in Figure 6.3 - was significantly higher than that which would be expected to occur by chance.

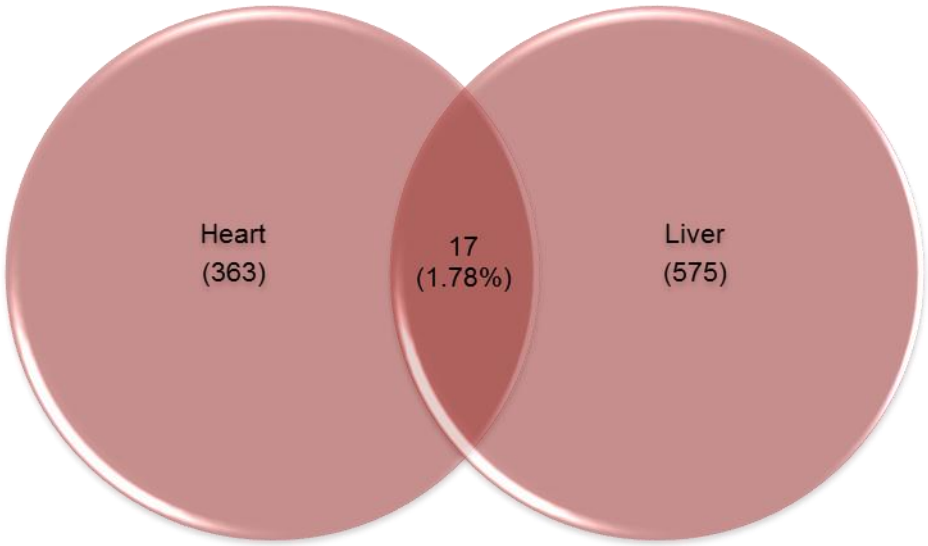

A

red = hypermethylation;
blue = hypomethylation

B

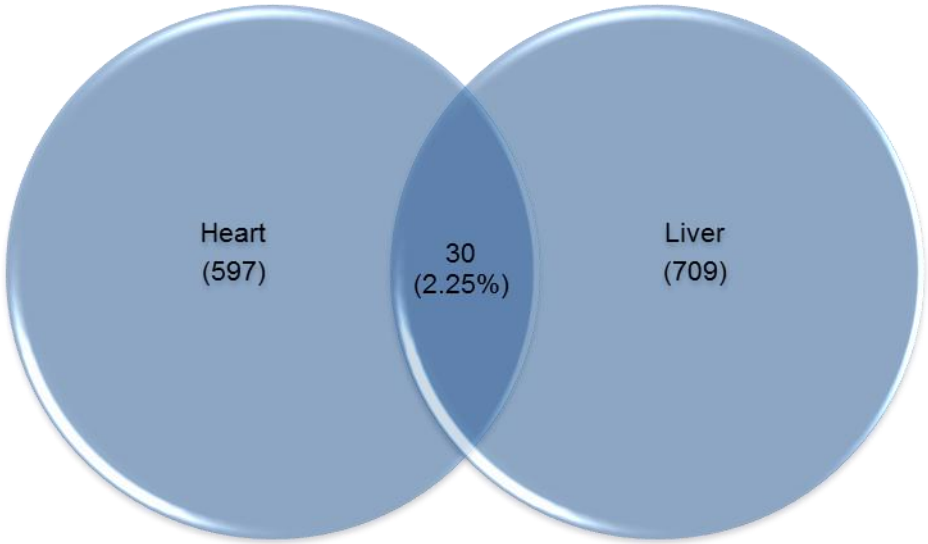
Heart
(597)
30
(2.25%)
Liver
(709)

C

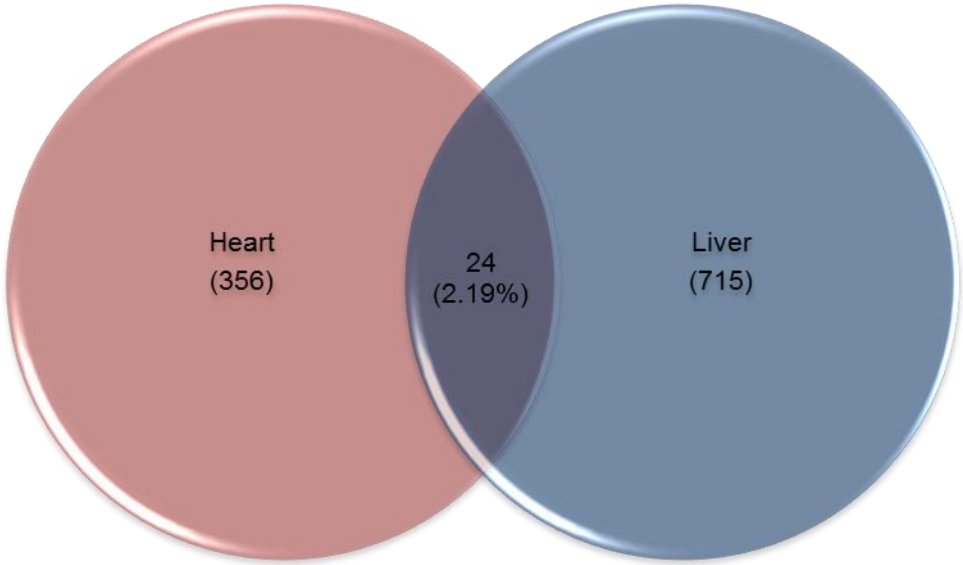
Heart
(356)
24
(2.19%)
Liver
(715)

D

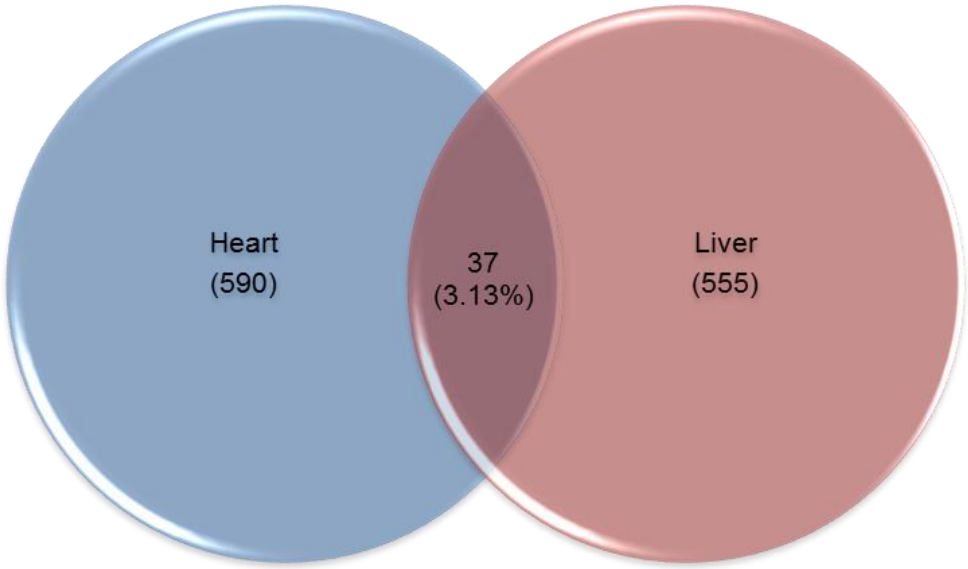
Heart
(590)
37
(3.13%)
Liver
(555)

Figure 6.3. Common and opposite behaviour for age-related promoter methylation changes in murine heart and liver shown as Venn diagrams. Panel A shows number and percentage of significantly hypermethylated Entrez Gene IDs in both heart and liver tissue from older animals in each case compared with young animals; panel B shows number and percentage of significantly hypomethylated Entrez Gene IDs in both heart and liver tissue tissue from older animals in each case compared with young animals; panel C shows the intersection between significantly hypermethylated Entrez Gene IDs in heart tissue from older animals and significantly hypomethylated Entrez Gene IDs in liver tissue from older animals in each case compared with young animals; panel D shows the intersection between the significantly hypomethylated Entrez Gene IDs in heart tissue from older animals and significantly hypermethylated Entrez Gene IDs in liver tissue from older animals in each case compared with young animals.

6.2.2 Pathway analysis for those genes which were differentially methylated in response to ageing and for which ageing effects were concordant in both liver and heart tissues

The IDs and official gene symbols which appeared in the intersections shown in Figure 6.3 are given in Table 6.1 and Table 6.2. Table 6.1 summarises those genes which showed the same methylation response to ageing in both tissues whereas Table 6.2 summarises those genes which showed contrasting methylation responses to ageing in the two tissue i.e. hypomethylation in liver but hypermethylation in heart and vice versa.

Table 6.1. Genes which showed the same methylation response to ageing in both heart and liver. Hypermethylated genes are listed on the left and hypomethylated genes on the right. In each case the Entrez Gene IDs and gene symbols are shown. The annotation (Gene ID withdrawn) indicates that the record has been discontinued and it is not in the current genome assembly.

Hypermethylation		Hypomethylation	
Entrez Gene ID	**Gene symbol**	**Entrez Gene ID**	**Gene symbol**
17880	Myh11	12315	Calm3
22418	Wnt5a	14113	Fbl
66061	Tctex1d2	14630	Gclm
67711	Nsmce1	18769	Pkig
70261	Chp2	19118	Prm1
71947	2310067B10Rik	19331	Rab19

73991	Atl1	19395	Rasgrp2
93873	Pcdhb2	54673	Sh3glb1
112415	C030039L03Rik	59029	Psmd14
226791	Lyplal1	67111	Naaa
245884	Fam71f2	72144	Slc37a3
269344	Ell3	74648	S100pbp
399510	Map4k5	75083	Usp50
494504	Apcdd1	76498	Paqr4
624124	Gm6472	77521	Mtus2
634044	(Gene ID withdrawn)	78625	1700061G19Rik
670550	Gm11565	107271	Yars
		140482	Zfp358
		209478	Tbc1d12
		218877	Sema3g
		223435	Trio
		228410	Cstf3
		258462	Olfr1392
		259300	Ehd2
		328845	Acsbg2
		380705	Tmem102
		380755	Gm889
		622568	Gm6334
		100044829	LOC100044829
		100044867	(Gene ID withdrawn)

Table 6.2. Genes which showed contrasting methylation responses to ageing in heart and liver. Genes which are hypermethylated in ageing hearts but hypomethylated in ageing livers are listed on the left whilst genes which are hypomethylated in ageing hearts but hypermethylated in ageing livers are listed on the right. In each case, the Entrez Gene IDs and gene symbols are shown. The annotation (Gene ID withdrawn) indicates that the record has been discontinued and it is not in the current genome assembly.

Hypermethylation in heart and Hypomethylation in liver		Hypomethylation in heart and Hypermethylation in liver	
Entrez Gene ID	**Gene symbol**	**Entrez Gene ID**	**Gene symbol**
11474	Actn3	11702	Amd1
13521	Slc26a2	14179	Fgf8
14594	Ggta1	14562	Gdf3

22235	Ugdh
23879	Fxr2
54369	Nme6
67116	Cuedc2
67381	Med4
70605	Zdhhc24
75146	Tmem180
104174	Gldc
104725	Sptssa
229906	Gtf2b
231932	Gimap7
244179	Ubqlnl
258268	Olfr1511
258536	Olfr1360
269587	Epb4.1
317757	Gimap5
320415	Gchfr
381126	Garem
435529	Gpr111
640370	Gm7292
100046163	(Gene ID withdrawn)

14744	Gpr65
17183	Matn4
20618	Sncg
20983	Syt4
22062	Trp73
22247	Umps
54003	Nell2
56380	Arid3b
59002	Wrap73
63959	Slc29a1
69241	Polr2d
71395	5430419D17Rik
75986	Agmat
80876	Ifitm2
83995	Mmp1a
94180	Acsbg1
105450	Mmrn2
107652	Uap1
108013	Celf4
110175	Ggct
113865	Vmn1r25
170639	Olfr78
171195	Vmn1r30
193053	Olfr384
211550	Tifa
235854	Mrgpra4
238395	Serpina3j
238680	Cntnap3
241263	Gpr158
381809	Clec4b2
631287	LOC631287
637082	(Gene ID withdrawn)
100043304	Amd-ps3
100047905	(Gene ID withdrawn)

To investigate the biological significance of my findings, I performed canonical pathways analysis and signal transduction pathways enrichment analysis using the Genomatix platform (http://www.genomatix.de/). This analysis revealed significant effects for three out of four of the intersections lists (Table 6.3). This was not surprising, as those lists

were made up by a small number of hits; in addition, some of the hits were predicted or inferred genes, whose biological function is still to be elucidated.

Table 6.3. Canonical and signal transduction pathway analyses for common and opposite promoter methylation changes in ageing heart and liver. Panel A lists the significant signal transduction pathways for the common hypermethylated Entrez Gene IDs in ageing heart and liver; panel B lists the significant canonical pathways for the common hypomethylated Entrez Gene IDs in ageing heart and liver; panel C lists the significant signal transduction pathways for the intersection between hypermethylated Entrez Gene IDs in ageing heart and hypomethylated Entrez Gene IDs in ageing liver.

A

Signal Transduction Pathway	**p value**	**Genes observed/total**	**Genes official symbol**
Wingless type	2.90E-03	3/451	Map4k5, Apcdd1, Wnt5a
Nuclear factor of activated T cells, cytoplasmic, calcineurin dependentT	3.25E-03	2/121	Chp2, Wnt5a
Glycogen synthase kinase	6.78E-03	2/176	Map4k5, Wnt5a
Ryk receptor like tyrosine kinase	7.60E-03	1/10	Wnt5a

B

Canonical Pathway	**p value**	**Genes observed/total**	**Genes official symbol**
Regulation of Ras family activation	9.37E-04	2/34	Calm3, Rasgrp2

C

Signal Transduction Pathway	**p value**	**Genes observed/total**	**Genes official symbol**
Cell division cycle 2, G1 to S and G2 to M	5.49E-03	2/158	Cuedc2, Epb4.1

For those genes which were hypermethylated in both heart and liver tissue from the older mice, analysis of the Entrez Gene IDs lists yielded 4 significantly enriched signal transduction pathways viz. the Wnt signalling pathway, the nuclear factor of activated T cells signalling pathway, the glycogen synthase kinase and the Ryk receptor like tyrosine kinase signalling pathways (Table 6.3, panel A). Similarly, for those genes which were hypomethylated in both heart and liver tissue from the older mice, analysis of the Entrez Gene IDs lists yielded a single enriched canonical pathway, i.e. the regulation of Ras

family activation pathway (Table 6.3, panel B). Next, I considered those genes showing discordant changes in methylation in liver and heart in response to ageing. For those genes (Entrez Gene IDs) which were hypermethylated in ageing hearts but were hypomethylated in ageing livers, this analysis revealed a single significantly enriched signal transduction pathway i.e. that for the cell division cycle 2, G1 to S and G2 to M signalling (Table 6.3, panel C). Finally, for those genes (Entrez Gene IDs) which were hypomethylated in ageing hearts but hypermethylated in ageing liver, no significantly enriched pathways were detected.

6.3 Effects of short-term dietary energy restriction and of ageing on methylation patterns in DNA from mouse liver

6.3.1 Overview of methylation changes occurring in murine liver in response to short-term dietary energy restriction

Genomic DNA from 3 animals for each diet group was prepared. Livers were obtained from male C57Bl/6 mice aged 17 months old; dietary energy restricted (ER) mice were fed 60% of the *ad libitum* (AL) diet for 3 months, starting at the age of 14 months. DNA samples were processed using the MeDIP technique, whole genome amplified, subjected to quality control to test for methylation enrichment and hybridized to Nimblegen promoter arrays (see sections 2.6, 2.7, 2.8 and 2.11 for experimental details). Figure 6.4 summarises the significant effects of dietary energy restriction on liver genome-wide methylation, where "hypomethylation" indicated that DNA from the tissue from ER fed animals was significantly less methylated than that from the AL fed animals, whereas the converse was true for "hypermethylation". A total of 1078 genomic regions (genes) corresponding to 5.41% of the array probes showed significantly different methylation in DNA from ER fed animals vs AL fed animals. A greater proportion of the differentially methylated genes in tissue from ER fed animals was hypomethylated compared with tissue from AL fed animals (60.02% of all significant methylation changes). For a complete list of all the significant hits, see CD insert.

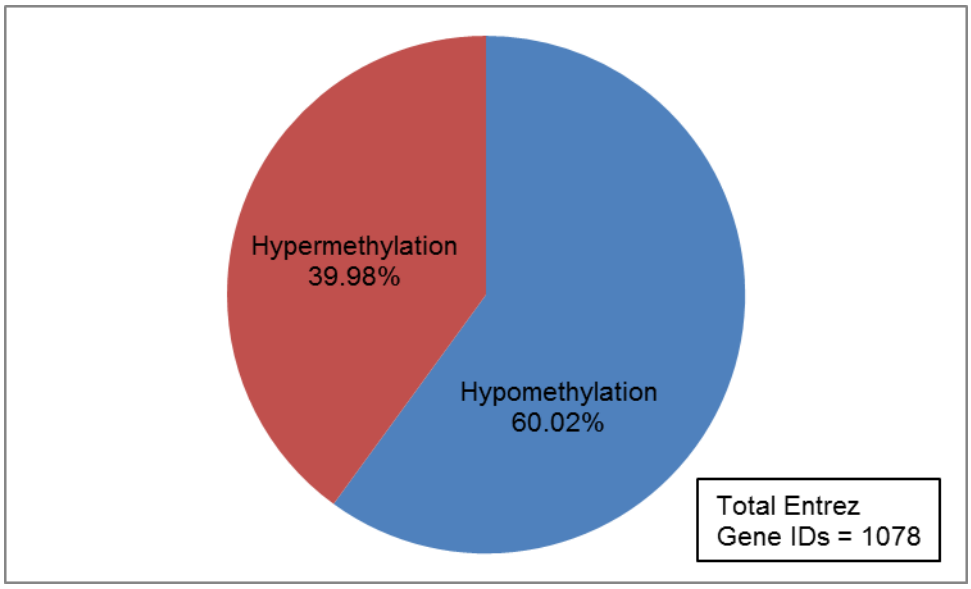

Figure 6.4. Significant effect of short-term dietary energy restriction on DNA methylation in mouse liver. The box in the pie chart area indicates the total number of significant Entrez Gene IDs for which significant methylation changes were detected ($p < 0.05$ for student's unpaired t-test).

The list of common Entrez Gene IDs promoters affected by significant age-related and dietary energy restriction-related DNA methylation changes in murine livers contained 82 hits (Figure 6.5); this number exceeded what would be expected by chance, although by a small amount; in fact, calculated representation factor and hypergeometric probability were 1.14 and 2.21×10^{-2}, respectively.

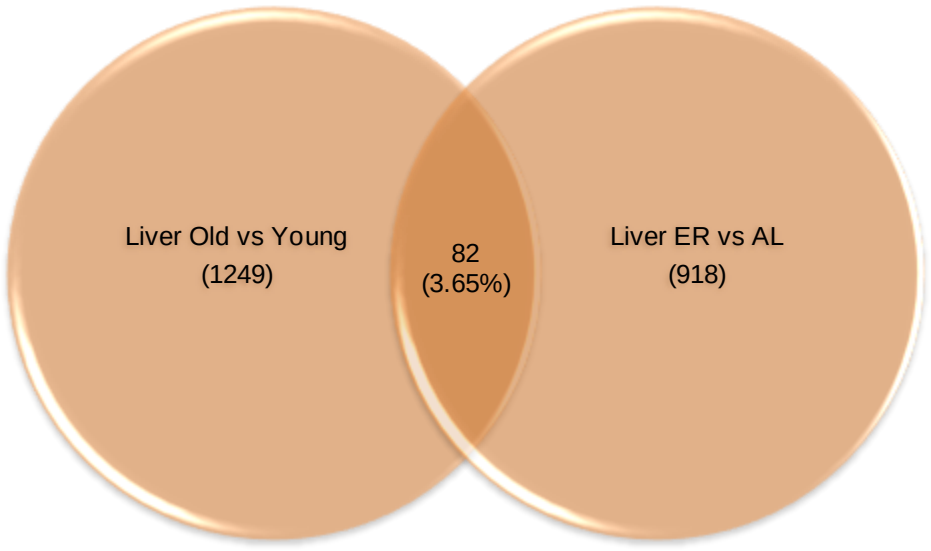

Figure 6.5. Common Entrez Gene IDs promoters affected by age-related and short-term dietary energy restriction-related DNA methylation changes in murine liver shown as Venn diagram. Representation factor = 1.14; hypergeometric probability = 2.21 x 10^{-2}.

These data indicated there were more genes showing altered promoter methylation with ageing and in response to ER than would have occurred by chance. The next step was to determine whether these methylation changes occurred in the same or opposite direction (i.e. hypermethylation or hypomethylation) and whether the numbers of same-direction or opposite-direction changes were significant. To address this issue, I used the lists of significantly hypermethylated and hypomethylated Entrez Gene IDs promoters separately and compared each pair of data as described below. The analyses yielded the following results:

- Entrez Gene IDs which were significantly hypermethylated in both tissue from older animals compared with tissue from young animals AND in tissue from ER fed animals compared with tissue from AL fed animals = 15 hits; representation factor = 1.17, not statistically significant (Figure 6.6, panel A);
- Entrez Gene IDs which were significantly hypomethylated in in both tissue from older animals compared with tissue from young animals AND in tissue from ER fed animals compared with tissue from AL fed animals = 27 hits; representation factor = 1.13, not statistically significant (Figure 6.6, panel B);
- Entrez Gene IDs which were significantly hypermethylated in tissue from older animals compared with tissue from young animals AND significantly hypomethylated Entrez Gene IDs in tissue from ER fed animals compared with tissue from AL fed animals = 16 hits; representation factor = 0.83, not statistically significant (Figure 6.6, panel C);
- Entrez Gene IDs which were significantly hypomethylated in tissue from older animals compared with tissue from young animals AND significantly hypermethylated Entrez Gene IDs in tissue from ER fed animals compared with tissue from AL fed animals = 24 hits; representation factor = 1.50 and hypergeometric probability = 1.13 x 10^{-2} (Figure 6.6, panel D).

A

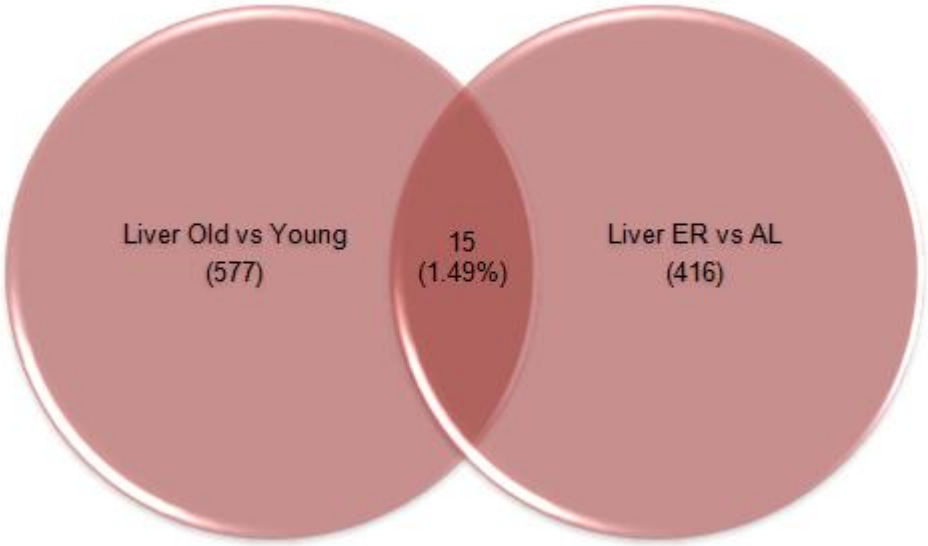

red = hypermethylation;
blue = hypomethylation

B

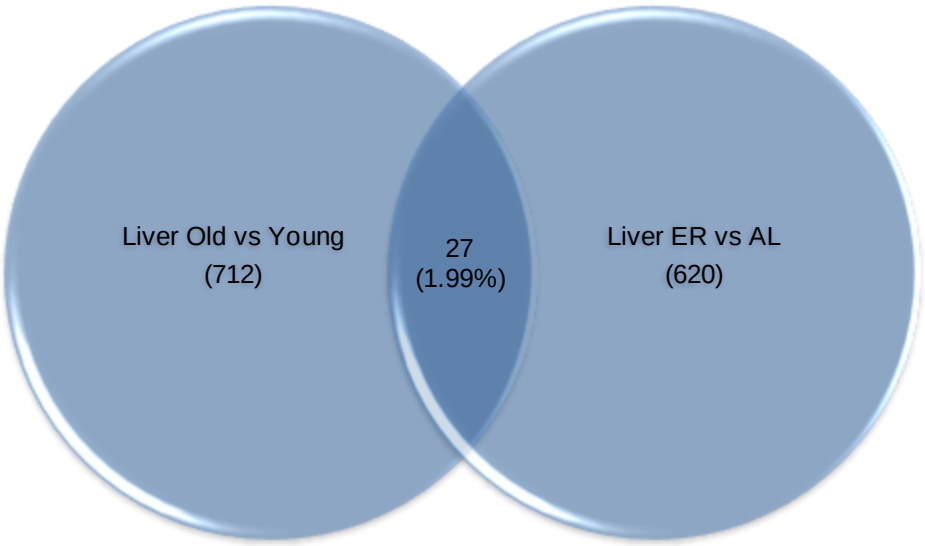

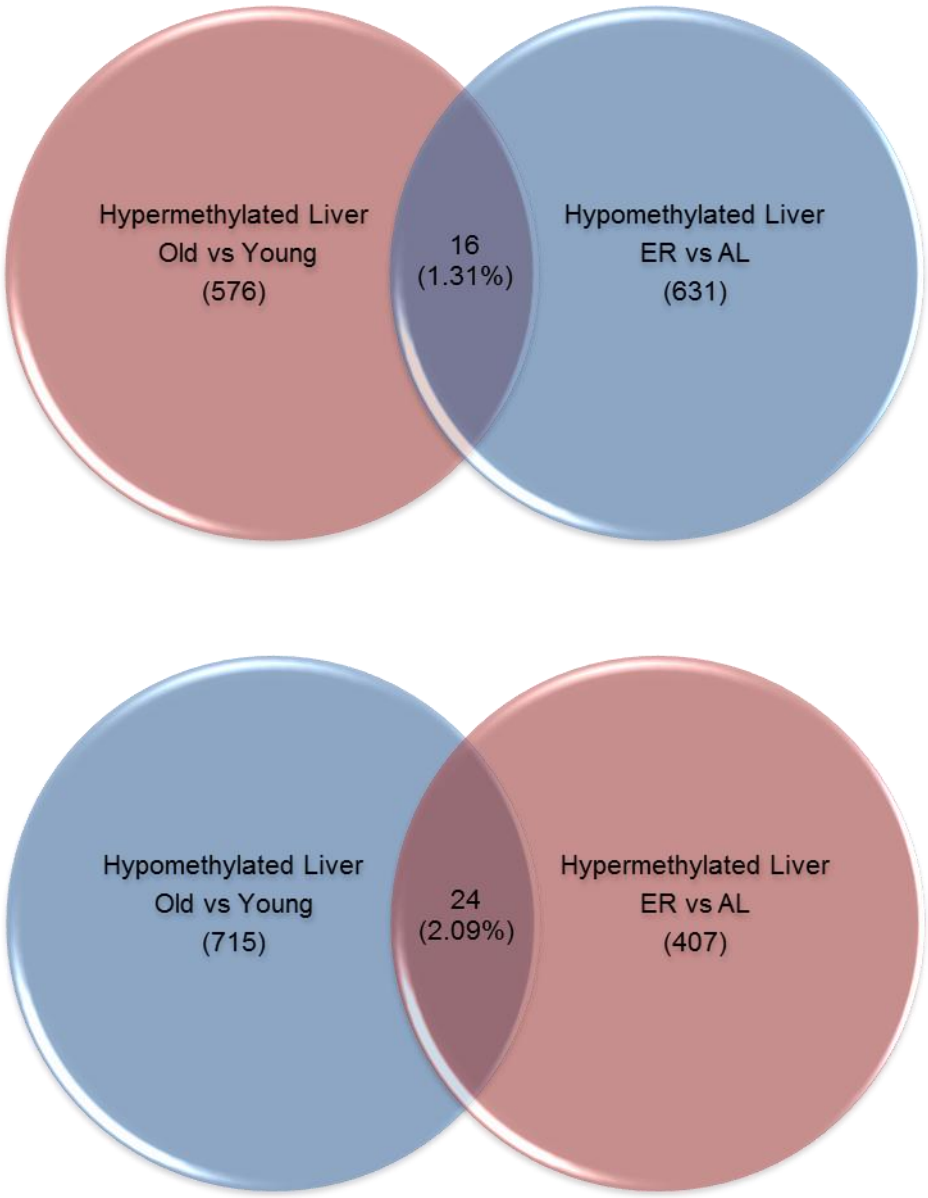

Figure 6.6. Effects of short-term dietary energy restriction on age-related DNA methylation changes in murine liver shown as Venn diagrams. Panel A shows common significantly hypermethylated Entrez Gene IDs in tissue from older animals compared with tissue from young animals and in tissue from ER fed animals compared with tissue from AL fed animal; panel B shows common significantly hypomethylated Entrez Gene IDs in tissue from older animals compared with tissue from young animals and in tissue from ER fed animals compared with tissue from AL fed animals; panel C shows intersection between hypermethylated Entrez Gene IDs in tissue from older animals compared with tissue from young animals and hypomethylated Entrez Gene IDs in tissue from ER fed animals compared with tissue from AL fed animals; panel D shows intersection between hypomethylated Entrez Gene IDs in tissue from older animals

compared with tissue from young animals and hypermethylated Entrez Gene IDs in tissue from ER fed animals compared with tissue from AL fed animals.

These data indicated that the number of hits in the intersections was significantly higher than what would be expected to be found by chance only in the fourth intersection; for this reason, I provide below the hits list for this case, but not for all other cases (Table 6.4).

6.3.2 Pathway analysis for those genes which were differentially methylated in response to ageing and to short-term dietary energy restriction

The IDs and official gene symbols which appeared in the intersections shown in Figure 6.4, panel D are given in Table 6.4, which summarises those genes which were significantly hypomethylated in tissue from older animals compared with tissue from young animals and hypermethylated in tissue from ER fed animals compared with tissue from AL fed animals.

Table 6.4. Genes which showed opposite methylation response to ageing and short-term dietary energy restriction in murine liver. Genes which are hypomethylated in liver tissue from older animals compared with liver tissue from young animals but hypermethylated in liver tissue from ER fed animals compared with AL fed animals are listed. The Entrez Gene IDs and gene symbols are shown. The annotation (Gene ID withdrawn) indicates that the record has been discontinued and it is not in the current genome assembly.

Hypomethylation in ageing liver
and Hypermethylation in ER liver

Entrez Gene ID	Gene symbol
13491	Drd4
14113	Fbl
14297	Fxn
14594	Ggta1
15900	Irf8
19337	Rab33a
19411	Rarg
26926	Aifm1
27274	Zfp354b

60613	Kcnq4
64685	Nmi
68877	Maf1
74525	8430419L09Rik
140482	Zfp358
214305	Hhipl1
215387	Ncaph
230909	Gm572
231932	Gimap7
246177	Myo1g
246728	Oas2
317757	Gimap5
100039672	Msmp
100044605	(Gene ID withdrawn)
100044829	LOC100044829

Similarly to what previously done for the ageing vs young comparisons, I performed canonical pathways analysis and signal transduction pathways analysis using the list of genes in Table 6.4; this was because this intersection showed a representation factor higher than 1 and significant hypergeometric probability, indicating more overlap than expected of two independent groups. Results of such analyses are reported in Table 6.5 and show one significantly enriched canonical pathway (opposing roles of aif in apoptosis and cell survival) and one significantly enriched signal transduction pathway (redox signalling).

Table 6.5. Canonical (panel A) and signal transduction pathway analyses (panel B) for opposite promoter methylation changes in ageing and dietary energy restricted fed mice livers.

A

Canonical Pathway	**p value**	**Genes observed/total**	**Genes official symbol**
opposing roles of aif in apoptosis and cell survival	6.11E-03	1/3	Aifm1

B

Signal Transduction Pathway	**p value**	**Genes observed/total**	**Genes official symbol**
REDOX	9.49E-03	2/126	Aifm1, Irf8

6.4 Discussion

This study was designed to use genome-wide array-based approaches to identify: i) common aberrantly methylated genomic regions in DNA from two different tissues (heart and liver) obtained from older mice when compared with tissue obtained from young mice and ii) common aberrantly methylated genomic regions in DNA from liver from mice exposed to short-term dietary energy restriction when compared with tissue obtained from *ad libitum* fed mice and in DNA from liver obtained from older mice when compared with tissue obtained from young mice.

6.4.1 Age-related DNA methylation changes in mouse heart and liver

For the first part of the study, I chose 2 tissues with different proliferative capacities i.e. heart and liver. To a large extent, cardiomyocytes are post-mitotic cells, i.e. cells that unable to proliferate and that remain in an irreversible state of arrested cell cycle upon differentiation although it is recognised that the heart tissue can undergo limited repair and regeneration (Ellison et al., 2012). In contrast, hepatocytes are mitotic cells, that is cells capable of proliferation when stimulated to renew in response to damage (Campisi and d'Adda di Fagagna, 2007). It has been proposed that some of the processes contributing to the ageing phenotype may be different in mitotic and post-mitotic tissues (Campisi and Warner, 2001). In fact, post-mitotic cells are not replaced after death due to malfunction or progressive accumulation of damage whilst cells in mitotic tissues develop a senescent phenotype over time, thus compromising surrounding cells and the homeostasis of the whole tissue. More recently, it has been shown that cells in post-mitotic tissues also develop a senescent phenotype and that this contributes to the accumulation of oxidative and inflammatory damage and which may exacerbate ageing of the whole tissue (Jurk et al., 2012).

Given the evidence that some of the mechanisms contributing to the ageing process are shared among different tissues, I wanted to assess the extent to which different tissues showed the same changes in DNA methylation during ageing and thus identify genes whose methylation status may be particularly susceptible to age-dependent alteration and which may play a major role in the ageing process. This is the first study that has compared age-related site-specific aberrant DNA methylation in ageing heart and liver in mice.

Using the MeDIP technique followed by hybridisation to whole genome promoter methylation arrays, I found a that a similar proportion of gene promoters (around 5% or >1000 genes) were affected by ageing in both tissues and that more gene promoters showed hypomethylation than hypermethylation in both ageing heart and liver. Despite the relatively small number of gene promoters (n = 108) which were differentially methylated in ageing and the limited number of available animals (n = 3), over-representation analyses yielded statistical significance for all of the intersections cases taken into consideration (see section 6.2.1). Thus, there is evidence that the observed same-direction and opposite-direction alteration of methylation patterns may not be totally stochastic. It should be noted that the statistical analyses provided reassurance that the number of genes featured in the various intersections was higher than what would be expected by chance but did not indicate, of course, which of these specific gene changes were truly in common since some of those gene showing methylation changes in common could have occurred by chance. In addition, a limitation of the present study design is that it does not allow me to distinguish between those methylation changes which might be causal for the ageing process and which are consequences of ageing. Hence, further experimental approaches are needed to be able to identify the genes which are relevant for the biology of ageing. However, whether causal or consequential, the genes which I've discovered show age-related aberrant DNA methylation could be potential markers of the ageing process.

DNA methylation changes which occurred in the opposite direction in the 2 tissues (n = 61) i.e. hypomethylated in one but hypermethylated in the other may be ascribed to the tissue-specificity of the DNA methylation patterns in ageing, which has already been documented (Thompson et al., 2010). In their study, (Thompson et al., 2010) compared age-related methylation changes in rat liver and adipose tissue and found that most of the high tissue-specificity resided at inter-genic sequences and conserved non-coding elements and not at gene promoters. Therefore, I hypothesize that concordant (or conserved) gene promoters aberrant DNA methylation (n = 41) may be of particular interest in the epigenetics of ageing in multiple species.

Interpretation of the functional consequences of the observed methylation changes in the present study was limited by the lack of gene expression data from the same samples. As a result I was unable to determine whether the detected changes in DNA methylation were associated with altered gene expression and to establish if similar gene expression changes occurred in both tissues (heart and liver).

Performing pathway analysis on the concordant DNA methylation changes in DNA from the two tissues revealed that the genes whose promoters where affected by ageing were involved in intercellular communication, cellular development/proliferation control, stress response (*Wnt5a*, *Map4k5*, *Apcdd1*) and malignant transformation (*Chp2*) for genes exhibiting hypermethylation and involved in cell growth/differentiation and survival (*Rasgrp2*) for genes exhibiting hypomethylation. Down-regulation of expression of the *Wnt5a* gene has been shown in mature osteoblasts from aged mice (Rauner et al., 2008) and this decreased *Wnt5a* expression could be consistent with the promoter hypermethylation detected in my study. Importantly, *Wnt5a* hypermethylation has been described in several cancers, including acute lymphoblastic leukaemia (Roman-Gomez et al., 2007), acute myeloid leukaemia (Martin et al., 2010), colorectal cancer (Rawson et al., 2011) and gastric carcinoma (Liu et al., 2013), which are amongst the most common cancers in older people (Hansen, 1998). To my knowledge, there have been no previous reports of changes in DNA methylation or in gene expression in ageing for the *Map4k5*, *Apcdd1*, *Chp2* and *Rasgrp2* genes so these are among the potential interesting targets for further investigation in the field of epigenetics of ageing.

A number of different mechanisms may be responsible for the altered DNA methylation patterns observed in this study. For example, age-related hypomethylation could be the result of the incorrect functioning of the maintenance methyltransferase (Dnmt1) on hemimethylated DNA in liver cells during the DNA replication process. In addition, hydrolytic deamination of 5'-methylCytosine to Thymine, described by (Wang et al., 1982) might be responsible for methylation changes in heart cells. On the other hand, age-related hypermethylation in both tissues probably occurs due to incorrect targeting of the DNA Methyltransferases enzymes, as described in (Casillas et al., 2003).

6.4.2 Effect of dietary energy restriction on age-related aberrant DNA methylation in mouse liver

In the second part of this study, I found that the predominance of hypomethylation in DNA from liver in old vs young animals was also apparent in the DNA from liver from dietary energy restricted vs *ad libitum* fed animals. The number of genes in intersection between age-affected and ER-affected genes showing altered promoter methylation was small but significant. About half of these genes (n = 42) showed concordant DNA methylation changes and for half (n = 40) the methylation changes occurred in the

opposite direction in response to ageing and to ER in DNA from liver. Given that mice used for the ageing study were killed at 30 months of age and mice used for the dietary intervention study were killed at 17 months of age, I hypothesize that same-direction DNA methylation changes may have been early-onset ageing related events which were unaffected by the short-term dietary energy restriction regimen. On the other hand, those genes showing changes in methylation in opposite directions in response to ageing and to ER may be responsible for mediating the beneficial effects of the dietary energy restriction regimen in slowing the ageing process.

Genes for which the promoters were hypomethylated in ageing samples and hypermethylated following dietary energy restriction were used in subsequent pathways analyses. The results of this bioinformatics analysis revealed that short-term dietary energy restriction affected promoter methylation of genes which play roles in apoptosis regulation (*Aifm1*) and in inflammatory responses to viral infection (*Irf8*). Previous studies have shown that even short-term dietary energy restriction affects the expression of genes involved in apoptosis in mouse hepatocytes (James et al., 1998) and liver (Cao et al., 2001), in human *in vitro* cell models and in *C. elegans* (Morselli et al., 2010) and genes involved in inflammation in mouse liver (Cao et al., 2001) and adipose tissue (Higami et al., 2006). Since both *Aifm1* and *Irf8* genes are included in the redox signaling transduction pathway, my observation that they show discordant changes in promoter methylation in response to ageing and to ER may be functionally important. This could suggest a possible epigenetic mechanism through which ER modulates the ageing process because ROS accumulation contributes to the biology of ageing through promotion of molecular damage, as outlined in Chapter 1 and reviewed in (Stadtman, 2004). However, to my knowledge, there have been no previous published studies of the effects of ageing and of ER on promoter methylation of the *Aifm1* and *Irf8* genes nor have data for corresponding gene expression profiles been published. Further work is warranted to discover whether these two genes are potential novel targets whose aberrant methylation in ageing is counteracted by dietary energy restriction which may help in elucidating the mechanisms through which dietary energy restriction exerts its anti-ageing effect.

Other gene promoters for which age-related aberrant promoter methylation was counteracted by dietary energy restriction included genes involved in transcription regulation (*Rarg*), immune response to viral infection (*Nmi*, *Maf1*), vesicle trafficking (*Rab33a*) and mitochondrial iron transport and respiration (*Fxn*). I am not aware of any

previous studies which have reported changes in promoter methylation or gene expression patterns for these genes in ageing or following ER. Further studies including validation (by pyrosequencing) of the observed changes in DNA methylation integrated with gene expression studies may provide a molecular explanation for some of the beneficial effects of dietary energy restriction in delaying the ageing process and in reducing the risk of age-related diseases.

6.5 Conclusions

In the work described in this Chapter I found that:

- in both mouse heart and liver, there were >1000 genes showing age-related changes in promoter methylation changes and that most (about 95%) of these genes changes were tissue-specific;
- a significant proportion of the genes showing age-dependent changes in promoter methylation were common to both liver and to heart suggesting that these genes may be universally susceptible to age-related aberrant methylation;
- the ageing process in both mouse heart and liver is characterized by the dysregulation of normal DNA methylation profiles of promoters of genes involved in intercellular communication, stress response, malignant transformation, cellular development/proliferation control and cell growth/differentiation and survival;
- the promoters of *Wnt5a*, *Map4k5*, *Apcdd1*, *Chp2* and *Rasgrp2* show aberrant methylation in DNA from both mouse heart and liver in ageing;
- short-term dietary energy restriction of mice in mid-life (from 14 – 17 months of age) resulted in altered promoter methylation of 1078 genes in DNA from liver compared with that from ad libitum-fed counterparts;
- short-term dietary energy restriction appeared to counteract age-related methylation changes in the promoters of a significant proportion of the genes and the latter genes included those involved in apoptosis regulation, inflammatory and immune response to viral infections, transcription regulation, vesicle trafficking and mitochondrial iron transport and respiration;
- age-dependent methylation of the promoters of *Aifm1*, *Irf8*, *Rarg*, *Nmi*, *Maf1*, *Rab33a* and *Fxn* genes was counteracted by dietary energy restriction.

Chapter 7. Mitochondrial DNA methylation in senescence and ageing and in response to dietary energy restriction

7.1 Outline

The recent discovery of the presence of the *DNMT1/Dnmt1* proteins in human and murine mitochondria has raised interest in the study of methylation of mitochondrial DNA. (Shock et al., 2011) demonstrated that both human and murine genomes feature a mitochondrial importing sequence upstream of the *DNMT1* and *Dnmt1* genes; both importing sequences are transcribed and translated and are capable of translocating the related protein products into the mitochondria. In addition, the authors confirmed that both DNMT1 and Dnmt1 bind to mitochondrial DNA and that these are the only enzymes of the DNAMethylTransferases family that are found in the organelle. Their conclusion is that, given the presence of methylated Cytosines in the mitochondrial genome (Nass, 1973; Shmookler Reis and Goldstein, 1983), DNMT1 and Dnmt1 must be responsible for the CpG methylation patterns found in the mitochondrial genome.
Their hypothesis fits with the prior *in vitro* observation that human DNMT1 and murine Dnmt1 show, to a certain extent, *de novo* methyltransferase activity (Chen et al., 1998; Pradhan et al., 1997). In contrast, much previous work has been based on the assumption that DNMT1 and Dnmt1 behave as the maintenance DNA methyltransferases, which are responsible for copying DNA methylation patterns during DNA replication.

In this study, I chose 5 CpG-rich regions within the human mitochondrial genome and 2 within the murine mitochondrial genome and assessed their methylation status by BM-DNA PCR and direct sequencing. The DNA for these studies was extracted from i) YC, ESIPS and RS MRC-5 human lung fibroblasts, ii) liver from young and old mice and iii) liver from both *ad libitum* fed and dietary energy restricted mice. In this way, I investigated whether senescence/ageing or dietary intervention altered in the patterns of mtDNA methylation.

7.2 Bioinformatics analyses of the human mitochondrial DNA molecule and choice of candidate regions for methylation studies

The human mitochondrion genome is a 16569 bp circular double strand DNA molecule, present in several copies in each organelle. To select candidate regions for my methylation studies, I obtained its sequence from the PubMed database (http://www.ncbi.nlm.nih.gov/nuccore/NC_012920) and searched for putative CpG islands using the webtool CpG plot (http://www.ebi.ac.uk/Tools/seqstats/emboss_cpgplot/), focussing on the sequences of the 13 protein-encoding mitochondrial genes, the D-Loop regulatory region and a long non-protein-coding region at the 5' end of the *ND1* gene. Applying the default settings of the program (island of at least 200 bp, % of C + G of at least 50% and C + G observed/expected ratio of at least 0.6), I identified a unique region that met the selection criteria, the *COX2* gene encoding region. To identify a higher number of putative candidates for methylation analyses, I therefore decided to apply less stringent criteria, reducing the length of the islands to a minimum of 100 bp. By doing so, the following eight genomic regions were identified:

- MT-non-coding region (5' end of the MT-ND1 gene);
- MT-*ND1* coding region;
- MT-*COX1* coding region;
- MT-*COX2* coding region;
- MT-*ATP6* coding region;
- MT-*ND4* coding region;
- MT-*ND5* coding region;
- MT-*CYTB* coding region.

I designed, and attempted to optimize, primers for PCR amplification of bisulphite modified DNA, as described in section 2.18. However, the optimization failed to yield a unique product – or any product – in the PCR trials for the MT-*COX2*, the MT-*ATP6* and the MT-*CYTB* gene sequences. These were removed from the gene panel and I therefore pursued methylation analyses of the other 5 genomic regions. Results of these analyses are reported in the section 7.3 below.

7.3 Quantification of CpG methylation at a single CpG level for five genomic regions within the human mtDNA in early stress-induced premature senescence and in replicative senescence

After total genomic DNA extraction (see section 2.3), I performed bisulphite modification (see section 2.17), BM-PCR (see section 2.18) and sequencing (see section 2.19) on one sample from each YC, ESIPS and RS cells and performed statistical analyses on the measured methylation values across the analyzed genomic regions. For the latter a paired t-test was used which compared methylation values at each CpG site within the region of interest from each of the cell types.
In the following sections, I provide the sequences of the DNA sequences under investigation and the related results for CpG methylation analyses.

7.3.1 MT-COI mitochondrially encoded cytochrome c oxidase I [Homo sapiens], Gene ID: 4512

1 atgttcgccg accgttgact attctctaca aaccacaaag acattggaac actataccta
61 ttattcggcg catgagctgg agtcctaggc acagctctaa gcctccttat tcgagccgag
121 ctgggccagc caggcaacct tctaggtaac gaccacatct acaacgttat cgtcacagcc
181 catgcatttg taataatctt cttcatagta atacccatca taatcggagg ctttggcaac
241 tgactagttc ccctaataat cggtgccccc gatatggcgt ttcccgcat aaacaacata
301 agcttctgac tcttacctcc ctctctccta ctcctgctcg catctgctat agtggaggcc
361 ggagcaggaa caggttgaac agtctaccct cccttagcag ggaactactc ccaccctgga
421 gcctccgtag acctaaccat cttctcctta cacctagcag gtgtctcctc tatcttaggg
481 gccatcaatt tcatcacaac aattatcaat ataaaacccc ctgccataac ccaataccaa
541 acgcccctct tcgtctgatc cgtcctaatc acagcagtcc tacttctcct atctctccca
601 gtcctagctg ctggcatcac tatactacta acagaccgca acctcaacac caccttcttc
661 gaccccgccg gaggaggaga ccccattcta taccaacacc tattctgatt tttcggtcac
721 cctgaagttt atattcttat cctaccaggc ttcggaataa tctcccatat tgtaacttac
781 tactccggaa aaaaagaacc atttggatac ataggtatgg tctgagctat gatatcaatt
841 ggcttcctag ggtttatcgt gtgagcacac catatattta cagtaggaat agacgtagac
901 acacgagcat atttcacctc cgctaccata atcatcgcta tccccaccgg cgtcaaagta
961 tttagctgac tcgccacact ccacggaagc aatatgaaat gatctgctgc agtgctctga
1021 gccctaggat tcatctttct tttcaccgta ggtggcctga ctggcattgt attagcaaac
1081 tcatcactag acatcgtact acacgacacg tactacgttg tagcccactt ccactatgtc

1141 ctatcaatag gagctgtatt tgccatcata ggaggcttca ttcactgatt tcccctattc
1201 tcaggctaca ccctagacca aacctacgcc aaaatccatt tcactatcat attcatcggc
1261 gtaaatctaa ctttcttccc acaacacttt ctcggcctat ccggaatgcc ccgacgttac
1321 tcggactacc ccgatgcata caccacatga aacatcctat catctgtagg ctcattcatt
1381 tctctaacag cagtaatatt aataattttc atgatttgag aagccttcgc ttcgaagcga
1441 aaagtcctaa tagtagaaga accctccata aacctggagt gactatatgg atgccccca
1501 ccctaccaca cattcgaaga acccgtatac ataaaatcta ga

Figure 7.1. MT-COI gene sequence. Genomic regions used as priming sites for methylation studies are underlined; CpG sites investigated in this study are indicated in bold orange font.

Figure 7.2 shows the percentage of CpG methylation measured across 11 CpG sites within the *MT-COI* gene coding sequence in YC, ESIPS and RS MRC-5 cells: YC cells methylation ranged between 0% and 11% (median value = 4%), ESIPS cells methylation ranged between 0% and 38% (median value = 15%) and RS cells methylation ranged between 0% and 22% (median value = 5%). There was a statistically significant difference in methylation content between YC and ESIPS cells (p = 0.002) and between YC and RS cells (p = 0.025).

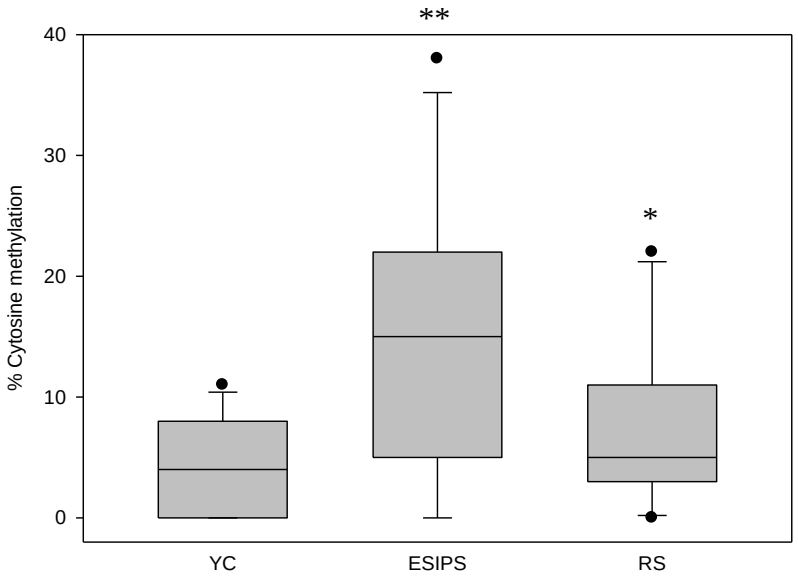

Figure 7.2. MT-COI CpG methylation measured by BM PCR direct sequencing. Box plots show the percentiles and the median of the percentages of Cytosine methylation. Box outlines define the 25th and 75th percentiles, with a line at the median, and whiskers

*indicate the 10th and 90th percentiles; dots indicate outliers. * = p < 0.05; ** = p < 0.01 for student's paired t-test in which methylation levels at individual CpG sites were compared across cell types.*

7.3.2 Homo sapiens mitochondrion genome, non-coding region, GenBank: J01415.2

901 ggtcacacga ttaacccaag tcaatagaag ccggcgtaaa gagtgtttta gatcaccccc
961 tccccaataa agctaaaact cacctgagtt gtaaaaaact ccagttgaca caaaatagac
1021 tacgaaagtg gctttaacat atctgaacac acaatagcta agacccaaac tgggattaga
1081 taccccacta tgcttagccc taaacctcaa cagttaaatc aacaaaactg ctcgccagaa
1141 cactacgagc cacagcttaa aactcaaagg acctggcggt gcttcatatc cctctagagg
1201 agcctgttct gtaatcgata aacccgatc aacctcacca cctcttgctc agcctatata
1261 ccgccatctt cagcaaaccc tgatgaaggc tacaaagtaa gcgcaagtac ccacgtaaag
1321 acgttaggtc aaggtgtagc ccatgaggtg gcaagaaatg ggctacattt tctaccccag
1381 aaaactacga tagcccttat gaaacttaag ggtcgaaggt ggatttagca gtaaactaag
1441 agtagagtgc ttagttgaac agggccctga agcgcgtaca caccgcccgt caccctcctc

Figure 7.3. Portion of the human mitochondrion genome non-protein-coding region. Genomic regions used as priming sites for methylation studies are underlined; CpG sites investigated in this study are indicated in bold orange font.

Figure 7.4 shows the percentage of CpG methylation measured across 9 CpG sites within the human mitochondrion genome non-coding region sequence in YC, ESIPS and RS MRC-5 cells: YC cells methylation ranged between 0% and 13% (median value = 1%), ESIPS cells methylation ranged between 0% and 15% (median value = 4%) and RS cells methylation ranged between 0% and 9% (median value = 3%). There was no statistically significant difference in methylation content between YC and ESIPS cells, nor between YC and RS cells.

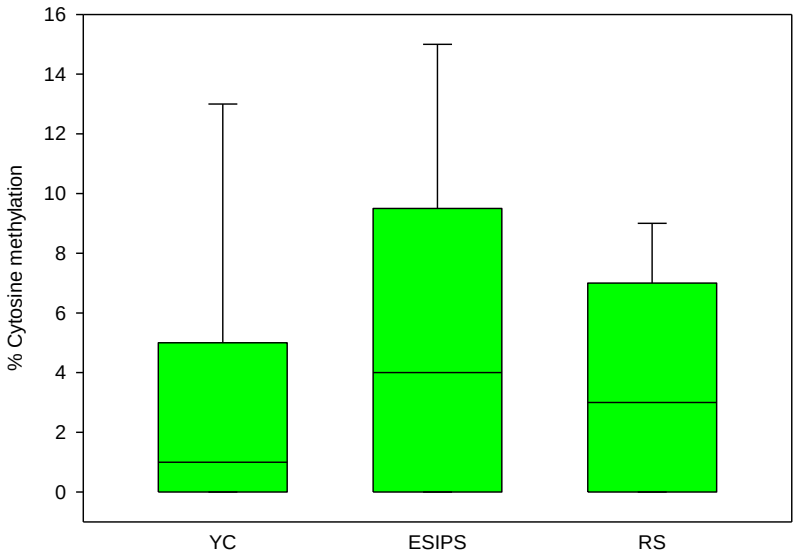

Figure 7.4. Human mitochondrion genome non-coding region CpG methylation measured by BM PCR direct sequencing. Box plots show the percentiles and the median of the percentages of Cytosine methylation. Box outlines define the 25th and 75th percentiles, with a line at the median, and whiskers indicate the 10th and 90th percentiles.

7.3.3. MT-ND1 mitochondrially encoded NADH dehydrogenase 1 [Homo sapiens], Gene ID: 4535

1 atacccatgg ccaacctcct actcctcatt gtacccattc taatcgcaat ggcattccta
61 atgcttaccg aacgaaaaat tctaggctat atacaactac gcaaaggccc caacgttgta
121 ggccccta cg ggctactaca acccttcgct gacgccataa aactcttcac caaagagccc
181 ctaaaaccg ccacatctac catcaccctc tacatcaccg cccgacctt agctctcacc
241 atcgctcttc tactatgaac ccccctcccc atacccaacc ccctggtcaa cctcaaccta
301 ggcctcctat ttattctagc cacctctagc ctagccgttt actcaatcct ctgatcaggg
361 tgagcatcaa actcaaacta cgccctgatc ggcgcactgc gagcagtagc ccaaacaatc
421 tcatatgaag tcaccctagc catcattcta ctatcaacat tactaataag tggctccttt
481 aacctctcca cccttatcac aacacaagaa cacctctgat tactcctgcc atcatgaccc
541 ttggccataa tatgatttat ctccacacta gcagagacca accgaacccc cttcgacctt
601 gccgaagggg agtccgaact agtctcaggc ttcaacatcg aatacgccgc aggccccttc
661 gccctattct tcatagccga atacacaaac attattataa taaacaccct caccactaca
721 atcttcctag gaacaacata tgacgcactc tcccctgaac tctacacaac atattttgtc
781 accaagaccc tacttctaac ctccctgttc ttatgaattc gaacagcata cccccgattc

841 cgctacgacc aactcataca cctcctatga aaaaacttcc taccactcac cctagcatta
901 cttatatgat atgtctccat acccattaca atctccagca ttccccctca aaccta

Figure 7.5. MT-ND1 gene sequence. Genomic regions used as priming sites for methylation studies are underlined; CpG sites investigated in this study are indicated in bold orange font.

Figure 7.6 shows the percentage of CpG methylation measured across 12 CpG sites within the *MT-ND1* gene coding sequence in YC, ESIPS and RS MRC-5 cells: YC cells methylation ranged between 0% and 29% (median value = 2%), ESIPS cells methylation ranged between 0% and 34% (median value = 7%) and RS cells methylation ranged between 0% and 38% (median value = 10%). There was a statistically significant difference in methylation content between YC and ESIPS cells (p = 0.011) and between YC and RS cells (p = 0.002).

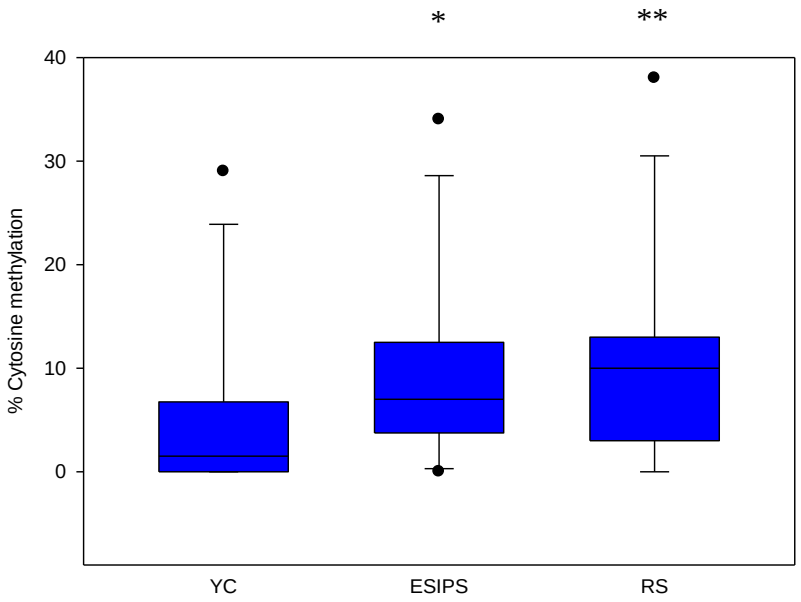

*Figure 7.6. MT-ND1 CpG methylation measured by BM PCR direct sequencing. Box plots show the percentiles and the median of the percentages of Cytosine methylation. Box outlines define the 25th and 75th percentiles, with a line at the median, and whiskers indicate the 10th and 90th percentiles; dots indicate outliers. * = p < 0.05; ** = p< 0.01 for student's paired t-test in which methylation levels at individual CpG sites were compared across cell types.*

7.3.4 MT-ND4 mitochondrially encoded NADH dehydrogenase 4 [Homo sapiens], Gene ID: 4538

1 atgctaaaac taatcgtccc aacaattata ttactaccac tgacatgact ttccaaaaaa
61 cacataattt gaatcaacac aaccacccac agcctaatta ttagcatcat ccctctacta
121 ttttttaacc aaatcaacaa caacctattt agctgttccc caacctttтc ctccgacccc
181 ctaacaaccc ccctcctaat actaactacc tgactcctac ccctcacaat catggcaagc
241 caacgccact tatccagtga accactatca cgaaaaaaac tctacctctc tatactaatc
301 tccctacaaa tctccttaat tataacattc acagccacag aactaatcat attttatatc
361 ttcttcgaaa ccacacttat ccccaccttg gctatcatca cccgatgagg caaccagcca
421 gaacgcctga acgcaggcac atacttccta ttctacaccc tagtaggctc ccttccccta
481 ctcatcgcac taatttacac tcacaacacc ctaggctcac taaacattct actactcact
541 ctcactgccc aagaactatc aaactcctga gccaacaact taatatgact agcttacaca
601 atagctttta tagtaaagat acctctttac ggactccact tatgactccc taaagcccat
661 gtcgaagccc ccatcgctgg gtcaatagta cttgccgcag tactcttaaa actaggcggc
721 tatggtataa tacgcctcac actcattctc aacccccтga caaaacacat agcctacccc
781 ttccttgtac tatccctatg aggcataatt ataacaagct ccatctgcct acgacaaaca
841 gacctaaaat cgctcattgc atactcttca atcagccaca tagccctcgt agtaacagcc
901 attctcatcc aaacccccтg aagcttcacc ggcgcagtca ttctcataat cgcccacggg
961 cttacatcct cattactatt ctgcctagca aactcaaact acgaacgcac tcacagtcgc
1021 atcataatcc tctctcaagg acttcaaact ctactcccac taatagcttt ttgatgactt
1081 ctagcaagcc tcgctaacct cgccttaccc cccactatta acctactggg agaactctct
1141 gtgctagtaa ccacgttctc ctgatcaaat atcactctcc tacttacagg actcaacata
1201 ctagtcacag ccctatactc cctctacata tttaccacaa cacaatgggg ctcactcacc
1261 caccacatta acaacataaa accctcattc acacgagaaa acaccctcat gttcatacac
1321 ctatccccca ttctcctcct atccctcaac cccgacatca ttaccgggtt ttcctctt

Figure 7.7. MT-ND4 gene sequence. Genomic regions used as priming sites for methylation studies are underlined; CpG sites investigated in this study are indicated in bold orange font.

Figure 7.8 shows the percentage of CpG methylation measured across 8 CpG sites within the *MT-ND4* gene coding sequence in YC, ESIPS and RS MRC-5 cells: YC cells methylation ranged between 0% and 9% (median value = 6%), ESIPS cells methylation ranged between 0% and 15% (median value = 4%) and RS cells methylation ranged

between 0% and 9% (median value = 3%). There was no statistically significant difference in methylation content between YC and ESIPS cells, nor between YC and RS cells.

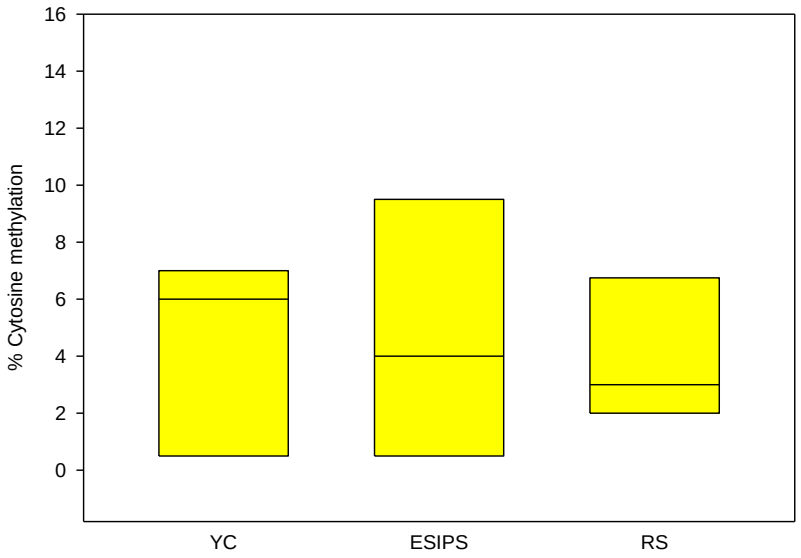

Figure 7.8. MT-ND4 CpG methylation measured by BM PCR direct sequencing. Box plots show the percentiles and the median of the percentages of Cytosine methylation. Box outlines define the 25th and 75th percentiles, with a line at the median.

7.3.5. MT-ND5 mitochondrially encoded NADH dehydrogenase 5 [Homo sapiens], Gene ID: 4540

1 ataaccatgc acactactat aaccacccta accctgactt ccctaattcc ccccatcctt
61 accaccctcg ttaaccctaa caaaaaaaac tcataccccc attatgtaaa atccattgtc
121 gcatccacct ttattatcag tctcttcccc acaacaatat tcatgtgcct agaccaagaa
181 gttattatct cgaactgaca ctgagccaca acccaaacaa cccagctctc cctaagcttc
241 aaactagact acttctccat aatattcatc cctgtagcat tgttcgttac atggtccatc
301 atagaattct cactgtgata tataaactca gacccaaaca ttaatcagtt cttcaaatat
361 ctactcatct tcctaattac catactaatc ttagttaccg ctaacaacct attccaactg
421 ttcatcggct gagagggcgt aggaattata tccttcttgc tcatcagttg atgatacgcc
481 cgagcagatg ccaacacagc agccattcaa gcaatcctat acaaccgtat cggcgatatc
541 ggtttcatcc tcgccttagc atgatttatc ctacactcca actcatgaga cccacaacaa
601 atagcccttc taaacgctaa tccaagcctc accccactac taggcctcct cctagcagca
661 gcaggcaaat cagcccaatt aggtctccac ccctgactcc cctcagccat agaaggcccc

721 accccagtct cagccctact ccactcaagc actatagttg tagcaggaat cttcttactc
781 atccgcttcc acccccctagc agaaaatagc ccactaatcc aaactctaac actatgctta
841 ggcgctatca ccactctgtt cgcagcagtc tgcgccctta cacaaaatga catcaaaaaa
901 atcgtagcct tctccacttc aagtcaacta ggactcataa tagttacaat cggcatcaac
961 caaccacacc tagcattcct gcacatctgt acccacgcct tcttcaaagc catactattt
1021 atgtgctccg ggtccatcat ccacaacctt aacaatgaac aagatattcg aaaaatagga
1081 ggactactca aaaccatacc tctcacttca acctccctca ccattggcag cctagcatta
1141 gcaggaatac ctttcctcac aggtttctac tccaaagacc acatcatcga aaccgcaaac
1201 atatcataca caaacgcctg agccctatct attactctca tcgctacctc cctgacaagc
1261 gcctatagca ctcgaataat tcttctcacc ctaacaggtc aacctcgctt ccccacccctt
1321 actaacatta acgaaaataa ccccacccta ctaaacccca ttaaacgcct ggcagccgga
1381 agcctattcg caggatttct cattactaac aacatttccc ccgcatcccc cttccaaaca
1441 acaatccccc tctacctaaa actcacagcc ctcgctgtca ctttcctagg acttctaaca
1501 gccctagacc tcaactacct aaccaacaaa cttaaaataa aatccccact atgcacattt
1561 tatttctcca acatactcgg attctaccct agcatcacac accgcacaat cccctatcta
1621 ggccttctta cgagccaaaa cctgccccta ctcctcctag acctaacctg actagaaaag
1681 ctattaccta aaacaatttc acagcaccaa atctccacct ccatcatcac ctcaacccaa
1741 aaaggcataa ttaaacttta cttcctctct ttcttcttcc cactcatcct aaccctactc
1801 ctaatcacat aa

Figure 7.9. MT-ND5 gene sequence. Genomic regions used as priming sites for methylation studies are underlined; CpG sites investigated in this study are indicated in bold orange font.

Figure 7.10 shows the percentage of CpG methylation measured across 10 CpG sites within the *MT-ND5* gene coding sequence in YC, ESIPS and RS MRC-5 cells: YC cells methylation ranged between 0% and 17% (median value = 8%), ESIPS cells methylation ranged between 0% and 13% (median value = 2%) and RS cells methylation ranged between 0% and 17% (median value = 7%). There was no statistically significant difference in methylation content between YC and ESIPS cells, nor between YC and RS cells.

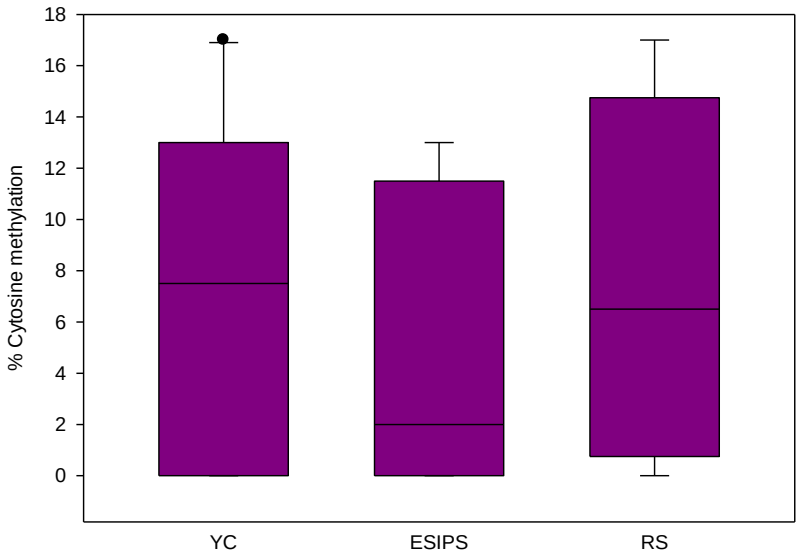

Figure 7.10. MT-ND5 CpG methylation measured by BM PCR direct sequencing. Box plots show the percentiles and the median of the percentages of Cytosine methylation. Box outlines define the 25th and 75th percentiles, with a line at the median, and whiskers indicate the 10th and 90th percentiles; dots indicate outliers.

7.4 Bioinformatics analyses of the murine mitochondrial DNA molecule and choice of candidate regions for methylation studies

The murine mitochondrion genome is a 16300 bp circular double strand DNA molecule, present in several copies in each organelle. To select candidate regions for my methylation studies, I obtained its sequence from the PubMed database (http://www.ncbi.nlm.nih.gov/nuccore/NC_010339) and looked for putative CpG islands using the webtool CpG plot (http://www.ebi.ac.uk/Tools/seqstats/emboss_cpgplot/), focussing on the sequences of the 13 mitochondria-encoded genes, the D-Loop regulatory region and a long non-protein-coding region at the 5' end of the *Nd1* gene. Applying the default settings of the program (island of at least 200 bp, % of C + G of at least 50% and C + G observed/expected ratio of at least 0.6), I was not able to identify regions that met the selection criteria; I therefore decided to apply less stringent criteria, lowering the length of the islands to a minimum of 100 bp. By doing so, only one CpG island was identified, included in the genomic region non-coding region at the 5' end of the *Nd1* gene was identified. In an additional attempt to identify more candidate regions, I further

lowered the length of the islands to a minimum of 50 bp; this process yielded a total of 4 regions:

- Mt-non-coding region (5' end of the Mt-*Nd1* gene);
- Mt-*Nd4* coding region;
- Mt-*Cytb* coding region;
- Mt-D-Loop.

I designed, and attempted to optimize, primers for PCR amplification of bisulphite modified DNA, as described in section 2.18. However, the optimization failed to yield a unique product – or any product – in the PCR trials for the Mt-*Nd4* and the Mt-*Cytb* sequences. These were removed from the gene panel and I therefore pursued methylation analyses of the other 2 genomic regions. Results of these analyses are reported in section 7.5 below.

7.5 Quantification of methylation at the single CpG level of resolution for two genomic regions within the murine mtDNA in liver samples from ageing and from dietary energy restricted mice

After total genomic DNA extraction (see section 2.3), I performed bisulphite modification (see section 2.17), BM-PCR (see section 2.18) and sequencing (see section 2.19) on 3 liver samples from each of the following groups: young vs old and *ad libitum* fed vs short-term dietary energy restricted mice. I then performed statistical analyses on the measured methylation values using an unpaired t-tests to compare methylation levels between treatment groups at each CpG site within the analysed genomic regions These data are reported in section 7.5.1.

7.5.1 Mus musculus musculus mitochondrion genome, non-coding region, NCBI Reference Sequence: NC_010339.1

1741 gagtaacaag aattctaatt ctccaggcat acacatataa caactcggat aaccattgtt
1801 agttaatcag actataggca ataattacac tataaataat tcacctataa cttctctgtt
1861 aacccaacac cggaatgcct aaaggaaaga tctaaaaaga taaaaggaac tcggcaaaca
1921 agaacccgc ctgtttacca aaaacatcac ctctagcatt acaagtatta gaggcactgc
1981 ctgcccagtg actaaagttt aacggccgcg gtatcctgac cgtgcaaagg tagcataatc

2041 acttgttcct taattaggga ctagcatgaa **cg**gctaaa**cg** agggtccaac tgtctcttat

2101 ctttaatcag tgaaattgac ctttcagtga agaggctgaa atataataat aagacgagaa

2161 gaccctatgg agcttaaatt atatgactta tctatttaat ttatttaaac ctaatggccc

Figure 7.11. Portion of the murine mitochondrion genome non-protein-coding region. Genomic regions used as priming sites for methylation studies are underlined; CpG sites investigated in this study are indicated in bold orange font.

Figure 7.12 shows the percentage of CpG methylation measured for each of the 8 CpG sites within the murine mitochondrion D-Loop sequence in DNA from young and old mouse livers (panel A) and from *ad libitum* and dietary energy restricted mouse livers (panel B). Regardless of experimental treatments, there were marked differences in extent of methylation at individual CpG sites. There was no detectable methylation at CpG sites 6 and 7 and methylation was very low for CpG site1 (see Figure 7.12). In contrast, methylation levels were consistently high (around 40%) for CpG site 3 with intermediate values at the other 4 CpG sites. At CpG site 5 methylation was 5 times higher in the older compared with the yonger mice ($p = 0.002$; see Figure 7.12, panel A). There were no significant age-related effects at the other 7 CpG sites. In addition, dietary energy restriction had no detectable effects on methylation at any of the CpG sites investigated (see Figure 7.12, panel B).

A

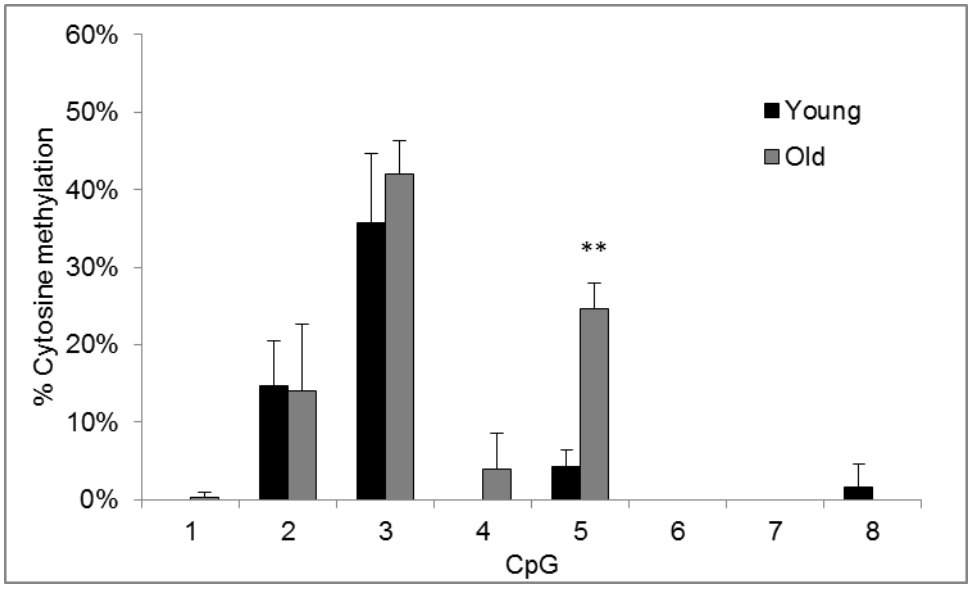

B

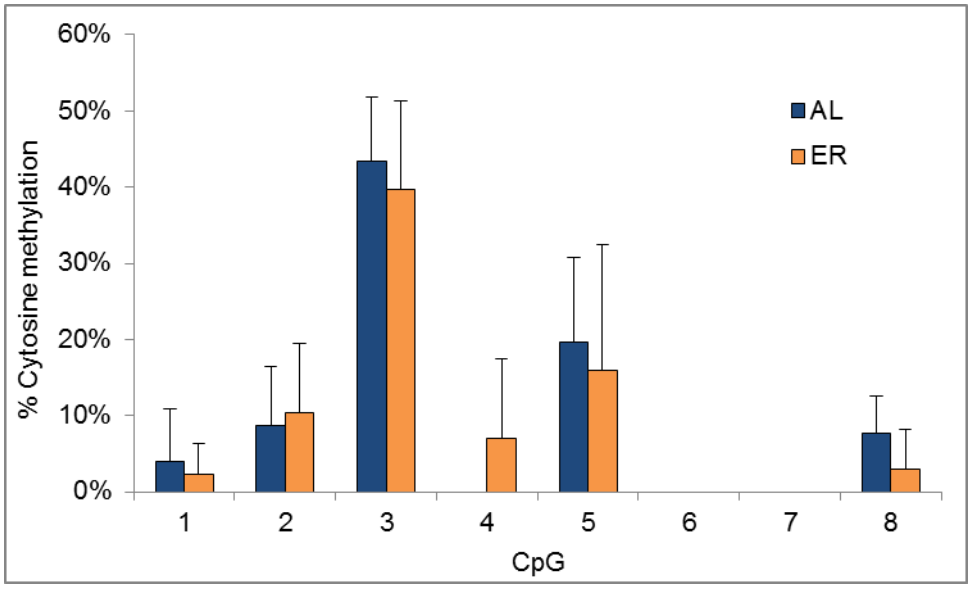

*Figure 7.12. Murine mitochondrion genome non-coding region CpG methylation measured by BM PCR direct sequencing in livers. Panel A compares methylation levels in young and old mouse liver samples; panel B shows effects of ad libitum (AL) compared with dietary energy restriction (ER) feeding on mouse liver samples. Data are mean ± SD, n = 3 biological replicates. ** = p < 0.01 for student's unpaired t-test.*

7.5.2 Mus musculus musculus mitochondrion genome, D-Loop, NCBI Reference Sequence: NC_010339.1

15426 cgtac ataaatttac atagtacaat agtacattta tgtatatcgt acattaaact
15481 attatcccca agcatataag caagtacatt taatcaatga tataggccat aaaacaatta
15541 tcaacataaa ctgatacaaa ccatgaatat tatactaata catcaaatta atgctttaaa
15601 gacatatctg tgttatctga catacaccat acagtcataa actcttctct tccatatgac
15661 tatccccttc cccatttggt ctattaatct accatcctcc gtgaaaccaa caaccgccc
15721 accaatgccc ctcttctcgc tccggccca ttaaacttgg gggtagctaa actgaaactt
15781 tatcagacat ctggttctta cttcagggcc atcaaatgcg ttatcgccca tacgttcccc
15841 ttaaataaga catctcgatg gtatcgggtc taatcagccc atgaccaaca taactgtggt
15901 gtcatgcatt tggtattttt ttattttggc ctactttcat caacatagcc gtcaaggcat
15961 gaaaggacag cacacagtct agacgcacct acggtgaaga atcattagtc cgcaaaaccc
16021 aatcacctaa ggctaattat tcatgcttgt tagacataaa tgctactcaa taccaaattt
16081 taactctcca aacccccaa ccccctcctc ttaatgccaa accccaaaaa cactaagaac
16141 ttgaaagaca tatattatta actatcaaac cctatgtcct gatcgattct agtagttccc

16201 aaaatatgac tcatatttta gtacttgtaa aaattttaca aaatcatgct ccgtgaacca
16261 aaactctaat cacactctat tacgcaataa atattaacaa

Figure 7.13.Murine mtDNA D-Loop sequence. Genomic regions used as priming sites for methylation studies are underlined; CpG sites investigated in this study are indicated in bold orange font.

Figure 7.14 shows the percentage of CpG methylation measured for each of the 5 CpG sites within a murine mitochondrion genome non-protein-coding region sequence in DNA from young and old mouse livers (panel A) and from *ad libitum* and dietary energy restricted mice livers (panel B). Regardless of experimental treatments, there were marked differences in extent of methylation at individual CpG sites. There was no detectable methylation at CpG sites 4 and 5 and methylation was very low for CpG site 1, but showed high biological variability among livers from dietary energy restricted animals (see Figure 7.14). In contrast, methylation levels were consistently high (around 30%-40%) for CpG site 2 with intermediate values at CpG site 3 (around 10%-20%). There were no significant age-related or dietary energy restriction effects at any of the CpG sites investigated (see Figure 7.14, panel A and B).

A

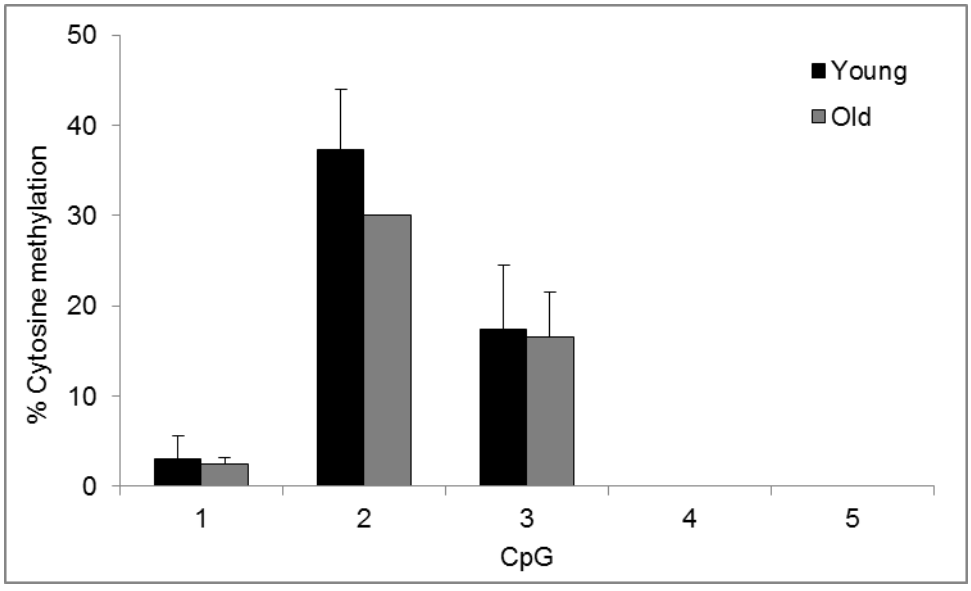

B

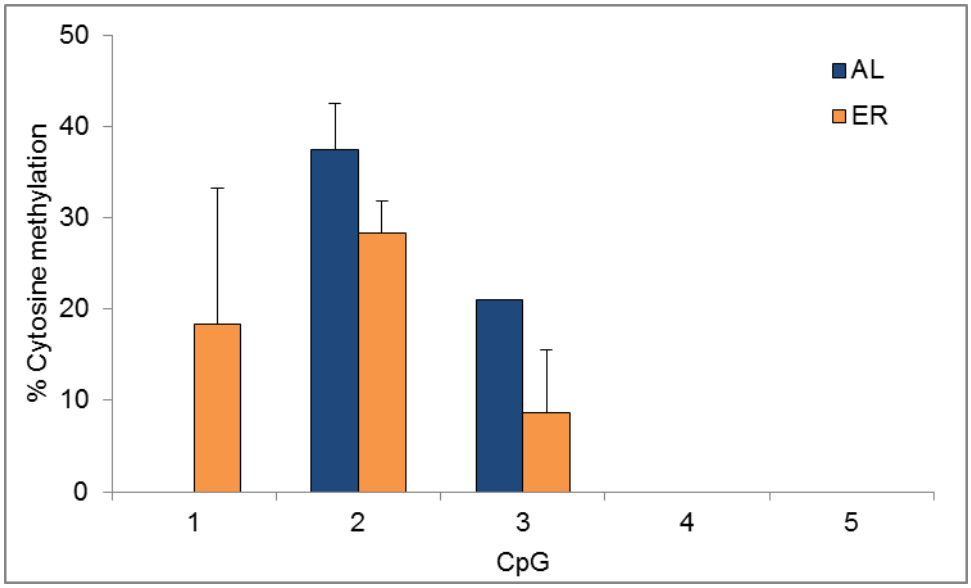

Figure 7.14. mtDNA D-Loop CpG methylation in murine livers measured by BM PCR direct sequencing. Panel A compares methylation levels in young and old mouse liver samples; panel B shows effects of ad libitum (AL) compared with dietary energy restriction (ER) feeding on mouse liver samples. Data are mean ± SD, n = 3 biological replicates.

7.6 Discussion

MtDNA is present in multiple copies in the mitochondria of each cell. This copy number is variable in a tissue specific manner (Naviaux, 2008; Kelly et al., 2012) and there is evidence that it progressively decreases with ageing in some tissues, in a proportional way to the tissue oxidative capacity (Barazzoni et al., 2000). However, there is limited and contrasting scientific evidence that mtDNA copy number per organelle/cell affects the extent of mitochondrial-encoded genes expression (Barazzoni et al., 2000; Hartmann et al., 2011). Hence, mechanisms other than gene dosage may be involved in the expression of mitochondrial genes. As for nuclear-encoded genes, regulation of mitochondrial gene expression relies on the activity of nuclear-encoded transcription factors (Leigh-Brown et al., 2010), as well as post-translational modifications (Taylor et al., 2003). Other mechanisms might involve snRNA, srpRNA and snoRNA – whose import into the mitochondria has been demonstrated recently (Sripada et al., 2012) – and DNA methylation.

Mitochondria DNA methylation has been investigated since the early 1970s. The first studies were conducted in rodents (Nass, 1973) and human cells *in vitro* models (Shmookler Reis and Goldstein, 1983) and revealed limited 5'-methylCytosine content (3% to 5%). These studies were performed using sensitive techniques, e.g. radioactive assays or methylation-sensitive restriction enzymes-based assays, allowing the detection of very small amounts of 5'-methylated Cytosines. However, their main limitation was that they could not detect the specific methylation sites/patterns of methylation and so provide information on global mtDNA methylation content only.

More recent observational studies have been performed to investigate alterations in the mtDNA methylation patterns at specific loci and whether these would correlate with cancer onset or progression (Maekawa et al., 2004) - with no success - and to exposure to airborne pollutants (Byun et al., 2013); the latter study provided evidence that metal-rich particulate matter exposure increased methylation in specific mtDNA genomic regions.

To my knowledge, this is the first study which has investigated the effects of senescence, ageing and dietary energy restriction on site-specific mtDNA methylation patterns. We observed that CpG methylation was higher in ESIPS compared with YC and in RS compared with YC across the MT-*COI* and MT-*ND1* coding sequences - in human MRC-5 fibroblasts. These genes belong to Complex IV and to Complex I of the mitochondrial electron transport chain, respectively, and their dysregulation can lead to accumulation of hazardous superoxide species. Such increase in superoxide species has been well

documented in ageing cells, but a causal role in the biology of ageing is still controversial, as reviewed in (Cui et al., 2012). In addition, we observed that ageing was associated with significantly increased methylation at one single CpG site within the D-Loop mitochondrial regulatory region (Figure 7.12). The D-Loop region is the starting point for the mitochondrial DNA replication process (Fish et al., 2004), so it is possible that increased methylation within it may impair the efficiency of such process by hindering the binding of the enzymes responsible for mtDNA replication. This hypothesis is consistent with the findings of previous studies that showed a progressive fall in mtDNA copy number in ageing tissues (Barazzoni et al., 2000). Since the D-Loop region is also involved in the mitochondrial DNA organization because it is recognized, and bound, by DNA binding proteins to form nucleoids (He et al., 2007), hypermethylation of this mitochondrial region may impair nucleoids formation. In the present study, there was no evidence that ER had any effect on methylation at any of the investigated CpG sites within the D-Loop region

Measured methylation values were higher than the ones found in the literature, which are estimated to be around 2% to 5% of the total CpG sites (Shmookler Reis and Goldstein, 1983). In my case, measured CpG methylation spanned from 0% to 38% for human cells and between 0% and 43% for murine samples; however, it is to noted that published data are based on much larger numbers of CpG sites compared with what analysed in my study, hence I believe that lower values might be due to a "dilution effect".

Bioinformatics analyses of the human and murine mitochondria genome applying one of the most commonly used criteria for the definiton of CpG island (Takai and Jones, 2002) revealed only one potential CpG island within the human mtDNA molecule (lying within the coding sequence of the *MT-COX2* gene) and no CpG islands within the murine mtDNA. Application of less stringent criteria, i.e. shorter minimum island lengths, allowed the identification of regions relatively dense in CpG sites (CpG rich regions) which were worth of investigation with BM-DNA PCR and direct sequencing. Surprisingly, these regions did not correspond with any of the known mitochondria regulatory sites, i.e. the transcription termination region (TERM) within the $tRNA^{Leu(UUR)}$, the heavy and light strand promoters (HSP and LSP) or the origin of replication of the light strand (O_L) (Rebelo et al., 2009). This observation suggests that these newly identified mtDNA regions could be involved in the epigenetic regulation of gene expression through DNA methylation, if this occurs within the mitochondria.

Based on established understanding of the regulation of expression of genes encoded in nuclear DNA, it is logical to postulate that the presence of methylated Cytosines could modulate the binding/occupancy of transcriptional regulators (e.g. by remodelling the mtDNA molecule) and therefore regulate transcription of mitochondrially-encoded genes. Another putative function of mtDNA methylation could be the protection against deleterious mutation. Ageing is associated with accumulation of point mutations and deletions in mtDNA – for example linked to respiratory chain defects in replicating tissues (Greaves et al., 2010; Nooteboom et al., 2010) - (reviewed in (Trifunovic, 2006) and (Desler et al., 2011)). In this context, hypomethylation of Cytosine residues methylation could facilitate the accumulation of spontaneous point mutations C > T and C > G/A (very frequent within the nuclear genome) (Cooper and Krawczak, 1989) and hypermethylation of Cytosine residues could contribute to the accumulation of spontaneous 5mC > T transitions (Mazin, 2009).

7.7 Conclusions

In summary, this study has shown for the first time that:

- *in vitro* replicative senescence and early stress-induced premature senescence are associated with changes in mtDNA methylation, specifically in the MT-*COI* and MT-*ND1* gene coding sequences, which belong to Complex IV and to Complex I respectively. These changes may contribute to the accumulation of hazardous superoxide species, which is widely documented in ageing cells;
- ageing is associated with aberrant methylation of the mtDNA D-Loop region in mouse liver. I hypothesize that this aberrant methylation may affect mtDNA replication and nucleoids formation;
- aberrant methylation of the mitochondrial D-Loop observed in ageing mouse liver was not reversed by dietary energy restriction.

Chapter 8. Conclusions

Although DNA methylation has been the subject of studies for more than fifty years, much work still needs to be done to completely elucidate its biological functions and its implications in the ageing process. Growing evidence, including results from this study, points to CpG methylation as a potential marker for ageing and age-related diseases. In addition, the fact that aberrant DNA methylation occurs at promoters of genes involved in the maintenance of cellular and tissue homeostasis and whose expression is altered in senescence and ageing suggests a potential causal role for altered CpG methylation in the aetiology of ageing. In parallel, this study has demonstrated that dietary energy restriction - at least in the short-term - can affect CpG methylation of several gene promoters in mouse tissues and, in some cases, can reverse the aberrant methylation associated with ageing. These findings suggest that some of the effects of dietary energy restriction in slowing down the ageing process and also delaying the onset of age-related diseases may occur via epigenetic mechanisms including amelioration of age-related aberrations in patterns of DNA methylation.

8.1 Methodological issues in determining DNA methylation

At the beginning of my study, I identified methodological issues in determining DNA methylation both at the global and at site-specific levels. In fact, when comparing various methods for the study of global DNA methylation, I found that results obtained by means of different methods for the same sample were often not comparable. However, some of the surrogate methods used for estimation of global DNA methylation level proved sufficiently sensitive to be able to detect small, but significant differences between samples in a particular experimental context. Each assay had its merits and none was clearly the best surrogate for total CpG methylation content quantified by HPLC. However, when chosen carefully, individual assays can be used as fast, cheap and good markers for the estimation of global DNA methylation in the samples under investigation (Chapter 3).

Continuing with my study, I also identified a major limitation of the MeDIP technique, a method aimed at the study of site-specific DNA methylation. The specific issue in this case consisted in the sequence-specific partial loss (about one third) of enrichment of certain DNA fragments during the WGA step. The quality assurance steps which I

developed and validated provide users of the MeDIP technique with ways to address this issue. Further, these quality assurance steps allow the assessment of the overall quality of single experiments and the estimation of intra-experimental and inter-experimental variability. These improvements to the MeDIP method proved cost-effective and were easy to apply in routine assays (Chapter 4).

With the inclusion of the modification described in Chapter 4, the MeDIP technique is a relatively cheap and reliable method for the preparation of samples for the genome-wide screening of CpG methylation and the identification of novel aberrantly methylated genomic regions under a variety of experimental conditions. In the present project, I used it in preparation for analysis using whole genome methylation arrays, but the approach would be equally applicable to methylation analysis by next generation sequencing.

8.2 Genome-wide searches for senescence and age-dependent DNA methylation changes

In contrast with the considerable overlap in gene expression changes between cells undergoing replicative senescence and those irradiated to induce premature senescence, there was quite limited overlap among genes showing changes in DNA methylation (Chapter 5). Given that altered DNA methylation is associated with changes in gene expression, this finding may appear unexpected. However, this finding may be explained if we consider the complexity of the transcription regulation process in which epigenetic mechanisms are just one set of regulators. In addition, it is possible that the specific CpG sites showing altered methylation in this study are not the most critical for regulating expression of the corresponding genes. It should be noted that the specific microarrays chosen for this study included probes for gene promoter regions only. It is now known that methylation at other sites including CpGs within island shores, shelves and open sea, within gene bodies and within inter-genic regions may be involved in the regulation of gene expression. Further, CpG sites in such genomic regions are also affected by senescence and by age-related DNA methylation in addition to methylation changes at gene promoters. In the future, study of methylation at these other genomic locations may give new insight into the regulation of gene transcription in senescence and ageing and may explain some of the changes in gene expression found in both premature and replicative senescence.

The same considerations apply to the ageing mice tissue samples, in which there were >1000 genes showing age-related changes in promoter methylation in both heart and in

liver, but few of these genes showing methylation changes were in common between the two tissues. One of the limitations of the present study is that I did not have data on age-related changes in expression profiles of the tissues under investigation and so I was unable to assess whether the genes showing changes in DNA methylation also showed changes in gene expression (Chapter 6). This issue is being addressed in follow up work by colleagues in Newcastle University.

Costs in terms of money and time limited the number of genes for which methylation changes observed in the microarray data could be validated by pyrosequencing. This is because pyrosequencing assays can investigate only a few CpG sites at a time since it is restricted to interrogation of amplicons of up to 200 bp within a genomic region. For this reason, multiple pyrosequencing assays need to be set up and run to cover the whole genomic region for which there are probes on the methylation arrays. In my study, although I did not confirm all the changes in DNA methylation for the selected candidates in terms of direction (increase or decrease) or extent (fold change) in the groups of comparisons, I was able to detect changes in methylation at specific CpG sites with the chosen pyrosequencing assays. These methylation changes may be causal for gene expression changes, as supported by the literature (Chapter 5).

A valid alternative to array-based studies is high-throughput (next generation) sequencing of MeDIP samples or bisulphite modified DNA samples. Using this method, single aberrantly methylated CpG sites could be identified and validation by pyrosequencing would be more time and cost effective. Unfortunately, when this project started, such technology was still novel and expensive and I therefore opted for the more widely used hybridization of MeDIP prepared samples to DNA microarrays.

8.3 Dietary energy restriction modulation of DNA methylation changes

Restriction of dietary energy intake by 40% compared with that of *ad libitum*-fed animals for 3 months counteracted some of the age-related DNA methylation changes occurring in mouse liver (Chapter 6). However, although significant, the number of identified changes was small. This finding may be due: i) to the chosen array design which included gene promoters only (see section 8.2); ii) to the small number of animals used in this study - including more animals may attenuate biological variability and increase statistical power - and iii) to the relatively short time of the dietary intervention. Nonetheless, this study

showed that dietary energy restriction has the potential of modulating DNA methylation alterations associated with ageing, thus confirming previous published results that have indicated this dietary intervention as a possible preventative measure for age-related diseases and for slowing down the ageing process itself. Future gene expression studies may help in focusing on those candidate genes which could be functionally important for the ageing process and may help in elucidating the molecular mechanisms responsible for the effects of dietary energy restriction.

8.4 Epigenetic dysregulation of mitochondrial function in ageing

The pilot study on mtDNA methylation showed aberrant methylation at some inter-genic regions occurring with premature senescence and replicative senescence in MRC-5 fibroblasts and in mouse liver during ageing. These are novel findings that may indicate the involvement of aberrant CpG methylation in the dysregulation of mitochondrially-encoded genes and, in turn, in age-related mitochondrial dysfunction. However, no effect of dietary energy restriction on methylation changes was found at the regions investigated. In future studies, the isolation of mtDNA molecules from cells/tissues samples followed by deep sequencing, may help in the identification of additional CpG sites whose methylation is affected by dietary energy restriction. This approach would overcome the main limitation of the present study i.e. the small number of CpG sites under investigation. Further studies should include determination of mitochondrial protein expression in senescence whilst a study of mitochondrial protein expression in mice liver during ageing and under dietary energy restriction has just been completed by other group members. These data will help in establishing the relationship (if any) between changes in mtDNA methylation and mitochondrial protein expression and, possibly, elucidating the role of mtDNA methylation in the ageing process.

References

AALBERTS, M., VAN DISSEL-EMILIANI, F. M., VAN ADRICHEM, N. P., VAN WIJNEN, M., WAUBEN, M. H., STOUT, T. A. & STOORVOGEL, W. 2012. Identification of distinct populations of prostasomes that differentially express prostate stem cell antigen, annexin A1, and GLIPR2 in humans. *Biol Reprod,* 86, 82.

ABAD, M. A., ENGUITA, M., DEGREGORIO-ROCASOLANO, N., FERRER, I. & TRULLAS, R. 2006. Neuronal pentraxin 1 contributes to the neuronal damage evoked by amyloid-beta and is overexpressed in dystrophic neurites in Alzheimer's brain. *J Neurosci,* 26, 12735-47.

ABALLAY, L. R., EYNARD, A. R., DIAZ MDEL, P., NAVARRO, A. & MUNOZ, S. E. 2013. Overweight and obesity: a review of their relationship to metabolic syndrome, cardiovascular disease, and cancer in South America. *Nutr Rev,* 71, 168-79.

ABDOLLAHI, A. 2007. LOT1 (ZAC1/PLAGL1) and its family members: mechanisms and functions. *J Cell Physiol,* 210, 16-25.

ACOSTA, J. C., O'LOGHLEN, A., BANITO, A., GUIJARRO, M. V., AUGERT, A., RAGUZ, S., FUMAGALLI, M., DA COSTA, M., BROWN, C., POPOV, N., TAKATSU, Y., MELAMED, J., D'ADDA DI FAGAGNA, F., BERNARD, D., HERNANDO, E. & GIL, J. 2008. Chemokine signaling via the CXCR2 receptor reinforces senescence. *Cell,* 133, 1006-18.

ADRIAENS, M. E., JAILLARD, M., EIJSSEN, L. M., MAYER, C. D. & EVELO, C. T. 2012. An evaluation of two-channel ChIP-on-chip and DNA methylation microarray normalization strategies. *BMC Genomics,* 13, 42.

AHUJA, N., LI, Q., MOHAN, A. L., BAYLIN, S. B. & ISSA, J. P. 1998. Aging and DNA methylation in colorectal mucosa and cancer. *Cancer Res,* 58, 5489-94.

ALDHAHI, W. & HAMDY, O. 2003. Adipokines, inflammation, and the endothelium in diabetes. *Curr Diab Rep,* 3, 293-8.

AMARAL, P. P., CLARK, M. B., GASCOIGNE, D. K., DINGER, M. E. & MATTICK, J. S. 2011. lncRNAdb: a reference database for long noncoding RNAs. *Nucleic Acids Res,* 39, D146-51.

ANDERSON, R. M., SHANMUGANAYAGAM, D. & WEINDRUCH, R. 2009. Caloric restriction and aging: studies in mice and monkeys. *Toxicol Pathol,* 37, 47-51.

ANDERSON, R. M. & WEINDRUCH, R. 2010. Metabolic reprogramming, caloric restriction and aging. *Trends Endocrinol Metab,* 21, 134-41.

ANDERSON, S., BANKIER, A. T., BARRELL, B. G., DE BRUIJN, M. H., COULSON, A. R., DROUIN, J., EPERON, I. C., NIERLICH, D. P., ROE, B. A., SANGER, F., SCHREIER, P. H., SMITH, A. J., STADEN, R. & YOUNG, I. G. 1981. Sequence and organization of the human mitochondrial genome. *Nature,* 290, 457-65.

ANTEQUERA, F. & BIRD, A. 1993. Number of CpG islands and genes in human and mouse. *Proc Natl Acad Sci U S A,* 90, 11995-9.

ANTWIH, D. A., GABBARA, K. M., LANCASTER, W. D., RUDEN, D. M. & ZIELSKE, S. P. 2013. Radiation-induced epigenetic DNA methylation modification of radiation-response pathways. *Epigenetics,* 8.

AUSTAD, S. N. 2012. Ageing: Mixed results for dieting monkeys. *Nature,* 489, 210-11.

AZZALIN, C. M., REICHENBACH, P., KHORIAULI, L., GIULOTTO, E. & LINGNER, J. 2007. Telomeric repeat containing RNA and RNA surveillance factors at mammalian chromosome ends. *Science,* 318, 798-801.

BAILEY, S. M. & MURNANE, J. P. 2006. Telomeres, chromosome instability and cancer. *Nucleic Acids Res,* 34, 2408-17.

BAKER, D. G. 1998. Natural pathogens of laboratory mice, rats, and rabbits and their effects on research. *Clin Microbiol Rev,* 11, 231-66.

BAKER, D. J., WIJSHAKE, T., TCHKONIA, T., LEBRASSEUR, N. K., CHILDS, B. G., VAN DE SLUIS, B., KIRKLAND, J. L. & VAN DEURSEN, J. M. 2011. Clearance of p16Ink4a-positive senescent cells delays ageing-associated disorders. *Nature,* 479, 232-6.

BANERJEE, T. & CHAKRAVARTI, D. 2011. A peek into the complex realm of histone phosphorylation. *Mol Cell Biol,* 31, 4858-73.

BARAZZONI, R., SHORT, K. R. & NAIR, K. S. 2000. Effects of aging on mitochondrial DNA copy number and cytochrome c oxidase gene expression in rat skeletal muscle, liver, and heart. *J Biol Chem,* 275, 3343-7.

BARBOT, W., DUPRESSOIR, A., LAZAR, V. & HEIDMANN, T. 2002. Epigenetic regulation of an IAP retrotransposon in the aging mouse: progressive demethylation and de-silencing of the element by its repetitive induction. *Nucleic Acids Res,* 30, 2365-73.

BARTKE, A. 2005. Minireview: role of the growth hormone/insulin-like growth factor system in mammalian aging. *Endocrinology,* 146, 3718-23.

BASS, T. M., GRANDISON, R. C., WONG, R., MARTINEZ, P., PARTRIDGE, L. & PIPER, M. D. 2007. Optimization of dietary restriction protocols in Drosophila. *J Gerontol A Biol Sci Med Sci,* 62, 1071-81.

BAUR, J. A., PEARSON, K. J., PRICE, N. L., JAMIESON, H. A., LERIN, C., KALRA, A., PRABHU, V. V., ALLARD, J. S., LOPEZ-LLUCH, G., LEWIS, K., PISTELL, P. J., POOSALA, S., BECKER, K. G., BOSS, O., GWINN, D., WANG, M., RAMASWAMY, S., FISHBEIN, K. W., SPENCER, R. G., LAKATTA, E. G., LE COUTEUR, D., SHAW, R. J., NAVAS, P., PUIGSERVER, P., INGRAM, D. K., DE CABO, R. & SINCLAIR, D. A. 2006. Resveratrol improves health and survival of mice on a high-calorie diet. *Nature,* 444, 337-42.

BAXTER, R. M., CROWELL, T. P., GEORGE, J. A., GETMAN, M. E. & GARDNER, H. 2007. The plant pathogenesis related protein GLIPR-2 is highly expressed in fibrotic kidney and promotes epithelial to mesenchymal transition in vitro. *Matrix Biol,* 26, 20-9.

BEDFORD, M. T. & CLARKE, S. G. 2009. Protein arginine methylation in mammals: who, what, and why. *Mol Cell,* 33, 1-13.

BELL, J. T., TSAI, P. C., YANG, T. P., PIDSLEY, R., NISBET, J., GLASS, D., MANGINO, M., ZHAI, G., ZHANG, F., VALDES, A., SHIN, S. Y., DEMPSTER, E. L., MURRAY, R. M., GRUNDBERG, E., HEDMAN, A. K., NICA, A., SMALL, K. S., DERMITZAKIS, E. T., MCCARTHY, M. I., MILL, J., SPECTOR, T. D. & DELOUKAS, P. 2012. Epigenome-wide scans identify differentially methylated regions for age and age-related phenotypes in a healthy ageing population. *PLoS Genet,* 8, e1002629.

BELLIZZI, D., D'AQUILA, P., MONTESANTO, A., CORSONELLO, A., MARI, V., MAZZEI, B., LATTANZIO, F. & PASSARINO, G. 2012. Global DNA methylation in old subjects is correlated with frailty. *Age (Dordr),* 34, 169-79.

BELTRAN, M., PUIG, I., PENA, C., GARCIA, J. M., ALVAREZ, A. B., PENA, R., BONILLA, F. & DE HERREROS, A. G. 2008. A natural antisense transcript regulates Zeb2/Sip1 gene expression during Snail1-induced epithelial-mesenchymal transition. *Genes Dev,* 22, 756-69.

BEN-PORATH, I. & WEINBERG, R. A. 2005. The signals and pathways activating cellular senescence. *Int J Biochem Cell Biol,* 37, 961-76.

BENDER, A., KRISHNAN, K. J., MORRIS, C. M., TAYLOR, G. A., REEVE, A. K., PERRY, R. H., JAROS, E., HERSHESON, J. S., BETTS, J., KLOPSTOCK, T., TAYLOR, R. W. & TURNBULL, D. M. 2006. High levels of mitochondrial DNA deletions in substantia nigra neurons in aging and Parkinson disease. *Nat Genet,* 38, 515-7.

BEREZIKOV, E., CHUNG, W. J., WILLIS, J., CUPPEN, E. & LAI, E. C. 2007. Mammalian mirtron genes. *Mol Cell,* 28, 328-36.

BERNSTEIN, E., CAUDY, A. A., HAMMOND, S. M. & HANNON, G. J. 2001. Role for a bidentate ribonuclease in the initiation step of RNA interference. *Nature,* 409, 363-6.

BISHOP, J. O. 1979. A DNA sequence cleaved by restriction endonuclease R.EcoRI in only one strand. *J Mol Biol,* 128, 545-9.

BJARTMAR, L., HUBERMAN, A. D., ULLIAN, E. M., RENTERIA, R. C., LIU, X., XU, W., PREZIOSO, J., SUSMAN, M. W., STELLWAGEN, D., STOKES, C. C., CHO, R., WORLEY, P., MALENKA, R. C., BALL, S., PEACHEY, N. S., COPENHAGEN, D., CHAPMAN, B., NAKAMOTO, M., BARRES, B. A. & PERIN, M. S. 2006. Neuronal pentraxins mediate synaptic refinement in the developing visual system. *J Neurosci,* 26, 6269-81.

BLENNOW, K., DE LEON, M. J. & ZETTERBERG, H. 2006. Alzheimer's disease. *Lancet,* 368, 387-403.

BLOMMAART, E. F., LUIKEN, J. J., BLOMMAART, P. J., VAN WOERKOM, G. M. & MEIJER, A. J. 1995. Phosphorylation of ribosomal protein S6 is inhibitory for autophagy in isolated rat hepatocytes. *J Biol Chem,* 270, 2320-6.

BLUWSTEIN, A., KUMAR, N., LEGER, K., TRAENKLE, J., OOSTRUM, J., REHRAUER, H., BAUDIS, M. & HOTTIGER, M. O. 2013. PKC signaling prevents irradiation-induced apoptosis of primary human fibroblasts. *Cell Death Dis,* 4, e498.

BOCK, C., REITHER, S., MIKESKA, T., PAULSEN, M., WALTER, J. & LENGAUER, T. 2005. BiQ Analyzer: visualization and quality control for DNA methylation data from bisulfite sequencing. *Bioinformatics,* 21, 4067-8.

BODE, J., STENGERT-IBER, M., KAY, V., SCHLAKE, T. & DIETZ-PFEILSTETTER, A. 1996. Scaffold/matrix-attached regions: topological switches with multiple regulatory functions. *Crit Rev Eukaryot Gene Expr,* 6, 115-38.

BODNAR, A. G., OUELLETTE, M., FROLKIS, M., HOLT, S. E., CHIU, C. P., MORIN, G. B., HARLEY, C. B., SHAY, J. W., LICHTSTEINER, S. & WRIGHT, W. E. 1998. Extension of life-span by introduction of telomerase into normal human cells. *Science,* 279, 349-52.

BOECKLE, S., PFISTER, H. & STEGER, G. 2002. A new cellular factor recognizes E2 binding sites of papillomaviruses which mediate transcriptional repression by E2. *Virology,* 293, 103-17.

BOLLATI, V., SCHWARTZ, J., WRIGHT, R., LITONJUA, A., TARANTINI, L., SUH, H., SPARROW, D., VOKONAS, P. & BACCARELLI, A. 2009. Decline in genomic DNA methylation through aging in a cohort of elderly subjects. *Mech Ageing Dev,* 130, 234-9.

BONAFE, M., BARBIERI, M., MARCHEGIANI, F., OLIVIERI, F., RAGNO, E., GIAMPIERI, C., MUGIANESI, E., CENTURELLI, M., FRANCESCHI, C. & PAOLISSO, G. 2003. Polymorphic variants of insulin-like growth factor I (IGF-I) receptor and phosphoinositide 3-kinase genes affect IGF-I plasma levels and human longevity: cues for an evolutionarily conserved mechanism of life span control. *J Clin Endocrinol Metab,* 88, 3299-304.

BONKOWSKI, M. S., ROCHA, J. S., MASTERNAK, M. M., AL REGAIEY, K. A. & BARTKE, A. 2006. Targeted disruption of growth hormone receptor interferes with the beneficial actions of calorie restriction. *Proc Natl Acad Sci U S A,* 103, 7901-5.

BORK, S., PFISTER, S., WITT, H., HORN, P., KORN, B., HO, A. D. & WAGNER, W. 2010. DNA methylation pattern changes upon long-term culture and aging of human mesenchymal stromal cells. *Aging Cell,* 9, 54-63.

BOURC'HIS, D., XU, G. L., LIN, C. S., BOLLMAN, B. & BESTOR, T. H. 2001. Dnmt3L and the establishment of maternal genomic imprints. *Science,* 294, 2536-9.

BROSH, R. M., JR. & BOHR, V. A. 2002. Roles of the Werner syndrome protein in pathways required for maintenance of genome stability. *Exp Gerontol,* 37, 491-506.

BROWN-BORG, H. M. & BARTKE, A. 2012. GH and IGF1: roles in energy metabolism of long-living GH mutant mice. *J Gerontol A Biol Sci Med Sci,* 67, 652-60.

BRUNET, A., SWEENEY, L. B., STURGILL, J. F., CHUA, K. F., GREER, P. L., LIN, Y., TRAN, H., ROSS, S. E., MOSTOSLAVSKY, R., COHEN, H. Y., HU, L. S., CHENG, H. L., JEDRYCHOWSKI, M. P., GYGI, S. P., SINCLAIR, D. A., ALT, F. W. & GREENBERG, M. E. 2004. Stress-dependent regulation of FOXO transcription factors by the SIRT1 deacetylase. *Science,* 303, 2011-5.

BRUNNER, Y., COUTE, Y., IEZZI, M., FOTI, M., FUKUDA, M., HOCHSTRASSER, D. F., WOLLHEIM, C. B. & SANCHEZ, J. C. 2007. Proteomics analysis of insulin secretory granules. *Mol Cell Proteomics,* 6, 1007-17.

BURNS, K. H. & BOEKE, J. D. 2012. Human transposon tectonics. *Cell,* 149, 740-52.

BUSTIN, S. A., BENES, V., GARSON, J. A., HELLEMANS, J., HUGGETT, J., KUBISTA, M., MUELLER, R., NOLAN, T., PFAFFL, M. W., SHIPLEY, G. L., VANDESOMPELE, J. & WITTWER, C. T. 2009. The MIQE guidelines: minimum

information for publication of quantitative real-time PCR experiments. *Clin Chem,* 55, 611-22.

BUTCHER, L. M. & BECK, S. 2010. AutoMeDIP-seq: a high-throughput, whole genome, DNA methylation assay. *Methods,* 52, 223-31.

BYRNE, E. M., CARRILLO-ROA, T., HENDERS, A. K., BOWDLER, L., MCRAE, A. F., HEATH, A. C., MARTIN, N. G., MONTGOMERY, G. W., KRAUSE, L. & WRAY, N. R. 2013. Monozygotic twins affected with major depressive disorder have greater variance in methylation than their unaffected co-twin. *Transl Psychiatry,* 3, e269.

BYUN, H. M., PANNI, T., MOTTA, V., HOU, L., NORDIO, F., APOSTOLI, P., BERTAZZI, P. A. & BACCARELLI, A. A. 2013. Effects of airborne pollutants on mitochondrial DNA Methylation. *Part Fibre Toxicol,* 10, 18.

CAMERON, K. M., GOLIGHTLY, A., MIWA, S., SPEAKMAN, J., BOYS, R. & VON ZGLINICKI, T. 2011. Gross energy metabolism in mice under late onset, short term caloric restriction. *Mech Ageing Dev,* 132, 202-9.

CAMPION, J., MILAGRO, F. I., GOYENECHEA, E. & MARTINEZ, J. A. 2009. TNF-alpha promoter methylation as a predictive biomarker for weight-loss response. *Obesity (Silver Spring),* 17, 1293-7.

CAMPISI, J. 2005. Senescent cells, tumor suppression, and organismal aging: good citizens, bad neighbors. *Cell,* 120, 513-22.

CAMPISI, J. & D'ADDA DI FAGAGNA, F. 2007. Cellular senescence: when bad things happen to good cells. *Nat Rev Mol Cell Biol,* 8, 729-40.

CAMPISI, J. & WARNER, H. R. 2001. Aging in mitotic and post-mitotic cells. *In:* BARBARA A. GILCHREST, V. A. B. (ed.) *Advances in Cell Aging and Gerontology.* Elsevier.

CANTARA, W. A., CRAIN, P. F., ROZENSKI, J., MCCLOSKEY, J. A., HARRIS, K. A., ZHANG, X., VENDEIX, F. A., FABRIS, D. & AGRIS, P. F. 2010. The RNA Modification Database, RNAMDB: 2011 update. *Nucleic Acids Res,* 39, D195-201.

CANTONE, I. & FISHER, A. G. 2013. Epigenetic programming and reprogramming during development. *Nat Struct Mol Biol,* 20, 282-9.

CAO, S. X., DHAHBI, J. M., MOTE, P. L. & SPINDLER, S. R. 2001. Genomic profiling of short- and long-term caloric restriction effects in the liver of aging mice. *Proc Natl Acad Sci U S A,* 98, 10630-5.

CARNINCI, P., KASUKAWA, T., KATAYAMA, S., GOUGH, J., FRITH, M. C., MAEDA, N., OYAMA, R., RAVASI, T., LENHARD, B., WELLS, C., KODZIUS,

R., SHIMOKAWA, K., BAJIC, V. B., BRENNER, S. E., BATALOV, S., FORREST, A. R., ZAVOLAN, M., DAVIS, M. J., WILMING, L. G., AIDINIS, V., ALLEN, J. E., AMBESI-IMPIOMBATO, A., APWEILER, R., ATURALIYA, R. N., BAILEY, T. L., BANSAL, M., BAXTER, L., BEISEL, K. W., BERSANO, T., BONO, H., CHALK, A. M., CHIU, K. P., CHOUDHARY, V., CHRISTOFFELS, A., CLUTTERBUCK, D. R., CROWE, M. L., DALLA, E., DALRYMPLE, B. P., DE BONO, B., DELLA GATTA, G., DI BERNARDO, D., DOWN, T., ENGSTROM, P., FAGIOLINI, M., FAULKNER, G., FLETCHER, C. F., FUKUSHIMA, T., FURUNO, M., FUTAKI, S., GARIBOLDI, M., GEORGII-HEMMING, P., GINGERAS, T. R., GOJOBORI, T., GREEN, R. E., GUSTINCICH, S., HARBERS, M., HAYASHI, Y., HENSCH, T. K., HIROKAWA, N., HILL, D., HUMINIECKI, L., IACONO, M., IKEO, K., IWAMA, A., ISHIKAWA, T., JAKT, M., KANAPIN, A., KATOH, M., KAWASAWA, Y., KELSO, J., KITAMURA, H., KITANO, H., KOLLIAS, G., KRISHNAN, S. P., KRUGER, A., KUMMERFELD, S. K., KUROCHKIN, I. V., LAREAU, L. F., LAZAREVIC, D., LIPOVICH, L., LIU, J., LIUNI, S., MCWILLIAM, S., MADAN BABU, M., MADERA, M., MARCHIONNI, L., MATSUDA, H., MATSUZAWA, S., MIKI, H., MIGNONE, F., MIYAKE, S., MORRIS, K., MOTTAGUI-TABAR, S., MULDER, N., NAKANO, N., NAKAUCHI, H., NG, P., NILSSON, R., NISHIGUCHI, S., NISHIKAWA, S., et al. 2005. The transcriptional landscape of the mammalian genome. *Science,* 309, 1559-63.

CARTHARIUS, K., FRECH, K., GROTE, K., KLOCKE, B., HALTMEIER, M., KLINGENHOFF, A., FRISCH, M., BAYERLEIN, M. & WERNER, T. 2005. MatInspector and beyond: promoter analysis based on transcription factor binding sites. *Bioinformatics,* 21, 2933-42.

CASILLAS, M. A., JR., LOPATINA, N., ANDREWS, L. G. & TOLLEFSBOL, T. O. 2003. Transcriptional control of the DNA methyltransferases is altered in aging and neoplastically-transformed human fibroblasts. *Mol Cell Biochem,* 252, 33-43.

CASTEL, S. E. & MARTIENSSEN, R. A. 2013. RNA interference in the nucleus: roles for small RNAs in transcription, epigenetics and beyond. *Nat Rev Genet,* 14, 100-12.

CASTRO, R., RIVERA, I., STRUYS, E. A., JANSEN, E. E., RAVASCO, P., CAMILO, M. E., BLOM, H. J., JAKOBS, C. & TAVARES DE ALMEIDA, I. 2003. Increased homocysteine and S-adenosylhomocysteine concentrations and DNA hypomethylation in vascular disease. *Clin Chem,* 49, 1292-6.

CEDAR, H. & BERGMAN, Y. 2012. Programming of DNA methylation patterns. *Annu Rev Biochem,* 81, 97-117.

CENTONZE, D., ROSSI, S., NAPOLI, I., MERCALDO, V., LACOUX, C., FERRARI, F., CIOTTI, M. T., DE CHIARA, V., PROSPERETTI, C., MACCARRONE, M., FEZZA, F., CALABRESI, P., BERNARDI, G. & BAGNI, C. 2007. The brain cytoplasmic RNA BC1 regulates dopamine D2 receptor-mediated transmission in the striatum. *J Neurosci,* 27, 8885-92.

CHAKHPARONIAN, M. & WELLINGER, R. J. 2003. Telomere maintenance and DNA replication: how closely are these two connected? *Trends Genet,* 19, 439-46.

CHAMBERS, S. M., SHAW, C. A., GATZA, C., FISK, C. J., DONEHOWER, L. A. & GOODELL, M. A. 2007. Aging hematopoietic stem cells decline in function and exhibit epigenetic dysregulation. *PLoS Biol,* 5, e201.

CHAPMAN, T. & PARTRIDGE, L. 1996. Female fitness in Drosophila melanogaster: an interaction between the effect of nutrition and of encounter rate with males. *Proc Biol Sci,* 263, 755-9.

CHEDIN, F., LIEBER, M. R. & HSIEH, C. L. 2002. The DNA methyltransferase-like protein DNMT3L stimulates de novo methylation by Dnmt3a. *Proc Natl Acad Sci U S A,* 99, 16916-21.

CHEN, Q. & AMES, B. N. 1994. Senescence-like growth arrest induced by hydrogen peroxide in human diploid fibroblast F65 cells. *Proc Natl Acad Sci U S A,* 91, 4130-4.

CHEN, Q., FISCHER, A., REAGAN, J. D., YAN, L. J. & AMES, B. N. 1995. Oxidative DNA damage and senescence of human diploid fibroblast cells. *Proc Natl Acad Sci U S A,* 92, 4337-41.

CHEN, R. Z., PETTERSSON, U., BEARD, C., JACKSON-GRUSBY, L. & JAENISCH, R. 1998. DNA hypomethylation leads to elevated mutation rates. *Nature,* 395, 89-93.

CHINNERY, P. F., ELLIOTT, H. R., HUDSON, G., SAMUELS, D. C. & RELTON, C. L. 2012. Epigenetics, epidemiology and mitochondrial DNA diseases. *Int J Epidemiol,* 41, 177-87.

CHOI, M. R., IN, Y. H., PARK, J., PARK, T., JUNG, K. H., CHAI, J. C., CHUNG, M. K., LEE, Y. S. & CHAI, Y. G. 2012. Genome-scale DNA methylation pattern profiling of human bone marrow mesenchymal stem cells in long-term culture. *Exp Mol Med,* 44, 503-12.

CHRISTENSEN, K., JOHNSON, T. E. & VAUPEL, J. W. 2006. The quest for genetic determinants of human longevity: challenges and insights. *Nat Rev Genet,* 7, 436-48.

CHU, S. 2012. Transcriptional regulation by post-transcriptional modification--role of phosphorylation in Sp1 transcriptional activity. *Gene,* 508, 1-8.

CIVITARESE, A. E., UKROPCOVA, B., CARLING, S., HULVER, M., DEFRONZO, R. A., MANDARINO, L., RAVUSSIN, E. & SMITH, S. R. 2006. Role of adiponectin in human skeletal muscle bioenergetics. *Cell Metab,* 4, 75-87.

CLARK, S. J., HARRISON, J., PAUL, C. L. & FROMMER, M. 1994. High sensitivity mapping of methylated cytosines. *Nucleic Acids Res,* 22, 2990-7.

CLAYTON, A. L., HAZZALIN, C. A. & MAHADEVAN, L. C. 2006. Enhanced histone acetylation and transcription: a dynamic perspective. *Mol Cell,* 23, 289-96.

CLAYTON, K. B., PODLESNIY, P., FIGUEIRO-SILVA, J., LOPEZ-DOMENECH, G., BENITEZ, L., ENGUITA, M., ABAD, M. A., SORIANO, E. & TRULLAS, R. 2012. NP1 regulates neuronal activity-dependent accumulation of BAX in mitochondria and mitochondrial dynamics. *J Neurosci,* 32, 1453-66.

COLMAN, R. J., ANDERSON, R. M., JOHNSON, S. C., KASTMAN, E. K., KOSMATKA, K. J., BEASLEY, T. M., ALLISON, D. B., CRUZEN, C., SIMMONS, H. A., KEMNITZ, J. W. & WEINDRUCH, R. 2009. Caloric restriction delays disease onset and mortality in rhesus monkeys. *Science,* 325, 201-4.

COMFORT, A. 1964. *Ageing: the biology of senescence,* London, Routledge & Kegan Paul.

CONDE-PEREZPRINA, J. C., LUNA-LOPEZ, A., LOPEZ-DIAZGUERRERO, N. E., DAMIAN-MATSUMURA, P., ZENTELLA, A. & KONIGSBERG, M. 2008. Msh2 promoter region hypermethylation as a marker of aging-related deterioration in old retired female breeder mice. *Biogerontology,* 9, 325-34.

COOPER, D. N. & GERBER-HUBER, S. 1985. DNA methylation and CpG suppression. *Cell Differ,* 17, 199-205.

COOPER, D. N. & KRAWCZAK, M. 1989. Cytosine methylation and the fate of CpG dinucleotides in vertebrate genomes. *Hum Genet,* 83, 181-8.

COOPER, D. N. & YOUSSOUFIAN, H. 1988. The CpG dinucleotide and human genetic disease. *Hum Genet,* 78, 151-5.

COPPE, J. P., PATIL, C. K., RODIER, F., SUN, Y., MUNOZ, D. P., GOLDSTEIN, J., NELSON, P. S., DESPREZ, P. Y. & CAMPISI, J. 2008. Senescence-associated secretory phenotypes reveal cell-nonautonomous functions of oncogenic RAS and the p53 tumor suppressor. *PLoS Biol,* 6, 2853-68.

CORRAL-DEBRINSKI, M., HORTON, T., LOTT, M. T., SHOFFNER, J. M., BEAL, M. F. & WALLACE, D. C. 1992. Mitochondrial DNA deletions in human brain: regional variability and increase with advanced age. *Nat Genet,* 2, 324-9.

CORTOPASSI, G. A., SHIBATA, D., SOONG, N. W. & ARNHEIM, N. 1992. A pattern of accumulation of a somatic deletion of mitochondrial DNA in aging human tissues. *Proc Natl Acad Sci U S A,* 89, 7370-4.

COSTELLO, J. F., PLASS, C. & CAVENEE, W. K. 2002. Restriction landmark genome scanning. *Methods Mol Biol,* 200, 53-70.

COUNTS, J. L., KAZNOWSKI, J. M., MCCLAIN, R. M. & GOODMAN, J. I. 1997. 5-methylcytosine is present in the 5' flanking region of Ha-ras in mouse liver and increases with ageing. *Int J Cancer,* 72, 491-7.

CRANDALL, J. P., ORAM, V., TRANDAFIRESCU, G., REID, M., KISHORE, P., HAWKINS, M., COHEN, H. W. & BARZILAI, N. 2012. Pilot study of resveratrol in older adults with impaired glucose tolerance. *J Gerontol A Biol Sci Med Sci,* 67, 1307-12.

CRAWFORD, D. C., ACUNA, J. M. & SHERMAN, S. L. 2001. FMR1 and the fragile X syndrome: human genome epidemiology review. *Genet Med,* 3, 359-71.

CRISTOFALO, V. J., LORENZINI, A., ALLEN, R. G., TORRES, C. & TRESINI, M. 2004. Replicative senescence: a critical review. *Mech Ageing Dev,* 125, 827-48.

CROWTHER, P. J., DOHERTY, J. P., LINSENMEYER, M. E., WILLIAMSON, M. R. & WOODCOCK, D. M. 1991. Revised genomic consensus for the hypermethylated CpG island region of the human L1 transposon and integration sites of full length L1 elements from recombinant clones made using methylation-tolerant host strains. *Nucleic Acids Res,* 19, 2395-401.

CUI, H., KONG, Y. & ZHANG, H. 2012. Oxidative stress, mitochondrial dysfunction, and aging. *J Signal Transduct,* 2012, 646354.

D'ADDA DI FAGAGNA, F., REAPER, P. M., CLAY-FARRACE, L., FIEGLER, H., CARR, P., VON ZGLINICKI, T., SARETZKI, G., CARTER, N. P. & JACKSON, S. P. 2003. A DNA damage checkpoint response in telomere-initiated senescence. *Nature,* 426, 194-8.

DAI, M., WANG, P., BOYD, A. D., KOSTOV, G., ATHEY, B., JONES, E. G., BUNNEY, W. E., MYERS, R. M., SPEED, T. P., AKIL, H., WATSON, S. J. & MENG, F. 2005. Evolving gene/transcript definitions significantly alter the interpretation of GeneChip data. *Nucleic Acids Res,* 33, e175.

DE MAGALHAES, J. P., CURADO, J. & CHURCH, G. M. 2009. Meta-analysis of age-related gene expression profiles identifies common signatures of aging. *Bioinformatics,* 25, 875-81.

DEMIDENKO, Z. N., ZUBOVA, S. G., BUKREEVA, E. I., POSPELOV, V. A., POSPELOVA, T. V. & BLAGOSKLONNY, M. V. 2009. Rapamycin decelerates cellular senescence. *Cell Cycle,* 8, 1888-95.

DESLER, C., MARCKER, M. L., SINGH, K. K. & RASMUSSEN, L. J. 2011. The importance of mitochondrial DNA in aging and cancer. *J Aging Res,* 2011, 407536.

DHAHBI, J. M., SPINDLER, S. R., ATAMNA, H., YAMAKAWA, A., GUERRERO, N., BOFFELLI, D., MOTE, P. & MARTIN, D. I. 2013. Deep sequencing identifies circulating mouse miRNAs that are functionally implicated in manifestations of aging and responsive to calorie restriction. *Aging (Albany NY),* 5, 130-41.

DI LEONARDO, A., LINKE, S. P., CLARKIN, K. & WAHL, G. M. 1994. DNA damage triggers a prolonged p53-dependent G1 arrest and long-term induction of Cip1 in normal human fibroblasts. *Genes Dev,* 8, 2540-51.

DIEZ, J. J. & IGLESIAS, P. 2003. The role of the novel adipocyte-derived hormone adiponectin in human disease. *Eur J Endocrinol,* 148, 293-300.

DIMRI, G. P., LEE, X., BASILE, G., ACOSTA, M., SCOTT, G., ROSKELLEY, C., MEDRANO, E. E., LINSKENS, M., RUBELJ, I., PEREIRA-SMITH, O. & ET AL. 1995. A biomarker that identifies senescent human cells in culture and in aging skin in vivo. *Proc Natl Acad Sci U S A,* 92, 9363-7.

DINGER, M. E., GASCOIGNE, D. K. & MATTICK, J. S. 2011. The evolution of RNAs with multiple functions. *Biochimie,* 93, 2013-8.

DINGER, M. E., PANG, K. C., MERCER, T. R. & MATTICK, J. S. 2008. Differentiating protein-coding and noncoding RNA: challenges and ambiguities. *PLoS Comput Biol,* 4, e1000176.

DOWN, T. A., RAKYAN, V. K., TURNER, D. J., FLICEK, P., LI, H., KULESHA, E., GRAF, S., JOHNSON, N., HERRERO, J., TOMAZOU, E. M., THORNE, N. P., BACKDAHL, L., HERBERTH, M., HOWE, K. L., JACKSON, D. K., MIRETTI, M. M., MARIONI, J. C., BIRNEY, E., HUBBARD, T. J., DURBIN, R., TAVARE, S. & BECK, S. 2008. A Bayesian deconvolution strategy for immunoprecipitation-based DNA methylome analysis. *Nat Biotechnol,* 26, 779-85.

DRENOS, F. & KIRKWOOD, T. B. 2005. Modelling the disposable soma theory of ageing. *Mech Ageing Dev,* 126, 99-103.

DUAN, S., MI, S., ZHANG, W. & DOLAN, M. E. 2009. Comprehensive analysis of the impact of SNPs and CNVs on human microRNAs and their regulatory genes. *RNA Biol,* 6, 412-25.

EADS, C. A., DANENBERG, K. D., KAWAKAMI, K., SALTZ, L. B., BLAKE, C., SHIBATA, D., DANENBERG, P. V. & LAIRD, P. W. 2000. MethyLight: a high-throughput assay to measure DNA methylation. *Nucleic Acids Res,* 28, E32.

EBERLE, H. B., SERRANO, R. L., FULLEKRUG, J., SCHLOSSER, A., LEHMANN, W. D., LOTTSPEICH, F., KALOYANOVA, D., WIELAND, F. T. & HELMS, J. B. 2002. Identification and characterization of a novel human plant pathogenesis-related protein that localizes to lipid-enriched microdomains in the Golgi complex. *J Cell Sci,* 115, 827-38.

EDWARDS, M. G., ANDERSON, R. M., YUAN, M., KENDZIORSKI, C. M., WEINDRUCH, R. & PROLLA, T. A. 2007. Gene expression profiling of aging reveals activation of a p53-mediated transcriptional program. *BMC Genomics,* 8, 80.

EHRICH, M., NELSON, M. R., STANSSENS, P., ZABEAU, M., LILOGLOU, T., XINARIANOS, G., CANTOR, C. R., FIELD, J. K. & VAN DEN BOOM, D. 2005. Quantitative high-throughput analysis of DNA methylation patterns by base-specific cleavage and mass spectrometry. *Proc Natl Acad Sci U S A,* 102, 15785-90.

EIJSSEN, L. M., JAILLARD, M., ADRIAENS, M. E., GAJ, S., DE GROOT, P. J., MULLER, M. & EVELO, C. T. 2013. User-friendly solutions for microarray quality control and pre-processing on ArrayAnalysis.org. *Nucleic Acids Res,* 41, W71-6.

EISENBERG, I., BARASH, M., KAHAN, T. & MITRANI-ROSENBAUM, S. 2002. Cloning and characterization of a human novel gene C9orf19 encoding a conserved putative protein with an SCP-like extracellular protein domain. *Gene,* 293, 141-8.

EL-MAARRI, O., BECKER, T., JUNEN, J., MANZOOR, S. S., DIAZ-LACAVA, A., SCHWAAB, R., WIENKER, T. & OLDENBURG, J. 2007. Gender specific differences in levels of DNA methylation at selected loci from human total blood: a tendency toward higher methylation levels in males. *Hum Genet,* 122, 505-14.

ELLISON, G. M., NADAL-GINARD, B. & TORELLA, D. 2012. Optimizing cardiac repair and regeneration through activation of the endogenous cardiac stem cell compartment. *J Cardiovasc Transl Res,* 5, 667-77.

ESQUELA-KERSCHER, A. & SLACK, F. J. 2006. Oncomirs - microRNAs with a role in cancer. *Nat Rev Cancer,* 6, 259-69.

ESTELLER, M., LEVINE, R., BAYLIN, S. B., ELLENSON, L. H. & HERMAN, J. G. 1998. MLH1 promoter hypermethylation is associated with the microsatellite instability phenotype in sporadic endometrial carcinomas. *Oncogene,* 17, 2413-7.

EVERITT, A. V., HILMER, S. N., BRAND-MILLER, J. C., JAMIESON, H. A., TRUSWELL, A. S., SHARMA, A. P., MASON, R. S., MORRIS, B. J. & LE

COUTEUR, D. G. 2006. Dietary approaches that delay age-related diseases. *Clin Interv Aging,* 1, 11-31.

FEBER, A., WILSON, G. A., ZHANG, L., PRESNEAU, N., IDOWU, B., DOWN, T. A., RAKYAN, V. K., NOON, L. A., LLOYD, A. C., STUPKA, E., SCHIZA, V., TESCHENDORFF, A. E., SCHROTH, G. P., FLANAGAN, A. & BECK, S. 2011. Comparative methylome analysis of benign and malignant peripheral nerve sheath tumors. *Genome Res,* 21, 515-24.

FEINBERG, A. P. & VOGELSTEIN, B. 1983. Hypomethylation distinguishes genes of some human cancers from their normal counterparts. *Nature,* 301, 89-92.

FERNANDEZ-REAL, J. M., LOPEZ-BERMEJO, A., CASAMITJANA, R. & RICART, W. 2003. Novel interactions of adiponectin with the endocrine system and inflammatory parameters. *J Clin Endocrinol Metab,* 88, 2714-8.

FERRUCCI, L., GIALLAURIA, F. & GURALNIK, J. M. 2008. Epidemiology of aging. *Radiol Clin North Am,* 46, 643-52, v.

FISH, J., RAULE, N. & ATTARDI, G. 2004. Discovery of a major D-loop replication origin reveals two modes of human mtDNA synthesis. *Science,* 306, 2098-101.

FLAJOLLET, S., PORAS, I., CAROSELLA, E. D. & MOREAU, P. 2009. RREB-1 is a transcriptional repressor of HLA-G. *J Immunol,* 183, 6948-59.

FONTANA, L., MEYER, T. E., KLEIN, S. & HOLLOSZY, J. O. 2004. Long-term calorie restriction is highly effective in reducing the risk for atherosclerosis in humans. *Proc Natl Acad Sci U S A,* 101, 6659-63.

FONTANA, L., PARTRIDGE, L. & LONGO, V. D. 2010. Extending healthy life span--from yeast to humans. *Science,* 328, 321-6.

FONTANA, L., VILLAREAL, D. T., WEISS, E. P., RACETTE, S. B., STEGER-MAY, K., KLEIN, S. & HOLLOSZY, J. O. 2007. Calorie restriction or exercise: effects on coronary heart disease risk factors. A randomized, controlled trial. *Am J Physiol Endocrinol Metab,* 293, E197-202.

FONTANA, L., WEISS, E. P., VILLAREAL, D. T., KLEIN, S. & HOLLOSZY, J. O. 2008. Long-term effects of calorie or protein restriction on serum IGF-1 and IGFBP-3 concentration in humans. *Aging Cell,* 7, 681-7.

FOREMAN, K. E. & TANG, J. 2003. Molecular mechanisms of replicative senescence in endothelial cells. *Exp Gerontol,* 38, 1251-7.

FRAGA, M. F., BALLESTAR, E., PAZ, M. F., ROPERO, S., SETIEN, F., BALLESTAR, M. L., HEINE-SUNER, D., CIGUDOSA, J. C., URIOSTE, M., BENITEZ, J., BOIX-CHORNET, M., SANCHEZ-AGUILERA, A., LING, C.,

CARLSSON, E., POULSEN, P., VAAG, A., STEPHAN, Z., SPECTOR, T. D., WU, Y. Z., PLASS, C. & ESTELLER, M. 2005. Epigenetic differences arise during the lifetime of monozygotic twins. *Proc Natl Acad Sci U S A,* 102, 10604-9.

FRAGA, M. F. & ESTELLER, M. 2007. Epigenetics and aging: the targets and the marks. *Trends Genet,* 23, 413-8.

FRANKLIN, R. B., LEVY, B. A., ZOU, J., HANNA, N., DESOUKI, M. M., BAGASRA, O., JOHNSON, L. A. & COSTELLO, L. C. 2012. ZIP14 zinc transporter downregulation and zinc depletion in the development and progression of hepatocellular cancer. *J Gastrointest Cancer,* 43, 249-57.

FRIDMAN, A. L. & TAINSKY, M. A. 2008. Critical pathways in cellular senescence and immortalization revealed by gene expression profiling. *Oncogene,* 27, 5975-87.

FROMMER, M., MCDONALD, L. E., MILLAR, D. S., COLLIS, C. M., WATT, F., GRIGG, G. W., MOLLOY, P. L. & PAUL, C. L. 1992. A genomic sequencing protocol that yields a positive display of 5-methylcytosine residues in individual DNA strands. *Proc Natl Acad Sci U S A,* 89, 1827-31.

FUJITA, K., MONDAL, A. M., HORIKAWA, I., NGUYEN, G. H., KUMAMOTO, K., SOHN, J. J., BOWMAN, E. D., MATHE, E. A., SCHETTER, A. J., PINE, S. R., JI, H., VOJTESEK, B., BOURDON, J. C., LANE, D. P. & HARRIS, C. C. 2009. p53 isoforms Delta133p53 and p53beta are endogenous regulators of replicative cellular senescence. *Nat Cell Biol,* 11, 1135-42.

FURUYA, S., MASUMORI, N., FURUYA, R., TSUKAMOTO, T., ISOMURA, H. & TAMAKAWA, M. 2005. Characterization of localized seminal vesicle amyloidosis causing hemospermia: an analysis using immunohistochemistry and magnetic resonance imaging. *J Urol,* 173, 1273-7.

GAO, Z. H., SUPPOLA, S., LIU, J., HEIKKILA, P., JANNE, J. & VOUTILAINEN, R. 2002. Association of H19 promoter methylation with the expression of H19 and IGF-II genes in adrenocortical tumors. *J Clin Endocrinol Metab,* 87, 1170-6.

GENTLEMAN, R. C., CAREY, V. J., BATES, D. M., BOLSTAD, B., DETTLING, M., DUDOIT, S., ELLIS, B., GAUTIER, L., GE, Y., GENTRY, J., HORNIK, K., HOTHORN, T., HUBER, W., IACUS, S., IRIZARRY, R., LEISCH, F., LI, C., MAECHLER, M., ROSSINI, A. J., SAWITZKI, G., SMITH, C., SMYTH, G., TIERNEY, L., YANG, J. Y. & ZHANG, J. 2004. Bioconductor: open software development for computational biology and bioinformatics. *Genome Biol,* 5, R80.

GILES, R. E., BLANC, H., CANN, H. M. & WALLACE, D. C. 1980. Maternal inheritance of human mitochondrial DNA. *Proc Natl Acad Sci U S A,* 77, 6715-9.

GIRIJASHANKER, K., HE, L., SOLEIMANI, M., REED, J. M., LI, H., LIU, Z., WANG, B., DALTON, T. P. & NEBERT, D. W. 2008. Slc39a14 gene encodes ZIP14, a metal/bicarbonate symporter: similarities to the ZIP8 transporter. *Mol Pharmacol,* 73, 1413-23.

GOLBUS, J., PALELLA, T. D. & RICHARDSON, B. C. 1990. Quantitative changes in T cell DNA methylation occur during differentiation and ageing. *Eur J Immunol,* 20, 1869-72.

GOLDSTEIN, S. 1990. Replicative senescence: the human fibroblast comes of age. *Science,* 249, 1129-33.

GOLDSTONE, A. P. 2004. Prader-Willi syndrome: advances in genetics, pathophysiology and treatment. *Trends Endocrinol Metab,* 15, 12-20.

GOLL, M. G. & BESTOR, T. H. 2005. Eukaryotic cytosine methyltransferases. *Annu Rev Biochem,* 74, 481-514.

GOLL, M. G., KIRPEKAR, F., MAGGERT, K. A., YODER, J. A., HSIEH, C. L., ZHANG, X., GOLIC, K. G., JACOBSEN, S. E. & BESTOR, T. H. 2006. Methylation of tRNAAsp by the DNA methyltransferase homolog Dnmt2. *Science,* 311, 395-8.

GOMEZ, C. R., NOMELLINI, V., FAUNCE, D. E. & KOVACS, E. J. 2008. Innate immunity and aging. *Exp Gerontol,* 43, 718-28.

GOODRICH, J. A. & KUGEL, J. F. 2006. Non-coding-RNA regulators of RNA polymerase II transcription. *Nat Rev Mol Cell Biol,* 7, 612-6.

GORGOULIS, V. G. & HALAZONETIS, T. D. 2010. Oncogene-induced senescence: the bright and dark side of the response. *Curr Opin Cell Biol,* 22, 816-27.

GREAVES, L. C., BARRON, M. J., PLUSA, S., KIRKWOOD, T. B., MATHERS, J. C., TAYLOR, R. W. & TURNBULL, D. M. 2010. Defects in multiple complexes of the respiratory chain are present in ageing human colonic crypts. *Exp Gerontol,* 45, 573-9.

GRIFFITHS-JONES, S., SAINI, H. K., VAN DONGEN, S. & ENRIGHT, A. J. 2008. miRBase: tools for microRNA genomics. *Nucleic Acids Res,* 36, D154-8.

GRILLARI, J. & GRILLARI-VOGLAUER, R. 2010. Novel modulators of senescence, aging, and longevity: Small non-coding RNAs enter the stage. *Exp Gerontol,* 45, 302-11.

GRUENBAUM, Y., CEDAR, H. & RAZIN, A. 1982. Substrate and sequence specificity of a eukaryotic DNA methylase. *Nature,* 295, 620-2.

GUARENTE, L. & PICARD, F. 2005. Calorie restriction--the SIR2 connection. *Cell,* 120, 473-82.

GUTTMAN, M., AMIT, I., GARBER, M., FRENCH, C., LIN, M. F., FELDSER, D., HUARTE, M., ZUK, O., CAREY, B. W., CASSADY, J. P., CABILI, M. N., JAENISCH, R., MIKKELSEN, T. S., JACKS, T., HACOHEN, N., BERNSTEIN, B. E., KELLIS, M., REGEV, A., RINN, J. L. & LANDER, E. S. 2009. Chromatin signature reveals over a thousand highly conserved large non-coding RNAs in mammals. *Nature,* 458, 223-7.

HAGIHARA, A., MIYAMOTO, K., FURUTA, J., HIRAOKA, N., WAKAZONO, K., SEKI, S., FUKUSHIMA, S., TSAO, M. S., SUGIMURA, T. & USHIJIMA, T. 2004. Identification of 27 5' CpG islands aberrantly methylated and 13 genes silenced in human pancreatic cancers. *Oncogene,* 23, 8705-10.

HAHNE, J. C., KUMMER, S., HEUKAMP, L. C., FUCHS, T., GUN, M., LANGER, B., VON RUECKER, A. & WERNERT, N. 2009. Regulation of protein tyrosine kinases in tumour cells by the transcription factor Ets-1. *Int J Oncol,* 35, 989-96.

HALLE, J. P., SCHMIDT, C. & ADAM, G. 1995. Changes of the methylation pattern of the c-myc gene during in vitro aging of IMR90 human embryonic fibroblasts. *Mutat Res,* 316, 157-71.

HALLEN, A. 2002. Accumulation of insoluble protein and aging. *Biogerontology,* 3, 307-16.

HAMEETMAN, L., ROZEMAN, L. B., LOMBAERTS, M., OOSTING, J., TAMINIAU, A. H., CLETON-JANSEN, A. M., BOVEE, J. V. & HOGENDOORN, P. C. 2006. Peripheral chondrosarcoma progression is accompanied by decreased Indian Hedgehog signalling. *J Pathol,* 209, 501-11.

HANDSCHIN, C. & SPIEGELMAN, B. M. 2008. The role of exercise and PGC1alpha in inflammation and chronic disease. *Nature,* 454, 463-9.

HANSEN, J. 1998. Common cancers in the elderly. *Drugs Aging,* 13, 467-78.

HARRISON, D. E., STRONG, R., SHARP, Z. D., NELSON, J. F., ASTLE, C. M., FLURKEY, K., NADON, N. L., WILKINSON, J. E., FRENKEL, K., CARTER, C. S., PAHOR, M., JAVORS, M. A., FERNANDEZ, E. & MILLER, R. A. 2009. Rapamycin fed late in life extends lifespan in genetically heterogeneous mice. *Nature,* 460, 392-5.

HARTMANN, N., REICHWALD, K., WITTIG, I., DROSE, S., SCHMEISSER, S., LUCK, C., HAHN, C., GRAF, M., GAUSMANN, U., TERZIBASI, E., CELLERINO, A., RISTOW, M., BRANDT, U., PLATZER, M. & ENGLERT, C. 2011. Mitochondrial DNA copy number and function decrease with age in the short-lived fish Nothobranchius furzeri. *Aging Cell,* 10, 824-31.

HASS, B. S., HART, R. W., LU, M. H. & LYN-COOK, B. D. 1993. Effects of caloric restriction in animals on cellular function, oncogene expression, and DNA methylation in vitro. *Mutat Res,* 295, 281-9.

HATA, K., OKANO, M., LEI, H. & LI, E. 2002. Dnmt3L cooperates with the Dnmt3 family of de novo DNA methyltransferases to establish maternal imprints in mice. *Development,* 129, 1983-93.

HAY, N. & SONENBERG, N. 2004. Upstream and downstream of mTOR. *Genes Dev,* 18, 1926-45.

HAYFLICK, L. 1965. The Limited in Vitro Lifetime of Human Diploid Cell Strains. *Exp Cell Res,* 37, 614-36.

HAYFLICK, L. 1979. The cell biology of aging. *J Invest Dermatol,* 73, 8-14.

HAYFLICK, L. & MOORHEAD, P. S. 1961. The serial cultivation of human diploid cell strains. *Exp Cell Res,* 25, 585-621.

HE, J., MAO, C. C., REYES, A., SEMBONGI, H., DI RE, M., GRANYCOME, C., CLIPPINGDALE, A. B., FEARNLEY, I. M., HARBOUR, M., ROBINSON, A. J., REICHELT, S., SPELBRINK, J. N., WALKER, J. E. & HOLT, I. J. 2007. The AAA+ protein ATAD3 has displacement loop binding properties and is involved in mitochondrial nucleoid organization. *J Cell Biol,* 176, 141-6.

HEARD, E. & DISTECHE, C. M. 2006. Dosage compensation in mammals: fine-tuning the expression of the X chromosome. *Genes Dev,* 20, 1848-67.

HECHT, N. B., LIEM, H., KLEENE, K. C., DISTEL, R. J. & HO, S. M. 1984. Maternal inheritance of the mouse mitochondrial genome is not mediated by a loss or gross alteration of the paternal mitochondrial DNA or by methylation of the oocyte mitochondrial DNA. *Dev Biol,* 102, 452-61.

HECTOR, K. L., LAGISZ, M. & NAKAGAWA, S. 2012. The effect of resveratrol on longevity across species: a meta-analysis. *Biol Lett,* 8, 790-3.

HEILBRONN, L. K., DE JONGE, L., FRISARD, M. I., DELANY, J. P., LARSON-MEYER, D. E., ROOD, J., NGUYEN, T., MARTIN, C. K., VOLAUFOVA, J., MOST, M. M., GREENWAY, F. L., SMITH, S. R., DEUTSCH, W. A., WILLIAMSON, D. A. & RAVUSSIN, E. 2006. Effect of 6-month calorie restriction on biomarkers of longevity, metabolic adaptation, and oxidative stress in overweight individuals: a randomized controlled trial. *JAMA,* 295, 1539-48.

HEILBRONN, L. K. & RAVUSSIN, E. 2003. Calorie restriction and aging: review of the literature and implications for studies in humans. *Am J Clin Nutr,* 78, 361-9.

HERBIG, U., FERREIRA, M., CONDEL, L., CAREY, D. & SEDIVY, J. M. 2006. Cellular senescence in aging primates. *Science,* 311, 1257.

HERMAN, J. G., GRAFF, J. R., MYOHANEN, S., NELKIN, B. D. & BAYLIN, S. B. 1996. Methylation-specific PCR: a novel PCR assay for methylation status of CpG islands. *Proc Natl Acad Sci U S A,* 93, 9821-6.

HERMANN, A., GOWHER, H. & JELTSCH, A. 2004a. Biochemistry and biology of mammalian DNA methyltransferases. *Cell Mol Life Sci,* 61, 2571-87.

HERMANN, A., GOYAL, R. & JELTSCH, A. 2004b. The Dnmt1 DNA-(cytosine-C5)-methyltransferase methylates DNA processively with high preference for hemimethylated target sites. *J Biol Chem,* 279, 48350-9.

HEWITT, G., JURK, D., MARQUES, F. D., CORREIA-MELO, C., HARDY, T., GACKOWSKA, A., ANDERSON, R., TASCHUK, M., MANN, J. & PASSOS, J. F. 2012. Telomeres are favoured targets of a persistent DNA damage response in ageing and stress-induced senescence. *Nat Commun,* 3, 708.

HIGAMI, Y., BARGER, J. L., PAGE, G. P., ALLISON, D. B., SMITH, S. R., PROLLA, T. A. & WEINDRUCH, R. 2006. Energy restriction lowers the expression of genes linked to inflammation, the cytoskeleton, the extracellular matrix, and angiogenesis in mouse adipose tissue. *J Nutr,* 136, 343-52.

HIRST, M. & MARRA, M. A. 2009. Epigenetics and human disease. *Int J Biochem Cell Biol,* 41, 136-46.

HOAGLAND, M. B., STEPHENSON, M. L., SCOTT, J. F., HECHT, L. I. & ZAMECNIK, P. C. 1958. A soluble ribonucleic acid intermediate in protein synthesis. *J Biol Chem,* 231, 241-57.

HOEK, H. W., BROWN, A. S. & SUSSER, E. 1998. The Dutch famine and schizophrenia spectrum disorders. *Soc Psychiatry Psychiatr Epidemiol,* 33, 373-9.

HOJYO, S., FUKADA, T., SHIMODA, S., OHASHI, W., BIN, B. H., KOSEKI, H. & HIRANO, T. 2011. The zinc transporter SLC39A14/ZIP14 controls G-protein coupled receptor-mediated signaling required for systemic growth. *PLoS One,* 6, e18059.

HOLBROOK, M. A. & MENNINGER, J. R. 2002. Erythromycin slows aging of Saccharomyces cerevisiae. *J Gerontol A Biol Sci Med Sci,* 57, B29-36.

HOLEMON, H., KORSHUNOVA, Y., ORDWAY, J. M., BEDELL, J. A., CITEK, R. W., LAKEY, N., LEON, J., FINNEY, M., MCPHERSON, J. D. & JEDDELOH, J. A. 2007. MethylScreen: DNA methylation density monitoring using quantitative PCR. *Biotechniques,* 43, 683-93.

HOLLIDAY, R. 1996. The current status of the protein error theory of aging. *Exp Gerontol,* 31, 449-52.

HOLLOSZY, J. O. & FONTANA, L. 2007. Caloric restriction in humans. *Exp Gerontol,* 42, 709-12.

HORNEBECK, W. 2003. Down-regulation of tissue inhibitor of matrix metalloprotease-1 (TIMP-1) in aged human skin contributes to matrix degradation and impaired cell growth and survival. *Pathol Biol (Paris),* 51, 569-73.

HOSSAIN, M. A., RUSSELL, J. C., O'BRIEN, R. & LATERRA, J. 2004. Neuronal pentraxin 1: a novel mediator of hypoxic-ischemic injury in neonatal brain. *J Neurosci,* 24, 4187-96.

HOTCHKISS, R. D. 1948. The quantitative separation of purines, pyrimidines, and nucleosides by paper chromatography. *J Biol Chem,* 175, 315-32.

HOWITZ, K. T., BITTERMAN, K. J., COHEN, H. Y., LAMMING, D. W., LAVU, S., WOOD, J. G., ZIPKIN, R. E., CHUNG, P., KISIELEWSKI, A., ZHANG, L. L., SCHERER, B. & SINCLAIR, D. A. 2003. Small molecule activators of sirtuins extend Saccharomyces cerevisiae lifespan. *Nature,* 425, 191-6.

HU, M., YAO, J., CAI, L., BACHMAN, K. E., VAN DEN BRULE, F., VELCULESCU, V. & POLYAK, K. 2005. Distinct epigenetic changes in the stromal cells of breast cancers. *Nat Genet,* 37, 899-905.

ILLINGWORTH, R., KERR, A., DESOUSA, D., JORGENSEN, H., ELLIS, P., STALKER, J., JACKSON, D., CLEE, C., PLUMB, R., ROGERS, J., HUMPHRAY, S., COX, T., LANGFORD, C. & BIRD, A. 2008. A novel CpG island set identifies tissue-specific methylation at developmental gene loci. *PLoS Biol,* 6, e22.

INOKI, K., ZHU, T. & GUAN, K. L. 2003. TSC2 mediates cellular energy response to control cell growth and survival. *Cell,* 115, 577-90.

IRIZARRY, R. A., LADD-ACOSTA, C., WEN, B., WU, Z., MONTANO, C., ONYANGO, P., CUI, H., GABO, K., RONGIONE, M., WEBSTER, M., JI, H., POTASH, J. B., SABUNCIYAN, S. & FEINBERG, A. P. 2009. The human colon cancer methylome shows similar hypo- and hypermethylation at conserved tissue-specific CpG island shores. *Nat Genet,* 41, 178-86.

ISSA, J. P., OTTAVIANO, Y. L., CELANO, P., HAMILTON, S. R., DAVIDSON, N. E. & BAYLIN, S. B. 1994. Methylation of the oestrogen receptor CpG island links ageing and neoplasia in human colon. *Nat Genet,* 7, 536-40.

ISSA, J. P., VERTINO, P. M., BOEHM, C. D., NEWSHAM, I. F. & BAYLIN, S. B. 1996. Switch from monoallelic to biallelic human IGF2 promoter methylation during aging and carcinogenesis. *Proc Natl Acad Sci U S A,* 93, 11757-62.

JACOBS, J. P., JONES, C. M. & BAILLE, J. P. 1970. Characteristics of a human diploid cell designated MRC-5. *Nature,* 227, 168-70.

JAMES, S. J., MUSKHELISHVILI, L., GAYLOR, D. W., TURTURRO, A. & HART, R. 1998. Upregulation of apoptosis with dietary restriction: implications for carcinogenesis and aging. *Environ Health Perspect,* 106 Suppl 1, 307-12.

JEONG, K. S. & LEE, S. 2005. Estimating the total mouse DNA methylation according to the B1 repetitive elements. *Biochem Biophys Res Commun,* 335, 1211-6.

JIANG, H., SHUKLA, A., WANG, X., CHEN, W. Y., BERNSTEIN, B. E. & ROEDER, R. G. 2011. Role for Dpy-30 in ES cell-fate specification by regulation of H3K4 methylation within bivalent domains. *Cell,* 144, 513-25.

JIANG, M., ZHANG, Y., FEI, J., CHANG, X., FAN, W., QIAN, X., ZHANG, T. & LU, D. Rapid quantification of DNA methylation by measuring relative peak heights in direct bisulfite-PCR sequencing traces. *Lab Invest,* 90, 282-90.

JIANG, Y., YU, V. C., BUCHHOLZ, F., O'CONNELL, S., RHODES, S. J., CANDELORO, C., XIA, Y. R., LUSIS, A. J. & ROSENFELD, M. G. 1996. A novel family of Cys-Cys, His-Cys zinc finger transcription factors expressed in developing nervous system and pituitary gland. *J Biol Chem,* 271, 10723-30.

JOHNSON, T. E. 2002. A personal retrospective on the genetics of aging. *Biogerontology,* 3, 7-12.

JOHNSON, T. E. 2008. Caenorhabditis elegans 2007: the premier model for the study of aging. *Exp Gerontol,* 43, 1-4.

JONES, P. A. & BAYLIN, S. B. 2002. The fundamental role of epigenetic events in cancer. *Nat Rev Genet,* 3, 415-28.

JOSHI, P. C., MEHTA, A., JABBER, W. S., FAN, X. & GUIDOT, D. M. 2009. Zinc deficiency mediates alcohol-induced alveolar epithelial and macrophage dysfunction in rats. *Am J Respir Cell Mol Biol,* 41, 207-16.

JUKES, T. H. & OSAWA, S. 1993. Evolutionary changes in the genetic code. *Comp Biochem Physiol B,* 106, 489-94.

JURK, D., WANG, C., MIWA, S., MADDICK, M., KOROLCHUK, V., TSOLOU, A., GONOS, E. S., THRASIVOULOU, C., SAFFREY, M. J., CAMERON, K. & VON ZGLINICKI, T. 2012. Postmitotic neurons develop a p21-dependent senescence-like phenotype driven by a DNA damage response. *Aging Cell,* 11, 996-1004.

KAEBERLEIN, M., POWERS, R. W., 3RD, STEFFEN, K. K., WESTMAN, E. A., HU, D., DANG, N., KERR, E. O., KIRKLAND, K. T., FIELDS, S. & KENNEDY, B. K. 2005. Regulation of yeast replicative life span by TOR and Sch9 in response to nutrients. *Science,* 310, 1193-6.

KANAYA, T., KYO, S., TAKAKURA, M., ITO, H., NAMIKI, M. & INOUE, M. 1998. hTERT is a critical determinant of telomerase activity in renal-cell carcinoma. *Int J Cancer,* 78, 539-43.

KAPAHI, P., CHEN, D., ROGERS, A. N., KATEWA, S. D., LI, P. W., THOMAS, E. L. & KOCKEL, L. 2010. With TOR, less is more: a key role for the conserved nutrient-sensing TOR pathway in aging. *Cell Metab,* 11, 453-65.

KARIJOLICH, J., KANTARTZIS, A. & YU, Y. T. 2010. Quantitative analysis of RNA modifications. *Methods Mol Biol,* 629, 21-32.

KARIMI, M., JOHANSSON, S. & EKSTROM, T. J. 2006a. Using LUMA: a Luminometric-based assay for global DNA-methylation. *Epigenetics,* 1, 45-8.

KARIMI, M., JOHANSSON, S., STACH, D., CORCORAN, M., GRANDER, D., SCHALLING, M., BAKALKIN, G., LYKO, F., LARSSON, C. & EKSTROM, T. J. 2006b. LUMA (LUminometric Methylation Assay)--a high throughput method to the analysis of genomic DNA methylation. *Exp Cell Res,* 312, 1989-95.

KAUFFMANN, A., GENTLEMAN, R. & HUBER, W. 2009. arrayQualityMetrics--a bioconductor package for quality assessment of microarray data. *Bioinformatics,* 25, 415-6.

KAWANISHI, S. & OIKAWA, S. 2004. Mechanism of telomere shortening by oxidative stress. *Ann N Y Acad Sci,* 1019, 278-84.

KELLY, R. D., MAHMUD, A., MCKENZIE, M., TROUNCE, I. A. & ST JOHN, J. C. 2012. Mitochondrial DNA copy number is regulated in a tissue specific manner by DNA methylation of the nuclear-encoded DNA polymerase gamma A. *Nucleic Acids Res,* 40, 10124-38.

KENYON, C. 2005. The plasticity of aging: insights from long-lived mutants. *Cell,* 120, 449-60.

KHANNA, A., MUTHUSAMY, S., LIANG, R., SAROJINI, H. & WANG, E. 2011. Gain of survival signaling by down-regulation of three key miRNAs in brain of calorie-restricted mice. *Aging (Albany NY),* 3, 223-36.

KIM, E. K., KANG, J. Y., RHO, Y. H., KIM, Y. S., KIM, D. S. & BAE, Y. S. 2009a. Silencing of the CKII alpha and CKII alpha' genes during cellular senescence is mediated by DNA methylation. *Gene,* 431, 55-60.

KIM, G. D., NI, J., KELESOGLU, N., ROBERTS, R. J. & PRADHAN, S. 2002. Co-operation and communication between the human maintenance and de novo DNA (cytosine-5) methyltransferases. *EMBO J,* 21, 4183-95.

KIM, J. K., SAMARANAYAKE, M. & PRADHAN, S. 2009b. Epigenetic mechanisms in mammals. *Cell Mol Life Sci,* 66, 596-612.

KIRKPATRICK, L. L., MATZUK, M. M., DODDS, D. C. & PERIN, M. S. 2000. Biochemical interactions of the neuronal pentraxins. Neuronal pentraxin (NP) receptor binds to taipoxin and taipoxin-associated calcium-binding protein 49 via NP1 and NP2. *J Biol Chem,* 275, 17786-92.

KIRKWOOD, T. B. 1977. Evolution of ageing. *Nature,* 270, 301-4.

KLAGSBRUN, M. 1973. An evolutionary study of the methylation of transfer and ribosomal ribonucleic acid in prokaryote and eukaryote organisms. *J Biol Chem,* 248, 2612-20.

KNOELL, D. L., JULIAN, M. W., BAO, S., BESECKER, B., MACRE, J. E., LEIKAUF, G. D., DISILVESTRO, R. A. & CROUSER, E. D. 2009. Zinc deficiency increases organ damage and mortality in a murine model of polymicrobial sepsis. *Crit Care Med,* 37, 1380-8.

KOCH, C. M., JOUSSEN, S., SCHELLENBERG, A., LIN, Q., ZENKE, M. & WAGNER, W. 2012. Monitoring of cellular senescence by DNA-methylation at specific CpG sites. *Aging Cell,* 11, 366-9.

KOCH, C. M., RECK, K., SHAO, K., LIN, Q., JOUSSEN, S., ZIEGLER, P., WALENDA, G., DRESCHER, W., OPALKA, B., MAY, T., BRUMMENDORF, T., ZENKE, M., SARIC, T. & WAGNER, W. 2013. Pluripotent stem cells escape from senescence-associated DNA methylation changes. *Genome Res,* 23, 248-59.

KOCH, C. M., SUSCHEK, C. V., LIN, Q., BORK, S., GOERGENS, M., JOUSSEN, S., PALLUA, N., HO, A. D., ZENKE, M. & WAGNER, W. 2011. Specific age-associated DNA methylation changes in human dermal fibroblasts. *PLoS One,* 6, e16679.

KOCH, C. M. & WAGNER, W. 2013. Epigenetic biomarker to determine replicative senescence of cultured cells. *Methods Mol Biol,* 1048, 309-21.

KOUZARIDES, T. 2007. Chromatin modifications and their function. *Cell,* 128, 693-705.

KRAYTSBERG, Y., KUDRYAVTSEVA, E., MCKEE, A. C., GEULA, C., KOWALL, N. W. & KHRAPKO, K. 2006. Mitochondrial DNA deletions are abundant and cause functional impairment in aged human substantia nigra neurons. *Nat Genet,* 38, 518-20.

KRISTAN, D. M. 2008. Calorie restriction and susceptibility to intact pathogens. *Age (Dordr),* 30, 147-56.

KRTOLICA, A., PARRINELLO, S., LOCKETT, S., DESPREZ, P. Y. & CAMPISI, J. 2001. Senescent fibroblasts promote epithelial cell growth and tumorigenesis: a link between cancer and aging. *Proc Natl Acad Sci U S A,* 98, 12072-7.

KUILMAN, T., MICHALOGLOU, C., MOOI, W. J. & PEEPER, D. S. 2010. The essence of senescence. *Genes Dev,* 24, 2463-79.

KUILMAN, T., MICHALOGLOU, C., VREDEVELD, L. C., DOUMA, S., VAN DOORN, R., DESMET, C. J., AARDEN, L. A., MOOI, W. J. & PEEPER, D. S. 2008. Oncogene-induced senescence relayed by an interleukin-dependent inflammatory network. *Cell,* 133, 1019-31.

KUO, K. C., MCCUNE, R. A., GEHRKE, C. W., MIDGETT, R. & EHRLICH, M. 1980. Quantitative reversed-phase high performance liquid chromatographic determination of major and modified deoxyribonucleosides in DNA. *Nucleic Acids Res,* 8, 4763-76.

LANGLEY, E., PEARSON, M., FARETTA, M., BAUER, U. M., FRYE, R. A., MINUCCI, S., PELICCI, P. G. & KOUZARIDES, T. 2002. Human SIR2 deacetylates p53 and antagonizes PML/p53-induced cellular senescence. *EMBO J,* 21, 2383-96.

LAPLANTE, M. & SABATINI, D. M. 2012. mTOR signaling in growth control and disease. *Cell,* 149, 274-93.

LAWLESS, C., JURK, D., GILLESPIE, C. S., SHANLEY, D., SARETZKI, G., VON ZGLINICKI, T. & PASSOS, J. F. 2012. A stochastic step model of replicative senescence explains ROS production rate in ageing cell populations. *PLoS One,* 7, e32117.

LAWLESS, C., WANG, C., JURK, D., MERZ, A., ZGLINICKI, T. & PASSOS, J. F. 2010. Quantitative assessment of markers for cell senescence. *Exp Gerontol,* 45, 772-8.

LEAKEY, T. I., ZIELINSKI, J., SIEGFRIED, R. N., SIEGEL, E. R., FAN, C. Y. & COONEY, C. A. 2008. A simple algorithm for quantifying DNA methylation levels on multiple independent CpG sites in bisulfite genomic sequencing electropherograms. *Nucleic Acids Res,* 36, e64.

LEE, C. K., WEINDRUCH, R. & PROLLA, T. A. 2000. Gene-expression profile of the ageing brain in mice. *Nat Genet,* 25, 294-7.

LEE, Y., KIM, M., HAN, J., YEOM, K. H., LEE, S., BAEK, S. H. & KIM, V. N. 2004. MicroRNA genes are transcribed by RNA polymerase II. *EMBO J,* 23, 4051-60.

LEIGH-BROWN, S., ENRIQUEZ, J. A. & ODOM, D. T. 2010. Nuclear transcription factors in mammalian mitochondria. *Genome Biol,* 11, 215.

LENSTRA, T. L., BENSCHOP, J. J., KIM, T., SCHULZE, J. M., BRABERS, N. A., MARGARITIS, T., VAN DE PASCH, L. A., VAN HEESCH, S. A., BROK, M. O., GROOT KOERKAMP, M. J., KO, C. W., VAN LEENEN, D., SAMEITH, K., VAN HOOFF, S. R., LIJNZAAD, P., KEMMEREN, P., HENTRICH, T., KOBOR, M. S., BURATOWSKI, S. & HOLSTEGE, F. C. 2011. The specificity and topology of chromatin interaction pathways in yeast. *Mol Cell,* 42, 536-49.

LESAGE, S. & BRICE, A. 2009. Parkinson's disease: from monogenic forms to genetic susceptibility factors. *Hum Mol Genet,* 18, R48-59.

LEVINE, B. & KROEMER, G. 2008. Autophagy in the pathogenesis of disease. *Cell,* 132, 27-42.

LEWIN, J., SCHMITT, A. O., ADORJAN, P., HILDMANN, T. & PIEPENBROCK, C. 2004. Quantitative DNA methylation analysis based on four-dye trace data from direct sequencing of PCR amplificates. *Bioinformatics,* 20, 3005-12.

LI, L. C. & DAHIYA, R. 2002. MethPrimer: designing primers for methylation PCRs. *Bioinformatics,* 18, 1427-31.

LI, L. C., OKINO, S. T., ZHAO, H., POOKOT, D., PLACE, R. F., URAKAMI, S., ENOKIDA, H. & DAHIYA, R. 2006. Small dsRNAs induce transcriptional activation in human cells. *Proc Natl Acad Sci U S A,* 103, 17337-42.

LI, Y., DANIEL, M. & TOLLEFSBOL, T. O. 2011. Epigenetic regulation of caloric restriction in aging. *BMC Med,* 9, 98.

LI, Y., LIU, L. & TOLLEFSBOL, T. O. 2010. Glucose restriction can extend normal cell lifespan and impair precancerous cell growth through epigenetic control of hTERT and p16 expression. *FASEB J,* 24, 1442-53.

LI, Y. & TOLLEFSBOL, T. O. 2011. p16(INK4a) suppression by glucose restriction contributes to human cellular lifespan extension through SIRT1-mediated epigenetic and genetic mechanisms. *PLoS One,* 6, e17421.

LIANG, X. W., ZHU, J. Q., MIAO, Y. L., LIU, J. H., WEI, L., LU, S. S., HOU, Y., SCHATTEN, H., LU, K. H. & SUN, Q. Y. 2008. Loss of methylation imprint of Snrpn in postovulatory aging mouse oocyte. *Biochem Biophys Res Commun,* 371, 16-21.

LIAO, C. Y., JOHNSON, T. E. & NELSON, J. F. 2013. Genetic variation in responses to dietary restriction - An unbiased tool for hypothesis testing. *Exp Gerontol*.

LICHTEN, L. A., LIUZZI, J. P. & COUSINS, R. J. 2009. Interleukin-1beta contributes via nitric oxide to the upregulation and functional activity of the zinc transporter Zip14

(Slc39a14) in murine hepatocytes. *Am J Physiol Gastrointest Liver Physiol,* 296, G860-7.

LIN, S. J., DEFOSSEZ, P. A. & GUARENTE, L. 2000. Requirement of NAD and SIR2 for life-span extension by calorie restriction in Saccharomyces cerevisiae. *Science,* 289, 2126-8.

LISANTI, S., VON ZGLINICKI, T. & MATHERS, J. C. 2012. Standardization and quality controls for the methylated DNA immunoprecipitation technique. *Epigenetics,* 7, 615-25.

LIU, X., WANG, Y., WANG, X., SUN, Z., LI, L., TAO, Q. & LUO, B. 2013. Epigenetic silencing of WNT5A in Epstein-Barr virus-associated gastric carcinoma. *Arch Virol,* 158, 123-32.

LIUZZI, J. P., LICHTEN, L. A., RIVERA, S., BLANCHARD, R. K., AYDEMIR, T. B., KNUTSON, M. D., GANZ, T. & COUSINS, R. J. 2005. Interleukin-6 regulates the zinc transporter Zip14 in liver and contributes to the hypozincemia of the acute-phase response. *Proc Natl Acad Sci U S A,* 102, 6843-8.

LIVAK, K. J. & SCHMITTGEN, T. D. 2001. Analysis of relative gene expression data using real-time quantitative PCR and the 2(-Delta Delta C(T)) Method. *Methods,* 25, 402-8.

LONGO, V. D., ELLERBY, L. M., BREDESEN, D. E., VALENTINE, J. S. & GRALLA, E. B. 1997. Human Bcl-2 reverses survival defects in yeast lacking superoxide dismutase and delays death of wild-type yeast. *J Cell Biol,* 137, 1581-8.

LOPEZ-OTIN, C., BLASCO, M. A., PARTRIDGE, L., SERRANO, M. & KROEMER, G. 2013. The hallmarks of aging. *Cell,* 153, 1194-217.

LOSSIE, A. C., WHITNEY, M. M., AMIDON, D., DONG, H. J., CHEN, P., THERIAQUE, D., HUTSON, A., NICHOLLS, R. D., ZORI, R. T., WILLIAMS, C. A. & DRISCOLL, D. J. 2001. Distinct phenotypes distinguish the molecular classes of Angelman syndrome. *J Med Genet,* 38, 834-45.

LOUNEVA, N., COHEN, J. W., HAN, L. Y., TALBOT, K., WILSON, R. S., BENNETT, D. A., TROJANOWSKI, J. Q. & ARNOLD, S. E. 2008. Caspase-3 is enriched in postsynaptic densities and increased in Alzheimer's disease. *Am J Pathol,* 173, 1488-95.

LOWE, S. W., CEPERO, E. & EVAN, G. 2004. Intrinsic tumour suppression. *Nature,* 432, 307-15.

LU, T. & FINKEL, T. 2008. Free radicals and senescence. *Exp Cell Res,* 314, 1918-22.

LUGER, K., MADER, A. W., RICHMOND, R. K., SARGENT, D. F. & RICHMOND, T. J. 1997. Crystal structure of the nucleosome core particle at 2.8 A resolution. *Nature,* 389, 251-60.

LUO, J., NIKOLAEV, A. Y., IMAI, S., CHEN, D., SU, F., SHILOH, A., GUARENTE, L. & GU, W. 2001. Negative control of p53 by Sir2alpha promotes cell survival under stress. *Cell,* 107, 137-48.

MACHWE, A., ORREN, D. K. & BOHR, V. A. 2000. Accelerated methylation of ribosomal RNA genes during the cellular senescence of Werner syndrome fibroblasts. *FASEB J,* 14, 1715-24.

MAEKAWA, M., TANIGUCHI, T., HIGASHI, H., SUGIMURA, H., SUGANO, K. & KANNO, T. 2004. Methylation of mitochondrial DNA is not a useful marker for cancer detection. *Clin Chem,* 50, 1480-1.

MAIR, W. & DILLIN, A. 2008. Aging and survival: the genetics of life span extension by dietary restriction. *Annu Rev Biochem,* 77, 727-54.

MALONE, C. D. & HANNON, G. J. 2009. Small RNAs as guardians of the genome. *Cell,* 136, 656-68.

MARTIN, G. M. 2005. Genetic modulation of senescent phenotypes in Homo sapiens. *Cell,* 120, 523-32.

MARTIN, V., VALENCIA, A., AGIRRE, X., CERVERA, J., SAN JOSE-ENERIZ, E., VILAS-ZORNOZA, A., RODRIGUEZ-OTERO, P., SANZ, M. A., HERRERA, C., TORRES, A., PROSPER, F. & ROMAN-GOMEZ, J. 2010. Epigenetic regulation of the non-canonical Wnt pathway in acute myeloid leukemia. *Cancer Sci,* 101, 425-32.

MATHERS, J. C. 2006. Nutritional modulation of ageing: genomic and epigenetic approaches. *Mech Ageing Dev,* 127, 584-9.

MATTISON, J. A., ROTH, G. S., BEASLEY, T. M., TILMONT, E. M., HANDY, A. M., HERBERT, R. L., LONGO, D. L., ALLISON, D. B., YOUNG, J. E., BRYANT, M., BARNARD, D., WARD, W. F., QI, W., INGRAM, D. K. & DE CABO, R. 2012. Impact of caloric restriction on health and survival in rhesus monkeys from the NIA study. *Nature,* 489, 318-21.

MAYS-HOOPES, L., CHAO, W., BUTCHER, H. C. & HUANG, R. C. 1986. Decreased methylation of the major mouse long interspersed repeated DNA during aging and in myeloma cells. *Dev Genet,* 7, 65-73.

MAZIN, A. L. 1995. [Methylation of the factor IX gene--a basic reason for the mutation causing hemophilia B]. *Mol Biol (Mosk),* 29, 71-90.

MAZIN, A. L. 2009. Suicidal function of DNA methylation in age-related genome disintegration. *Ageing Res Rev,* 8, 314-27.

MCCAY, C. M., CROWELL, M. F. & MAYNARD, L. A. 1989. The effect of retarded growth upon the length of life span and upon the ultimate body size. 1935. *Nutrition,* 5, 155-71; discussion 172.

MCKAY, J. A. & MATHERS, J. C. 2011. Diet induced epigenetic changes and their implications for health. *Acta Physiol (Oxf),* 202, 103-18.

MEDAWAR, P. B. 1952. *An Unsolved Problem of Biology*, London, H. K. Lewis.

MEIER, U. & GRESSNER, A. M. 2004. Endocrine regulation of energy metabolism: review of pathobiochemical and clinical chemical aspects of leptin, ghrelin, adiponectin, and resistin. *Clin Chem,* 50, 1511-25.

MEISSNER, C., BRUSE, P., MOHAMED, S. A., SCHULZ, A., WARNK, H., STORM, T. & OEHMICHEN, M. 2008. The 4977 bp deletion of mitochondrial DNA in human skeletal muscle, heart and different areas of the brain: a useful biomarker or more? *Exp Gerontol,* 43, 645-52.

MEYDANI, M., DAS, S., BAND, M., EPSTEIN, S. & ROBERTS, S. 2011. The effect of caloric restriction and glycemic load on measures of oxidative stress and antioxidants in humans: results from the CALERIE Trial of Human Caloric Restriction. *J Nutr Health Aging,* 15, 456-60.

MEYERSON, M., COUNTER, C. M., EATON, E. N., ELLISEN, L. W., STEINER, P., CADDLE, S. D., ZIAUGRA, L., BEIJERSBERGEN, R. L., DAVIDOFF, M. J., LIU, Q., BACCHETTI, S., HABER, D. A. & WEINBERG, R. A. 1997. hEST2, the putative human telomerase catalytic subunit gene, is up-regulated in tumor cells and during immortalization. *Cell,* 90, 785-95.

MEYNE, J., RATLIFF, R. L. & MOYZIS, R. K. 1989. Conservation of the human telomere sequence (TTAGGG)n among vertebrates. *Proc Natl Acad Sci U S A,* 86, 7049-53.

MILAGRO, F. I., CAMPION, J., CORDERO, P., GOYENECHEA, E., GOMEZ-URIZ, A. M., ABETE, I., ZULET, M. A. & MARTINEZ, J. A. 2011. A dual epigenomic approach for the search of obesity biomarkers: DNA methylation in relation to diet-induced weight loss. *FASEB J,* 25, 1378-89.

MILLER, R. A., HARRISON, D. E., ASTLE, C. M., BAUR, J. A., BOYD, A. R., DE CABO, R., FERNANDEZ, E., FLURKEY, K., JAVORS, M. A., NELSON, J. F., ORIHUELA, C. J., PLETCHER, S., SHARP, Z. D., SINCLAIR, D., STARNES, J. W., WILKINSON, J. E., NADON, N. L. & STRONG, R. 2011. Rapamycin, but not

resveratrol or simvastatin, extends life span of genetically heterogeneous mice. *J Gerontol A Biol Sci Med Sci,* 66, 191-201.

MISHRA, P. J. & BERTINO, J. R. 2009. MicroRNA polymorphisms: the future of pharmacogenomics, molecular epidemiology and individualized medicine. *Pharmacogenomics,* 10, 399-416.

MISHRA, P. K., TYAGI, N., KUMAR, M. & TYAGI, S. C. 2009. MicroRNAs as a therapeutic target for cardiovascular diseases. *J Cell Mol Med,* 13, 778-89.

MOHN, F. & SCHUBELER, D. 2009. Genetics and epigenetics: stability and plasticity during cellular differentiation. *Trends Genet,* 25, 129-36.

MOISEEVA, O., BOURDEAU, V., ROUX, A., DESCHENES-SIMARD, X. & FERBEYRE, G. 2009. Mitochondrial dysfunction contributes to oncogene-induced senescence. *Mol Cell Biol,* 29, 4495-507.

MOREY, C., NAVARRO, P., DEBRAND, E., AVNER, P., ROUGEULLE, C. & CLERC, P. 2004. The region 3' to Xist mediates X chromosome counting and H3 Lys-4 dimethylation within the Xist gene. *EMBO J,* 23, 594-604.

MORI, Y., OLARU, A. V., CHENG, Y., AGARWAL, R., YANG, J., LUVSANJAV, D., YU, W., SELARU, F. M., HUTFLESS, S., LAZAREV, M., KWON, J. H., BRANT, S. R., MAROHN, M. R., HUTCHEON, D. F., DUNCAN, M. D., GOEL, A. & MELTZER, S. J. 2011. Novel candidate colorectal cancer biomarkers identified by methylation microarray-based scanning. *Endocr Relat Cancer,* 18, 465-78.

MORSELLI, E., MAIURI, M. C., MARKAKI, M., MEGALOU, E., PASPARAKI, A., PALIKARAS, K., CRIOLLO, A., GALLUZZI, L., MALIK, S. A., VITALE, I., MICHAUD, M., MADEO, F., TAVERNARAKIS, N. & KROEMER, G. 2010. Caloric restriction and resveratrol promote longevity through the Sirtuin-1-dependent induction of autophagy. *Cell Death Dis,* 1, e10.

MOTORIN, Y., LYKO, F. & HELM, M. 2009. 5-methylcytosine in RNA: detection, enzymatic formation and biological functions. *Nucleic Acids Res,* 38, 1415-30.

MOTTA, M. C., DIVECHA, N., LEMIEUX, M., KAMEL, C., CHEN, D., GU, W., BULTSMA, Y., MCBURNEY, M. & GUARENTE, L. 2004. Mammalian SIRT1 represses forkhead transcription factors. *Cell,* 116, 551-63.

MOYZIS, R. K., BUCKINGHAM, J. M., CRAM, L. S., DANI, M., DEAVEN, L. L., JONES, M. D., MEYNE, J., RATLIFF, R. L. & WU, J. R. 1988. A highly conserved repetitive DNA sequence, (TTAGGG)n, present at the telomeres of human chromosomes. *Proc Natl Acad Sci U S A,* 85, 6622-6.

MUNOZ-NAJAR, U. & SEDIVY, J. M. 2011. Epigenetic control of aging. *Antioxid Redox Signal,* 14, 241-59.

MYLLYKANGAS, S., BOHLING, T. & KNUUTILA, S. 2007. Specificity, selection and significance of gene amplifications in cancer. *Semin Cancer Biol,* 17, 42-55.

NABILSI, N. H., BROADDUS, R. R. & LOOSE, D. S. 2009. DNA methylation inhibits p53-mediated survivin repression. *Oncogene,* 28, 2046-50.

NASS, M. M. 1973. Differential methylation of mitochondrial and nuclear DNA in cultured mouse, hamster and virus-transformed hamster cells. In vivo and in vitro methylation. *J Mol Biol,* 80, 155-75.

NAVIAUX, R. K. 2008. Mitochondrial control of epigenetics. *Cancer Biol Ther,* 7, 1191-3.

NELSON, G., WORDSWORTH, J., WANG, C., JURK, D., LAWLESS, C., MARTIN-RUIZ, C. & VON ZGLINICKI, T. 2012. A senescent cell bystander effect: senescence-induced senescence. *Aging Cell,* 11, 345-9.

NICCOLI, T. & PARTRIDGE, L. 2012. Ageing as a risk factor for disease. *Curr Biol,* 22, R741-52.

NICHOLLS, R. D. & KNEPPER, J. L. 2001. Genome organization, function, and imprinting in Prader-Willi and Angelman syndromes. *Annu Rev Genomics Hum Genet,* 2, 153-75.

NIKI, E., YOSHIDA, Y., SAITO, Y. & NOGUCHI, N. 2005. Lipid peroxidation: mechanisms, inhibition, and biological effects. *Biochem Biophys Res Commun,* 338, 668-76.

NISHIO, K., INOUE, A., QIAO, S., KONDO, H. & MIMURA, A. 2001. Senescence and cytoskeleton: overproduction of vimentin induces senescent-like morphology in human fibroblasts. *Histochem Cell Biol,* 116, 321-7.

NISHIOKA, M., BUNDO, M., KASAI, K. & IWAMOTO, K. 2012. DNA methylation in schizophrenia: progress and challenges of epigenetic studies. *Genome Med,* 4, 96.

NOOTEBOOM, M., JOHNSON, R., TAYLOR, R. W., WRIGHT, N. A., LIGHTOWLERS, R. N., KIRKWOOD, T. B., MATHERS, J. C., TURNBULL, D. M. & GREAVES, L. C. 2010. Age-associated mitochondrial DNA mutations lead to small but significant changes in cell proliferation and apoptosis in human colonic crypts. *Aging Cell,* 9, 96-9.

NYSTROM, T. 2002. Translational fidelity, protein oxidation, and senescence: lessons from bacteria. *Ageing Res Rev,* 1, 693-703.

OLIVEIRA, A. M., HEMSTEDT, T. J. & BADING, H. 2012. Rescue of aging-associated decline in Dnmt3a2 expression restores cognitive abilities. *Nat Neurosci,* 15, 1111-3.

ONGENAERT, M., WISMAN, G. B., VOLDERS, H. H., KONING, A. J., ZEE, A. G., VAN CRIEKINGE, W. & SCHUURING, E. 2008. Discovery of DNA methylation markers in cervical cancer using relaxation ranking. *BMC Med Genomics,* 1, 57.

ONO, T., TAKAHASHI, N. & OKADA, S. 1989. Age-associated changes in DNA methylation and mRNA level of the c-myc gene in spleen and liver of mice. *Mutat Res,* 219, 39-50.

ONO, T., TAWA, R., SHINYA, K., HIROSE, S. & OKADA, S. 1986. Methylation of the c-myc gene changes during aging process of mice. *Biochem Biophys Res Commun,* 139, 1299-304.

OROM, U. A., LIM, M. K., SAVAGE, J. E., JIN, L., SALEH, A. D., LISANTI, M. P. & SIMONE, N. L. 2012. MicroRNA-203 regulates caveolin-1 in breast tissue during caloric restriction. *Cell Cycle,* 11, 1291-5.

OSAWA, S., JUKES, T. H., WATANABE, K. & MUTO, A. 1992. Recent evidence for evolution of the genetic code. *Microbiol Rev,* 56, 229-64.

OUCHI, N., KIHARA, S., FUNAHASHI, T., MATSUZAWA, Y. & WALSH, K. 2003. Obesity, adiponectin and vascular inflammatory disease. *Curr Opin Lipidol,* 14, 561-6.

PALADE, G. E. 1955. A small particulate component of the cytoplasm. *J Biophys Biochem Cytol,* 1, 59-68.

PARADIS, E., DOUILLARD, H., KOUTROUMANIS, M., GOODYER, C. & LEBLANC, A. 1996. Amyloid beta peptide of Alzheimer's disease downregulates Bcl-2 and upregulates bax expression in human neurons. *J Neurosci,* 16, 7533-9.

PARK, S. K. & PROLLA, T. A. 2005. Lessons learned from gene expression profile studies of aging and caloric restriction. *Ageing Res Rev,* 4, 55-65.

PARTRIDGE, L. & MANGEL, M. 1999. Messages from mortality: the evolution of death rates in the old. *Trends Ecol Evol,* 14, 438-442.

PASCAL, T., DEBACQ-CHAINIAUX, F., CHRETIEN, A., BASTIN, C., DABEE, A. F., BERTHOLET, V., REMACLE, J. & TOUSSAINT, O. 2005. Comparison of replicative senescence and stress-induced premature senescence combining differential display and low-density DNA arrays. *FEBS Lett,* 579, 3651-9.

PASSOS, J. F., NELSON, G., WANG, C., RICHTER, T., SIMILLION, C., PROCTOR, C. J., MIWA, S., OLIJSLAGERS, S., HALLINAN, J., WIPAT, A., SARETZKI, G., RUDOLPH, K. L., KIRKWOOD, T. B. & VON ZGLINICKI, T. 2010. Feedback

between p21 and reactive oxygen production is necessary for cell senescence. *Mol Syst Biol,* 6, 347.

PASSOS, J. F. & VON ZGLINICKI, T. 2005. Mitochondria, telomeres and cell senescence. *Exp Gerontol,* 40, 466-72.

PAULER, F. M., KOERNER, M. V. & BARLOW, D. P. 2007. Silencing by imprinted noncoding RNAs: is transcription the answer? *Trends Genet,* 23, 284-92.

PAULL, T. T., ROGAKOU, E. P., YAMAZAKI, V., KIRCHGESSNER, C. U., GELLERT, M. & BONNER, W. M. 2000. A critical role for histone H2AX in recruitment of repair factors to nuclear foci after DNA damage. *Curr Biol,* 10, 886-95.

PEARSON, K. J., BAUR, J. A., LEWIS, K. N., PESHKIN, L., PRICE, N. L., LABINSKYY, N., SWINDELL, W. R., KAMARA, D., MINOR, R. K., PEREZ, E., JAMIESON, H. A., ZHANG, Y., DUNN, S. R., SHARMA, K., PLESHKO, N., WOOLLETT, L. A., CSISZAR, A., IKENO, Y., LE COUTEUR, D., ELLIOTT, P. J., BECKER, K. G., NAVAS, P., INGRAM, D. K., WOLF, N. S., UNGVARI, Z., SINCLAIR, D. A. & DE CABO, R. 2008. Resveratrol delays age-related deterioration and mimics transcriptional aspects of dietary restriction without extending life span. *Cell Metab,* 8, 157-68.

PENAGARIKANO, O., MULLE, J. G. & WARREN, S. T. 2007. The pathophysiology of fragile x syndrome. *Annu Rev Genomics Hum Genet,* 8, 109-29.

PFAFFL, M. W. 2001. A new mathematical model for relative quantification in real-time RT-PCR. *Nucleic Acids Res,* 29, e45.

PHILLIPS, D. M. 1963. The presence of acetyl groups of histones. *Biochem J,* 87, 258-63.

PIPER, M. D., SELMAN, C., MCELWEE, J. J. & PARTRIDGE, L. 2008. Separating cause from effect: how does insulin/IGF signalling control lifespan in worms, flies and mice? *J Intern Med,* 263, 179-91.

POLLACK, Y., KASIR, J., SHEMER, R., METZGER, S. & SZYF, M. 1984. Methylation pattern of mouse mitochondrial DNA. *Nucleic Acids Res,* 12, 4811-24.

POUREBRAHIM, R., HOUTMEYERS, R., GHOGOMU, S., JANSSENS, S., THELIE, A., TRAN, H. T., LANGENBERG, T., VLEMINCKX, K., BELLEFROID, E., CASSIMAN, J. J. & TEJPAR, S. 2011. Transcription factor Zic2 inhibits Wnt/beta-catenin protein signaling. *J Biol Chem,* 286, 37732-40.

POWERS, R. W., 3RD, KAEBERLEIN, M., CALDWELL, S. D., KENNEDY, B. K. & FIELDS, S. 2006. Extension of chronological life span in yeast by decreased TOR pathway signaling. *Genes Dev,* 20, 174-84.

PRADHAN, S., TALBOT, D., SHA, M., BENNER, J., HORNSTRA, L., LI, E., JAENISCH, R. & ROBERTS, R. J. 1997. Baculovirus-mediated expression and characterization of the full-length murine DNA methyltransferase. *Nucleic Acids Res,* 25, 4666-73.

PRICE, J. S., WATERS, J. G., DARRAH, C., PENNINGTON, C., EDWARDS, D. R., DONELL, S. T. & CLARK, I. M. 2002. The role of chondrocyte senescence in osteoarthritis. *Aging Cell,* 1, 57-65.

PROSPECTIVE STUDIES, C., WHITLOCK, G., LEWINGTON, S., SHERLIKER, P., CLARKE, R., EMBERSON, J., HALSEY, J., QIZILBASH, N., COLLINS, R. & PETO, R. 2009. Body-mass index and cause-specific mortality in 900 000 adults: collaborative analyses of 57 prospective studies. *Lancet,* 373, 1083-96.

QIN, W., ZHAO, W., HO, L., WANG, J., WALSH, K., GANDY, S. & PASINETTI, G. M. 2008. Regulation of forkhead transcription factor FoxO3a contributes to calorie restriction-induced prevention of Alzheimer's disease-type amyloid neuropathology and spatial memory deterioration. *Ann N Y Acad Sci,* 1147, 335-47.

R-CORE-TEAM 2012. *R: A language and environment for statistical computing*.

RACETTE, S. B., WEISS, E. P., VILLAREAL, D. T., ARIF, H., STEGER-MAY, K., SCHECHTMAN, K. B., FONTANA, L., KLEIN, S. & HOLLOSZY, J. O. 2006. One year of caloric restriction in humans: feasibility and effects on body composition and abdominal adipose tissue. *J Gerontol A Biol Sci Med Sci,* 61, 943-50.

RAHMAN, A. & ISENBERG, D. A. 2008. Systemic lupus erythematosus. *N Engl J Med,* 358, 929-39.

RATTAN, S. I. 1996. Synthesis, modifications, and turnover of proteins during aging. *Exp Gerontol,* 31, 33-47.

RATTAN, S. I. 2006. Theories of biological aging: genes, proteins, and free radicals. *Free Radic Res,* 40, 1230-8.

RATTAN, S. I. & CLARK, B. F. 2005. Understanding and modulating ageing. *IUBMB Life,* 57, 297-304.

RAUNER, M., SIPOS, W. & PIETSCHMANN, P. 2008. Age-dependent Wnt gene expression in bone and during the course of osteoblast differentiation. *Age (Dordr),* 30, 273-82.

RAWSON, J. B., MRKONJIC, M., DAFTARY, D., DICKS, E., BUCHANAN, D. D., YOUNGHUSBAND, H. B., PARFREY, P. S., YOUNG, J. P., POLLETT, A., GREEN, R. C., GALLINGER, S., MCLAUGHLIN, J. R., KNIGHT, J. A. & BAPAT, B. 2011. Promoter methylation of Wnt5a is associated with microsatellite instability

and BRAF V600E mutation in two large populations of colorectal cancer patients. *Br J Cancer,* 104, 1906-12.

RAY, D., WU, A., WILKINSON, J. E., MURPHY, H. S., LU, Q., KLUVE-BECKERMAN, B., LIEPNIEKS, J. J., BENSON, M., YUNG, R. & RICHARDSON, B. 2006. Aging in heterozygous Dnmt1-deficient mice: effects on survival, the DNA methylation genes, and the development of amyloidosis. *J Gerontol A Biol Sci Med Sci,* 61, 115-24.

RAZIN, A. & CEDAR, H. 1991. DNA methylation and gene expression. *Microbiol Rev,* 55, 451-8.

REBELO, A. P., WILLIAMS, S. L. & MORAES, C. T. 2009. In vivo methylation of mtDNA reveals the dynamics of protein-mtDNA interactions. *Nucleic Acids Res,* 37, 6701-15.

REED, M. J., PENN, P. E., LI, Y., BIRNBAUM, R., VERNON, R. B., JOHNSON, T. S., PENDERGRASS, W. R., SAGE, E. H., ABRASS, I. B. & WOLF, N. S. 1996. Enhanced cell proliferation and biosynthesis mediate improved wound repair in refed, caloric-restricted mice. *Mech Ageing Dev,* 89, 21-43.

REIK, W., DEAN, W. & WALTER, J. 2001. Epigenetic reprogramming in mammalian development. *Science,* 293, 1089-93.

RENALDI, O., PRAMONO, B., SINORITA, H., PURNOMO, L. B., ASDIE, R. H. & ASDIE, A. H. 2009. Hypoadiponectinemia: a risk factor for metabolic syndrome. *Acta Med Indones,* 41, 20-4.

RIBARIC, S. 2012. Diet and aging. *Oxid Med Cell Longev,* 2012, 741468.

RICHARDSON, B. 2003. Impact of aging on DNA methylation. *Ageing Res Rev,* 2, 245-61.

RINN, J. L., KERTESZ, M., WANG, J. K., SQUAZZO, S. L., XU, X., BRUGMANN, S. A., GOODNOUGH, L. H., HELMS, J. A., FARNHAM, P. J., SEGAL, E. & CHANG, H. Y. 2007. Functional demarcation of active and silent chromatin domains in human HOX loci by noncoding RNAs. *Cell,* 129, 1311-23.

RITTLING, S. R., BROOKS, K. M., CRISTOFALO, V. J. & BASERGA, R. 1986. Expression of cell cycle-dependent genes in young and senescent WI-38 fibroblasts. *Proc Natl Acad Sci U S A,* 83, 3316-20.

ROBERTSON, K. D. & WOLFFE, A. P. 2000. DNA methylation in health and disease. *Nat Rev Genet,* 1, 11-9.

ROBLES, S. J. & ADAMI, G. R. 1998. Agents that cause DNA double strand breaks lead to p16INK4a enrichment and the premature senescence of normal fibroblasts. *Oncogene,* 16, 1113-23.

ROCHON, J., BALES, C. W., RAVUSSIN, E., REDMAN, L. M., HOLLOSZY, J. O., RACETTE, S. B., ROBERTS, S. B., DAS, S. K., ROMASHKAN, S., GALAN, K. M., HADLEY, E. C. & KRAUS, W. E. 2011. Design and conduct of the CALERIE study: comprehensive assessment of the long-term effects of reducing intake of energy. *J Gerontol A Biol Sci Med Sci,* 66, 97-108.

RODIER, F., COPPE, J. P., PATIL, C. K., HOEIJMAKERS, W. A., MUNOZ, D. P., RAZA, S. R., FREUND, A., CAMPEAU, E., DAVALOS, A. R. & CAMPISI, J. 2009. Persistent DNA damage signalling triggers senescence-associated inflammatory cytokine secretion. *Nat Cell Biol,* 11, 973-9.

RODRIGUEZ, J., FRIGOLA, J., VENDRELL, E., RISQUES, R. A., FRAGA, M. F., MORALES, C., MORENO, V., ESTELLER, M., CAPELLA, G., RIBAS, M. & PEINADO, M. A. 2006. Chromosomal instability correlates with genome-wide DNA demethylation in human primary colorectal cancers. *Cancer Res,* 66, 8462-9468.

ROLLINS, R. A., HAGHIGHI, F., EDWARDS, J. R., DAS, R., ZHANG, M. Q., JU, J. & BESTOR, T. H. 2006. Large-scale structure of genomic methylation patterns. *Genome Res,* 16, 157-63.

ROMAN-GOMEZ, J., JIMENEZ-VELASCO, A., CORDEU, L., VILAS-ZORNOZA, A., SAN JOSE-ENERIZ, E., GARATE, L., CASTILLEJO, J. A., MARTIN, V., PROSPER, F., HEINIGER, A., TORRES, A. & AGIRRE, X. 2007. WNT5A, a putative tumour suppressor of lymphoid malignancies, is inactivated by aberrant methylation in acute lymphoblastic leukaemia. *Eur J Cancer,* 43, 2736-46.

RONAGHI, M., KARAMOHAMED, S., PETTERSSON, B., UHLEN, M. & NYREN, P. 1996. Real-time DNA sequencing using detection of pyrophosphate release. *Anal Biochem,* 242, 84-9.

ROWLATT, C. 1979. Problems associated with the development of a colony of aged mice for experimental purposes. *Age Ageing,* 8, 237-42.

ROZHON, W., BAUBEC, T., MAYERHOFER, J., MITTELSTEN SCHEID, O. & JONAK, C. 2008. Rapid quantification of global DNA methylation by isocratic cation exchange high-performance liquid chromatography. *Anal Biochem,* 375, 354-60.

SANGER, F. & COULSON, A. R. 1975. A rapid method for determining sequences in DNA by primed synthesis with DNA polymerase. *J Mol Biol,* 94, 441-8.

SATOH, M. & KUROIWA, T. 1991. Organization of multiple nucleoids and DNA molecules in mitochondria of a human cell. *Exp Cell Res,* 196, 137-40.

SCACHERI, P. C., CRAWFORD, G. E. & DAVIS, S. 2006. Statistics for ChIP-chip and DNase hypersensitivity experiments on NimbleGen arrays. *Methods Enzymol,* 411, 270-82.

SCHILLING, M. M., OESER, J. K., BOUSTEAD, J. N., FLEMMING, B. P. & O'BRIEN, R. M. 2006. Gluconeogenesis: re-evaluating the FOXO1-PGC-1alpha connection. *Nature,* 443, E10-1.

SCHMITGES, F. W., PRUSTY, A. B., FATY, M., STUTZER, A., LINGARAJU, G. M., AIWAZIAN, J., SACK, R., HESS, D., LI, L., ZHOU, S., BUNKER, R. D., WIRTH, U., BOUWMEESTER, T., BAUER, A., LY-HARTIG, N., ZHAO, K., CHAN, H., GU, J., GUT, H., FISCHLE, W., MULLER, J. & THOMA, N. H. 2011. Histone methylation by PRC2 is inhibited by active chromatin marks. *Mol Cell,* 42, 330-41.

SCHOENHERR, C. J., PAQUETTE, A. J. & ANDERSON, D. J. 1996. Identification of potential target genes for the neuron-restrictive silencer factor. *Proc Natl Acad Sci U S A,* 93, 9881-6.

SCHULZ, W. A., STEINHOFF, C. & FLORL, A. R. 2006. Methylation of endogenous human retroelements in health and disease. *Curr Top Microbiol Immunol,* 310, 211-50.

SCHVARTZ, D., COUTE, Y., BRUNNER, Y., WOLLHEIM, C. B. & SANCHEZ, J. C. 2012. Modulation of neuronal pentraxin 1 expression in rat pancreatic beta-cells submitted to chronic glucotoxic stress. *Mol Cell Proteomics,* 11, 244-54.

SETO, A. G., KINGSTON, R. E. & LAU, N. C. 2007. The coming of age for Piwi proteins. *Mol Cell,* 26, 603-9.

SHADEL, G. S. & CLAYTON, D. A. 1997. Mitochondrial DNA maintenance in vertebrates. *Annu Rev Biochem,* 66, 409-35.

SHANDILYA, J., WANG, Y. & ROBERTS, S. G. 2012. TFIIB dephosphorylation links transcription inhibition with the p53-dependent DNA damage response. *Proc Natl Acad Sci U S A,* 109, 18797-802.

SHARMA, A., SINGH, K. & ALMASAN, A. 2012. Histone H2AX phosphorylation: a marker for DNA damage. *Methods Mol Biol,* 920, 613-26.

SHELTON, D. N., CHANG, E., WHITTIER, P. S., CHOI, D. & FUNK, W. D. 1999. Microarray analysis of replicative senescence. *Curr Biol,* 9, 939-45.

SHEN, L., KONDO, Y., HAMILTON, S. R., RASHID, A. & ISSA, J. P. 2003. P14 methylation in human colon cancer is associated with microsatellite instability and wild-type p53. *Gastroenterology,* 124, 626-33.

SHEN, L. & WATERLAND, R. A. 2007. Methods of DNA methylation analysis. *Curr Opin Clin Nutr Metab Care,* 10, 576-81.

SHERR, C. J. 2000. Cell cycle control and cancer. *Harvey Lect,* 96, 73-92.

SHIN, K. H., KANG, M. K., DICTEROW, E. & PARK, N. H. 2003. Hypermethylation of the hTERT promoter inhibits the expression of telomerase activity in normal oral fibroblasts and senescent normal oral keratinocytes. *Br J Cancer,* 89, 1473-8.

SHINMURA, K., TAMAKI, K., SAITO, K., NAKANO, Y., TOBE, T. & BOLLI, R. 2007. Cardioprotective effects of short-term caloric restriction are mediated by adiponectin via activation of AMP-activated protein kinase. *Circulation,* 116, 2809-17.

SHMOOKLER REIS, R. J. & GOLDSTEIN, S. 1983. Mitochondrial DNA in mortal and immortal human cells. Genome number, integrity, and methylation. *J Biol Chem,* 258, 9078-85.

SHOCK, L. S., THAKKAR, P. V., PETERSON, E. J., MORAN, R. G. & TAYLOR, S. M. 2011. DNA methyltransferase 1, cytosine methylation, and cytosine hydroxymethylation in mammalian mitochondria. *Proc Natl Acad Sci U S A,* 108, 3630-5.

SHOJI-KAWATA, S., SUMPTER, R., LEVENO, M., CAMPBELL, G. R., ZOU, Z., KINCH, L., WILKINS, A. D., SUN, Q., PALLAUF, K., MACDUFF, D., HUERTA, C., VIRGIN, H. W., HELMS, J. B., EERLAND, R., TOOZE, S. A., XAVIER, R., LENSCHOW, D. J., YAMAMOTO, A., KING, D., LICHTARGE, O., GRISHIN, N. V., SPECTOR, S. A., KALOYANOVA, D. V. & LEVINE, B. 2013. Identification of a candidate therapeutic autophagy-inducing peptide. *Nature,* 494, 201-6.

SIEGFRIED, Z. & SIMON, I. 2010. DNA methylation and gene expression. *Wiley Interdiscip Rev Syst Biol Med,* 2, 362-71.

SILAR, P. & PICARD, M. 1994. Increased longevity of EF-1 alpha high-fidelity mutants in Podospora anserina. *J Mol Biol,* 235, 231-6.

SILAR, P., ROSSIGNOL, M., HAEDENS, V., DERHY, Z. & MAZABRAUD, A. 2000. Deletion and dosage modulation of the eEF1A gene in Podospora anserina: effect on the life cycle. *Biogerontology,* 1, 47-54.

SIMONETTI, S., CHEN, X., DIMAURO, S. & SCHON, E. A. 1992. Accumulation of deletions in human mitochondrial DNA during normal aging: analysis by quantitative PCR. *Biochim Biophys Acta,* 1180, 113-22.

SINGH, K. & PRASAD, S. 2008. Age- and sex-related analysis of methylation of 5'-upstream sequences of Fmr-1 gene in mouse brain and modulation by sex steroid hormones. *Biogerontology,* 9, 455-65.

SINGHAL, R. P., MAYS-HOOPES, L. L. & EICHHORN, G. L. 1987. DNA methylation in aging of mice. *Mech Ageing Dev,* 41, 199-210.

SIOMI, M. C., SATO, K., PEZIC, D. & ARAVIN, A. A. 2011. PIWI-interacting small RNAs: the vanguard of genome defence. *Nat Rev Mol Cell Biol,* 12, 246-58.

SMITH, D. L., JR., MCCLURE, J. M., MATECIC, M. & SMITH, J. S. 2007. Calorie restriction extends the chronological lifespan of Saccharomyces cerevisiae independently of the Sirtuins. *Aging Cell,* 6, 649-62.

SMYTH, G. K. 2004. Linear models and empirical bayes methods for assessing differential expression in microarray experiments. *Stat Appl Genet Mol Biol,* 3, Article3.

SOFI, F., ABBATE, R., GENSINI, G. F. & CASINI, A. 2010. Accruing evidence on benefits of adherence to the Mediterranean diet on health: an updated systematic review and meta-analysis. *Am J Clin Nutr,* 92, 1189-96.

SPAHN, L. & BARLOW, D. P. 2003. An ICE pattern crystallizes. *Nat Genet,* 35, 11-2.

SRIPADA, L., TOMAR, D., PRAJAPATI, P., SINGH, R., SINGH, A. K. & SINGH, R. 2012. Systematic analysis of small RNAs associated with human mitochondria by deep sequencing: detailed analysis of mitochondrial associated miRNA. *PLoS One,* 7, e44873.

STADTMAN, E. R. 2004. Role of oxidant species in aging. *Curr Med Chem,* 11, 1105-12.

STEARNS, T. M., CARIO, C. L., SAVAGE, H. S., SUNDBERG, J. P., PAIGEN, B. & BERNDT, A. 2012. Early gene expression differences in inbred mouse strains with susceptibility to pulmonary adenomas. *Exp Mol Pathol,* 93, 455-61.

SUH, Y., ATZMON, G., CHO, M. O., HWANG, D., LIU, B., LEAHY, D. J., BARZILAI, N. & COHEN, P. 2008. Functionally significant insulin-like growth factor I receptor mutations in centenarians. *Proc Natl Acad Sci U S A,* 105, 3438-42.

SUJI, G. & SIVAKAMI, S. 2004. Glucose, glycation and aging. *Biogerontology,* 5, 365-73.

SUSSER, E., NEUGEBAUER, R., HOEK, H. W., BROWN, A. S., LIN, S., LABOVITZ, D. & GORMAN, J. M. 1996. Schizophrenia after prenatal famine. Further evidence. *Arch Gen Psychiatry,* 53, 25-31.

SWINDELL, W. R. 2012. Dietary restriction in rats and mice: a meta-analysis and review of the evidence for genotype-dependent effects on lifespan. *Ageing Res Rev,* 11, 254-70.

SWISSHELM, K., DISTECHE, C. M., THORVALDSEN, J., NELSON, A. & SALK, D. 1990. Age-related increase in methylation of ribosomal genes and inactivation of chromosome-specific rRNA gene clusters in mouse. *Mutat Res,* 237, 131-46.

TADDEI, A., HEDIGER, F., NEUMANN, F. R. & GASSER, S. M. 2004. The function of nuclear architecture: a genetic approach. *Annu Rev Genet,* 38, 305-45.

TAKAI, D. & JONES, P. A. 2002. Comprehensive analysis of CpG islands in human chromosomes 21 and 22. *Proc Natl Acad Sci U S A,* 99, 3740-5.

TAPP, H. S., COMMANE, D. M., BRADBURN, D. M., ARASARADNAM, R., MATHERS, J. C., JOHNSON, I. T. & BELSHAW, N. J. 2013. Nutritional factors and gender influence age-related DNA methylation in the human rectal mucosa. *Aging Cell,* 12, 148-55.

TAVERNA, S. D., LI, H., RUTHENBURG, A. J., ALLIS, C. D. & PATEL, D. J. 2007. How chromatin-binding modules interpret histone modifications: lessons from professional pocket pickers. *Nat Struct Mol Biol,* 14, 1025-40.

TAYLOR, C. G. & BRAY, T. M. 1991. Effect of hyperoxia on oxygen free radical defense enzymes in the lung of zinc-deficient rats. *J Nutr,* 121, 460-6.

TAYLOR, K. M., MORGAN, H. E., JOHNSON, A. & NICHOLSON, R. I. 2005. Structure-function analysis of a novel member of the LIV-1 subfamily of zinc transporters, ZIP14. *FEBS Lett,* 579, 427-32.

TAYLOR, S. W., FAHY, E., MURRAY, J., CAPALDI, R. A. & GHOSH, S. S. 2003. Oxidative post-translational modification of tryptophan residues in cardiac mitochondrial proteins. *J Biol Chem,* 278, 19587-90.

THOMPSON, R. F., ATZMON, G., GHEORGHE, C., LIANG, H. Q., LOWES, C., GREALLY, J. M. & BARZILAI, N. 2010. Tissue-specific dysregulation of DNA methylation in aging. *Aging Cell,* 9, 506-18.

THORSEN, K., MANSILLA, F., SCHEPELER, T., OSTER, B., RASMUSSEN, M. H., DYRSKJOT, L., KARNI, R., AKERMAN, M., KRAINER, A. R., LAURBERG, S., ANDERSEN, C. L. & ORNTOFT, T. F. 2011. Alternative splicing of SLC39A14 in colorectal cancer is regulated by the Wnt pathway. *Mol Cell Proteomics,* 10, M110 002998.

TIMMERS, S., KONINGS, E., BILET, L., HOUTKOOPER, R. H., VAN DE WEIJER, T., GOOSSENS, G. H., HOEKS, J., VAN DER KRIEKEN, S., RYU, D., KERSTEN, S., MOONEN-KORNIPS, E., HESSELINK, M. K., KUNZ, I., SCHRAUWEN-HINDERLING, V. B., BLAAK, E. E., AUWERX, J. & SCHRAUWEN, P. 2011.

Calorie restriction-like effects of 30 days of resveratrol supplementation on energy metabolism and metabolic profile in obese humans. *Cell Metab,* 14, 612-22.

TOMINAGA, K., KAGATA, T., JOHMURA, Y., HISHIDA, T., NISHIZUKA, M. & IMAGAWA, M. 2005. SLC39A14, a LZT protein, is induced in adipogenesis and transports zinc. *FEBS J,* 272, 1590-9.

TOYAMA, B. H. & HETZER, M. W. 2013. Protein homeostasis: live long, won't prosper. *Nat Rev Mol Cell Biol,* 14, 55-61.

TRIFUNOVIC, A. 2006. Mitochondrial DNA and ageing. *Biochim Biophys Acta,* 1757, 611-7.

TYBURCZY, M. E., KOTULSKA, K., POKAROWSKI, P., MIECZKOWSKI, J., KUCHARSKA, J., GRAJKOWSKA, W., ROSZKOWSKI, M., JOZWIAK, S. & KAMINSKA, B. 2010. Novel proteins regulated by mTOR in subependymal giant cell astrocytomas of patients with tuberous sclerosis complex and new therapeutic implications. *Am J Pathol,* 176, 1878-90.

UEHARA, Y., ONO, T., KURISHITA, A., KOKURYU, H. & OKADA, S. 1989. Age-dependent and tissue-specific changes of DNA methylation within and around the c-fos gene in mice. *Oncogene,* 4, 1023-8.

UKKOLA, O. & SANTANIEMI, M. 2002. Adiponectin: a link between excess adiposity and associated comorbidities? *J Mol Med (Berl),* 80, 696-702.

VALENZANO, D. R., TERZIBASI, E., GENADE, T., CATTANEO, A., DOMENICI, L. & CELLERINO, A. 2006. Resveratrol prolongs lifespan and retards the onset of age-related markers in a short-lived vertebrate. *Curr Biol,* 16, 296-300.

VAN ROSSUM, A. G., VAN BRAGT, M. P., SCHUURING-SCHOLTES, E., VAN DER PLOEG, J. C., VAN KRIEKEN, J. H., KLUIN, P. M. & SCHUURING, E. 2006. Transgenic mice with mammary gland targeted expression of human cortactin do not develop (pre-malignant) breast tumors: studies in MMTV-cortactin and MMTV-cortactin/-cyclin D1 bitransgenic mice. *BMC Cancer,* 6, 58.

VAQUERO, A. & REINBERG, D. 2009. Calorie restriction and the exercise of chromatin. *Genes Dev,* 23, 1849-69.

VARGAS, J., FELTES, B. C., POLONI JDE, F., LENZ, G. & BONATTO, D. 2012. Senescence; an endogenous anticancer mechanism. *Front Biosci,* 17, 2616-43.

VAZIRI, H. & BENCHIMOL, S. 1998. Reconstitution of telomerase activity in normal human cells leads to elongation of telomeres and extended replicative life span. *Curr Biol,* 8, 279-82.

VAZIRI, H., DESSAIN, S. K., NG EATON, E., IMAI, S. I., FRYE, R. A., PANDITA, T. K., GUARENTE, L. & WEINBERG, R. A. 2001. hSIR2(SIRT1) functions as an NAD-dependent p53 deacetylase. *Cell,* 107, 149-59.

VEGA, R. B., HUSS, J. M. & KELLY, D. P. 2000. The coactivator PGC-1 cooperates with peroxisome proliferator-activated receptor alpha in transcriptional control of nuclear genes encoding mitochondrial fatty acid oxidation enzymes. *Mol Cell Biol,* 20, 1868-76.

VISWANATHAN, M., KIM, S. K., BERDICHEVSKY, A. & GUARENTE, L. 2005. A role for SIR-2.1 regulation of ER stress response genes in determining C. elegans life span. *Dev Cell,* 9, 605-15.

VON ZGLINICKI, T. 2002. Oxidative stress shortens telomeres. *Trends Biochem Sci,* 27, 339-44.

VON ZGLINICKI, T. 2003. Replicative senescence and the art of counting. *Exp Gerontol,* 38, 1259-64.

VON ZGLINICKI, T., SARETZKI, G., DOCKE, W. & LOTZE, C. 1995. Mild hyperoxia shortens telomeres and inhibits proliferation of fibroblasts: a model for senescence? *Exp Cell Res,* 220, 186-93.

WAKELING, L. A., IONS, L. J. & FORD, D. 2009. Could Sirt1-mediated epigenetic effects contribute to the longevity response to dietary restriction and be mimicked by other dietary interventions? *Age (Dordr),* 31, 327-41.

WALSH, C. P. & XU, G. L. 2006. Cytosine methylation and DNA repair. *Curr Top Microbiol Immunol,* 301, 283-315.

WANG, C., JURK, D., MADDICK, M., NELSON, G., MARTIN-RUIZ, C. & VON ZGLINICKI, T. 2009. DNA damage response and cellular senescence in tissues of aging mice. *Aging Cell,* 8, 311-23.

WANG, R. Y., KUO, K. C., GEHRKE, C. W., HUANG, L. H. & EHRLICH, M. 1982. Heat- and alkali-induced deamination of 5-methylcytosine and cytosine residues in DNA. *Biochim Biophys Acta,* 697, 371-7.

WANG, Y. & LEUNG, F. C. 2004. An evaluation of new criteria for CpG islands in the human genome as gene markers. *Bioinformatics,* 20, 1170-7.

WEAVER, A. M. 2008. Cortactin in tumor invasiveness. *Cancer Lett,* 265, 157-66.

WEBER, M., DAVIES, J. J., WITTIG, D., OAKELEY, E. J., HAASE, M., LAM, W. L. & SCHUBELER, D. 2005. Chromosome-wide and promoter-specific analyses identify sites of differential DNA methylation in normal and transformed human cells. *Nat Genet,* 37, 853-62.

WEBER, M., HELLMANN, I., STADLER, M. B., RAMOS, L., PAABO, S., REBHAN, M. & SCHUBELER, D. 2007. Distribution, silencing potential and evolutionary impact of promoter DNA methylation in the human genome. *Nat Genet,* 39, 457-66.

WEI, M., FABRIZIO, P., HU, J., GE, H., CHENG, C., LI, L. & LONGO, V. D. 2008. Life span extension by calorie restriction depends on Rim15 and transcription factors downstream of Ras/PKA, Tor, and Sch9. *PLoS Genet,* 4, e13.

WEINDRUCH, R., KAYO, T., LEE, C. K. & PROLLA, T. A. 2001. Microarray profiling of gene expression in aging and its alteration by caloric restriction in mice. *J Nutr,* 131, 918S-923S.

WEINDRUCH, R., KAYO, T., LEE, C. K. & PROLLA, T. A. 2002. Gene expression profiling of aging using DNA microarrays. *Mech Ageing Dev,* 123, 177-93.

WERLE, E., SCHNEIDER, C., RENNER, M., VOLKER, M. & FIEHN, W. 1994. Convenient single-step, one tube purification of PCR products for direct sequencing. *Nucleic Acids Res,* 22, 4354-5.

WHO 2013. *World Health Statistics 2013,* Geneva, Switzerland.

WILSON, V. L. & JONES, P. A. 1983. DNA methylation decreases in aging but not in immortal cells. *Science,* 220, 1055-7.

WILSON, V. L., SMITH, R. A., MA, S. & CUTLER, R. G. 1987. Genomic 5-methyldeoxycytidine decreases with age. *J Biol Chem,* 262, 9948-51.

WOJDACZ, T. K. & DOBROVIC, A. 2007. Methylation-sensitive high resolution melting (MS-HRM): a new approach for sensitive and high-throughput assessment of methylation. *Nucleic Acids Res,* 35, e41.

WOOD, J. G., ROGINA, B., LAVU, S., HOWITZ, K., HELFAND, S. L., TATAR, M. & SINCLAIR, D. 2004. Sirtuin activators mimic caloric restriction and delay ageing in metazoans. *Nature,* 430, 686-9.

WRIGHT, W. E. & SHAY, J. W. 2000. Telomere dynamics in cancer progression and prevention: fundamental differences in human and mouse telomere biology. *Nat Med,* 6, 849-51.

WRIGHT, W. E. & SHAY, J. W. 2001. Cellular senescence as a tumor-protection mechanism: the essential role of counting. *Curr Opin Genet Dev,* 11, 98-103.

WU, F., LEVCHENKO, I. & FILUTOWICZ, M. 1995. A DNA segment conferring stable maintenance on R6K gamma-origin core replicons. *J Bacteriol,* 177, 6338-45.

WU, H. C., DELGADO-CRUZATA, L., FLOM, J. D., KAPPIL, M., FERRIS, J. S., LIAO, Y., SANTELLA, R. M. & TERRY, M. B. 2011. Global methylation profiles in DNA from different blood cell types. *Epigenetics,* 6, 76-85.

WU, Z. & IRIZARRY, R. A. 2004. Preprocessing of oligonucleotide array data. *Nat Biotechnol,* 22, 656-8; author reply 658.

WYZYKOWSKI, J. C., WINATA, T. I., MITIN, N., TAPAROWSKY, E. J. & KONIECZNY, S. F. 2002. Identification of novel MyoD gene targets in proliferating myogenic stem cells. *Mol Cell Biol,* 22, 6199-208.

XIONG, Z. & LAIRD, P. W. 1997. COBRA: a sensitive and quantitative DNA methylation assay. *Nucleic Acids Res,* 25, 2532-4.

YANG, A. S., ESTECIO, M. R., DOSHI, K., KONDO, Y., TAJARA, E. H. & ISSA, J. P. 2004. A simple method for estimating global DNA methylation using bisulfite PCR of repetitive DNA elements. *Nucleic Acids Res,* 32, e38.

YANG, J., CHANG, E., CHERRY, A. M., BANGS, C. D., OEI, Y., BODNAR, A., BRONSTEIN, A., CHIU, C. P. & HERRON, G. S. 1999. Human endothelial cell life extension by telomerase expression. *J Biol Chem,* 274, 26141-8.

YANG, N., EIJSINK, J. J., LENDVAI, A., VOLDERS, H. H., KLIP, H., BUIKEMA, H. J., VAN HEMEL, B. M., SCHUURING, E., VAN DER ZEE, A. G. & WISMAN, G. B. 2009. Methylation markers for CCNA1 and C13ORF18 are strongly associated with high-grade cervical intraepithelial neoplasia and cervical cancer in cervical scrapings. *Cancer Epidemiol Biomarkers Prev,* 18, 3000-7.

YEN, W. L. & KLIONSKY, D. J. 2008. How to live long and prosper: autophagy, mitochondria, and aging. *Physiology (Bethesda),* 23, 248-62.

YOUNG, A. R., NARITA, M., FERREIRA, M., KIRSCHNER, K., SADAIE, M., DAROT, J. F., TAVARE, S., ARAKAWA, S., SHIMIZU, S. & WATT, F. M. 2009. Autophagy mediates the mitotic senescence transition. *Genes Dev,* 23, 798-803.

YUE, M. X., FU, X. W., ZHOU, G. B., HOU, Y. P., DU, M., WANG, L. & ZHU, S. E. 2012. Abnormal DNA methylation in oocytes could be associated with a decrease in reproductive potential in old mice. *J Assist Reprod Genet,* 29, 643-50.

ZAHN, J. M., POOSALA, S., OWEN, A. B., INGRAM, D. K., LUSTIG, A., CARTER, A., WEERARATNA, A. T., TAUB, D. D., GOROSPE, M., MAZAN-MAMCZARZ, K., LAKATTA, E. G., BOHELER, K. R., XU, X., MATTSON, M. P., FALCO, G., KO, M. S., SCHLESSINGER, D., FIRMAN, J., KUMMERFELD, S. K., WOOD, W. H., 3RD, ZONDERMAN, A. B., KIM, S. K. & BECKER, K. G. 2007. AGEMAP: a gene expression database for aging in mice. *PLoS Genet,* 3, e201.

ZALEWSKI, P. D. 2006. Zinc metabolism in the airway: basic mechanisms and drug targets. *Curr Opin Pharmacol,* 6, 237-43.

ZENTNER, G. E. & HENIKOFF, S. 2013. Regulation of nucleosome dynamics by histone modifications. *Nat Struct Mol Biol,* 20, 259-66.

ZHANG, F., NAKANISHI, G., KUREBAYASHI, S., YOSHINO, K., PERANTONI, A., KIM, Y. S. & JETTEN, A. M. 2002a. Characterization of Glis2, a novel gene encoding a Gli-related, Kruppel-like transcription factor with transactivation and repressor functions. Roles in kidney development and neurogenesis. *J Biol Chem,* 277, 10139-49.

ZHANG, H., PAN, K. H. & COHEN, S. N. 2003. Senescence-specific gene expression fingerprints reveal cell-type-dependent physical clustering of up-regulated chromosomal loci. *Proc Natl Acad Sci U S A,* 100, 3251-6.

ZHANG, L., LIN, Q. L., LU, L., YANG, C. C., LI, Y. L., SUN, F. L., WANG, D. H., CAI, Y. N. & LI, L. 2013. Tissue-specific modification of clock methylation in aging mice. *Eur Rev Med Pharmacol Sci,* 17, 1874-80.

ZHANG, L., WU, C., CARTA, R., BAGGERLY, K. & COOMBES, K. R. 2004. Response to Preprocessing of oligonucleotide array data. *Nat Biotechnol,* 22, 658.

ZHANG, R., CHEN, W. & ADAMS, P. D. 2007. Molecular dissection of formation of senescence-associated heterochromatin foci. *Mol Cell Biol,* 27, 2343-58.

ZHANG, W., JI, W., YANG, J., YANG, L., CHEN, W. & ZHUANG, Z. 2008. Comparison of global DNA methylation profiles in replicative versus premature senescence. *Life Sci,* 83, 475-80.

ZHANG, Y., LV, J., LIU, H., ZHU, J., SU, J., WU, Q., QI, Y., WANG, F. & LI, X. 2010. HHMD: the human histone modification database. *Nucleic Acids Res,* 38, D149-54.

ZHANG, Z., DENG, C., LU, Q. & RICHARDSON, B. 2002b. Age-dependent DNA methylation changes in the ITGAL (CD11a) promoter. *Mech Ageing Dev,* 123, 1257-68.

ZHENG, Q. H., MA, L. W., ZHU, W. G., ZHANG, Z. Y. & TONG, T. J. 2006. p21Waf1/Cip1 plays a critical role in modulating senescence through changes of DNA methylation. *J Cell Biochem,* 98, 1230-48.

ZHU, M., LEE, G. D., DING, L., HU, J., QIU, G., DE CABO, R., BERNIER, M., INGRAM, D. K. & ZOU, S. 2007. Adipogenic signaling in rat white adipose tissue: modulation by aging and calorie restriction. *Exp Gerontol,* 42, 733-44.

ZID, B. M., ROGERS, A. N., KATEWA, S. D., VARGAS, M. A., KOLIPINSKI, M. C., LU, T. A., BENZER, S. & KAPAHI, P. 2009. 4E-BP extends lifespan upon dietary restriction by enhancing mitochondrial activity in Drosophila. *Cell,* 139, 149-60.

ZIN'KOVSKAIA, G. G., BERDYSHEV, G. D. & VANIUSHIN, B. F. 1978. [Tissue-specific decrease and change in the character of DNA methylation in cattle with aging]. *Biokhimiia,* 43, 1883-92.

ZOU, X., MA, W., SOLOV'YOV, I. A., CHIPOT, C. & SCHULTEN, K. 2012. Recognition of methylated DNA through methyl-CpG binding domain proteins. *Nucleic Acids Res,* 40, 2747-58.

Appendix A: Dilution curves and melt curves for qPCR and RT-qPCR assays

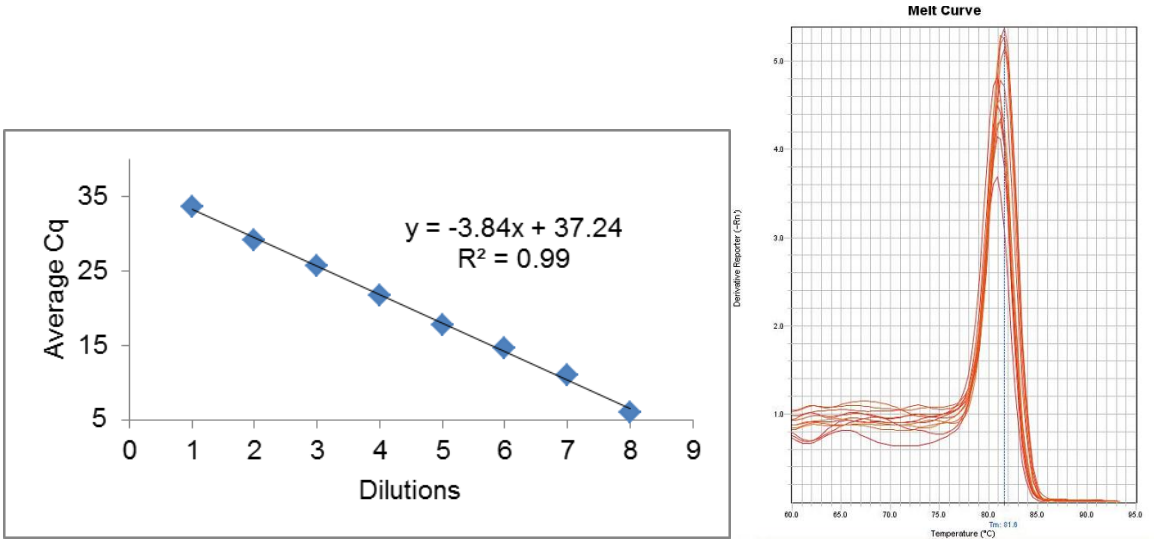

E = 0.82

Figure A.1. Dilution curve (left) and melt curve (right) for λ-Phage DNA Positive Control (Fragment A pair 2) primer pair. Dilution curve was obtained by plotting the average Cq of three replicates of 10-fold serial dilutions, with dilution 8 being equal to 500 ng/µL. "E" indicates the efficiency of amplification.

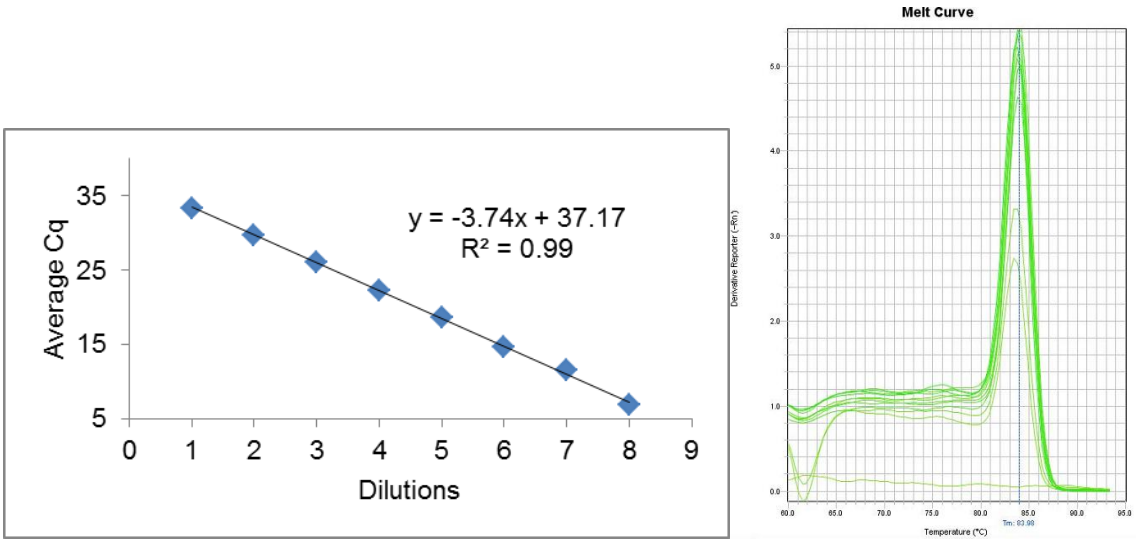

E = 0.85

Figure A.2. Dilution curve (left) and melt curve (right) for λ-Phage DNA Negative Control (Fragment B pair 2) primer pair. Dilution curve was obtained by plotting the average Cq of three replicates of 10-fold serial dilutions, with dilution 8 being equal to 500 ng/µL. "E" indicates the efficiency of amplification.

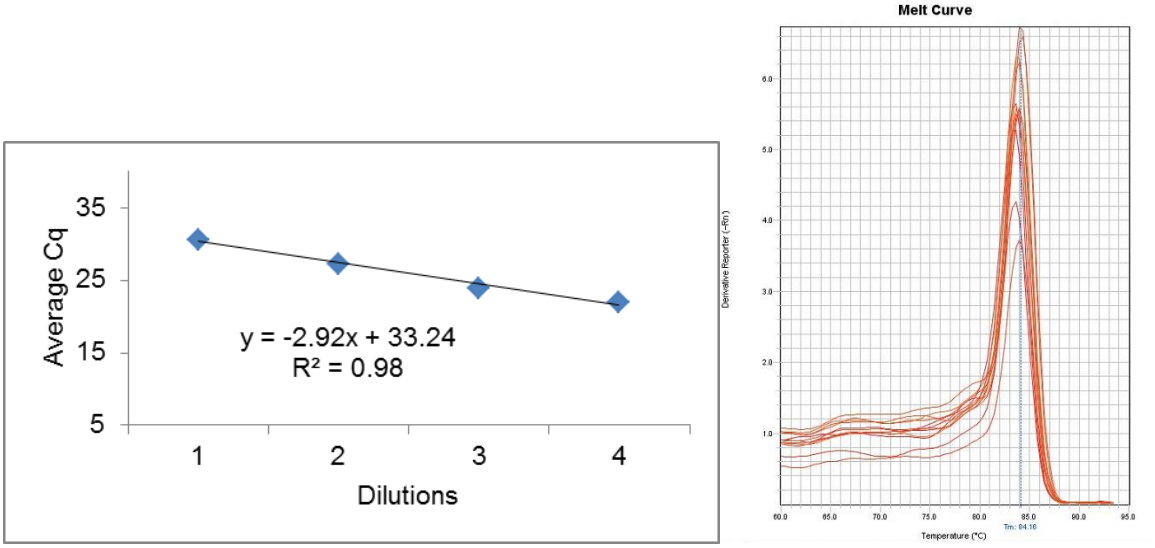

E = 1.20

Figure A.3. Dilution curve (left) and melt curve (right) for human H19 ICR primer pair. Dilution curve was obtained by plotting the average Cq of three replicates of 10-fold serial dilutions of genomic DNA, with dilution 4 being equal to 200 ng/µL. "E" indicates the efficiency of amplification.

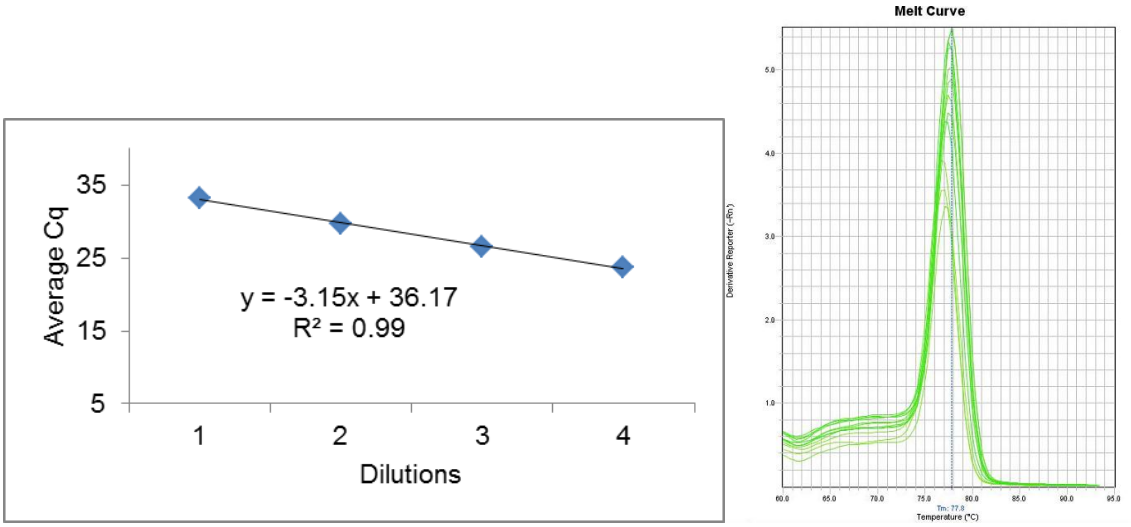

E = 1.08

Figure A.4. Dilution curve (left) and melt curve (right) for human HIST1H2BA primer pair. Dilution curve was obtained by plotting the average Cq of three replicates of 10-fold serial dilutions of genomic DNA, with dilution 4 being equal to 200 ng/µL. "E" indicates the efficiency of amplification.

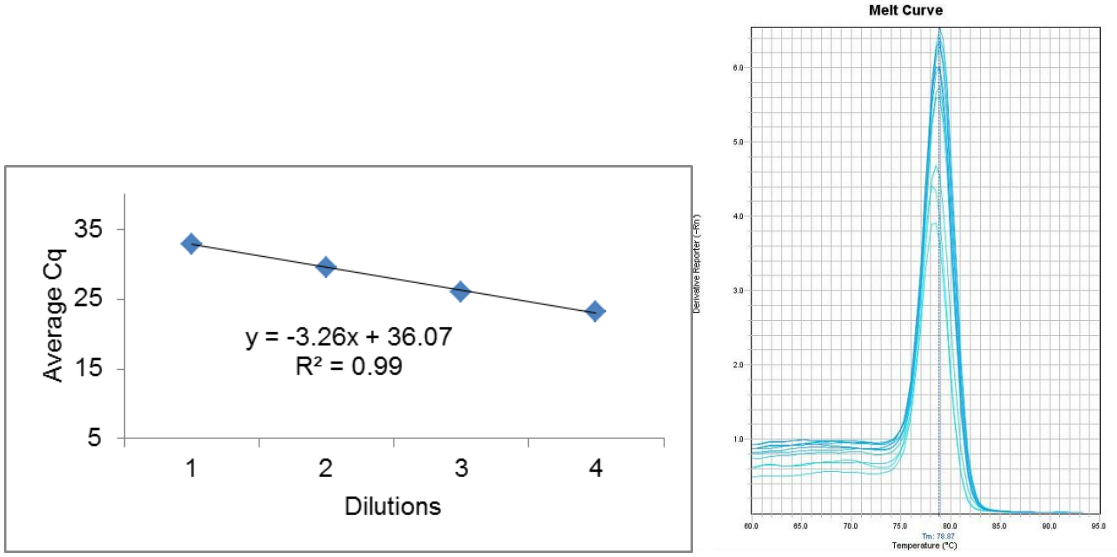

E = 1.03

Figure A.5. Dilution curve (left) and melt curve (right) for human GAPDH primer pair. Dilution curve was obtained by plotting the average Cq of three replicates of 10-fold serial dilutions of genomic DNA, with dilution 4 being equal to 200 ng/µL. "E" indicates the efficiency of amplification.

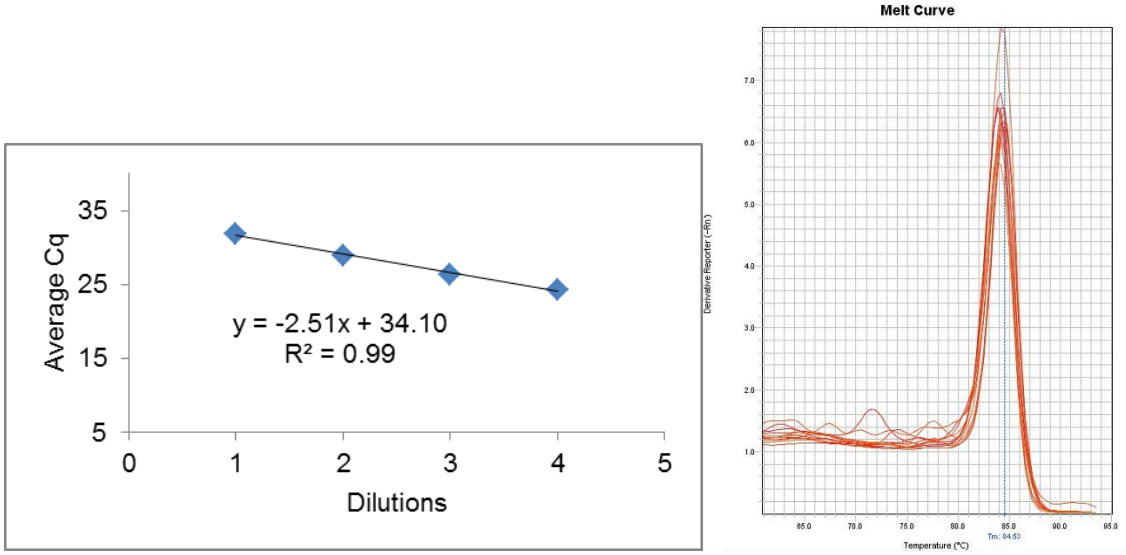

E = 0.89

Figure A.6. Dilution curve (left) and melt curve (right) for human CD7 primer pair. Dilution curve was obtained by plotting the average Cq of three replicates of 5-fold serial dilutions of genomic DNA, with dilution 4 being equal to 50 ng/µL. "E" indicates the efficiency of amplification.

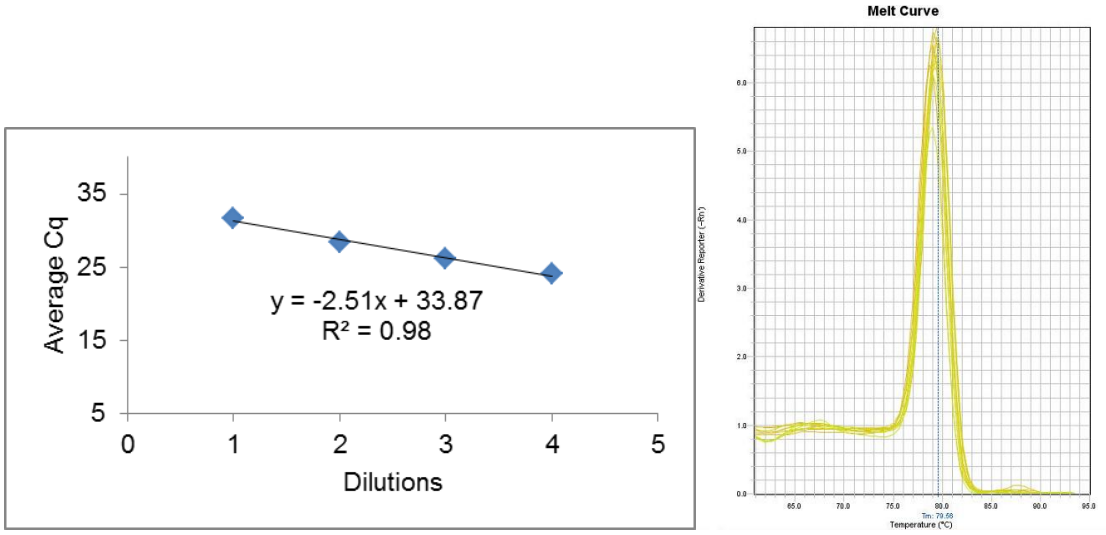

E = 0.90

Figure A.7. Dilution curve (left) and melt curve (right) for human DCHS1 primer pair. Dilution curve was obtained by plotting the average Cq of three replicates of 5-fold serial dilutions of genomic DNA, with dilution 4 being equal to 50 ng/µL. "E" indicates the efficiency of amplification.

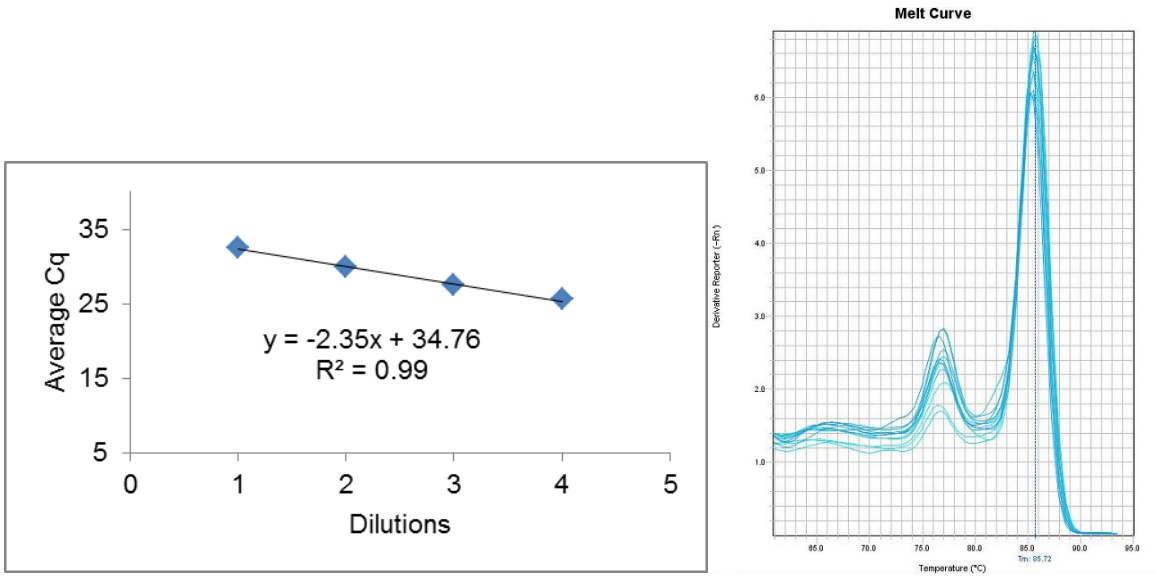

E = 0.98

Figure A.8. Dilution curve (left) and melt curve (right) for human MLNR primer pair. Dilution curve was obtained by plotting the average Cq of three replicates of 5-fold serial dilutions of genomic DNA, with dilution 4 being equal to 50 ng/µL. "E" indicates the efficiency of amplification.

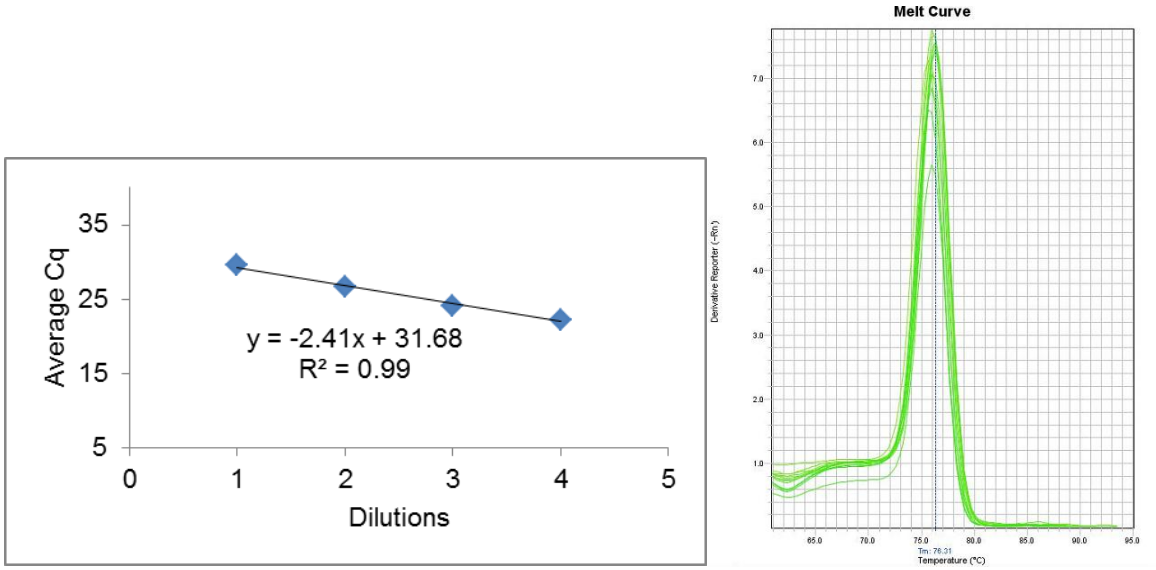

E = 0.95

Figure A.9. Dilution curve (left) and melt curve (right) for human OR5AP2 primer pair. Dilution curve was obtained by plotting the average Cq of three replicates of 5-fold serial dilutions of genomic DNA, with dilution 4 being equal to 50 ng/µL. "E" indicates the efficiency of amplification.

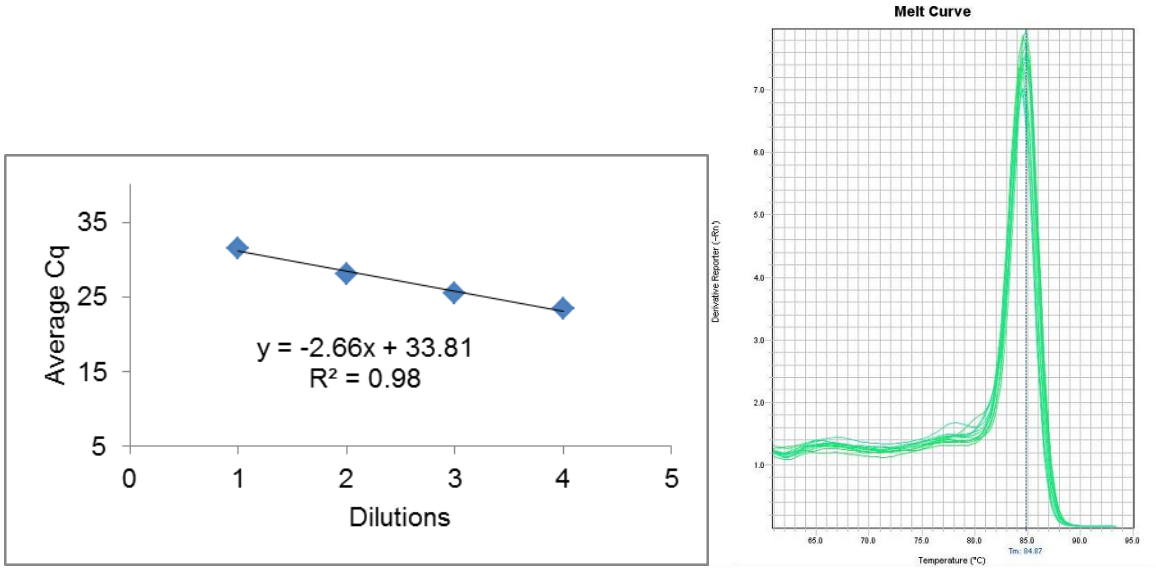

E = 0.83

Figure A.10. Dilution curve (left) and melt curve (right) for human PRDM8 primer pair. Dilution curve was obtained by plotting the average Cq of three replicates of 5-fold serial dilutions of genomic DNA, with dilution 4 being equal to 50 ng/µL. "E" indicates the efficiency of amplification.

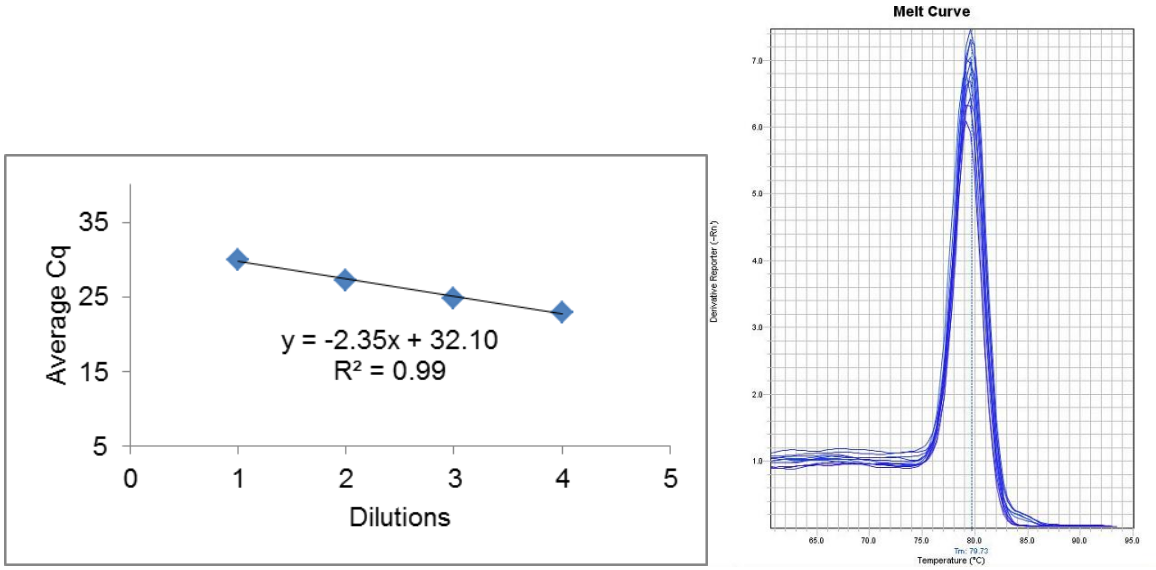

E = 0.98

Figure A.11. Dilution curve (left) and melt curve (right) for human RAB5C primer pair. Dilution curve was obtained by plotting the average Cq of three replicates of 5-fold serial dilutions of genomic DNA, with dilution 4 being equal to 50 ng/µL. "E" indicates the efficiency of amplification.

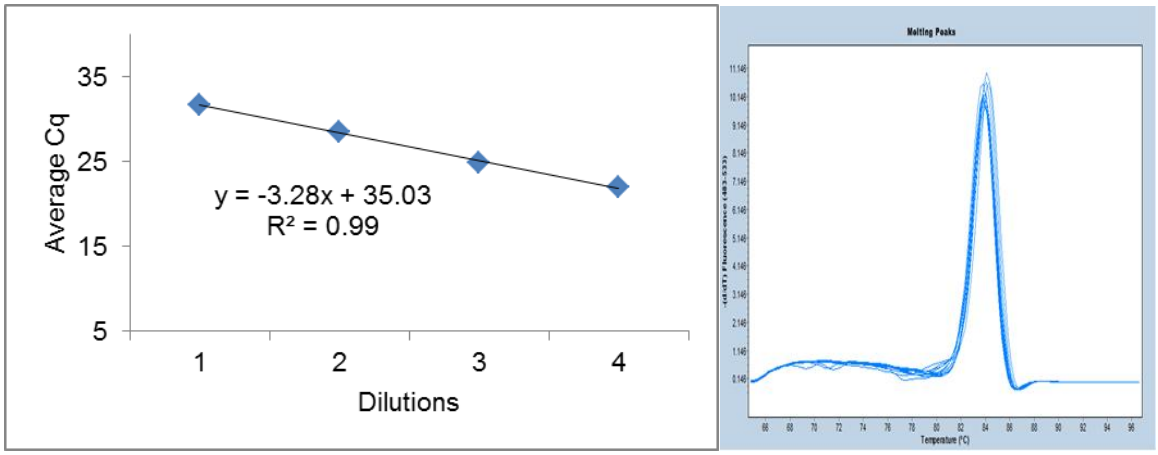

E = 1.01

Figure A.12. Dilution curve (left) and melt curve (right) for murine H19 primer pair. Dilution curve was obtained by plotting the average Cq of three replicates of 10-fold serial dilutions of genomic DNA, with dilution 4 being equal to 200 ng/µL. "E" indicates the efficiency of amplification.

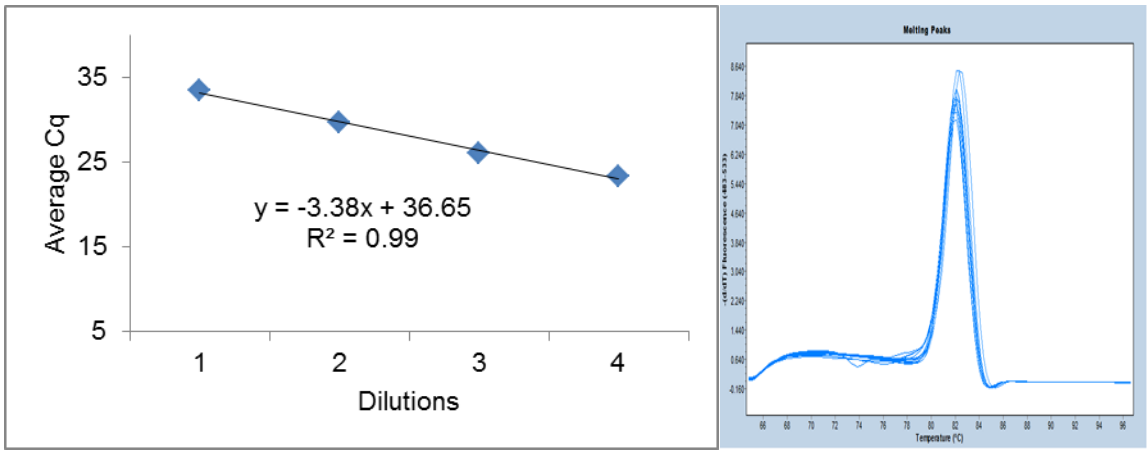

E = 0.98

Figure A.13. Dilution curve (left) and melt curve (right) for murine Hist1h2ba primer pair. Dilution curve was obtained by plotting the average Cq of three replicates of 10-fold serial dilutions of genomic DNA, with dilution 4 being equal to 200 ng/µL. "E" indicates the efficiency of amplification.

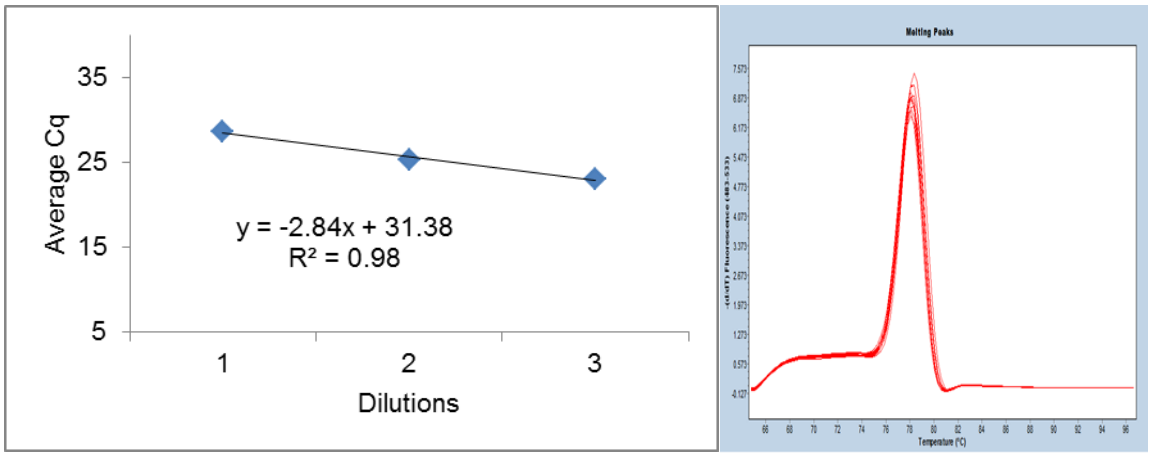

E = 1.01

Figure A.14. Dilution curve (left) and melt curve (right) for murine Actb primer pair. Dilution curve was obtained by plotting the average Cq of three replicates of 10-fold serial dilutions of genomic DNA, with dilution 4 being equal to 200 ng/µL. "E" indicates the efficiency of amplification.

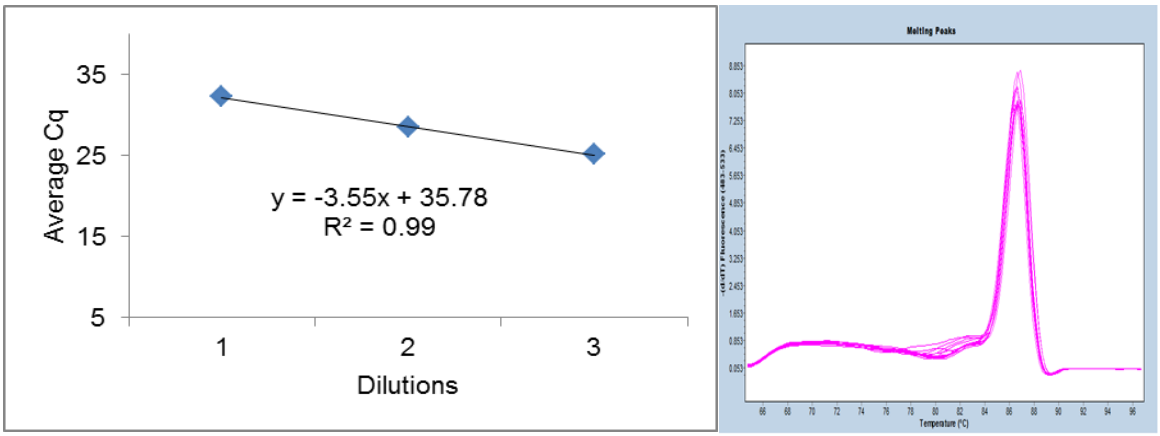

E = 0.91

Figure A.15. Dilution curve (left) and melt curve (right) for murine Gapdh primer pair. Dilution curve was obtained by plotting the average Cq of three replicates of 10-fold serial dilutions of genomic DNA, with dilution 4 being equal to 200 ng/µL. "E" indicates the efficiency of amplification.

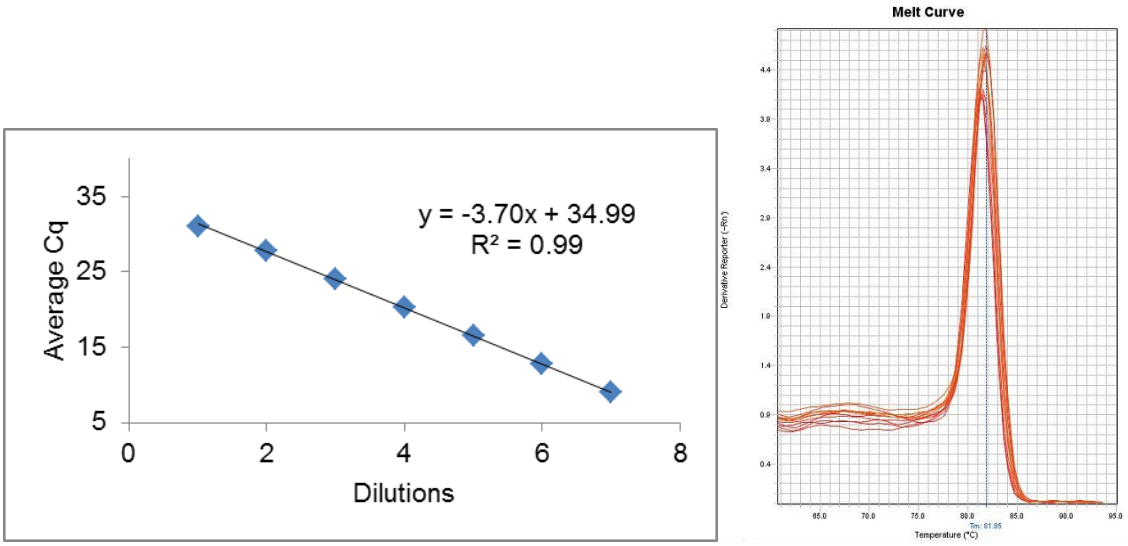

E = 0.86

Figure A.16. Dilution curve (left) and melt curve (right) for λ Phage DNA Spike 208 primer pair 2. Dilution curve was obtained by plotting the average Cq of three replicates of 10-fold serial dilutions of genomic DNA, with dilution 7 being equal to 50pg/µL. "E" indicates the efficiency of amplification.

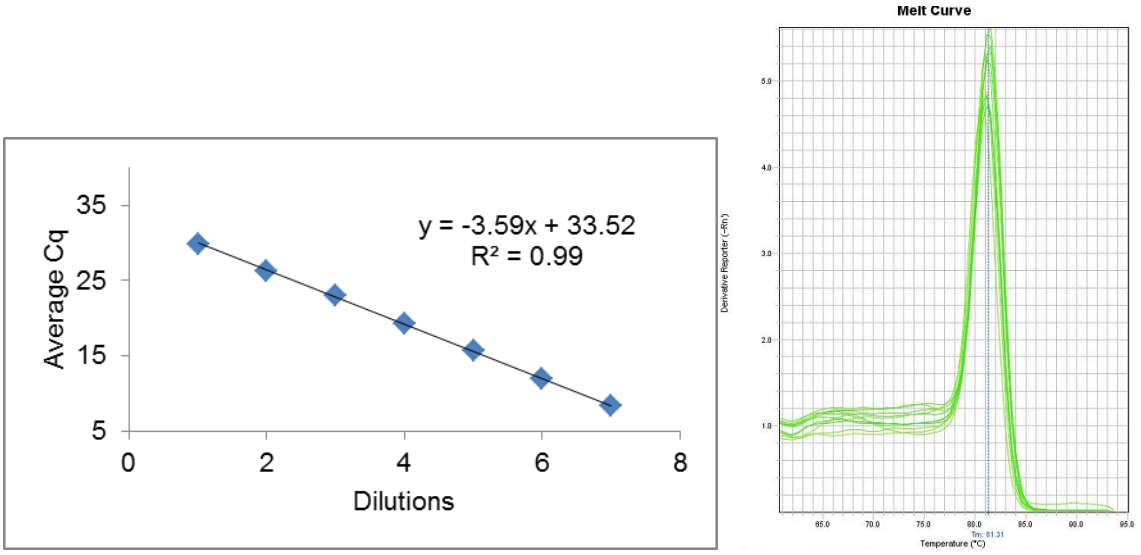

E = 0.90

Figure A.17. Dilution curve (left) and melt curve (right) for λ Phage DNA Spike 400 primer pair 2. Dilution curve was obtained by plotting the average Cq of three replicates of 10-fold serial dilutions of genomic DNA, with dilution 7 being equal to 50pg/µL. "E" indicates the efficiency of amplification.

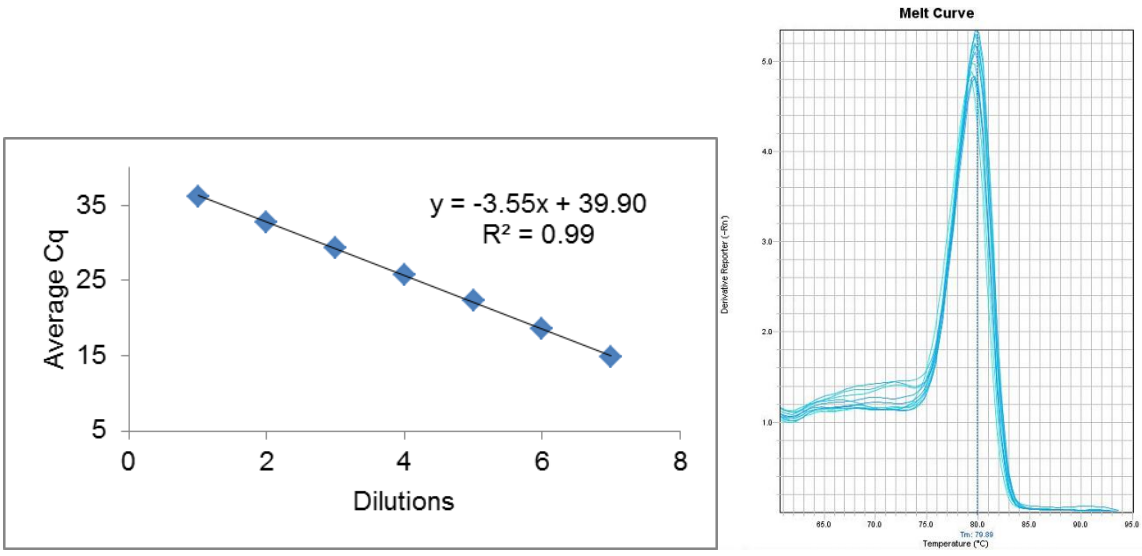

E = 0.91

Figure A.18. Dilution curve (left) and melt curve (right) for λ Phage DNA Spike 800 primer pair 2. Dilution curve was obtained by plotting the average Cq of three replicates of 10-fold serial dilutions of genomic DNA, with dilution 7 being equal to 50pg/µL. "E" indicates the efficiency of amplification.

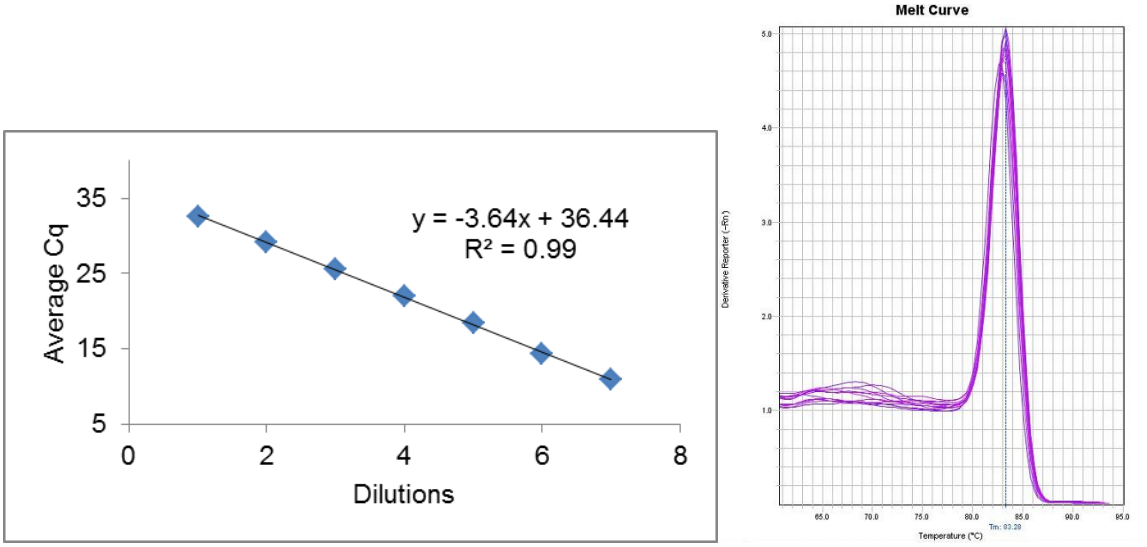

E = 0.88

Figure A.19. Dilution curve (left) and melt curve (right) for λ Phage DNA Spike 1000 primer pair 2. Dilution curve was obtained by plotting the average Cq of three replicates of 10-fold serial dilutions of genomic DNA, with dilution 7 being equal to 50pg/µL. "E" indicates the efficiency of amplification.

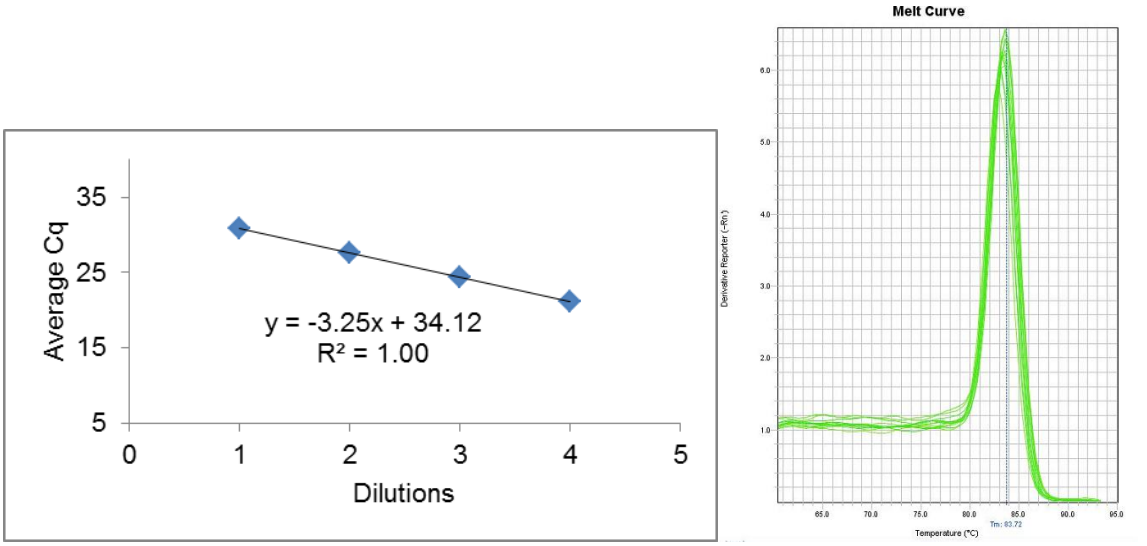

E = 1.03

Figure A.20. Dilution curve (left) and melt curve (right) for human DNMT1 primer pair. Dilution curve was obtained by plotting the average Cq of three replicates of 10-fold serial dilutions of cDNA obtained by reverse transcription of 500 ng of total RNA, with dilution 4 being a dilution 1:2. "E" indicates the efficiency of amplification.

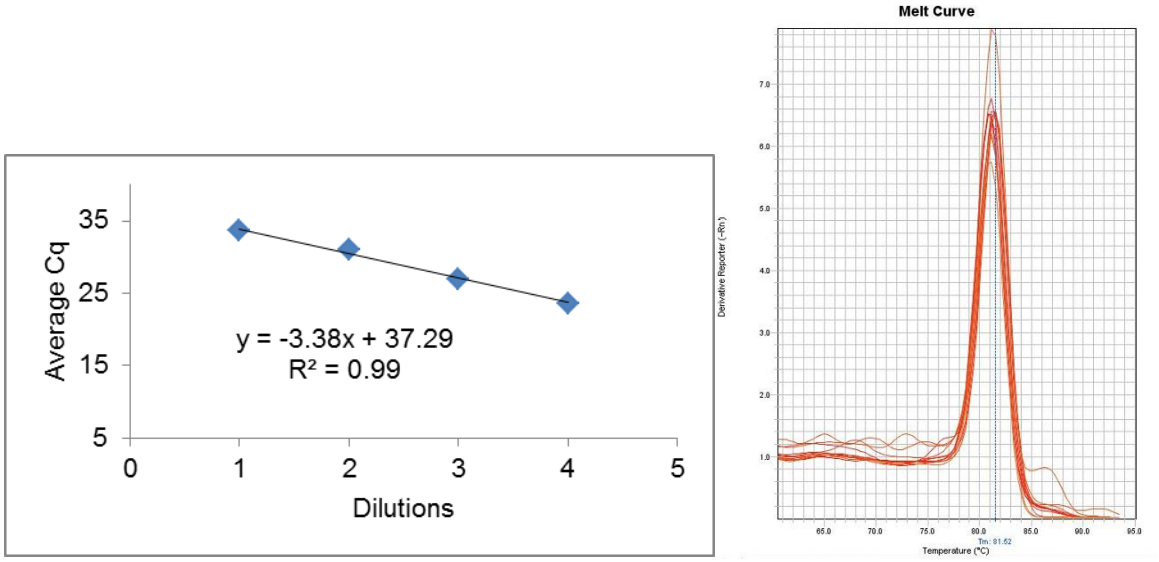

E =0.97

Figure A.21. Dilution curve (left) and melt curve (right) for human DNMT3A primer pair. Dilution curve was obtained by plotting the average Cq of three replicates of 10-fold serial dilutions of cDNA obtained by reverse transcription of 500 ng of total RNA, with dilution 4 being a dilution 1:2. "E" indicates the efficiency of amplification.

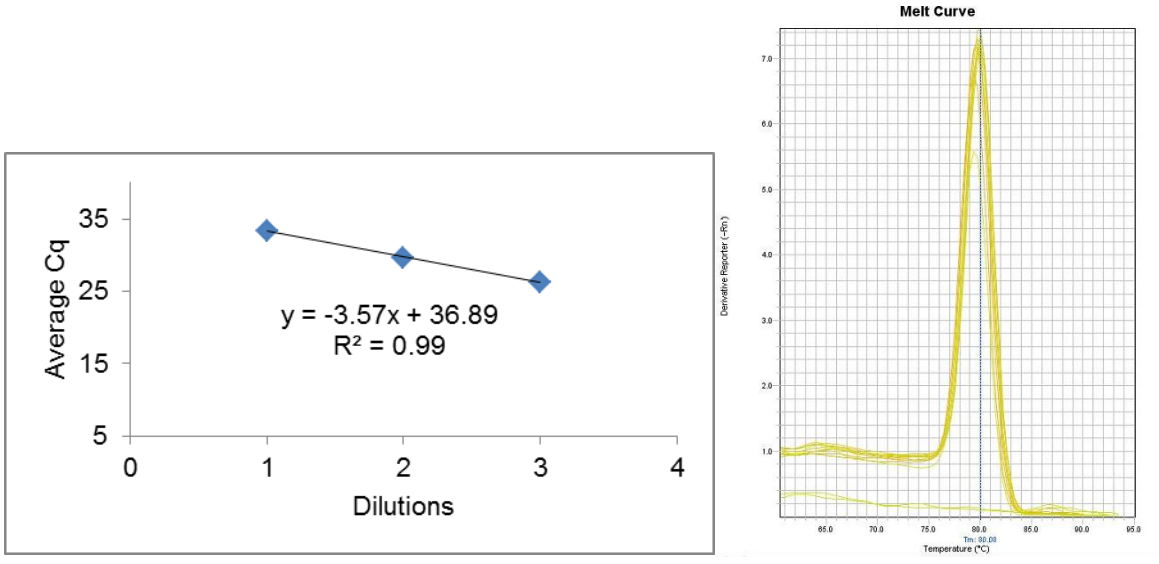

E = 0.90

Figure A.22. Dilution curve (left) and melt curve (right) for human DNMT3B primer pair. Dilution curve was obtained by plotting the average Cq of three replicates of 10-fold serial dilutions of cDNA obtained by reverse transcription of 500 ng of total RNA, with dilution 4 being a dilution 1:2. "E" indicates the efficiency of amplification.

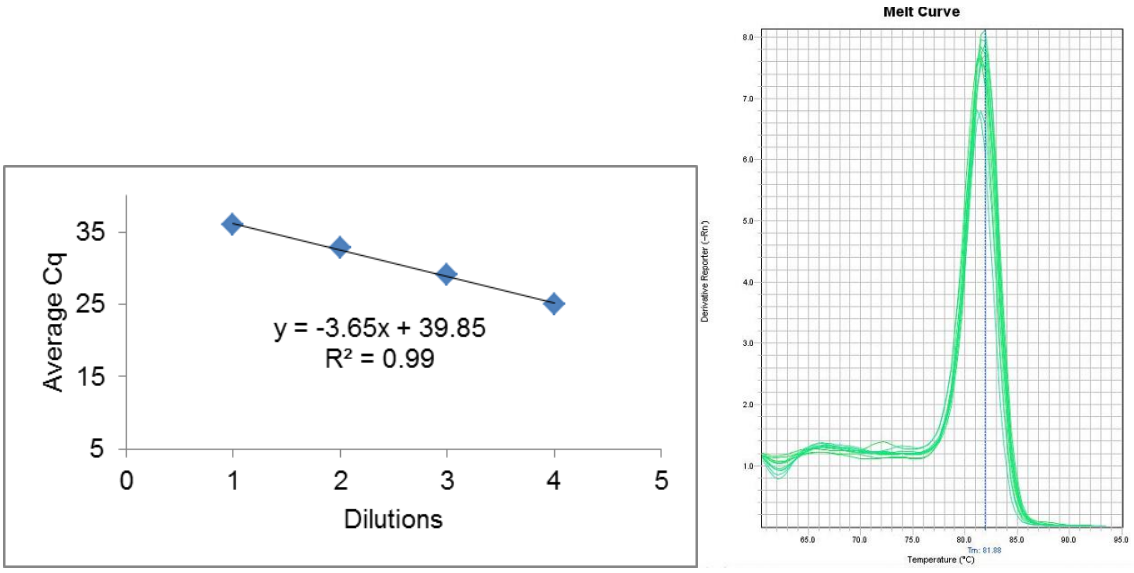

E = 0.88

Figure A.23. Dilution curve (left) and melt curve (right) for murine Dnmt1 primer pair. Dilution curve was obtained by plotting the average Cq of three replicates of 10-fold serial dilutions of cDNA obtained by reverse transcription of 500 ng of total RNA, with dilution 4 being a dilution 1:2. "E" indicates the efficiency of amplification.

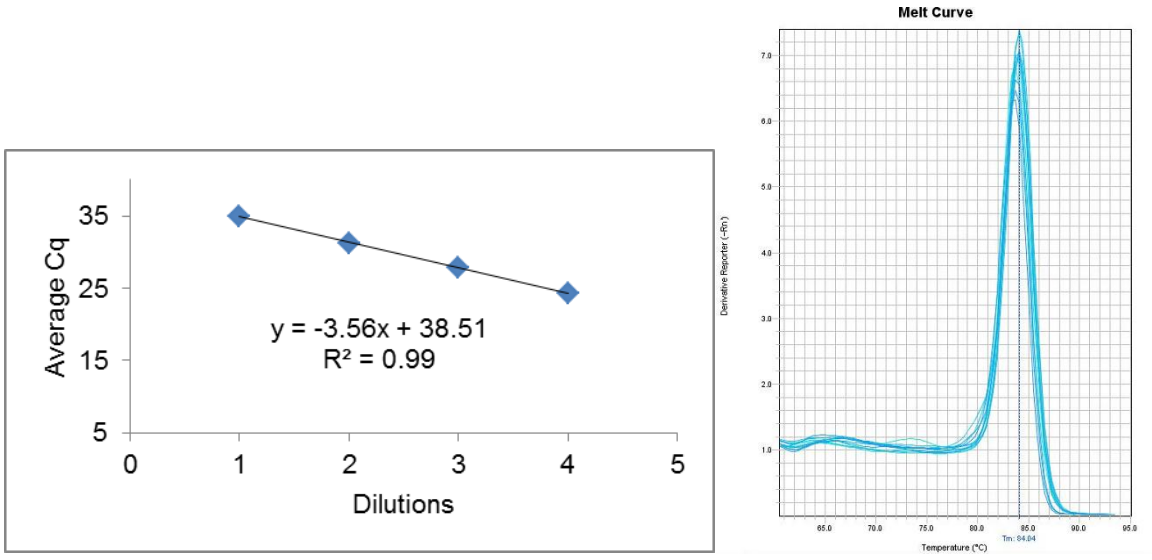

E = 0.91

Figure A.24. Dilution curve (left) and melt curve (right) for murine Dnmt3a primer pair. Dilution curve was obtained by plotting the average Cq of three replicates of 10-fold serial dilutions of cDNA obtained by reverse transcription of 500 ng of total RNA, with dilution 4 being a dilution 1:2. "E" indicates the efficiency of amplification.

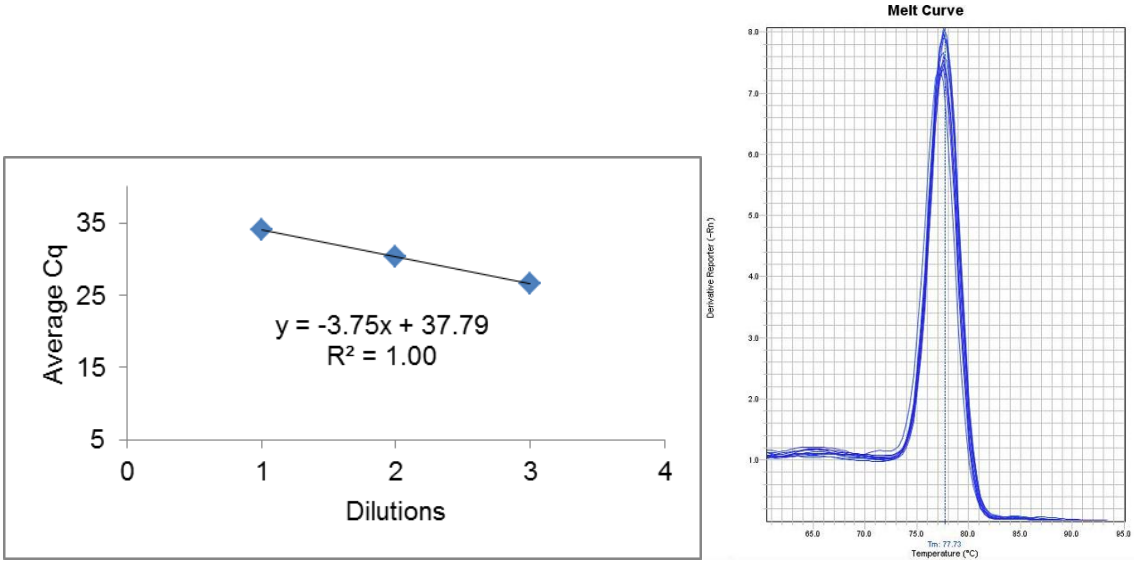

E = 0.85

Figure A.25. Dilution curve (left) and melt curve (right) for murine Dnmt3b primer pair. Dilution curve was obtained by plotting the average Cq of three replicates of 10-fold serial dilutions of cDNA obtained by reverse transcription of 500 ng of total RNA, with dilution 3 being a dilution 1:2. "E" indicates the efficiency of amplification.

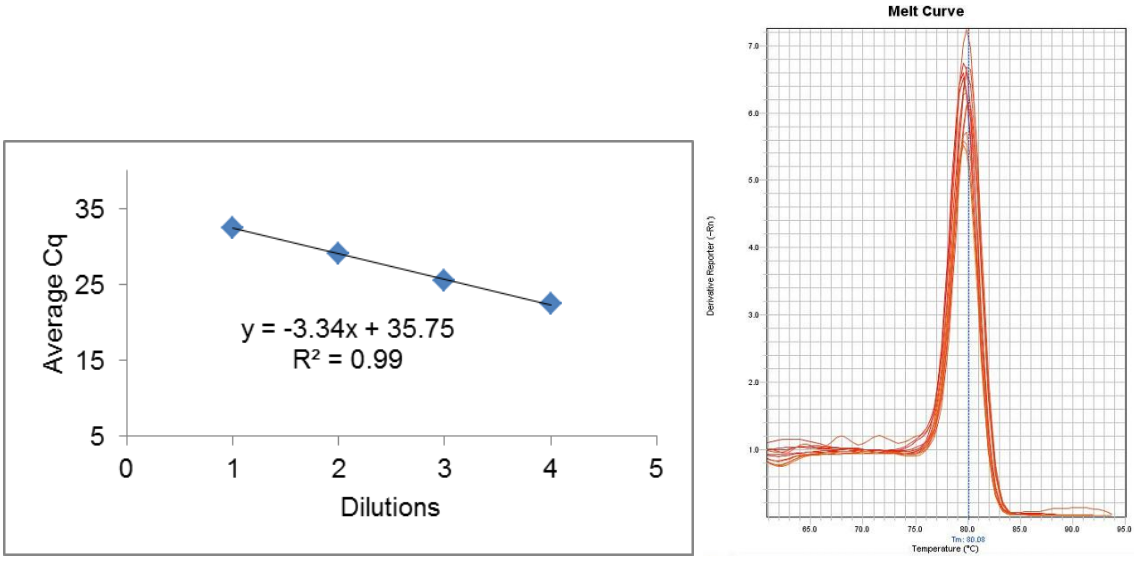

E = 0.99

Figure A.26. Dilution curve (left) and melt curve (right) for human CCNB2 primer pair. Dilution curve was obtained by plotting the average Cq of three replicates of 10-fold serial dilutions of cDNA obtained by reverse transcription of 500 ng of total RNA, with dilution 4 being a dilution 1:2. "E" indicates the efficiency of amplification.

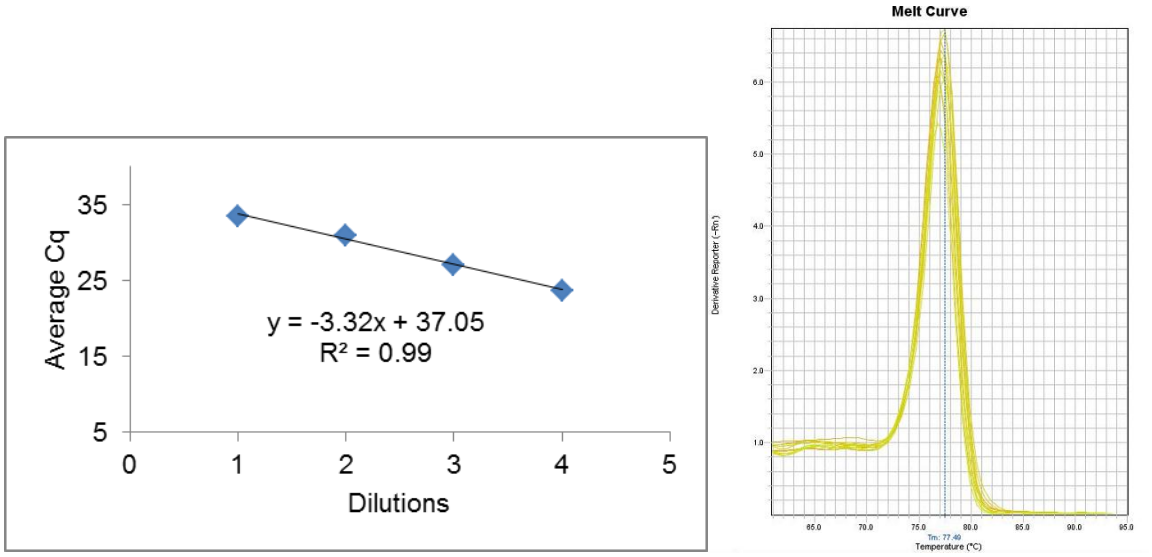

E = 1.00

Figure A.27. Dilution curve (left) and melt curve (right) for human DLGAP5 primer pair. Dilution curve was obtained by plotting the average Cq of three replicates of 10-fold serial dilutions of cDNA obtained by reverse transcription of 500 ng of total RNA, with dilution 4 being a dilution 1:2. "E" indicates the efficiency of amplification.

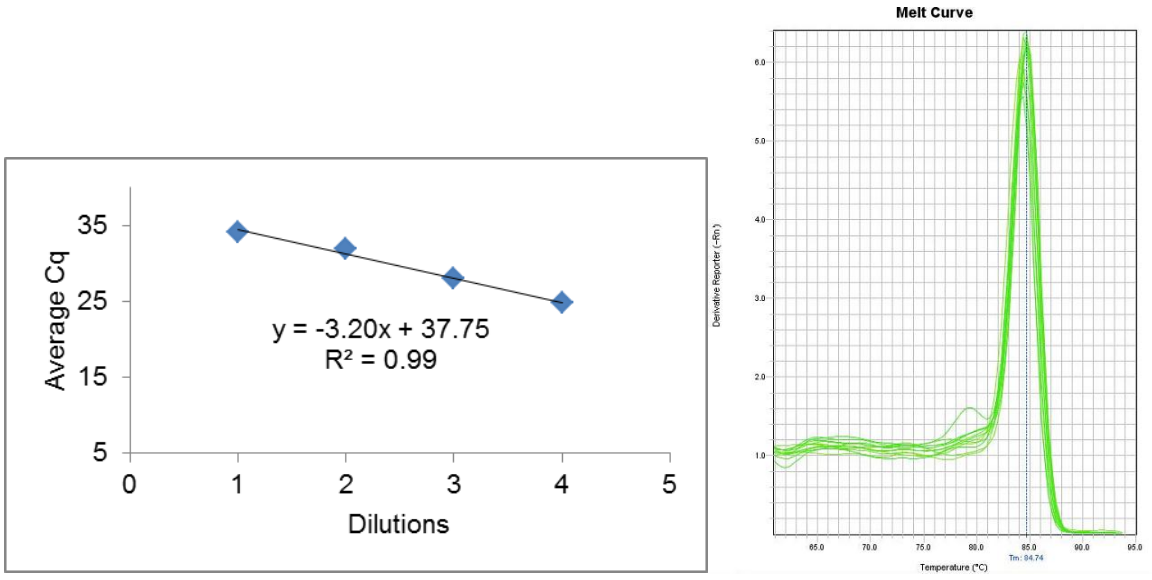

E = 1.05

Figure A.28. Dilution curve (left) and melt curve (right) for human FANCG primer pair. Dilution curve was obtained by plotting the average Cq of three replicates of 10-fold serial dilutions of cDNA obtained by reverse transcription of 500 ng of total RNA, with dilution 4 being a dilution 1:2. "E" indicates the efficiency of amplification.

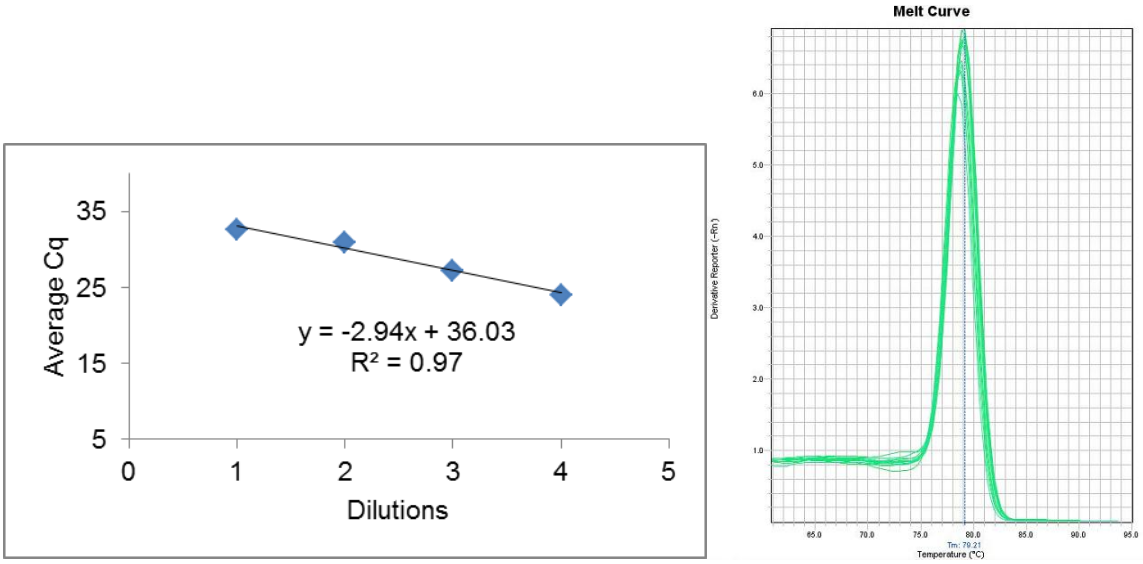

E = 1.19

Figure A.29. Dilution curve (left) and melt curve (right) for human MMP3 primer pair. Dilution curve was obtained by plotting the average Cq of three replicates of 10-fold serial dilutions of cDNA obtained by reverse transcription of 500 ng of total RNA, with dilution 4 being a dilution 1:2. "E" indicates the efficiency of amplification.

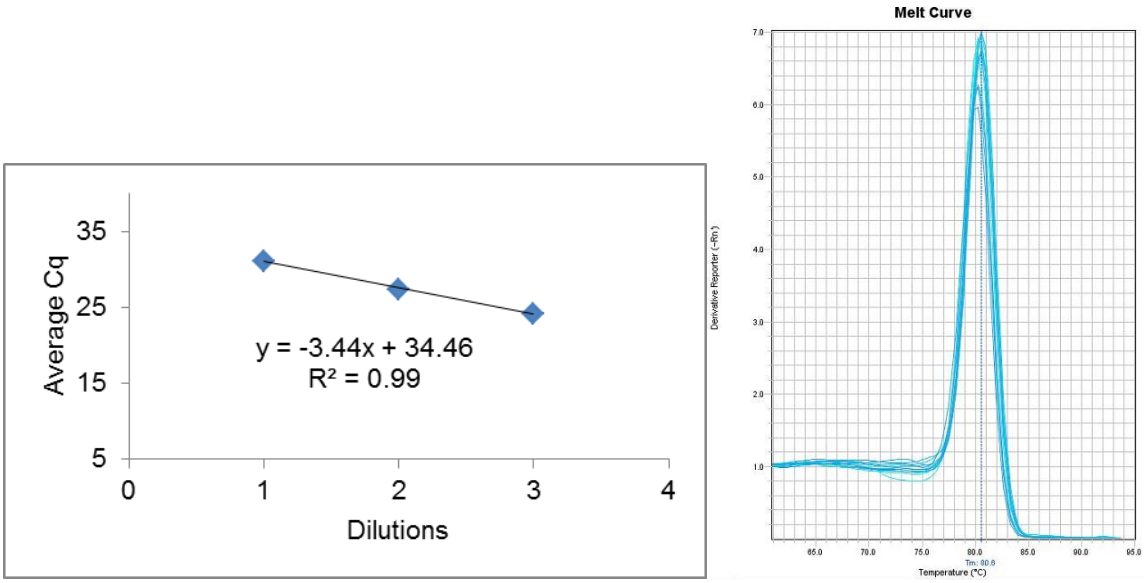

E = 0.95

Figure A.30. Dilution curve (left) and melt curve (right) for human PNMA2 primer pair. Dilution curve was obtained by plotting the average Cq of three replicates of 10-fold serial dilutions of cDNA obtained by reverse transcription of 500 ng of total RNA, with dilution 3 being a dilution 1:2. "E" indicates the efficiency of amplification.

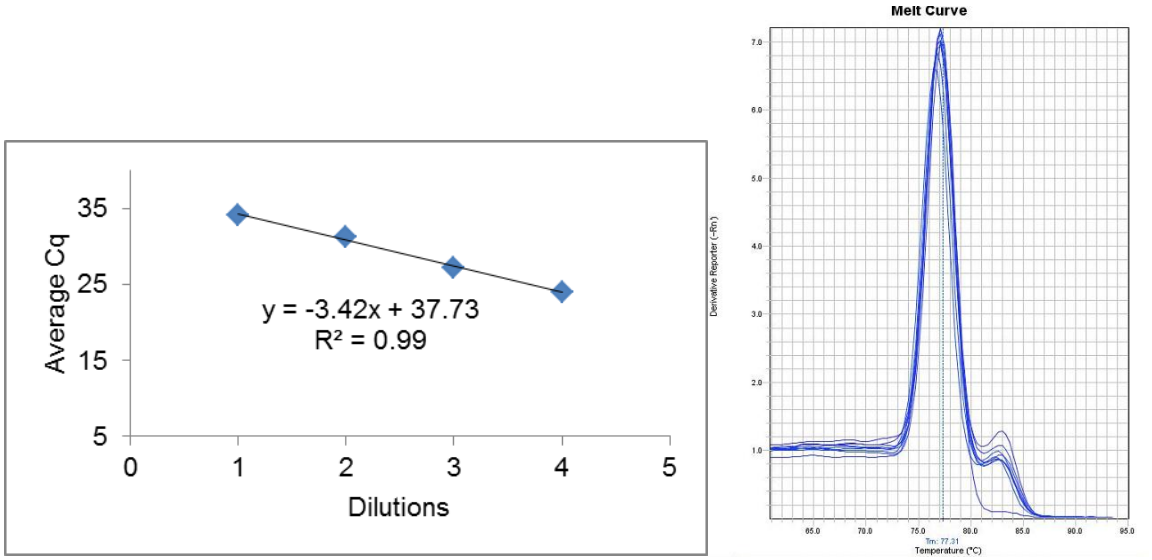

E = 0.96

Figure A.31. Dilution curve (left) and melt curve (right) for human TMSB15A primer pair. Dilution curve was obtained by plotting the average Cq of three replicates of 10-fold serial dilutions of cDNA obtained by reverse transcription of 500 ng of total RNA, with dilution 4 being a dilution 1:2. "E" indicates the efficiency of amplification.

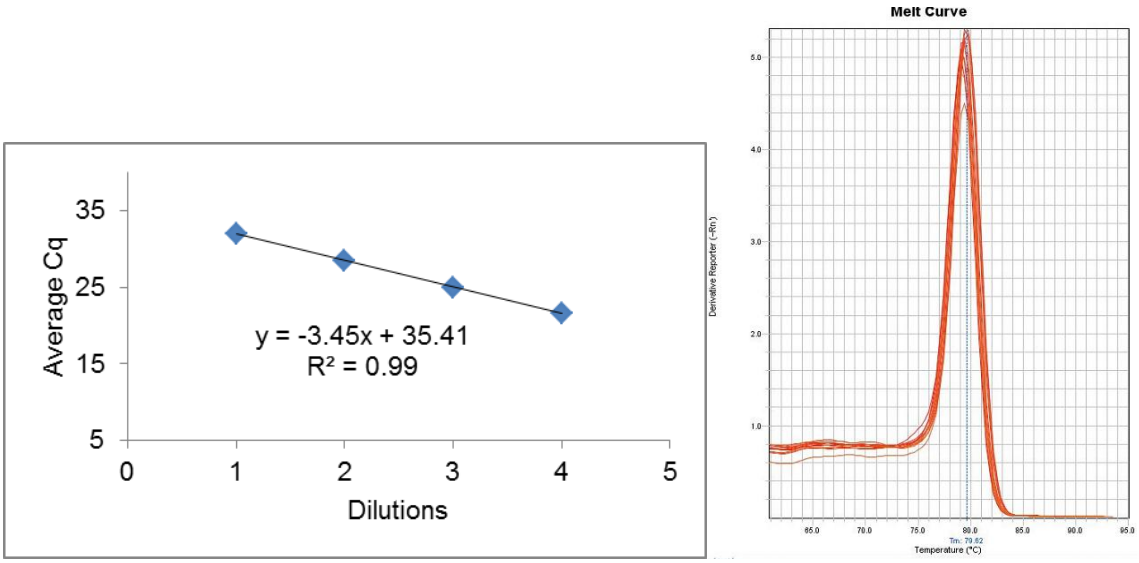

E = 0.95

Figure A.32. Dilution curve (left) and melt curve (right) for human CTTN primer pair. Dilution curve was obtained by plotting the average Cq of three replicates of 10-fold serial dilutions of cDNA obtained by reverse transcription of 500 ng of total RNA, with dilution 4 being a dilution 1:2. "E" indicates the efficiency of amplification.

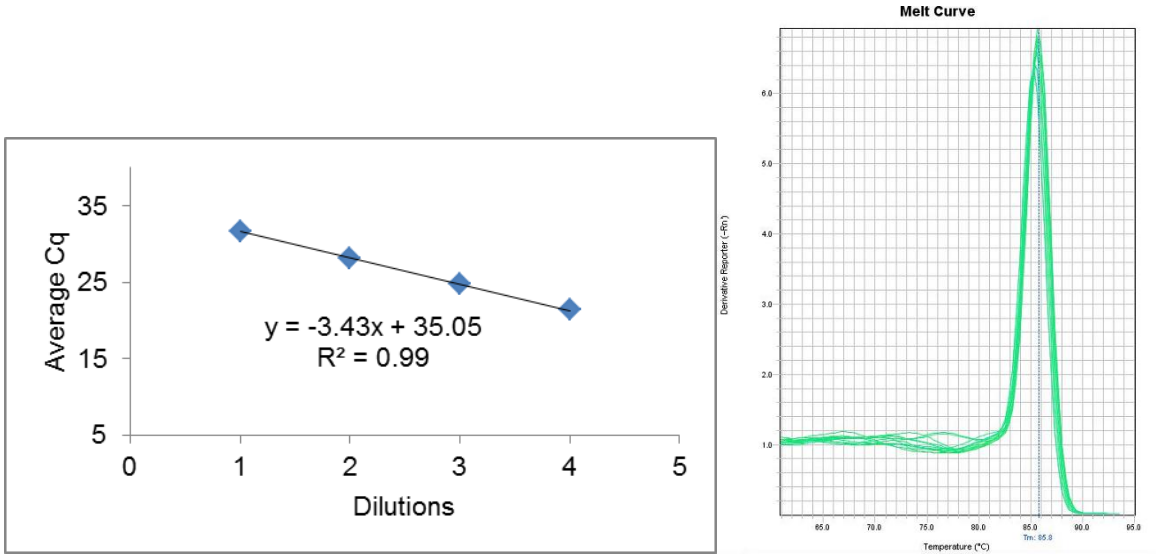

E = 0.95

Figure A.33. Dilution curve (left) and melt curve (right) for human GLIPR2 primer pair. Dilution curve was obtained by plotting the average Cq of three replicates of 10-fold serial dilutions of cDNA obtained by reverse transcription of 500 ng of total RNA, with dilution 4 being a dilution 1:2. "E" indicates the efficiency of amplification.

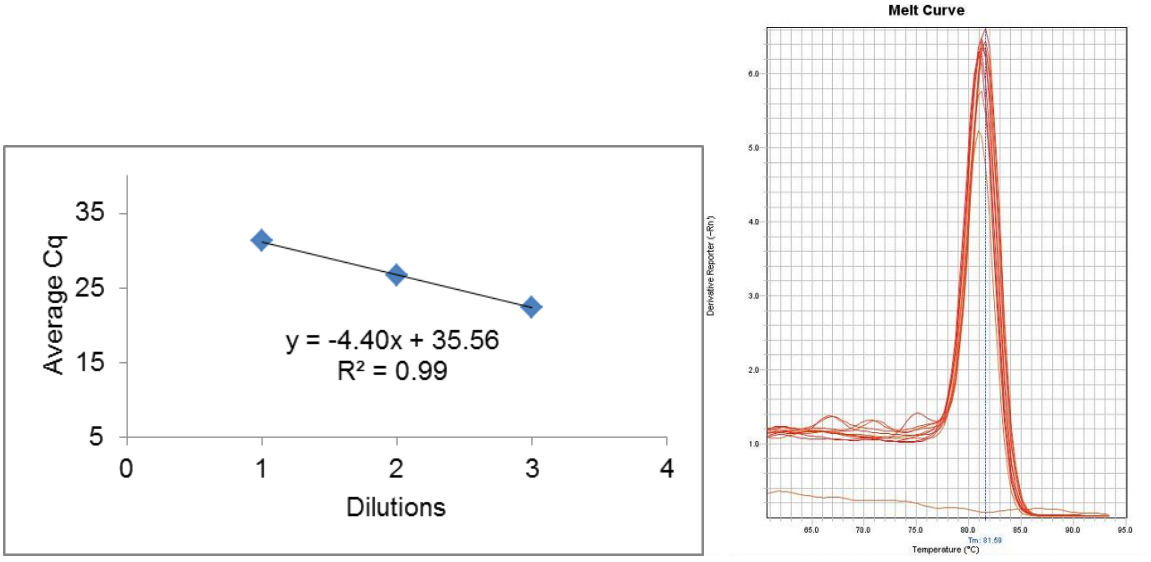

E = 0.98

Figure A.34. Dilution curve (left) and melt curve (right) for human NPTX1 primer pair. Dilution curve was obtained by plotting the average Cq of three replicates of 20-fold serial dilutions of cDNA obtained by reverse transcription of 500 ng of total RNA, with dilution 3 being a dilution 1:2. "E" indicates the efficiency of amplification.

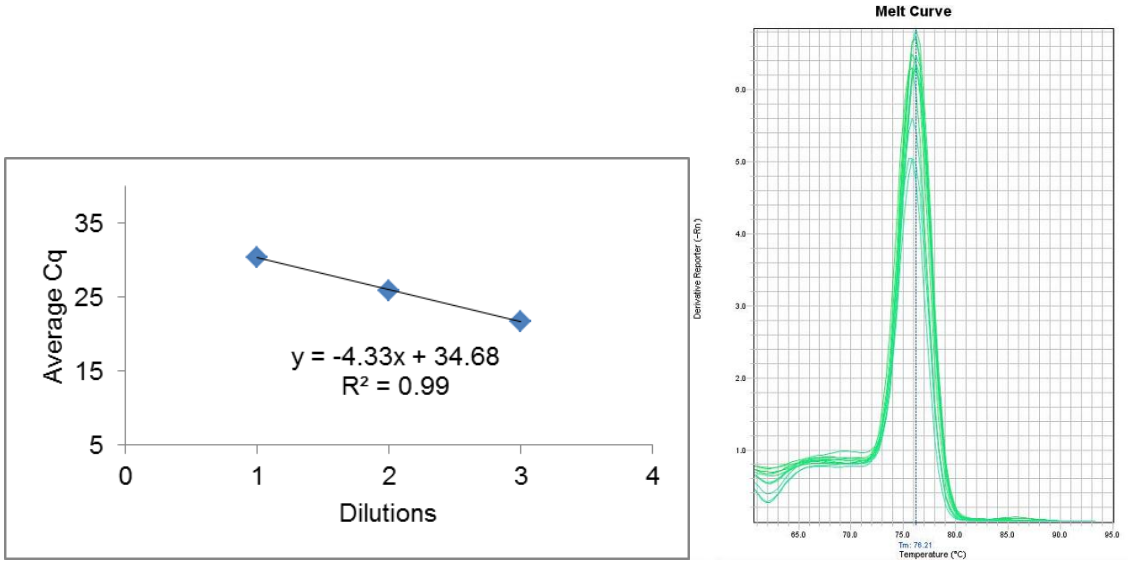

E = 1.00

Figure A.35. Dilution curve (left) and melt curve (right) for human SLC39A14 primer pair. Dilution curve was obtained by plotting the average Cq of three replicates of 20-fold serial dilutions of cDNA obtained by reverse transcription of 500 ng of total RNA, with dilution 3 being a dilution 1:2. "E" indicates the efficiency of amplification.

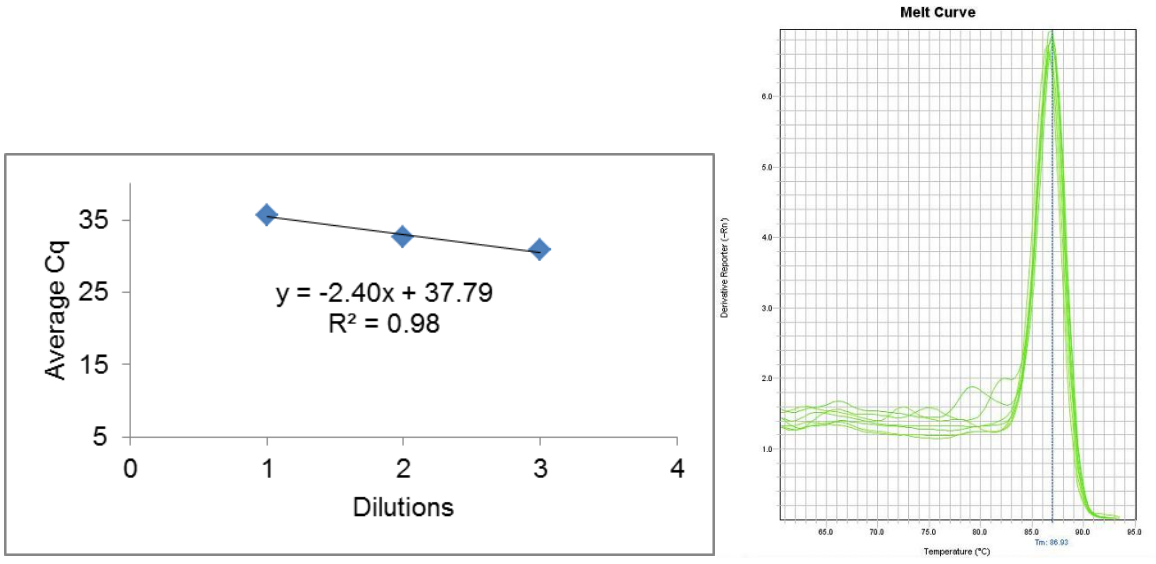

E = 1.61

Figure A.36. Dilution curve (left) and melt curve (right) for human mtDNMT1 primer pair. Dilution curve was obtained by plotting the average Cq of three replicates of 10-fold serial dilutions of cDNA obtained by reverse transcription of 500 ng of total RNA, with dilution 3 being a dilution 1:2. "E" indicates the efficiency of amplification.

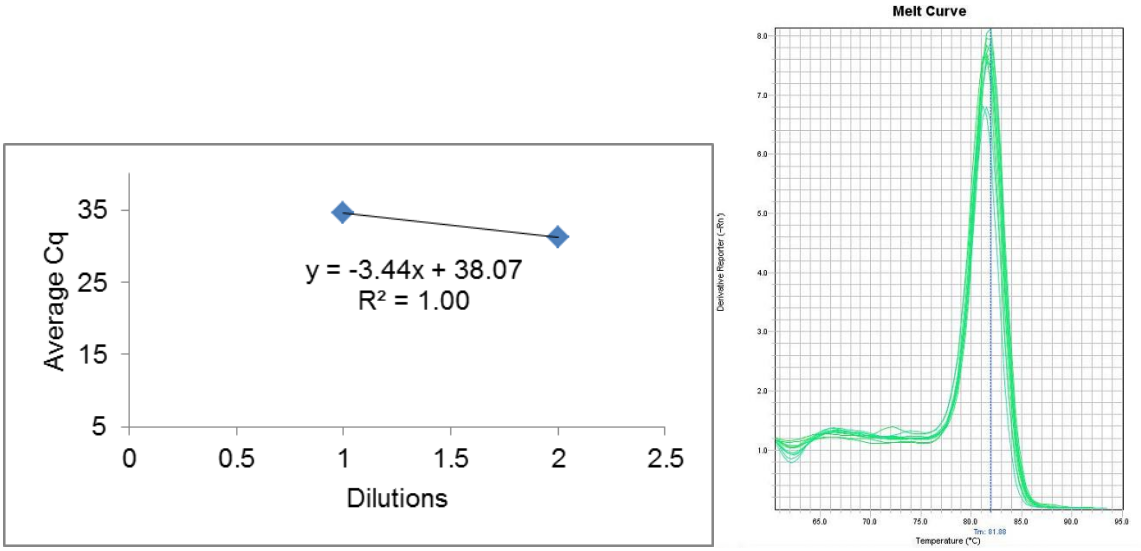

E = 0.95

Figure A.37. Dilution curve (left) and melt curve (right) for murine mtDnmt1 primer pair. Dilution curve was obtained by plotting the average Cq of three replicates of 10-fold serial dilutions of cDNA obtained by reverse transcription of 500 ng of total RNA, with dilution 2 being a dilution 1:2. "E" indicates the efficiency of amplification.

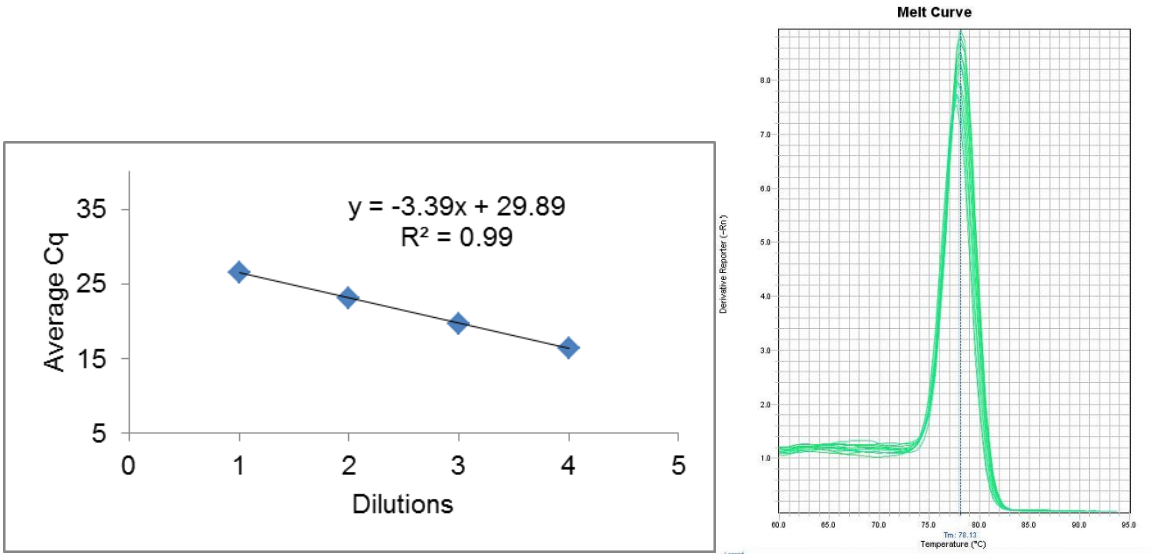

E = 0.97

Figure A.38. Dilution curve (left) and melt curve (right) for human B2M primer pair. Dilution curve was obtained by plotting the average Cq of three replicates of 10-fold serial dilutions of cDNA obtained by reverse transcription of 500 ng of total RNA, with dilution 4 being a dilution 1:2. "E" indicates the efficiency of amplification.

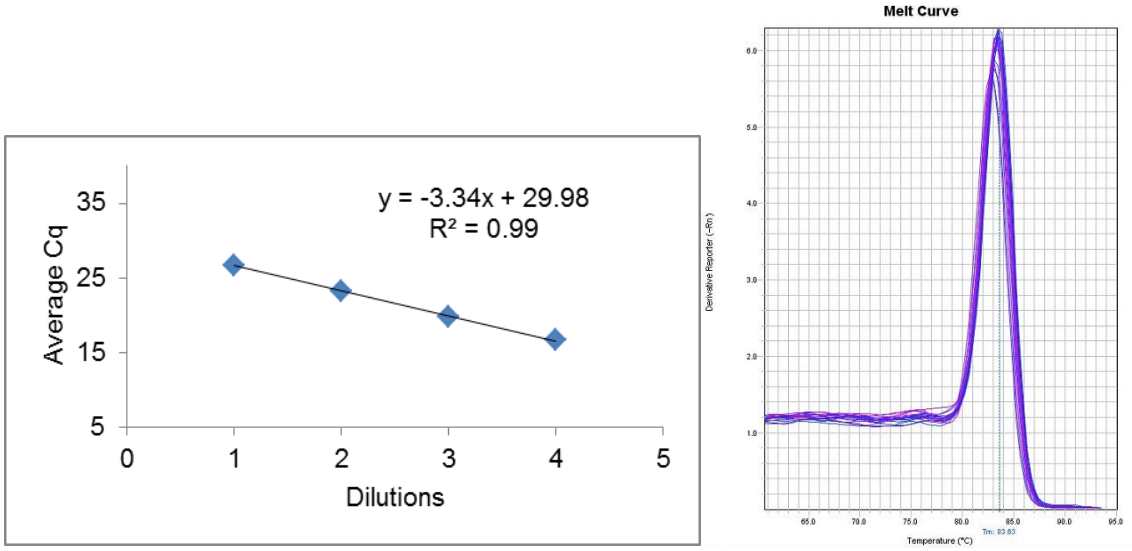

E = 0.99

Figure A.39. Dilution curve (left) and melt curve (right) for human GAPDH primer pair. Dilution curve was obtained by plotting the average Cq of three replicates of 10-fold serial dilutions of cDNA obtained by reverse transcription of 500 ng of total RNA, with dilution 4 being a dilution 1:2. "E" indicates the efficiency of amplification.

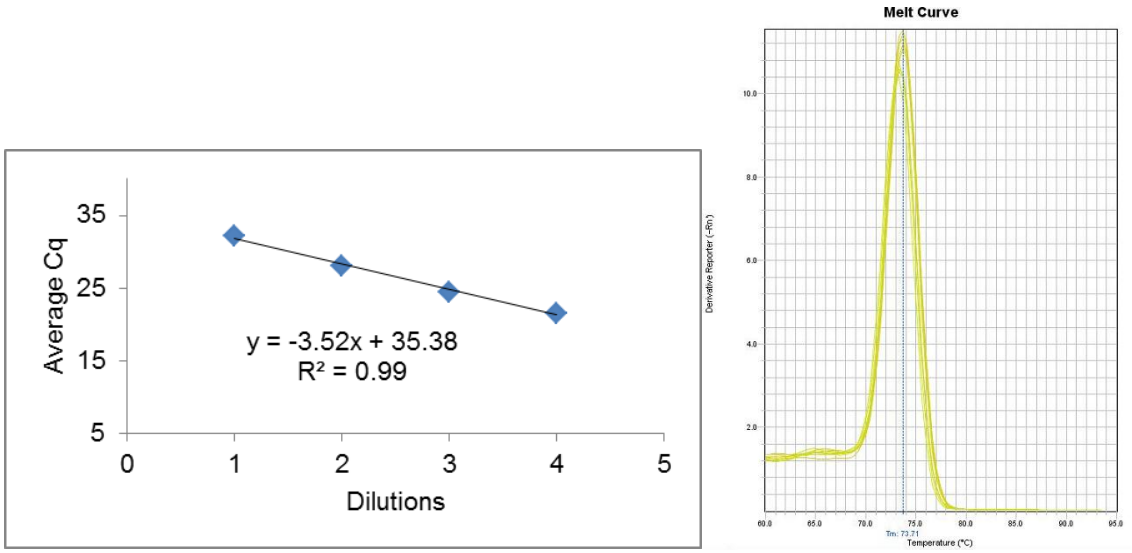

E = 0.92

Figure A.40. Dilution curve (left) and melt curve (right) for human HPRT1 primer pair. Dilution curve was obtained by plotting the average Cq of three replicates of 10-fold serial dilutions of cDNA obtained by reverse transcription of 500 ng of total RNA, with dilution 4 being a dilution 1:2. "E" indicates the efficiency of amplification.

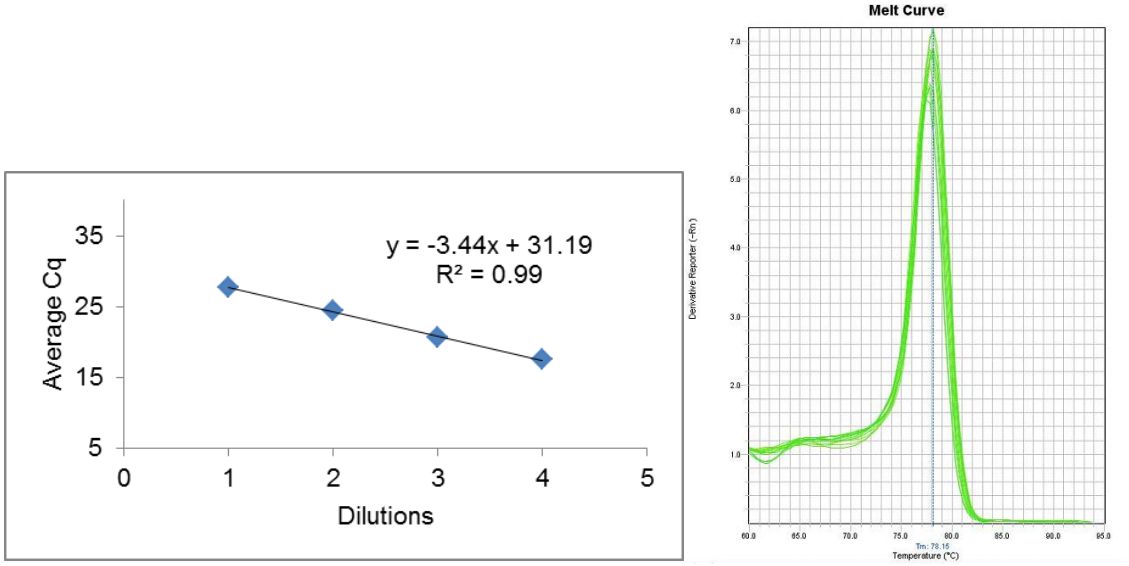

E = 0.95

Figure A.41. Dilution curve (left) and melt curve (right) for human UBE2B primer pair. Dilution curve was obtained by plotting the average Cq of three replicates of 10-fold serial dilutions of cDNA obtained by reverse transcription of 500 ng of total RNA, with dilution 4 being a dilution 1:2. "E" indicates the efficiency of amplification.

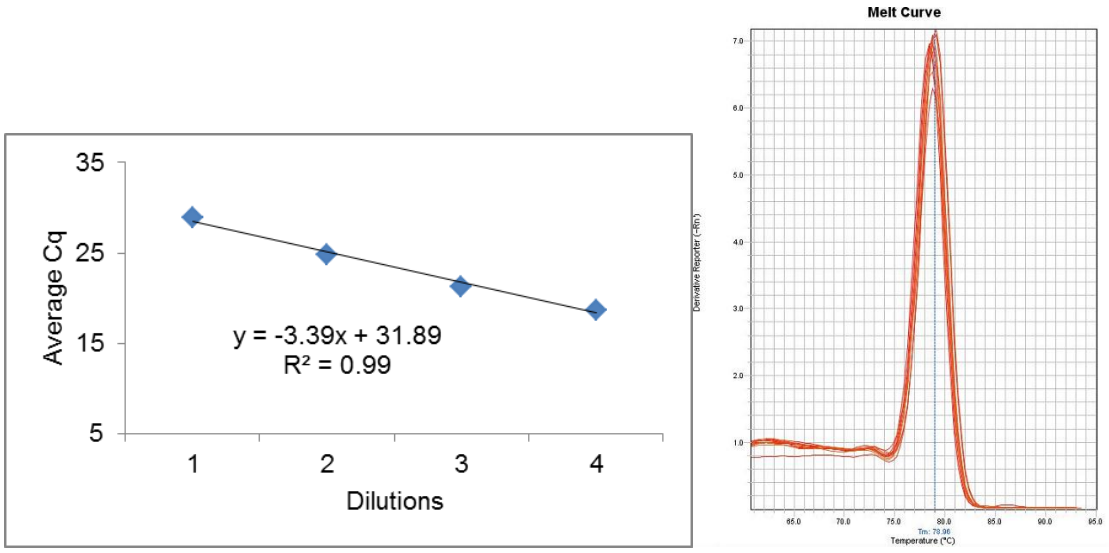

E = 0.97

Figure A.42. Dilution curve (left) and melt curve (right) for murine Actb primer pair. Dilution curve was obtained by plotting the average Cq of three replicates of 10-fold serial dilutions of cDNA obtained by reverse transcription of 500 ng of total RNA, with dilution 4 being the undiluted cDNA. "E" indicates the efficiency of amplification.

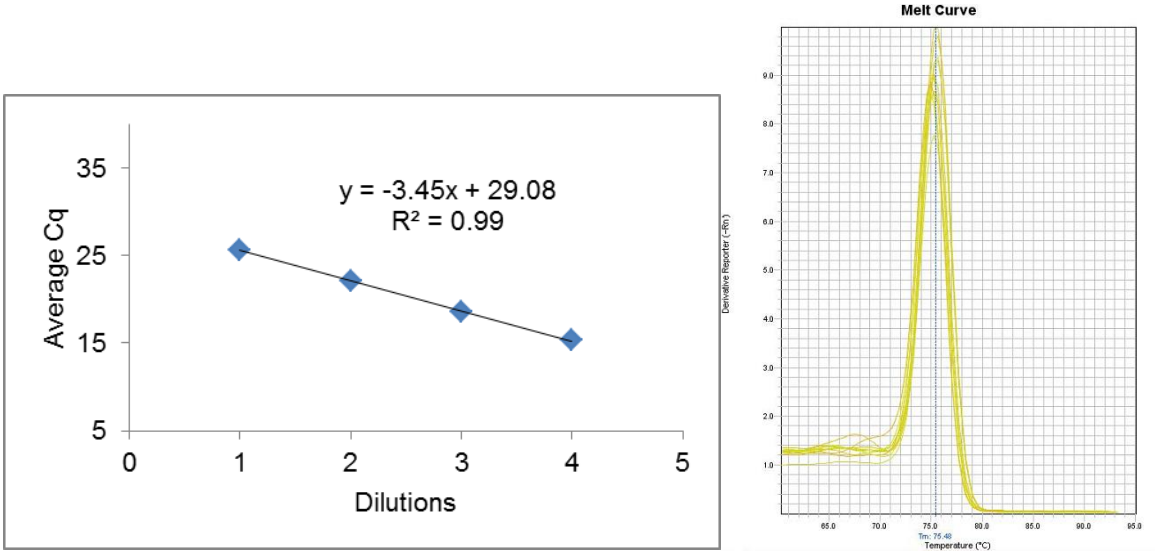

E = 0.95

Figure A.43. Dilution curve (left) and melt curve (right) for murine B2m primer pair. Dilution curve was obtained by plotting the average Cq of three replicates of 10-fold serial dilutions of cDNA obtained by reverse transcription of 500 ng of total RNA, with dilution 4 being a dilution 1:2. "E" indicates the efficiency of amplification.

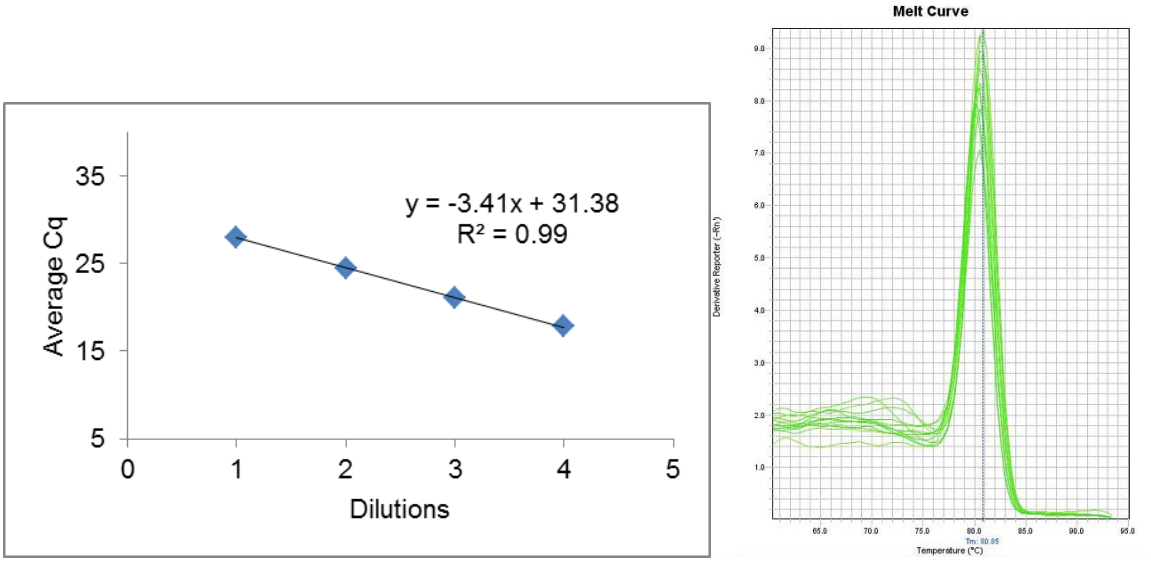

E = 0.96

Figure A.44. Dilution curve (left) and melt curve (right) for murine Gapdh primer pair. Dilution curve was obtained by plotting the average Cq of three replicates of 10-fold serial dilutions of cDNA obtained by reverse transcription of 500 ng of total RNA, with dilution 4 being a dilution 1:2. "E" indicates the efficiency of amplification.

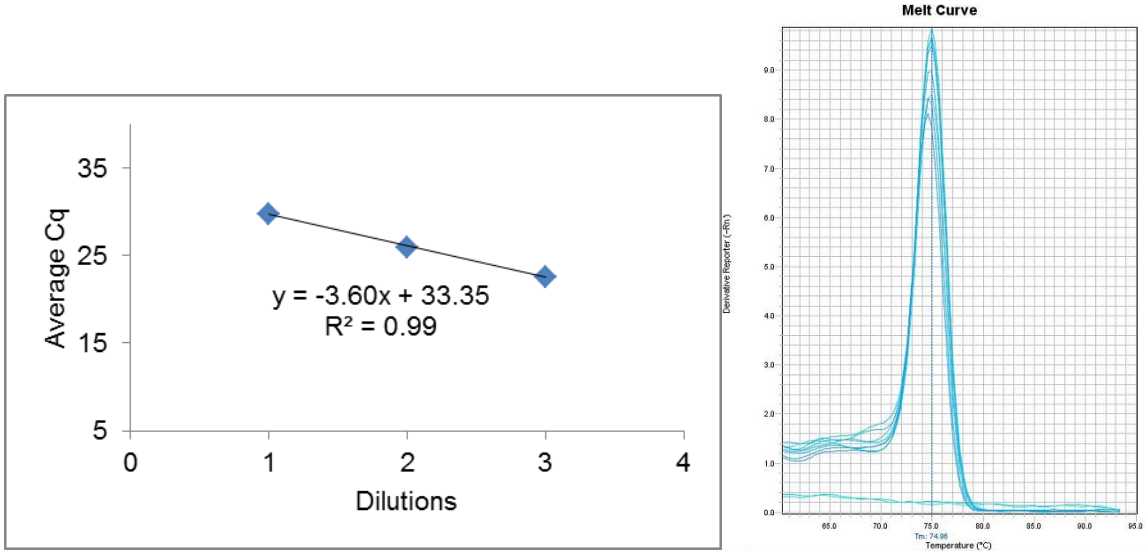

E = 0.89

Figure A.45. Dilution curve (left) and melt curve (right) for murine Hprt primer pair. Dilution curve was obtained by plotting the average Cq of three replicates of 10-fold serial dilutions of cDNA obtained by reverse transcription of 500 ng of total RNA, with dilution 3 being a dilution 1:2. "E" indicates the efficiency of amplification.

Appendix B: Quality control outputs for BM-DNA PCR direct sequencing

Table B.1. Quality control output for BM-DNA PCR sequences analyzed by BiQ BioAnalyzer software (Bock et al., 2005).

Specificity	BM-DNA PCR product	Sequence alignment	Bisulphite conversion rate
Human	LINE-1 MRC-5 YC A	95%	95%
Human	LINE-1 MRC-5 YC B	95%	95%
Human	LINE-1 MRC-5 YC C	95%	94%
Human	LINE-1 MRC-5 ESIPS A	95%	95%
Human	LINE-1 MRC-5 ESIPS B	95%	97%
Human	LINE-1 MRC-5 ESIPS C	96%	95%
Human	LINE-1 MRC-5 RS A	95%	95%
Human	LINE-1 MRC-5 RS B	95%	94%
Human	LINE-1 MRC-5 RS C	95%	95%
Mouse	B1 Heart 3 m. o. A	78%	95%
Mouse	B1 Heart 3 m. o. B	78%	100%
Mouse	B1 Heart 3 m. o. C	79%	95%
Mouse	B1 Heart 32 m. o. A	80%	100%
Mouse	B1 Heart 32 m. o. B	78%	94%
Mouse	B1 Heart 32 m. o. C	78%	100%
Mouse	B1 Liver 6 Young	79%	100%
Mouse	B1 Liver 7 Young	84%	100%
Mouse	B1 Liver 8 Young	76%	95%
Mouse	B1 Liver 6 Old	82%	100%
Mouse	B1 Liver 7 Old	79%	95%
Mouse	B1 Liver 8 Old	78%	100%
Mouse	B1 Colon 3 m. o. A	85%	100%
Mouse	B1 Colon 3 m. o. B	87%	100%
Mouse	B1 Colon 3 m. o. C	82%	100%
Mouse	B1 Colon 32 m. o. A	86%	100%

Mouse	B1 Colon 32 m. o. B	82%	100%
Mouse	B1 Colon 32 m. o. C	88%	100%
Mouse	B1 Liver 6(B)AL	85%	100%
Mouse	B1 Liver 6(4)AL	77%	100%
Mouse	B1 Liver 7(1)AL	81%	100%
Mouse	B1 Liver 14(2)CR	81%	100%
Mouse	B1 Liver 14(3)CR	76%	100%
Mouse	B1 Liver 14(4)CR	80%	100%
Human	H19 ICR MRC-5 YC	89%	100%
Human	H19 ICR MRC-5 ESIPS	91%	97%
Human	H19 ICR MRC-5 RS	91%	100%
Human	HIST1H2BA MRC-5 YC	95%	100%
Human	HIST1H2BA MRC-5 ESIPS	92%	94%
Human	HIST1H2BA MRC-5 RS	95%	100%
Human	GAPDH MRC-5 YC	90%	100%
Human	GAPDH MRC-5 ESIPS	85%	96%
Human	GAPDH MRC-5 RS	86%	100%
Mouse	H19 ICR Colon 3 m. o. A	89%	100%
Mouse	H19 ICR Colon 3 m. o. B	89%	100%
Mouse	H19 ICR Colon 3 m. o. C	85%	100%
Mouse	H19 ICR Colon 32 m. o. A	82%	100%
Mouse	H19 ICR Colon 32 m. o. B	81%	93%
Mouse	H19 ICR Colon 32 m. o. C	83%	100%
Mouse	Hist1h2ba Colon 3 m. o. A	95%	98%
Mouse	Hist1h2ba Colon 3 m. o. B	95%	98%
Mouse	Hist1h2ba Colon 3 m. o. C	96%	98%
Mouse	Hist1h2ba Colon 32 m. o. A	96%	98%
Mouse	Hist1h2ba Colon 32 m. o. B	95%	98%
Mouse	Hist1h2ba Colon 32 m. o. C	95%	98%
Mouse	Actb Colon 3 m. o. A	79%	100%
Mouse	Actb Colon 3 m. o. B	85%	87%

Mouse	Actb Colon 3 m. o. C	82%	93%
Mouse	Actb Colon 32 m. o. A	84%	92%
Mouse	Actb Colon 32 m. o. B	77%	91%
Mouse	Actb Colon 32 m. o. C	66%	92%
Mouse	Gapdh Colon 3 m. o. A	90%	97%
Mouse	Gapdh Colon 3 m. o. B	90%	100%
Mouse	Gapdh Colon 3 m. o. C	93%	100%
Mouse	Gapdh Colon 32 m. o. A	90%	93%
Mouse	Gapdh Colon 32 m. o. B	89%	100%
Mouse	Gapdh Colon 32 m. o. C	92%	100%

Table B.2. Quality control output for BM-DNA PCR and cloning sequences analyzed by BiQ BioAnalyzer software (Bock et al., 2005).

Specificity	**BM-DNA PCR product**	**Sequence alignment**	**Bisulphite conversion rate**
Mouse	Actb Heart 3 m. o. B clone 2	100%	100%
Mouse	Actb Heart 3 m. o. B clone 3	100%	100%
Mouse	Actb Heart 3 m. o. B clone 4	100%	100%
Mouse	Actb Heart 3 m. o. B clone 5	100%	100%
Mouse	Actb Heart 3 m. o. B clone 6	100%	100%
Mouse	Actb Heart 3 m. o. B clone 7	100%	100%
Mouse	Actb Heart 3 m. o. B clone 8	100%	100%
Mouse	Actb Heart 3 m. o. B clone 9	100%	100%
Mouse	Actb Heart 3 m. o. B clone 10	100%	100%
Mouse	Actb Heart 3 m. o. B clone 11	100%	100%
Mouse	Actb Colon 3 m. o. B clone 11	100%	100%
Mouse	Actb Colon 3 m. o. B clone 12	100%	100%
Mouse	Actb Colon 3 m. o. B clone 13	100%	100%
Mouse	Actb Colon 3 m. o. B clone 14	100%	100%
Mouse	Actb Colon 3 m. o. B clone 15	100%	100%
Mouse	Actb Colon 3 m. o. B clone 16	100%	100%

Mouse	Actb Colon 3 m. o. B clone 17	100%	100%
Mouse	Actb Colon 3 m. o. B clone 18	100%	100%
Mouse	Actb Colon 3 m. o. B clone 19	100%	100%
Mouse	Actb Colon 3 m. o. B clone 20	100%	100%

Table B.3. Quality control output for BM-DNA PCR sequences analyzed by ESME software (Lewin et al., 2004).

Specificity	**BM-PCR product**	**Alignment error**	**Signal admixtures**
λ-Phage	Fragment A 0% methylation	1%	4%
λ-Phage	Fragment A 5% methylation	2%	6%
λ-Phage	Fragment A 25% methylation	6%	15%
λ-Phage	Fragment A 50% methylation	22%	22%
λ-Phage	Fragment A 75% methylation	1%	11%
λ-Phage	Fragment A 95% methylation	2%	3%
λ-Phage	Fragment A 100% methylation	2%	3%
Human	MT-COI YC	4%	23%
Human	MT-COI ESIPS	1%	25%
Human	MT-COI RS	2%	23%
Human	MT-non coding region YC	0%	4%
Human	MT-non coding region ESIPS	0%	7%
Human	MT-non coding region RS	0%	5%
Human	MT-ND1 YC	0%	15%
Human	MT-ND1 ESIPS	1%	14%
Human	MT-ND1 RS	0%	14%
Human	MT-ND4 YC	2%	12%
Human	MT-ND4 ESIPS	0%	11%
Human	MT-ND4 RS	1%	11%
Human	MT-ND5 YC	1%	10%
Human	MT-ND5 ESIPS	0%	10%
Human	MT-ND5 RS	1%	11%

Mouse	Mt-D-Loop Liver 6 Young	1%	10%
Mouse	Mt-D-Loop Liver 7 Young	0%	9%
Mouse	Mt-D-Loop Liver 8 Young	1%	10%
Mouse	Mt-D-Loop Liver 6 Old	2%	8%
Mouse	Mt-D-Loop Liver 7 Old	1%	9%
Mouse	Mt-D-Loop Liver 8 Old	1%	8%
Mouse	Mt-D-Loop Liver 6(B)AL	1%	8%
Mouse	Mt-D-Loop Liver 6(4)AL	1%	8%
Mouse	Mt-D-Loop Liver 7(1)AL	1%	10%
Mouse	Mt-D-Loop Liver 14(2)ER	1%	9%
Mouse	Mt-D-Loop Liver 14(3)ER	1%	14%
Mouse	Mt-D-Loop Liver 14(4)ER	0%	9%
Mouse	Mt-non coding region Liver 6 Young	4%	11%
Mouse	Mt-non coding region Liver 7 Young	4%	11%
Mouse	Mt-non coding region Liver 8 Young	3%	15%
Mouse	Mt-non coding region Liver 6 Old	3%	10%
Mouse	Mt-non coding region Liver 7 Old	3%	17%
Mouse	Mt-non coding region Liver 8 Old	4%	8%
Mouse	Mt-non coding region Liver 6(B)AL	4%	9%
Mouse	Mt-non coding region Liver 6(4)AL	5%	10%
Mouse	Mt-non coding region Liver 7(1)AL	5%	9%
Mouse	Mt-non coding region Liver 14(2)ER	5%	7%
Mouse	Mt-non coding region Liver 14(3)ER	1%	19%
Mouse	Mt-non coding region Liver 14(4)ER	5%	14%

Appendix C: Pyrograms for pyrosequencing assays controls

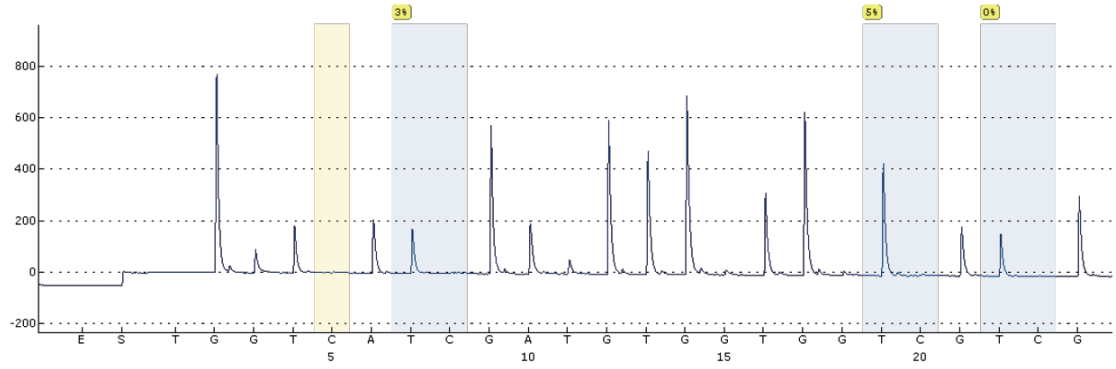

Figure C.1. 0% methylation control pyrogram for the Hs_CTTN_01 assay (Qiagen, catalog number PM00151844). Blue columns indicate the CpGs under investigation and the yellow column indicates the site for completion of the bisulphite treatment control.

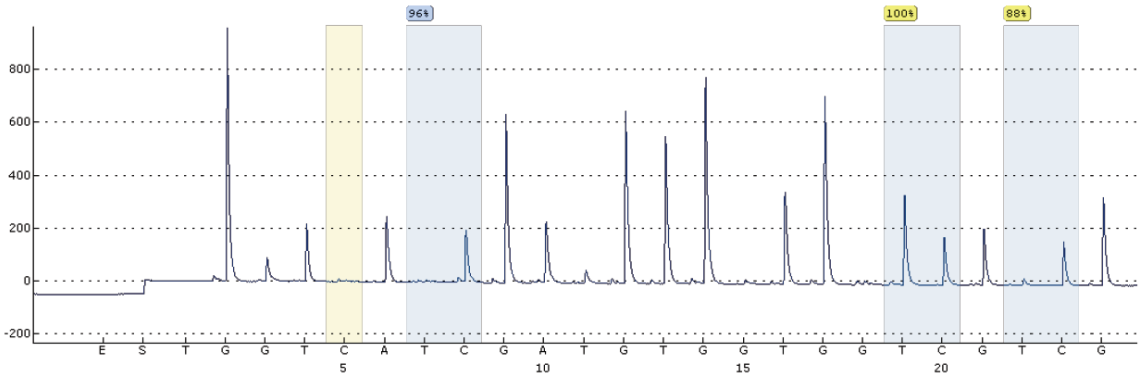

Figure C.2. 100% methylation control pyrogram for the Hs_CTTN_01 assay (Qiagen, catalog number PM00151844). Blue columns indicate the CpGs under investigation and the yellow column indicates the site for completion of the bisulphite treatment control.

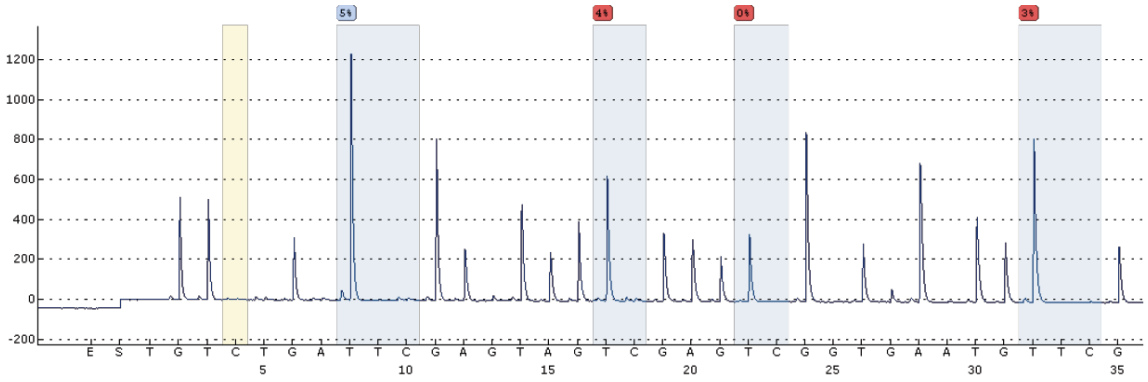

Figure C.3. 0% methylation control pyrogram for the Hs_GLIPR2_01 assay (Qiagen, catalog number PM00141176). Blue columns indicate the CpGs under investigation and the yellow column indicates the site for completion of the bisulphite treatment control. The red boxes on the top refer to sites that did not pass the quality controls and were excluded from further analyses.

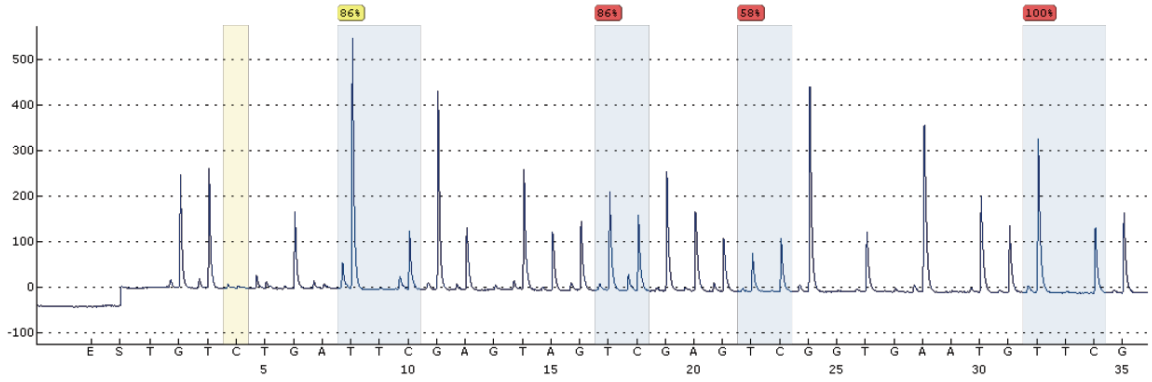

Figure C.4. 100% methylation control pyrogram for the Hs_GLIPR2_01 assay (Qiagen, catalog number PM00141176). Blue columns indicate the CpGs under investigation and the yellow column indicates the site for completion of the bisulphite treatment control. The red boxes on the top refer to sites that did not pass the quality controls and were excluded from further analyses.

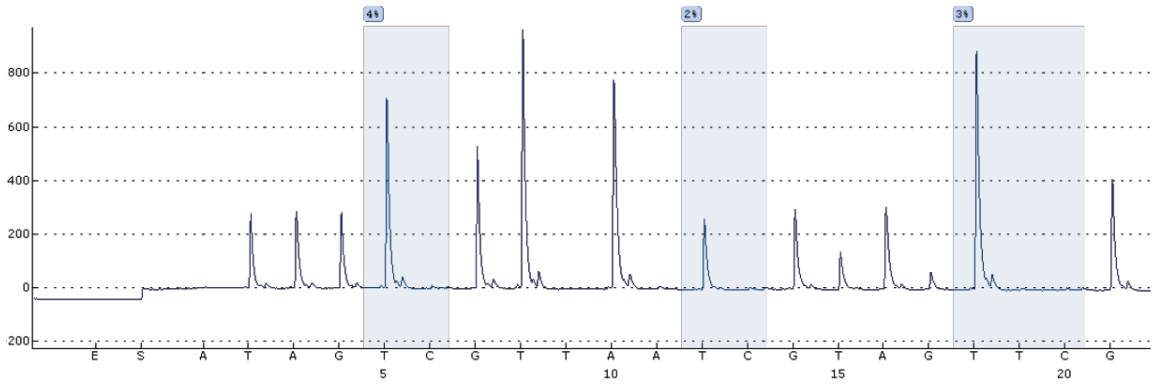

Figure C.5. 0% methylation control pyrogram for the Hs_NPTX1_03 assay (Qiagen, catalog number PM00182035). Blue columns indicate the CpGs under investigation.

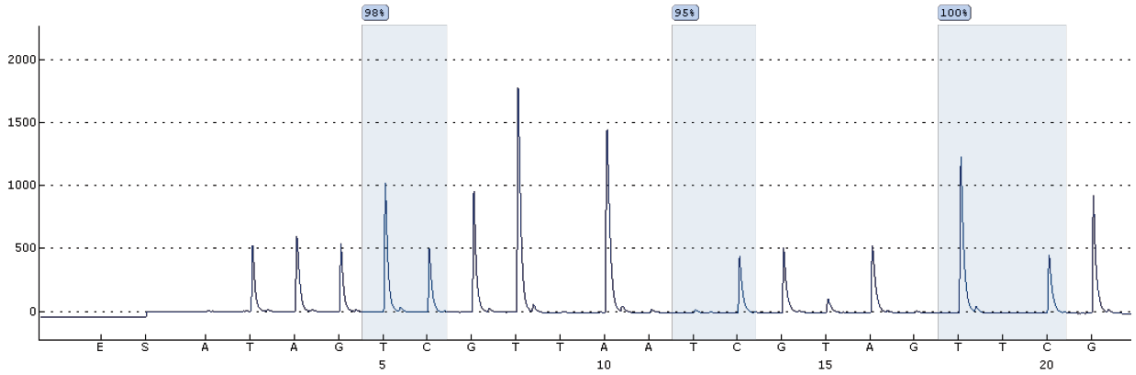

Figure C.6. 100% methylation control pyrogram for the Hs_NPTX1_03 assay (Qiagen, catalog number PM00182035). Blue columns indicate the CpGs under investigation.

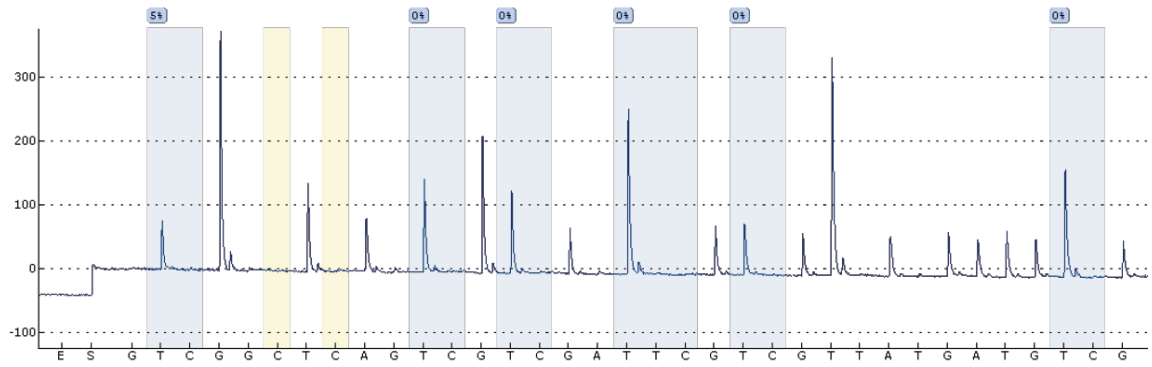

Figure C.7. 0% methylation control pyrogram for the Hs_NPTX1_07 assay (Qiagen, catalog number PM00182063). Blue columns indicate the CpGs under investigation and yellow columns indicate sites for completion of the bisulphite treatment control.

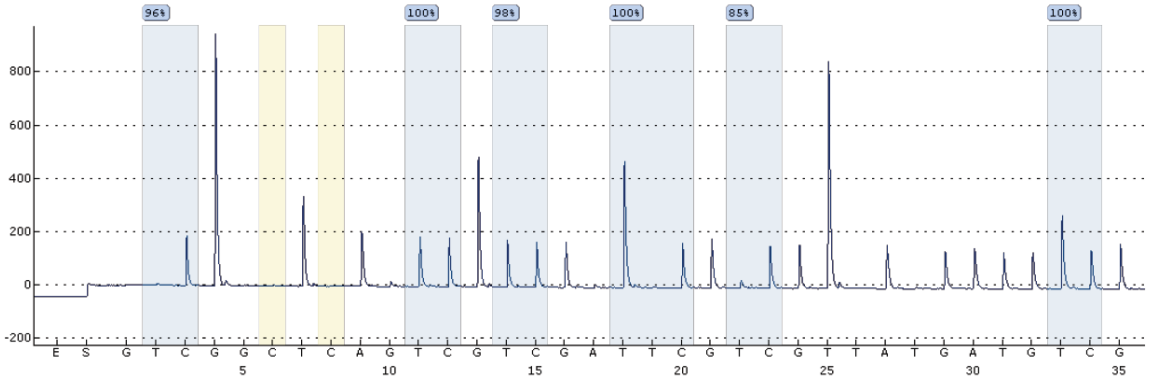

Figure C.8. 100% methylation control pyrogram for the Hs_NPTX1_07 assay (Qiagen, catalog number PM00182063). Blue columns indicate the CpGs under investigation and yellow columns indicate sites for completion of the bisulphite treatment control.

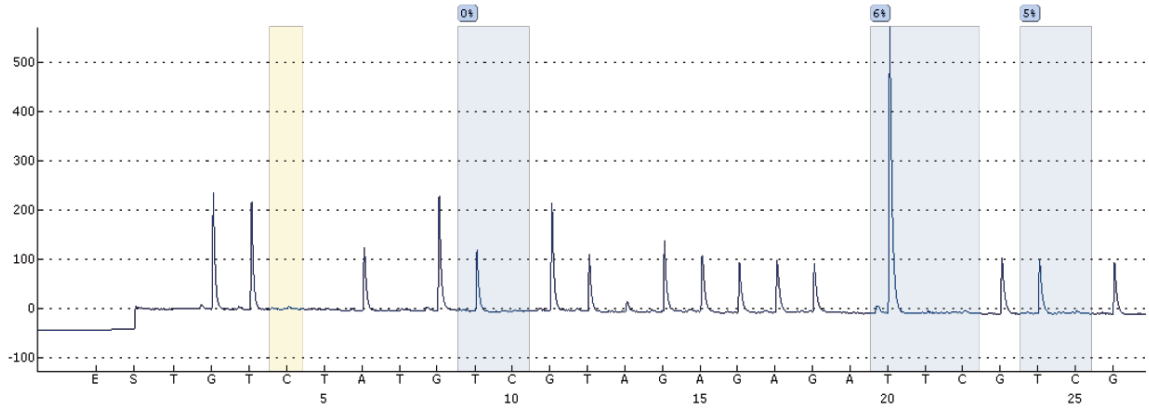

Figure C.9. 0% methylation control pyrogram for the Hs_SLC39A14_01 assay (Qiagen, catalog number PM00136598). Blue columns indicate the CpGs under investigation and the yellow column indicates a site for completion of the bisulphite treatment control.

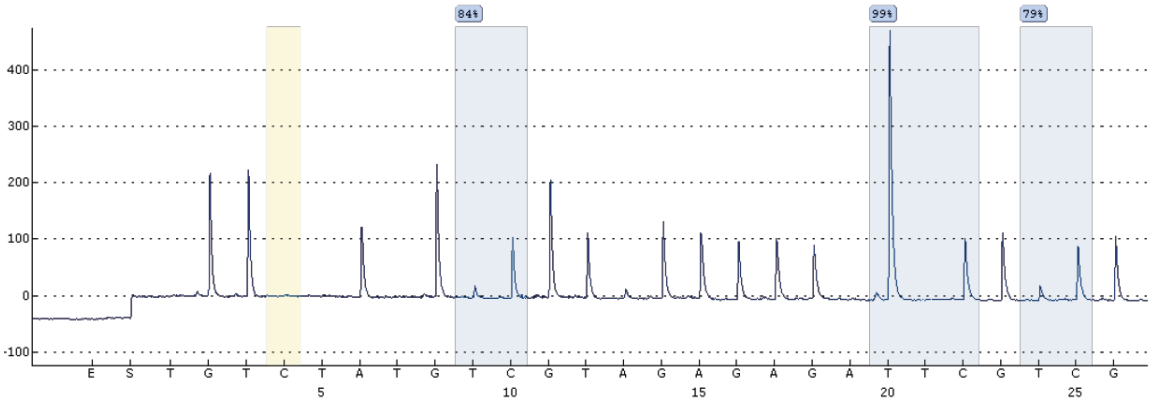

Figure C.10. 100% methylation control pyrogram for the Hs_SLC39A14_01 assay (Qiagen, catalog number PM00136598). Blue columns indicate the CpGs under investigation and the yellow column indicates a site for completion of the bisulphite treatment control.

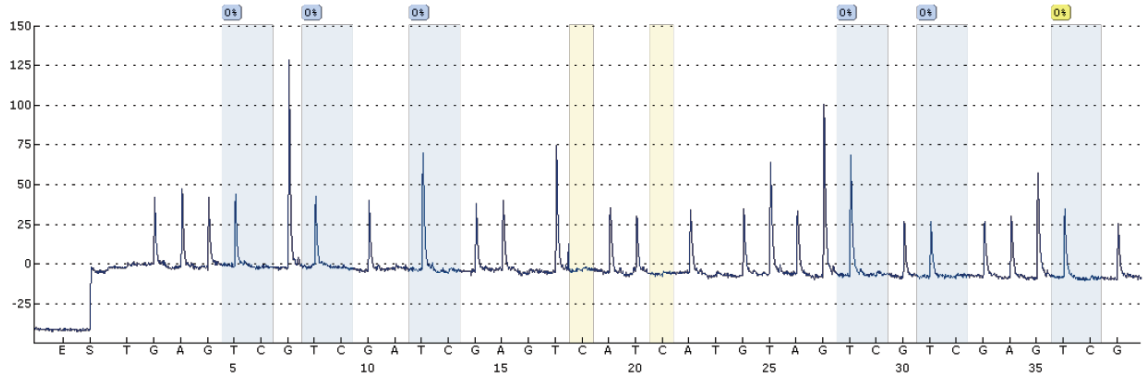

Figure C.11. 0% methylation control pyrogram for the Hs_SLC39A14_02 assay (Qiagen, catalog number PM00136605). Blue columns indicate the CpGs under investigation and yellow columns indicate sites for completion of the bisulphite treatment control.

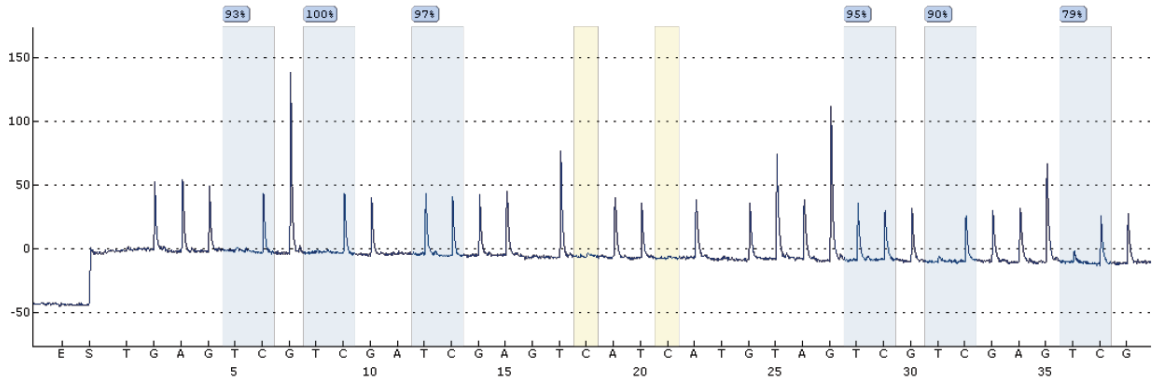

Figure C.12. 100% methylation control pyrogram for the Hs_SLC39A14_02 assay (Qiagen, catalog number PM00136605). Blue rectangles indicate the CpGs under investigation and yellow columns indicate sites for completion of the bisulphite treatment control.

Appendix D: Confirmation of specificity of qPCR products used for calculations of methylation enrichments

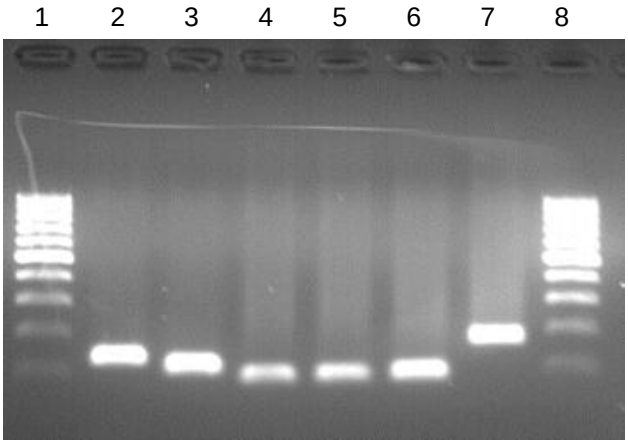

Figure D.1. Agarose/TBE gel run of human qPCR products for MeDIP enrichment calculations. Lanes 1 and 8 = 100 bp DNA Ladder, lane 2 = H19 PCR product, lane 4 = HIST1H2BA PCR product, lane 6 = GAPDH PCR product. The remaining lanes show runs of PCR products not related to this study.

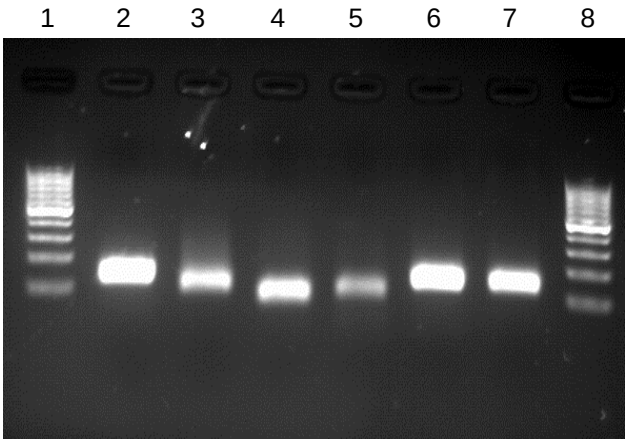

Figure D.2. Agarose/TBE gel run of murine qPCR products for MeDIP enrichment calculations. Lanes 1 and 8 = 100 bp DNA Ladder, lane 2 = H19 PCR product, lane 4 = Hist1h2ba PCR product, lane 5 = Actb PCR product, lane 7 = Gapdh PCR product. The remaining lanes show runs of PCR products not related to this study.

H19 = chr11:2020940-2021073. 100% sequence match

Human genome assembly GRCh37/h19

```
0000023 gagccgcaccagatcttcaggtcgggcattatccacagccccgtggcccc 0000072
<<<<<<< |||||||||||||||||||||||||||||||||||||||||||||||||| <<<<<<<
2021073 gagccgcaccagatcttcaggtcgggcattatccacagccccgtggcccc 2021024

0000073 gggtcacactccgagggcttcagtgtcatggcctgggactcaagtcacgc 0000122
<<<<<<< |||||||||||||||||||||||||||||||||||||||||||||||||| <<<<<<<
2021023 gggtcacactccgagggcttcagtgtcatggcctgggactcaagtcacgc 2020974

0000123 ctacttatgtgatgatcacagtgtgttccaccaaa.tctt 0000161
<<<<<<< |||||||||||||||||||||||||||||||||| |||| <<<<<<<
2020973 ctacttatgtgatgatcacagtgtgttccaccaaaatctt 2020934
```

HIST1H2BA = chr6:25727004+25727094. 100% sequence match

Human genome assembly GRCh37/h19

```
00000035 tgtttgtttacttggcgagacttggagctgaggtcatttggagctgttta 00000084
>>>>>>>> |||||||||||||||||||||||||||||||||||||||||||||||||| >>>>>>>>
25727004 tgtttgtttacttggcgagacttggagctgaggtcatttggagctgttta 25727053

00000085 atactgaagagctgttgagcactggaaagtgctgtgtaacc 00000125
>>>>>>>> ||||||||||||||||||||||||||||||||||||||| >>>>>>>>
25727054 atactgaagagctgttgagcactggaaagtgctgtgtaacc 25727094
```

GAPDH = chr12:6645023+6645112. 100% sequence match

Human genome assembly GRCh37/h19

```
0000024 ctctctcccatcccttctccccacacacatgcacttacctgtgctcccac 0000073
>>>>>>> |||||||||||||||||||||||||||||||||||||||||||||||||| >>>>>>>
6645023 ctctctcccatcccttctccccacacacatgcacttacctgtgctcccac 6645072

0000074 tcctgatttctggaaaagagctaggaaggacaggcaactt 0000113
>>>>>>> ||||||||||||||||||||||||||||||||||||||| >>>>>>>
6645073 tcctgatttctggaaaagagctaggaaggacaggcaactt 6645112
```

Figure D.3. BLAT (BLAST-Like Alignment Tool) analyses output for cloned human qPCR products used for methylation enrichment calculations in Chapter 4.

H19 = chr7:149767910-149768055. 99.4% sequence match

Mouse genome assembly NCBI37/mm9

```
000000032 tacattcacacgagcatccaggaggcataagaattctgcaaggagaccat 000000081
<<<<<<<<< |||||||||||||||||||||||||||||||||||||||||||||||||| <<<<<<<<<
149768056 tacattcacacgagcatccaggaggcataagaattctgcaaggagaccat 149768007

000000082 gccctactcttggacgtctgctgaatcagttgtggggtttatacgcggga 000000131
<<<<<<<<< |||||| |||||||||||||||||||||||||||||||||||||||||| <<<<<<<<<
149768006 gccctattcttggacgtctgctgaatcagttgtggggtttatacgcggga 149767957

000000132 gttgccgcgtggtggcagcaaaatcgattgcgccaaacctaaagagc 000000178
<<<<<<<<< |||||||||||||||||||||||||||||||||||||||||||| <<<<<<<<<
149767956 gttgccgcgtggtggcagcaaaatcgattgcgccaaacctaaagagc 149767910
```

Hist1h2ba = chr13:24025814-24025892. 100% sequence match

Mouse genome assembly NCBI37/mm9

```
00000041 aggtgctg.aacaagtgcaccccgacaccggcatctcctccaaggccatg 00000089
<<<<<<<< |||||||| |||||||||||||||||||||||||||||||||||| <<<<<<<<
24025892 aggtgctgaaacaagtgcaccccgacaccggcatctcctccaaggccatg 24025843

00000090 agcatcatgaactcctttgtgacagacat 00000118
<<<<<<<< |||||||||||||||||||||||||||| <<<<<<<<
24025842 agcatcatgaactcctttgtgacagacat 24025814
```

Actb = chr5:143665852-143665948. 100% of sequence match

Mouse genome assembly NCBI37/mm9

```
000000025 tttctgtcactcttctcttaggtatggaatcctgtggcatccatgaaact 000000074
<<<<<<<<< |||||||||||||||||||||||||||||||||||||||||||||||||| <<<<<<<<<
143665948 tttctgtcactcttctcttaggtatggaatcctgtggcatccatgaaact 143665899

000000075 acattcaattccatcatgaagtgtgacgttgacatccgtaaagacct 000000121
<<<<<<<<< |||||||||||||||||||||||||||||||||||||||||||||||| <<<<<<<<<
143665898 acattcaattccatcatgaagtgtgacgttgacatccgtaaagacct 143665852
```

Gapdh = chr6:125115488-125115620. 97.8% sequence match

Mouse genome assembly NCBI37/mm9

```
00000107 ctggcactgcacaagaagatgcggccgtctctggaacagggaggagcaga 00000156
<<<<<<<< ||||||  |||||||||||||||| |||| | |||| |||||||||||| <<<<<<<<
47061869 ctggcaaagcacaagaagatgcggctgtctgttgaac.gggaggagcaga 47061821

00000157 ga 00000158
<<<<<<<< || <<<<<<<<
47061820 ga 47061819
```

Figure D.4. BLAT (BLAST-Like Alignment Tool) analyses output for cloned murine qPCR products used for methylation enrichment calculations in Chapter 4.

Appendix E: Differentially methylated Entrez Gene IDs in replicative senescent and early stress premature induced senescent compared with young confluent MRC-5 cells

Table E1. Significant differentially methylated Entrez Gene ID between replicative senescent and young confluent MRC-5 cells.

Entrez Gene ID	Gene symbol	Delta enrichment	Entrez Gene ID	Gene symbol	Delta enrichment
2	A2M	3.11	1535	CYBA	-2.32
21	ABCA3	-1.95	1548	CYP2A6	1.87
21	ABCA3	-3.73	1548	CYP2A6	0.37
118	ADD1	-1.63	1553	CYP2A13	0.77
182	JAG1	1.50	1553	CYP2A13	0.38
398	ARHGDIG	-2.41	1634	DCN	-0.19
475	ATOX1	0.62	1656	DDX6	3.14
479	ATP12A	3.65	1773	DNASE1	-4.41
481	ATP1B1	-1.75	1837	DTNA	0.83
514	ATP5E	-2.47	1843	DUSP1	-2.59
547	KIF1A	-2.11	1870	E2F2	-1.08
658	BMPR1B	-1.27	1875	E2F5	-2.31
678	ZFP36L2	-1.31	1902	LPAR1	1.07
757	TMEM50B	-2.95	1908	EDN3	-1.35
766	CA7	-3.63	1908	EDN3	-2.14
766	CA7	-4.59	1952	CELSR2	-4.20
793	CALB1	1.02	1991	ELA2	-3.25
800	CALD1	0.18	2017	CTTN	-2.15
800	CALD1	0.15	2035	EPB41	1.81
818	CAMK2G	-2.76	2046	EPHA8	-2.49
866	SERPINA6	-0.05	2051	EPHB6	-0.35
924	CD7	0.00	2069	EREG	-0.05
1147	CHUK	1.64	2109	ETFB	2.54
1159	CKMT1A	1.51	2178	FANCE	-2.42
1159	CKMT1A	1.22	2213	FCGR2C	0.93
1191	CLU	0.63	2244	FGB	0.01
1297	COL9A1	-2.60	2268	FGR	-3.03
1301	COL11A1	0.96	2302	FOXJ1	-2.88
1393	CRHBP	0.32	2527	FUT5	3.09
1396	CRIP1	-0.90	2664	GDI1	-0.98
1429	CRYZ	-0.10	2689	GH2	1.48
1435	CSF1	-0.87	2898	GRIK2	0.60

1468	SLC25A10	-1.05	2915	GRM5	0.00
1486	CTBS	3.06	2961	GTF2E2	3.85
1497	CTNS	-2.31	2972	BRF1	-1.95
3000	GUCY2D	-2.71	6154	RPL26	-1.76
3149	HMGB3	1.91	6154	RPL26P6	-1.76
3149	HMGB3	0.07	6232	RPS27	-1.74
3201	HOXA4	-1.57	6310	ATXN1	-1.47
3337	DNAJB1	-1.42	6310	ATXN1	-2.84
3484	IGFBP1	0.32	6432	SFRS7	0.52
3642	INSM1	-1.14	6506	SLC1A2	2.11
3642	INSM1	-1.94	6553	SLC9A5	-1.15
3732	CD82	-1.81	6570	SLC18A1	0.59
3769	KCNJ13	0.04	6614	SIGLEC1	1.88
3895	KTN1	-2.26	6620	SNCB	1.22
3909	LAMA3	3.00	6622	SNCA	1.91
3918	LAMC2	1.54	6643	SNX2	0.79
3918	LAMC2	0.06	6760	SS18	-2.94
4033	LRMP	0.85	6818	SULT1A3	-1.91
4062	LY6H	-1.88	6919	TCEA2	-5.60
4099	MAG	-2.56	7107	GPR137B	-1.77
4121	MAN1A1	-0.20	7138	TNNT1	1.53
4121	MAN1A1	-0.67	7465	IE1	-0.64
4359	MPZ	0.30	7483	WNT9A	-2.58
4482	MSRA	-0.38	7512	XPNPEP2	0.66
4833	NME4	-1.47	7536	SF1	-1.80
4833	NME4	-1.93	7580	ZNF32	0.69
4884	NPTX1	-2.27	7587	ZNF37A	1.05
4900	NRGN	0.30	7587	ZNF37A	0.56
4935	GPR143	1.26	7629	ZNF76	1.24
4967	OGDH	0.59	8110	DPF3	-0.81
5052	PRDX1	0.54	8284	JARID1D	-0.02
5105	PCK1	-4.14	8290	HIST3H3	-1.25
5127	PCTK1	-4.00	8313	AXIN2	3.86
5274	SERPINI1	-3.00	8322	FZD4	-2.91
5321	PLA2G4A	0.75	8471	IRS4	-1.95
5465	PPARA	-1.64	8622	PDE8B	-1.93
5493	PPL	-1.25	8644	AKR1C3	0.03
5534	PPP3R1	-1.97	8655	DYNLL1	-1.73
5654	HTRA1	2.88	8717	TRADD	6.95
5726	TAS2R38	-0.15	8767	RIPK2	-0.42
5793	PTPRG	-2.44	8776	MTMR1	-2.78

5795	PTPRJ	-1.59	8913	CACNA1G	-3.38
5830	PEX5	-2.03	8934	RAB7L1	2.95
5878	RAB5C	3.75	8934	RAB7L1	0.29
8938	BAIAP3	-2.47	22841	RAB11FIP2	1.02
8997	KALRN	0.14	22853	LMTK2	-1.75
9045	RPL14	1.34	22883	CLSTN1	-2.14
9085	CDY1B	-0.02	22883	CLSTN1	-2.97
9103	FCGR2C	0.93	22884	WDR37	-2.64
9144	SYNGR2	1.28	22897	CEP164	-1.14
9261	MAPKAPK2	0.87	22911	WDR47	-2.04
9308	CD83	-0.92	22978	NT5C2	1.35
9604	RNF14	1.08	22978	NT5C2	0.37
9622	KLK4	2.57	23126	POGZ	-0.82
9788	MTSS1	0.63	23126	POGZ	-1.33
9844	ELMO1	1.22	23303	KIF13B	-1.24
9942	XYLB	-1.88	23498	HAAO	1.42
9942	XYLB	-2.11	23516	SLC39A14	-3.28
9962	SLC23A2	-1.35	23521	RPL13A	-1.16
10073	SNUPN	-0.43	23530	NNT	-3.61
10098	TSPAN5	1.65	23530	NNT	-3.61
10120	ACTR1B	-0.51	23598	PATZ1	-0.65
10225	CD96	1.14	23641	LDOC1	-4.94
10312	TCIRG1	-2.71	23729	SHPK	-2.31
10312	TCIRG1	-4.43	23761	PISD	1.94
10455	PECI	0.16	26012	NELF	-0.24
10463	SLC30A9	-2.39	26022	TMEM98	-2.13
10509	SEMA4B	-1.15	26059	ERC2	0.65
10541	ANP32B	0.91	26059	ERC2	0.22
10591	C6orf108	4.07	26136	TES	0.68
10591	C6orf108	0.13	26249	KLHL3	0.56
10602	CDC42EP3	-0.51	26292	MYCBP	-1.48
10668	CGRRF1	-1.25	26534	OR10G2	-1.70
10762	NUP50	-1.04	26534	OR10G2	-2.93
10797	MTHFD2	-1.27	27031	NPHP3	-1.11
10808	HSPH1	-1.34	27031	ACAD11	-1.11
10927	SPIN1	-1.88	27071	DAPP1	0.58
10963	STIP1	-0.92	27071	DAPP1	0.48
11072	DUSP14	-3.28	27164	SALL3	-0.29
11085	ADAM30	4.48	28985	MCTS1	0.28
11098	PRSS23	-0.69	29109	FHOD1	-1.15
11228	RASSF8	-1.70	29761	USP25	-2.00

11228	RASSF8	-2.76	29801	ZDHHC8	-2.74
11235	PDCD10	-3.00	30061	SLC40A1	3.27
11326	VSIG4	-0.29	30819	KCNIP2	1.42
30837	SOCS7	-2.74	57161	PELI2	-2.71
50964	SOST	1.50	57182	ANKRD50	-1.68
51083	GAL	2.11	57215	THAP11	-2.39
51084	CRYL1	-1.89	57402	S100A14	1.86
51087	YBX2	-2.66	57473	ZNF512B	-0.80
51151	SLC45A2	1.40	57473	ZNF512B	-1.45
51151	SLC45A2	0.00	57488	FAM62B	-0.93
51176	LEF1	0.86	57488	FAM62B	-1.10
51435	SCARA3	3.50	57509	MTUS1	0.78
51646	YPEL5	-3.36	57529	RGAG1	-2.55
51669	TMEM66	0.40	57563	KLHL8	0.98
54361	WNT4	-2.04	57567	ZNF319	-0.45
54463	FAM134B	0.35	57718	PPP4R4	-3.39
54522	ANKRD16	0.70	60487	TRMT11	-0.41
54537	FAM35A	-0.04	60494	CCDC81	0.40
54765	TRIM44	-1.00	63940		0.82
54899	PXK	3.32	64064	OXCT2	0.00
54899	PXK	2.18	64423	INF2	-1.74
54970	TTC12	-0.48	64579	NDST4	0.01
54984		-2.17	64856	VWA1	-2.51
55080	TAPBPL	3.66	65059	RAPH1	1.38
55105	GPATCH2	0.87	79058	ASPSCR1	-0.33
55112	WDR60	-1.62	79091	C16orf68	0.22
55160	ARHGEF10L	-1.20	79258	MMEL1	1.02
55196	C12orf35	-1.74	79650	C16orf57	-0.45
55303	GIMAP4	0.29	79671	NLRX1	1.02
55336	FBXL8	6.95	79671	NLRX1	0.92
55558	PLXNA3	-1.70	79698	ZMAT4	0.87
55608	ANKRD10	-1.57	79921	TCEAL4	0.66
55608	ANKRD10	-1.94	79948		-3.43
55624	POMGNT1	-1.38	80212	CCDC92	-3.17
55786	ZNF415	2.35	80235	PIGZ	-4.03
55852	TEX2	-0.93	80274	SCUBE1	-2.52
56122	PCDHB14	5.26	80305	TRABD	-3.55
56132	PCDHB3	0.42	80323	CCDC68	-0.80
56172	ANKH	-2.64	80331	DNAJC5	-1.50
56888	KCMF1	-0.86	80709	AKNA	1.24
56978	PRDM8	2.56	81566	CSRNP2	-0.71

57055	DAZ2	-3.61	81615	TMEM163	-0.86
57088	PLSCR4	-0.65	81615	TMEM163	-1.08
57156	TMEM63C	-0.84	81618	ITM2C	2.31
81894	SLC25A28	-2.18	158131	OR1Q1	0.72
83737	ITCH	-1.22	162517	FBXO39	-2.16
83935	TMEM133	-0.05	163183	C19orf46	0.00
83992	CTTNBP2	-2.51	192670	EIF2C4	-0.39
84263	HSDL2	0.28	192670	EIF2C4	-1.08
84309	NUDT16L1	-3.86	196883	ADCY4	2.11
84309	NUDT16L1	-4.19	201633	TIGIT	0.06
84504	NKX6-2	-0.78	202459	OSTCL	-0.54
84800	INF2	-1.74	219409	GSX1	-2.93
84893	FBXO18	0.70	219429	OR4C11	0.01
85474	LBX2	2.27	220988	HNRNPA3	-2.54
90423	ATP6V1E2	0.62	246330	PELI3	-1.99
91782	CHMP7	0.55	253175	CDY1B	-0.02
93010	B3GNT7	-1.21	253582	C6orf191	-0.87
93343	FAM125A	-0.71	253582	C6orf191	-1.10
94081	SFXN1	-1.33	283643	C14orf80	-0.90
115209	OMA1	1.76	284312	ZSCAN1	-2.69
123876	ACSM2A	1.15	284340	CXCL17	2.06
126123	C19orf41	-3.69	326624	RAB37	-2.09
126328	NDUFA11	3.09	343071	PRAMEF10	0.00
127253	TYW3	-0.10	343990	C2orf55	-1.05
128372	OR6N1	-3.00	348093	RBPMS2	1.80
130271	PLEKHH2	-2.69	348487	FAM131C	1.65
130814	PQLC3	-2.80	374407	DNAJB13	0.60
130951	C2orf65	2.67	374470	C12orf42	-1.58
136259	KLF14	-1.23	374928	ZNF773	4.74
138881	OR1L8	2.07	375607	C7orf52	2.47
138881	OR1L8	1.57	378832	C21orf123	-3.30
140731	ANKRD60	-1.06	389136	VGLL3	-3.79
144348	ZNF664	-3.17	390152	OR8H3	-0.77
145497	C14orf166B	-5.86	400509	RUNDC2B	5.63
145781	GRINL1A	-2.26	400509	RUNDC2B	5.62
146712	B3GNTL1	-1.45	440348		0.81
147199	SCGB1C1	-1.98	440435	GPR179	2.57
147339	C18orf25	-1.65	445329	SULT1A3	-1.91
149175	MANEAL	0.79	448834	KPRP	0.74
149650		-2.14	448834	KPRP	0.44
151449	GDF7	-2.55	548596	CKMT1A	1.51

151473	SLC16A14	1.01	548596	CKMT1A	1.22
644511	RPL13A	-1.16			
648581	ASPSCR1	-0.33			
151835	CPNE9	-0.81			
152007	GLIPR2	-2.20			
652251	GPSM1	-2.36			
728513	PNMA6A	-1.05			
100129905	RPS27	-1.74			
100130070	RPS27	-1.74			
100131572	RPS27	-1.74			
100132291	RPS27	-1.74			
100132353	GDI2	-0.78			
100133623	CKMT1A	1.51			
100133623	CKMT1A	1.22			
100134295	SLCO4A1	-2.14			

Table E2. Significant differentially methylated Entrez Gene ID between early stress-induced premature senescent and young confluent MRC-5 cells.

Entrez Gene ID	**Gene symbol**	**Delta enrichment**	**Entrez Gene ID**	**Gene symbol**	**Delta enrichment**
24	ABCA4	-3.65	820	CAMP	-2.86
24	ABCA4	-3.78	831	CAST	-1.39
118	ADD1	-1.73	831	CAST	-1.96
132	ADK	-1.52	840	CASP7	-5.17
320	APBA1	1.38	911	CD1C	-3.65
331	XIAP	-3.36	924	CD7	0.00
366	AQP9	-2.72	928	CD9	0.00
366	AQP9	-3.77	1025	CDK9	-1.66
430	ASCL2	-3.66	1063	CENPF	-3.86
522	ATP5J	-3.69	1260	CNGA2	-0.63
551	AVP	-1.94	1267	CNP	-2.28
701	BUB1B	1.24	1298	COL9A2	-2.99
722	C4BPA	-4.37	1390	CREM	-4.02
727	C5	0.00	1572	CYP2F1	1.03
745	C11orf9	-3.61	1634	DCN	-0.19
801	CALM2	-5.44	1727	CYB5R3	-3.09
805	CALM2	-5.69	1727	CYB5R3	-3.10
808	CALM2	-5.69	1780	DYNC1I1	0.45
818	CAMK2G	-3.40	1811	SLC26A3	-0.30

820	CAMP	-1.59	1917	EEF1A2	1.59
1967	EIF2B1	-5.26	2797	GNRH2	-4.54
2049	EPHB3	0.00	2811	GP1BA	0.00
2059	EPS8	-3.77	2848	GPR25	-2.76
2059	EPS8	-5.07	2862	MLNR	-5.08
2060	EPS15	-4.99	2901	GRIK5	-2.69
2119	ETV5	-3.52	2960	GTF2E1	-4.64
2119	ETV5	-3.70	2967	GTF2H3	-1.43
2245	FGD1	0.00	2972	BRF1	-2.63
2268	FGR	-3.56	3052	HCCS	0.00
2551	GABPA	-3.69	3052	HCCS	-2.90
2576	GAGE2C	0.00	3149	HMGB3	0.73
2576	GAGE7	0.00	3158	HMGCS2	0.00
2576	GAGE6	0.00	3158	HMGCS2	-4.11
2576	GAGE3	0.00	3185	HNRNPF	-0.16
2576	GAGE12I	-0.48	3297	HSF1	-2.22
2576	GAGE5	-0.48	3417	IDH1	-1.61
2576	GAGE4	-0.48	3481	IGF2	-0.53
2577	GAGE12I	0.00	3481	IGF2	-3.16
2577	GAGE5	0.00	3508	IGHMBP2	0.00
2577	GAGE4	0.00	3587	IL10RA	-4.33
2577	GAGE2C	-0.48	3592	IL12A	0.00
2577	GAGE7	-0.48	3611	ILK	-6.57
2577	GAGE6	-0.48	3658	IREB2	-3.16
2577	GAGE3	-0.48	3661	IRF3	-3.21
2578	GAGE2C	0.00	3704	ITPA	-1.42
2578	GAGE7	0.00	3708	ITPR1	-3.26
2578	GAGE6	0.00	3748	KCNC3	-2.07
2578	GAGE3	0.00	3883	KRT33A	0.00
2578	GAGE12I	-0.48	3883	KRT33A	-3.22
2578	GAGE5	-0.48	3895	KTN1	-2.88
2578	GAGE4	-0.48	3904	LAIR2	-2.88
2579	GAGE12I	0.00	3958	LGALS3	-1.05
2579	GAGE5	0.00	3992	FADS1	-1.29
2579	GAGE4	0.00	4048	LTA4H	-4.20
2579	GAGE2C	-0.48	4121	MAN1A1	-0.76
2579	GAGE7	-0.48	4209	MEF2D	4.94
2579	GAGE6	-0.48	4240	MFGE8	-0.85
2579	GAGE3	-0.48	4325	MMP16	-3.43
2596	GAP43	-2.14	4338	MOCS2	-1.31
2627	GATA6	-3.35	4354	MPP1	-0.51

2764	GMFB	1.03	4359	MPZ	-6.42
4697	NDUFA4	0.00	7508	XPC	-3.86
4744	NEFH	-3.60	7580	ZNF32	0.95
4833	NME4	-2.27	7592	ZNF41	-3.38
4867	NPHP1	-3.64	7644	ZNF91	2.04
4884	NPTX1	-2.01	7743	ZNF189	-2.96
4914	NTRK1	-0.97	7762	ZNF215	-6.37
4978	OPCML	-0.19	7905	REEP5	-3.71
5032	P2RY11	-4.44	8263	F8A2	-2.62
5188	PET112L	-2.80	8294	HIST1H4C	-1.89
5191	PEX7	-5.24	8317	CDC7	-2.43
5335	PLCG1	-1.34	8359	HIST1H4C	-1.89
5335	PLCG1	-3.69	8360	HIST1H4C	-1.89
5435	POLR2F	0.00	8361	HIST1H4C	-1.89
5534	PPP3R1	-2.28	8362	HIST1H4C	-1.89
5582	PRKCG	-5.06	8363	HIST1H4C	-1.89
5648	MASP1	0.44	8364	HIST1H4C	-1.89
5653	KLK6	-3.17	8365	HIST1H4C	-1.89
5683	PSMA2	0.31	8366	HIST1H4C	-1.89
5830	PEX5	-3.03	8367	HIST1H4C	-1.89
5872	RAB13	-1.03	8368	HIST1H4C	-1.89
5877	RABIF	-1.81	8370	HIST1H4C	-1.89
5898	RALA	-5.79	8479	HIRIP3	0.00
5908	RAP1B	-0.37	8493	PPM1D	0.00
5922	RASA2	-2.02	8519	IFITM1	-3.03
5930	RBBP6	-6.08	8521	GCM1	-4.61
6035	RNASE1	0.80	8614	STC2	-2.60
6046	BRD2	-2.52	8638	OASL	-1.82
6228	RPS23	0.00	8642	DCHS1	-1.83
6228	RPS23	-2.91	8773	SNAP23	-0.70
6295	SAG	1.79	8774	NAPG	-5.77
6507	SLC1A3	-1.24	8879	SGPL1	-4.85
6817	SULT1A1	-1.70	9047	SH2D2A	-0.97
7094	TLN1	-5.36	9099	USP2	-4.38
7094	TLN1	-5.91	9131	AIFM1	-1.57
7141	TNP1	-2.51	9232	PTTG1	-1.06
7319	UBE2A	-3.12	9232	PTTG2	-1.06
7329	UBE2I	-1.99	9352	TXNL1	-6.06
7350	UCP1	-3.21	9362	CPNE6	-0.88
7409	VAV1	-3.50	9425	CDYL	-6.25
7434	VIPR2	-4.66	9435	CHST2	-4.53

7483	WNT9A	-0.68	9532	BAG2	-2.28
9532	BAG2	-3.93	23127	GLT25D2	-2.50
9542	NRG2	-4.68	23189	KANK1	-1.06
9589	WTAP	-0.78	23216	TBC1D1	-2.02
9665	KIAA0430	-1.24	23246	BOP1	-4.07
9742	IFT140	-1.72	23281	KIAA0774	0.44
9847	KIAA0528	-3.72	23308	ICOSLG	0.53
9848	MFAP3L	-1.22	23316	CUX2	-1.01
9853	RUSC2	-0.95	23317	DNAJC13	-1.53
10013	HDAC6	-3.19	23366	KIAA0895	-6.90
10169	SERF2	-3.89	23373	CRTC1	-0.14
10401	PIAS3	-0.48	23378	KIAA0409	-6.57
10422	UBAC1	-1.94	23411	SIRT1	-2.49
10455	PECI	0.50	23436	ELA3B	0.30
10488	CREB3	-5.36	23436	ELA3B	0.00
10488	CREB3	-5.91	23559	WBP1	-0.48
10509	SEMA4B	-1.20	23598	PATZ1	-0.80
10512	SEMA3C	-3.67	23609	MKRN2	-2.85
10512	SEMA3C	-3.86	23633	KPNA6	-2.36
10540	DCTN2	-2.63	23641	LDOC1	-6.09
10569	SLU7	-1.06	24140	FTSJ1	0.00
10608	MXD4	1.68	24140	FTSJ1	-0.85
10635	RAD51AP1	0.00	25819	CCRN4L	-1.69
10693	CCT6B	-2.41	25824	PRDX5	-3.73
10887	PROKR1	-0.92	25917	THUMPD3	-1.63
10919	EHMT2	-1.74	25984	KRT23	-2.26
10926	DBF4	-3.12	25988	MIZF	-3.82
10930	APOBEC2	-4.51	26000	TBC1D10B	-3.15
10989	IMMT	-3.06	26015	RPAP1	-4.68
10989	IMMT	-3.07	26053	AUTS2	-1.79
11064	CEP110	-4.93	26128	KIAA1279	0.61
11079	RER1	-4.01	26166	RGS22	-2.58
11083	DIDO1	0.00	26292	MYCBP	-1.40
11083	DIDO1	-2.82	26524	LATS2	-4.38
11170	FAM107A	-5.42	26524	LATS2	-5.69
11341		-4.93	26575	RGS17	-0.30
22884	WDR37	-1.12	26748	GAGE12I	0.00
22884	WDR37	-1.30	26748	GAGE5	0.00
22884	WDR37	-1.84	26748	GAGE4	0.00
22889	KIAA0907	-2.78	26748	GAGE2C	-0.48
22948	CCT5	0.64	26748	GAGE7	-0.48

23035	PHLPPL	-5.34	26748	GAGE6	-0.48
26748	GAGE3	-0.48	54839	LRRC49	-2.42
26749	GAGE2E	-0.48	54840	APTX	-0.70
26985	AP3M1	-1.52	54840	APTX	-1.52
27040	LAT	-0.40	54893	MTMR10	-1.40
27071	DAPP1	0.52	54960	GEMIN8	-1.04
27101	CACYBP	-2.11	54960	GEMIN8	-1.88
27106	ARRDC2	1.21	54994	C20orf11	0.00
27164	SALL3	-1.10	54994	C20orf11	-2.82
27164	SALL3	-1.88	55101	ATP5SL	-3.83
27238	GPKOW	-2.89	55176	SEC61A2	-1.30
27258	LSM3	-1.48	55223	TRIM62	-3.99
27309	ZNF330	-4.88	55293	UEVLD	1.48
28991	COMMD5	-1.23	55293	UEVLD	-0.26
50508	NOX3	-2.96	55293	UEVLD	-3.14
50619	DEF6	2.56	55529	TMEM55A	-3.87
51175	TUBE1	-2.34	55608	ANKRD10	-1.09
51214	IGF2AS	-0.53	55608	ANKRD10	-1.44
51301	GCNT4	0.00	55626	AMBRA1	-7.34
51315	KRCC1	-6.32	55630	SLC39A4	-1.55
51315	KRCC1	-8.23	55686	MREG	0.00
51318	MRPL35	-3.06	55793	FAM63A	-1.75
51447	IP6K2	0.00	55894	DEFB103A	-3.85
51447	IP6K2	-0.90	55924	C1orf183	-2.48
51493	C22orf28	-1.47	55929	DMAP1	-3.05
51493	C22orf28	-2.87	56125	PCDHB11	0.57
51504		-3.73	56172	ANKH	-3.25
51601	LIPT1	-4.28	56267	CCBL2	0.00
51601	LIPT1	-5.91	56267	RBMXL1	0.00
51646	YPEL5	-2.32	56548	CHST7	-4.60
53339	BTBD1	3.78	56906	THAP10	-2.42
54205	CYCS	1.65	57001	ACN9	-3.64
54207	KCNK10	-3.08	57030	SLC17A7	0.00
54496	PRMT7	-6.16	57030	SLC17A7	-0.30
54518	APBB1IP	-1.58	57102		0.00
54518	APBB1IP	-5.37	57154	SMURF1	-0.85
54534	MRPL50	-2.96	57156	TMEM63C	-1.12
54550	NECAB2	-4.04	57167	SALL4	-2.63
54680	ZNHIT6	-0.89	57181	SLC39A10	-2.29
54820	NDE1	-1.24	57468	SLC12A5	-1.99
54834	GDAP2	-3.14	57473	ZNF512B	-1.99

54834	GDAP2	-3.64	57585	CRAMP1L	-1.72
57728	WDR19	-4.28	84138	SLC7A6OS	-6.16
58497	PRUNE	-1.75	84141	FAM176A	0.00
59351	PBOV1	-4.08	84146	ZNF644	-2.57
60370	AVPI1	-2.97	84188	FAR1	-1.82
60468	BACH2	-1.41	84311	MRPL45	-4.66
60485	SAV1	0.00	84332	DYDC2	-1.28
60485	SAV1	-0.70	84504	NKX6-2	-1.47
64232	MS4A5	0.37	84557	MAP1LC3A	-4.05
64332	NFKBIZ	-4.94	84557	MAP1LC3A	-4.59
64763	ZNF574	-2.69	84645	C22orf23	0.00
64949	MRPS26	-4.54	84645	C22orf23	-5.43
64965	MRPS9	0.49	84909	C9orf3	-4.61
64983	MRPL32	0.31	84910	TMEM87B	-3.95
65078	RTN4R	-2.49	84922	FIZ1	0.00
79646	PANK3	-2.03	84935	C13orf33	-4.84
79651	RHBDF2	-1.36	85438	C4orf35	-0.52
79712	GTDC1	-4.83	85455	DISP2	-8.13
79730	NSUN7	-3.02	85465		-1.03
79898	ZNF613	0.38	85480	TSLP	-2.99
79903	NAT15	-0.05	89846	FGD3	2.71
79906	MORN1	-4.01	89857	KLHL6	-4.42
79935	CNTD2	-2.04	91147	TMEM67	-1.97
80237	ELL3	-3.89	91147	TMEM67	-3.24
80305	TRABD	-2.01	91353	IGLL3	-4.47
80318	GKAP1	-4.86	91603	ZNF830	-2.41
80323	CCDC68	-0.45	91801	ALKBH8	-7.74
80331	DNAJC5	-1.99	91862	MARVELD3	-3.08
80705	TSGA10	-4.28	92014	MCART1	-2.09
80705	TSGA10	-5.91	92270		0.00
80739	C6orf25	-4.35	92270		-2.91
80740	LY6G6C	-4.35	92715	WDR85	-1.68
80760	ITIH5	2.57	93426	SYCE1	-2.26
81542	TXNDC1	-3.67	93663	ARHGAP18	-4.09
81542	TXNDC1	-3.95	93973	ACTR8	0.00
81557	MAGED4B	-4.62	94032	CAMK2N2	-0.97
83444	INO80B	-0.48	112950	MED8	-3.07
83550	GPR101	-7.58	114987	WDR31	-2.86
83640	FAM103A1	-5.87	115416	C7orf30	-4.54
83740	H2AFB2	-2.62	116224	FAM122A	0.00
116224	FAM122A	-0.30	196483	FAM86A	-2.65

117248	GALNTL2	-0.70	219844	HYLS1	-2.05
118813	ZFYVE27	-1.81	219927	MRPL21	0.00
119774	OR52K2	-3.12	220988	HNRNPA3	-3.15
120066	OR5P3	-3.67	246330	PELI3	-0.80
120066	OR5P3	-4.64	255239	ANKK1	0.04
121504	HIST1H4C	-1.89	255324	EPGN	-0.07
124583	CANT1	-2.37	266812	NAP1L5	-0.48
124583	CANT1	-4.32	283294	C11orf47	-2.34
128372	OR6N1	-4.08	283899	INO80E	0.00
129868	TRIM43	-1.31	284119	PTRF	-0.97
130271	PLEKHH2	-2.47	284207	METRNL	-1.71
130271	PLEKHH2	-3.71	284309	ZNF776	0.96
130535	KCTD18	-2.35	284309	ZNF776	0.54
131474	CHCHD4	-4.55	284309	ZNF776	-0.11
134145	FAM173B	0.64	284611	FAM102B	-3.59
140467	ZNF358	-2.53	285242	HTR3E	-1.20
143241	DYDC1	-1.28	285282	RABL3	-4.64
143279	HECTD2	-4.01	285349	ZNF660	-6.77
143496	OR52B4	-0.98	286187	LRRC67	-3.75
144165	PRICKLE1	2.40	338675	OR5AP2	-3.63
147807	ZNF524	0.00	339345	NANOS2	0.65
149469	KIAA0467	-3.07	340252	ZNF680	0.87
152926	PPM1K	-1.97	341676	NEK5	-2.61
152926	PPM1K	-2.66	342538	NACA2	-4.45
152926	PPM1K	-4.27	344807	CD200R1L	-3.17
158399	ZNF483	-2.50	345079	ANKRD56	-6.01
160428	ALDH1L2	-2.58	347468	OR13H1	-2.96
162605	KRT28	0.00	353164	TAS2R42	-1.52
162605	KRT28	-2.43	375704	ENHO	-4.74
163126	EID2	0.80	387103	C6orf173	0.00
164091	PAQR7	-1.95	387328	ZNF322B	-1.48
164237	WFDC13	0.01	387758	FIBIN	-1.38
165082	GPR113	-1.03	388228	SBK1	-3.60
165140	OXER1	-2.21	388533	KRTDAP	-5.82
170506	DHX36	-5.17	388650	FAM69A	-3.45
170685	NUDT10	-2.64	388677	NOTCH2NL	-1.66
170692	ADAMTS18	-1.09	388759		-1.04
192668	CYS1	-0.83	389136	VGLL3	-3.65
192668	CYS1	-1.21	389151		-3.64
389658	FAM150A	-0.83	391358		-3.73
390063	OR51I1	-6.30	391370	RPS12	0.02

390144	OR5D16	0.00	391723	HELT	-0.95
390151	OR8H2	-0.82	399947	C11orf87	-7.81
391123	C1orf204	0.00	400360	C15orf54	-0.95
391123	VSIG8	0.00	400823	FAM177B	-4.16
391358		-3.73	402415	XKRX	1.28
391370	RPS12	0.02	408029		0.04
391723	HELT	-0.95	414325	DEFB103A	-3.85
399947	C11orf87	-7.81	440107	PLEKHG7	-2.01
400360	C15orf54	-0.95	440275	EIF2AK4	0.00
400823	FAM177B	-4.16	474381	H2AFB2	-2.62
402415	XKRX	1.28	474383	F8A2	-2.62
408029		0.04	474384	F8A2	-2.62
414325	DEFB103A	-3.85	554313	HIST1H4C	-1.89
440107	PLEKHG7	-2.01	574016	CLLU1OS	-1.18
440275	EIF2AK4	0.00	642265	FAM75A2	1.24
474381	H2AFB2	-2.62	643736		-1.13
474383	F8A2	-2.62	645073	GAGE2C	0.00
474384	F8A2	-2.62	645073	GAGE7	0.00
554313	HIST1H4C	-1.89	645073	GAGE6	0.00
574016	CLLU1OS	-1.18	645073	GAGE3	0.00
642265	FAM75A2	1.24	645073	GAGE12I	-0.48
643736		-1.13	645073	GAGE5	-0.48
645073	GAGE2C	0.00	645073	GAGE4	-0.48
645073	GAGE7	0.00	653333	FAM86B2	-2.65
645073	GAGE6	0.00	653506	METRNL	-1.71
645073	GAGE3	0.00	654258	LRRC49	-2.42
645073	GAGE12I	-0.48	728401		0.00
645073	GAGE5	-0.48	729627		-3.64
645073	GAGE4	-0.48	729915		0.00
653333	FAM86B2	-2.65	100008586	GAGE2C	0.00
653506	METRNL	-1.71	391123	VSIG8	0.00
654258	LRRC49	-2.42	391358		-3.73
728401		0.00	391370	RPS12	0.02
729627		-3.64	391723	HELT	-0.95
729915		0.00	399947	C11orf87	-7.81
100008586	GAGE2C	0.00	400360	C15orf54	-0.95
391123	VSIG8	0.00	400823	FAM177B	-4.16
402415	XKRX	1.28	474383	F8A2	-2.62
408029		0.04	474384	F8A2	-2.62
414325	DEFB103A	-3.85	554313	HIST1H4C	-1.89
440107	PLEKHG7	-2.01	574016	CLLU1OS	-1.18

440275	EIF2AK4	0.00
474381	H2AFB2	-2.62
474383	F8A2	-2.62
474384	F8A2	-2.62
554313	HIST1H4C	-1.89
574016	CLLU1OS	-1.18
642265	FAM75A2	1.24
643736		-1.13
645073	GAGE2C	0.00
645073	GAGE7	0.00
645073	GAGE6	0.00
645073	GAGE3	0.00
645073	GAGE12I	-0.48
645073	GAGE5	-0.48
645073	GAGE4	-0.48
653333	FAM86B2	-2.65
653506	METRNL	-1.71
654258	LRRC49	-2.42
728401		0.00
729627		-3.64
729915		0.00
100008586	GAGE2C	0.00
391123	VSIG8	0.00
391358		-3.73
391370	RPS12	0.02
391723	HELT	-0.95
399947	C11orf87	-7.81
400360	C15orf54	-0.95
400823	FAM177B	-4.16
402415	XKRX	1.28
408029		0.04
414325	DEFB103A	-3.85
440107	PLEKHG7	-2.01
440275	EIF2AK4	0.00
474381	H2AFB2	-2.62
643736		-1.13
645073	GAGE2C	0.00
645073	GAGE7	0.00
645073	GAGE6	0.00
645073	GAGE3	0.00
645073	GAGE12I	-0.48

642265	FAM75A2	1.24
645073	GAGE4	-0.48
653333	FAM86B2	-2.65
653506	METRNL	-1.71
654258	LRRC49	-2.42
728401		0.00
729627		-3.64
729915		0.00
100008586	GAGE2C	0.00
100008586	GAGE7	0.00
100008586	GAGE6	0.00
100008586	GAGE3	0.00
100008586	GAGE12I	-0.48
100008586	GAGE5	-0.48
100008586	GAGE4	-0.48
100130430		-1.99
100131294	RAB13	-1.03
100131390		1.23
100133501	FAM75A2	1.24
100133913	CXorf24	-3.38
100134431		-1.99

645073	GAGE5	-0.48